UNIVERSITY OF SOUTHERN QUEENSLAND

MEASURING, MODELLING AND UNDERSTANDING THE MECHANICAL BEHAVIOUR OF BAGASSE

A Dissertation submitted by

Floren Plaza BE (Civil Hons)

For the award of

Doctor of Philosophy

September, 2002

Vol 1 of 2

ABSTRACT

In the Australian sugar industry, sugar cane is smashed into a straw like material by hammers before being squeezed between large rollers to extract the sugar juice. The straw like material is initially called prepared cane and then bagasse as it passes through successive roller milling units. The sugar cane materials are highly compressible, have high moisture content, are fibrous, and they resemble some peat soils in both appearance and mechanical behaviour.

A promising avenue to improve the performance of milling units for increased throughput and juice extraction, and to reduce costs is by modelling of the crushing process. To achieve this, it is believed necessary that milling models should be able to reproduce measured bagasse behaviour.

This investigation sought to measure the mechanical (compression, shear, and volume) behaviour of prepared cane and bagasse, to identify limitations in currently used material models, and to progress towards a material model that can predict bagasse behaviour adequately.

Tests were carried out using a modified direct shear test equipment and procedure at most of the large range of pressures occurring in the crushing process. The investigation included an assessment of the performance of the direct shear test for measuring bagasse behaviour. The assessment was carried out using finite element modelling.

It was shown that prepared cane and bagasse exhibited critical state behaviour similar to that of soils and the magnitudes of material parameters were determined. The measurements were used to identify desirable features for a bagasse material model. It was shown that currently used material models had major limitations for reproducing bagasse behaviour. A model from the soil mechanics literature was modified and shown to achieve improved reproduction while using magnitudes of material parameters that better reflected the measured values. Finally, a typical three roller mill pressure feeder configuration was modelled. The predictions and limitations were assessed by comparison to measured data from a sugar factory.

CERTIFICATION OF DISSERTATION

I certify that the ideas, experimental work, results, analyses, software and conclusions reported in this dissertation are entirely my own effort, except where otherwise acknowledged. I also certify that the work is original and has not been previously submitted for any other award.

Eleonor Plaza — Signature of Candidate

19/09/02 — Date

ENDORSEMENT

N. Harris — Signature of Supervisor

04/09/02 — Date

Signature of Supervisor

16/9/02 — Date

ACKNOWLEDGMENTS

I wish to thank my supervisors, Assoc. Prof. Harry Harris from the University of Southern Queensland, and Dr. Mac Kirby from the CSIRO Land and Water, for their guidance and patience throughout the project, and for their friendship. Their advice has been invaluable to me.

I would like to thank John Williams for his major contribution in the design and preparation of the equipment, and in carrying out the tests safely and efficiently. Neil McKenzie ensured that the press equipment was fixed in time to carry out the experimental tests. Neil McKenzie and Allan Connor both supervised and carried out the required electronic and hydraulic work. Peter Everitt provided measurement and control advice.

The assistance of Gordon Ingram, Steven Pennisi, Anthony Mann, Gaye Davy, and Ramesh Ponnuswami in carrying out the 1998 tests, and Letitia Langens in carrying out the 2001 tests, is acknowledged. Letitia Langens was also the co-author of several conference papers. The staff of Pleystowe Mill and Racecourse Mill provided assistance in obtaining the cane and also cane analysis information.

Matt Schembri provided support and advice particularly in the early stages of this work.

Geoff Kent provided advice, and also assistance in running several computer packages.

The following people were of great help to me during this investigation and I thank them: Anthony Mann for mathematical advice. Ann Ellis in finding and obtaining publications. Stewart McKinnon, Col Benson, and Geoff Kent provided assistance with numerous computer applications and problems.

Christine Bartlett at the Research and Higher Degrees Office at USQ provided help in progress and administrative matters.

Mike Cox at the Bureau of Sugar Experiment Stations in Bundaberg gave advice and information on cane varieties.

CSR Limited gave permission to publish operating mill data from one of its factories.

I would like to thank: Terry Dixon for championing the funding of this investigation, and for his encouragement. The Sugar Research Institute Board for its vision in the initial funding. The Faculty of Engineering and Surveying at the University of Southern Queensland for its scholarship, which allowed the investigation to be progressed. The Australian sugar mills for providing additional funds through Sugar Research Institute levy funding; and the Sugar Research and Development Corporation for part funding of the 2001 experimental tests.

This thesis is dedicated to Allan Connor, who passed away suddenly in September 2002.

This thesis is also dedicated to my mum and dad, my grandmother Antonia, my sister Miren, and my brother John. Euzkaldunak Australian.

Measuring, modelling and understanding the mechanical behaviour of bagasse

Contents

List of Tables

List of Figures

Notation

a , P_a	Position of critical state line
β	Extension of Modified Cam Clay model
D_e	Elastic matrix
D_{ep}	Elastic-plastic matrix
E	Young's Modulus
G	Shear Modulus
e	Void ratio
σ	Stress
ε	Strain
v	Specific volume
λ	Slope of normal compression line
κ	Slope of elastic unloading-reloading line
χ	Hardening constant
ϕ_{cs}	Equivalent critical state friction angle
F	Yield surface
Q	Plastic potential surface
H	Plastic hardening modulus
K_o	At rest earth pressure coefficient, horizontal effective stress divided by the vertical effective stress
M	Slope of critical state line in pressure-shear stress plane
OCR	Over Consolidation Ratio, ratio of maximum stress experienced previously to current stress,
P_c , P_b	Size of yield surface, pre-consolidation pressure, pressure at the intersection of the current elastic loading reloading line with the normal compression line
R	Extension of Drucker Prager Cap model
d	Cohesion for Drucker Prager Cap model
p	Pressure (or stress)
p'	Effective pressure (or stress)
q , t	Deviator stress

r	spacing ratio for CASM model
n	stress state coefficient for CASM model
υ	Poisson's ratio
C	Compression ratio
γ	Compaction
f	Fibre content
ρ_f	Fibre density
ρ_j	Juice density
μ	Coefficient of friction
θ	Angle between line connecting a roll pair and location on the roll surface
D	Diameter of roll
L	Length of roll
G	Total torque on one roll
H	Force on rolls parallel to the movement of bagasse
R	Separating force on rolls

1 Chapter 1 – The need for a better understanding of bagasse behaviour

1.1 Introduction – the hypothesis

The project sets out to improve the understanding of the generalised stress-strain relationships (ie. the constitutive equations) that characterise the way in which cane fibres behave during the milling process. Put in more detailed terms, the project seeks to show that bagasse exhibits critical state behaviour, to determine material parameters for prepared cane and bagasse, and to make progress towards a robust material model that can reproduce the compression, shear, and volume behaviour over the range of stresses and strains relevant to the milling process to which sugar cane is subjected.

1.2 Background

The Australian sugar industry is one of Australia's largest rural industries and one of the world's largest exporters of raw sugar, contributing directly and indirectly over $4 billion to the Australian economy. The 40 Mt of sugarcane produced in Australia each year generates about $2 billion from the sale of raw sugar, of which about 80% is exported. To remain competitive in the world market, the cost of production of raw sugar has had to continually decrease at a long term average rate of approximately 2% each year (Fry, 1996). Cost reductions have been achieved through growth of the industry to reduce the unit costs of production and through continued research and development to reduce costs and increase the efficiency of the raw sugar manufacturing process.

Raw sugar is manufactured in 30 raw sugar factories, mostly situated in regional areas of Queensland and northern New South Wales. The raw sugar manufacturing process involves firstly the extraction of sugar juice from sugarcane, followed by the clarification and concentration of the juice and then the crystallisation of sugar from the juice. The extraction process is one of the highest cost operations in the factory and results in the second largest source of sugar loss in the sugar manufacturing process. The extraction of sugar juice from sugarcane is mostly achieved in a series of six-roll milling units. A schematic of an Australian six roll milling unit is shown in Figure 1.1.

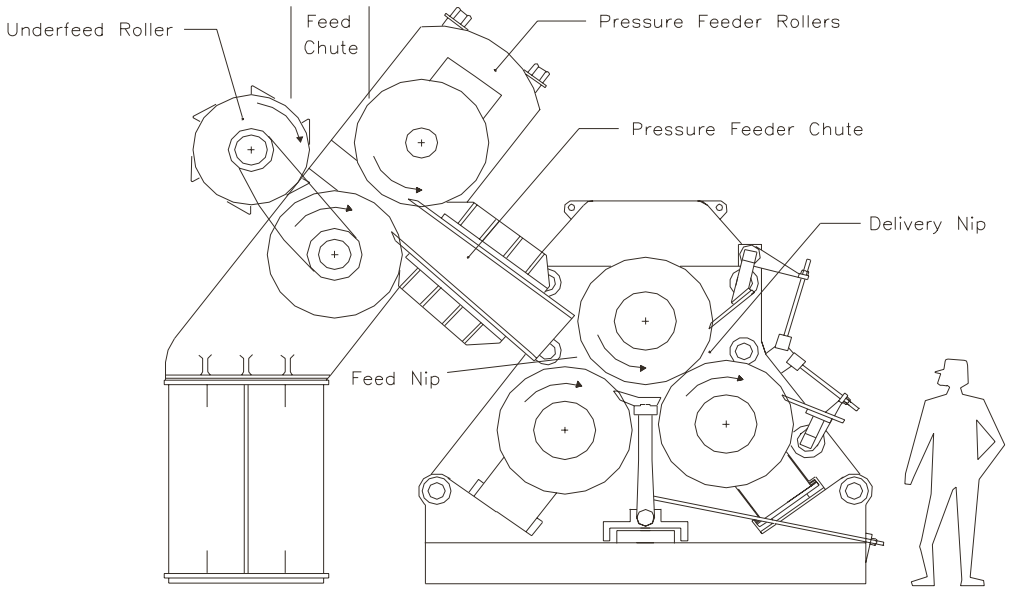

Figure 1.1. Standard six roll mill unit used in the Australian sugar industry (Neill et al., 1996).

Sugar cane is prepared for milling in a hammer mill, which reduces the cane to a mixture of juice, storage cells and lengths of multiple and individual fibres. When freshly prepared, this is quite similar to moist straw, but when handled it is not readily apparent that there is a high level of moisture (mass of water divided by total mass equal to 70%) in the material (shown in Figure 1.2). This prepared cane is then compressed between pairs of rollers in a six roll milling unit to extract the maximum possible quantity of sugar juice. The solid material leaving this milling unit is called bagasse. The bagasse is then sprayed or soaked with dilute juice and then passed through up to five further mills, in a counter current extraction process, with a further spraying or soaking process occurring before each subsequent mill (the initial hot water is usually added just before the final milling unit). The final bagasse (shown in Figure 1.3), still containing about 2% sugar and 50% water (mass divided by total mass), is then burnt to provide self-sufficient power to the factory.

Improved juice extraction performance has benefits in terms of increased sugar production and results in lower moisture fuel and hence higher boiler capacity for steam generation. Milling units and boilers have the highest capital costs of any individual items of sugar factory plant.

Figure 1.2. Prepared cane.

Figure 1.3. Final bagasse.

Increases in mill and boiler capacity through improved operational settings will have significant financial benefit to the industry. Incremental milling capacity has a capital cost of about $100,000 for every tonne of cane per hour increase in capacity, so there is a substantial incentive for the industry to improve the capacity of existing mills without the need for new capital expenditure. An avenue for improved performance is through computer modelling. Based on the experience gained from the modelling of other factory processes, for example, clarifier modelling (Steindl, 1995, Steindl et al., 1998) and boiler modelling (Dixon and Plaza, 1995, Plaza et al., 1999), it is expected that improved modelling of the milling process will result in increased throughput through existing milling units and improved juice extraction performance.

The milling process consists of three distinct but coupled phenomena: 1. The fibrous skeleton of the prepared cane or bagasse is subjected to pressures from typically 2 kPa to 20 MPa. This results in large compressive and shear strains that reorient, distort and break the fibres. 2. The juice flows within the porous matrix of this skeleton at rates governed by the void ratio and therefore its degree of compression and pressure differential. 3. Juice flows through the boundaries of the bagasse, where compressive and frictional stresses are applied. The interaction of all these processes influences the roll loads, the roll torques, and the percentage juice extraction.

1.3 Previous work on the milling process

Much of the industry's knowledge of the milling process originates from a series of PhD projects undertaken at The University of Queensland in the 1950s and 1960s. Empirical models for roll load, roll torque and sugar extraction were developed then and are still used today (Murry & Holt, 1967). These models identified many of the important milling parameters such as the roll speed and the prepared cane or bagasse compaction. While these models have served the industry well, they do not identify the detailed mechanisms occurring within the milling process and so do not provide a fundamental understanding of the process. It is considered unlikely that further substantial improvements in terms of cost reductions or improvements in process efficiencies will be made to the milling process without this more fundamental understanding.

In 1989 the Sugar Research Institute in Mackay and the Sugar Research and Development Corporation began funding the development of a milling model at the University College of Swansea in Wales. The milling model was to incorporate the fundamental equations that describe the mechanisms occurring in the milling process. The development of the model of a two roll mill by Zhao (1993) and Owen et al. (1995) at the University College of Swansea involved the use of porous media mechanics and finite element methods to describe the behaviour of prepared cane. The model is based on the governing equations for saturated - unsaturated porous media and has been simplified somewhat by assuming that accelerations can be neglected. Darcy's law is used to describe the flow of the juice through the fibrous skeleton. The bagasse has a degree of water saturation of at least 85% at most of the locations in a milling unit, except at the feed chute and underfeed rolls, and after the delivery nip. A significant amount of air is also present in the bagasse at feed chute conditions. Terzaghi's principle of effective stress is assumed to apply. The material is essentially described with a two-phase model, consisting of the fibrous skeleton and the juice.

The model offered the potential for an improved understanding of the milling process. Garson (1992a, 1992b) evaluated the progress made by Zhao towards the end of his study. Garson identified two immediate impediments to further progress: ‘a general lack of reliable property data for prepared cane and bagasses and the failure to yet define appropriate boundary conditions. In particular, a stress-strain relation for the fibrous skeleton component of cane and bagasse and the prescribed boundary condition at the roll surface are required’. Garson further commented on a proposal by Swansea to ‘back calculate an effective stress-strain relation for the fibrous skeleton from constrained uniaxial test data’. As a side issue relevant to the current investigation, Garson commented that ‘of great interest was the apparent ability of the model to represent reabsorption as internal shearing of the material being crushed. This was evidenced by the change in sign of the tangential load on the roll surface and in the velocity field produced by the program. The result does not conclusively identify this as the mechanism of reabsorption but it demonstrated one of the desired capabilities of the new model’.

Crucial to this model is a suitable material (constitutive) description for the stress-strain behaviour of the fibrous skeleton. The model developed by Zhao (1993) used a linear elastic material model that was unsuitable for bagasse, which experiences large unrecoverable strains when loaded. The lack of a suitable material model has hindered the development and application of the finite element model to real milling situations. A more suitable family of material models applicable to bagasse, called critical state models, was identified by Leitch (1996) and adopted by Adam (1997). Further development of Zhao's model was undertaken by Zhao at Swansea and Adam (1997) at James Cook University. The development of the model has been monitored and assessed periodically, for example, by Edwards et al. (1995) and Kent et al. (1998).

1.4 Explanation of the critical state concept

Critical state models were developed for saturated soils, which are similar (to a degree) to prepared cane, in that they exhibit elastic and plastic behaviour, large strains and compressive behaviour at yield. Prepared cane is also saturated with water at many locations in a milling unit. The critical state models had their origin at the Cambridge Soil Mechanics Group in the United Kingdom, see Roscoe et al. (1958), Schofield and Wroth (1968), Atkinson and Bransby (1978), following and building on the measurements carried out by Rendulic (1936) and Henkel (1960). Further development and description of critical state models in soil mechanics is given, for example, in Britto and Gunn (1987) and Muir Wood (1990). Critical state models unify the compression, shear and volume behaviour of soils. Critical state models are formulated in three dimensional p:q:v space where p is the average of the normal stresses acting on the body, q (the deviatoric axis) is related to the shear stresses, and v is the specific volume (or some other appropriate volumetric measure such as e, the void ratio). Constitutive models of particular interest have been the Modified Cam Clay (MCC) model, the Crushable Foam model and the Drucker-Prager Cap (DPC) model.

More detailed summaries of the application of Modified Cam Clay, Crushable Foam and Drucker-Prager Cap models to prepared cane can be found in Adam (1997). The models themselves (and extensions of them) are described in detail in publications such as Desai and Siriwardane (1984) or Hibbit et al. (2001) and will

not be repeated here. A short description of the relevant features is given below. Extensions of the MCC and DPC models are described in Chapter 8.

Figure 1.4 shows the plastic and elastic compression behaviour in the p:e plane. Initial loading takes place along the normal compression line (NCL), also known as the normal consolidation line, and is shown in Figure 1.4 as the line with a plastic slope. The unloading and reloading behaviour takes place along the elastic line that is shown in Figure 1.4 as the line with an elastic slope. When reloading along the elastic line reaches the NCL it continues along the NCL line. At a relatively low level of unload (the 'wet' side of critical state) the material will decrease in volume during shearing. At a relatively high level of unload (the 'dry' side of critical state) the material will increase in volume during shearing. Between these two extremes is the location of the critical state where no change in volume or stress occurs with ongoing shear deformation (not shown in Figure 1.4).

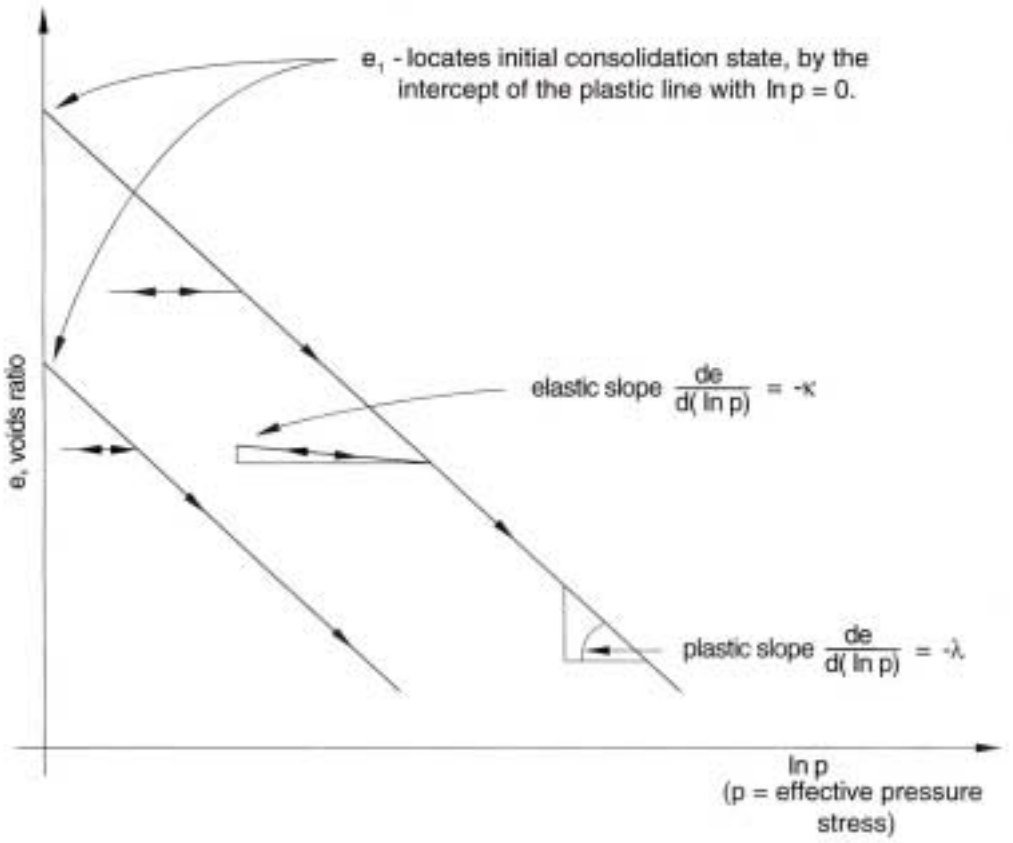

Figure 1.4. Compression loading and unloading behaviour in the p-e plane (after Hibbit et al., 2001).

When viewed in the p:q plane, the Modified Cam Clay critical state model has an elliptical yield surface (see Figure 1.5, where q is given as t, following Hibbit et al., 2001), and an associated plastic flow rule, which defines the plastic strain vector as being orthogonal to the point on the yield surface intersected by the material's stress path. The plastic strain vector has two components: the plastic volumetric strain parallel to the p axis, and the plastic shear or shape strain parallel to the q axis. Critical state occurs at the apex of the ellipse, where there is (ongoing) shape change at constant volume and stress. The material's hydrostatic pressure-volume relationship (the normal compression line) governs the growth and contraction of the yield surface. The shape of the elliptical yield surface is dependent on M, the slope of the critical state line in the p:q plane. The M parameter is normally obtained by taking the material to critical state in a triaxial test, or is estimated in direct shear box tests. An extension of the Modified Cam Clay model is given in Hibbit et al. (2001) whereby the shape of the yield surface (in particular, the right hand side of the ellipse) can be further modified by the use of a β parameter.

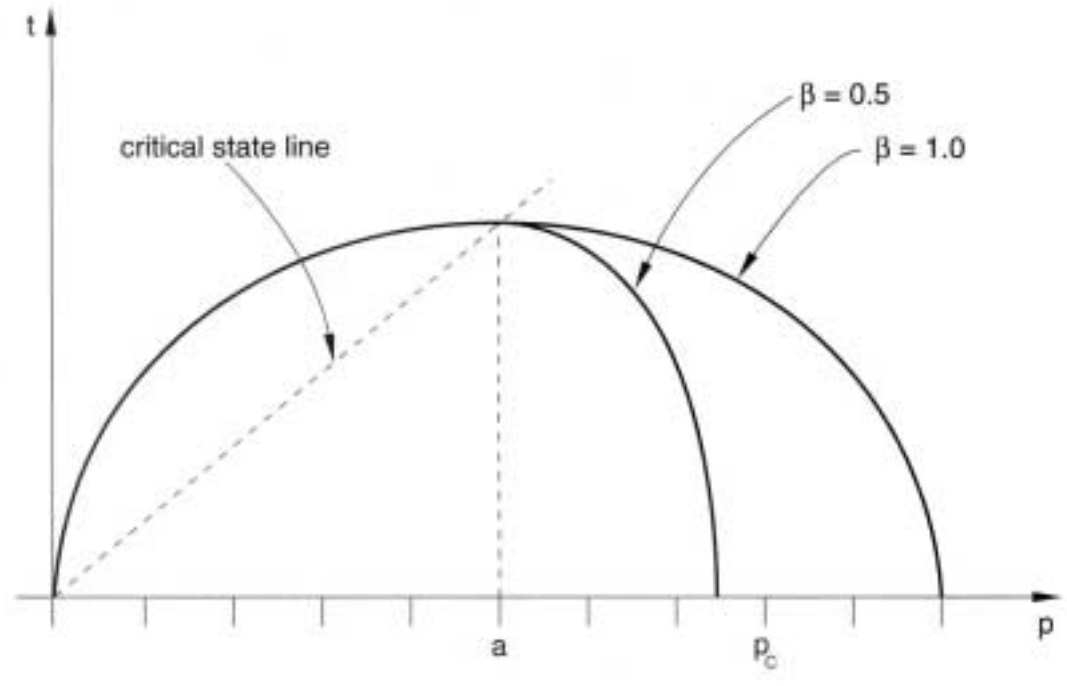

Figure 1.5. Clay yield surfaces in the p-t plane (after Hibbit et al., 2001).

The Crushable Foam model was developed for the analysis of materials such as foams and honeycombed structures. It is a variation on the Modified Cam Clay model. It uses a non-associated elliptical flow potential centred about the deviatoric stress axis. This flow potential is based on the observation of negligible radial plastic strains in simple compression tests. 'Associated' means that (post-yield) flow is perpendicular to the yield surface. 'Non-associated' means the flow is not perpendicular to the yield surface.

The Drucker-Prager Cap model has an elliptical yield surface on the 'wet' side of critical state, and a Mohr-Coulomb type shear failure surface on the 'dry' side (shown in Figure 1.6). The elliptical yield surface has an associated flow rule governing the plastic strain vector, whilst the shear failure surface has non-associated flow, that is the plastic strain vector is associated with another potential surface which intersects the yield surface at the point where the material has commenced plastic flow.

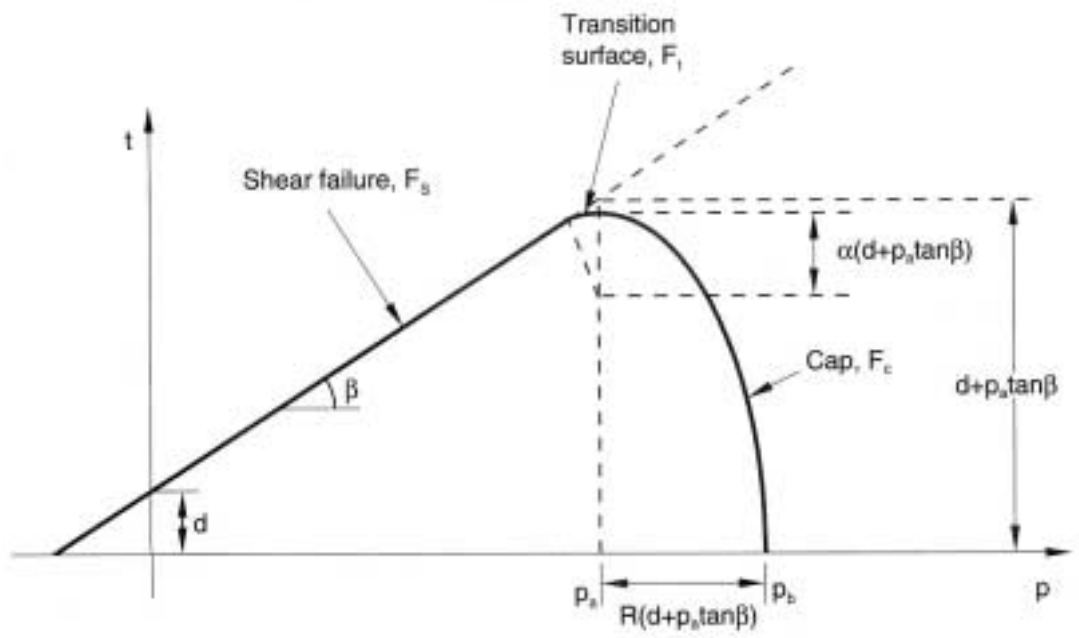

Figure 1.6. Drucker Prager Cap yield surfaces in the p-t plane (after Hibbit et al., 2001).

Leitch et al. (1997) carried out a search of available constitutive models including isotropic elasticity, isotropic elasto-plastic models and anisotropic models. They concluded that anisotropic models were too complex at the time to be coded into a computer model and recommended the model for coding to be a modified isotropic associated flow Crushable Foam model. Adam (1997) discontinued the use of the Crushable Foam plasticity model due to severe numerical convergence difficulties and used the Drucker-Prager Cap and Modified Cam-clay models such that they basically represented the same model by using an inverse calibration procedure based on uniaxial compression tests. Loughran and Adam (1998) presented an inverse calibration procedure using the Drucker-Prager Cap plasticity model in combination with uniaxial compression tests to determine material parameters such as M, the slope of the critical state line.

1.5 Experimental investigation of critical state models

The yield surfaces and plastic flow rules of Modified Cam Clay and Capped Drucker-Prager models were developed after extensive testing of soil samples in p:q:v space (Schofield and Wroth, 1968; Muir Wood, 1990; Hibbitt et al, 2001). Numerous stress probes were carried out to define the yield surfaces, and ascertain the direction of the plastic strain vectors.

Similar stress probes were not performed for prepared cane or bagasse. An attempt to measure parameters for a critical state model for prepared cane in p:q:v space was carried out by Leitch (1996). He used a soil mechanics triaxial cell to apply both isotropic and deviatoric compression to samples of cane. Leitch's isotropic tests were used to describe the normal consolidation line, while his deviatoric tests were aimed at defining a shear and compression relation. The isotropic compression results were reasonably reliable, but the experimental results for the deviatoric tests had major problems. The cylindrical samples experienced large deformations along the axis of the cylinder during the isotropic compression part of the tests while much smaller deformation took place along the radial direction, such that the aspect ratio of the sample changed dramatically. Aspect ratios less than one were obtained which are quite undesirable. During the deviatoric loading the ram ran out of travel. High juice pressures developed in the nominally drained tests.

Leitch concluded that, for the purpose of developing a material model, 'the test results were considered to be unreliable'. Therefore, although critical state material parameters have been obtained by several investigators from analysing the deviatoric part of the triaxial tests as reported below, these parameters must be treated with a great deal of caution.

1.6 Derivation of critical state parameters

Loughran and Adam (1998) and Owen et al. (1998) summarised their derivations of the parameters of prepared cane. In order to improve their predictions of simple uniaxial compression, the parameter M (slope of the critical state line) was set at 3.8 to 4.0. This range of values was stated to be derived from inverse calibration of uniaxial test data and from the Leitch (1996) triaxial results. It is noted that values of M as high as 3.8 and 4.0 imply physically impossible friction angles. A maximum value for M is 3.0, for which the corresponding friction angle for triaxial compression is 90 degrees. Following Carter (2003), the physical absurdity of values of M of 3.8 and 4.0 is noted. However, since these values have been extensively used in many modelling papers, it has been necessary in this investigation to address the use of such values and the results of their use.

Kirby (1997) calculated estimates of M from the Leitch data to be from 0.07 to 2.0. Schembri et al. (1998) concluded that, on the basis of the Leitch data, 'M is unlikely to be greater than 2 and may be much less'. Considering the above, and Leitch's own conclusions on the quality of the measured data, it is unlikely that a value of M can be obtained with confidence from the Leitch (1996) data. Kirby (1997) calculated M values of about 1.0 as derived from direct shear box tests of Plaza and Kent (1997). The value of M used in the Drucker Prager Cap (or the MCC) material model has important implications for the kind of material behaviour that a milling model can reproduce. There is a major discrepancy between the values of M quoted by Loughran and Adam (1998) and Owen et al. (1998) and those quoted by Kirby (1997) and Schembri et al. (1998).

Schembri et al. (1998) tested a Modified Cam-Clay model against the available experimental data including constrained uniaxial, triaxial and direct shear tests. The Modified Cam-Clay model was basically the same model as the Drucker Prager Cap

model as calibrated by Loughran and Adam (1998). These modelling tests concluded that adjustments to the M value can be used in some situations (such as uniaxial compression loading) to improve the predictions to the detriment of other predictions (such as loading in shear). This suggests that the model and procedure adopted by Loughran and Adam is suited to only a narrow range of stress states, and should be viewed with caution when considering its application to a milling simulation, which is believed to involve complex stress conditions. Although large portions of the milling process are believed to subject the fibrous skeleton to uniaxial compression, there is also evidence that there are locations in a mill in which the bagasse experiences significant shear strains (Plaza and Kent, 1997, Schembri et al., 1998). Chapter 5 in this investigation describes a limitation in the MCC and DPC models that explains the reason for the above modelling problems.

1.7 Inverse methods for obtaining material parameters

The inverse method topic for obtaining material parameters is touched upon because it has been referred to, used by, and modified, by several authors in the milling research field in the last 10 years. Zhao (1993) adopted this approach when confronted with the fact that a constitutive relationship relating stresses and strains (a material model) was not available for bagasse. He refers to previous work on inverse methods including Mehta (1984), Kubo (1988), Maniatty and Zabaras (1989), Zabaras and Ruan (1989) and Schnur and Zabaras (1990).

Zhao developed an inverse problem solution to an experimental compression stress versus strain curve (a normal compression line in soil mechanics terms) supplied to him by the Sugar Research Institute. It is noted that there seems to have been an error made in what this compression curve represented because Zhao stated that 'this curve is very different from the stress-strain curves for other porous media (e.g. soil, concrete)'. However, the supplied curve is actually very similar to the normal compression line observed in soil tests.

The statement seems to have its origin in Progress Report 5 to the Sugar Research Institute (Owen and Zhao, ca. 1991), where the stress-strain curve for prepared cane is shown in their Figure 5.1 (also shown in Figure 2.1 of Research Report 7 to the Sugar Research Institute (Owen and Zhao, ca. 1991) and reproduced here in Figure

1.7) (it is noted that the Swansea research reports are compiled in the appendices of Garson, 1992b). The curve is reproduced here in Figure 1.8 with the stress plotted on a natural log scale (basically the normal compression curve usually plotted in soil mechanics, except strain is plotted instead of specific volume or void ratio, and therefore the slope of the line is reversed). A linear relation is evident, as is the case for soils (see, for example, Figure 4.20 in Craig, 1987). The result provides strong evidence that the behaviour of prepared cane in uniaxial compression is very similar to that of soils.

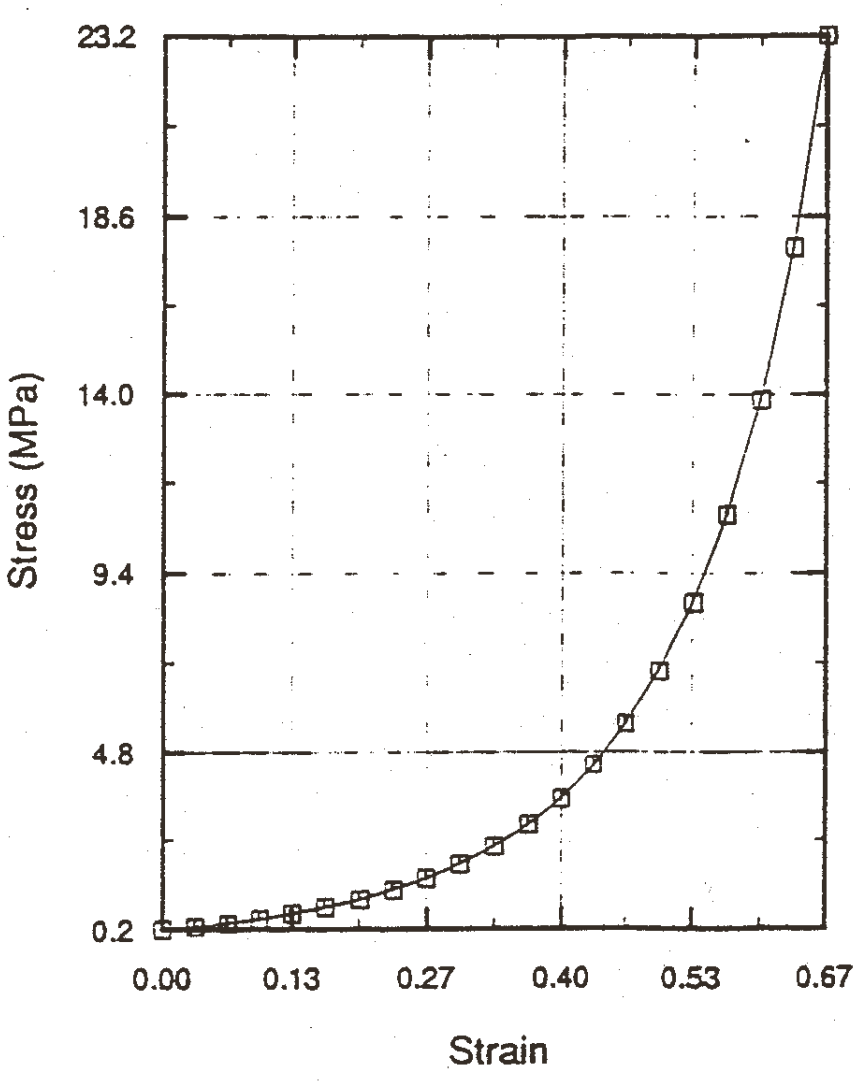

Figure 1.7. Stress-strain curve for prepared cane (reproduced from Owen and Zhao, ca. 1991).

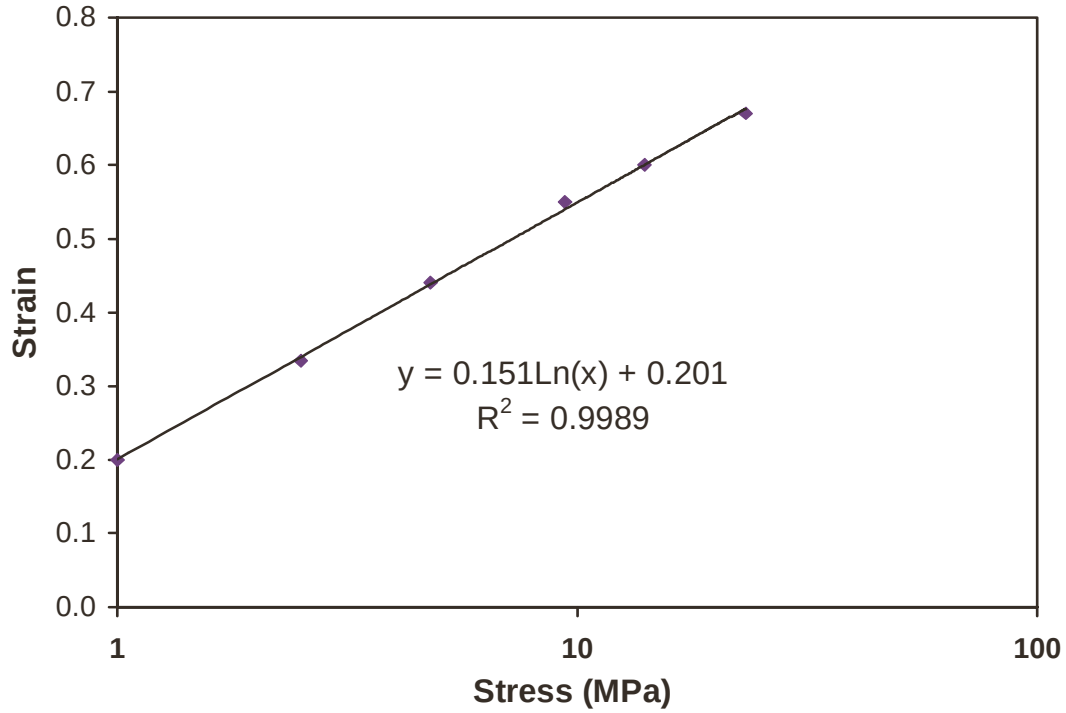

Figure 1.8. Stress-strain curve for prepared cane (reproduced from Owen and Zhao, ca. 1991) with the stress plotted on a natural log scale).

Zhao commented that no constitutive relation exists for bagasse but then stated that 'the form of the constitutive relations for other porous materials such as soil and concrete is far removed from that needed for prepared cane'. The same statement is made by Owen at al. (1994a) and Owen et al. (1995). However, no details of results or references were given to justify the statement. These statements are believed to be the result of the error made in what the compression curve represented, and the resultant erroneous conclusion that the behaviour of prepared cane is very different from that of soil. Experimental evidence is provided in Chapters 3, 4 and 7 of this thesis that shows that the form of the constitutive relations for prepared cane are quite similar to those for soil.

Over the following eight years the use of uniaxial compression tests and inverse calibration procedures was emphasized (Owen et al., 1994a, Owen et al., 1994b, Owen et al., 1995, Loughran and Adam, 1995, Adam, 1997, Adam et al., 1997a, Adam et al., 1997b, De Souza Neto et al., 1997, Adam and Loughran, 1998,

Loughran and Adam, 1998, Owen et al., 1998, Downing, 1999, Downing et al., 1999a, Downing et al., 1999b, Loughran and Kannapiran, 2002).

Indeed, De Souza Neto et al. (1997) stated that 'Before the developed computational tool can be applied to industrial simulation, a necessary prerequisite is identification of the material parameters of the solid phase by numerical experiments, since it is impossible to undertake material tests on samples in the dry state. Therefore, an inverse procedure in which the material properties of the solid phase are deduced by computationally replicating the actual experimental material tests must be undertaken'. The statement is repeated in Owen et al. (1998). However, it is believed to be incorrect. Tests to obtain material parameters (for example, triaxial tests, direct shear tests, ring shear tests, vane tests) have been carried out for soils over at least the last 100 years on materials that are wet, whether the materials are drained or not, saturated or not and both in the laboratory and the field, without the need for an inverse calculation procedure (see for example, Craig, 1987, Muir Wood, 1990).

Most of the literature on the solution of inverse problems (Mehta, 1984, Kubo, 1988, Maniatty and Zabaras, 1989, Zabaras and Ruan, 1989, and Schnur and Zabaras, 1990) has been devoted to inverse heat transfer problems, with some other application to static elastic problems. Inverse methods are still in their infancy in terms of development and in comparison to, for example, the material parameter development work carried out in the soil mechanics field. In combination with the material parameter development work, inverse analysis methods have been applied in the soil mechanics field for example by Kirby et al. (1998) and Kirby (1998b), and have recently been applied to prepared cane and bagasse (Kent, 2001; Plaza et al., 2001).

The use of inverse calculation methods is not discounted as an aid (or as a check) to calculate material parameters from the measured bagasse experimental data (and is used in Chapter 5 to gain valuable insights into the limitations of material models), but this investigation will apply much less emphasis to inverse calibration methods.

1.8 The current state of material models for prepared cane

The situation at the middle of 1998 was that the Drucker-Prager Cap model had been successfully used to predict some of the empirical trends relating to roll loads, roll torques and juice extraction in a milling unit, but not some others and not together in a simulation using the same parameters. Its inability to model some known aspects of the fibrous skeleton behaviour left concern that the model did not capture some important mechanisms and hence could not lead to an improved understanding of the milling process. To resolve this doubt, an improved material model for the fibrous skeleton and improved methods of determining parameters for the material model are required. Prepared cane has been fitted into the critical state models Modified Cam Clay and Drucker-Prager Cap by manipulation of the parameters, but a reliable and consistent material model has not been achieved. Indeed, all experimental test methods up to this time have failed to measure the basic behaviour for prepared cane or bagasse which is required to develop a reliable critical state model, or even to identify bagasse as a critical state material (as shown for soil, for example, in Craig 1987, Muir Wood 1990). Although the parameter M has been used as an example, there are many other parameters that require identification (such as the position of the critical state line relative to the normal consolidation line) in order to build a reliable critical state model for bagasse.

1.9 Review of available test methods to measure critical state behaviour

There are two widely used test methods for soil engineering design that can measure critical state behaviour. They are the triaxial test method and the direct shear test method (a third method, known as the simple shear test method, can also be used although that equipment is not as widely available). The triaxial test is the more appropriate of the two tests. It measures the full state of stress in a cylindrical sample as well as the volume change and the pore water pressure. The standard geotechnical triaxial test rig cannot cope with the large volume deformations that occur when bagasse is loaded. The large deformations occur because of the low stiffness of bagasse. At least two attempts have been made (Cullen, 1965, and Leitch, 1996) to test prepared cane using standard soil test equipment. Cullen also built a true triaxial test rig that was not successful. The result is that reliable data

from deviatoric tests are not available either for normally consolidated samples or over-consolidated samples.

The direct shear test method is less time consuming and less expensive than the triaxial test. It is widely used to test frictional materials, i.e. sands. Its drawbacks are that the full stress state is not known and it does not allow the measurement of pore water pressure. However, it is very successfully used in soil mechanics engineering and design in combination with the triaxial test. For example, both the direct shear test and the triaxial test can be used to measure the Mohr-Coulomb parameters for soils.

In a direct shear test (shown in Figure 1.9) the material is confined in a box split into top and bottom sections. A vertical pressure is applied and shear stress is applied by moving one section of the box horizontally relative to the other, inducing internal shear.

Plaza and Kent (1997) presented normal consolidation tests carried out on prepared cane using a modified direct shear test and show that prepared cane does meet the Coulomb failure criterion. Interestingly there are two linear segments in the Coulomb line over the very large range of vertical pressures (200 kPa to 20000 kPa) tested. Pressures present in the milling process range from typically 2 kPa to as much as 20000 kPa. Soil tests usually only go to about 500 kPa vertical stress.

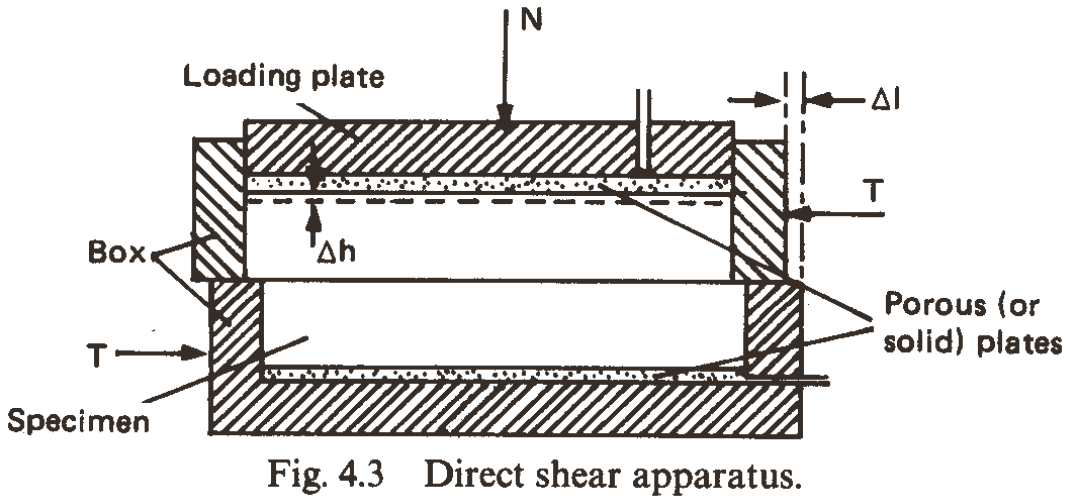

Figure 1.9. Schematic of a direct shear test (reproduced from Craig, 1987).

Plaza and Kent (1997) also discussed the problems associated with testing prepared cane and bagasse, specifically the low stiffness of prepared cane and its much higher water content compared to soils. The low stiffness of the material makes testing difficult at relatively lower pressures (below 4000 kPa). Modified test geometries from the standard direct shear test have been used to deal with the low stiffness. Plaza and Kent (1998) described such a test geometry that was successful in differentiating between the level of grip provided by three surfaces on prepared cane at low compactions (40 $kg.m^{-3}$ to 110 $kg.m^{-3}$ corresponding to pressures from 5 kPa to 200 kPa for prepared cane). Compaction is defined as the fibre density (mass of fibre in the volume occupied by the bagasse). These compactions correspond to the bottom of the feed chute, at the underfeed roll and towards the pressure feeder nip, depending on whether a light duty pressure feeder or a heavy duty pressure feeder is present. The results showed that for this restricted pressure range prepared cane did meet the Coulomb failure criterion.

Since the Coulomb failure criterion is incorporated within critical state theory, the above results indicated that the direct shear test method showed promise in being able to demonstrate and measure critical state behaviour for prepared cane and bagasse. It is noted that, because the stress state in a direct shear test is not fully known, the results were not expected to be as accurate or conclusive as those obtained if an adequate triaxial testing rig for prepared cane and bagasse were available. However, the direct shear test rig looked to be a promising option for bagasse and was supported by Kirby (1998a), who had a high level of experience in using a direct shear test to measure critical state behaviour of soils and reproduce the same behaviour using computer models. Kirby (1994) demonstrated that direct shear box results yielded material parameters that could be used to predict the critical state behaviour of clays. Kirby (1998b) developed a method of estimating critical state parameters from a single shear box test, both saving much labour and providing more information than traditional analyses, which required several shear box tests and a uniaxial compression test to yield the same information. Kirby (1998b) showed that the constant stress test (constant pressure on the sample during shearing) 'led to the better and more stable estimates of the critical state parameters, particularly λ and κ'. Since Kirby (1998b) and Plaza and Kent (1997), (1998) had

used a constant pressure during the direct shear test to achieve two quite different objectives on two quite dissimilar materials, one material being a clay and one material being prepared cane, it seemed logical that such a test should be attempted first.

1.10 Summary of objectives

The project seeks to show that bagasse exhibits critical state behaviour, determine material parameters for prepared cane and bagasse, and make progress towards a robust material model that can reproduce the compression, shear, and volume behaviour for any combination of stresses and strains.

2 Chapter 2 – A search for similar materials, related tests, and promising models

2.1 Introduction

A series of literature searches was carried out throughout the course of this investigation focussing on three separate but related topics. The first topic was finding similar materials to prepared cane and bagasse in order to compare their parameters, experimental test methods, and modelling capabilities. The second topic was finding experimental test methods, and the outcome was that this section focusses on the direct shear test. The third topic was finding material models, focussing mainly on critical state models. The results presented here follow that division with a significant overlap between the topics.

2.2 Similar materials to prepared cane and bagasse

2.2.1 Peat – an organic soil

Peat is a soil material that is quite abundant throughout the world. It has some properties such as high compressibility and low strength that make it less suitable for supporting man made structures such as buildings and roads. As available land becomes scarcer, there has been increasing pressure to build on peat regions and this has resulted in research into understanding the behaviour of peat. A comparison between peat and bagasse is carried out below.

Prepared cane and bagasse are organic, fibrous, highly compressible, saturated materials. Prepared cane is made up of plant cellulose and lignin, sugar, water, and soil, in the typical proportions shown in Table 2.1. A small amount of other dissolved material may also be present.

Table 2.1 Typical make up of prepared cane

Cellulose and Lignin	Sugar	Water	Soil
13 % to 16 %	12 % to 16 %	70 %	1.0 % to 2.0 %

In appearance, the fibrous cellulose is most readily apparent, with stringy fibres ranging from 1 mm to 100 mm or more in length and having length to diameter ratios ranging from 1 to about 30. The prepared cane is similar to the Radforth

peats described by Landva and La Rochelle (1983). Radforth peats is a term used to describe peats with a negligible content of mineral matter. Landva and La Rochelle described the Sphagnum peat in their paper as consisting 'mostly of fibrous particles such as stems, leaves, fiber hairs, etc'.

The similarity of peat behaviour and bagasse behaviour is quite striking. Farrell and Hebib (1998) stated that 'Peat and organic soils can be extremely difficult materials to test owing to the presence of fibres, their anisotropy and very high compressibility'. During the deviatoric part of a drained triaxial test on Irish peat, Farrel and Hebib showed that the deviatoric stress continued to increase even at 35% axial strain and a failure stress could not be defined, with a decrease in height of the specimen involving little lateral strain. Prepared cane is made up of fibres, is anisotropic (Murry, 1960), and over the pressure range experienced in a milling unit, its volume decreases by a factor of eight. Leitch (1996) carried out some nominally drained deviatoric triaxial tests on prepared cane and observed a similar continual increase in deviatoric stress with strain, and stated that 'during deviatoric compression testing, the triaxial samples did not fail in shear'. During both isotropic and deviatoric loading, large axial and small lateral strains were observed in the prepared cane samples.

Landva and La Rochelle (1983) discussed the testing of Radforth peat and observed that 'in general, failure in peat brought about with equipment having rigid shear boundaries, such as plate and cone shear, as well as vane shear, is associated with excessive local compression. These modes of failure are therefore not representative of the stress conditions in peat under embankments'. The excessive local compression caused by equipment with rigid boundaries also applies to the testing of prepared cane and bagasse. Bernhardt (1995) carried out modified vane shear tests on bagasse, with four paddles rotating in a container with eight cutting baffles mounted on the sides. The bagasse compacted into a ball between the paddle and baffle edges and shear strength could not be measured. Cullen (1965) and Plaza and Kent (1997) describe investigations carried out to determine the roughness required on the surface of sugar mill rollers, which have circumferential grooves typically 50 mm deep at 38 mm pitch with an included angle of 35°, with the tips of the grooves roughened to increase grip. Direct shear tests were carried

out on prepared cane and non-uniform compression occurred at the sides (next to the sideways moving walls) relative to the middle of the sample. It is noted that the top and bottom surfaces in the split boxes they used were smooth mild steel (and therefore the split box test geometry was not ideal).

Plaza and Kent (1997) also showed that, although prepared cane has some cohesion, it is essentially a frictional material (see their Figure 10, included in Chapter 9 as Figure 9.6). Similarly, it was concluded by Adams (1961,1965) and Hanrahan et al (1967) that peat is also an essentially frictional material. A summary of values of the cohesion (C), friction angle (ϕ), and ratio of vertical to lateral stress (K_o) for peat and prepared cane is given in Table 2.2 for comparison (compiled from Landva and La Rochelle, 1983[A], Adams, 1961[B], 1965[B], Krieg and Goldscheider, 1994[C], Plaza and Kent, 1997[D], 1998[E], Adam, 1997[F]). For prepared cane the pressure ranges at which the tests were carried out are also provided because of the large range of pressures present in a milling unit.

Table 2.2 A comparison of typical parameter values for peat and prepared cane.

Parameter	Peat	Prepared cane
C (kPa)	2 to 6[A]	17[E], 50[D]
ϕ (degrees)	27 to 32[A], 48[B]	38[E], 26[D]
K_o	0.18[B], 0.3 to 0.5[C]	0.1 to 0.2[F]

[D]Tests carried out at 300 to 4000 kPa normal pressures, [E]Tests carried out at 0 to 250 kPa normal pressures, [F]Tests carried out at 0 to 3000 kPa normal pressures

MacFarlane (1969) stated that peat has a very high natural water content and that 'large deformations occur as the peat develops its inherent resistance to applied loads'. Both are also true for bagasse. MacFarlane refers to the shear strength of peat and states that 'recent research has shown conclusively that it is essentially a frictional material and that it behaves closely in accordance with the principles of effective stress'. The frictional material observation is in agreement with Adams (1961,1965) and Hanrahan et al (1967). The comment on agreement with principles of effective stress is important since most (maybe all) modelling computer packages that hold promise for modelling bagasse adopt this principle. MacFarlane also

states that ‘There are reasons to doubt that the solid phase in peat can indeed be considered as inert and incompressible, for practical purposes, as is assumed for the inorganic soils’. The high compressibility of bagasse indicates a similar observation, that the decrease in volume is not fully explained by the reduction in voids.

The conclusion from considering all the above is that bagasse and peat are very similar, which is not surprising since they have the same origin, which is plant matter. Methods of measuring peat behaviour and conclusions are considered below. Particular attention is paid to the effect of fibre layering. This is because for prepared cane and bagasse fibre alignment and its effect on behaviour has been discussed frequently (Leitch, 1996, Adam, 1997), but there is little data available to quantify the effect.

Ekwue (1990) measured the shear strength of soils to which peat had been added using a drop cone penetrometer and concluded that adding peat to soils increased moisture retention, decreased bulk density, reduced aggregate stability and decreased soil shear strength (measured using a drop cone). Galvin (1976) carried out shear strength tests on undisturbed and remoulded peats and concluded that the strength of remoulded peat was less than that of undisturbed peat at higher moisture contents (60 to 70% by volume) but the opposite was true at low moisture contents (30% by volume).

Macfarlane and Williams (1974) noted that ‘anisotropy in strength behaviour is of considerable significance in some Canadian peats, however, with the strength in the vertical direction being up to twice as much as that in the horizontal direction’ and ‘imperfect as it is, the shear vane is the most useful instrument devised thus far for determining the shear strength of peat’. Boulanger et al (1998) noted that ‘strong cross-anisotropic behavior of the peat was clearly indicated by the effective stress paths during monotonic compression and extension loading, and this behaviour is consistent with the visible layering of fibres within the specimens’ when they tested Sherman Island Peat using triaxial equipment.

Landva and La Rochelle (1983) discussed the effect of fibre alignment with respect to the direction of principal stresses and its effect on shear strength, the observed

excessive local compression by equipment having rigid shear boundaries, and presented results of ring shear tests on remolded peat and undisturbed peat sheared both parallel and at right angles to the insitu bedding planes. It was concluded that 'tests on (1) remolded peat, (2) undisturbed peat sheared at right angles to the in situ bedding planes, and (3) undisturbed peat with a precut shear plane all gave results within the same range as normally consolidated peat sheared first time. This suggests that disturbance or remolding of peat samples is not critical and that it is the stress and deformation history of the sample that is important'. Such conclusions are quite important if they apply to bagasse since they imply that fibre alignment does not have a significant effect on properties. However, it is noted that the vertical stress for the tests ranged from 3 kPa to 50 kPa, which are very low (although they are included) compared to most of the stresses experienced by bagasse in a milling unit. These stress levels correspond to the bottom of the feed chute and towards the underfeed roll nip. It is also noted that Macfarlane and Williams (1974) found different bagasse strengths in the vertical and horizontal directions. Therefore no firm conclusions can be made on the effect of fibre alignment on peat behaviour.

Thun and Rautalin (1985) reported parameters for milled peat for bulk handling (the peat is used as a fuel source). An angle of repose of 48° and angles of friction between 33° and 38° on an inclined plane are reported, with the interesting comment that 'the finer the peat, the higher the value of friction coefficient'. They commented that, 'in general, the experiments carried out with the Jenike Cell indicated that the equipment was not specially suitable for milled peat, at least not for unscreened, fibrous and moist one'. However, the shear experiments with screened fine fractions with < 25% moisture content succeeded quite well. A Jenike Cell is used to measure material parameters for the design of bulk handling hoppers, etc.

Bouazza and Djafer-Khodja (1994) measured the friction characteristics of peat and the interface between peat and a geotextile using a direct shear test. They commented that the 'the contact between the geo-textile and the peat is perfect', implying there was no slip. A cohesion of 34 kPa and a friction angle of 26° were measured for the peat alone.

As noted previously in this section, for example with reference to Leitch (1996) for prepared cane and Farrell and Hebib (1998) for peat, it has been found difficult to measure meaningful parameters using drained triaxial tests. Hanrahan et al (1967) carried out triaxial tests on remoulded wholly organic peat and supported the difficulties experienced by stating that 'consolidated-drained tests are not feasible with peat with available apparatus due to the extremely lengthy time intervals involved'. However, Hanrahan et al (1967) also carried out undrained tests on normally consolidated peat at pressures ranging from 10 kPa to 200 kPa and appeared to have had considerable success in defining the critical state line projected on the p-q plane. The results are shown in their Figure 9 and a value of 1.55 for the slope of the critical state line (M) was determined. Similar tests on prepared cane and bagasse are well warranted.

Termaat and Topolnicki (1994) carried out tests on natural peat (and also an artificial peat, made from 50% clay and 50% paper pulp) using a specialised cubical biaxial apparatus and also appeared to have had considerable success in measuring the behaviour of peat. They concluded that an average M value for natural peat was approximately 1.35. Similar tests on prepared cane and bagasse are well warranted.

In summary, the behaviour of peat and bagasse is very similar. It was concluded that three types of tests held promise with respect to measuring the mechanical behaviour of bagasse: direct shear tests, undrained triaxial tests, and biaxial tests. Of these three tests, the equipment to carry out direct shear tests at most of the pressures occurring in milling was readily available.

2.2.2 Other similar materials to bagasse

Here, three different materials that have some commonalities with bagasse are discussed briefly. The three materials are apples, paper, and foams. Some reference papers that provide a description of the materials are given. The papers also include models of the materials' behaviour. Those models have been judged to be of less relevance (at the current time) for developing a bagasse model than the models that are discussed later in this chapter, and are not discussed further. They may have some characteristics that may be of interest in the future.

The similarities of apples to bagasse are that they are also organic, they contain a large amount of juice, and the juice can be expressed from thin apple slices by mechanical pressing through a screen. Schwartzberg et al (1996) provided equations for calculating pressures at varying compression speeds.

Paper (and paperboard) is formed by draining a suspension of fibres in a fluid through a filter screen to form a sheet. The sheet is then passed through the nip of a pair of rollers to remove moisture, in a similar manner to the squeezing of bagasse in a set of mill rolls. However, the blanket thickness of paper is usually much less than a millimetre, while bagasse blankets are in the order of 40 mm to 400 mm thick. The method of making paper results in a material that is anisotropic (its in-plane parameters are quite different to those in the through thickness direction). Descriptions of experimental results and mathematical models are given in Saliklis and Kuskowski (1998), Sawyer et al (1996), Sawyer et al (1998), Valentin (1999), and Xia et al (2002).

Foams and honeycombs are used in a wide range of applications, from aircraft wings to energy absorbing materials. The individual cells in sugarcane that hold the sugar juice have a honeycomb structure. Foams and honeycombs and bagasse show little sideways strain when they are compressed vertically. Schreyer et al (1994) provide a comparison of predictions from a material model with experimental results. Hibbitt et al (2001) included a Crushable Foam model that has been mentioned previously.

2.3 The soil direct shear test

'The direct shear test is a crude but simple engineering test which has a long and honourable history in soil mechanics' (Wroth, 1987). The direct shear test apparatus (shown in Figure 2.1) is successfully used in design, despite its shortcomings and the availability of more advanced test methods such as the triaxial test. In this section the advantages, disadvantages, and possible improvements of the direct shear test are discussed, while keeping in mind the desire to carry out tests on prepared cane and bagasse materials.

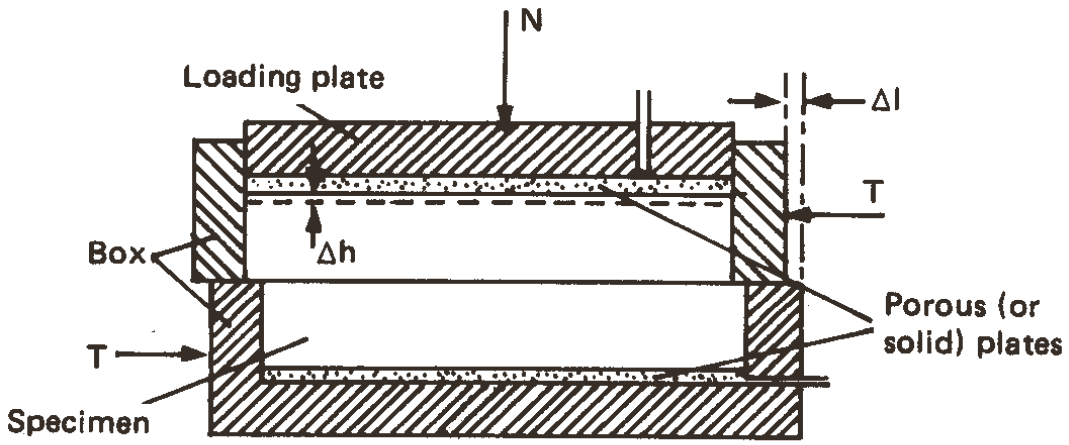

Fig. 4.3 Direct shear apparatus.

Figure 2.1. Schematic of a direct shear test apparatus (reproduced from Craig, 1987).

As noted in Chapter 1, modified versions of the direct shear test have been used previously to determine the required surface roughness to grip prepared cane (Plaza et al, 1993, Plaza and Edwards, 1994, Plaza and Kent, 1997, 1998). The soil mechanics literature available on the direct shear test is very large, and only a very small sample is referred to.

Craig (1987) described the advantages of the direct shear test as being its simplicity and, in the case of sands, the ease of sample preparation. The disadvantages are that the drainage conditions cannot be controlled, pore water cannot be measured, only an approximation to the state of pure shear is produced in the specimen, and shear stress on the failure plane is not uniform, with failure occurring progressively from the edges towards the centre of the specimen. Another disadvantage is that the full stress state is not known (since the side wall stresses are not measured).

There seem to be many disadvantages with the direct shear test. However, it is very successfully used in soil mechanics engineering and design in combination with the triaxial test. For example, both the direct shear test and the triaxial test are used to measure the Coulomb parameters for soils. The direct shear test method is less time consuming and less expensive than the triaxial test. This is quite attractive for

testing bagasse since a large number of tests are required because of the large range of pressures and materials present in the milling process.

Toolan (1987) commented that there has been a world wide revival of interest in shear tests. The revival is attributed to shear testing (both direct shear box and simple shear) being found to have provided better correlations in several field situations than triaxial tests. Also, although the above direct shear test is quite simple, there have been concerted efforts to develop better equipment, new applications, and more detailed interpretation. For example, de Campos and Carrillo (1995) used a suction controlled direct shear device able to control both air and water pressures. Shibuya et al (1997) presented improvements to the design and interpretation of the direct shear test. A conclusion is that direct shear tests will continue to be carried out to measure soil behaviour. A similar test to measure bagasse behaviour would be useful. The non-uniformity problem is discussed in more detail below since this is believed to be an important issue when testing a low stiffness material such as bagasse.

A major criticism of the direct shear box has been that the stresses and strains in the sample are non-uniform (Rowe, 1969, Potts et al., 1987). Improvements to the direct shear test, with the aim of reducing non-uniformity have been carried out, for example, by Jewell and Wroth (1987) and Shibuya et al (1997). Potts et al. (1987) stated that 'the stress state in an ideal shear box in which strains are uniform is that of simple shear' while Wroth (1987) stated that 'Roscoe (1953) devised the simple shear apparatus with the purpose of applying uniform conditions of simple shear'. Potts et al. (1987) compared the behaviour in a direct shear test to that in a simple shear test, including a detailed analysis using finite element models. Their conclusion was that 'the analyses thus show that the non-uniformities within the direct shear box sample have little effect, and with surprisingly little error the test may be interpreted as if it were a simple shear test'. However, they also concluded that the local state of stress and strain within the direct shear test was far from uniform and that 'highly stressed zones propagate from the edges of the box at an early stage of loading' while 'the strains and stresses within the failure zone at the peak in the direct shear box are surprisingly uniform'. Potts et al. attributed the uniformity at failure to the absence of progressive failure, and stated that

‘progressive failure occurs when loading produces non-uniform mobilisation of strength’.

It is believed that the issues of ‘highly stressed zones propagating from the edges of the box’ and ‘non-uniform mobilisation of strength’ are highly relevant and undesirable when testing a material which has high compressibility and low stiffness such as prepared cane and bagasse (or peat for that matter) in a direct shear test. Cullen (1965) and Plaza and Kent (1997) carried out direct shear tests on prepared cane and commented on extra compression at the side walls, which result in the prepared cane at the two cutting edges of the split box being more compacted than the prepared cane at the middle of the sample. It is noted that the geometries used for those split box tests were less than ideal, since both the top and bottom surfaces contacting the bagasse were smooth steel. Rough surfaces to grip the bagasse would have been far more suitable. Such ‘grid plates’ on the top and bottom surfaces, as noted by Head (1994), ‘enable the shearing forces to be transmitted uniformly along the length of the sample’. It is interesting to note that the use of these ‘grid plates’ is not mandatory in the British Standard (BS1377:Part 7:1990:4 and BS1377:Part 7:1990:5) and the Australian Standard (AS1289.6.2.2-1998). The British Standard is unclear about the use of such plates, which seem to be referred to as both spacer plates and grid plates. The gripping surfaces on the top and bottom surfaces when testing bagasse are described in Chapters 3, 4, and 7.

The top pushing plate used in the direct shear tests for prepared cane and bagasse (Plaza et al, 1993, Plaza and Edwards, 1994, Plaza and Kent, 1997, 1998) was attached rigidly to a vertical ram and was not able to rotate. This was also the case for the tests described in Chapters 3, 4, and 7. The main criteria for this setup were ease of use and safety. However, it is consistent with the findings that the non-uniformity in the sample is minimised (Wernick, 1977, Jewell and Wroth, 1987) and that the occurrence of progressive failure in the sample is reduced (Shibuya et al, 1997) when the top plate is not allowed to rotate.

One further complication is that large and persistent water (juice) pressures are observed when prepared cane or bagasse is compressed, which must be measured and/or controlled. As noted by De Campos and Carrillo (1995), the small height of

the sample in a direct shear device provides a faster moisture equalisation time within the sample, than, for example, the triaxial test. When high juice pressures are observed when testing prepared cane in a direct shear test, a procedure (explained in Chapter 3) can be implemented to drain the sample and reduce the juice pressure to a low level within a short time (minutes rather than hours or days, see Leitch (1996) triaxial tests).

2.4 Material models

The literature available on the understanding of material behaviour and the development of models to describe that behaviour is very large and it is being added to at a furious pace. The subset of soil behaviour and models, particularly critical state models, falls into that category. Several literature searches identified about fifteen papers of strong interest on the topic of computer models to predict material behaviour (from a collected group of about seventy papers). Those papers are noted here. Detailed study of the concepts, understanding the mathematics of the material models, the predictions obtained from the models, and their strengths and weaknesses, described in any one of the papers is a major undertaking. Many of the models are themselves works in progress. Some of the experimental data required for the models is not available for bagasse. This section should be read in the context that, prior to this investigation, it was not even known that bagasse exhibited critical state behaviour. As noted in Chapter 8, there are large gaps in bagasse data remaining after this investigation (such as the shapes of the yield and potential surfaces required for a critical state model, and the effect of anisotropy) that are required to identify a material model suitable for bagasse. The approach taken was to note papers of interest for future bagasse material model development and to adopt, modify and test one of the models (shown in Chapter 8).

The material models of interest are detailed in the following publications. In alphabetical order, the publications are: Brandt and Nilsson (1999), Davies and Newson (1992), Gajo and Muir Wood (1999a, 1999b), Heshmati (2000), Houlsby and Sharma (1999), Kabirul (1999), Kumbhojkar and Banerjee (1993), Liu and Carter (2000), Manzari and Dafalias (1997), Molenkamp (1994), Molenkamp et al (1996), Oka et al (1999), Pestana and Whittle (1999), Sellmeijer (1994), Seung and Seboong (1995), Stallebrass and Taylor (1997), Thomas and He (1998), Topolnicki

and Niemunis (1994), and Yu (1995, 1998). This list should by no means be considered complete since the literature available is very large and is being added to at a furious pace.

The prediction of stress anisotropy is considered first. Kumbhojkar and Banerjee (1993) considered the Casagrande and Carillo (1994) interpretation of material hardening. Kumbhojkar and Banerjee stated that it (the interpretation) distinguishes between the inherent anisotropy, developed during the initial formation of a soil, and induced anisotropy caused by subsequent loading. Their Figure 3, reproduced here as Figure 2.2, shows the change in the yield surface (initially at an isotropic stress state, and resembling the Modified Cam Clay yield surface shape) as the soil is loaded under the condition of no lateral strain (K_o consolidation). The final shape resembles the shape of the yield surface shown in Figure 1 of Topolnicki and Niemunis (1994), who presented a material model for reproducing the behaviour of peat in biaxial tests, using test data from Termaat and Topolnicki (1994). Since it has been concluded previously that peat and bagasse behave in a similar manner, material models for peat should also be appropriate for bagasse.

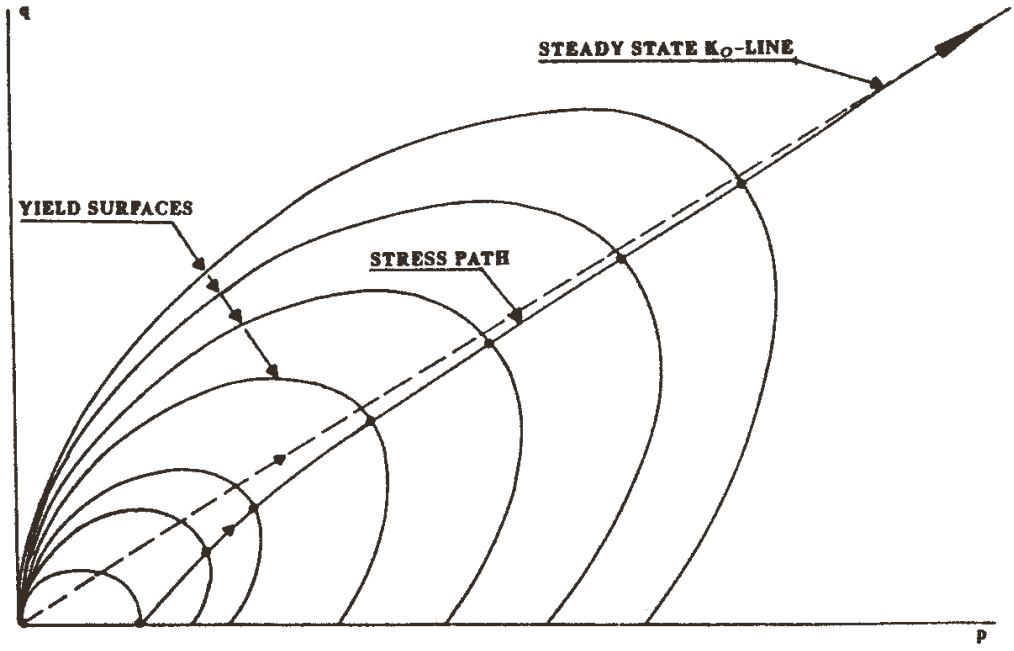

Figure 2.2. Development of the yield surface orientation towards K_o line (reproduced from Kumbhojkar and Banerjee (1993).

Also, other models with shapes for the yield surface (and/or potential surface) similar to that shown in Figure 2.2 must be considered as contenders for a bagasse material model. Similar yield surface shapes are shown in Brandt and Nilsson (1999), Davies and Newson (1992), Houlsby and Sharma (1999), Pestana and Whittle (1999), Seung and Seboong (1995), and Yu (1995,1998). All the models in these publications are based on classical concepts of elasto-plastic materials. They also have an advantage that, in many cases, the Modified Cam Clay model (the Drucker Prager Cap model in the case of Brandt and Nilsson) can be derived as a special case, and therefore their correct implementation can be checked fairly easily.

Brandt and Nilsson presented a model for the cold compaction of metal powders. Reproduction of clay behaviour was carried out by Davies and Newson (1992), Houlsby and Sharma (1999), Kumbhojkar and Banerjee (1993), Seung and Seboong (1995), and Stallebrass and Taylor (1997). Unified models for clays and sands were provided by Pestana and Whittle (1999), and Yu (1995, 1998). Models for sands were presented by Gajo and Muirwood (1999a, 1999b), Manzari and Dafalias (1997), and Oka et al (1999). The Thomas and He (1998) model was for unsaturated soils (and its features could be of use since there are stages in the milling process where bagasse is unsaturated). Kabirul (1999) produced a model for carbonate sand that can be considered a special case of the model presented by Yu (1995,1998) for clays and sands. Carbonate sand has some features, such as its high compressibility, that are quite similar to bagasse.

Liu and Carter (2000) presented three modifications that can be implemented in the Modified Cam Clay model, with a large body of work on the loading and unloading behaviour of reconstituted soil, both in compression and shear. The modifications are of interest since there are many locations at which unloading occurs in a milling unit. Also, as noted in Chapter 5, there are problems reproducing bagasse behaviour with critical state models at high degrees of unloading.

Molenkamp (1994), Molenkamp et al. (1996) and Heshmati (2000) presented a mainly theoretical study on an experimental test method and a mathematical model to measure and predict peat behaviour. Sellmeijer (1994) also presented a mainly

theoretical study on the development of an anisotropic peat model, which was considered to be a work in progress. Their approach had a large focus on fibre orientation, and it is believed that their approach is significantly different to others. The experimental data available for bagasse is not believed to be adequate, even at the end of this investigation, to test these models. The development of that work on peat should be monitored in the future.

The above publications may be of use, not only because of the models, but because they contain much information on the behaviour of materials. The model described in Yu (1998) was adopted in this investigation to progress the reproduction of bagasse behaviour (as well as extended versions of the Modified Cam Clay and Drucker Prager Cap models).

2.5 Summary of Chapter 2

A comparison of peat and bagasse showed that their behaviour is very similar. It was concluded that three types of tests held promise with respect to measuring the mechanical behaviour of bagasse: direct shear tests, undrained triaxial tests, and biaxial tests. Of these three tests, the equipment to carry out direct shear tests at most of the pressures occurring in milling was readily available. The advantages and disadvantages of a direct shear test were considered with regard to an improved test for bagasse. Publications containing material models that may be of use in understanding bagasse behaviour and to carry out bagasse modelling were identified and described briefly. A model was identified for adoption in Chapter 8.

3 Chapter 3 – Preliminary direct shear tests to measure bagasse behaviour

3.1 Introduction

An outcome from Chapter 1 and Chapter 2 was that a direct shear test method looked the most promising option for testing the material behaviour of bagasse. The aim of this project was to show and measure the behaviour required to build a material model. Due to the very large volume changes and range of pressures present in the crushing of cane, it was necessary to make a decision on the pressure range of the tests before any required equipment was designed or built. Figure 3.1 shows a standard six roll mill unit used in the Australian sugar industry. The range of pressures experienced by prepared cane and bagasse is shown in Figure 3.2 together with the locations in a milling unit. Pressure is plotted on the horizontal axis with compaction plotted on the vertical axis (note that the values of compaction only apply to prepared cane). Compaction is a measure of density used by mill engineers and is defined as the mass of dry fibre per unit volume of bagasse.

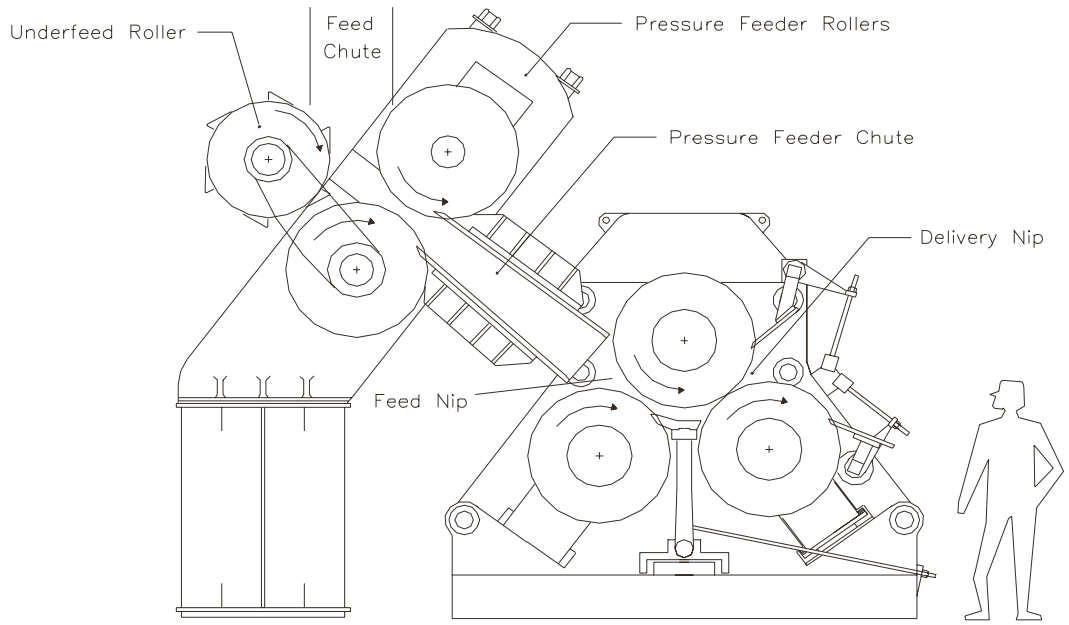

Figure 3.1. Standard six roll mill unit used in the Australian sugar industry (Neill et al, 1996).

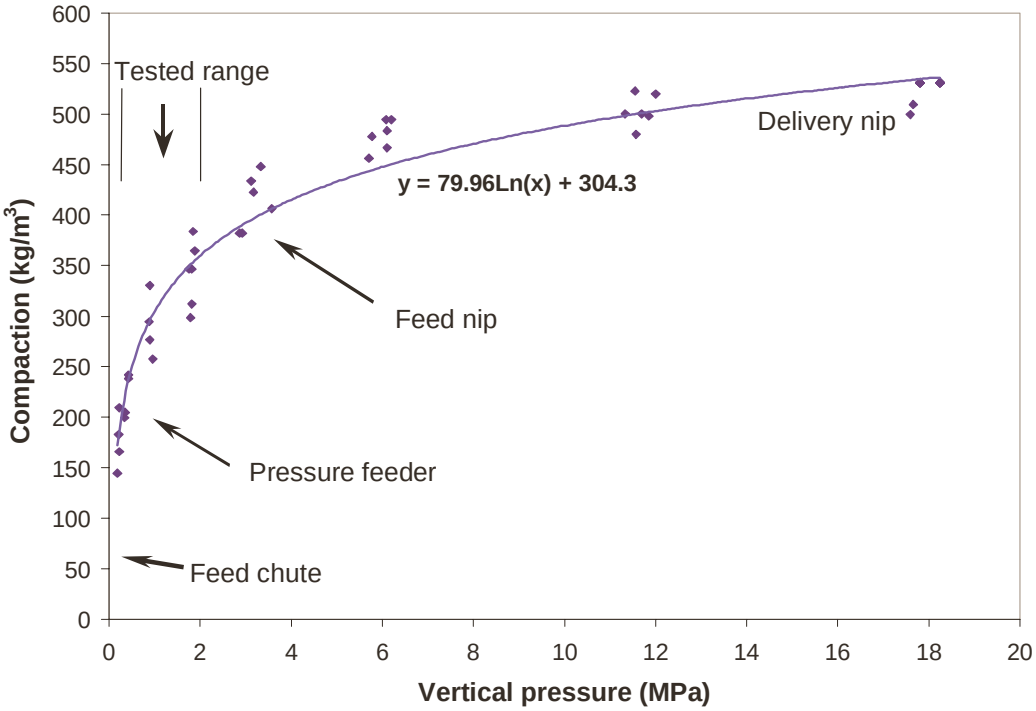

Figure 3.2. Typical compaction versus pressure plot for prepared cane showing tested pressure range in preliminary direct shear tests.

No single test equipment can measure material behaviour over the full range of pressures and densities of crushed cane. The test equipment used in this chapter and in Chapter 4 was designed to operate in the pressure range from 200 kPa to 3000 kPa, encompassing the pressure range that prepared cane and bagasse is subjected to in a pressure feeder. The general arrangement of the test equipment is shown in Figure 3.3 and is the same as that used by Plaza et al (1993) and Plaza and Kent (1998) for finding the required surface roughness to grip prepared cane. Basically the top part of the box was suspended above the bottom part of the box. The bottom part was mounted on linear bearings allowing it to move sideways with minimal frictional resistance. The general arrangement is the same as a typical direct shear test for soil except it is on a larger scale.

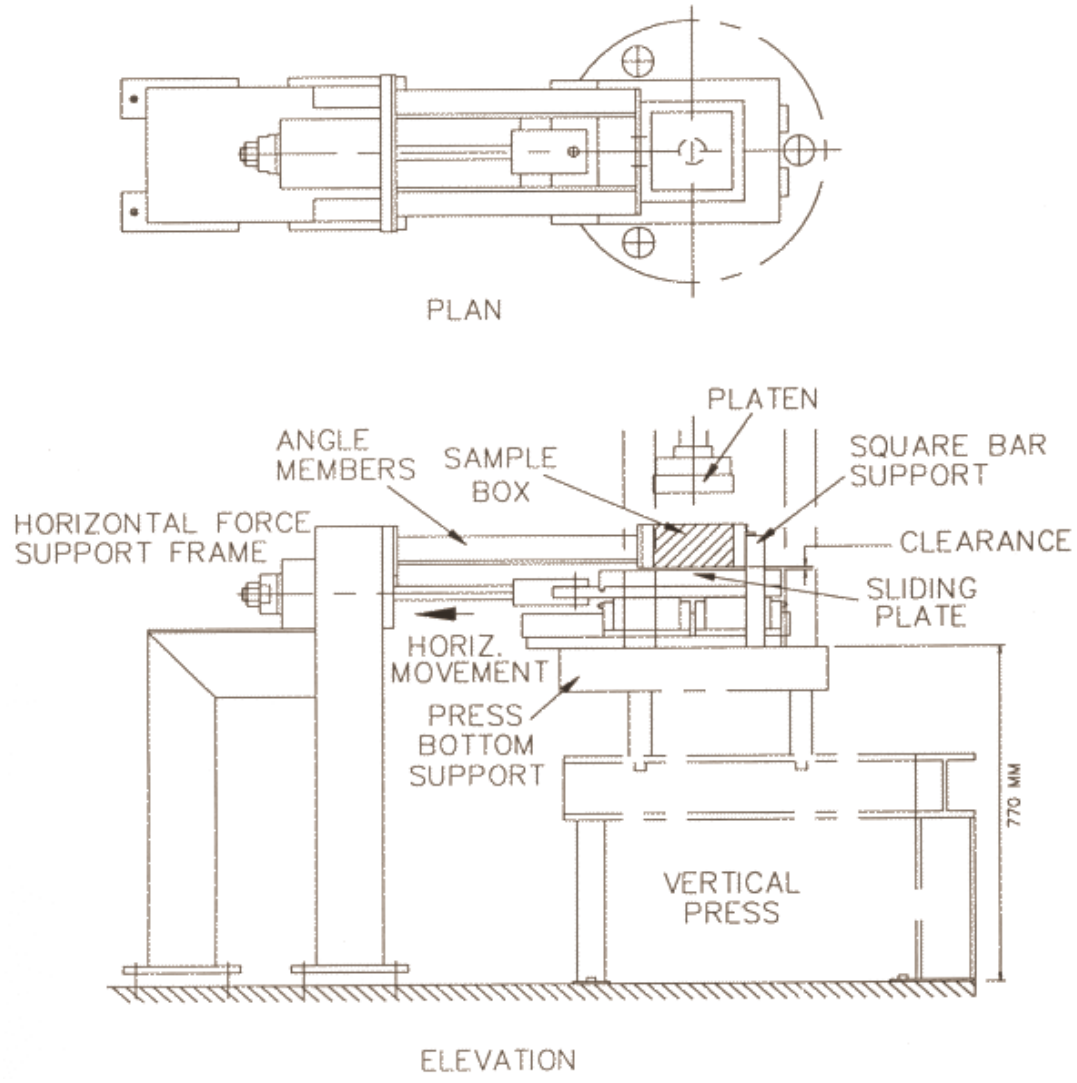

Figure 3.3. General arrangement of direct shear testing equipment (Plaza et al, 1993).

The detail of the box geometry is shown in Figure 3.4. The prepared cane or bagasse was placed by hand into an open-ended box suspended three millimetres above a bottom steel plate with a rough surface on its top surface, providing a gap of two millimetres between the box and the particles of the rough surface. Due to the space limitations in the test rig, a pre-compressor box on top of the open-ended box was used as an extension to place the required amount of prepared cane or bagasse inside the test box.

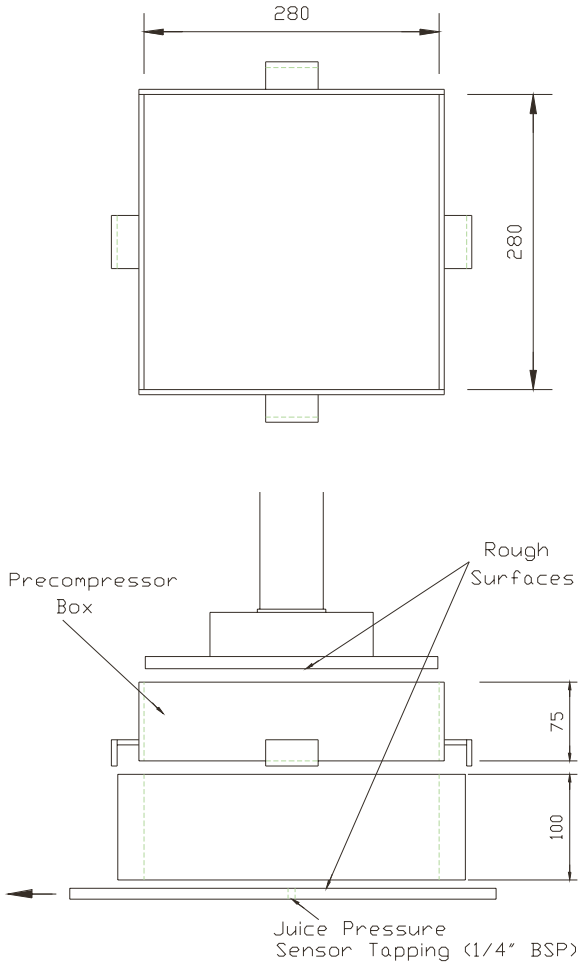

Figure 3.4. General arrangement of direct shear testing equipment.

At the beginning of a test, a top plate with a rough bottom surface was pushed through the pre-compressor box by a hydraulic cylinder, and the bagasse was compressed into the open-ended box until the top plate just intruded into the top of the open-ended box. The top plate was lifted up and the pre-compressor box was removed. The bottom of the top plate was then positioned just inside the top lip of the open-ended box at which time the test was ready to begin.

The shear test involved compression of the bagasse by the top plate and shear by the horizontal movement of the bottom plate. Juice pressure in the bagasse was measured though a 6.35 mm diameter hole at the middle of the bottom plate. Soil water pressure is not usually measured in direct shear tests on soil because drainage paths are short and the material (such as sand) has high permeability. Therefore the soil can be considered as drained. However, the permeabilities of prepared cane

and bagasse at the pressures used in the tests are quite low and are also strong functions of the pressure. Measurement of juice pressure was therefore considered important to ensure the juice pressure was (1.) kept to low levels, and (2.) known, so as to be able to calculate effective stress.

Initially, the top and bottom steel plates (as well as other equipment such as hydraulic pumps) were sourced from the equipment used by Plaza et al (1993) and Plaza and Kent (1998). A progression of preliminary tests was carried out in which the limitations of the existing equipment were identified, and problems due to the behaviour of prepared cane and bagasse were worked out and overcome. The preliminary tests are described below with examples of the test results.

3.2 Over-consolidated test on prepared cane using sandpaper as the rough surface.

A test was carried out using 9 kg of prepared cane as the test material and having P24 sandpaper surfaces on the top compressing plate and on the bottom support plate (refer to Figure 3.4). The sandpaper surface on the top and bottom plates was intended to distribute the shear stress uniformly into the prepared cane during shearing and is a very important part of the test geometry (see Chapter 2). The prepared cane was compressed to about 3000 kPa vertical pressure and held there for a short time (about 10 seconds). The vertical pressure was then reduced to 1500 kPa (allowing the sample to become over-consolidated), and held constant for about 60 seconds. The prepared cane was then sheared (while maintaining the vertical pressure constant) by moving the bottom plate sideways at constant speed. Figure 3.5 shows the vertical pressure, the water pressure (juice pressure) and the calculated effective vertical pressure before, during and after the shearing was carried out. Figure 3.6 shows the horizontal displacement of the bottom plate and the height of the sample (measured by the position of the sandpaper surface on the compressing plate). Figure 3.7 shows the height of the sample and the shear stress (the average horizontal stress) present during shearing.

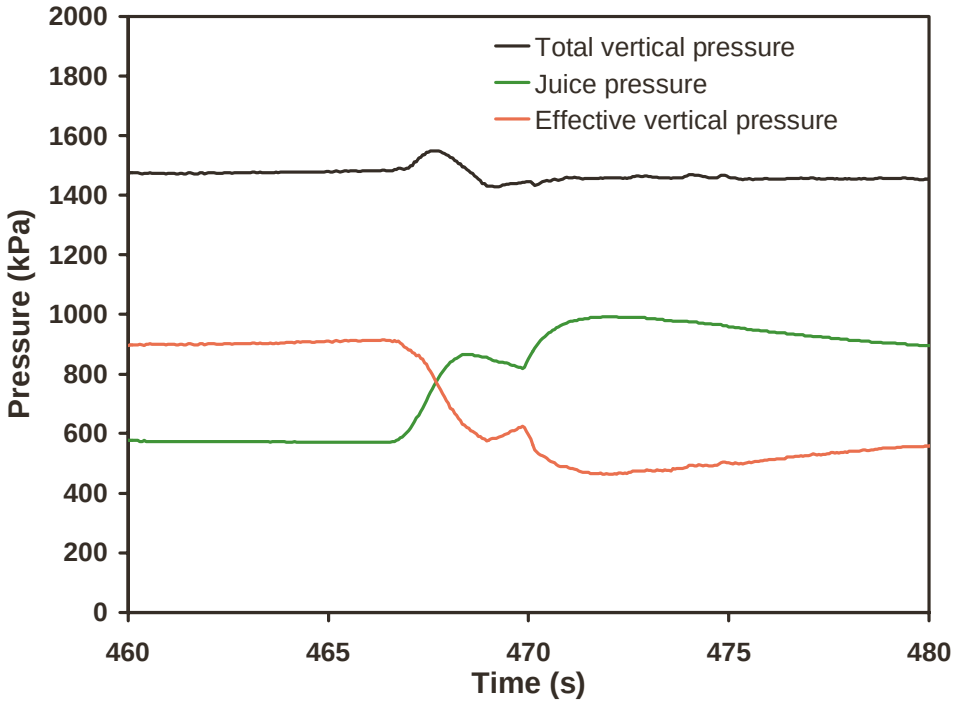

Figure 3.5. Pressures during shearing of over-consolidated prepared cane with sandpaper roughness.

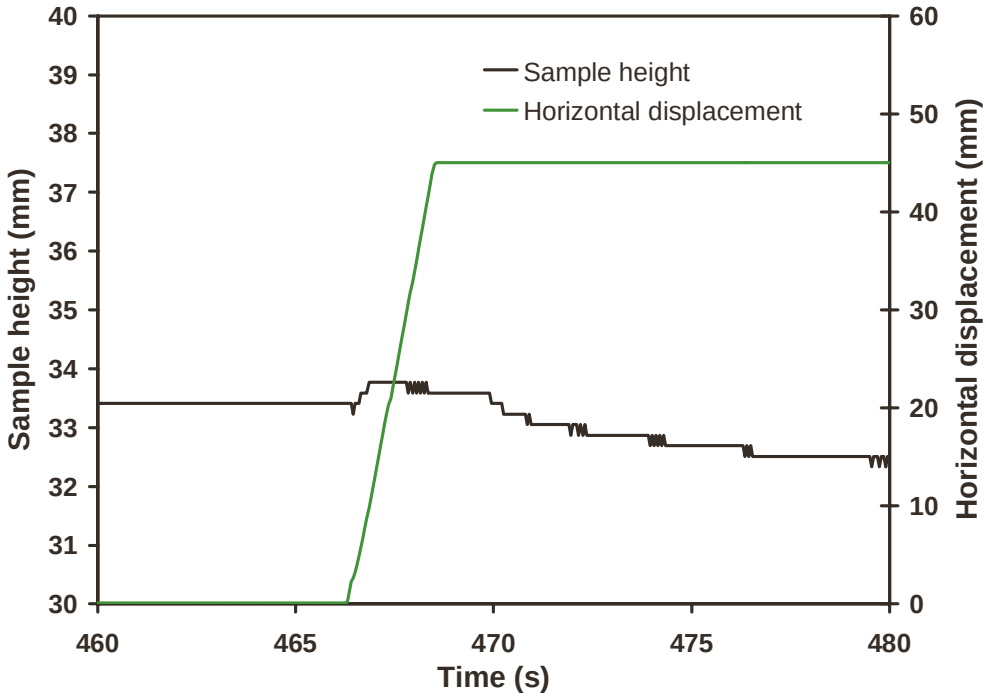

Figure 3.6. Horizontal displacement and sample height during shearing of over-consolidated prepared cane with sandpaper roughness.

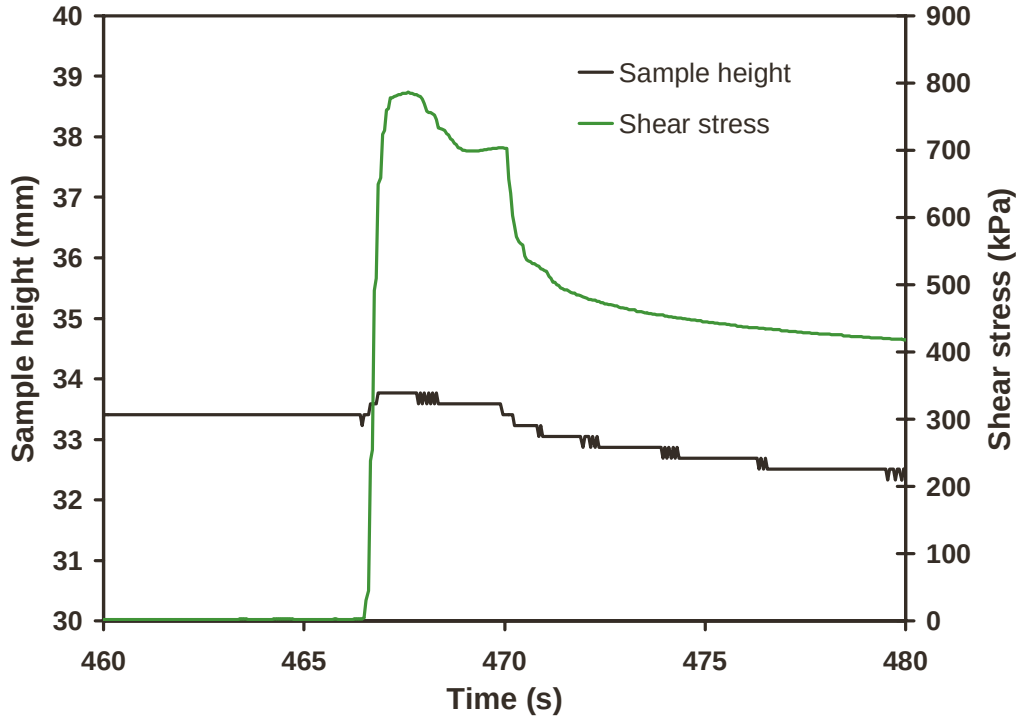

Figure 3.7. Shear stress and sample height during shearing of over-consolidated prepared cane with sandpaper roughness.

This test on prepared cane was noteworthy because it showed three deficiencies:

1. The resolution in the measurement of vertical height was inadequate, at about 0.2 mm in a change of 2.7 mm, giving an error of 7%.

2. High water pressures were measured. The test was supposed to be drained, with a 1 mm clearance between the top compressing plate and the sidewalls of the test box and a 2 mm clearance between the test box and the bottom plate available for drainage. The measurements showed that juice pressures in the order of nearly half the vertical pressure were present in the prepared cane during shearing. The presence of large juice pressure is highly undesirable because it may obscure the behaviour of the solid skeleton of the prepared cane, and also be a long way from constant effective vertical pressure. Since the juice pressure measurement point is outside the bagasse, even higher juice pressures may have been present inside the bagasse. The measurement of juice pressure was not ideal since the measurement location was restricted because of the large change in volume of the bagasse and the shearing action, which could easily damage any specialized equipment, such as

tubes into the bagasse. Note that the calculation of effective pressure was simply the measured (total) vertical pressure minus the measured juice pressure. It was judged highly desirable that the effective vertical pressure on the bagasse skeleton was close to the total vertical pressure in order to measure the behaviour of the solid skeleton of the bagasse, without any complications (such as flow of juice and its effects). For this scenario to occur the juice pressure had to be reduced greatly.

3. The horizontal displacement of the bottom plate was too fast, about 20 $mm.s^{-1}$. A drained test requires a slow shear strain rate to allow any generated water pressure during shearing to dissipate.

Notwithstanding the above problems, the test results gave some confidence that, with some further refinement, the material behaviour in combined shear and compression could be measured.

Similar tests were carried out on first bagasse (the residue that exits the first mill) and final bagasse (the residue that exits the final mill, which is usually the fifth mill). The lowest water pressure was developed in final bagasse, followed by first bagasse while prepared cane developed the largest water pressure. Therefore a method that reduced water pressure in prepared cane to a low level could be expected to have the same effect for first bagasse and final bagasse.

3.3 Tests showing effect of different surface plate geometries and test procedures on water pressure

As stated in the previous section, the presence of large water pressures is undesirable when the objective is to measure the behaviour of the solid skeleton (the fibre) of prepared cane and bagasse. Compression tests were carried out with differing test geometries with the aim of facilitating drainage from the boundaries of the prepared cane. After compression, the test samples measure 280 mm by 280 mm in plan by about 30 mm to 40 mm in height. Therefore the largest area available for drainage is at the top and bottom surfaces. Good drainage at the top and bottom surfaces would also reduce the internal drainage path lengths in the material. Therefore tests were carried out with a combination of sandpaper and grooved surface plates to verify the hypothesis that a major factor contributing towards the measured high water pressures was inadequate drainage at the

boundaries of the test sample. The combinations were governed by the surface plates already available from the equipment used by Plaza and Kent (1998). The combinations were: 1. Both top and bottom surfaces of P24 sandpaper, and 2. Top surface of P24 sandpaper surface and the bottom surface made up of 3 mm high, 45 degree grooves, with the axis of the grooves perpendicular to the direction of shear. The grooves were perpendicular to the direction of shear to provide uniform transfer of shear stress (grip) to the test material, as well as provide drainage.

Shown in Figure 3.8 are results from a test with sandpaper on the top and bottom surfaces, while Figure 3.9 shows the results from a test with sandpaper on the top surface and grooves on the bottom surface.

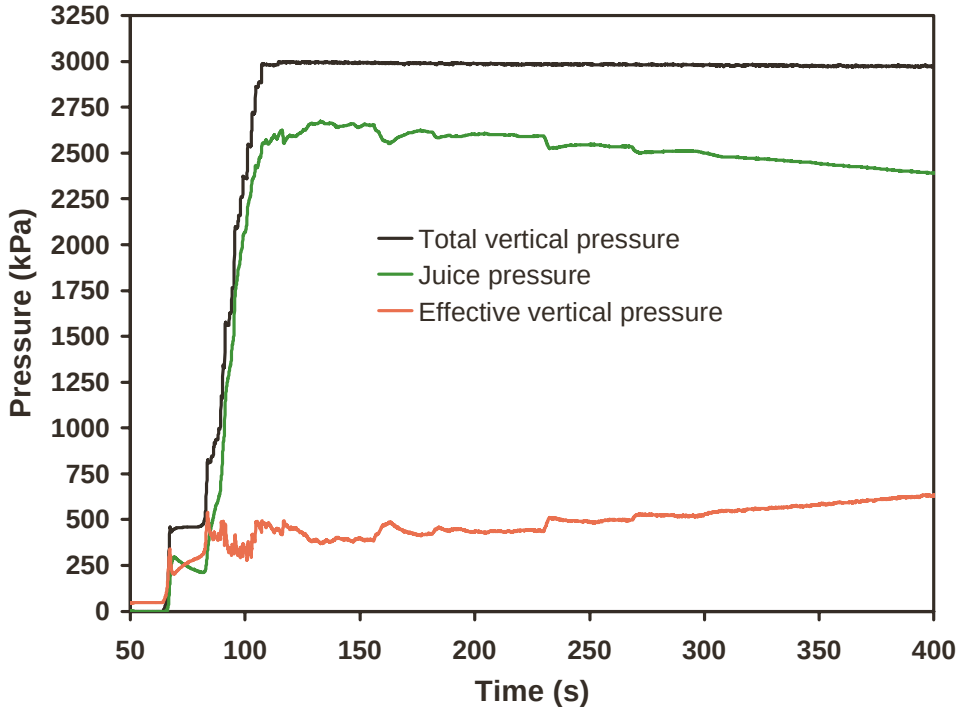

Figure 3.8. Prepared cane under compression using sandpaper as top and bottom surfaces.

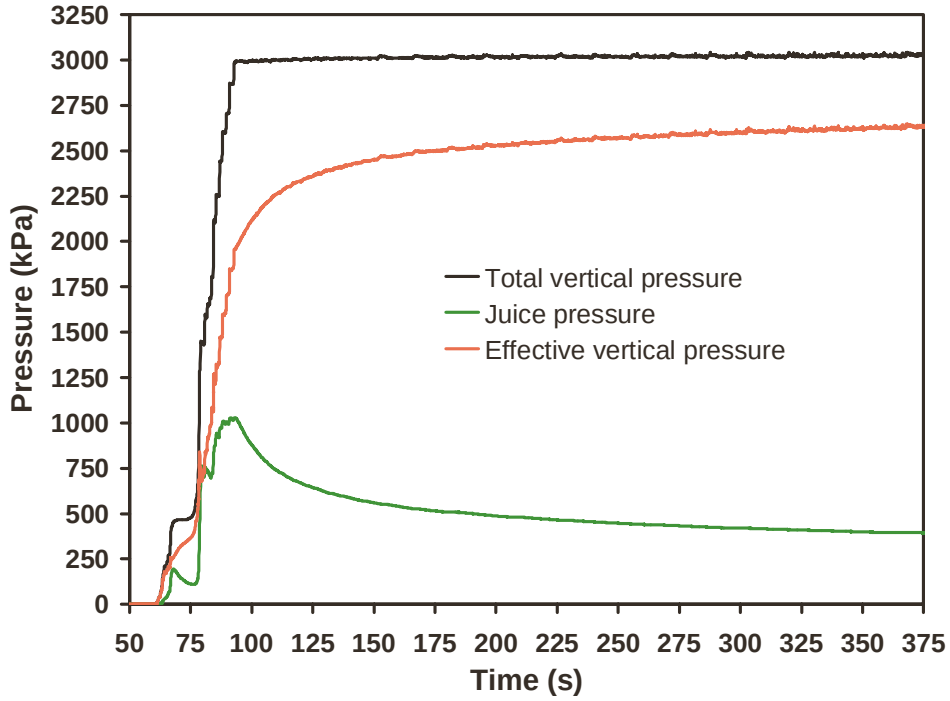

Figure 3.9. Prepared cane under compression using sandpaper as the top surface and 3 mm grooves as the bottom surface.

Clearly, the grooved plate has resulted in reduced water pressures on the bottom, drained boundary. The measured juice water pressure is less than a quarter for the test with the bottom grooved plate, indicating that the use of grooves should be adopted. However, high water pressures might have been present at the top boundary and within the cane. This was examined in later series of tests in this chapter and in Chapter 4.

While carrying out these tests, an interesting behaviour of prepared cane was observed. When prepared cane is loaded to a certain pressure, high water pressures are generated. If the vertical pressure is removed and reapplied, the new magnitude of the water pressure is significantly lower than the previous value. The change in vertical pressure is shown in Figure 3.10. A possible explanation for the difference in water pressure is that prepared cane becomes unsaturated during the unloading and reloading steps. The expressed juice was removed and was not available for reabsorption. Therefore not enough juice was available during the second compression for the cane to become saturated and for juice pressures to develop.

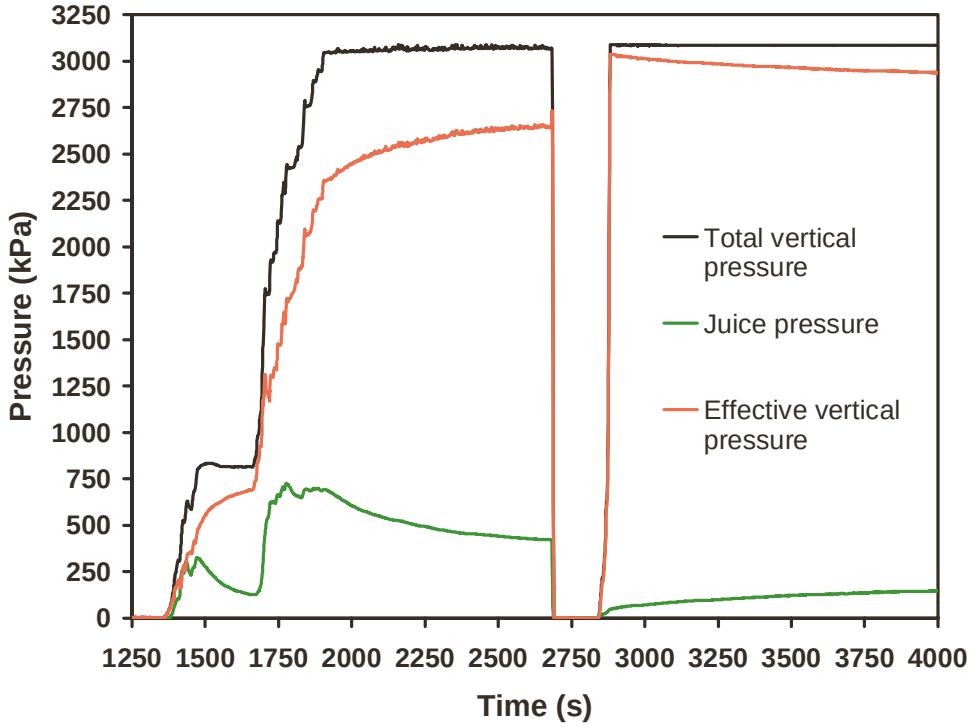

Figure 3.10. Magnitude of water pressure in prepared cane during the application, unloading and reloading of vertical pressure.

There is also a delay between when the vertical pressure is applied and the water pressure develops, which may indicate that more juice was being expressed from the cane cells.

The decrease in water pressure due to cycles of unloading and reloading was identified as being a useful method of reducing water pressure so that the behaviour of the solid skeleton could be measured. The behaviour of soils during the application of pressure, unloading and reloading is well established and soils that have experienced a higher pressure in the past than currently are known as being over-consolidated. As shown in Chapter 4, over-consolidation plays an important part in the tests carried out to work out material behaviour. The use of loading and unloading to reduce water pressures fitted in well with the procedure to establish material behaviour.

3.4 Towards finalising the test geometry and procedure

A grooved plate was identified in Section 3.3 as being beneficial to both drain juice and reduce juice pressures. The best position to put a draining grooved plate was judged to be at the top pushing surface, with the bottom surface being sandpaper. This geometry has many advantages:

1. By drilling holes at the bottom of the grooves through the top steel plate, the holes can drain the juice flowing into the bottom of the grooves. Because of the aspect ratio of the sample (280 mm by 280 mm in plan by 30 mm to 40 mm in height), the shortest drainage paths for most of the sample are towards the top and bottom of the sample (not the sides). The amount of juice being extracted can readily be observed and easily removed from the top of the plate through the use of a suction device such as a vacuum cleaner. The juice that is removed is no longer available for reabsorption when the vertical pressure is removed and the material expands. The removal of juice available to cause water pressure implies reduced water pressure.

2. A juice pressure tapping hole positioned at the middle of the bottom surface can measure the highest water pressure present in the sample (as the main flow of juice is towards the top draining plate then the highest water pressure is expected to be at the furthest point away from the top surface, that is, at the bottom surface). Therefore, there is no need to worry that high water pressures are present in the middle of the sample if low water pressures are measured at the middle of the bottom surface.

3. Since the water pressure tapping point is located flush with the bottom surface, there is no equipment that may be caught or damaged during the shearing action.

4. The gripping surfaces (the grooved surface at the top and the sandpaper surface at the bottom) appeared to distribute the shear stress uniformly during the horizontal movement of the bottom plate. The test equipment can therefore cope with the low stiffness of the prepared cane and bagasse by minimising non-uniform compaction that can be caused, for example, by the box sidewalls.

5. Importantly, the above geometry makes the equipment easy to use, taking into account limitations due to structural integrity and limited available working space.

Therefore 3 mm holes were drilled through an existing top plate that had 3 mm grooves at 45 degrees. Three rows of holes were drilled along the axis of the grooves: one row 25 mm away from each side of the plate and one row in the middle of the plate. Each row of holes started 25 mm away from the side of the plate and each hole was spaced approximately 15 mm away from its neighbour. Therefore only about half the grooves were drained directly by the holes. It would have been desirable for each groove to be drained individually but the plate was not strong enough to allow the drilling of more holes.

There were two objectives for the next set of tests: The first was to test the new geometry to decide whether a new top grooved surface plate needed to be designed and built. The second objective was to test the adequacy of the vertical press to provide a constant vertical load. The vertical load was controlled by manually adjusting the oil pressure in the vertical press system (that is, the oil pressure on the piston of the vertical press).

3.4.1 Testing the geometry and the vertical load

Seven tests were carried out on first bagasse with over-consolidation ratios ranging from 1.0 (normally consolidated) to 3.75. The tests were carried out by compressing the first bagasse up to a vertical pressure of 2000 kPa, then unloading fully, repeating the loading and unloading twice more, then unloading and reloading to the pressure at which the shear was to be carried out (the over-consolidation pressure). During each loading stage, the pressure was held at 2000 kPa, and the juice draining out of the sample through the top plate was removed by a vacuum cleaner, as well as the smaller amounts of juice draining from the edge clearances (about 2 mm) between the box and the bottom surface. Once the sample was compressed to the over-consolidation pressure, the sample was sheared at constant speed while the press oil pressure was manually adjusted to keep the vertical pressure constant.

First bagasse was used instead of prepared cane because lower water pressures would be generated, and attention could be focussed on the total vertical pressure and its control. Measurements for a normally consolidated test are shown in Figure 3.11 to Figure 3.16 while measurements for an over-consolidated test are shown in Figure 3.17 to Figure 3.22. These measurements are used to summarise the results from the seven tests.

Figure 3.11 and Figure 3.17 show the measured vertical pressure, the measured water pressure, and the calculated effective vertical pressure (equal to the measured vertical pressure minus the measured water pressure) for the duration of each test. It is apparent that the test geometry and procedure to reduce water pressure was highly successful, with water pressure being reduced to about 5% of the initial magnitude in a test time of about 15 minutes. It is also apparent that a much longer time would have been required to achieve a similar reduction by simply waiting for the water pressure to dissipate once the sample was loaded. Most probably the water pressure would have remained at a high level as the material continues to express juice at a slow rate while being held under pressure. The tests showed that it was worthwhile to manufacture a new top grooved surface plate to provide further improvement in drainage, provide grip, and be structurally adequate for the range of tested pressures.

Figure 3.12 and Figure 3.18 show the specific volume of the sample plotted against effective vertical pressure (an example calculation of specific volume is shown in Appendix A). Figure 3.12 and Figure 3.18 are basically identical in form to Figure 4.7b in Muir Wood (1990) where the idealised behaviour of a soil under compression is shown. The initial loading path is known as the normal compression line and involves both elastic and plastic deformations (plastic deformation is much larger). The cycles of unloading and reloading take an elastic path known as the unloading-reloading line. It has a much smaller slope than the normal compression line. If the material is loaded beyond the previous maximum vertical pressure the loading path will continue along the normal compression line.

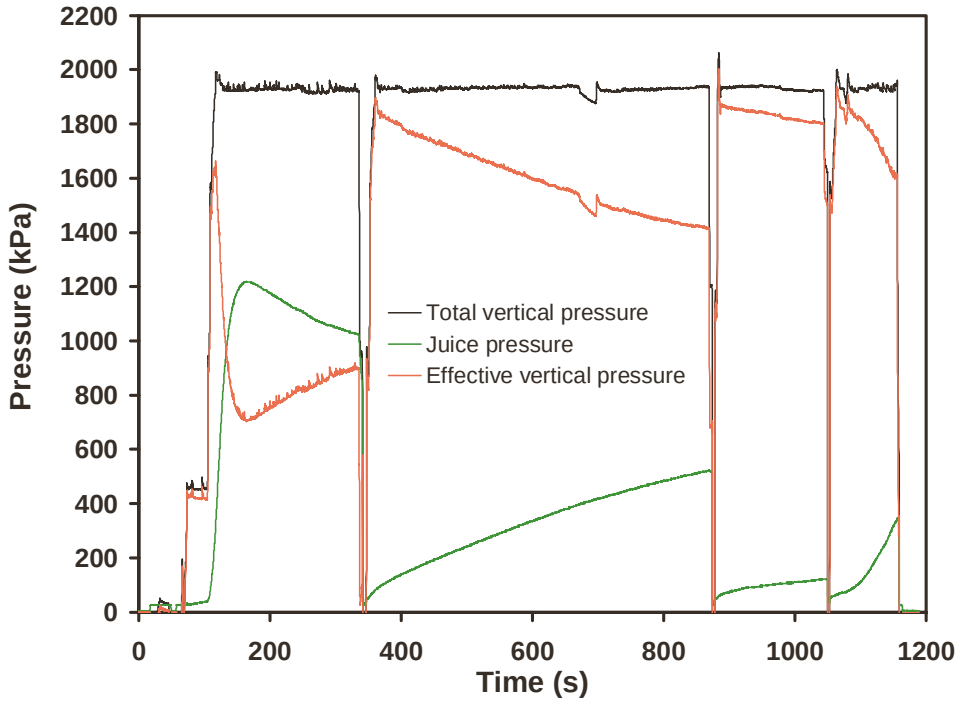

Figure 3.11. Measured pressures for normally consolidated first mill bagasse.

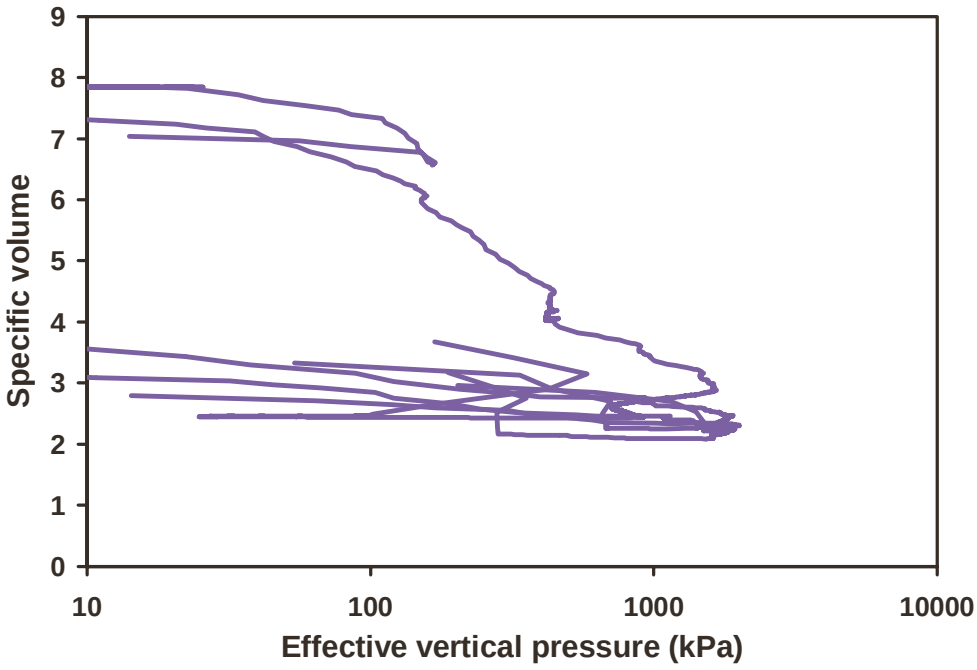

Figure 3.12. Measured normal compression line and unload reload lines for normally consolidated first mill bagasse.

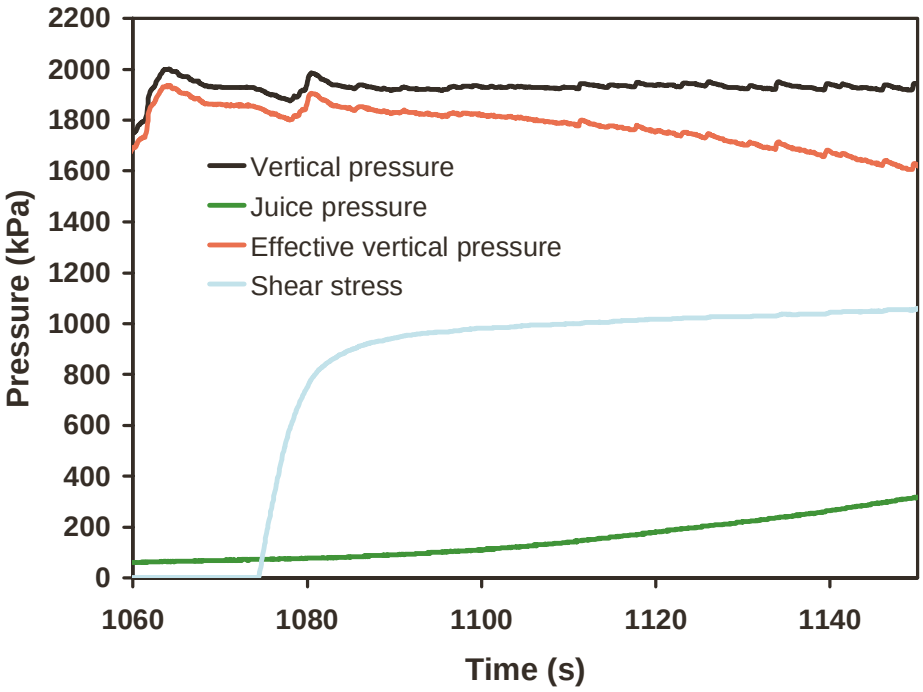

Figure 3.13. Measured pressures and shear stress during shearing for normally consolidated first mill bagasse.

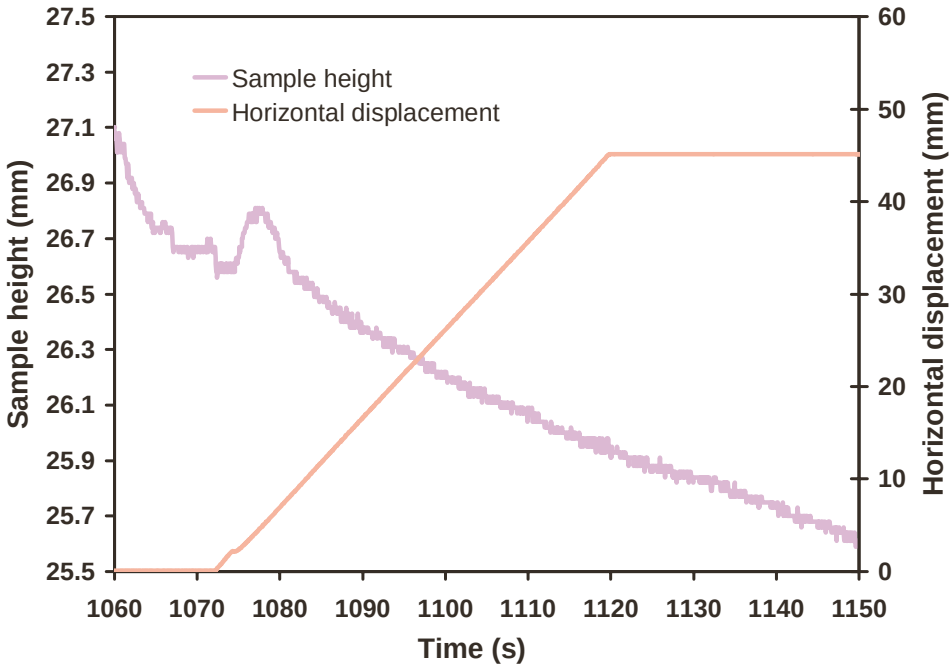

Figure 3.14. Measured sample height and horizontal displacement during shearing for normally consolidated first mill bagasse.

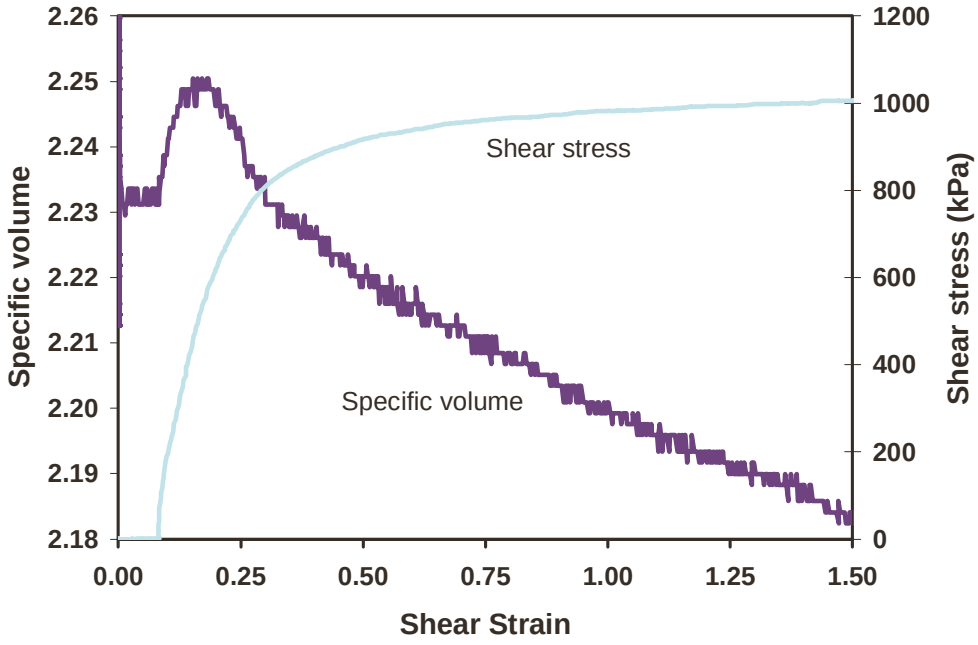

Figure 3.15. Specific volume and shear stress versus shear strain for normally consolidated first mill bagasse.

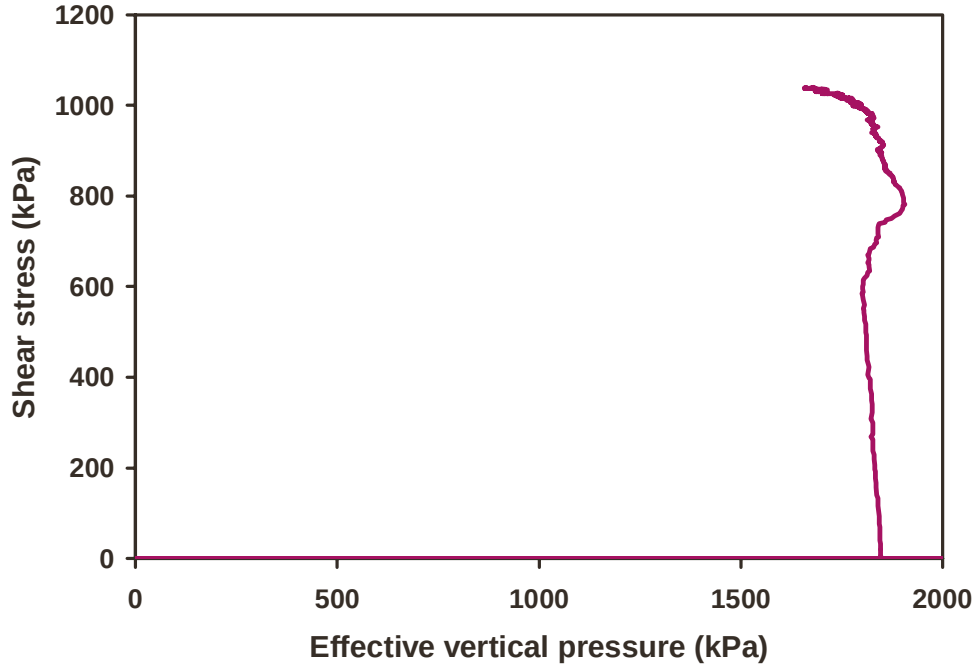

Figure 3.16. Measured shear stress versus effective vertical pressure for normally consolidated first mill bagasse.

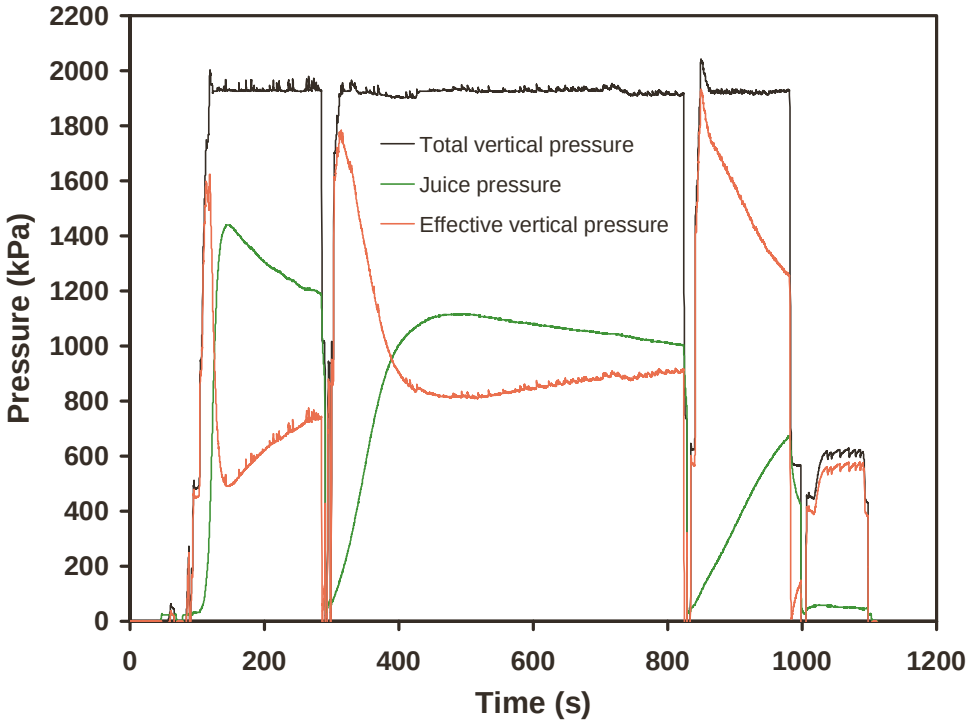

Figure 3.17. Measured pressures for over-consolidated first mill bagasse.

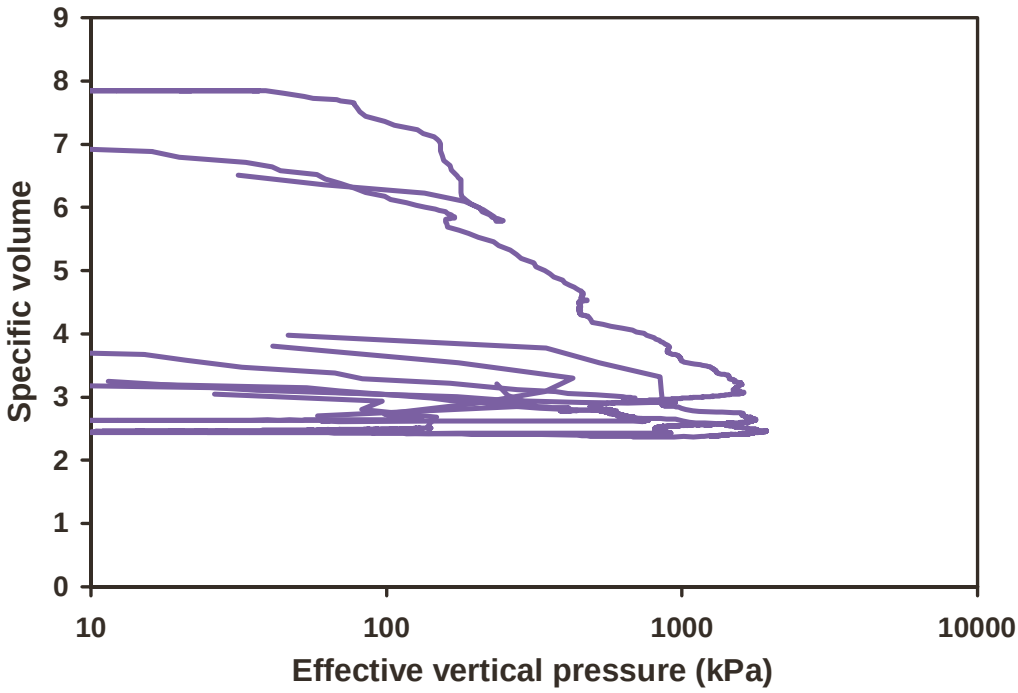

Figure 3.18. Normal compression line and unload reload lines for over-consolidated first mill bagasse.

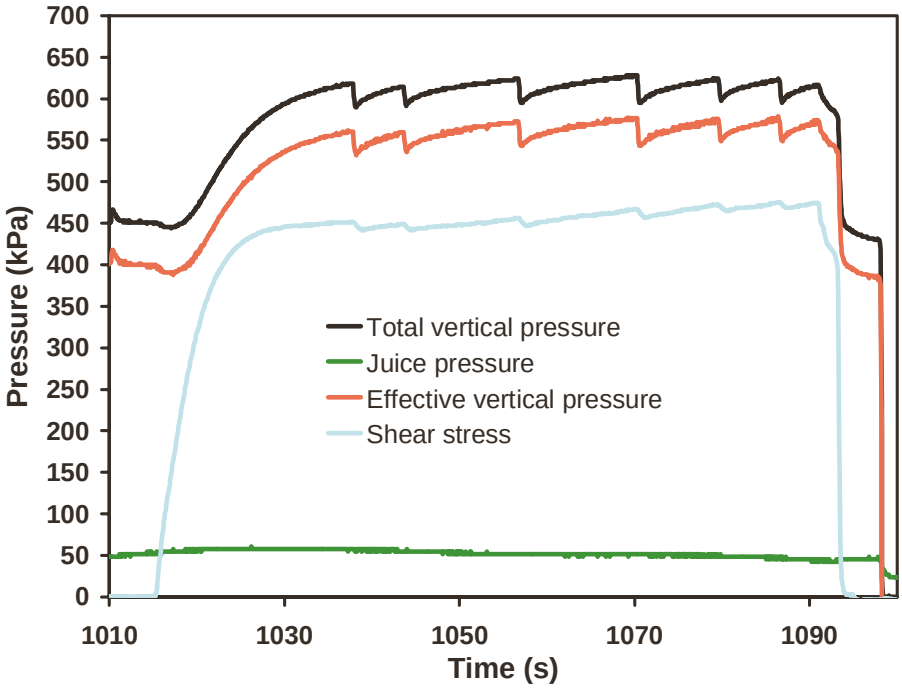

Figure 3.19. Measured pressures and shear stress during shearing for over-consolidated first mill bagasse.

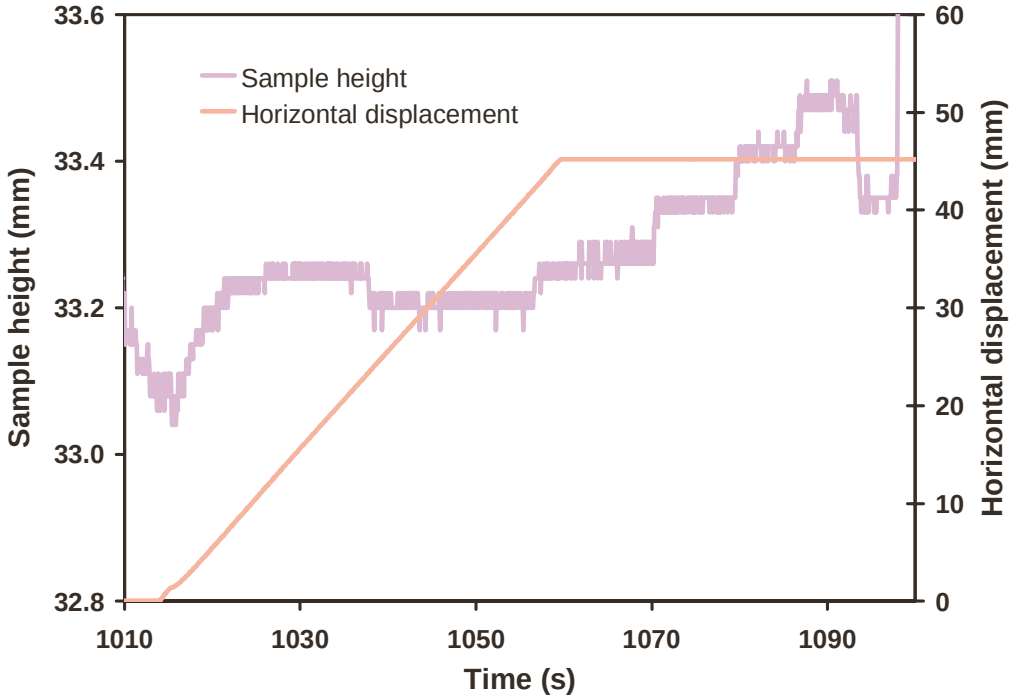

Figure 3.20. Measured sample height and horizontal displacement during shearing for over-consolidated first mill bagasse.

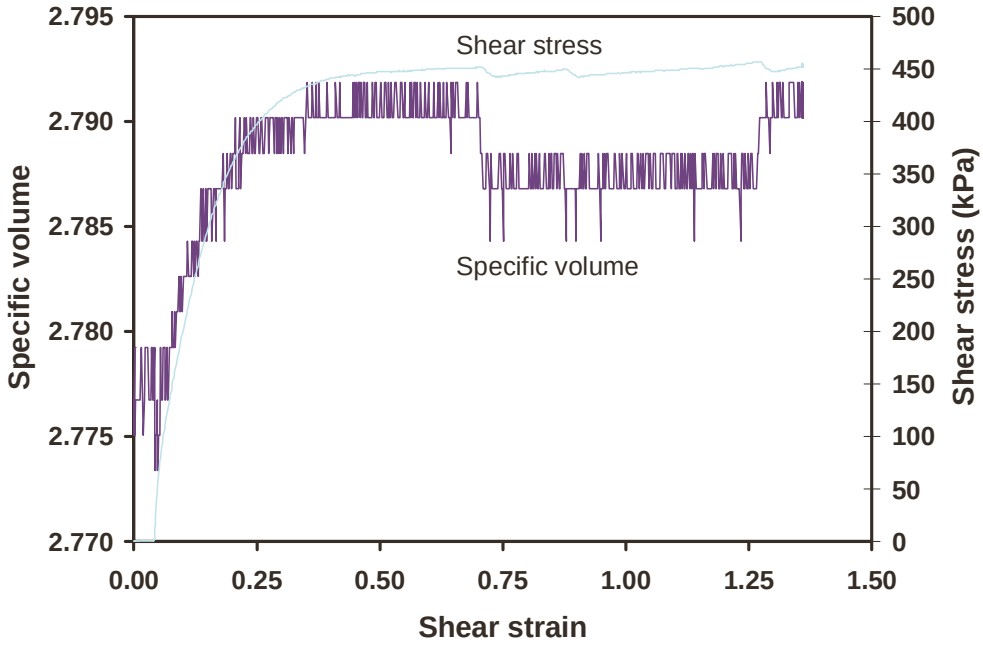

Figure 3.21. Specific volume and shear stress during shearing for over-consolidated first mill bagasse.

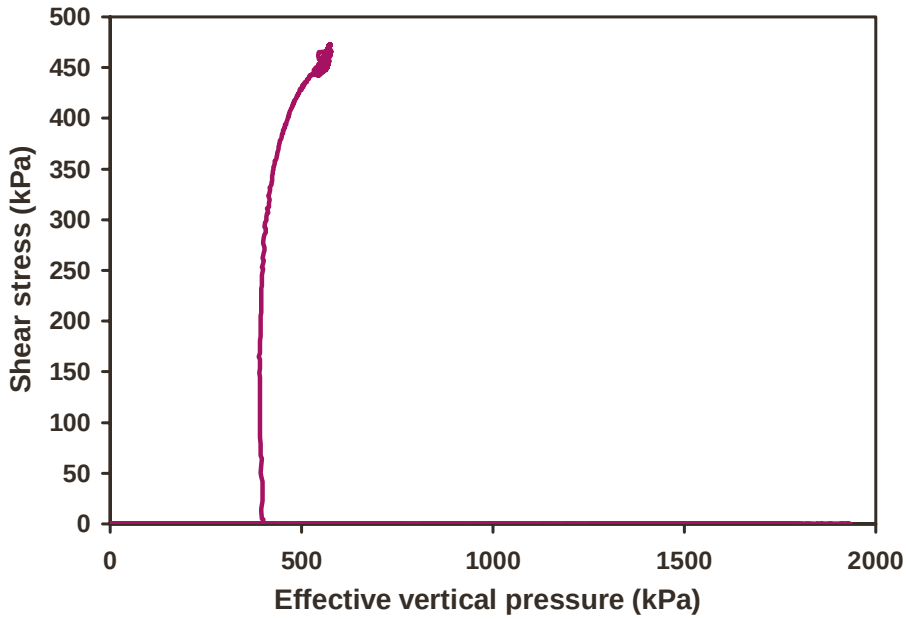

Figure 3.22. Shear stress versus effective vertical pressure for over-consolidated first mill bagasse.

It is noted here that the calculation of specific volume is carried out, as shown in Appendix A, using the full height of the sample. This is the case for all loading conditions, including shearing, and therefore relatively uniform stress and strain conditions are assumed throughout all the sample. A case is made in this investigation that the deformation of the bagasse samples, even during shearing, occurs throughout the sample (not just the thickness of the material at the two millimetre gap between the box and the rough surface on the bottom plate). Actual deformations inside the box could not be observed. A finite element analysis of the test method carried out in Chapter 6 supports this interpretation of the results.

Figure 3.13 and Figure 3.19 show pressures and shear stress during shearing for normally consolidated and over-consolidated first bagasse. The manual control to keep the vertical pressure constant was not entirely successful. For the normally consolidated test there were some significant disturbances in the vertical pressure (shown in Figure 3.13) just before and at the initial stages of shearing. For the over-consolidated sample the vertical pressure increased significantly (by about 35%) once shearing started (shown in Figure 3.19). Efforts to lower the magnitude to its previous level resulted in kinks.

Figure 3.14 and Figure 3.20 show the constant speed horizontal displacement of the bottom surface plate and the sample height (height is measured by the position of the top surface). It is noted that the constant speed horizontal displacement continued for approximately 28 seconds longer than shown in Figure 3.14 and Figure 3.20 due to the displacement sensor having a limited stroke.

Figure 3.15 and Figure 3.21 show the shear stress and specific volume plotted against shear strain. The decrease in volume during shear for the normally consolidated first bagasse sample is shown in Figure 3.15 and is similar to that shown in Figure 5.6d in Muir Wood (1990), which shows the decrease in volume during shear that occurs for a normally consolidated soil. The increase in volume during shear for an over-consolidated first bagasse sample is shown in Figure 3.21 and is similar to that shown in Figure 5.7d in Muir Wood (1990), which shows the increase in volume during shear that occurs for a highly over-consolidated soil. An expected peak in the shear stress versus time plot was not observed. It was thought

that the peak had been obscured due to the increase in vertical pressure (this was confirmed by the main sets of tests shown in Chapter 4). The above measurements were confirmed by other tests, including the other five on first bagasse that are not reported here. The observations of bagasse compressing and expanding during shearing at different over-consolidation pressures indicated that bagasse exhibited critical state behaviour.

Figure 3.16 and Figure 3.22 show shear stress plotted against effective vertical pressure, demonstrating how constant the effective vertical pressure stayed during shearing (until the later part of the tests). The figures are shown here for completeness. The set of plots shown in this section was adopted for further tests.

In summary, the tests showed that:

1. The manufacture of a new top grooved surface plate to provide further improvement in drainage, provide grip, and be structurally adequate for the range of tested pressures was required, and

2. Further improvement in the steady control of the vertical pressure was required to show some of the detail of the expected critical state behaviour (some of the behaviour was already shown, for example, the expansion and contraction behaviour).

3. The preliminary tests indicated that bagasse exhibited critical state behaviour and that the behaviour could be measured using a direct shear test.

3.4.2 Further tests to improve vertical pressure control

A control program using the ASYST data logging and process control software (and using a program modified from that used by Plaza et al, 1993) was tested. The result was that the measurement and control resolution required was better than what was available (for example, the 12 bit Analog to Digital cards provided only 4096 discrete values in the measuring span of the vertical height and the vertical pressure and in the control signal to achieve vertical load control). During these tests there were two major failures of the equipment: the main seals on the press

failed and the hydraulic pump for the vertical press failed. During the repair of the press and the replacement of the pump the hydraulic system was improved. The result was that the manual control that had been judged to be not quite good enough in the previous section was significantly improved and judged to be adequate.

3.5 Summary of Chapter 3

Preliminary direct shear tests were carried out on bagasse with a progression of improved test procedures, geometries and equipment. The following was achieved:

1. Direct shear test equipment for testing prepared cane and bagasse with adequate control of vertical pressure and adequate measurement of vertical force, shear force, maximum juice pressure, sample height and horizontal displacement.

2. Equipment design and testing methodology for reducing juice pressure.

3. The first evidence that bagasse exhibits critical state behaviour.

In summary, the preliminary tests indicated that bagasse exhibited critical state behaviour similar to that of soils and that the behaviour could be measured using a direct shear test.

It is noted that a case is made in this investigation that the deformation of the bagasse samples, even during shearing, occurs throughout the sample (not just the thickness of the material at the two millimetre gap between the box and the rough surface on the bottom plate). Actual deformations inside the box could not be observed. A finite element analysis of the test method carried out in Chapter 6 supports this interpretation of the results.

4 Chapter 4 – Experimental results at pressures in the pressure feeder

4.1 Introduction

The preliminary tests described in Chapter 3 resulted in the development of a test geometry and method that could cope with the large moisture content and very low stiffness of prepared cane, first bagasse and final bagasse. The test geometry and procedure made possible the reduction of juice pressure to a low level. The control and resolution were improved to an adequate level. This chapter describes the final geometry and the test procedure adopted, then presents the main series of test results followed by an analysis of the results to produce material parameters for bagasse.

4.2 Test geometry and equipment

The finalised overall geometry is shown in Figure 4.1. A box of internal dimensions 280 mm by 280 mm and 100 mm high was suspended above a bottom plate that could move sideways as it was mounted on linear bearings. The bottom plate had a P24 (~1 mm diameter particles) closed coat sandpaper surface attached, facing the box. The surface extended beyond the box such that as the bottom plate moved sideways the surface underneath the box remained a continuous sandpaper surface. There was a clearance of 2 to 3 mm between the box and the sandpaper surface on the bottom plate to ensure no contact occurred. A 6.35 mm (1/4 inch) diameter hole was present at the middle of the bottom surface through which water (juice) pressure was measured.

The bottom plate had two functions: to provide uniform grip on the material being tested, and to measure the juice pressure at the interface between the rough surface and the prepared cane or bagasse. As discussed in Chapter 3, this juice measurement was considered the maximum juice pressure in the sample.

The top plate is shown in Figure 4.2. A 1 mm clearance between the sides of the top plate and the box sidewalls allowed the top plate to move into the box to compress the material being tested.

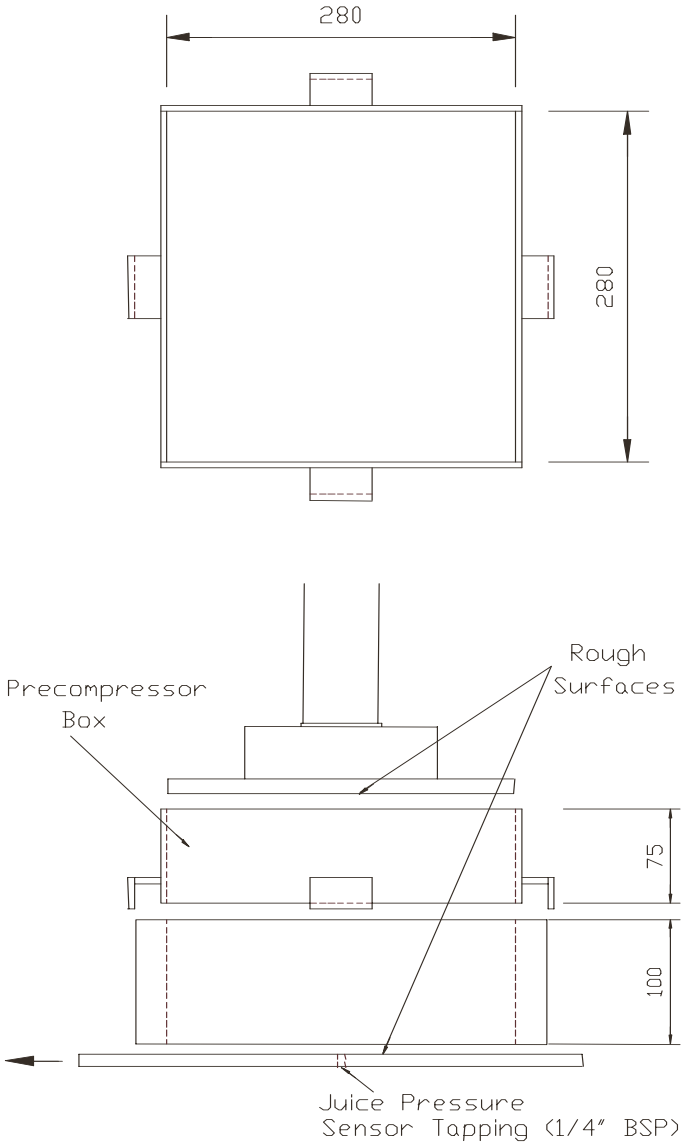

Figure 4.1. Overall geometry of direct shear test for measuring critical state behaviour of prepared cane and bagasse at pressure feeder compactions.

The bottom surface of the top plate had 4 mm deep grooves (8 mm pitch and 90°grooving) with their axis perpendicular to the direction of sideways movement of the bottom plate. The grooves were drained to the top surface of the top plate through 3 mm diameter holes in the bottom of the grooves. Each groove was drained by either two or three holes, with the positions of the sets of holes alternating for each groove to maintain the structural integrity of the plate.

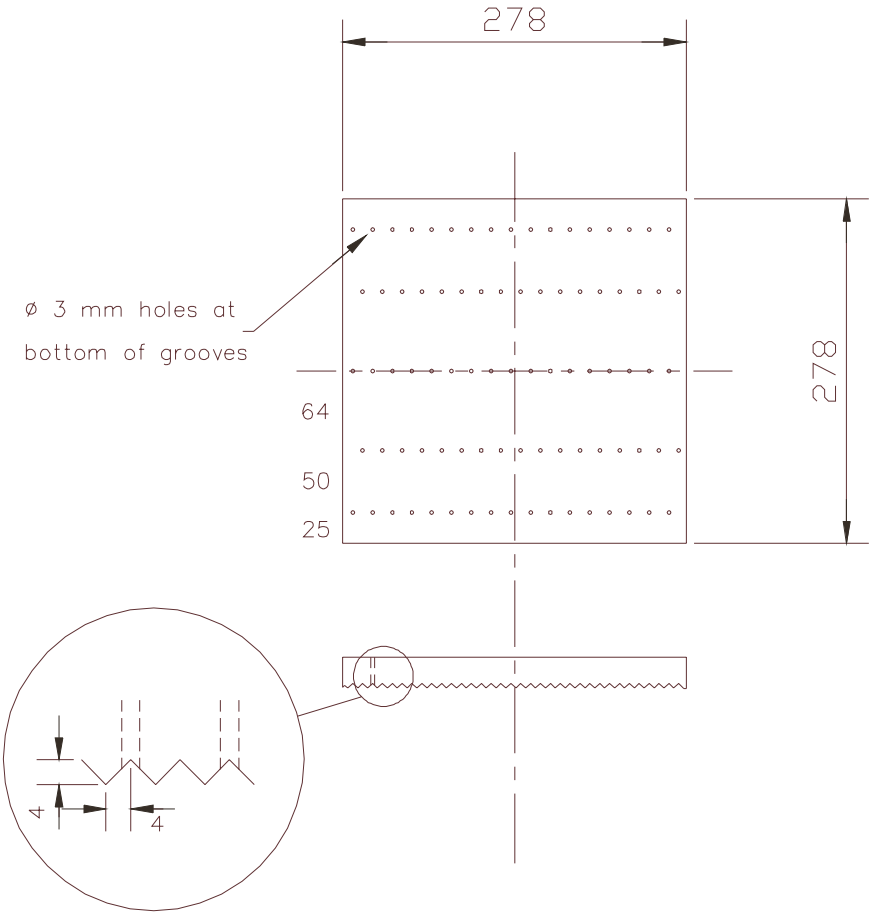

Figure 4.2. Arrangement of top plate and surface details.

The top plate had three functions: to compress the material, to provide uniform grip on the material being tested and to provide the main drainage path for the extracted juice.

The importance of the surfaces on the top and bottom surfaces is emphasized here. A case is made in this investigation that the deformation of the bagasse samples, even during shearing, occurs throughout the sample (not just the thickness of the material at the two millimetre gap between the box and the rough surface on the bottom plate). Actual deformations inside the box could not be observed. A finite element analysis of the test method carried out in Chapter 6 supports this interpretation of the results. The grip of the top and bottom surfaces on the bagasse is important in ensuring deformations occur throughout the sample.

Because of the large deformations present during the testing of a material such as prepared cane or bagasse, it is difficult to measure the highest juice pressure present in the material, which is presumably in the middle of the sample away from the draining boundaries. However, the overall design of the test geometry shown in Figure 4.1 and Figure 4.2 provided the means to measure the highest juice pressure inside the sample test box: as noted previously in Chapter 3, there was virtually no drainage at the clearances between the top and bottom plates and the box. The aspect ratio of the sample, beginning at 100 mm high and 280 mm by 280 mm in plan and decreasing to about 30 to 40 mm high during the shearing part of the test, ensured that the shortest drainage path through the prepared cane or bagasse sample was towards the grooves of the top of the box. It was observed that most of the juice expressed from the box occurred at the top plate. The juice (water) pressure at the bottom of the grooves was relatively very low as the juice oozed out of the holes on the top plate and there were never any spurts. No difference was observed in the distribution of the magnitude of out flowing juice from holes at different locations on the top plate (for example, if fibre orientation due to the direction of compression had caused preferential drainage towards the sides of the box). Therefore, it follows that the highest driving juice pressure occurred at the P24 sandpaper surface at the middle of the bottom plate, that is, where the juice/water pressure was measured. By measuring the highest juice pressure and ensuring that it had a relatively low magnitude compared to the total stress measurement (that is, most of the stress was effective stress), it was ensured that the drained behaviour of the solid skeleton of the prepared cane or bagasse was measured.

Also shown in Figure 4.1 is a pre-compressor box. This box was used to place enough prepared cane, first bagasse, or final bagasse in the test box to be able to carry out the tests within the limited working height of the vertical press used.

The vertical load on the top plate (measured using a load cell), the horizontal load on the bottom plate (measured using strain gauges on a steel rod), the vertical displacement of the top plate (measured using a magnetostrictive non-contact transducer), the horizontal displacement of the bottom plate (measured using a linear potentiometer), and the juice pressure (measured using a water pressure transducer) at the middle of the bottom plate were logged.

4.3 Test procedure

The test procedure was as follows:

1. The prepared cane, first bagasse, or final bagasse was collected from a mill in garbage bins that held 20 to 30 kg of material (usually 30 kg of prepared cane).

2. The material was mixed by the following procedure, following Method 5 in Anon (1991):

(a) dumped into a pile,

(b) split into two equal parts,

(c) any packed material brought to a loose state and all placed into a coned pile,

(d) the pile was given a 90 degree turn and split into two equal parts,

(e) the material was mixed by putting into a coned pile,

(f) steps d and e were repeated once more.

3. The required quantity of material was weighed.

4. The juice pressure line was topped up with water up to the level of the P24 sandpaper surface.

5. The sample was placed in handfuls inside the box with the fibres variably aligned (to avoid the sample becoming initially orientated in one direction) and was then pushed in as hard as finger pressure allowed.

6. Once the top of the box was reached the pre-compressor box was placed on top and the remaining material was placed into the combined box using the same procedure.

7. The logging program was started and the loads, displacements and juice pressure were displayed on a computer screen. The vertical load was also displayed on a LCD display next to a valve that, by manually varying the oil pressure in the press system, determined the load applied by the top plate.

8. The top platen was brought down through the pre-compressor box under manual control and low oil pressure and stopped just inside the test box. The top platen was then taken back up and the pre-compressor box was removed.

9. The top platen was brought down under low oil pressure and placed just inside the box. The manual piston displacement valve was then turned all the way telling the press to drive the top plate down. The top platen therefore compressed the prepared cane or bagasse down to the equivalent pressure on the press system. The corresponding load on the top plate was shown on the LCD display.

10. The oil pressure was increased manually by using the oil pressure valve until the LCD display showed the target maximum load.

11. While holding the load constant, a vacuum cleaner was used to suck the expressed juice from the top of the top plate and from the clearances between the side walls and the bottom plate.

12. The oil pressure was then reduced to low levels and the top plate lifted off the cane but not out of the box.

13. Steps 9 to 12 were repeated four, five or more times, depending on the level of the juice pressure displayed on the computer screen compared to the total vertical pressure (measured while the target maximum load was displayed). When the juice pressure was judged to be low enough (less than 10% of the total pressure) step 14 was undertaken.

14. Either the total load was reduced to the target over-consolidation load (over-consolidation in readiness for the shearing stage) by reducing the oil pressure, or the top plate was lifted off the cane at low oil pressure then put back and increased to the target load. It is believed that the second alternative ended up with slightly lower juice pressures at the over-consolidated target load.

15. The bottom plate was then moved sideways at constant speed by activating a hydraulic pump. During this time the target load (the LCD display) was kept nominally constant by adjusting the oil pressure manually.

16. Once the sideways movement of the bottom plate reached its maximum travel, logging was stopped, the test was stopped and the box was removed and cleaned.

Notes: 1. For the range of pressures tested, it is much easier to achieve low juice pressures for first bagasse then for prepared cane, and it is easier to achieve low juice pressures for final bagasse than for first bagasse. That is, it is much easier to work out the behaviour of the solid skeleton of final bagasse than of prepared cane. This is interesting because historically most tests have been carried out on prepared cane, which is the hardest material to test.

2. It is desirable for a milling unit to be drained but in many locations too much juice and low permeability of the mat result in high juice pressures, which are undesirable (for example, spurting of juice is quite commonly observed). One desirable aim of computer modelling is to find operating parameters for which the spurting does not occur. As noted above, tests on final bagasse achieve the best quality data on the mechanical behaviour of the material. Tests in a simple (for example, two rolls) milling unit without grooves (i.e. flat rolls with a sandpaper surface) using final bagasse without added water would be a logical progression from the direct shear tests.

4.4 Main test series

The pressure range targeted was 200 kPa to 2000 kPa. As shown in the procedure in the previous section, the tests were drained, over-consolidated, and had constant total vertical pressure during shearing. The over-consolidation ratios ranged from 10.0 to 1.0. The materials tested were prepared cane, first bagasse and final bagasse. The sample masses were 10.0 kg for prepared cane, 3.8 kg for first bagasse, and 3.8 kg for final bagasse. Each sample was only tested once. The effect of repeated testing of bagasse was not assessed. The overall description of the main set of direct shear tests is shown in Table 4.1.

The results for each test are shown in Appendix B. A set of six figures is shown for each test. A general description of the measurements and the bagasse behaviour is given below by referring to the first test in Appendix B (Figure B.1.1 to Figure B.1.6), reproduced here in Figure 4.3 to Figure 4.8.

Figure 4.3 shows the total vertical pressure, the juice pressure and the calculated effective vertical stress plotted against time for the duration of the test. The total vertical pressure is the vertical load divided by the plan area of the box. An area correction was not applied because as the bottom sandpaper surface moves sideways, the bottom sandpaper surface area remains constant. The effective vertical stress is calculated by subtracting the juice pressure from the total vertical pressure. This graph shows the quality of the vertical pressure control as well as the progressive development and reduction of juice pressure. Figure 4.3 shows that, for a final bagasse sample, juice pressure is close to zero when the vertical stress is applied and increases as the vertical stress is maintained (as juice is expressed and the material becomes closer to being saturated, and/or as the result of juice expression due to creep). After removing and replacing the vertical stress four times the juice pressure remains constant at a low pressure relative to the total vertical stress. Similar behaviour is shown in Appendix B for prepared cane. However, the juice pressures generated for prepared cane are much higher than those for final bagasse. For prepared cane, the vertical stress is removed and replaced seven times in order to reduce the juice pressure to a low level compared to the total vertical stress.

Table 4.1 Description of direct shear tests at pressure feeder compactions

Material type	Date	Mill	Test number	Nominal (or target) pressures and ratios		
				Maximum pressure (kPa)	Over-consolidation pressure (kPa)	Over-consolidation ratio
Final bagasse	4-12-98	Racecourse	C	2000.0	2000.0	1.0
			E		1600.0	1.25
			A		1200.0	1.67
			A1		1200.0	1.67
			F		1000.0	2.0
			B		800.0	2.5
			D		400.0	5.0
			G		400.0	5.0
First bagasse	3-12-98	Racecourse	3	2000.0	2000.0	1.0
			3A		2000.0	1.0
			5		1600.0	1.25
			1		1200.0	1.67
			6		1000.0	2.0
			2		800.0	2.5
			7		800.0	2.5
			4		400.0	5.0
	5-12-98	Pleystowe	8	1500.0	1500.0	1.0
			5		1500.0	1.0
			3		1200.0	1.25
			1		900.0	1.67
			6		750.0	2.0

Table 4.1 (cont.) Description of direct shear tests at pressure feeder compactions

Material type	Date	Mill	Test number	Nominal (or target) pressures and over-consolidation ratios		
				Maximum pressure (kPa)	Over-consolidation pressure (kPa)	Over-consolidation ratio
			2		600.0	2.5
			4		300.0	5.0
			7		300.0	5.0
Prepared cane	7-12-98	Pleystowe	6	1500.0	1500.0	1.0
			8		1500.0	1.0
			3		1200.0	1.25
			1		900.0	1.67
			5		750.0	2.0
			2		600.0	2.5
			7		600.0	2.5
			4		300.0	5.0
	8-12-98	Racecourse	E	2000.0	2000.0	1.0
			H		2000.0	1.0
			D		1600.0	1.25
			B		1200.0	1.67
			F		1000.0	2.0
			A		800.0	2.5
			C		400.0	5.0
			I		400.0	5.0
			G		200.0	10.0

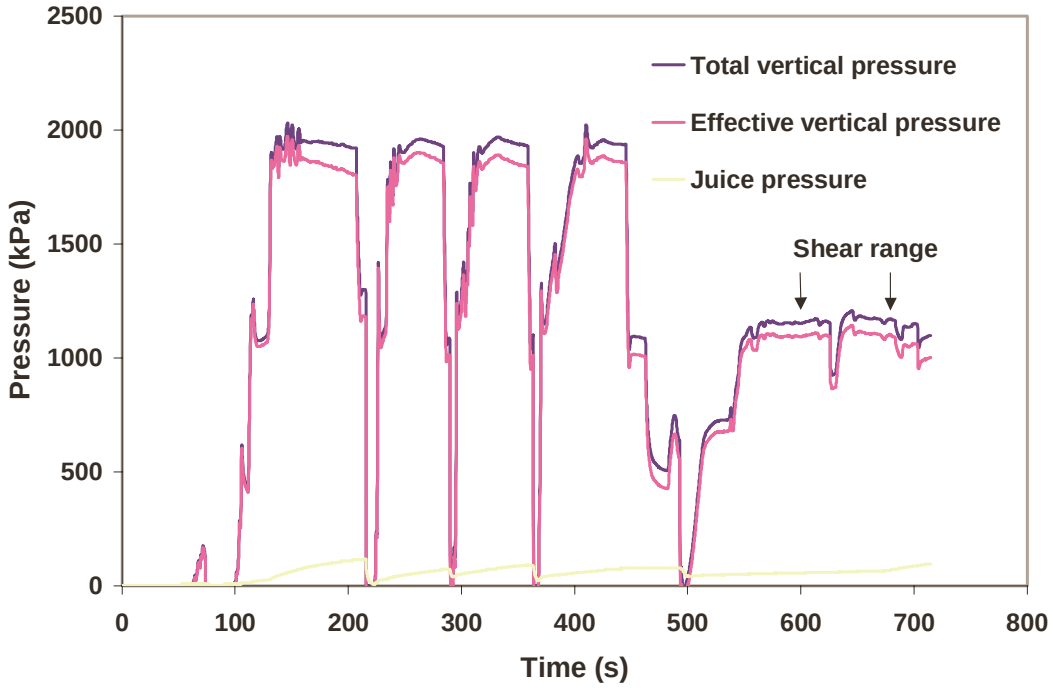

Figure 4.3. Example of measured pressures, Test A, final bagasse, 4-12-98.

Figure 4.4 shows the specific volume plotted against the natural log of effective vertical pressure (an example of the calculation of specific volume is given in Appendix A). The final bagasse had been previously compressed to a pressure of about 80 kPa by the use of the pre-compressing box. This previous loading is reflected in the initial flat loading line (marked as 1). The final bagasse was then unloaded and reloaded (marked 2 and 3). The continuation of the line marked 3 shows the measured normal compression line between 100 kPa and 2000 kPa. The line marked 4 is the initial unloading line from 2000 kPa and 5 represents a series of reloading and unloading lines to and from 2000 kPa. The normal compression line (between 100 kPa and 2000 kPa) and the elastic unloading-reloading lines from 2000 kPa (between 10 kPa and 2000 kPa) are shown, and a good case can be made that both lines are linear as is usually (although not always) observed for soils. It is noted that Butterfield (1979) has shown an improved representation of the normal compression line for soils by plotting the log of specific volume versus the log of pressure. However, for the purpose of this investigation, the conventional plot for soils of specific volume versus the log of pressure has been retained.

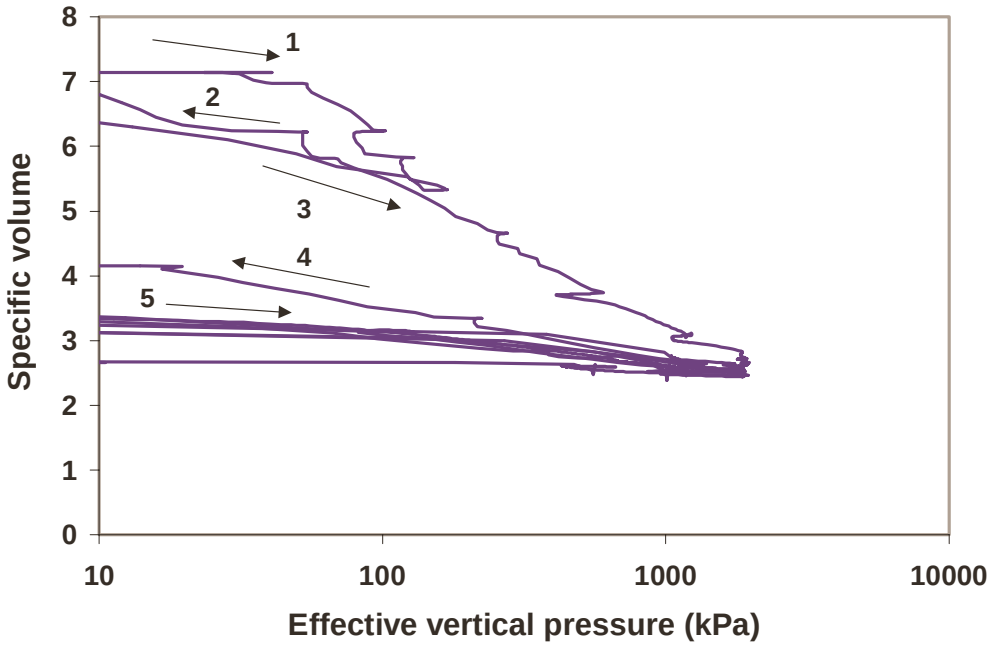

Figure 4.4. Example of normal compression line and unload reload lines, Test A, final bagasse, 4-12-98.

It is noted that the linearity of the normal compression curve for prepared cane (shown in Appendix B) is more difficult to identify because of the presence of large juice pressures during this stage (for example, see Figure B.4.1 and Figure B.4.2). The unloading-reloading lines for prepared cane are linear for the measured range of pressures. Comparison of the normal compression line and elastic unloading-reloading line for prepared cane with those for final bagasse and first bagasse indicate that it is reasonable to assume a linear relationship for the normal compression line of prepared cane at pressures from 80 kPa to 2000 kPa, noting that there will be a higher uncertainty in the measured slopes for prepared cane than for the bagasses. The graphs show that final bagasse, first bagasse and prepared cane are highly compressible with a small amount of rebound when the pressure is removed.

Figure 4.5 is a close up of the shearing part of the test. It shows the total vertical pressure, the juice pressure, the calculated effective vertical pressure, and the shear stress plotted versus time.

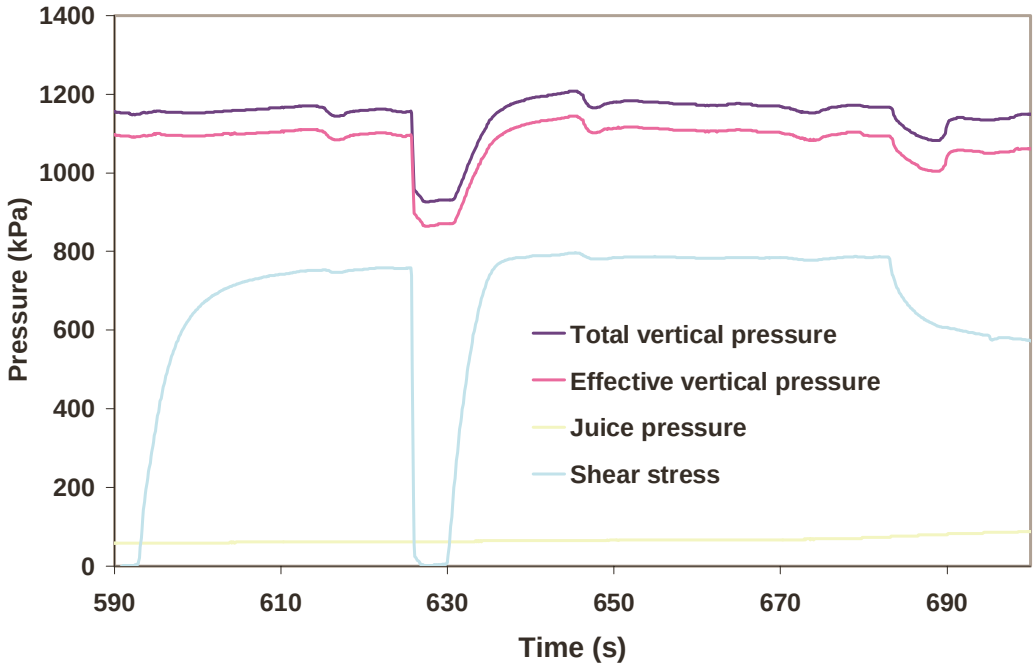

Figure 4.5. Example of measured pressures and shear stress during shearing stage, Test A, final bagasse, 4-12-98.

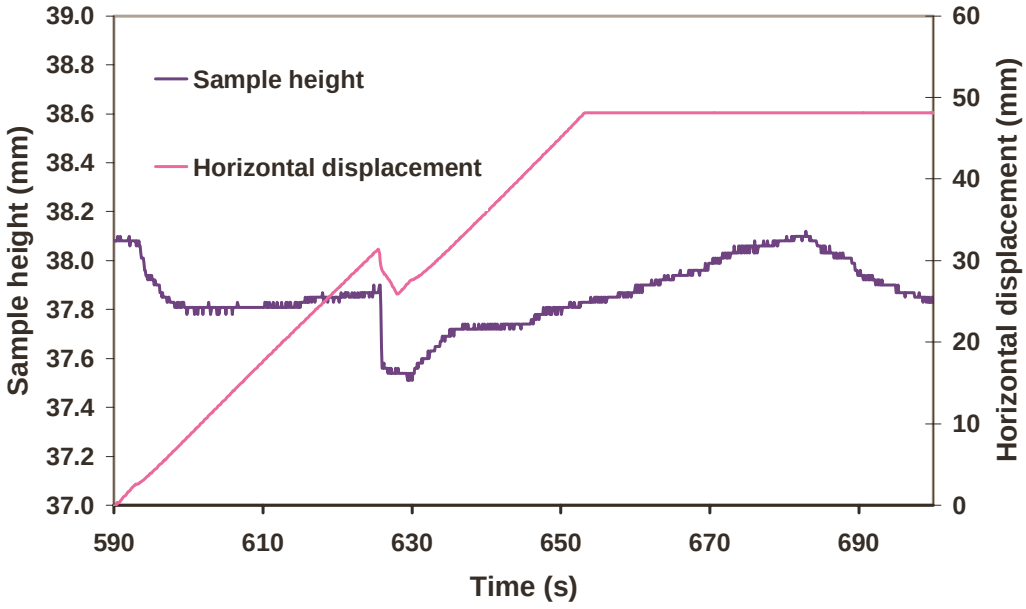

Figure 4.6. Example of measured sample height and horizontal displacement during shearing stage, Test A, final bagasse, 4-12-98.

Figure 4.6 is a companion to Figure 4.5 and shows the height of the sample and the horizontal displacement of the bottom plate versus time. These two plots show the differences in the shape of the shear stress curve and whether the sample compresses or expands during shearing.

If the shear stress reduces to zero during shearing, as shown in Figure 4.5 (for example, by the failure of the hydraulic pump driving the bottom plate horizontally), there is an almost instant decrease in the volume of the material, as shown in Figure 4.6. This decrease in volume when shearing is stopped seems to occur for samples at any level of over-consolidation. The understanding of this behaviour could potentially be used to increase compaction density and extract more juice by the use of different milling equipment and/or operating conditions.

Figure 4.7 shows the shear stress and specific volume plotted against shear strain. The shear strain is defined as the horizontal displacement divided by the height of the sample.

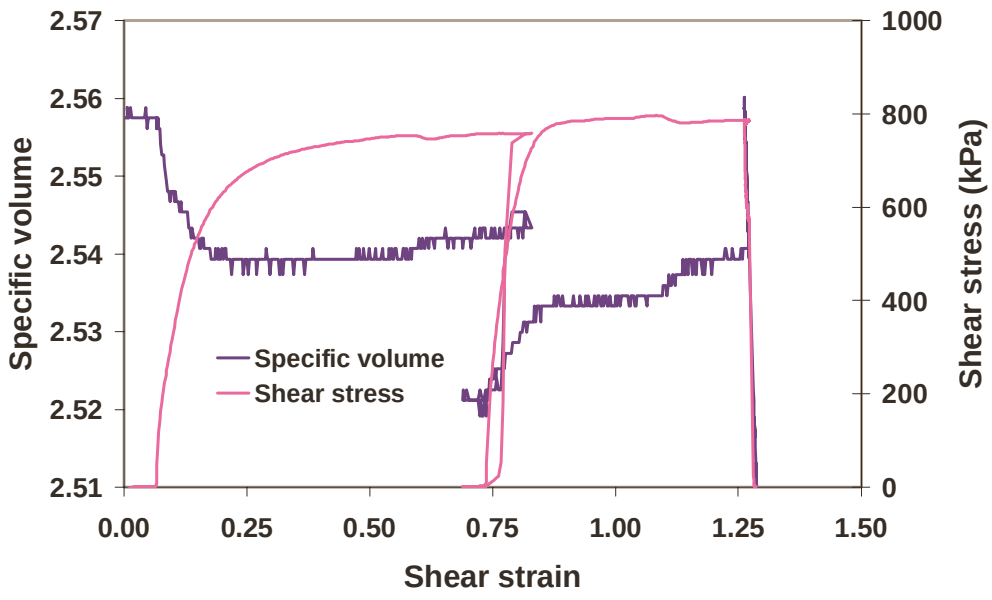

Figure 4.7. Example of specific volume and shear stress versus shear strain during shearing stage, Test A, final bagasse, 4-12-98.

Figure 4.8 shows the shear stress plotted against the effective vertical pressure. It provides a measure of the quality of the test: as the shear stress changes the effective vertical pressure should stay constant if good vertical pressure control and low juice pressure are achieved. It is shown that the effective vertical pressure is constant for a large proportion of the test, being upset only by the sudden stop in shearing. The plot also shows the continuation of shearing and final stop in shearing.

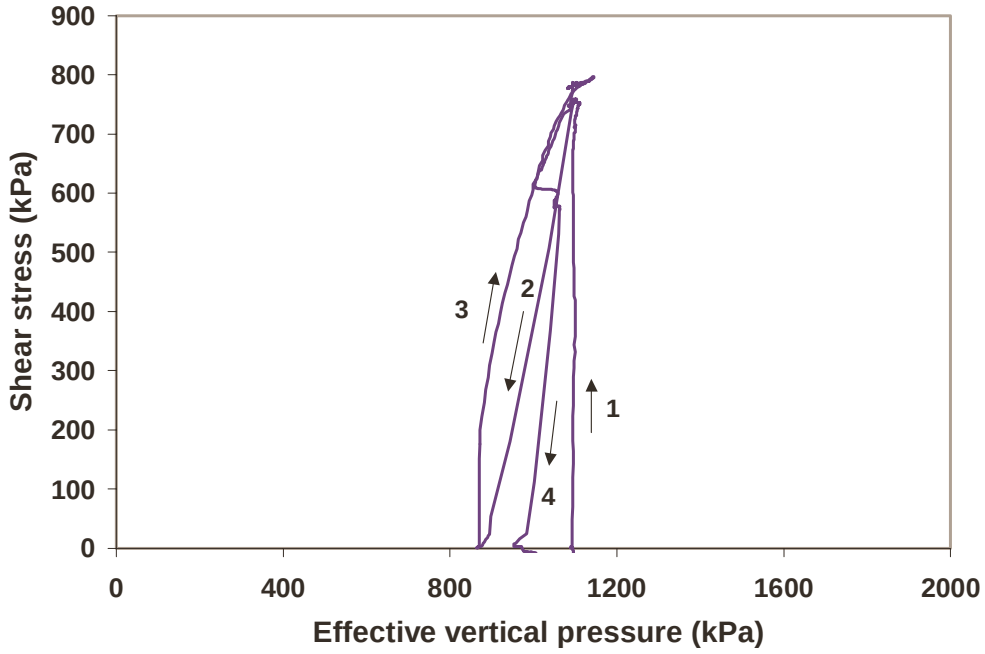

Figure 4.8. Example of shear stress versus effective vertical pressure during shearing stage, Test A, final bagasse, 4-12-98.

The measurements shown in Appendix B were summarised using analysis techniques given by Kirby (1998a) and Harris (1998), following for example Muir Wood (1990), and were divided into the five sets of tests shown in Table 4.1 (one set for final bagasse and two sets each for first bagasse and prepared cane). Seven plots for each set of tests are described below. Average values for the normal compression line are presented in Table 4.2 to Table 4.6. The determined material parameter values are summarised in Table 4.7. It is emphasised that the values should ideally only be used for the pressure range at which they were measured, and to be aware if any extrapolation is carried out during computer modelling. For

example, the values of λ are much higher at lower pressures (Kent and McKenzie, 2000).

Figure 4.9, Figure 4.16, Figure 4.23, Figure 4.30, and Figure 4.37 show specific volume plotted against the effective vertical pressure during the loading and unloading-reloading phases before the shearing stage, in order to show the normal compression line and the elastic unloading-reloading line. The normal compression line is an average from each set of tests as worked out in Table 4.2 to Table 4.6. The elastic unloading-reloading line was determined from a single value for each test in a set after over-consolidation and just before shearing started. There is a small discrepancy where the normal compression line and the unloading reloading line meet in the plots, reflecting that they were determined independently. This discrepancy is of little consequence: the important data for modelling is the slope of the unloading-reloading line. There was a trend of decreasing initial specific volume at low pressure (for example, 10 kPa) when going from prepared cane to first bagasse to final bagasse as well as an increase in the stiffness of the materials.

Figure 4.10, Figure 4.17, Figure 4.24, Figure 4.31, and Figure 4.38 show normalised shear stress plotted against shear strain for the duration of shearing. The normalised shear stress is the shear stress divided by the nominal maximum vertical pressure (1500 kPa or 2000 kPa). These graphs show the changing shape of the shear stress curve: a lightly over-consolidated material has a steep initial curve followed by a transition to a plateau, with a much lower shear stiffness, but with the shear stress continuing to increase slowly with further shear strain. A heavily over-consolidated material has a similar initial steep rise, but then has a peak in the shear stress, followed by reduction to a constant residual shear stress with further shear strain.

Figure 4.11, Figure 4.18, Figure 4.25, Figure 4.32, and Figure 4.39 show the volumetric strain plotted against the shear strain for the duration of shearing. These graphs show the striking difference in volume behaviour with the materials decreasing in volume when lightly over-consolidated and increasing in volume when highly over-consolidated.

Also shown, for example in Figure 4.10 and Figure 4.11 for Test a on final bagasse (Test a, OCR of 1.67), is the sudden decrease in volume when shearing stops during a test. Also worth mentioning is the excellent repeatability of the shear stress during the tests. The repeatability is demonstrated when a test has been repeated due to a problem such as electrical noise or loss of hydraulic pressure in the cylinder driving the bottom plate sideways (for example Test a and Test a1 in Figure 4.10 and Figure 4.11 for final bagasse, Test 3 and Test 3a in Figure 4.17 and Figure 4.18, Test 4 and Test 7 in Figure 4.24 and Figure 4.25 for first bagasse, Test 6 and Test 8 in Figure 4.31 and Figure 4.32 for prepared cane, and Test e and Test h in Figure 4.38 and Figure 4.39 for prepared cane), the shear stress lines coincide, even when the shear stress has been removed and reapplied. The volumetric strain also has good repeatability although not as good as the shear stress.

Figure 4.12, Figure 4.19, Figure 4.26, Figure 4.33, and Figure 4.40 show shear stress divided by effective vertical pressure plotted against volumetric strain. Again the difference in compressing and expanding behaviour can be seen. This plot is used to estimate the critical state equivalent friction angle, ϕ_{cs}, by determining the value of shear stress divided by effective vertical pressure between the expanding curves and the compressing curves [$\phi_{cs} = \tan^{-1}$ (shear stress / effective vertical pressure)]. An estimate of the critical state parameter $M = 2 \sin \phi_{cs}$ can be carried out (Naylor and Pande, 1981) assuming plane strain conditions.

Figure 4.13, Figure 4.20, Figure 4.27, Figure 4.34, and Figure 4.41 show the final volumetric strain of each test in a set of tests plotted against the average normalised effective vertical pressure during shearing. The effective vertical pressure is normalised by dividing by the nominal maximum vertical stress (1500 kPa or 2000 kPa). The normalised effective vertical pressure (and therefore the over-consolidation ratio by calculating the inverse) at which no volume change occurs are obtained from this plot and is shown in Table 4.7 (shown on page 95). The results indicate that the no volume change over-consolidation ratio decreases when going from prepared cane to first bagasse to final bagasse. As will be shown in Chapter 7, pressure has a large effect on this value for all three materials. The change in over-consolidation ratio has implications for which mathematical model

is suitable for reproducing prepared cane, first bagasse and final bagasse behaviour as this parameter can determine the shape of the yield surface. For example, for the Modified Cam Clay model the no volume change over-consolidation ratio is 2.0. The results indicate that a model where this parameter can be changed might be required to model the three different materials. The value of the no volume change over-consolidation ratio and its effect on modelling is discussed in greater detail in Chapter 7 and in Chapter 8. If the normalised total vertical pressure is used (instead of the effective pressure) in the calculations, the resultant no volume change over-consolidation ratios are reduced as shown in Table 4.7.

Figure 4.14, Figure 4.21, Figure 4.28, Figure 4.35, and Figure 4.42 show the maximum and final normalised shear stress values plotted against the average normalised effective vertical pressure during shearing (normalised by dividing by the nominal maximum vertical stress (1500 kPa or 2000 kPa)) to estimate the equivalent critical state friction line. The critical state equivalent friction angle, ϕ_{cs}, is determined, following Kirby (1991), by drawing a line from the origin and below and to the right of values where the maximum shear stress is higher than the final shear stress (corresponding to samples that expand in volume during shearing) and above and to the left of values where the maximum shear stress is the same as the final shear stress (corresponding to samples that compress in volume during shearing). As before, an estimate of the critical state parameter $M = 2 \sin \phi_{cs}$ is made.

Figure 4.15, Figure 4.22, Figure 4.29, Figure 4.36 and Figure 4.43 show the specific volume plotted against the effective vertical pressure to estimate the equivalent critical state line. The specific volume of each sample is plotted just before shearing starts and just before shearing stops to show whether a test sample expands or contracts during shearing. The equivalent critical state line in volume-pressure space can be estimated by drawing a line above and to the right of the expanding test values and below and to the left of the compressing test values. It is noted that this line is quite poorly defined (in comparison to the previous parameters).

Also shown in Table 4.7 (on page 95) and plotted in Figure 4.44 (on page 97) is the maximum shear stress measured for tests at an over-consolidation ratio of 1.0 (i.e.

the Mohr-Coulomb plot) for all three materials. Figure 4.44 is interesting because it indicates that the shear strengths of prepared cane, first bagasse, and final bagasse are similar (further measurements are given in Section 7.7 of Chapter 7 to confirm this).

Table 4.2 Normal compression line values for final bagasse, 4-12-98 tests

Test	υ_λ	λ
A	11.38	1.17
A1	11.34	1.15
B	11.07	1.11
C	11.02	1.11
D	11.21	1.13
E	10.68	1.04
F	11.38	1.17
G	10.77	1.06
Average	11.11	1.12
Standard Deviation	0.272	0.048

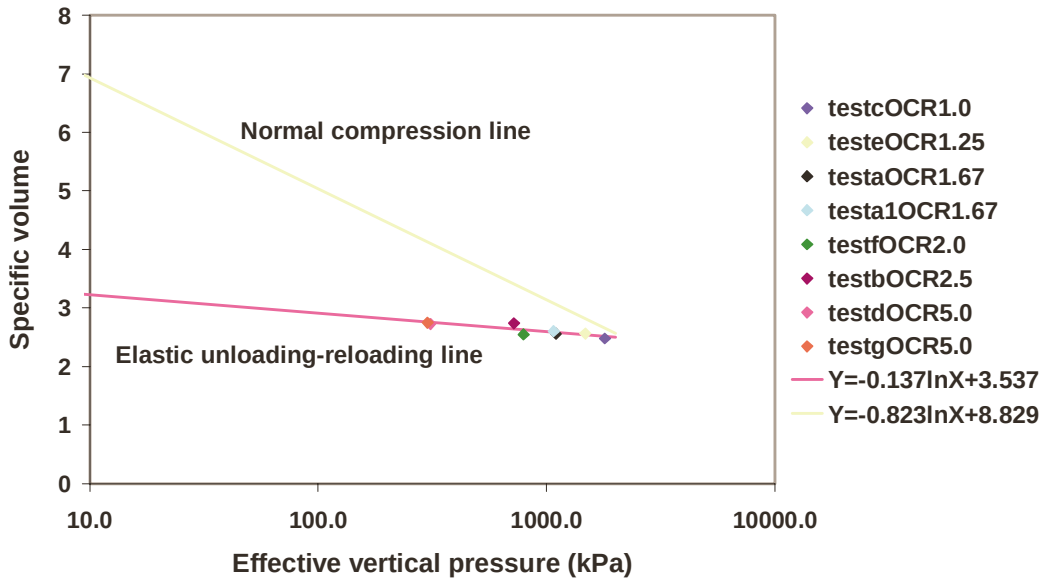

Figure 4.9. Normal compression line and elastic unloading reloading line for final bagasse, 4-12-98 tests.

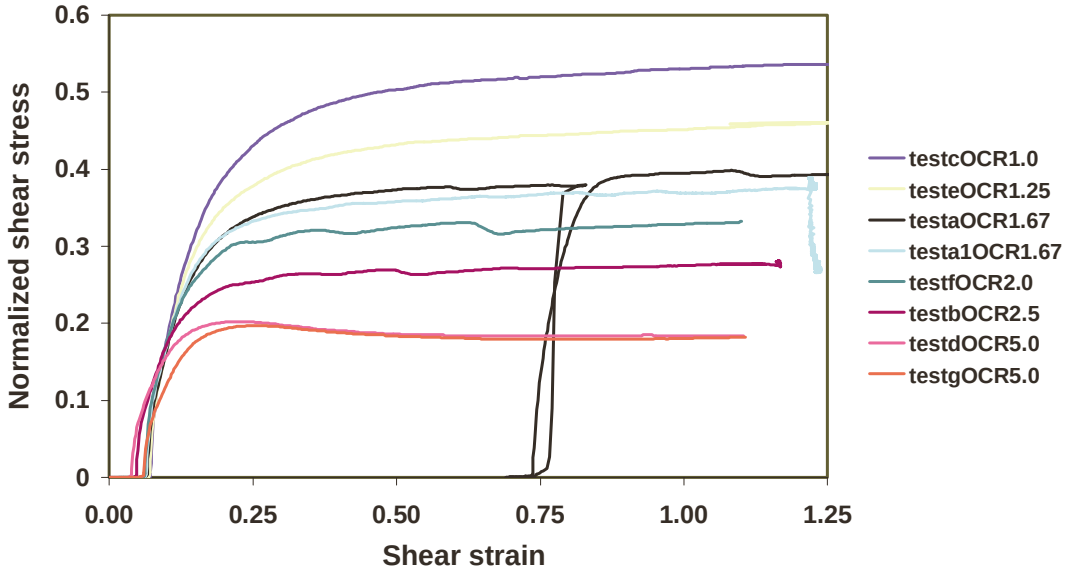

Figure 4.10. Normalized shear stress versus shear strain plot for final bagasse, 4-12-98 tests.

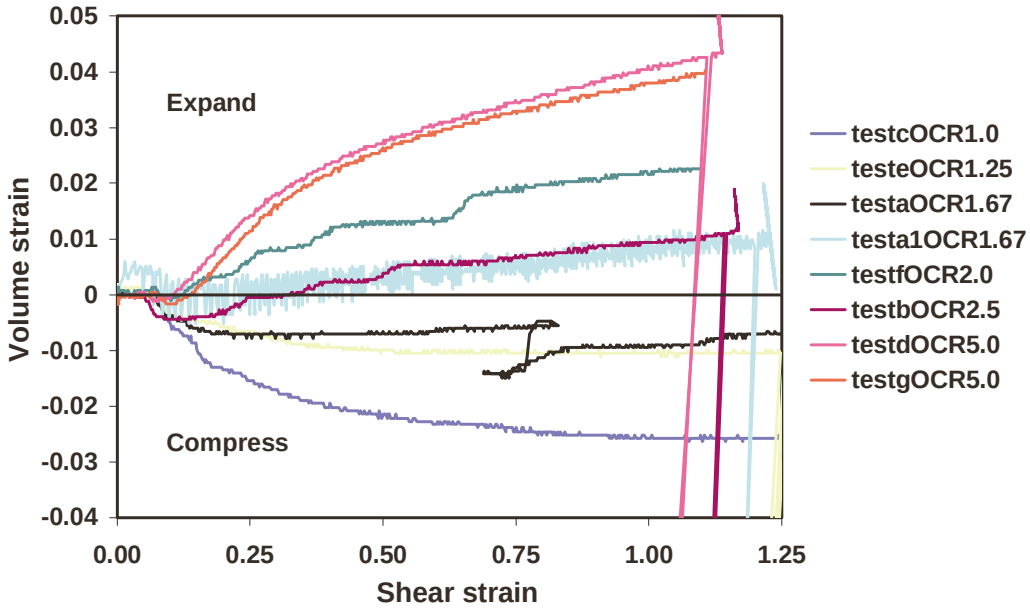

Figure 4.11. Volumetric strain versus shear strain plot for final bagasse, 4-12-98 tests.

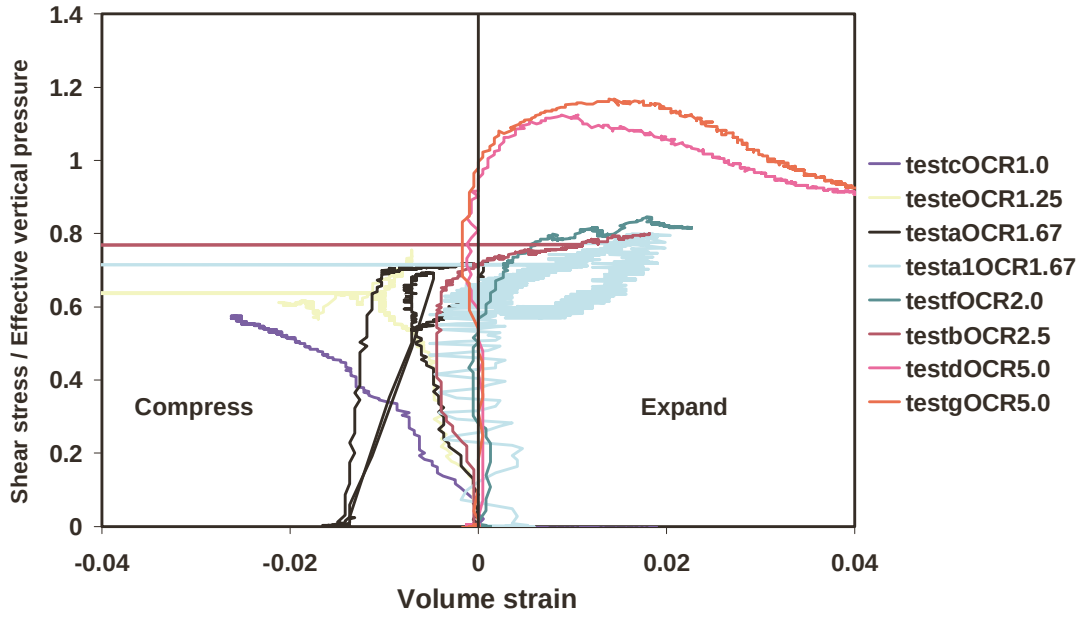

Figure 4.12. Plot of shear stress / effective vertical pressure versus volumetric strain to estimate M for final bagasse, 4-12-98 tests.

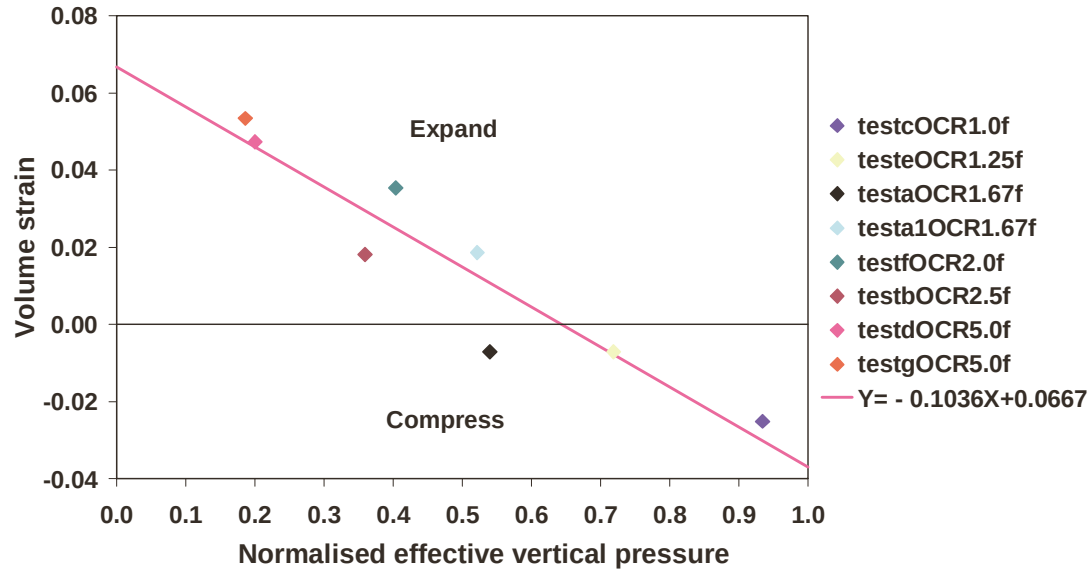

Figure 4.13. Plot of volumetric strain versus normalised effective vertical pressure to estimate the no volume change over-consolidation ratio for final bagasse, 4-12-98 tests.

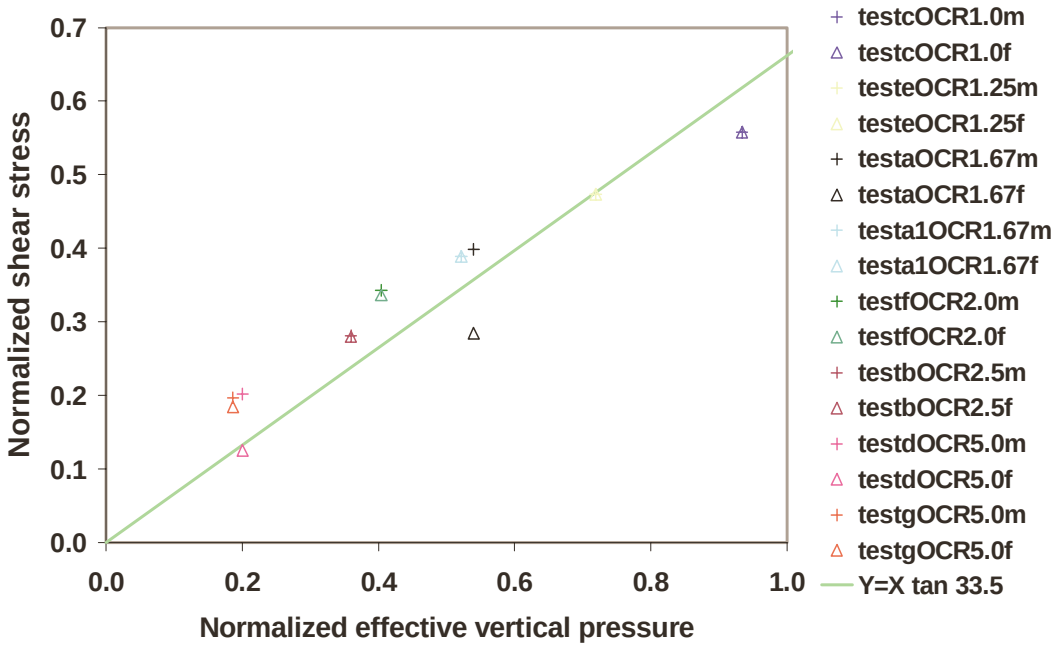

Figure 4.14. Plot of normalised shear stress versus normalised effective vertical pressure to estimate the equivalent critical state friction line and M for final bagasse, 4-12-98 tests.

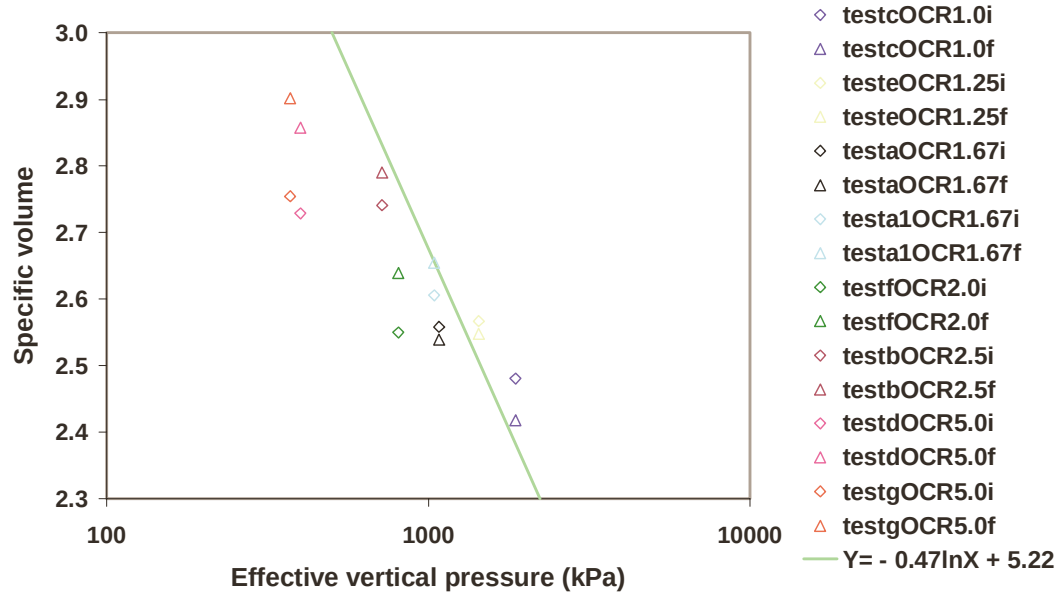

Figure 4.15. Plot of specific volume versus effective vertical pressure to estimate the critical state line for final bagasse, 4-12-98 tests.

Table 4.3 Normal compression line values for first bagasse, 3-12-98 tests

Test	υ_λ	λ
1	12.10	1.26
2	12.38	1.30
3	11.87	1.19
3A	11.88	1.22
4	12.07	1.24
5	11.97	1.24
6	11.77	1.19
Average	12.01	1.23
Standard Deviation	0.20	0.039

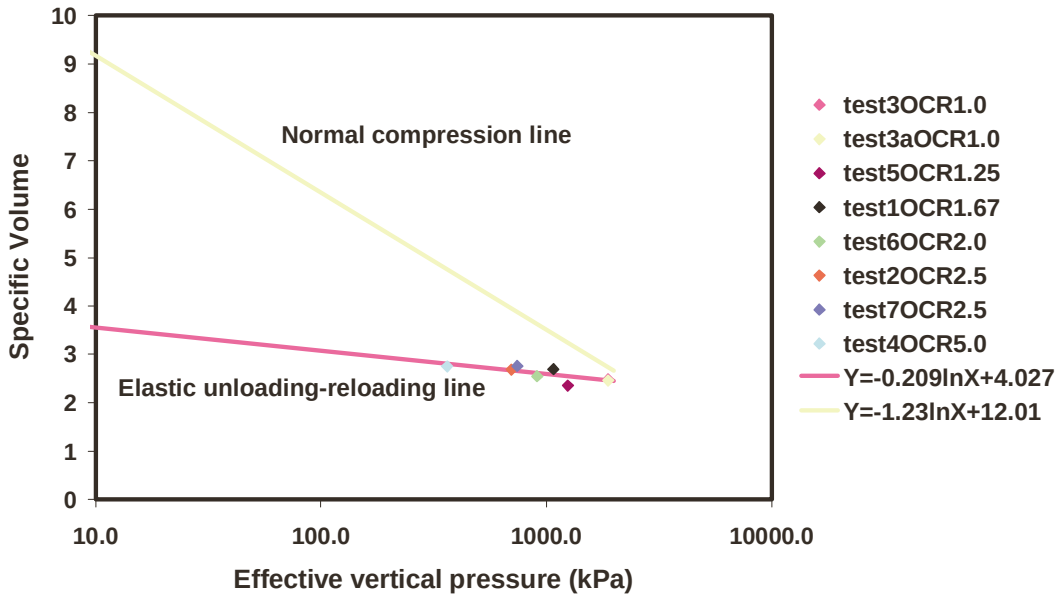

Figure 4.16. Normal compression line and elastic unloading-reloading line for first bagasse, 3-12-98 tests.

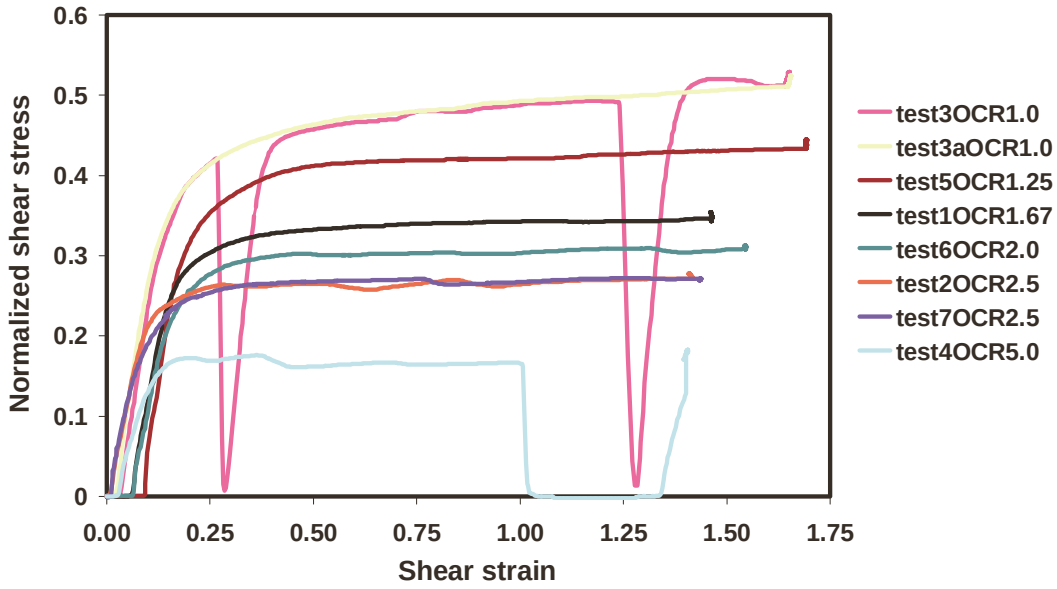

Figure 4.17. Normalised shear stress versus shear strain plot for first bagasse, 3-12-98 tests.

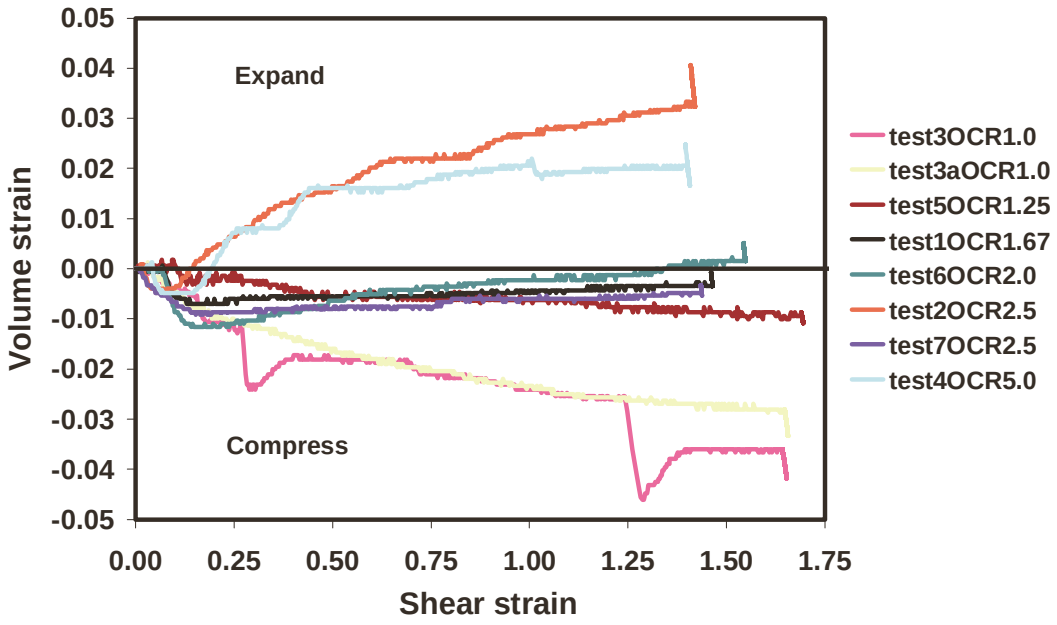

Figure 4.18. Volumetric strain versus shear strain plot for first bagasse, 3-12-98 tests.

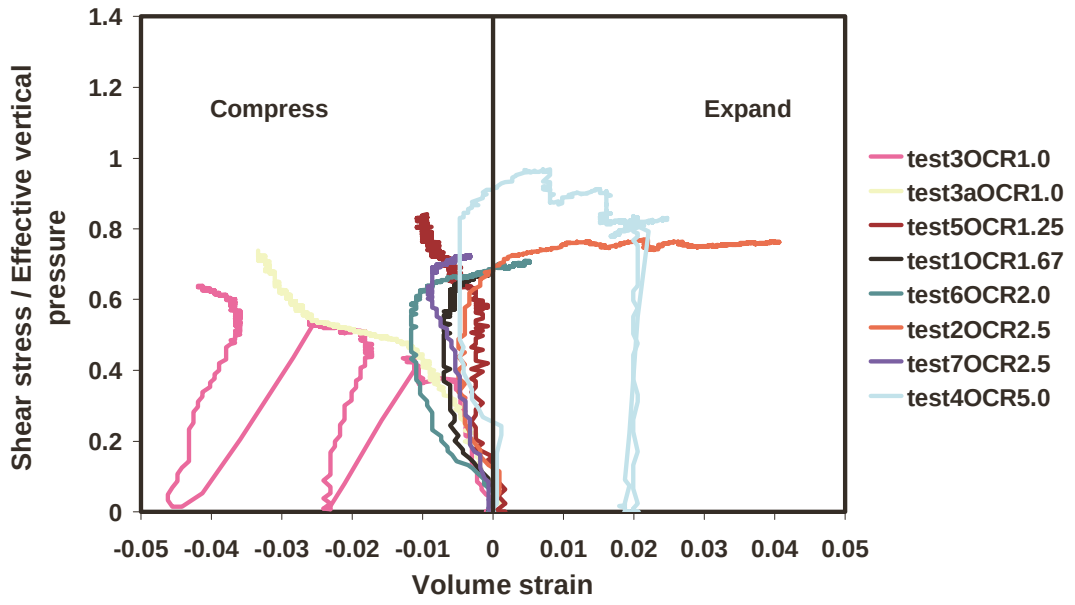

Figure 4.19. Plot of shear stress / effective vertical pressure versus volumetric strain to estimate M for first bagasse, 3-12-98 tests.

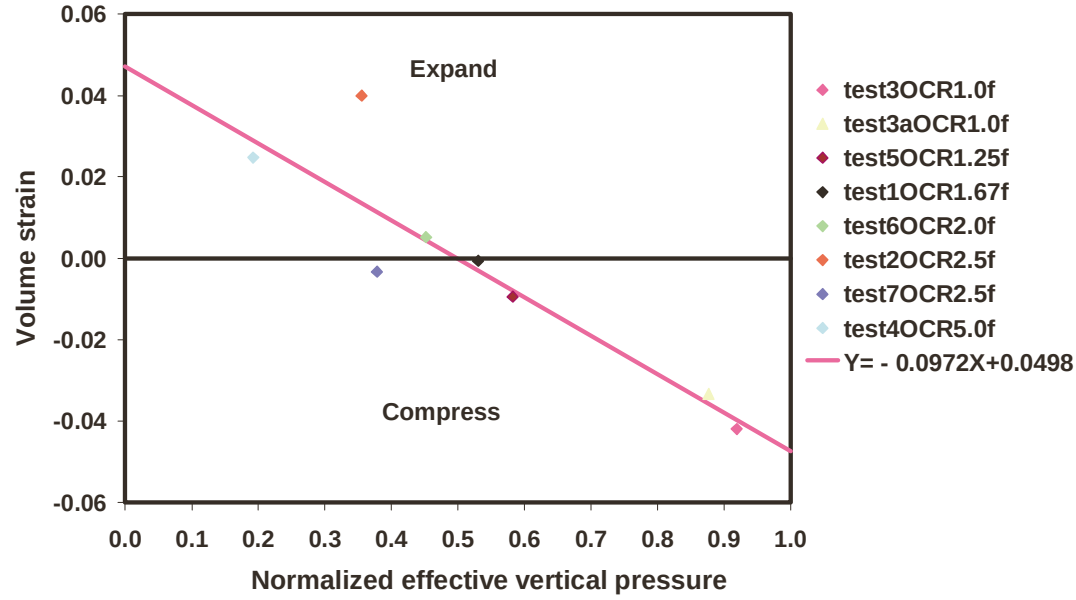

Figure 4.20. Plot of volumetric strain versus normalised effective vertical pressure to estimate the no volume change over-consolidation ratio for first bagasse, 3-12-98 tests.

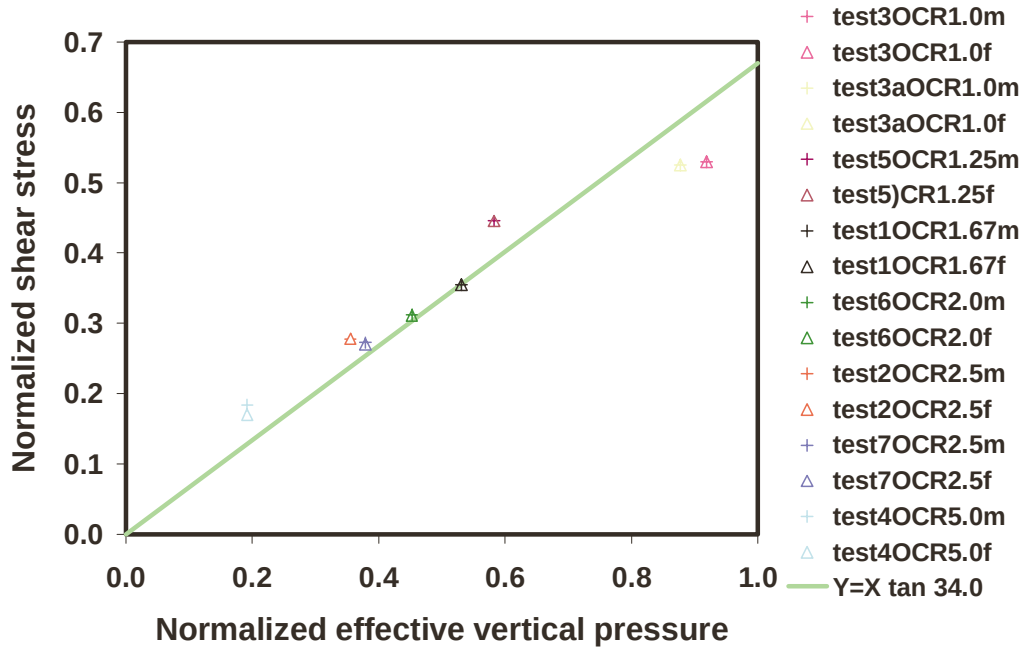

Figure 4.21. **Plot of normalised shear stress versus normalised effective vertical pressure to estimate the equivalent critical state friction line and M for first bagasse, 3-12-98 tests.**

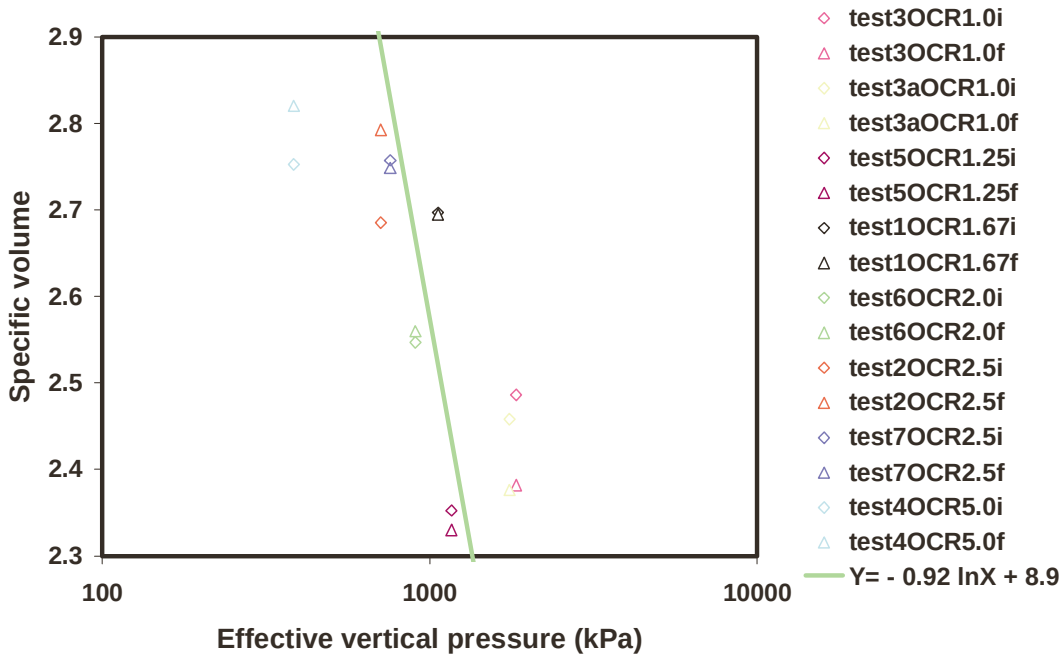

Figure 4.22. **Plot of specific volume versus effective vertical pressure to estimate the critical state line for first bagasse, 3-12-98 tests.**

Table 4.4 Normal compression line values for first bagasse, 5-12-98 tests

Test	υ_λ	λ
1	12.43	1.22
2	12.57	1.24
3	13.12	1.32
4	12.98	1.30
5	13.26	1.37
6	12.75	1.26
7	12.43	1.22
8	12.98	1.30
Average	12.82	1.28
Standard Deviation	0.32	0.053

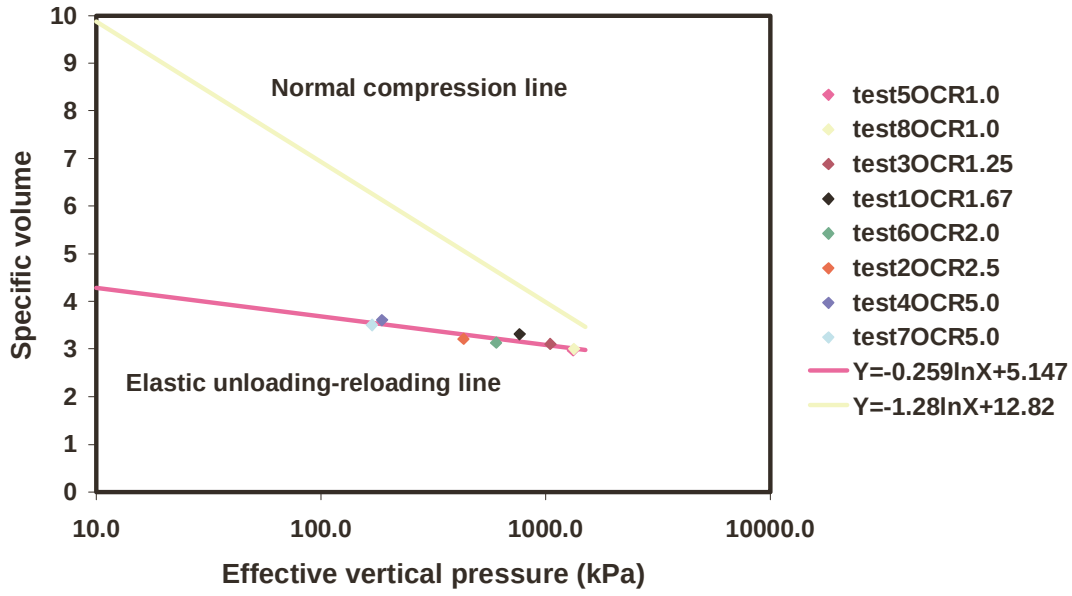

Figure 4.23. Normal compression line and elastic unloading-reloading line for first bagasse, 5-12-98 tests.

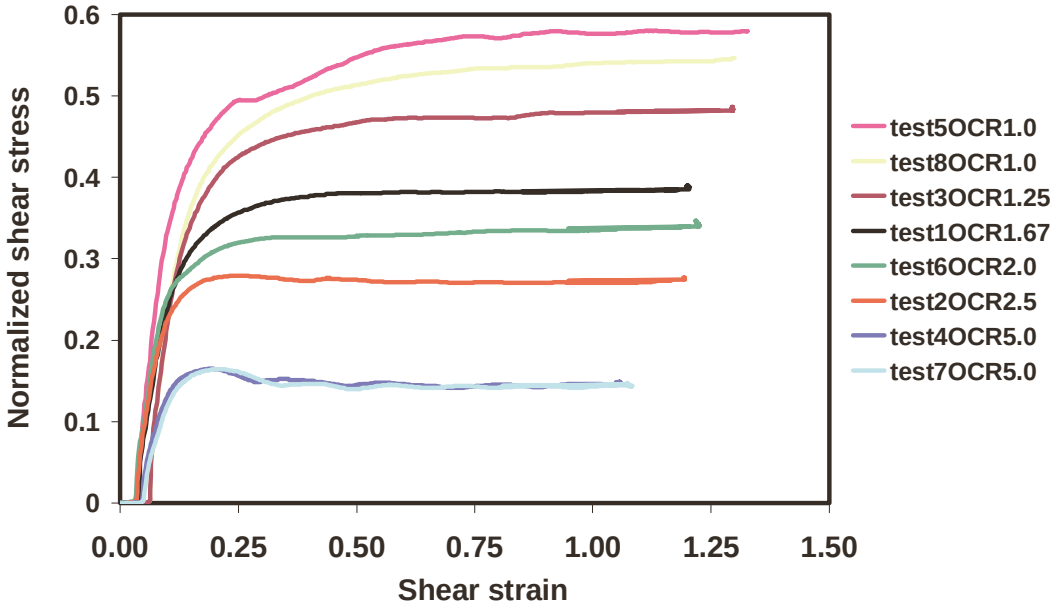

Figure 4.24. Normalised shear stress versus shear strain plot for first bagasse, 5-12-98 tests.

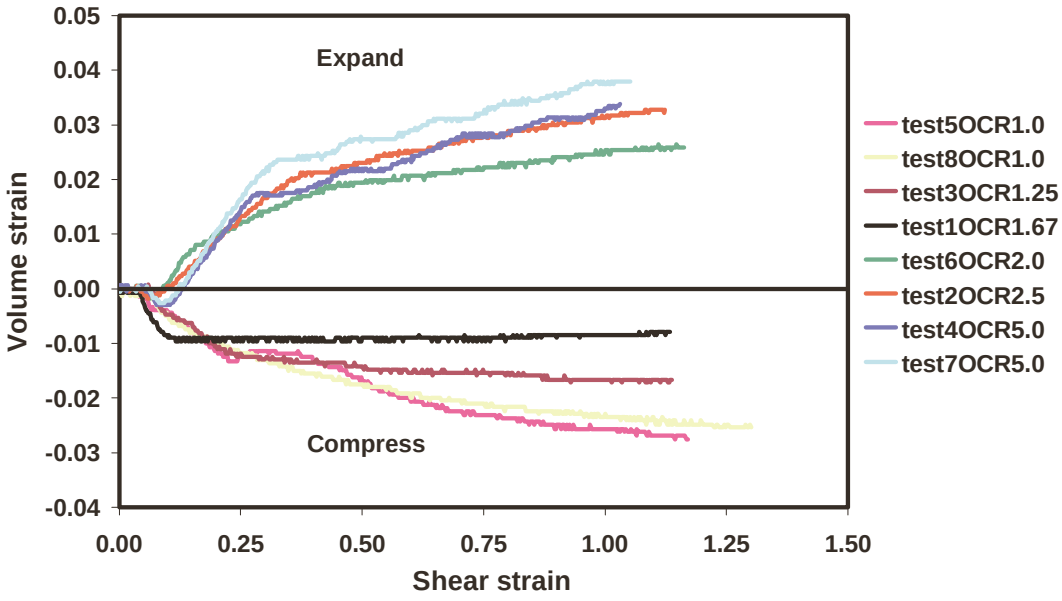

Figure 4.25. Volumetric strain versus shear strain plot for first bagasse, 5-12-98 tests.

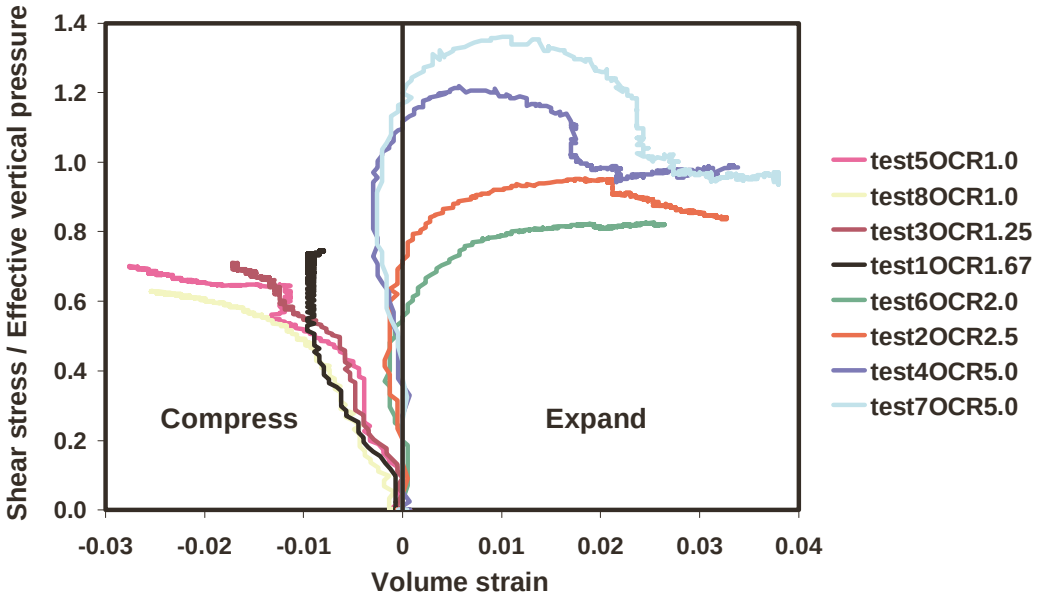

Figure 4.26. Plot of shear stress / effective vertical pressure versus volumetric strain to estimate M for first bagasse, 5-12-98 tests.

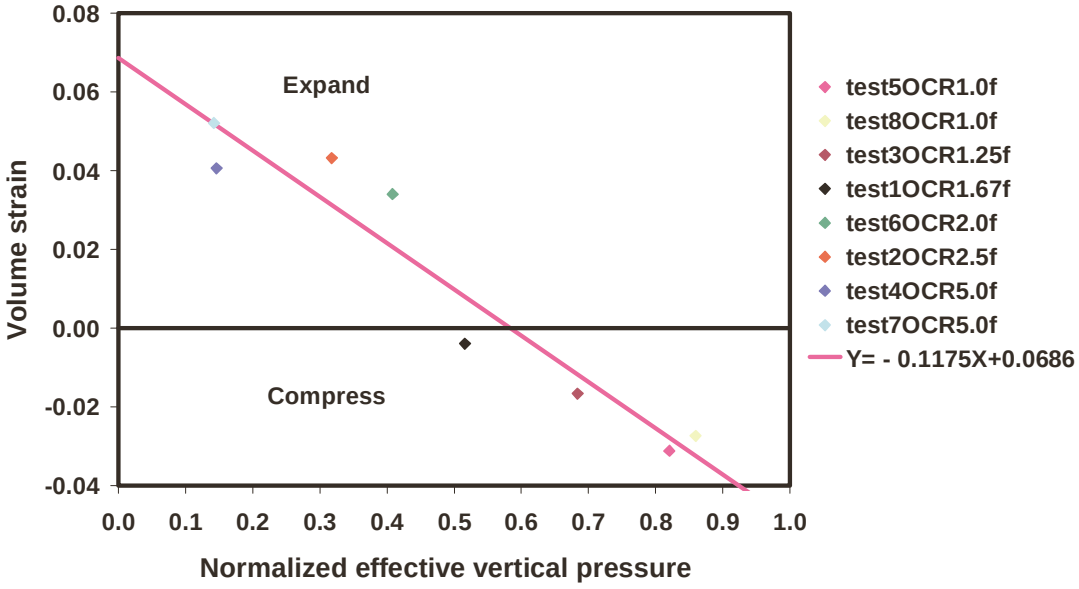

Figure 4.27. Plot of volumetric strain versus normalised effective vertical pressure to estimate the no volume change over-consolidation ratio for first bagasse, 5-12-98 tests.

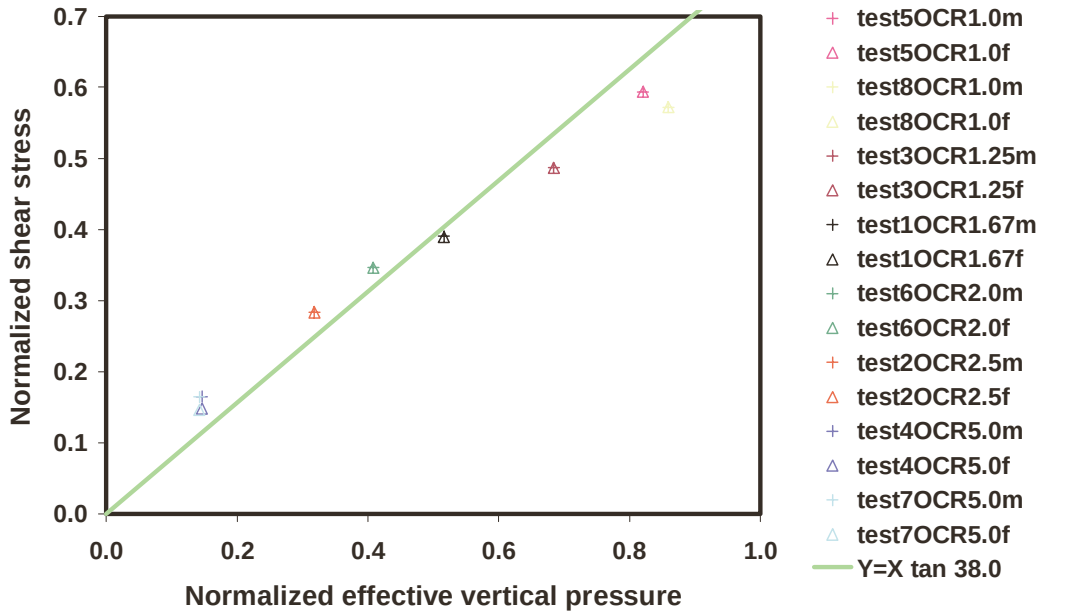

Figure 4.28. **Plot of normalised shear stress versus normalised effective vertical pressure to estimate the equivalent critical state friction line and M for first bagasse, 5-12-98 tests.**

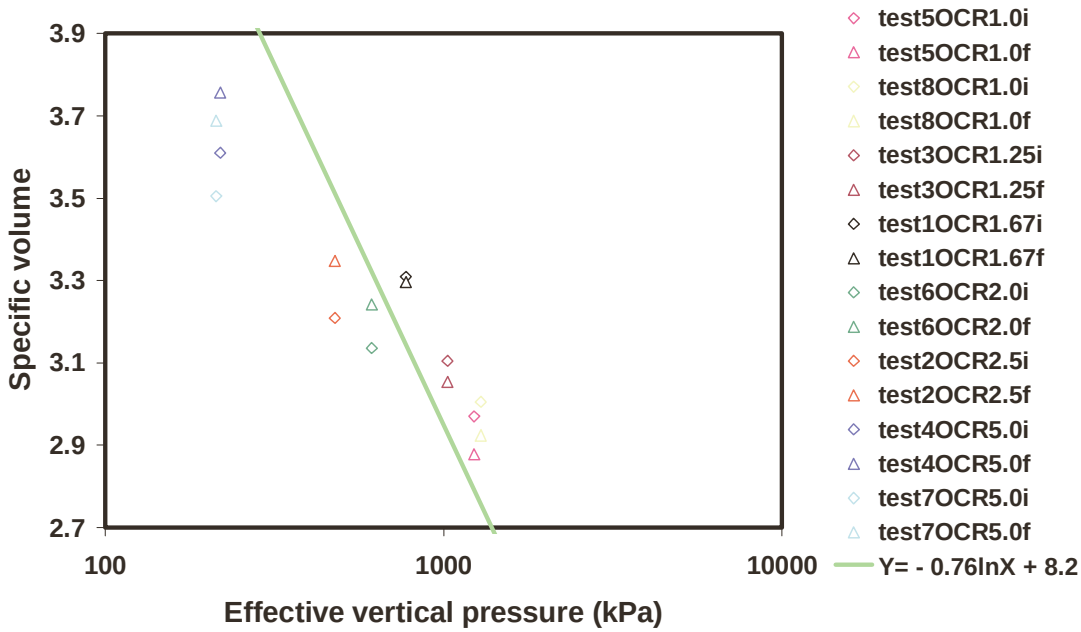

Figure 4.29. **Plot of specific volume versus effective vertical pressure to estimate the critical state line for first bagasse, 5-12-98 tests.**

Table 4.5 Normal compression line values for prepared cane, 7-12-98 tests

Test	υ_λ	λ
1	19.57	2.21
2	19.01	2.13
3	20.29	2.30
4	19.57	2.21
5	20.99	2.43
6	18.91	2.13
7	18.49	2.04
8	18.67	2.08
Average	19.44	2.19
Standard Deviation	0.86	0.13

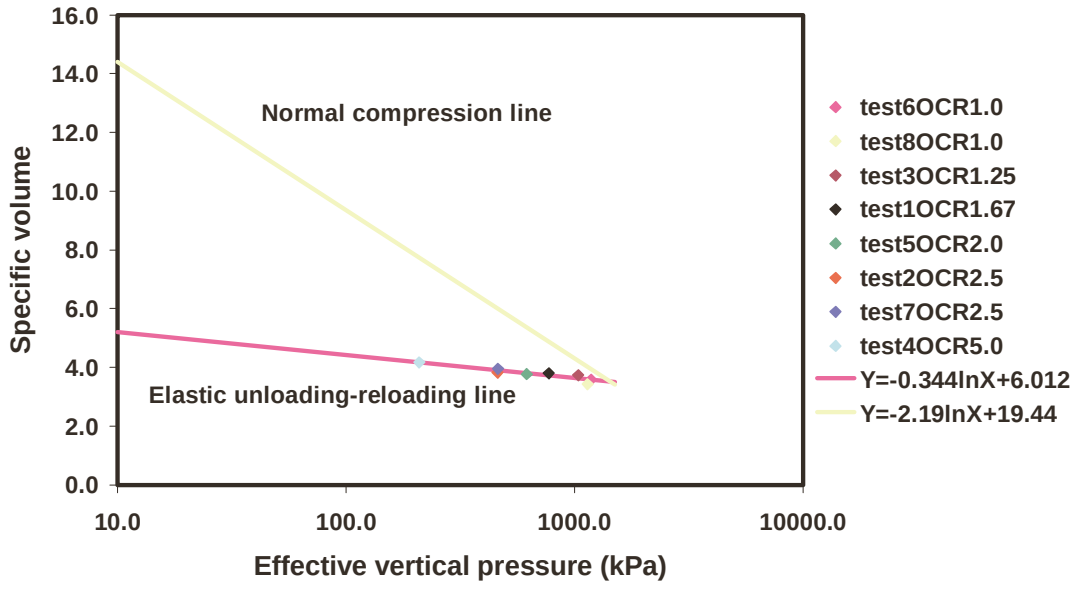

Figure 4.30. Normal compression line and elastic unloading-reloading line for prepared cane, 7-12-98 tests.

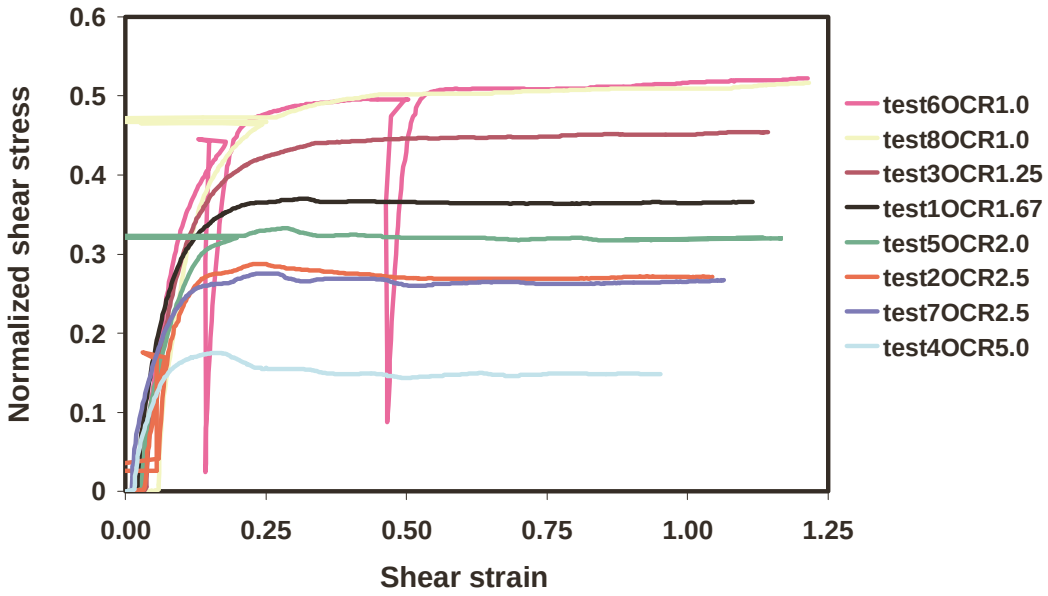

Figure 4.31. Normalised shear stress versus shear strain plot for prepared cane, 7-12-98 tests.

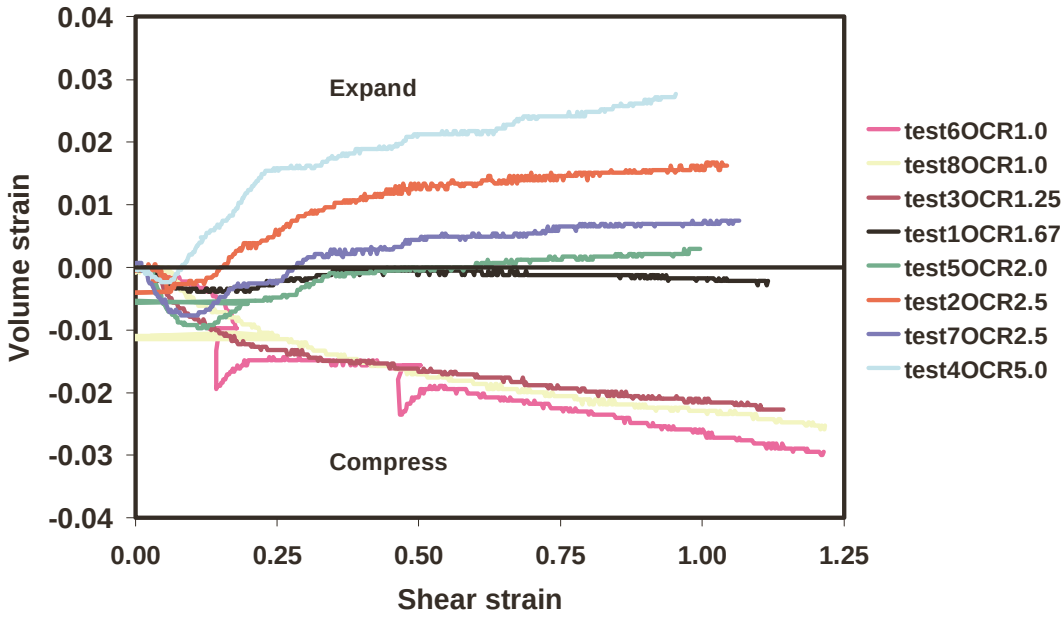

Figure 4.32. Volumetric strain versus shear strain plot for prepared cane, 7-12-98 tests.

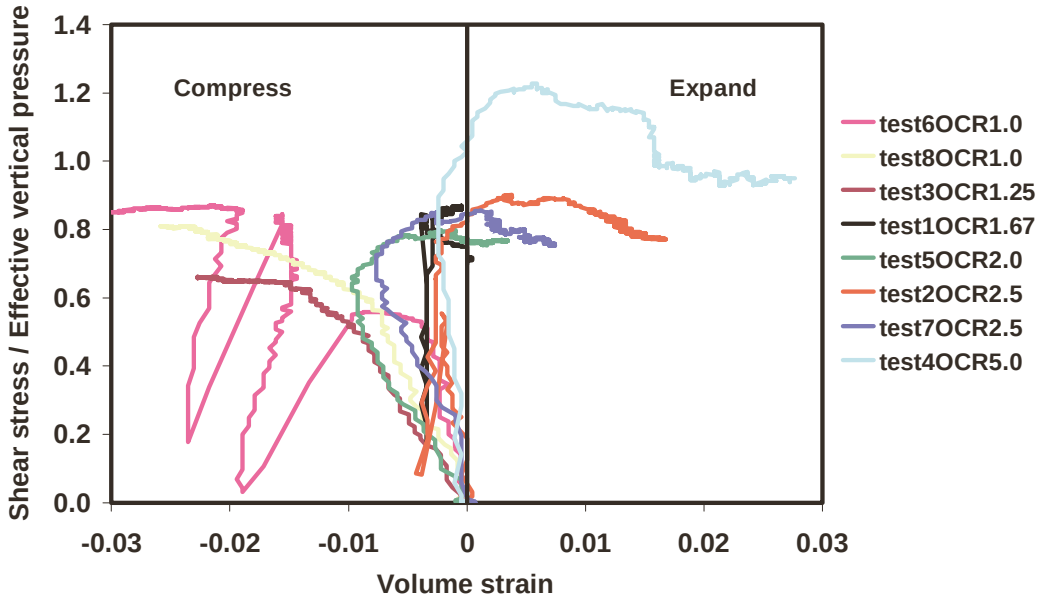

Figure 4.33. Plot of shear stress / effective vertical pressure versus volumetric strain to estimate M for prepared cane, 7-12-98 tests.

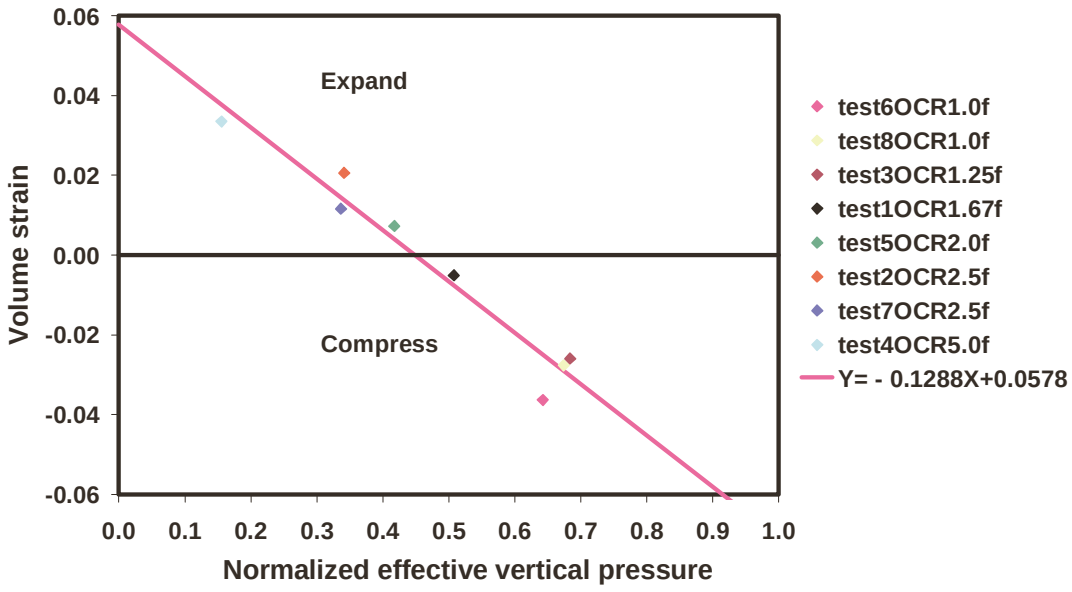

Figure 4.34. Plot of volumetric strain versus normalised effective vertical pressure to estimate the no volume change over-consolidation ratio for prepared cane, 7-12-98 tests.

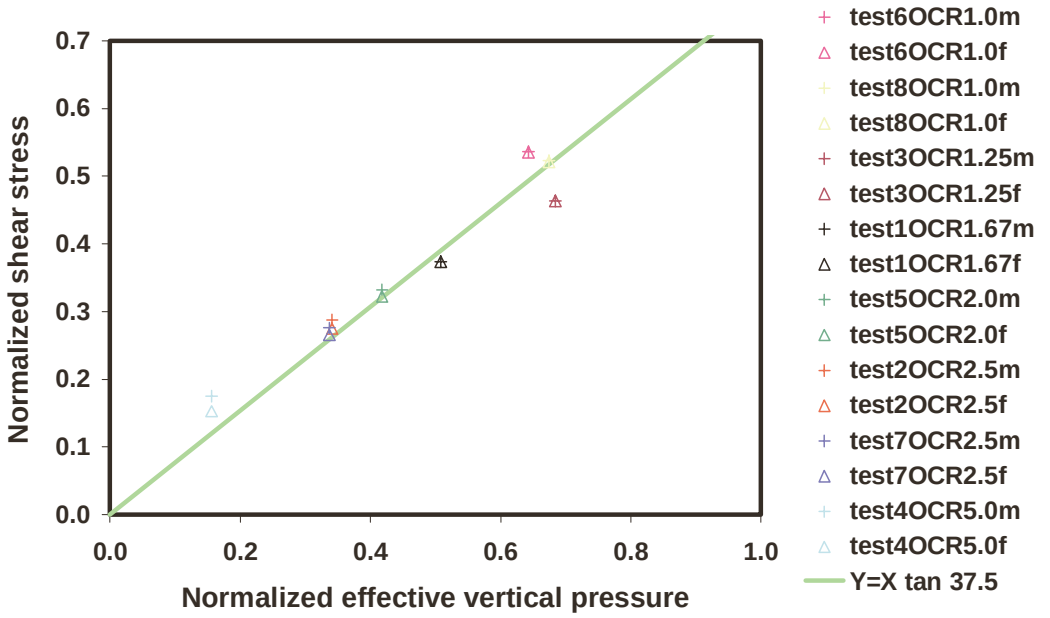

Figure 4.35. Plot of normalised shear stress versus normalised effective vertical pressure to estimate the equivalent critical state friction line and M for prepared cane, 7-12-98 tests.

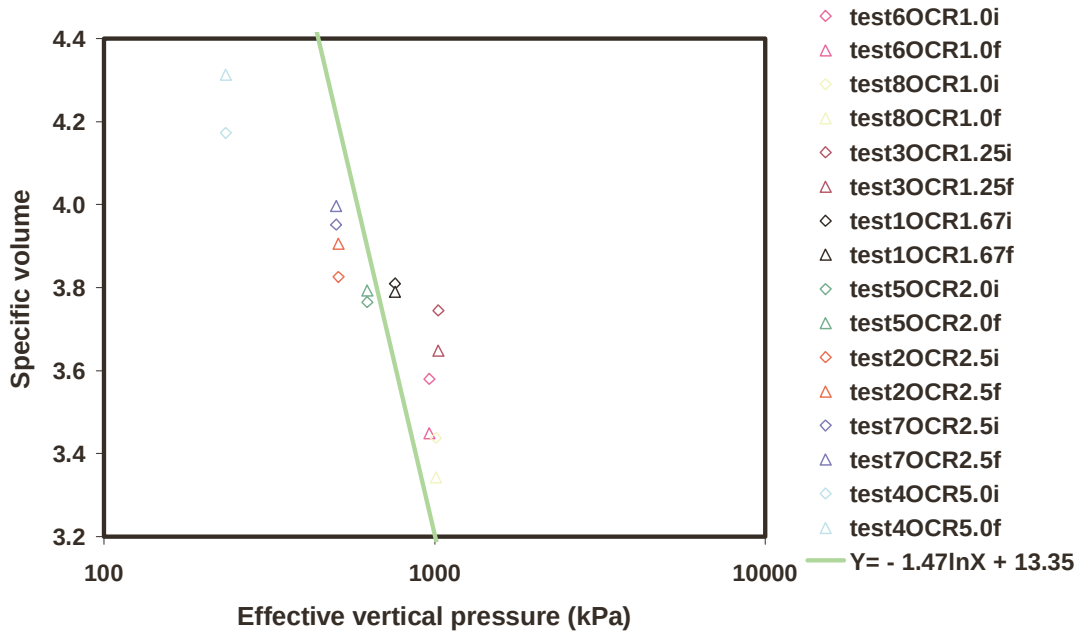

Figure 4.36. Plot of specific volume versus effective vertical pressure to estimate the critical state line for prepared cane, 7-12-98 tests.

Table 4.6 Normal compression line values for prepared cane, 8-12-98 tests

Test	υ_λ	λ
A	18.69	2.04
B	17.69	1.91
C	20.61	2.26
D	16.70	1.78
E	17.89	1.91
F	16.70	1.78
G	16.90	1.78
H	17.89	1.91
Average	17.88	1.92
Standard Deviation	1.30	0.16

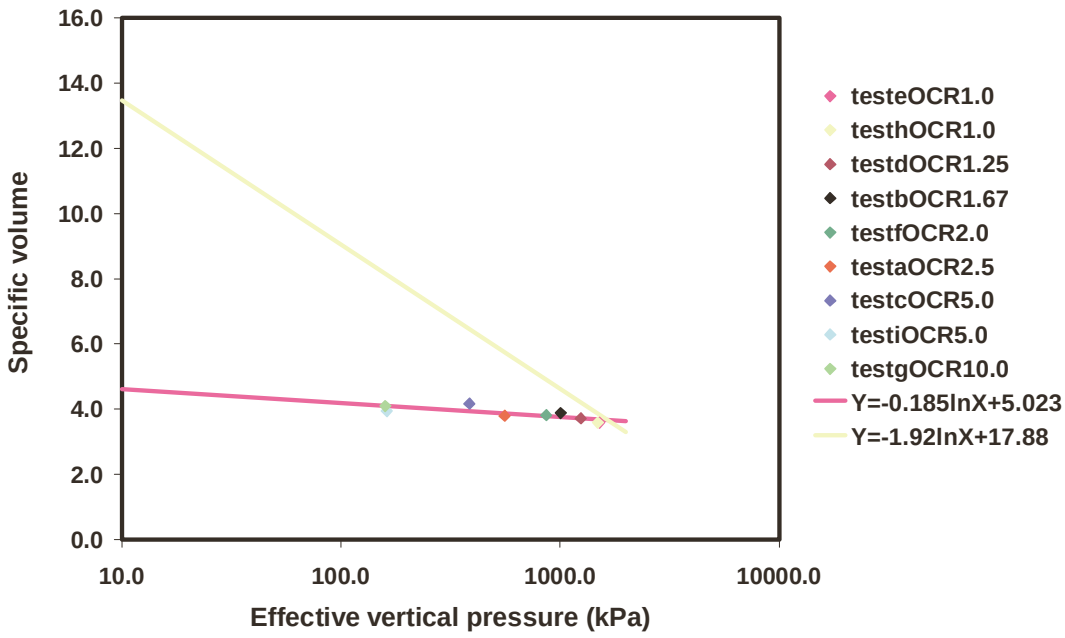

Figure 4.37. Normal compression line and elastic unloading-reloading line for prepared cane, 8-12-98 tests.

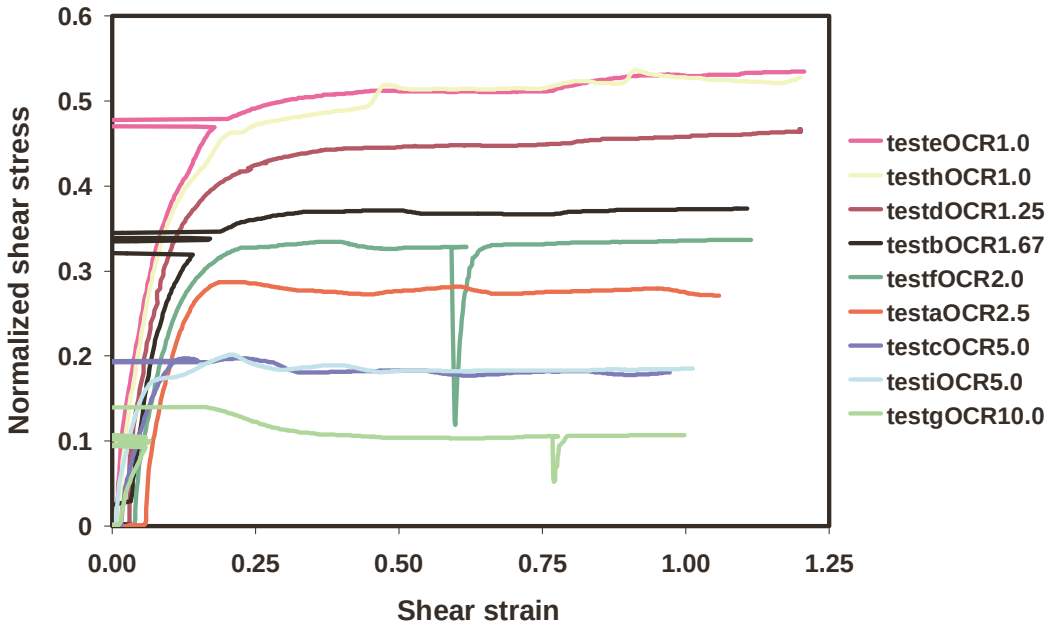

Figure 4.38. Normalised shear stress versus shear strain plot for prepared cane, 8-12-98 tests.

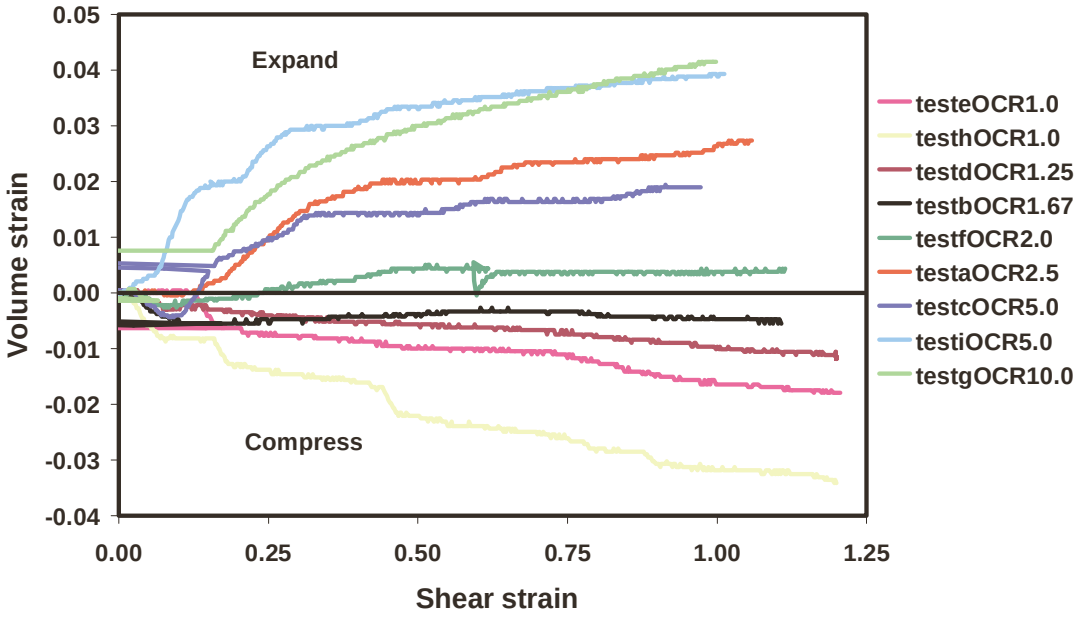

Figure 4.39. Volumetric strain versus shear strain plot for prepared cane, 8-12-98 tests.

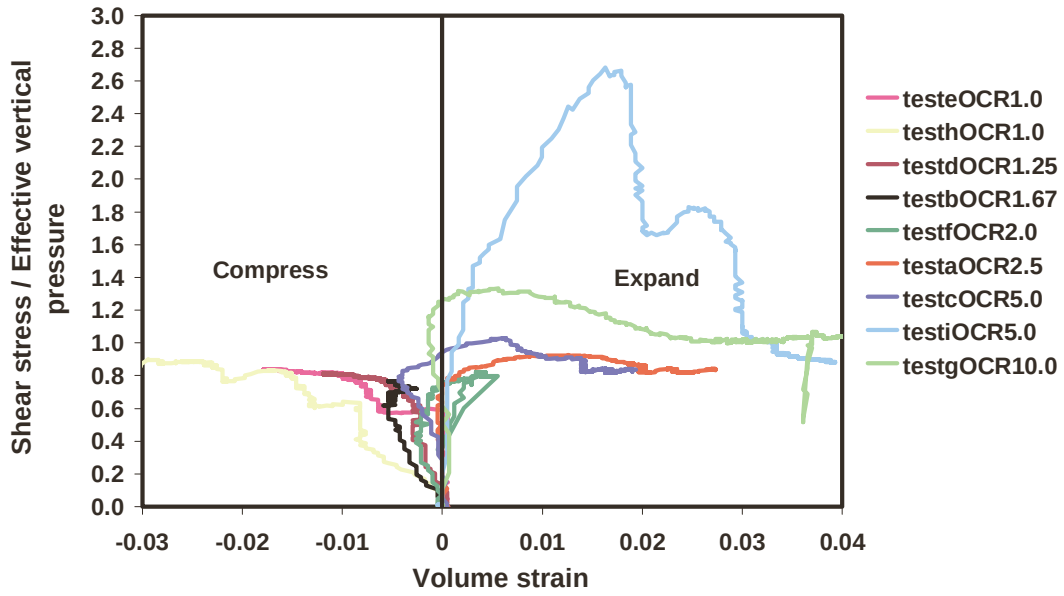

Figure 4.40. Plot of shear stress / effective vertical pressure versus volumetric strain to estimate M for prepared cane, 8-12-98 tests.

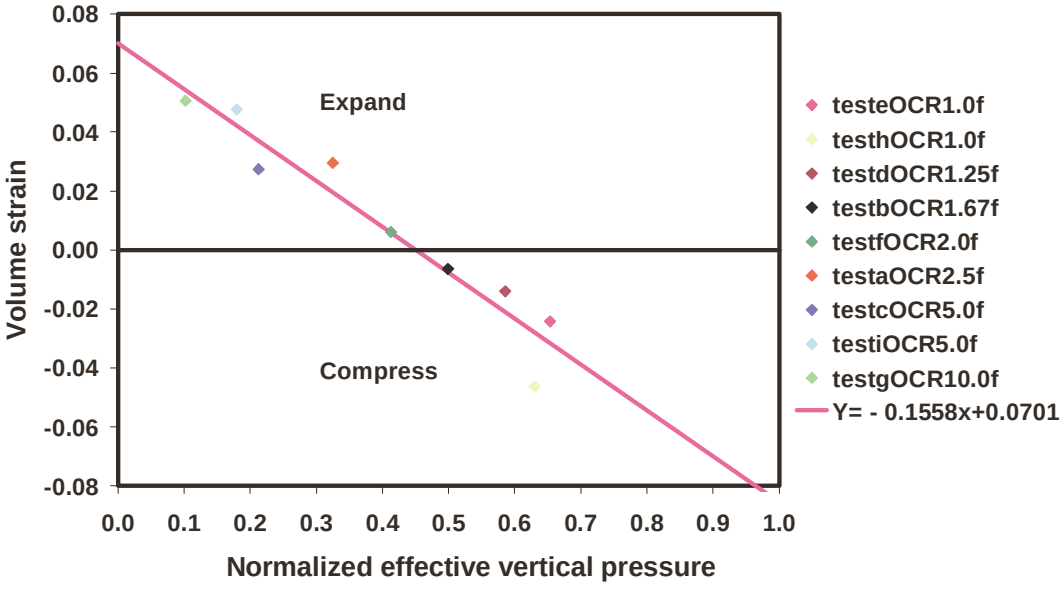

Figure 4.41. Plot of volumetric strain versus normalised effective vertical pressure to estimate the no volume change over-consolidation ratio for prepared cane, 8-12-98 tests.

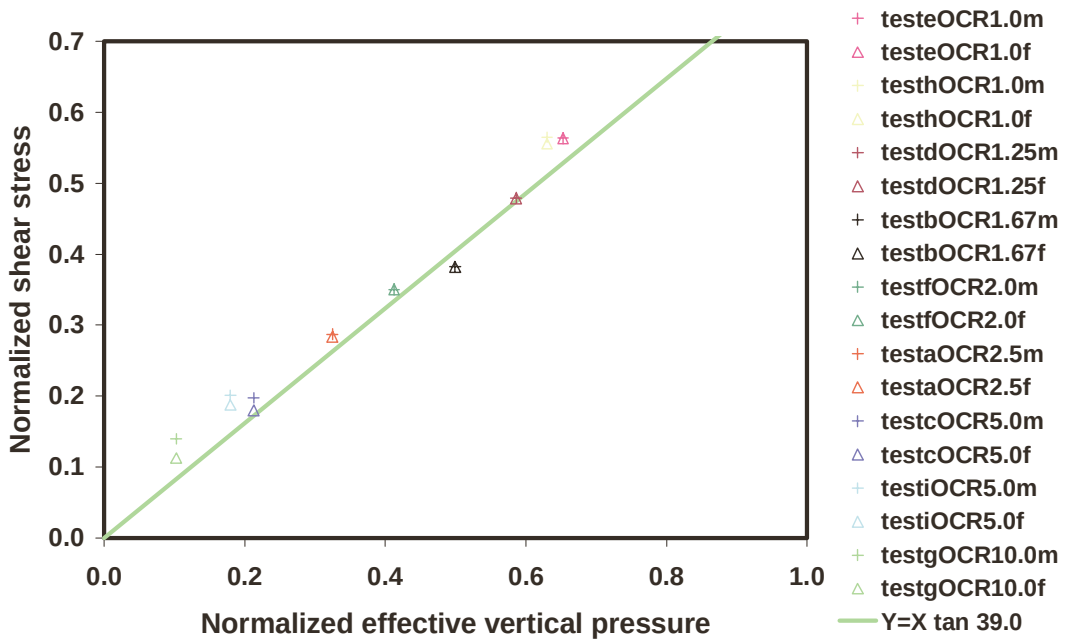

Figure 4.42. Plot of normalised shear stress versus normalised effective vertical pressure to estimate the equivalent critical state friction line and M for prepared cane, 8-12-98 tests.

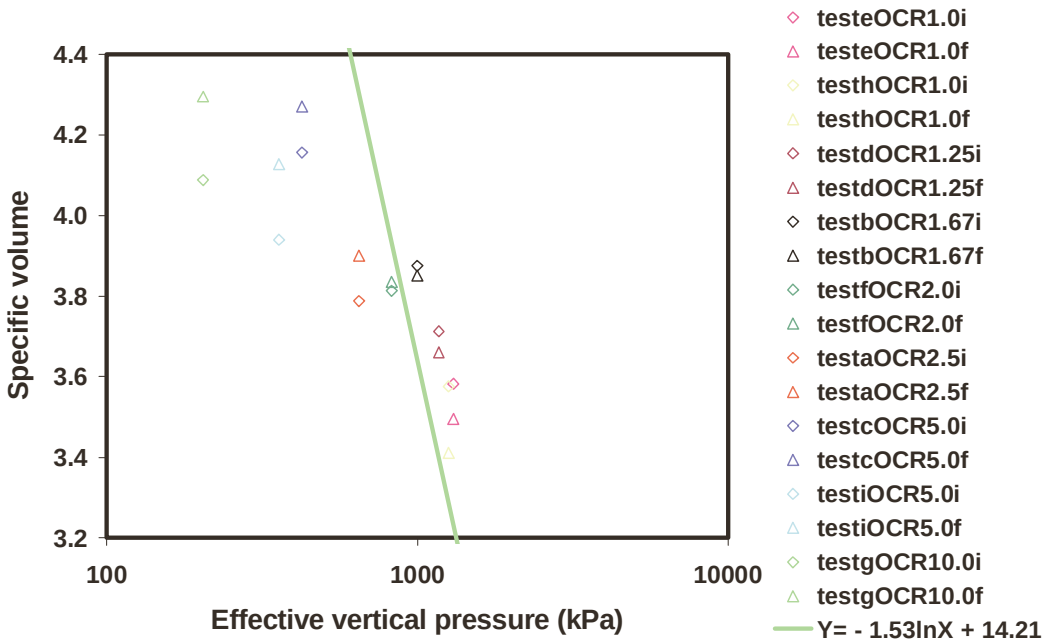

Figure 4.43. Plot of specific volume versus effective vertical pressure to estimate the critical state line for prepared cane, 8-12-98 tests.

Table 4.7 Summary of determined material parameters

		Prepared cane		First Bagasse		Final bagasse
Date of tests		7-12-98	8-12-98	5-12-98	3-12-98	4-12-98
Nominal maximum vertical pressure (kPa)		1500	2000	1500	2000	2000
Normal compression line $\upsilon=\upsilon_\lambda + \lambda \ln P'$	υ_λ	19.44	17.88	12.82	12.01	11.11
	λ	2.19	1.92	1.28	1.23	1.12
Elastic loading-unloading line $\upsilon=\upsilon_\kappa + \kappa \ln P'$	υ_κ	6.012	5.023	5.147	4.027	3.537
	κ	0.344	0.185	0.259	0.209	0.137
Equivalent critical state line $\upsilon=\Gamma + \lambda_{cs} \ln P'$	Γ	13.35	14.21	8.2	8.9	5.92
	λ_{cs}	1.47	1.53	0.76	0.92	0.47
Equivalent critical state friction angle ϕ_{cs}		37.5	39.0	38.0	34.0	33.5
Approximation of $M \approx 2 \sin \phi_{cs}$		1.22	1.26	1.23	1.12	1.10
Shear stress / effective vertical pressure ratio at which there is no volume change		0.83	0.89	0.75	0.71	0.72
Equivalent critical state friction angle $\phi_{cs} = \tan^{-1}$(shear stress/effective vertical pressure)		39.7	41.7	36.9	35.4	33.5
Approximation of $M \approx 2 \sin \phi_{cs}$		1.28	1.33	1.20	1.16	1.17

Table 4.7 (cont.) Summary of determined material parameters

	Prepared cane		First Bagasse		Final bagasse
Date of tests	7-12-98	8-12-98	5-12-98	3-12-98	4-12-98
Nominal maximum vertical pressure (kPa)	1500	2000	1500	2000	2000
Normalised effective vertical pressure at which no volume change occurs	0.45	0.45	0.58	0.51	0.64
Over-consolidation ratio at which no volume change occurs (inverse of above)	2.22	2.22	1.72	1.96	1.56
Normalised total vertical pressure at which no volume change occurs	0.54	0.61	0.65	0.57	0.69
Over-consolidation ratio at which no volume change occurs (inverse of above)	1.85	1.64	1.54	1.75	1.45
Maximum shear stress for no over-consolidation test (kPa)	795	1119	875	1055	1115
Effective vertical pressure at maximum shear stress for no over-consolidation test (kPa)	1012	1250	1165	1540	1820
“Coefficient of friction” for no over-consolidation test	0.79	0.89	0.75	0.69	0.61

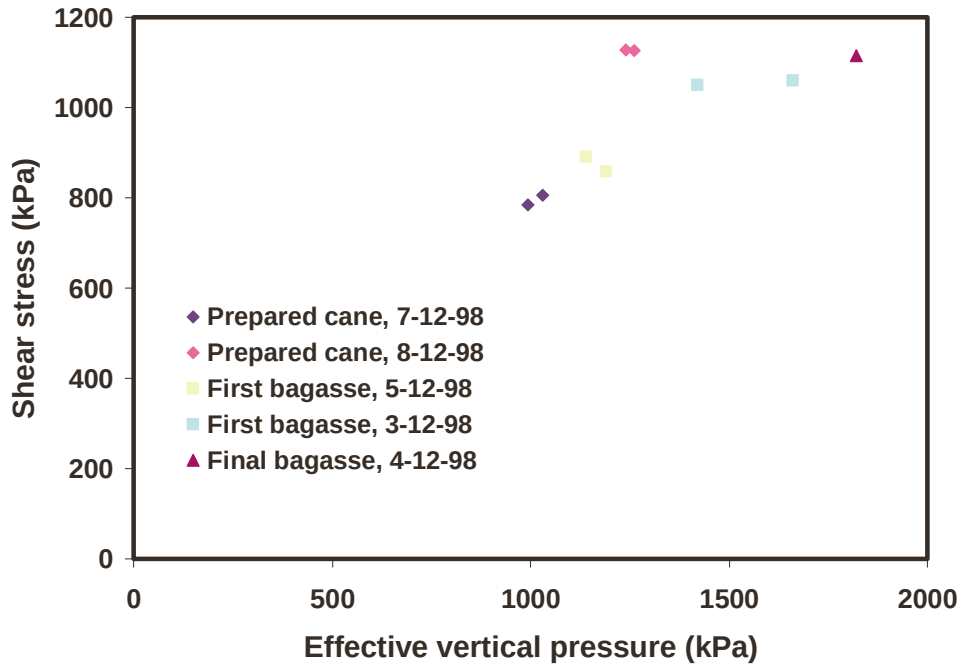

Figure 4.44. Maximum shear stress versus effective vertical pressure (Coulomb plot) for tests at an over-consolidation ratio of 1.0 for prepared cane, first bagasse and final bagasse.

4.5 Summary of Chapter 4

A test method and procedure based on the direct shear test used for testing soils, but specially modified to cope with the low stiffness and high moisture content of prepared cane, first bagasse, and final bagasse, has been successfully applied to estimate the critical state parameters of these materials at pressure feeder compactions (densities). The analysis shows that prepared cane, first bagasse and final bagasse behave in the same manner as soil (sand, clay) in combined compression and shear loading, despite their much higher moisture content and lower stiffness. This leads to the conclusion that the vast amount of well proven widely used theory developed for soils may be applicable (with modifications) to prepared cane, first bagasse, and final bagasse.

For the range of pressures tested, it is much easier to achieve low juice pressures for first bagasse then for prepared cane, and it is easier to achieve low juice pressures

for final bagasse than for first bagasse. That is, it is much easier to work out the behaviour of the solid skeleton of final bagasse than of prepared cane. This is interesting and useful because historically most tests have been carried out on prepared cane, which is the hardest material to test. The quality of the measured data of the mechanical behaviour of final bagasse is better than the data for prepared cane and first bagasse. Mainly for this reason, the modelling carried out in the following chapters focuses on comparisons between measured and predicted behaviour for final bagasse, while also carrying out checks for consistency using first bagasse data.

It is noted that the tests carried out have not determined the effect of loading direction and fibre alignment, broadly termed as anisotropy. It would be useful to carry out such tests in order to determine the similarities and differences between soil and bagasse, particularly for modelling purposes. Direct shear tests with the sample rotated 90 degrees have the potential to measure the anisotropy effects, as do the tests on peat that have been noted in the literature searches in Chapter 2 (such as the biaxial and undrained triaxial tests). The fibres could be deliberately aligned either parallel or perpendicular to the direction of shearing. However, all the above tests were judged to be beyond the scope of this investigation since additional equipment was required and was not available.

The analysis of the results has produced many parameters to be used for building a material model. The direct shear test method, because it does not measure the full state of stress in a test sample, provides an estimate only of the actual behaviour. What this means is that some of the measured parameters may not be accurate and/or may need adjustment/interpretation. Some parameters are well defined, such as the critical state equivalent friction angle. Some have a number of questions/deficiencies that need to be addressed, such as the critical state line slope in the pressure volume plane.

The next step was to adopt the determined material parameters and to attempt to reproduce the measured direct shear test behaviour using existing computer models, in order to progress towards a material model that can reproduce bagasse behaviour adequately.

5 Chapter 5 – Modelling the compression, shear and volume behaviour of bagasse

5.1 Introduction

This chapter considers two existing material models that have been previously used for mill modelling purposes, the Modified Cam Clay (MCC) model and the Drucker-Prager Cap (DPC) model. Initially, a single element Modified Cam Clay material model is employed and its predictions are compared to the experimental measurements for final bagasse. The predictions for the single element model are verified against a multi-element Modified Cam Clay model, using the software package ABAQUS, to determine under what conditions a single element model is adequate. This is followed by the use of a parameter estimation package called PEST (Watermark Numerical Computing, 2000) in combination with the single element Modified Cam Clay model, and the results of a single direct shear test to determine which material parameters can be found from each loading step of a direct shear test. The limitations of a Modified Cam Clay model with respect to reproducing bagasse behaviour are identified. It is verified that the same limitations are present in the Drucker-Prager Cap model. Finally, the performance of the multi-element Modified Cam Clay and Drucker-Prager Cap models in reproducing bagasse behaviour is assessed.

5.2 Fitting predictions to experimental results using a single element Modified Cam Clay model

The single element Modified Cam Clay model employed here is that presented by Kirby (1994). Kirby (1994) described a variant on the modification proposed by Naylor (1985) of the basic Modified Cam Clay model (Britto and Gunn, 1987, Lewis and Schrefler, 1987). The modification is a continuous plasticity extension that provides a gradual transition from elastic to plastic behaviour. The model incorporates linear elasticity (a linear relationship when void ratio or specific volume is plotted against isotropic pressure or vertical pressure during unloading or reloading stress states). As shown in Chapter 4, over the range of pressures tested this relationship for bagasse is actually linear when specific volume is plotted against the natural log of isotropic pressure or vertical pressure (called porous elasticity). As will be shown later, adopting linear elasticity or porous elasticity

makes little difference to the predictions when using the measured value of M of about 1.1. If higher values of M are used (in the order of 2.5 or 3.8) then the predictions are quite different for linear elasticity and porous elasticity.

The predictions were compared against measurements for the loading conditions:

1. Compression along the normal compression line.
2. Compression when unloading along the unloading-reloading line.
3. Compression when reloading along the unloading-reloading line.
4. Shearing of a normally consolidated sample.
5. Shearing of a highly over-consolidated sample.

Two versions of the single element Modified Cam Clay model were used: one that modelled constrained uniaxial compression, and one that modelled simple shearing. It is noted that the assumption of near uniform strain conditions throughout the sample is made (refer to Kirby, 1994). For loading condition 5 non-uniform strains are expected to occur. Modelling and discussion of uniform stress and strain conditions is carried out in Chapter 6.

For loading conditions 1 to 4, Test C for final bagasse carried out on the 4-12-98 was adopted. For loading condition 5 Test G for final bagasse was adopted. These two tests were representative of those carried out (a similar exercise, not reported, was also carried out using two first bagasse tests to verify the conclusions). The single element Modified Cam Clay model requires the plasticity model parameters λ, κ, and M and the elastic parameters Young's Modulus (E) and Poisson's ratio (ν). The material parameters used for the predictions were a combination of one parameter (M) derived previously in Chapter 4 for the set of final bagasse tests, the parameter λ derived in Chapter 4 for the individual Tests C and G, parameter κ from individual loading-reloading lines for Test C and Test G (Figures B.1.20 and B.1.44 in Appendix B), and the parameters E and ν which are obtained below.

Young's Modulus E was calculated at approximately 1800 kPa vertical pressure by plotting the elastic reloading line for Test C (shown in Figure B.1.20 in Appendix B) in terms of vertical strain versus effective vertical pressure (see Figure 5.1) and calculating E as the slope of a line drawn for the pressure range 1500 kPa to 2000

kPa. A value of 76000 kPa was obtained. It is noted that, by choosing a different pressure range, a different value of E can be obtained that can easily be 50% different (because E is pressure dependent). It is noted that for materials such as steel, E is determined from a test unconstrained at the sides. For the direct shear tests on bagasse, the elastic unload and reload was carried out in a box and therefore there was zero lateral strain at the walls, that is, the test was constrained. This inconsistency is noted. However, since there is little sideways strain and stress when bagasse is compressed, the effect of the presence of the sidewalls on the vertical strain versus effective vertical pressure behaviour during unloading and reloading is likely to be minimal. That is, similar results would be obtained if the sidewalls were removed before reloading (carrying out this exercise would be worthwhile). It is also noted, and shown in Chapters 8 and 9, that the critical state models in one particular commercial package only require the input of κ and ν, and if required, E and G (the shear modulus) are calculated internally.

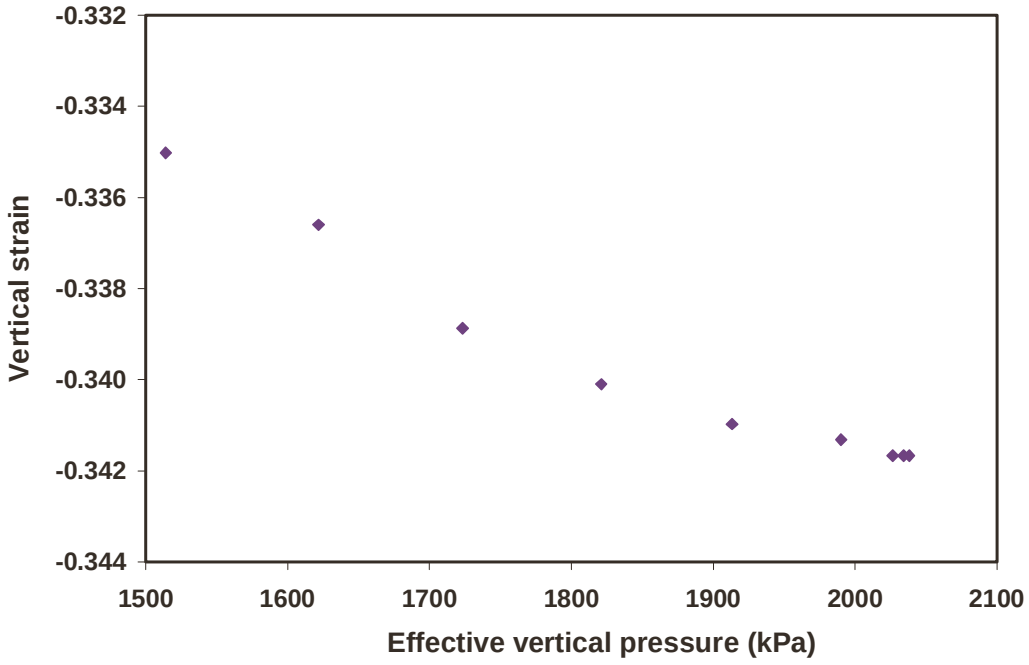

Figure 5.1 Vertical strain versus effective vertical pressure for final bagasse being reloaded in Test C.

In order to calculate Poisson's ratio, ν, the shear modulus G was calculated by dividing the change in shear stress by the change in shear strain during the shearing part of Test C (Figure B.1.23 in Appendix B). This plot is plotted in Figure 5.2 versus shear strain for the duration of the test. G is calculated from the initial tangent of the curve of shear stress versus shear strain (Popov, 1978; Potts et al., 1987) and is therefore the initial value in Figure 5.2. A value of 30000 kPa was adopted. It is noted that values of 20000 kPa and 40000 kPa could just as well have been chosen.

Poisson's ratio, ν, can then be calculated from the relationship $G=E/2(1 + \nu)$ (Jaeger, 1962). A value of 0.3 was obtained.

Similarly, for Test G, E was calculated at pressures close to 340 kPa by plotting the elastic reloading line (shown in Figure B.1.44 of Appendix B) in terms of vertical strain versus effective vertical pressure in Figure 5.3 (this time an unloading line was plotted) and calculating E as the slope of a line drawn for the pressure range 300 kPa to 450 kPa. A value of 12500 kPa was obtained.

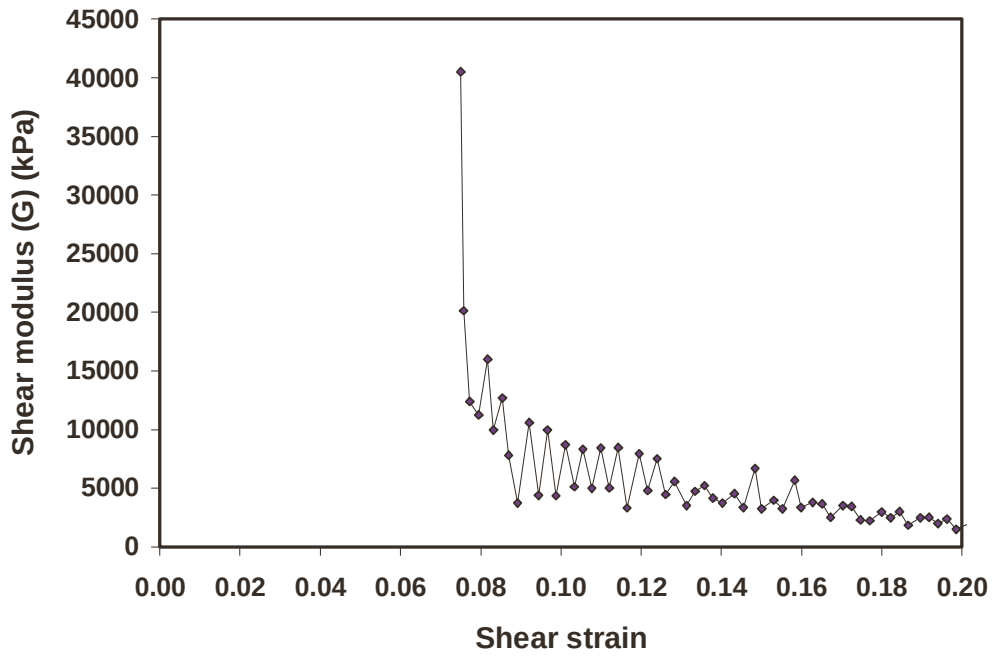

Figure 5.2. Shear modulus of normally consolidated final bagasse during shearing in Test C.

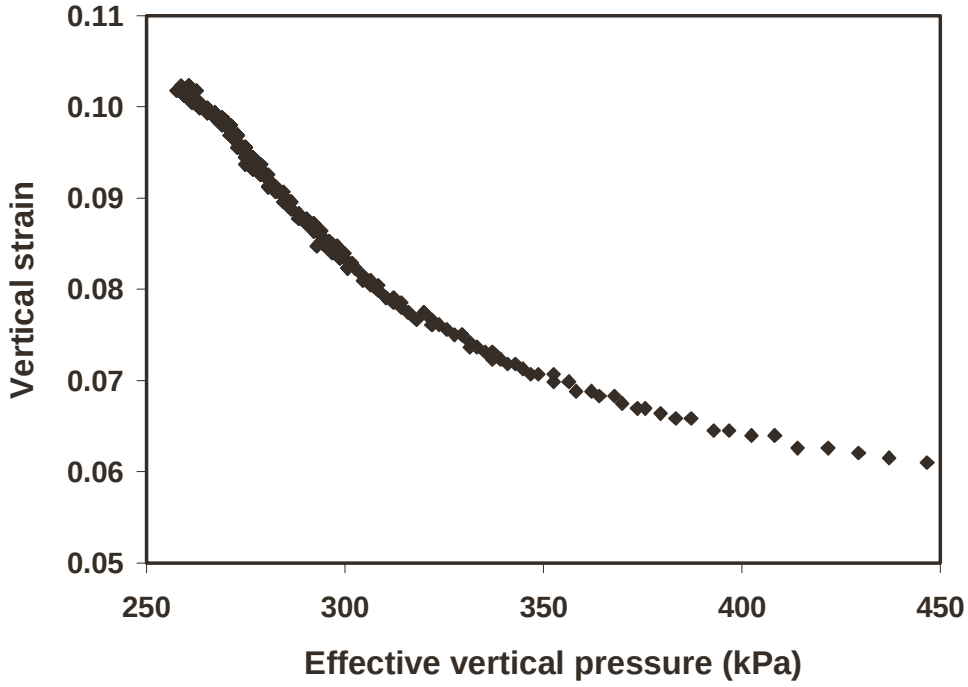

Figure 5.3. Vertical strain versus effective vertical pressure for final bagasse being unloaded in Test G.

The change in shear stress by the change in shear strain during the shearing part of Test G (Figure B.1.47 in Appendix B) was plotted in Figure 5.4. From the initial part of this curve, a value for G of 10000 kPa was adopted. Together with an E value of 12500 kPa, this results in a calculated value of ν of -0.4. As this value is unrealistic, the value of ν of 0.3 calculated in Test C was adopted. Using an E value of 12500 kPa, the value of ν of 0.3 corresponds to a G value of 4800 kPa. A summary of the material parameters used in the following predictions is shown in Table 5.1 for Test C and Test G. It is noted that the values of E are only used by the shearing version of the single element model. The values of E given in Table 5.1 correspond to a normally consolidated sample (Test C) at a vertical pressure of about 1800 kPa and a heavily over-consolidated sample (Test G) at a vertical pressure of about 340 kPa.

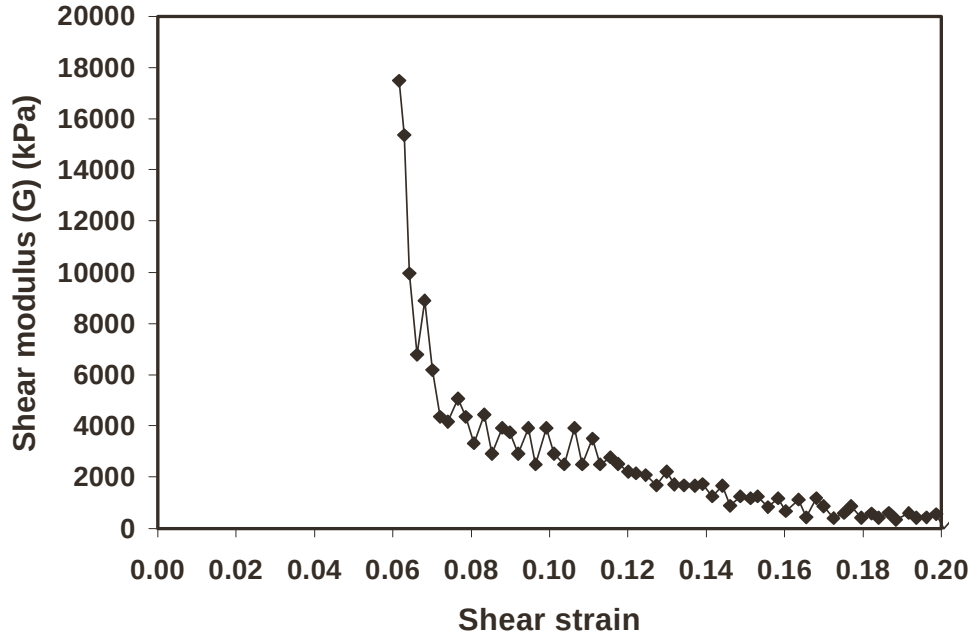

Figure 5.4. Shear modulus of highly over-consolidated final bagasse during shearing in Test G.

It is shown later in this chapter that the values of the material parameters can be determined, from particular loading conditions, by fitting predictions to measurements using a critical state model and a parameter estimation software package.

The value of Poisson's ratio, ν, has not been directly measured in this investigation. In the absence of measured values for bagasse, a value of 0.3 is usually used in modelling. This is consistent with the value of 0.3 adopted by Kirby (1998b) in modelling the behaviour of clay in a direct shear box, following common practice (Britto and Gunn, 1987). Since ν is required for most cases of computer modelling, its measurement for bagasse is deemed worthwhile in future work.

Table 5.1 Summary of material parameters for single element MCC predictions

Test	λ	κ	M	E (kPa)	ν
C*	0.93	0.17	1.1	76000	0.3
G*	1.06	0.17	1.1	12500	0.3

*Tests carried out on the 4-12-98 (refer to Table 4.1).

5.2.1 Compression along the normal compression line

Here the ratio of the horizontal effective stress to the vertical effective stress, K_o, is introduced. It is known as the 'at rest earth pressure coefficient' in the soil mechanics literature. K_o was not mentioned in Chapters 3 and 4 as it was not measured during the direct shear tests. K_o is not a material parameter as such (and it is not usually an input parameter to computer models, simply an input as an initial starting stress condition). However, the value of K_o measured for bagasse is lower than those for most soils (at approximately 0.2) and it is desirable for a model to reproduce such a stress condition at the same loading conditions in order to be confident that the behaviour of bagasse is modelled adequately.

Shown in Figure 5.5 are predictions of the normal compression line compared to the measured line. The predicted line shows an excellent fit to the experimental data. The predicted line was obtained with an initial stress condition of K_o equal to 0.69, which remained at this number during the simulation (not shown in Figure 5.5). As shown in Figure 5.5, if an initial stress condition with a different value of K_o, for example 0.2, is used, a poorer prediction is obtained. In uniaxial compression along the normal compression line, the Modified Cam Clay model changes the input value of K_o (from the input stress conditions) to a value dependent on the input value of the parameter M. For an M value of 1.1, the corresponding K_o is 0.69. This limitation present in the Modified Cam Clay model (and which, as will be shown later is also present in previous material models used in mill modelling such as the Drucker Prager Cap model) is quite well known. The limitation is shown for example by Brinkgreve et al (1994), where the yield condition results in equation (5.1).

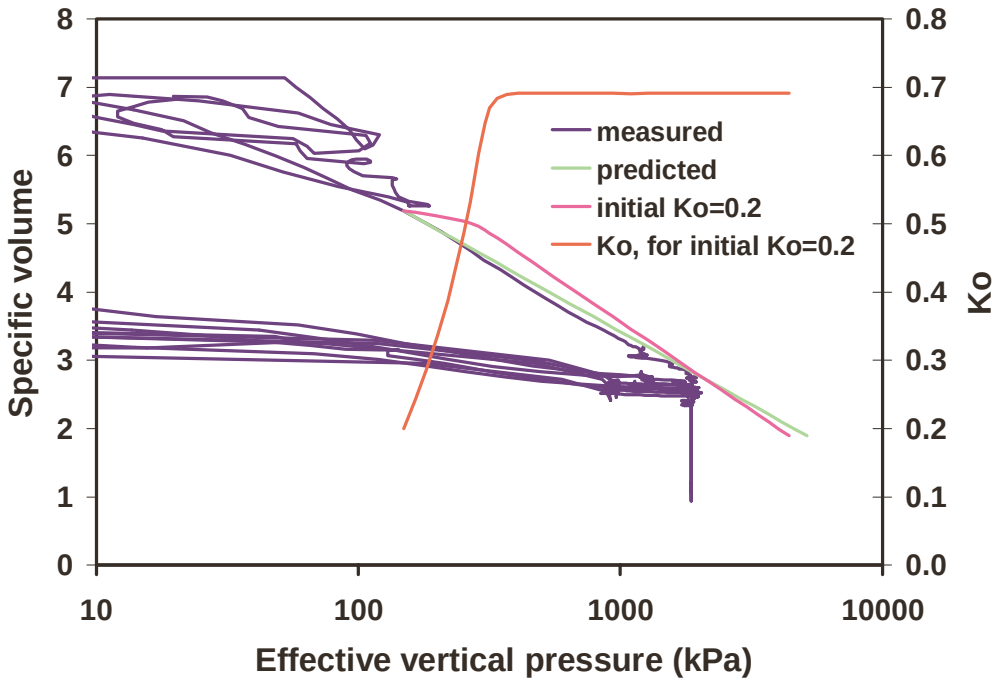

Figure 5.5. Prediction of uniaxial compression along the normal compression line for final bagasse.

$$\sigma_c = \frac{M^2(1+2K_o)}{\frac{1}{3}M^2(1+2K_o)^2 + 3(1-K_o)^2} P_c \qquad (5.1)$$

where σ_c is the vertical stress and P_c is the yield stress in hydrostatic compression (the size of the yield surface). In effect, the Modified Cam Clay model enforces a value of K_o for a given value of M if a stress state is present that involves compression along the normal compression line. Figure 5.6 shows this by plotting the K_o values enforced by the model in predicting uniaxial constrained compression loading along the normal compression line, while varying the input parameter M and keeping the other material parameters given in Table 5.1 constant.

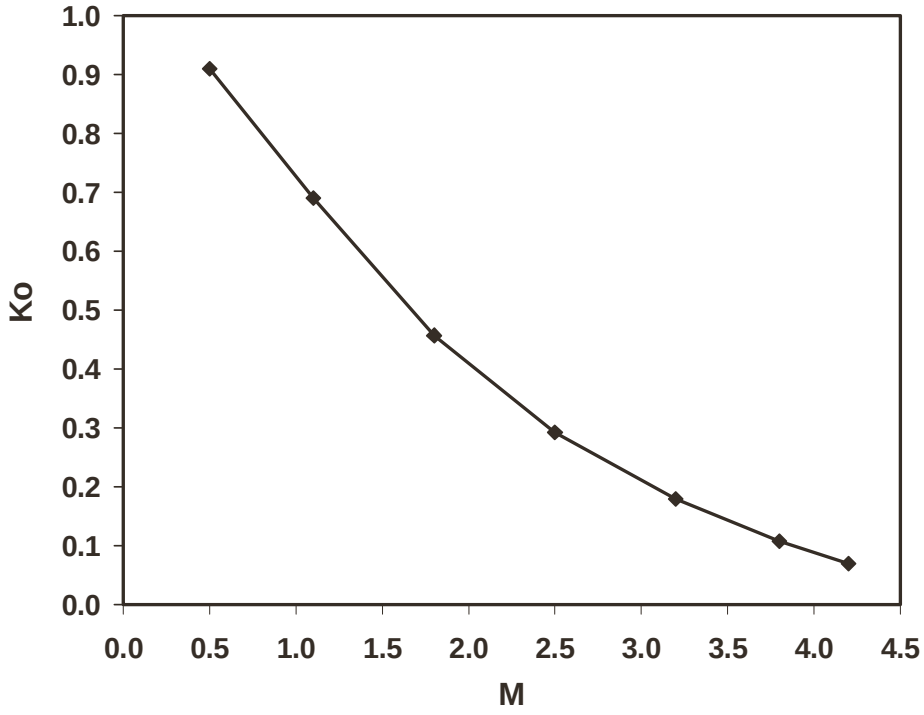

Figure 5.6. Values of K_o enforced by Modified Cam Clay model during uniaxial compression of final bagasse for varying input material parameter M.

Any combination of M and K_o along the line shown in Figure 5.6 will predict an excellent fit to the experimental normal compression line shown in Figure 5.5. It is also noted that at higher values of M such as 3.8, ν has a significant effect on the value of K_o predicted. For example, for an M value of 3.8, changing ν from 0.3 to 0.1 halves the predicted value of K_o from 0.1 to 0.05.

The limitation means that, to predict a small value of K_o such as the 0.2 as observed in the compression of bagasse, a high value of M (a value that cannot be justified from experimental measurements) must be input to the model.

5.2.2 Compression unloading of a bagasse sample

A prediction of the unloading behaviour of final bagasse was carried out using the input parameters that were previously successful in reproducing final bagasse behaviour in compression loading along the normal compression line. That is, for a value of M of 1.1, the simulation started with an initial stress state having a K_o

value of 0.69. A comparison of the prediction with the experimental measurements is shown in Figure 5.7. A poor prediction was obtained.

However, if the predicted specific volume is plotted against the mean effective stress (P, the average of the effective vertical pressure and the two horizontal stresses), instead of the effective vertical pressure, while the measured specific volume remains plotted against the measured effective vertical pressure, a much improved fit is obtained, as shown in Figure 5.8. If the experimental data were perfect and the corresponding κ was used as an input to the simulation, an excellent fit would be obtained. The poor fit shown in Figure 5.7 is due to a limitation in the definitions used in the Modified Cam Clay model, which is defined in terms of P.

At a high degree of unload numerical problems were experienced when the yield surface was reached on the dry side of the critical state line (the super-critical region). Similar numerical problems are expected when modelling the exit of bagasse from a nip in a mill, and need to be monitored.

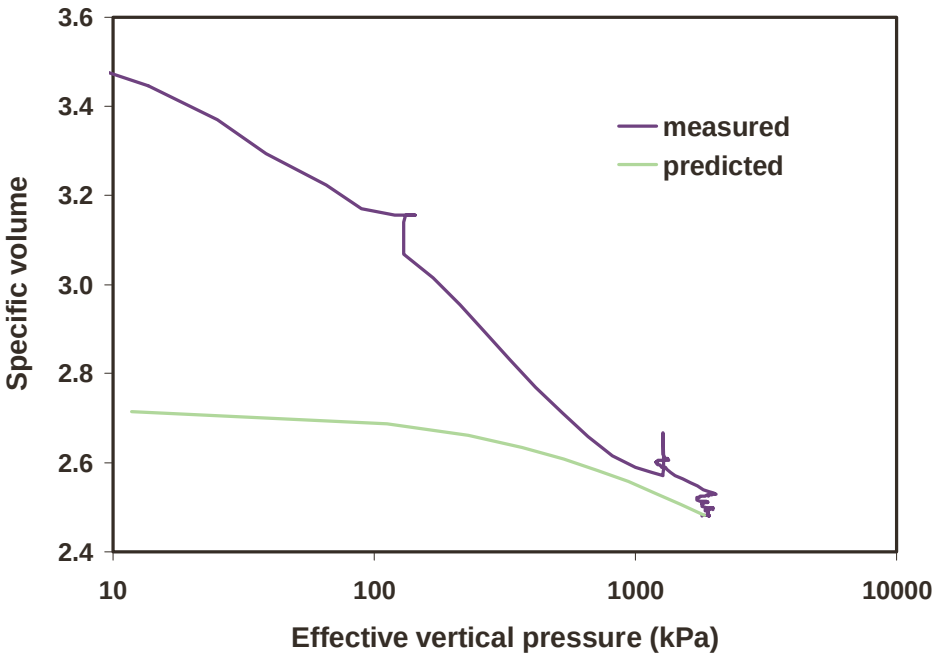

Figure 5.7. Prediction of compression behaviour during unloading of final bagasse.

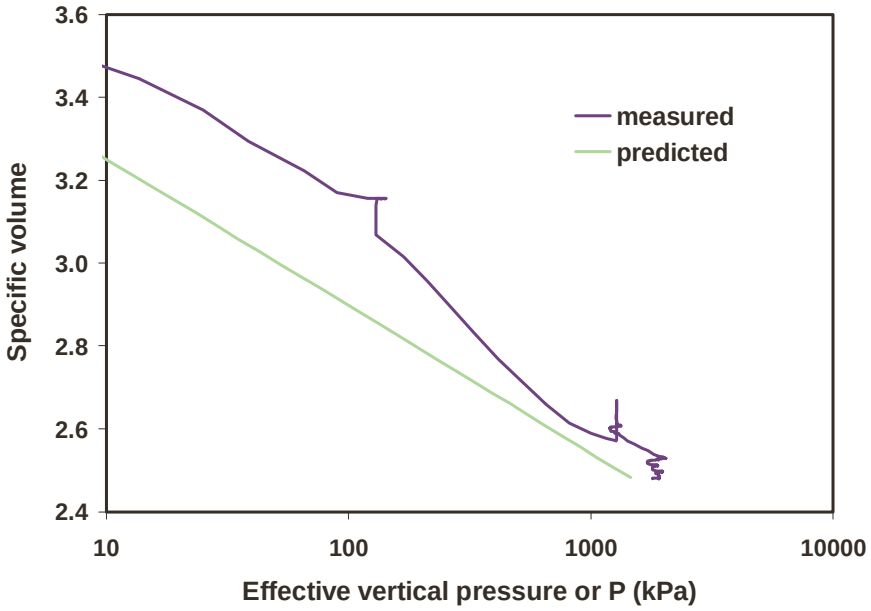

Figure 5.8. Modified prediction of compression behaviour during unloading of final bagasse by adopting mean effective stress (P).

5.2.3 Compression when reloading a final bagasse sample

The prediction of compression reloading behaviour of final bagasse is shown in Figure 5.9. With the same parameters, an excellent fit to the experimental measurements was achieved. When the normal compression line was reached (located by the end of experimental results at a pressure of 2000 kPa in Figure 5.9), it was followed by the predicted results. Therefore reloading is predicted well by the single element model.

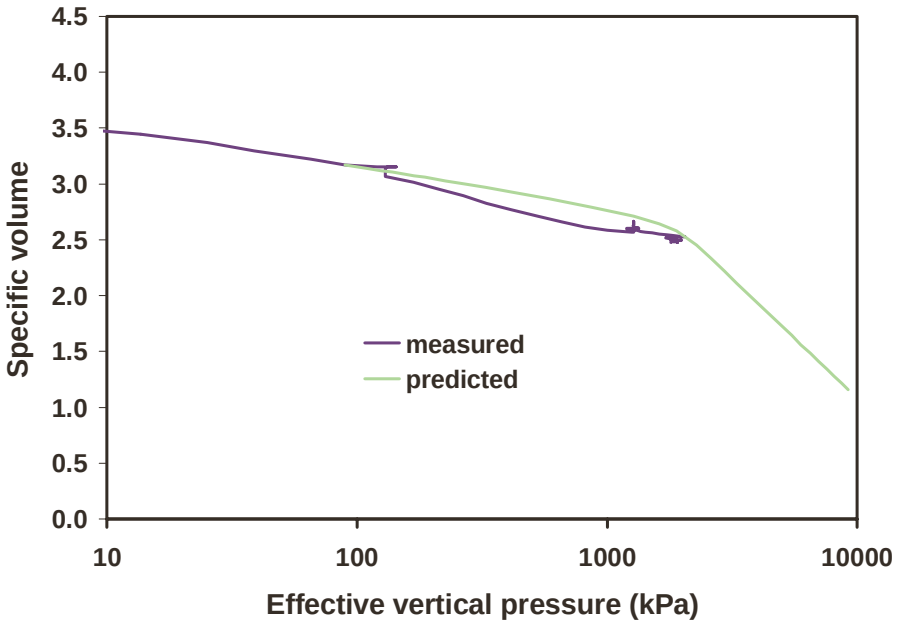

Figure 5.9. Prediction of compression behaviour during reloading of final bagasse.

5.2.4 Shearing of a normally consolidated bagasse sample.

With the same parameters (M of 1.1 and K_o of 0.69), poor predictions of the shearing behaviour of normally consolidated final bagasse were achieved. The poor predictions of shear stress and specific volume are shown later in Section 5.5 in Figure 5.35 and Figure 5.36. In this section, predictions are shown for an assumed initial K_o value of 0.2 (which has been measured for bagasse). Shown in Figure 5.10 and Figure 5.11 are the measured and predicted behaviour of normally consolidated final bagasse undergoing shearing at constant vertical pressure.

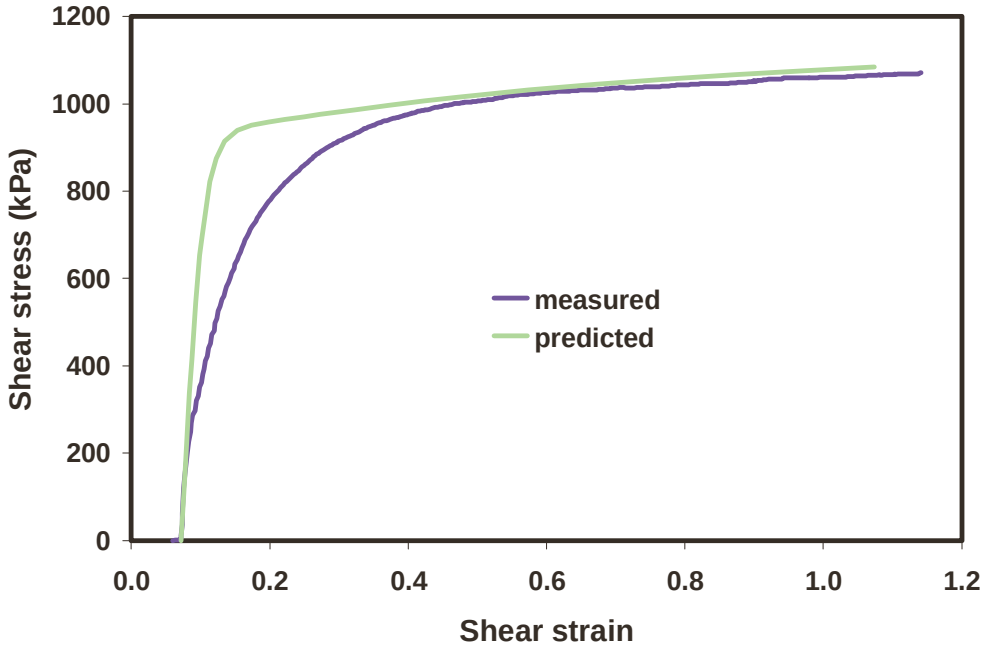

Figure 5.10. Prediction of shear stress during shearing of normally consolidated final bagasse.

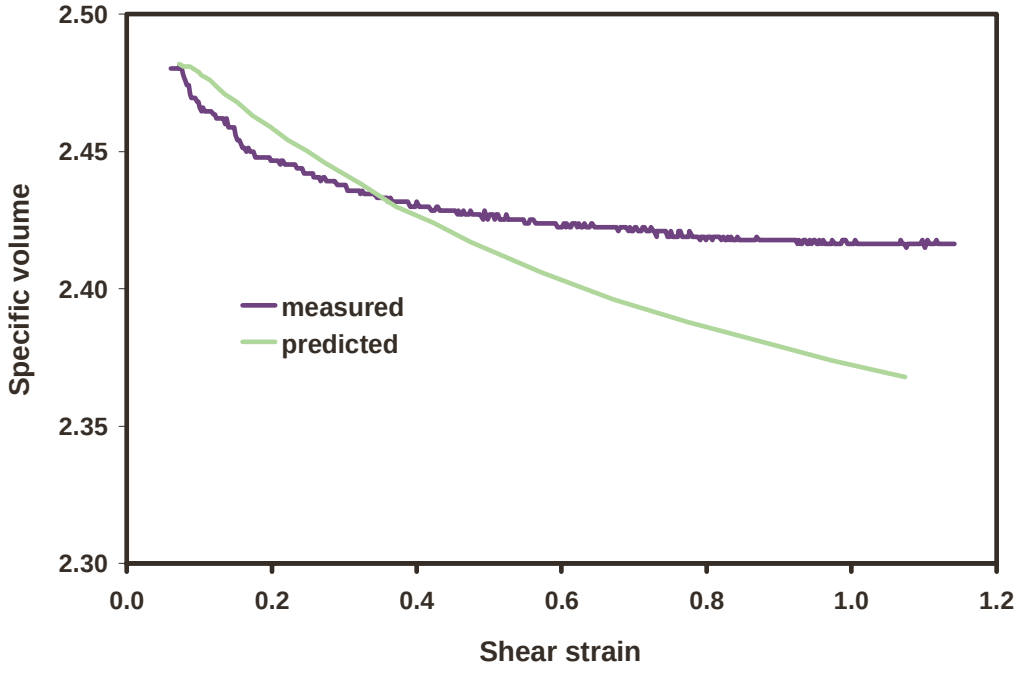

Figure 5.11. Prediction of specific volume during shearing of normally consolidated final bagasse.

Figure 5.10 shows the shear stress versus shear strain plot while Figure 5.11 shows the specific volume versus shear strain plot. The predicted results show that it is very likely that a single element Modified Cam Clay model can reproduce the shear behaviour of a normally consolidated sample, although some inadequacies can be identified: the predicted shear behaviour is too stiff at the beginning of the test and the predicted final decrease in volume is nearly twice that measured.

5.2.5 Shearing of an over-consolidated final bagasse sample

Shown in Figure 5.12 and Figure 5.13 are the measured and predicted behaviour of a final bagasse sample with an over-consolidation ratio of 5.0 (Test G) undergoing shearing at constant vertical pressure. Initial K_o values of 0.2 and 0.69 were used for the predictions. Figure 5.12 shows the shear stress versus shear strain plot, while Figure 5.13 shows the specific volume versus shear strain plot. Up to an initial shear strain of about 0.15 there is good agreement between the measured and predicted values for both shear stress and specific volume. However, after this stage far too much expansion is predicted (an increase in specific volume of 1.2, while the actual expansion was 0.05). The predicted final shear stress was a third of that measured.

The poor prediction of the shear behaviour of a final bagasse sample with an over-consolidation ratio of 5.0 may be a result of the Modified Cam Clay model or the use of a single element model or a combination of both. It is noted that Kirby (1994) showed that over-consolidated clay undergoes non-uniform deformations during shearing in a shear box. Similar non-uniform deformations may occur for over-consolidated bagasse. The measurements and predictions for over-consolidated bagasse have been presented here for completeness. A multi-element model is tested in Section 5.3 and compared to measurements in Chapter 6.

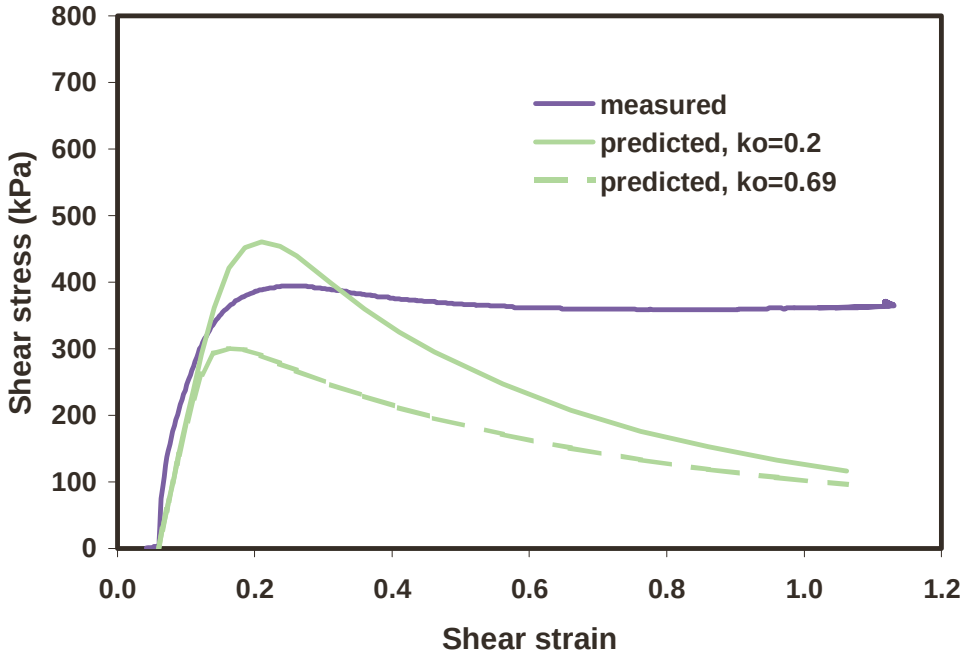

Figure 5.12. Prediction of shear stress during shearing of over-consolidated final bagasse (OCR of 5.0).

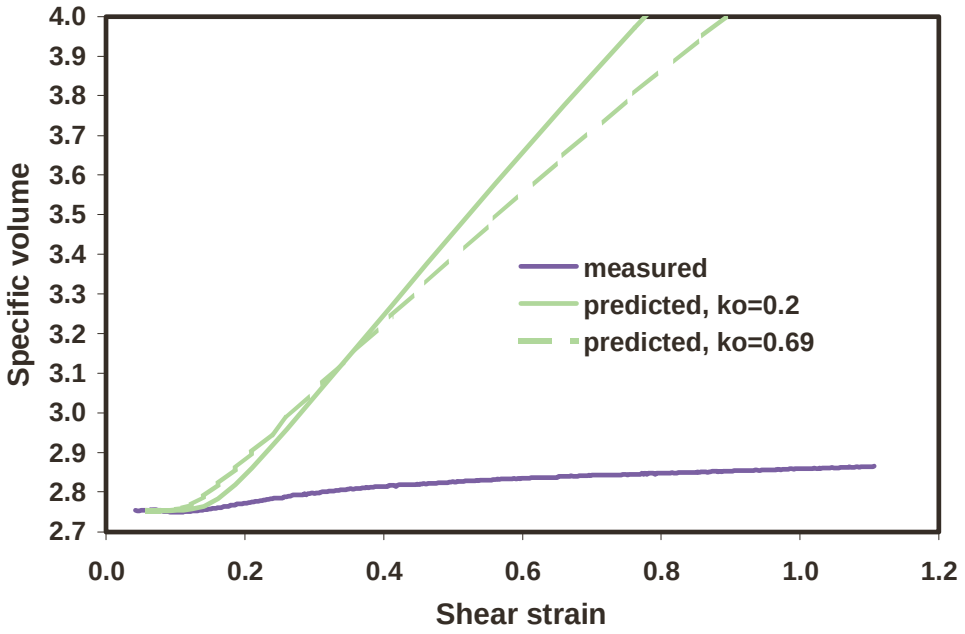

Figure 5.13. Prediction of specific volume during shearing of over-consolidated final bagasse (OCR of 5.0).

5.2.6 Summary of fitting predictions to experimental results using a single element Modified Cam Clay model

The single element Modified Cam Clay model was able to reproduce compression loading and re-loading well with the use of particular combinations of material parameters. The unloading behaviour was poorly reproduced because of a limitation in the definitions used by the Modified Cam Clay model, and not because of the use of a single element model. The predicted results show that it is likely that a single element Modified Cam Clay model can reproduce the shear behaviour of a normally consolidated final bagasse sample but not that of a sample with a fairly high degree of over-consolidation. Similar conclusions were found when the above exercise was repeated for two first bagasse tests (not reported).

5.3 Fitting predictions to experimental results using a multi-element Modified Cam Clay model.

The comparison of predictions against measurements carried out in Section 5.2 for five loading conditions was repeated, but this time a multi-element Modified Cam Clay model incorporating porous elasticity was used. This model was available in the software package ABAQUS (Hibbit et al, 2001). The elements adopted were two-dimensional plane strain. For compression, the initial sample dimensions were 77 mm vertical by 280 mm horizontal and for shearing 37 mm vertical by 280 mm horizontal. Shown in Figure 5.14 is the 36 element grid used for the compression simulations (3 elements vertical by 12 elements horizontal), while the same grid was used for the shearing simulation of a normally consolidated final bagasse sample. The elements are shown in blue while the nodes are shown in red. Both the 36 element grid and a 72 element grid (6 elements vertical by 12 elements horizontal) shown in Figure 5.15 were used for the shearing simulations of an over-consolidated final bagasse sample (OCR of 5.0). The two different grids were used to test for the prediction of the formation of a shear plane during shearing of the over-consolidated sample, as described later in this section. Note that the aspect ratio shown in Figure 5.14 is that at the start of the compression simulations while the aspect ratio shown in Figure 5.15 is that at the start of the shearing simulations.

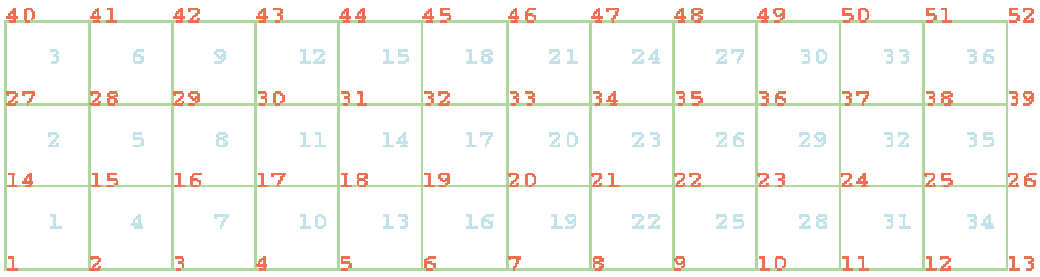

Figure 5.14. Grid of 36 elements used for compression and shearing simulations.

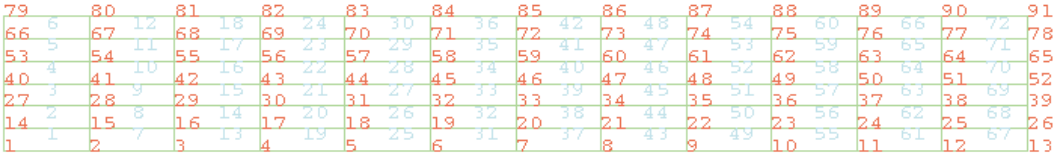

Figure 5.15. Grid of 72 elements used for shearing simulations of over-consolidated final bagasse sample (OCR of 5.0).

Example ABAQUS input files for compression loading along the normal compression line in the 36 element model and shearing of an over-consolidated (OCR of 5.0) sample in the 72 element model are given in Appendix C.

5.3.1 Predictions for loading conditions 1 to 4

The loading conditions 1 to 4 have been defined as:

1. Compression along the normal compression line.
2. Compression when unloading along the unloading-reloading line.
3. Compression when reloading along the unloading-reloading line.
4. Shearing of a normally consolidated sample.

For loading conditions 1 to 3 the bottom nodes of the sample were constrained vertically while the side nodes of the sample were constrained horizontally, and a vertical pressure was applied to the nodes on the top surface of the sample. For loading condition 4 the bottom nodes of the sample were constrained vertically and horizontally, and the nodes at each side of the sample and at the same height were

constrained horizontally to each other. A vertical pressure and a horizontal displacement were applied to the nodes on the top surface of the sample.

The simulations carried out with the multi-element Modified Cam Clay model incorporating porous elasticity predicted results either identical to or very similar to the results predicted by a single element Modified Cam Clay model incorporating linear elasticity. The development of stress and strain, including shear strain in the normally consolidated sample, was uniform throughout the multi-element model, except for perturbations at the edges. Shown in Figure 5.16 is an example of a normally consolidated final bagasse sample undergoing an imposed shear strain, with the shear stress (kPa) shown as coloured contours. For a sideways movement of 30 mm, the sample was predicted to decrease in height by 2.2 mm.

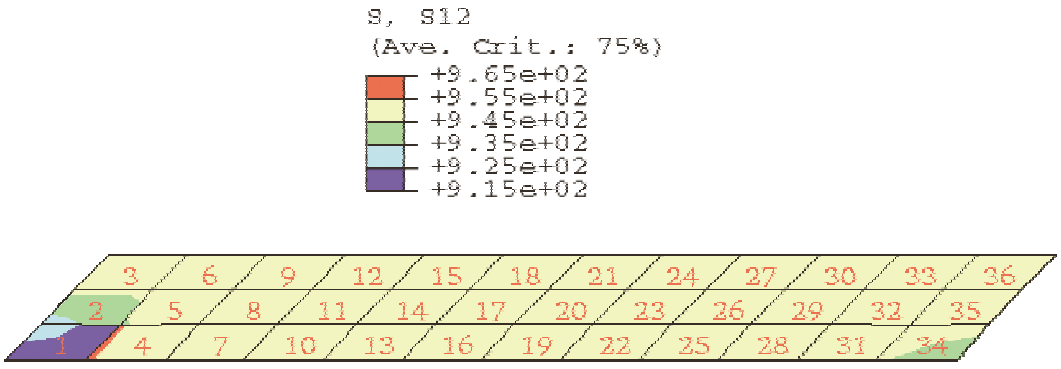

Figure 5.16. Normally consolidated final bagasse sample undergoing shear strain (shear stress shown in kPa).

Therefore, for the above four loading conditions, since the stresses and strains are uniform across all elements, a single element model is adequate for testing the performance of different material models.

5.3.2 Predictions for loading condition 5

Kirby (1991) showed experimentally the different shear behaviour of a normally consolidated (OCR of 1.0) soil and a highly over-consolidated soil (OCR of 10.0) in a direct shear box. The normally consolidated soil exhibited uniform shear deformation along the height of the sample while the highly over-consolidated sample exhibited the formation of a shear plane (a localized zone of failure). The

formation of such a shear plane in the direct shear test of the final bagasse sample with an OCR of 5.0 would require a simulation with a multi-element model and may account for some of the poor fit of the predicted behaviour using a single element model (observed in Section 5.2.5) to the measured behaviour.

Multi-element simulations of an over-consolidated (OCR of 5.0) final bagasse sample were carried out. Shown in Figure 5.17 is a simulation with 36 elements that shows the formation of a shear plane at the bottom row of elements, which have a greater shear angle than the top two rows. Similarly, shown in Figure 5.18 is a simulation with 72 elements that has badly distorted sides and a shear plane that makes its way from the sides and along the bottom row of cells.

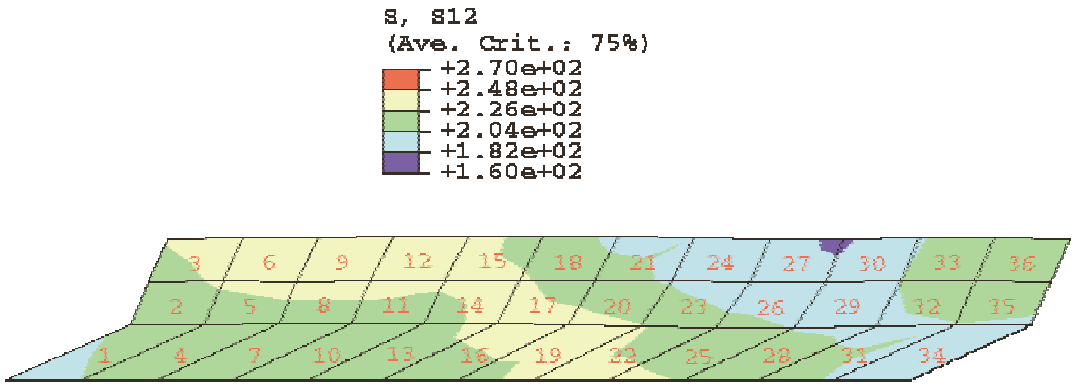

Figure 5.17. Over-consolidated (OCR of 5.0) final bagasse sample undergoing shear strain (shear stress in kPa) using a 36 element model.

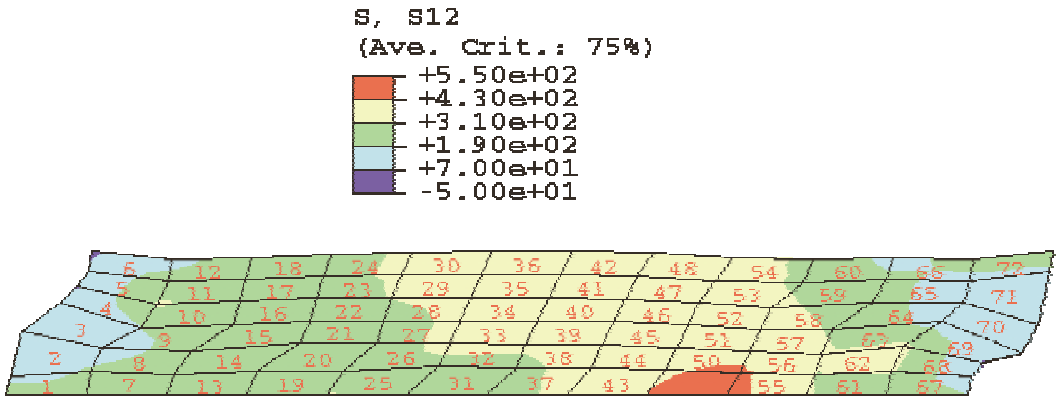

Figure 5.18. Over-consolidated (OCR of 5.0) final bagasse sample undergoing shear strain (shear stress in kPa) using a 72 element model.

The result of model predictions will be explained by comparing the predictions of elements 37 and 42 in the model shown in Figure 5.18. For individual elements in the multi-element model the magnitudes of the shear stress and specific volume plotted against shear strain of each individual element are similar. However, when a shear plane is predicted to form, the elements in the shear plane (element 37) continue to experience shear strain and continue to expand. The elements that are not in the shear plane (element 42) are predicted to experience a decrease in the shear strain (they relax a bit) and reduce in volume. Shown in Figure 5.19 is the shear stress versus shear strain behaviour for elements 37 and 42, which is identical until a shear strain of about 0.6, at which time element 37 continues shearing while element 42 relaxes. Then element 42 continues to undergo shear strain and follows the shear stress path of element 37. The final shear strain of element 42 is less than that of element 37, as can be seen in Figure 5.18. Shown in Figure 5.20 is the specific volume versus shear strain behaviour for elements 37 and 42. A slight decrease in volume can be seen for element 42 at a shear strain of 0.6.

The above shows that a single element model is not adequate to reproduce shear behaviour of a final bagasse sample at an over-consolidation ratio of 5.0. Also, the shear stress predictions are significantly less stiff than the measured behaviour (the predictions are poor). It is also noted that the shear stress prediction for individual elements using the Modified Cam Clay model incorporating porous elasticity for a final bagasse sample at an over-consolidation ratio of 5.0 is significantly less stiff than the prediction for a single element model using the Modified Cam Clay model incorporating linear elasticity.

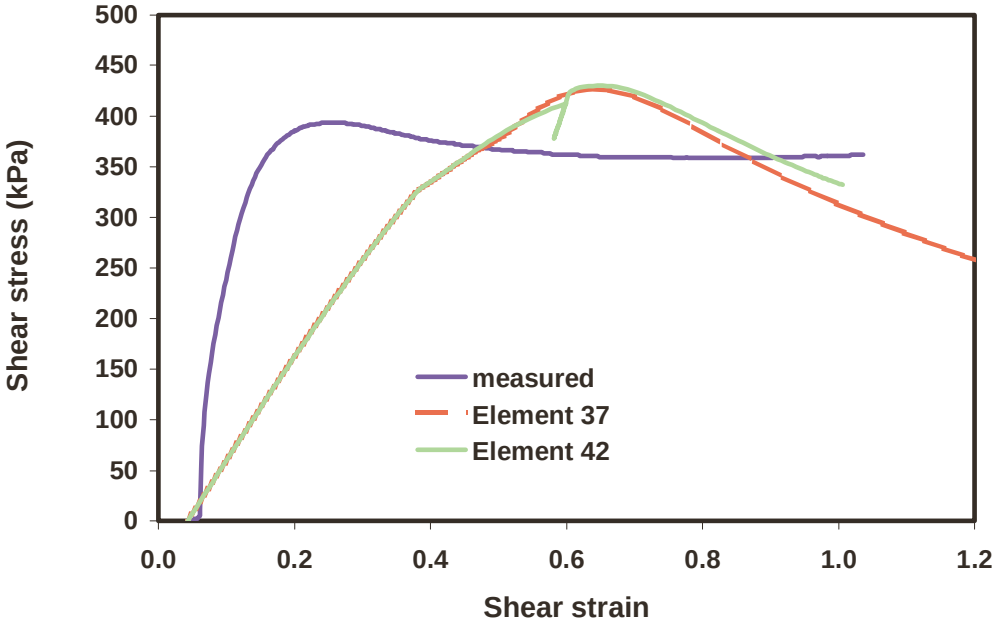

Figure 5.19. Multi-element prediction of shear stress versus shear strain during shearing of over-consolidated final bagasse (OCR of 5.0).

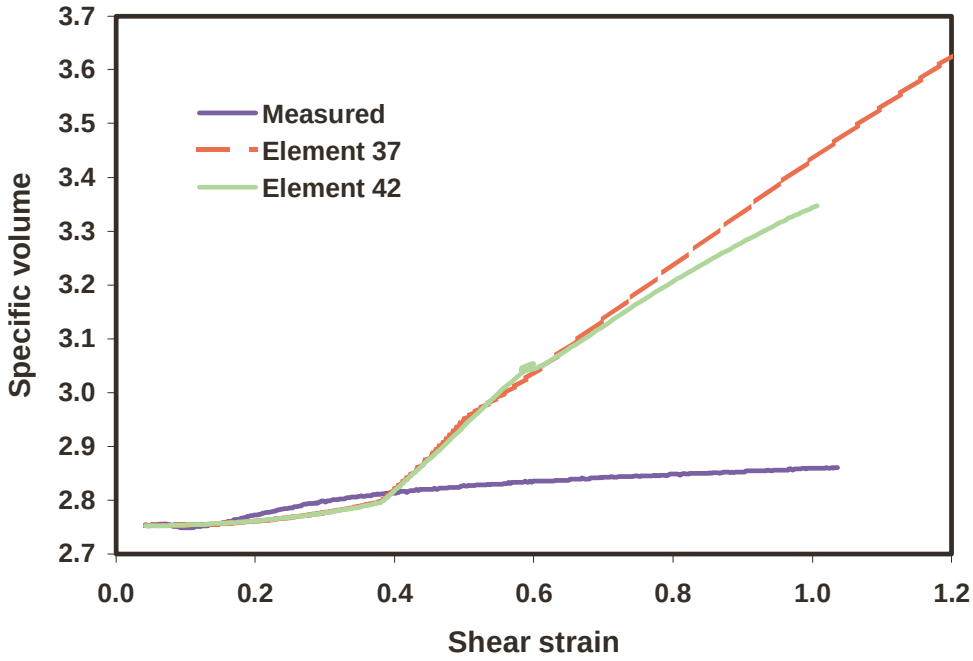

Figure 5.20. Multi-element prediction of specific volume versus shear strain during shearing of over-consolidated final bagasse (OCR of 5.0).

The results of the formation of a shear plane on simulations can be seen more dramatically by adopting a value of K_o of 0.69 and a ν value of 0.01. Such a prediction is shown in Figure 5.21, Figure 5.22 and Figure 5.23. Although such a value of K_o has been observed in highly over-consolidated soils, the results of this simulation for bagasse are reported simply to show the effect of the shear plane formation and to show that a stiffer shear prediction is obtained by the use of these parameter values. In Figure 5.21, element 32 is in a shear plane while element 33 just above it is not. The relaxation in shear strain and shear stress is shown dramatically in Figure 5.22 for element 33, and Figure 5.23 shows element 33 decreasing in volume to less than the original volume, while element 32 continues to undergo shear strain and volume expansion.

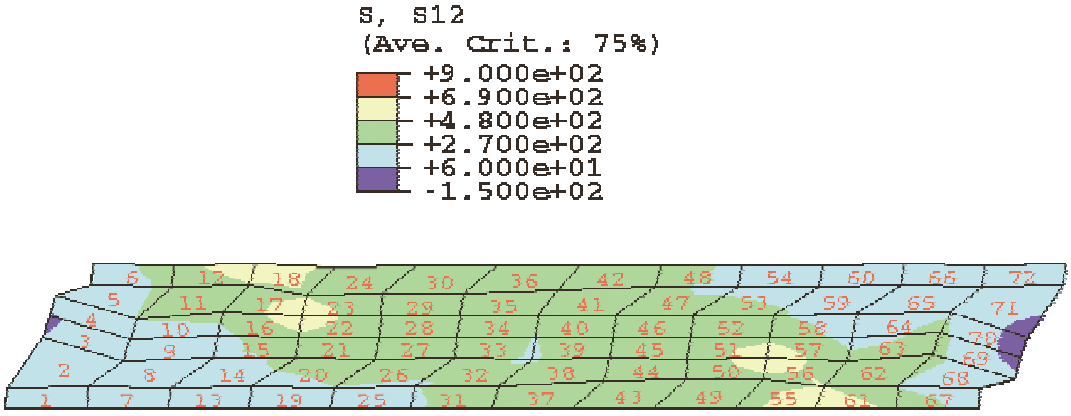

Figure 5.21. Over-consolidated (OCR of 5.0) final bagasse sample undergoing shear strain (shear stress shown in kPa) using a 72 element model and adopting a variation in input material parameters (K_o =0.69, ν=0.01).

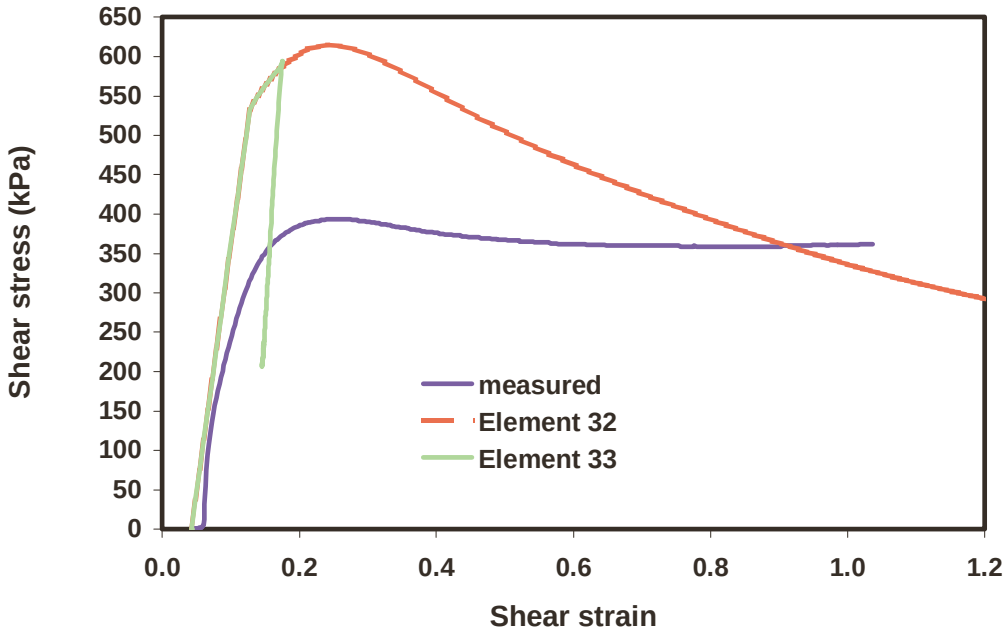

Figure 5.22. **Multi-element prediction of shear stress during shearing of over-consolidated final bagasse (OCR of 5.0) and adopting a variation in input material parameters (K_o =0.69, ν=0.01).**

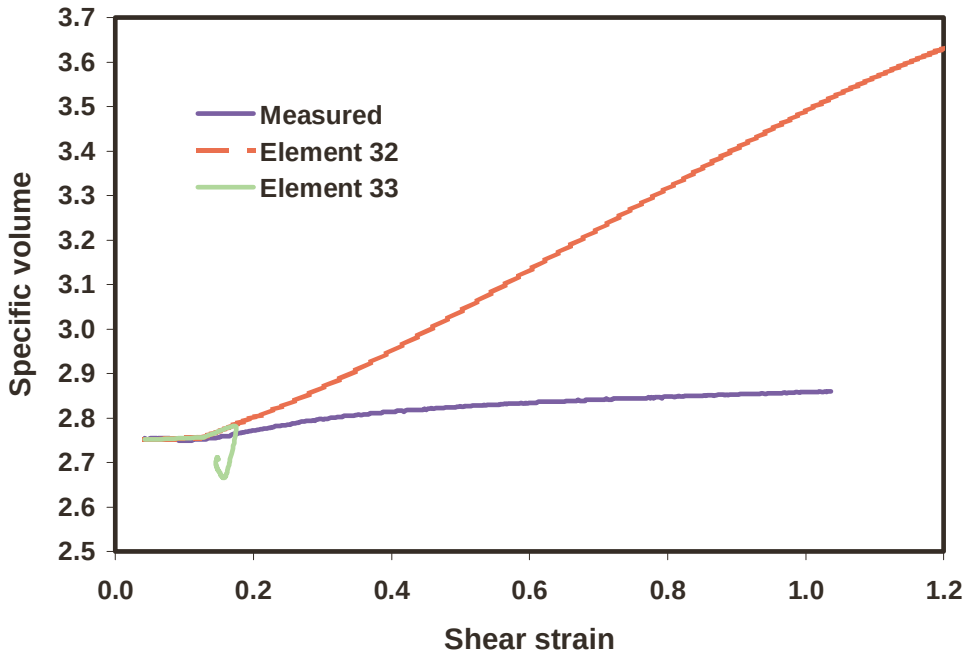

Figure 5.23. **Multi-element prediction of specific volume during shearing of over-consolidated final bagasse (OCR of 5.0) and adopting a variation in input material parameters (K_o =0.69, ν=0.01).**

5.3.3 Summary of multi-element simulations

The simulations carried out with the multi-element Modified Cam Clay models incorporating porous elasticity predicted results either identical to or very similar to the results predicted by a single element Modified Cam Clay model incorporating linear elasticity, for the four loading conditions:

1 Compression along the normal compression line.
2. Compression when unloading along the unloading-reloading line.
3. Compression when reloading along the unloading-reloading line.
4. Shearing of a normally consolidated sample.

The development of stress and strain was uniform throughout the multi-element model, except for perturbations at the edges. Therefore, for the above four loading conditions, a single element model is adequate for testing the performance of different material models.

For loading condition 5, the shearing of a final bagasse sample with an over-consolidation ratio of 5.0, modelling using multi-element models predicted the formation of a shear plane with non-uniform deformation throughout the sample. The non-uniform deformation means that a single element model is not capable of reproducing the shear behaviour for this loading condition.

5.4 Indirect material parameter estimation by model inversion

In Chapter 4 and in the previous sections of Chapter 5, material parameters were estimated simply by examining the experimental results for the sets of tests on prepared cane, first bagasse, and final bagasse. Kirby (1998b) showed that parameters can be estimated indirectly by matching critical state model results to experimental data, and adjusting the parameters until a good match is obtained. In this section, material parameters are estimated using a parameter estimation package called PEST from Watermark Numerical Computing (2000) in combination with a single element Modified Cam Clay (MCC) critical state model and the experimental results from a single direct shear test. The two versions of the single element Modified Cam Clay model were used: one that modelled constrained uniaxial compression (and used κ), and one that modelled shearing (and used E).

The single direct shear test adopted was Test C for final bagasse carried out on the 4-12-98.

As well as the five material parameters lambda (λ), kappa (κ), Young's Modulus (E), Poisson's ratio (ν), and the slope of the critical state line (M), the ratio of the horizontal stress to the vertical stress (K_o) in the direct shear box was included in the parameter estimation. Although it is not a material parameter as such, previous simulations have shown that initial condition values of K_o can have an effect on the predictions from a model, and that there is a relationship between K_o and, for example, the material parameter M.

For three loading conditions, which previously had been shown could be modelled using a single element model (compression along the normal compression line, compression along the elastic unloading-reloading line, and shearing of a normally consolidated sample), PEST was run in "parameter estimation mode". The set of material parameters was determined by PEST which reduced to a minimum the discrepancies between the measured behaviour and the corresponding model generated behaviour (that is, provided the best fit of the measured data by the predicted data). PEST indicated which material parameters could be determined from which loading step, by providing confidence limits for the magnitude of each parameter and a parameter correlation coefficient matrix. In addition, PEST was run in "predictive analysis mode" in combination with a companion program called SENSAN from Watermark Numerical Computing, in which a sensitivity analysis was carried out to determine the range of parameter values that provided a sum of squared deviations (SSD) value no more than 10% higher than the minimum SSD value. A value of 10% was chosen to be consistent with the analysis carried out by Kent (2001) who estimated prepared cane material parameters from a uniaxial compression test. Again, the sensitivity analysis was carried out using the experimental results from a single direct shear test (Test C for final bagasse carried out on the 4-12-98). The results are summarised in Sections 5.4.1, 5.4.2, and 5.4.3 respectively for three loading conditions: compression along the normal compression line, compression along the elastic unloading-reloading line, and shearing of a normally consolidated sample.

5.4.1 Indirect parameter estimation from normal compression loading step data

Shown in Table 5.2 are the material parameters found by PEST to give the best fit of the normal compression line. Shown in Figure 5.24 is the resultant fit, which is excellent. Table 5.3 shows the parameter correlation coefficient matrix for normal compression. The values in bold have a significance level of 95%.

Table 5.2 Summary of material parameters for best fit of normal compression line

Test	M	λ	κ	ν	K_o
C	1.2	0.97	0.28	0.28	0.61

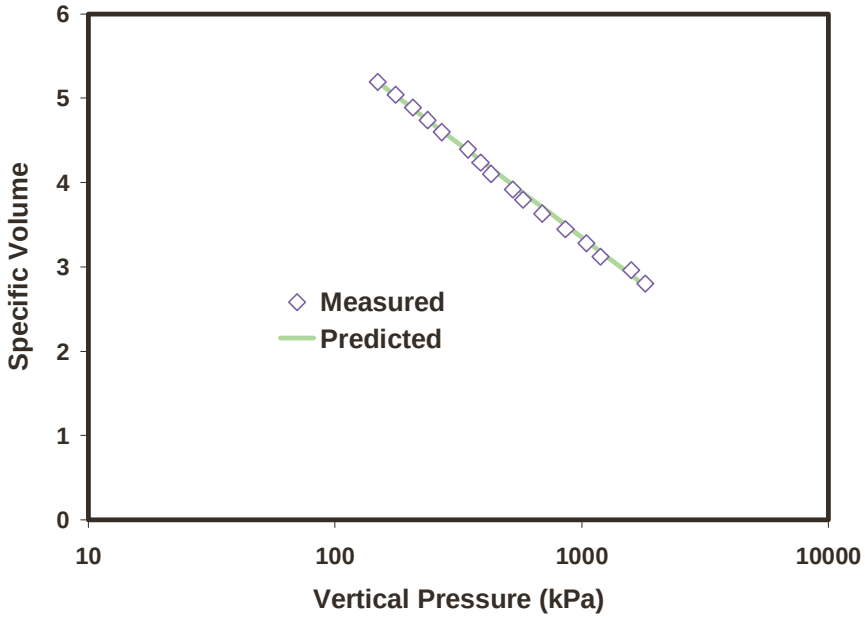

Figure 5.24. Fit of normal compression line using PEST best fit parameters.

Table 5.3 Correlation coefficient matrix for normal compression line

	M	λ	κ	ν	K_o
M	**1.0**	-0.10	**-0.79**	0.45	**-0.84**
λ		**1.0**	0.19	-0.21	-0.01
κ			**1.0**	**-0.90**	0.34
ν				**1.0**	0.10
K_o					**1.0**

Note: E had no effect on the calculations

The correlation coefficients in bold in Table 5.3 are those higher than the critical value of the correlation coefficient at a significance level of 95% (a value of 0.497 for the 16 experimental values given in Figure 5.24). During compression along the normal compression line, λ was not correlated with the other material parameters (magnitudes of correlation coefficients close to zero) and a unique value can be obtained. M, κ, and K_o were strongly correlated to each other (magnitudes of correlation coefficients near 1) and unique values for them cannot be confidently obtained, as they can be varied together to give a good fit to the experimental data. The relationship between M and K_o has already been described in Section 5.2.1 and gives strong confidence in the output from the PEST analysis.

A contour plot representation of the sensitivity analysis is shown in Figure 5.25 and follows the structure shown in Figure 8 of Kirby et al (1998).

Figure 5.25 shows the range of parameter values that provided a sum of squared deviations (SSD) value no more than 10% higher than the minimum SSD value for fitting the normal compression data. The ten subplots are very helpful in showing whether there is a relationship between material parameters and again show that λ is independent of the other parameters and a unique value of λ can be determined. The plots can also be very useful in the case that the PEST algorithm is not able to find the minimum (for example, if it becomes stuck in a local depression). In this case the presence of a lower minimum becomes obvious from the contour plot. Such a case is shown in Section 5.4.2.

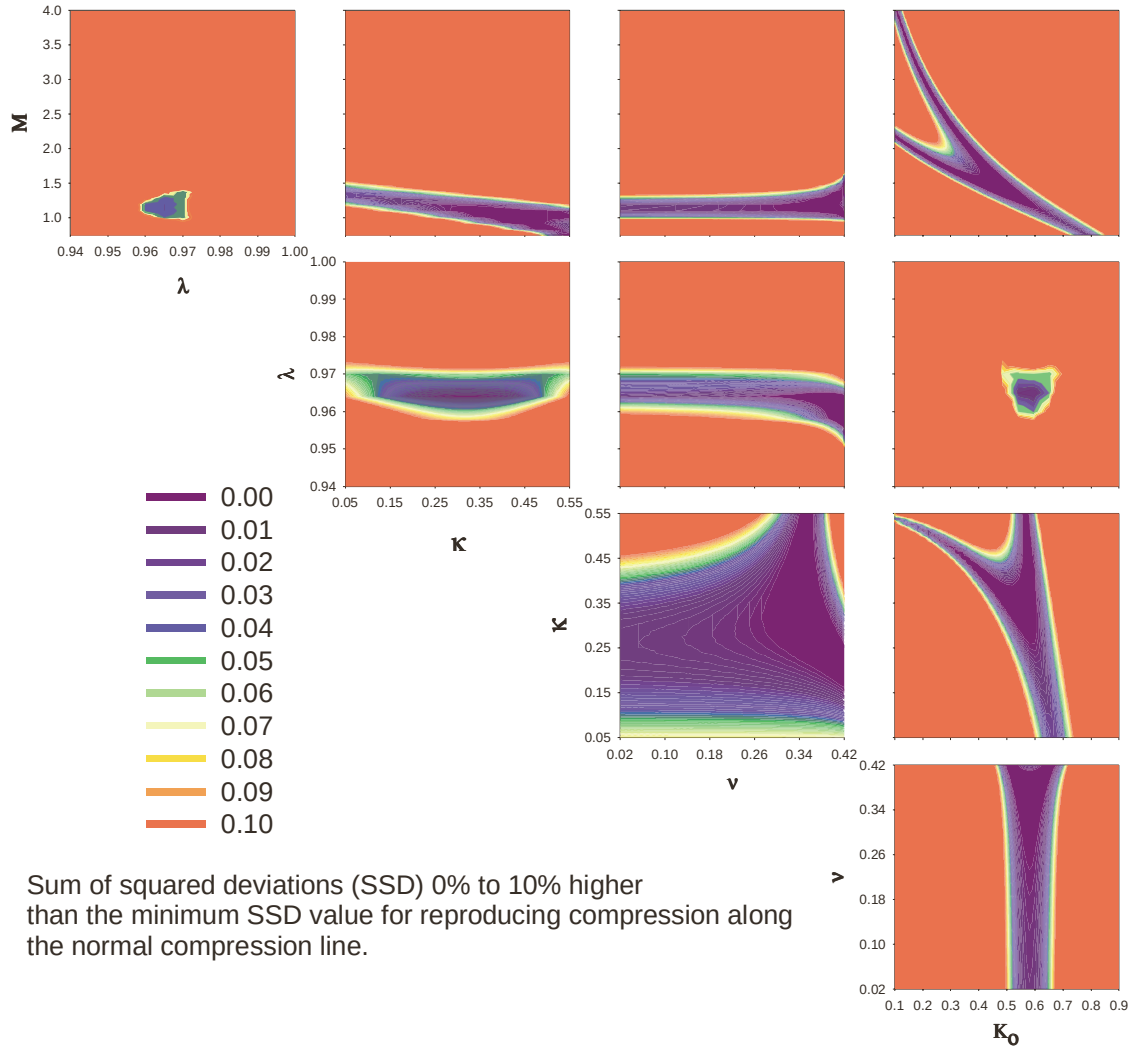

Figure 5.25 Sum of squared deviations for compression along normal compression line.

5.4.2 Indirect parameter estimation from elastic re-loading step data

Shown in Table 5.4 are the material parameters found by PEST to give the best fit of the elastic re-loading compression line. Shown in Figure 5.26 is the resultant fit (green line). The fit is fairly good, although the prediction has a kink that is not justified by the experimental data. Table 5.5 shows the parameter correlation coefficient matrix for elastic re-loading.

Table 5.4 Summary of material parameters for best fit of elastic re-loading compression line

Test	M	λ	κ	ν	K_o
C	2.2	0.48	0.23	0.29	0.33

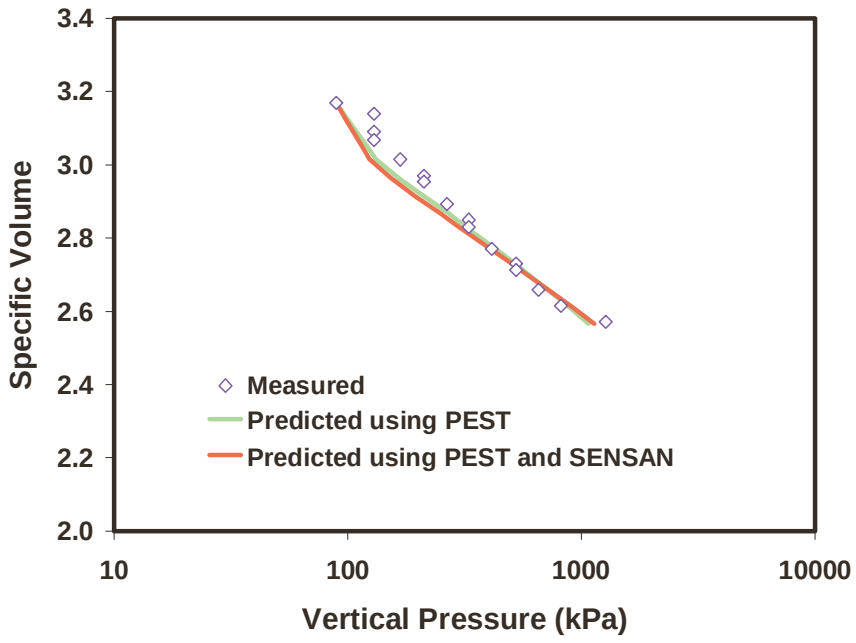

Figure 5.26. Fit of elastic re-loading compression line using PEST best fit parameters.

Table 5.5 Correlation coefficient matrix for compression along the elastic line

	M	λ	κ	ν	K_o
M	**1.0**	**0.99**	-0.08	0.27	0.51
λ		**1.0**	-0.13	0.26	0.48
κ			**1.0**	-0.24	0.22
ν				**1.0**	**0.85**
K_o					**1.0**

Note: E had no effect on the calculations

The correlation coefficients in bold in Table 5.5 are those higher than the critical value of the correlation coefficient at a significance level of 95% (a value of 0.497 for the 16 experimental values given in Figure 5.26). During compression along the elastic re-loading line, κ was not correlated to the other material parameters (magnitudes of correlation coefficients near 0) and a unique value can be obtained.

However, while carrying out the contour plot representation of the sum of squared deviations (SSD) values no more than 10% higher than the minimum SSD, it became apparent that a lower optimum than that found by PEST was present. This is shown in Figure 5.27, where the plot for material parameters K_o and κ shows that a large blue region exists below and to the left of the values of K_o of 0.33 and κ of 0.23 found by PEST.

Further investigation found a lower minimum (a sum of squared deviations of 40849 compared to 54988) did exist and the corresponding material parameters are given in Table 5.6. The corresponding fit is shown in Figure 5.26 in red and is very similar to the previous fit. The sensitivity analysis was carried out using these parameters as the minimum. Figure 5.28 shows the range of parameter values that provided a sum of squared deviations (SSD) value no more than 10% higher than the minimum SSD value for fitting the elastic re-loading compression line. The ten subplots show that κ is independent of the other material parameters and a unique value of κ can be determined.

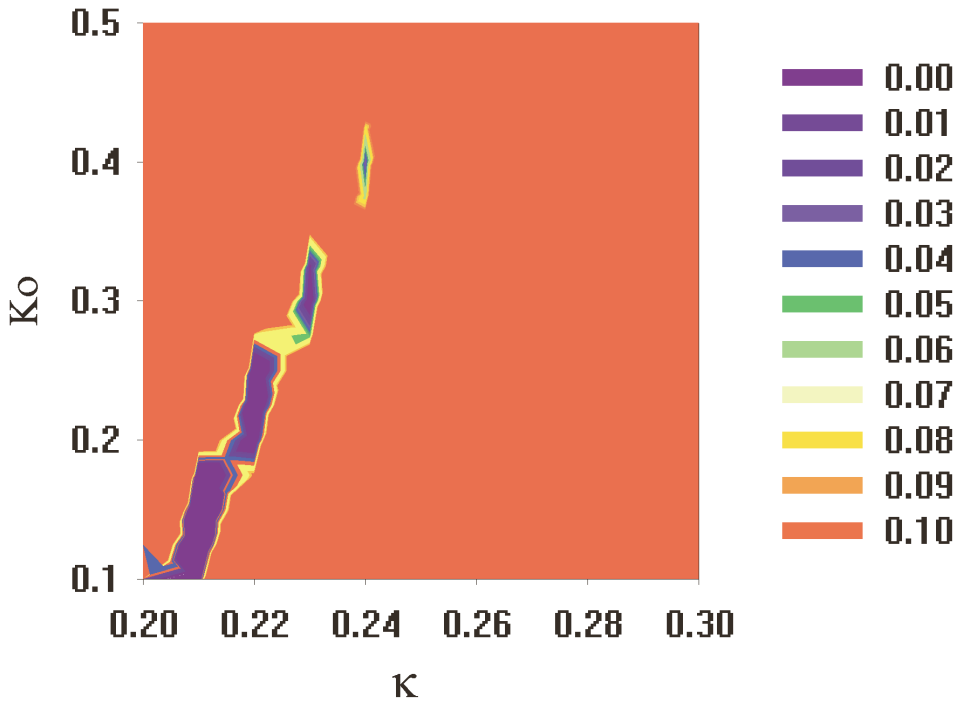

Figure 5.27. Sum of squared deviations (SSD) no more than 10% higher than the minimum SSD found by PEST (with varying K_o and κ).

Table 5.6 Revised summary of material parameters for best fit of elastic re-loading compression line

Test	M	λ	κ	ν	K_o
C	2.2	0.48	0.20	0.29	0.055

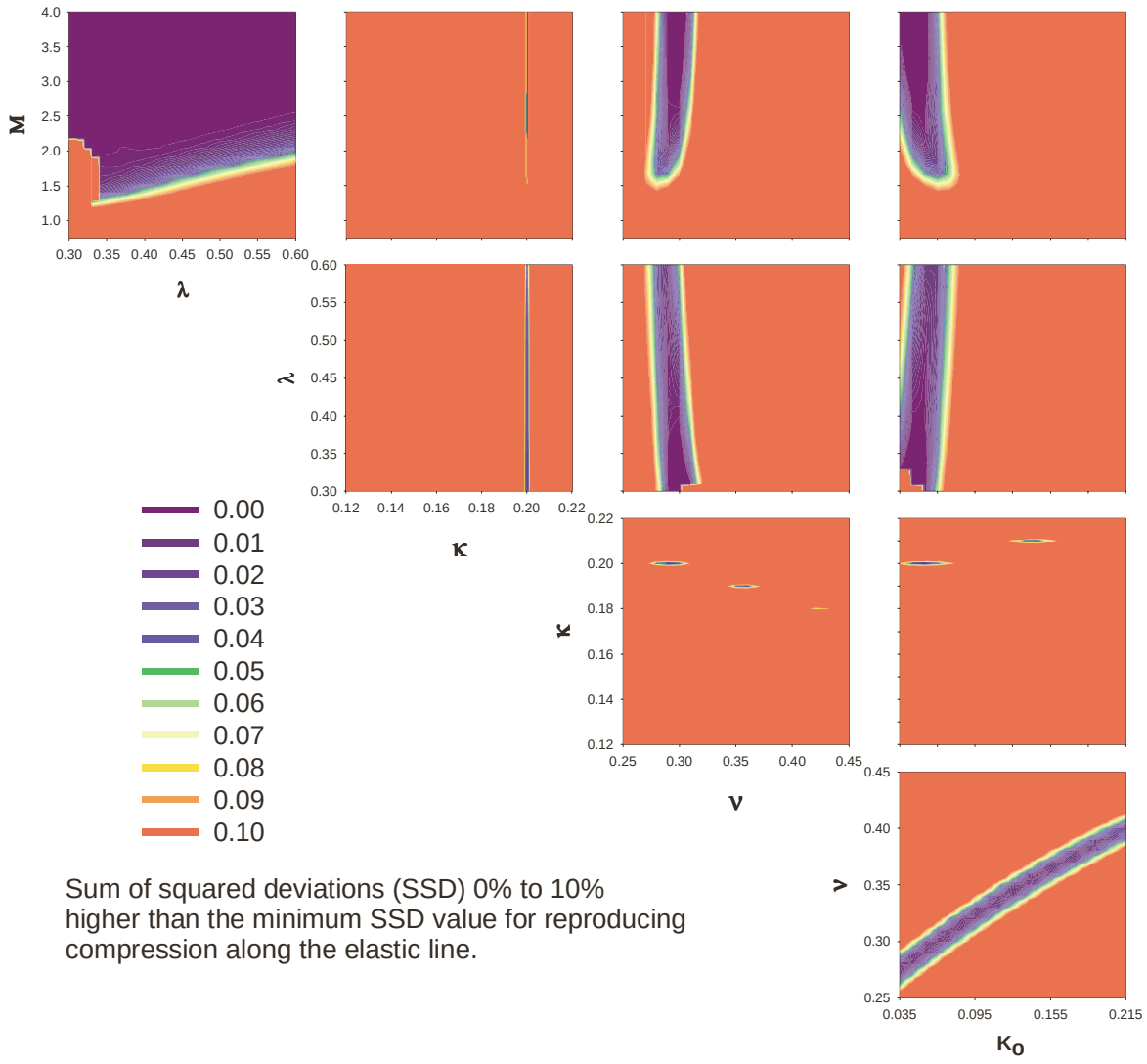

Figure 5.28 Sum of squared deviations for compression along the elastic line.

5.4.3 Indirect parameter estimation from shearing step data

Shown in Table 5.7 are the material parameters found by PEST to give the best fit of the shearing behaviour of a normally consolidated final bagasse sample (both the shear stress versus shear strain data and the specific volume versus shear strain data). Shown in Figure 5.29 and Figure 5.30 are the resultant fits.

Table 5.7 Summary of material parameters for best fit of the shearing behaviour of a normally consolidated final bagasse sample.

Test	M	λ	κ	$E^{\#}$ (kPa)	ν	K_o
C	0.98	1.67	1.49	39830	0.37	0.95

$^{\#}$only at 1800 kPa

The fits are quite good, although the shear stress prediction has a small kink that is not justified by the experimental data. Table 5.8 shows the parameter correlation coefficient matrix for shearing.

Table 5.8 Correlation coefficient matrix for shearing.

	M	λ	κ	E	ν	K_o
M	**1.0**	0.06	0.06	-0.22	-0.01	-0.11
λ		**1.0**	**0.99**	-0.20	**-0.66**	**-0.93**
κ			**1.0**	-0.20	**-0.66**	**-0.94**
E				**1.0**	0.27	0.18
ν					**1.0**	**0.54**
K_o						**1.0**

The correlation coefficients in bold in Table 5.8 are those higher than the critical value of the correlation coefficient at a significance level of 95% (a value of 0.37 for the 29 experimental values given in Figure 5.29 and Figure 5.30). During shearing, M and E were not correlated to the other material parameters (magnitudes of correlation coefficients near zero) and unique values can be obtained.

Note that κ and E are two ways of representing the same material parameter and can be worked out from the elastic unloading-reloading line during the step of uniaxial compression of bagasse in a direct shear test.

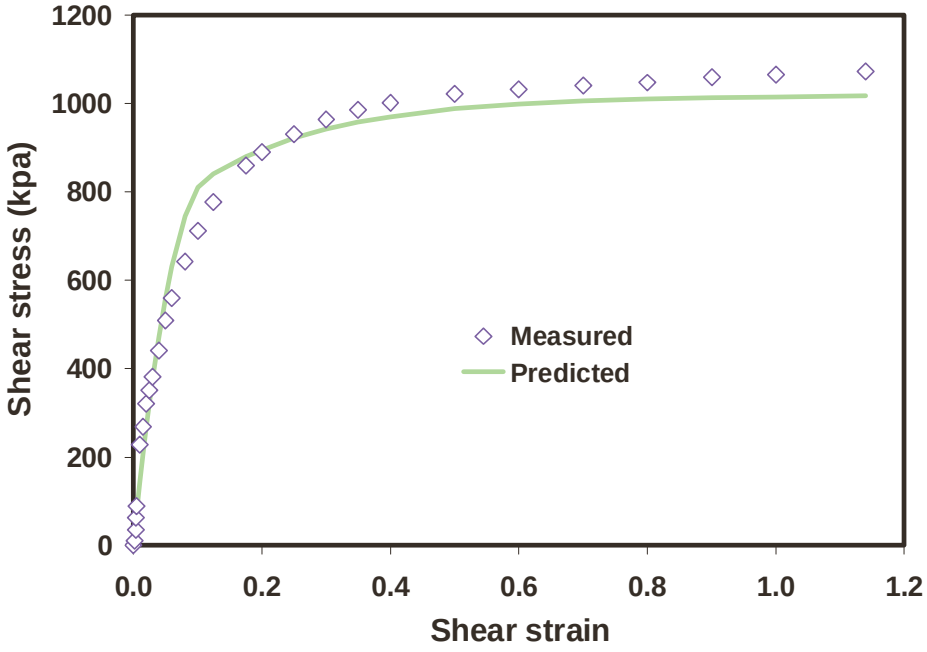

Figure 5.29. Fit of shear stress versus shear strain for normally consolidated final bagasse using PEST best fit parameters.

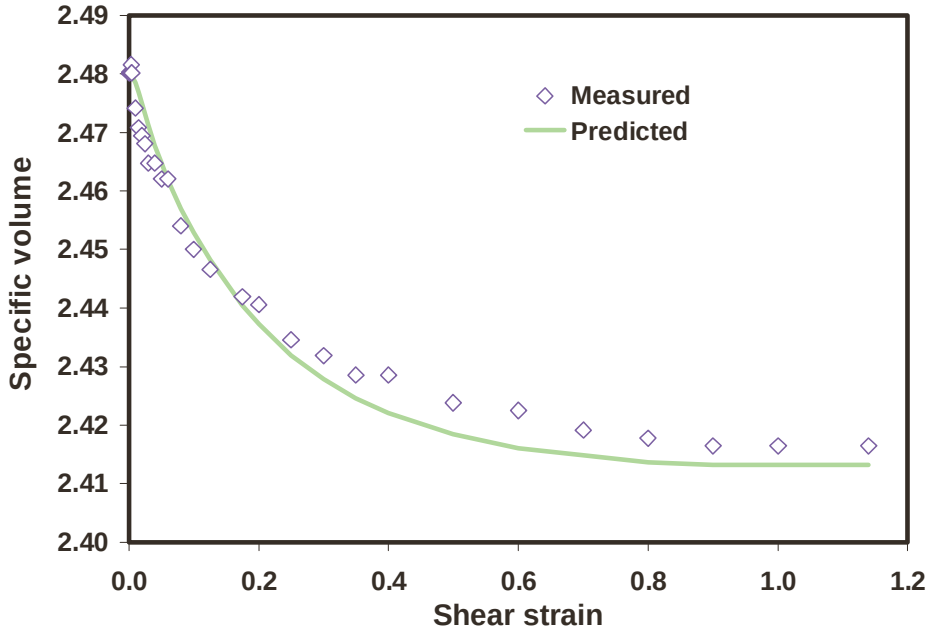

Figure 5.30. Fit of specific volume versus shear strain for normally consolidated final bagasse using PEST best fit parameters.

However, the analysis using the particular code of the Modified Cam Clay Model shows that E can also be determined from the shearing step in a direct shear test and the calculated value (40000 kPa) is quite reasonable compared to the value determined from just looking at the unloading compression data in Section 5.2 (76000 kPa), taking into account the error associated in calculating E at a particular pressure (it is strongly pressure/compaction dependent). This comes about because the shear modulus G can be calculated from the shearing step, there is a well known relationship between Young's Modulus, shear modulus and Poisson's ratio in the elastic region ($E=2G(1 + \nu)$), and the particular version of the Model uses E and ν as the two input material parameter inputs. Being able to determine E from two different steps of the direct shear test could be quite useful for checking purposes.

Figure 5.31 shows the range of parameter values that provided a sum of squared deviations (SSD) value no more than 10% higher than the minimum SSD value for fitting the shear stress and specific volume data. The fifteen subplots show that M and E are independent of the other material parameters and a limited range of values of M and E can be determined.

5.4.4 Summary of material parameters from indirect parameter estimation

The results of the indirect parameter estimation carried out in Section 5.4 are summarised here. The values of the material parameters, their limits, and the loading steps they can be determined from are shown in Table 5.9.

Table 5.9 Optimal parameter values and limits

Material Parameter	Value	Limits (SSD 10% higher than minimum)	Loading step
λ	0.97	0.96 to 0.97	Compression along normal compression line
κ^{+}	0.2	0.19 to 0.21	Compression along elastic line
E (kPa)$^{\#+}$	39830	30000 to 54000	Shearing
M	0.98	0.94 to 1.05	Shearing

$^{\#}$only at 1800 kPa, $^{+}\kappa$ and E represent the same information

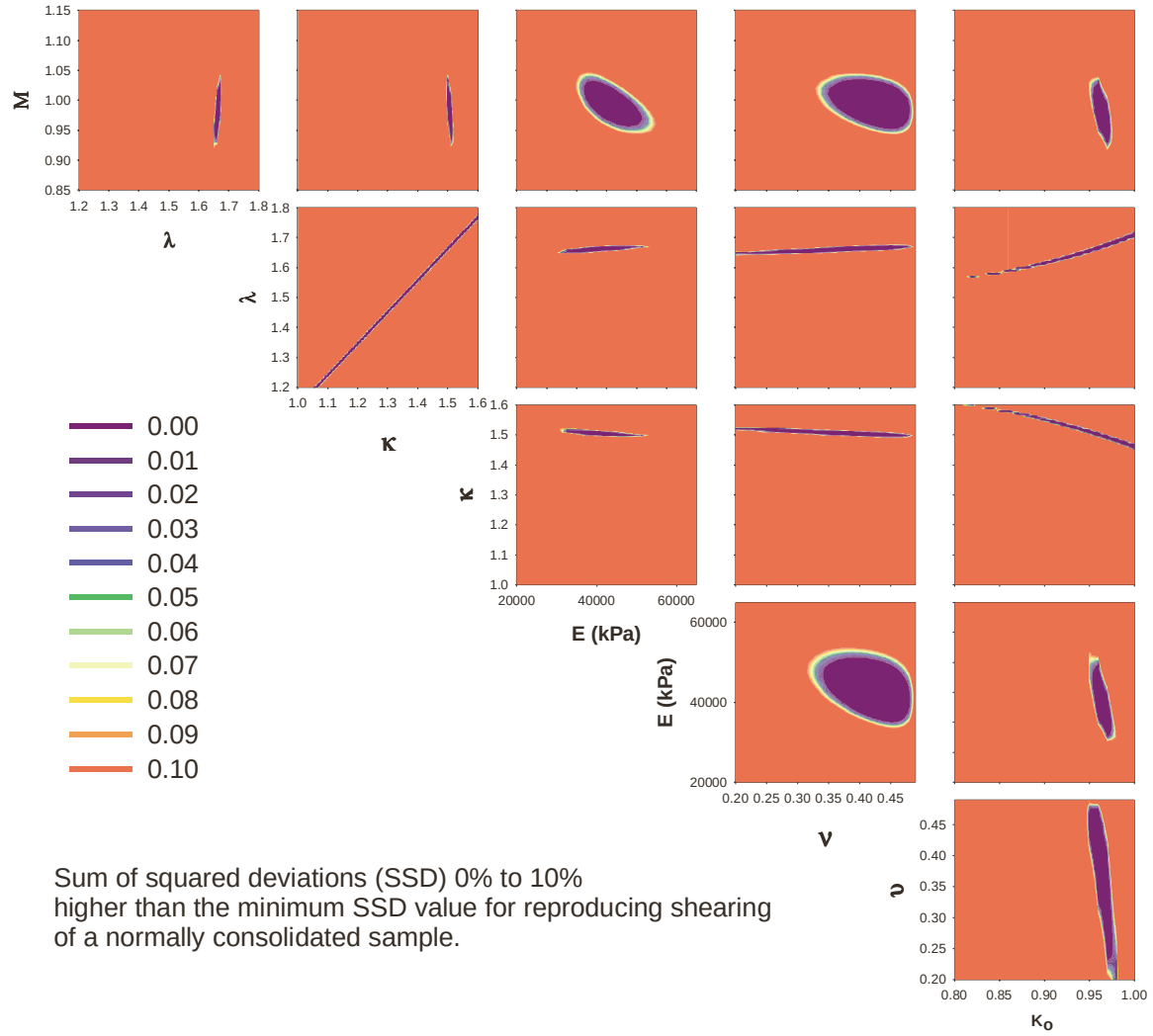

Figure 5.31 Sum of squared deviations for shearing of a normally consolidated sample.

There is quite good agreement between the values in Table 5.9 (obtained from considering only one test and using the MCC model) and the values in Table 5.1 (obtained from examining eight tests).

5.5 Performance of critical state models in use at this time

The performance and the deficiencies of two material models, the Modified Cam Clay (MCC) model and Drucker-Prager Cap (DPC) model, both including porous elasticity, were assessed. The assessment was carried out in terms of reproducing the final bagasse behaviour in the loading steps of a direct shear test (the conclusions were checked by carrying out the same exercise with first bagasse, the comparison for first bagasse was not presented). The two models are generally similar, but give slightly different predictions for expansion during shear (Hibbitt et al., 2001). Previous modelling work was discussed in Chapter 1. However, for clarity, a brief summary follows. The two models, the MCC and DPC models, had been previously used to model milling situations, with material parameter values modified from those used in soil modelling. In particular, a value for M of 3.8 had been used for prepared cane (Adam, 1997), while a value of about 1.0 is used in soil applications. Higher values for M of 2.5 and 3.8 had arisen from investigations at James Cook University (see papers by Adam (1997), Adam et al (1997a, b), Leitch et al. (1997), Loughran and Adam (1998), Owen et al (1998), Downing (1999) and Downing et al (1999)). Adam et al. (1997a, b) and Loughran and Adam (1998) used the same experimental data (uniaxial tests and triaxial tests) to derive values of either 2.5 and 3.8 for M. The triaxial tests were carried out by Leitch (1996), whose main body of work was isotropic compression triaxial tests, but also included a small number of deviatoric triaxial tests.

The values of M of 2.5 and 3.8 given in these references were explained by citing: a. experimentally observed behaviour of small lateral strains during uniaxial compression, b. no measurable shear failure in uniaxial or triaxial tests and c. the predictions from at least four critical state models, including the MCC and DPC models. However, Leitch (1996) referred to his deviatoric triaxial test results and, in his Section 4.6 entitled ‘Towards a constitutive relation for prepared cane’ stated that ‘as already noted, no quantitative results are presented because the test results were considered to be unreliable’. This was because of testing problems, including

the development of high juice pressures and small height to diameter ratios in the test sample. Schembri et al (1998) examined Leitch's results and estimated that the 'values of M ranged from 0.07 to 2.0'. Considering the above, it is unlikely that a value of M can be obtained with confidence from the Leitch (1996) deviatoric test results. Section 5.4 has shown that it is unlikely that M values can be determined from a uniaxial compression test on final bagasse or prepared cane, as M is strongly correlated to other parameters, including K_o. Consequently, it is unlikely that a value of M of 2.5 or 3.8 can be determined from the available experimental data. Values of M higher than the ones presented in Chapter 4 may be obtained from direct shear tests with the shearing parallel to the initial direction of compression. As stated previously, such tests should be carried out to investigate this possibility. Attempts to obtain funding to carry out such tests have been unsuccessful.

It is noted that values of M as high as 3.8 and 4.0 imply physically impossible friction angles. A maximum value for M is 3.0, for which the corresponding friction angle for triaxial compression is 90 degrees. Following Carter (2003), the physical absurdity of values of M of 3.8 and 4.0 is noted. However, since these values have been extensively used in many modelling papers, it has been necessary in this investigation to address the use of such values and the results of their use.

As shown in Table 4.7 in Chapter 4, experimental values were determined for M. The values were 1.1 for final bagasse, 1.2 for first bagasse, and 1.3 for prepared cane. In this section, the performance of both the MCC and DPC models will be examined for M values of 1.1 and 3.8, noting that these two values imply significantly different shapes for the yield surface. For the DPC Model with M=3.8, a friction angle of 75.26^o (which is difficult to justify, as noted by Williams, 2003) and a ratio of the minor to major ellipse axes of 0.2632 (R=1/M) were adopted (Downing, 1999). It is noted that Multi-element simulations were carried out using the ABAQUS finite element analysis software. The simulation predictions were compared against the final bagasse experimental data previously shown in this chapter.

Figure 5.32 shows a plot of specific volume versus effective vertical pressure for the initial compression of final mill bagasse. Also shown are predictions using the

DPC model (for this case, predictions from the MCC model were basically identical to those from the DPC model). It is shown that, for particular combinations of M and K_o, excellent fits to the measured values of the normal compression line were obtained. As stated previously in Section 5.2, in uniaxial compression the Modified Cam Clay (MCC) model and the Drucker-Prager Cap (DPC) model will enforce a value of K_o for a particular value of M.

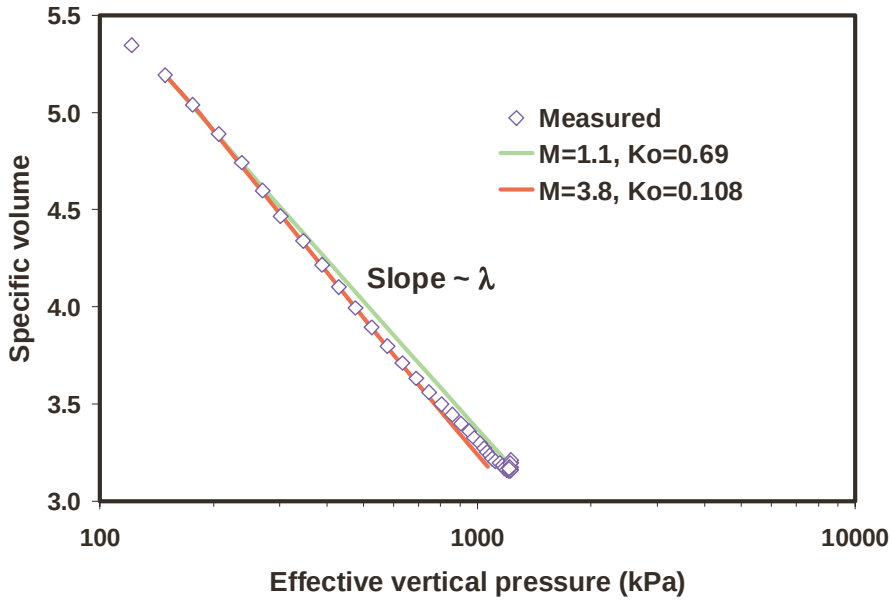

Figure 5.32. Reproducing compression behaviour of final mill bagasse using the DPC model.

Figure 5.33 shows the specific volume versus effective vertical pressure relationship for final bagasse unloaded from a pressure of 2000 kPa, with a slope of κ for the measurements. Also shown are the predictions for the MCC and DPC models, for the input parameters that were previously successful in reproducing final bagasse behaviour in compression loading along the normal compression line. It is shown that poor predictions for unloading were obtained in all cases. The use of M of 1.1 resulted in too little expansion being predicted at most pressures. A sudden increase in expansion in the DPC prediction is shown at a pressure of about 200 kPa, when the yield surface was reached in the shear failure region.

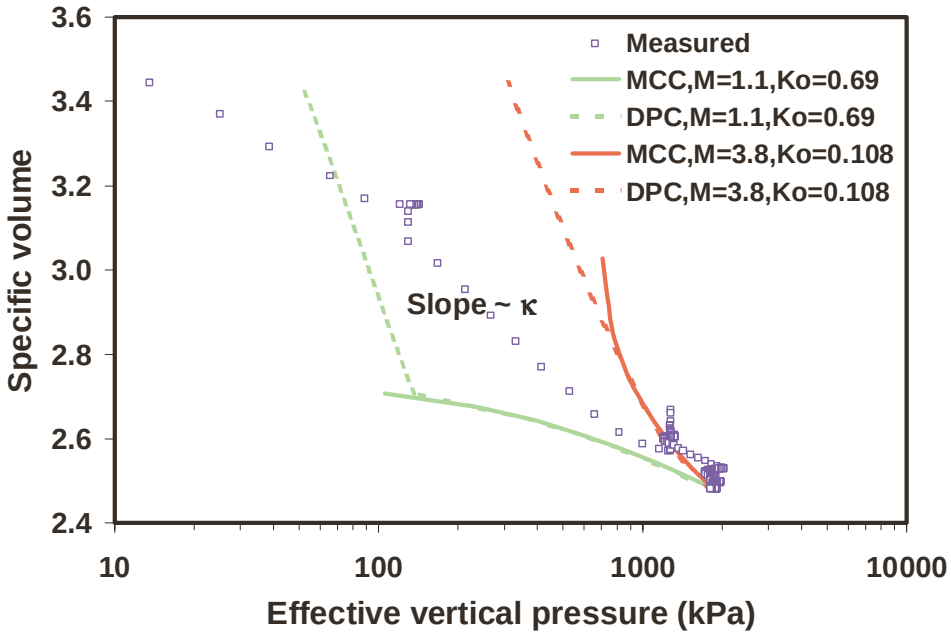

Figure 5.33. Reproducing compression unloading behaviour of final mill bagasse using the MCC and DPC models.

Numerical problems were experienced with both models at a high degree of unloading. The use of M of 3.8 resulted in far too much expansion being predicted. For both M=1.1 and M=3.8 the predictions should have followed the measured unloading line with a slope of κ. The MCC and DPC results eventually diverge because the yield surfaces on the 'dry' side are different. The DPC yield surface is reached first.

As shown in Figure 5.34, the DPC model gave excellent fits to the measured data in reloading (the MCC model predictions were very similar and are not shown). Once the maximum effective vertical pressure previously experienced by the bagasse was reached, the loading was predicted to continue along the normal compression line (as has been shown to occur experimentally).

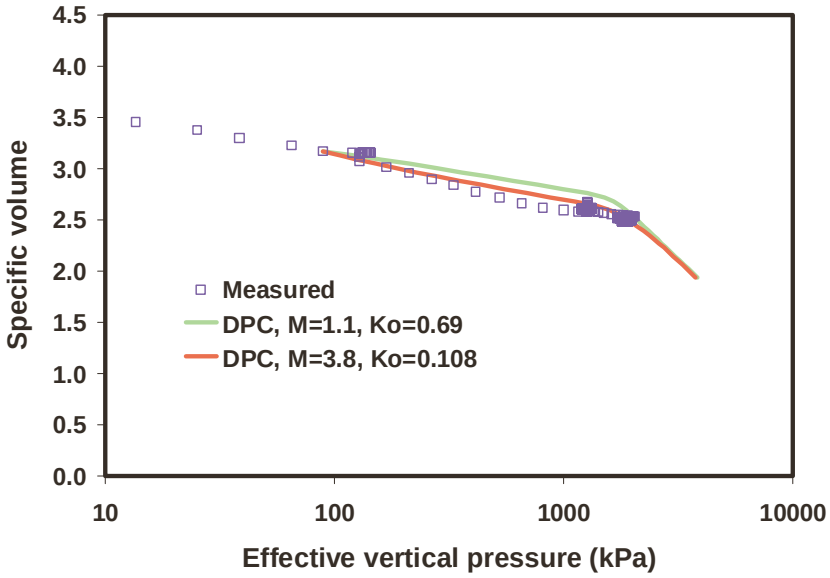

Figure 5.34. Reproducing compression re-loading behaviour of final mill bagasse using the DPC model.

The measured shear behaviour for a normally consolidated final bagasse sample is shown in Figure 5.35 and Figure 5.36 as are the predictions for the DPC model (the predictions for the MCC model are not shown since for an M of 1.1 they were very similar to the DPC model and for an M of 3.8 the predictions were identical). The shear stress was poorly predicted (Figure 5.35) while the change in specific volume due to shear strain was very poorly predicted (Figure 5.36). It is emphasised that better fits of the shear behaviour can be obtained by adjusting the value of, for example K_o, but not with the combinations of M and K_o enforced by the MCC and DPC models when modelling uniaxial compression of normally consolidated prepared cane or final bagasse. If linear elasticity was used instead of porous elasticity for an M value of 3.8 the predictions were worse still (not shown).

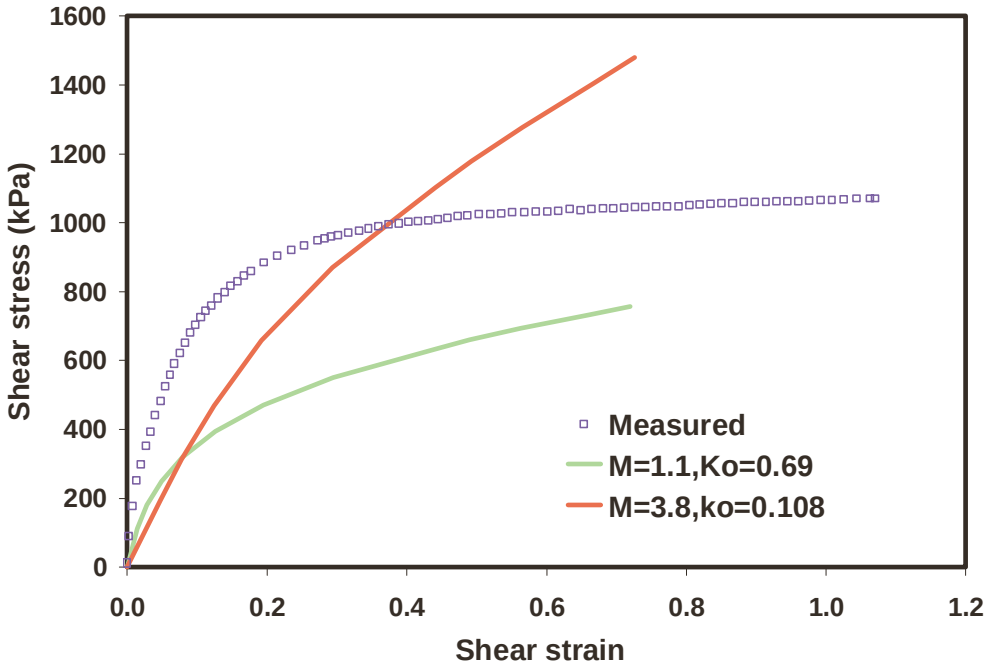

Figure 5.35. Reproducing shear stress versus shear strain behaviour of normally consolidated final mill bagasse using the DPC model.

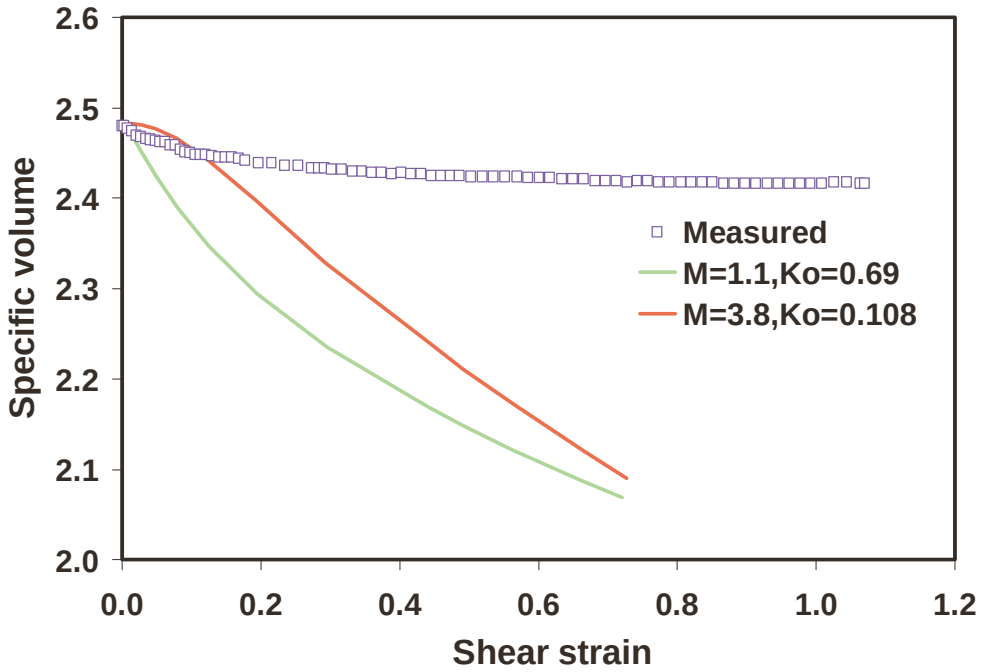

Figure 5.36. Reproducing specific volume versus shear strain behaviour of normally consolidated final mill bagasse using the DPC model.

In summary, the material models reproduce compression well, but are relatively poor at modelling unloading and shear. A major conclusion from this work is therefore that the MCC and DPC models cannot successfully model all the loading conditions relevant to milling with a single set of parameter values. It is consequently likely that behaviour after a nip and in shearing zones will not be well modelled using either the MCC or DPC models. A material model should be able to predict the four loading conditions described above fairly well in order to confidently predict milling behaviour.

In addition, the shear behaviour of a heavily consolidated bagasse sample needs to be predicted and tension behaviour may need to be modelled (Downing, 1999).

A better material model is required. In this chapter, a platform has been established to identify such a model by:

1. determining the magnitudes of physically meaningful material parameters, and
2. identifying the limitations of currently used models.

5.6 Summary of Chapter 5

Sections 5.2 and 5.3 showed which loading steps could be predicted using a single element Modified Cam Clay material model and which loading steps required the use of a multi-element model. These are:

The single element model predicted -

1. Compression along the normal compression line.
2. Compression when unloading along the unloading-reloading line.
3. Compression when reloading along the unloading-reloading line.
4. Shearing of a normally consolidated sample.

The multi-element model predicted -

Shearing of an over-consolidated sample with an over-consolidation ratio of 5.0.

In Section 5.4 material parameters were determined by using the experimental results from a single direct shear test in combination with a single element Modified Cam Clay model and a parameter estimation package called PEST. There was quite

good agreement with the magnitudes of the material parameters obtained simply by analysing the experimental results of the set of eight shear tests carried out in Chapter 4 and in Section 5.2. The analysis also showed which material parameters could be confidently determined from each of the loading steps in a direct shear test: lambda (λ, the slope of the normal compression line) from compression, kappa (κ, the slope of the elastic line) from unloading, and the slope of the critical state line (M) and Young's Modulus (E) from shear. The loading steps are analogous to those that occur during the crushing of cane.

The variation in the magnitudes of material parameters in loading situations where shearing is parallel to the direction of compression is still to be determined.

Section 5.5 showed that current models cannot with a single set of parameter values successfully model all the loading and unloading conditions relevant to milling. The Modified Cam Clay and Drucker-Prager Cap models can predict compression loading well by using particular combinations of parameter values, but the predictions of unloading behaviour, shear behaviour and the change in volume due to shear are poor. This is likely to result in poor predictions when modelling the whole mill, which involves complex loading conditions. For these circumstances, a material model will be required which will model different loading conditions using the same experimentally measured material parameters. A platform has been established on which the search for such a material model can be carried out.

6 Chapter 6 - Comparison of modified direct shear test geometry with classical split box geometry

6.1 Issues with modified direct shear test geometry

As discussed in Chapter 2 and further developed in Chapters 3 and 4, the geometry of the modified direct shear test used had a bottom plate with a rough surface on its top surface. The rough surface was P24 sandpaper above which the box containing the sample was suspended. The horizontal movement of the bottom plate provided the shearing action. In a classical soil direct shear test, the bottom plate has an insert such that there is as much sample below the shearing plane as there is above it. The use of the flat bottom plate with most of the sample above the shearing plane (apart from a layer that remained attached to the bottom rough sandpaper surface) in the experimental tests at pressure feeder compactions followed previous work on the surface roughness required to grip prepared cane. It was used to differentiate between internal shear of prepared cane and slip at the surface (Plaza et al, 1993, Plaza and Kent, 1998) and to show that the shear strength of prepared cane (Plaza et al, 1993, Plaza and Kent, 1997) could be represented by the Coulomb failure criterion (as described for soils by Craig, 1987). At the time (late 1998) when plans were being made to carry out direct shear tests to measure bagasse behaviour at pressure feeder compactions, it was felt that such a geometry had a good probability of measuring the critical state behaviour of prepared cane and bagasse, if such behaviour existed. Subsequently, as shown in Chapters 3 and 4, the geometry was successful in showing that bagasse exhibited critical state behaviour.

A case is made in this investigation that the deformation of the bagasse samples, even during shearing, occurs throughout the sample (not just the thickness of the material at the two millimetre gap between the box and the rough surface on the bottom plate). Actual deformations inside the box could not be observed. A finite element analysis of the test method carried out in this chapter supports this interpretation of the results.

The effect of the modified geometry on the experimental results was seen to be an issue. The experimental results were used to determine magnitudes of material parameters, to determine how adequate existing material models were, and in the

future were to be used to search for material models that better reproduced bagasse behaviour, as well as providing inputs to a model of a milling unit. An assessment of the performance of the test at this time was seen to be useful, both in understanding what happened to the bagasse sample inside the box during a test, and in understanding variations in the measurements due to the equipment used.

Also, as discussed in Chapter 2 (and repeated here for clarity), a major criticism of the direct shear box has been that the stresses and strains in the sample are non-uniform (Rowe, 1969, Potts et al., 1987). Improvements to the direct shear test, with the aim of reducing non-uniformity, have been reported in the soil mechanics literature, for example, by Jewell and Wroth (1987) and Shibuya et al (1997). Potts et al. (1987) stated that 'the stress state in an ideal shear box in which strains are uniform is that of simple shear' while Wroth (1987) stated that 'Roscoe (1953) devised the simple shear apparatus with the purpose of applying uniform conditions of simple shear'. Potts et al. (1987) compared the behaviour in a direct shear test to that in a simple shear test, including a detailed analysis using finite element models. Their conclusion was that 'the analyses thus show that the non-uniformities within the direct shear box sample have little effect, and with surprisingly little error the test may be interpreted as if it were a simple shear test'. However, they also concluded that the local state of stress and strain within the direct shear test was far from uniform and that 'highly stressed zones propagate from the edges of the box at an early stage of loading' while 'the strains and stresses within the failure zone at the peak in the direct shear box are surprisingly uniform'. Potts et al attributed the uniformity at failure to the absence of progressive failure, and stated that 'progressive failure occurs when loading produces non-uniform mobilisation of strength'. The issues of 'highly stressed zones propagating from the edges of the box' and 'non-uniform mobilisation of strength' are highly relevant and undesirable when testing a material which has high compressibility and low stiffness such as prepared cane and bagasse (or peat for that matter) in a direct shear test.

The computer modelling carried out in Chapter 4, both for quasi-analytical single element models and multi-element models, assumes that the shearing action is basically that of simple shear. In reality the stresses and strains in a direct shear test, whether a classical split box test or a modified geometry test, are not uniform.

Therefore, it was decided to investigate the performance of the modified geometry and classical split box geometry and to compare them against each other. The investigation was based on finite element modelling. The overall predictions were also compared to the predictions from the quasi-analytical single element model described in Chapter 5. This approach is believed to be sound: it was shown in Section 5.2.4 that a Modified Cam Clay material model with an M of 1.1 and a K_o of 0.2 (corresponding to bagasse) can model the main characteristics of shear stress and volume change during shearing of a normally consolidated final bagasse sample, even though some inadequacies were identified in the detail of the predictions.

Grid independence was tested by modelling a coarse mesh and a fine mesh, as well as the single element model.

The multi-element simulations of the split box geometry and modified geometry were carried out using the ABAQUS finite element analysis software (Hibbit et al., 2001). Computer simulations of the shear phase at constant vertical pressure were carried out. The side walls of the boxes and the bottom plate were modelled as rigid surfaces while the top plate was modelled as mild steel elements. The top plate was not allowed to rotate in the models. For both ease of use and safety, the top plate in the experimental direct shear tests on bagasse was rigidly fixed to the press ram and was not able to rotate. It is noted that the classical soil shear box had a top plate that could rotate. However, there is quite a bit of literature that concludes that a fixed top plate will result in improved uniformity in the sample and should be used, for example, Wernick (1977), Jewell and Wroth (1987), and Shibuya et al (1997). The use of a fixed top plate in the bagasse investigations is therefore consistent with those findings in the soil mechanics literature.

The modelling was carried out using two-dimensional plane strain elements. The investigation was split into two stages:

a. With a normally consolidated final bagasse sample, bottom part displaced horizontally by 13 mm for both the split box geometry and the modified geometry using a coarse mesh and a fine mesh. Subsequently, simulations

were carried out with the bottom part displaced horizontally by 19.5 mm and using a coarse mesh.

b. With an over-consolidated final bagasse sample, bottom part displaced horizontally by 16 mm for both the split box geometry and the modified geometry using a fine mesh.

6.2 Direct shear test simulations for normally consolidated final bagasse with a sideways displacement of 13 mm

The material modelled was a sample of normally consolidated final bagasse 36.95 mm high (after initial compression to a vertical pressure of 1800 kPa). The values of the input material parameters for the particular sample and initial stress conditions are shown in Table 6.1. The surfaces of the top plate and bottom plate contacting the bagasse had a coefficient of friction of 0.6 (P24 sandpaper) while the side walls had a coefficient of friction of 0.3 (smooth mild steel) (data from Plaza and Kent, 1997, and Plaza et al., 2001).

Table 6.1. Material parameters and initial stress conditions for normally consolidated final bagasse sample

M	λ	κ	ν	Vertical stress (kPa)	K_o
1.1	0.93	0.169	0.3	1800	0.2

Two different meshes were used. The coarse mesh was 6 elements high by 12 elements wide. For the coarse mesh, each element was initially approximately 6.2 mm vertically and 23.3 mm horizontally. The fine mesh was 13 elements high by 50 elements wide. For the fine mesh, each element was initially approximately 2.8 mm vertically and 5.6 mm horizontally.

A sideways displacement of 13 mm (a shear strain of about 0.35) was applied to the bottom part. The predictions are shown in Figure 6.1 to Figure 6.6 (coarse mesh) and in Figure 6.13 to Figure 6.18 (fine mesh) for the split box geometry, and in Figure 6.7 to Figure 6.12 (coarse mesh) and in Figure 6.19 to Figure 6.24 (fine mesh) for the modified box geometry. The vertical stress, horizontal stress, shear stress, shear strain, confining pressure (the average of the three normal stresses), and void ratio are shown on the predicted deformed geometry.

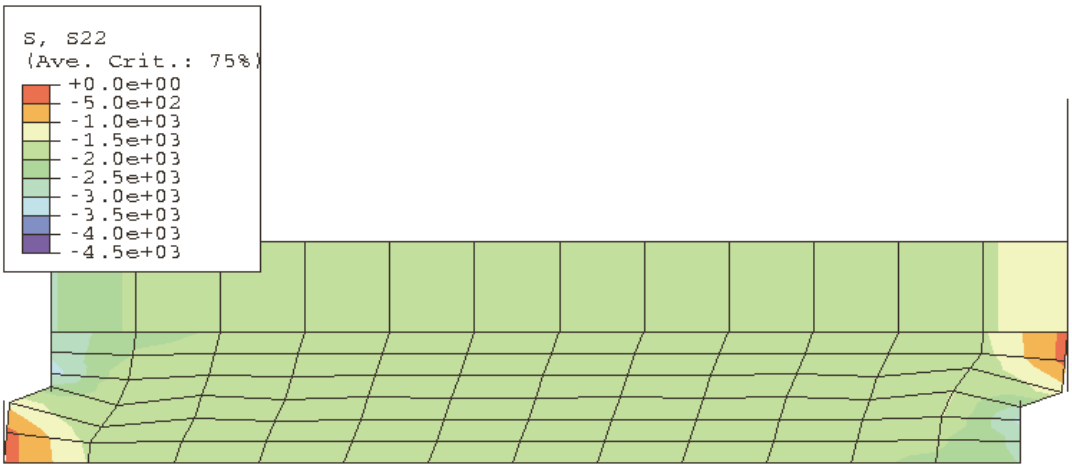

Figure 6.1. Vertical stress (kPa) for normally consolidated final bagasse, split box geometry, displacement 13 mm, coarse mesh.

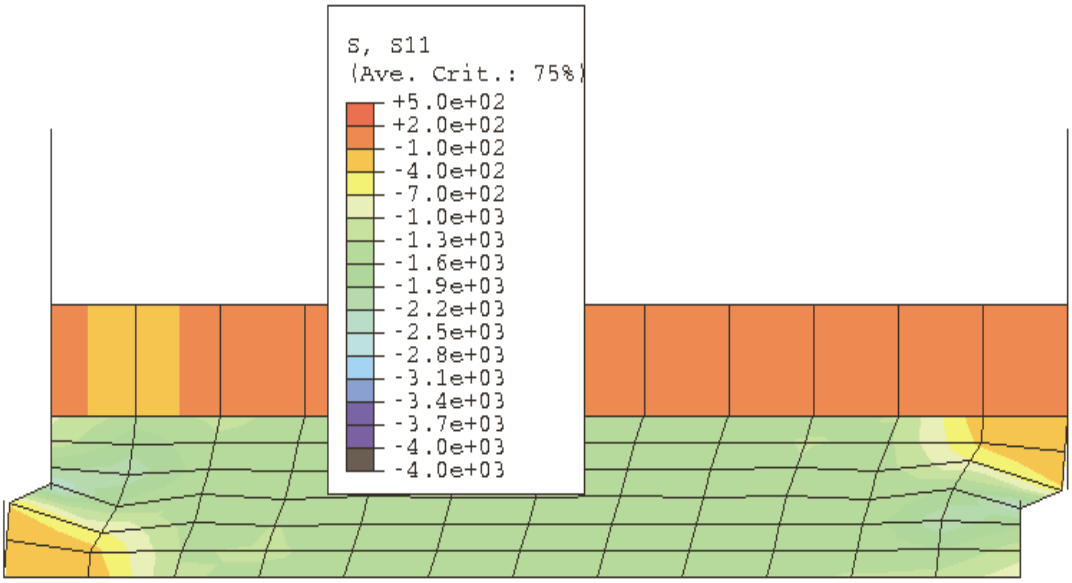

Figure 6.2. Horizontal stress (kPa) for normally consolidated final bagasse, split box geometry, displacement 13 mm, coarse mesh.

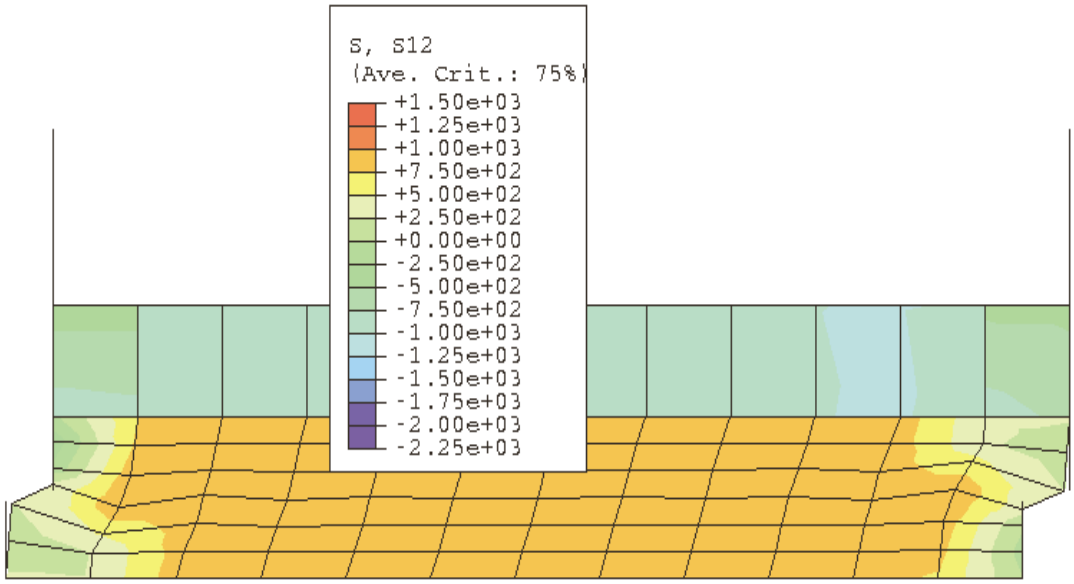

Figure 6.3. Shear stress (kPa) for normally consolidated final bagasse, split box geometry, displacement 13 mm, coarse mesh.

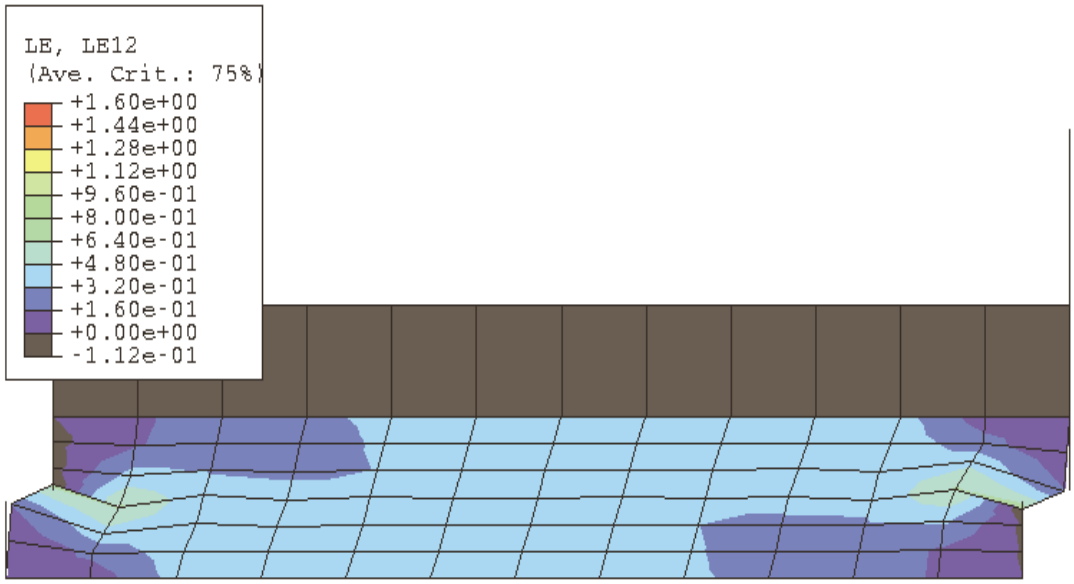

Figure 6.4. Shear strain for normally consolidated final bagasse, split box geometry, displacement 13 mm, coarse mesh.

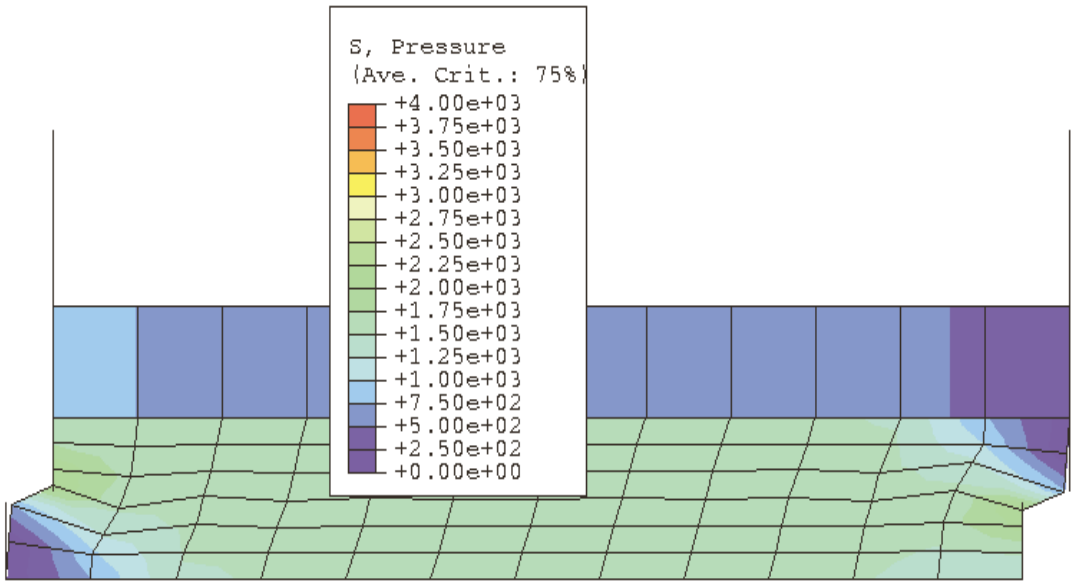

Figure 6.5. Confining pressure (kPa) for normally consolidated final bagasse, split box geometry, displacement 13 mm, coarse mesh.

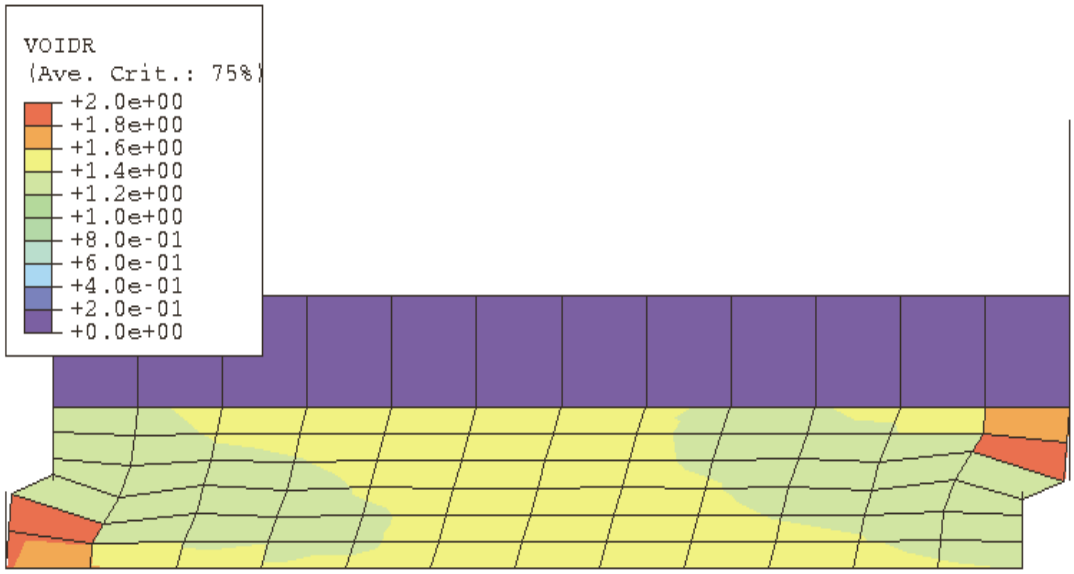

Figure 6.6. Void ratio for normally consolidated final bagasse, split box geometry, displacement 13 mm, coarse mesh.

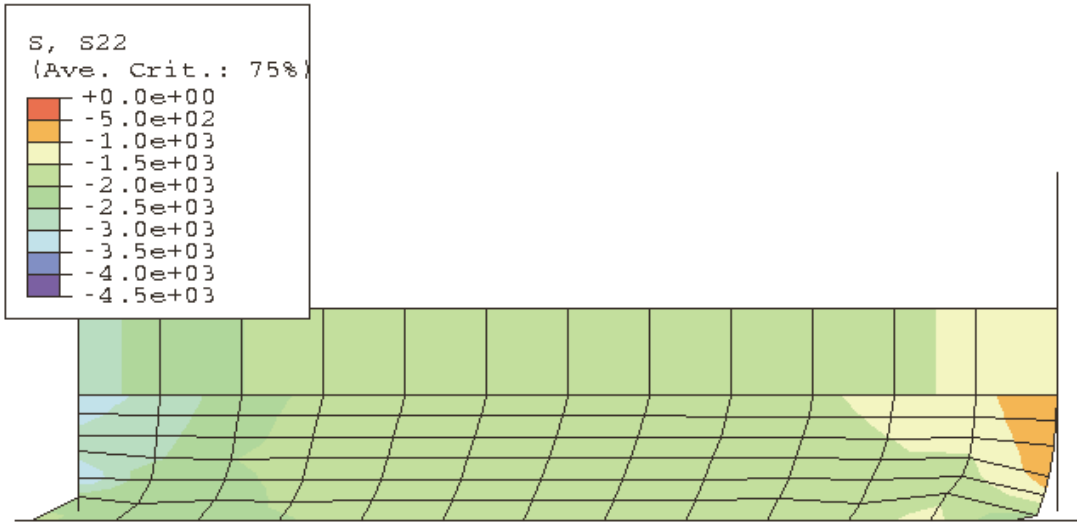

Figure 6.7. Vertical stress (kPa) for normally consolidated final bagasse, modified box geometry, displacement 13 mm, coarse mesh.

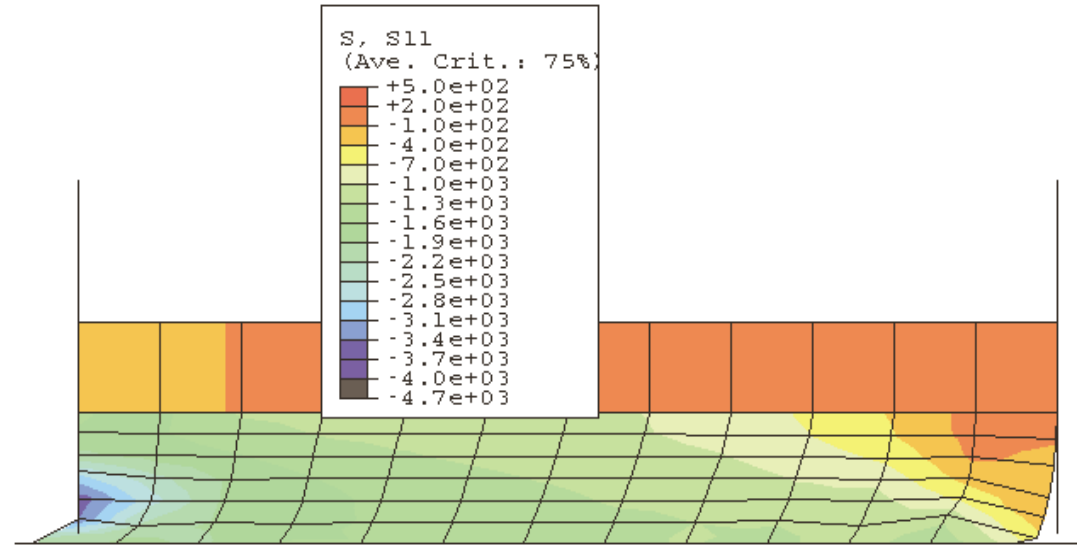

Figure 6.8. Horizontal stress (kPa) for normally consolidated final bagasse, modified box geometry, displacement 13 mm, coarse mesh.

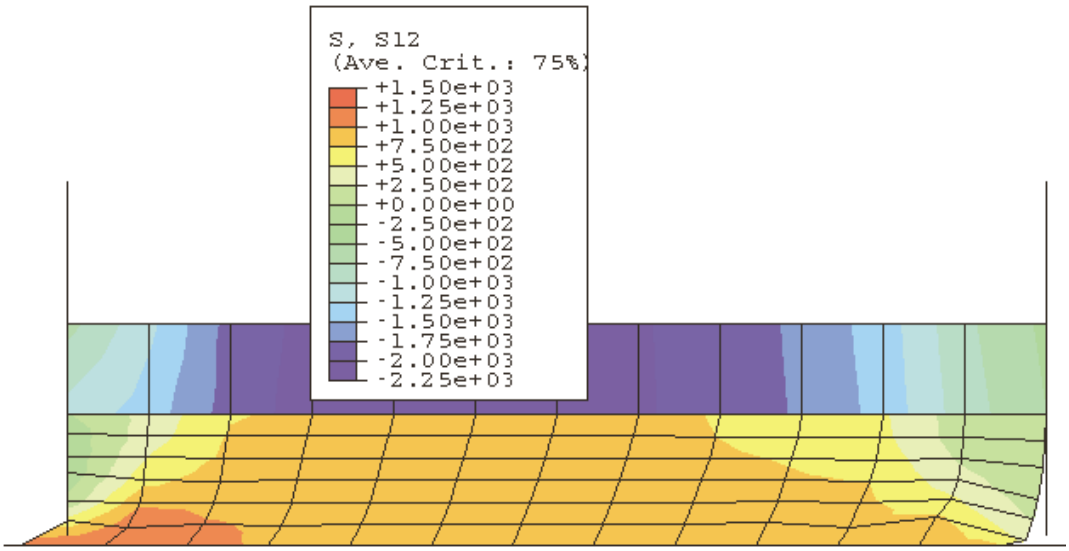

Figure 6.9. Shear stress (kPa) for normally consolidated final bagasse, modified box geometry, displacement 13 mm, coarse mesh.

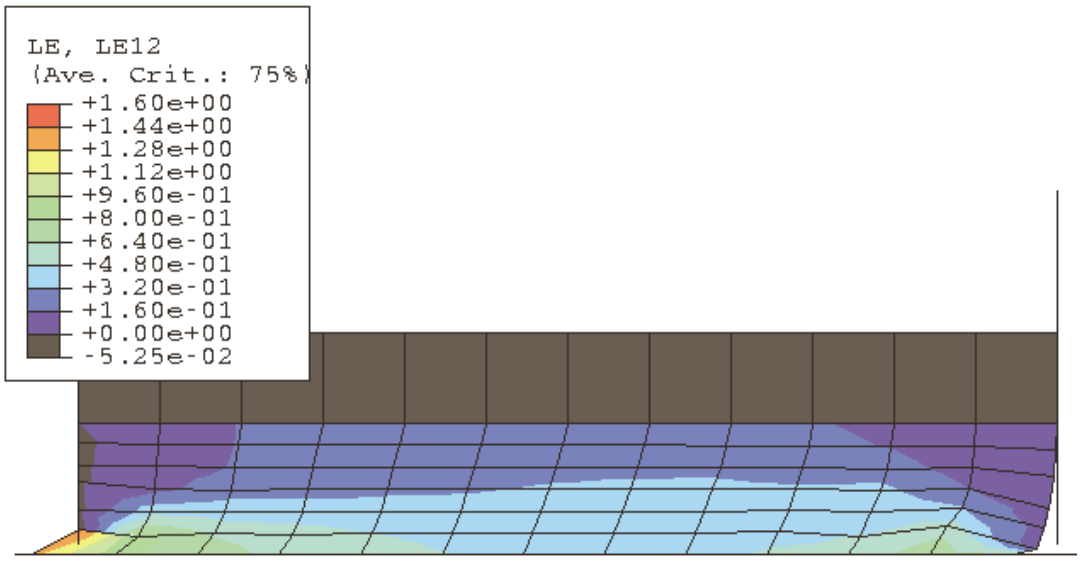

Figure 6.10. Shear strain for normally consolidated final bagasse, modified box geometry, displacement 13 mm, coarse mesh.

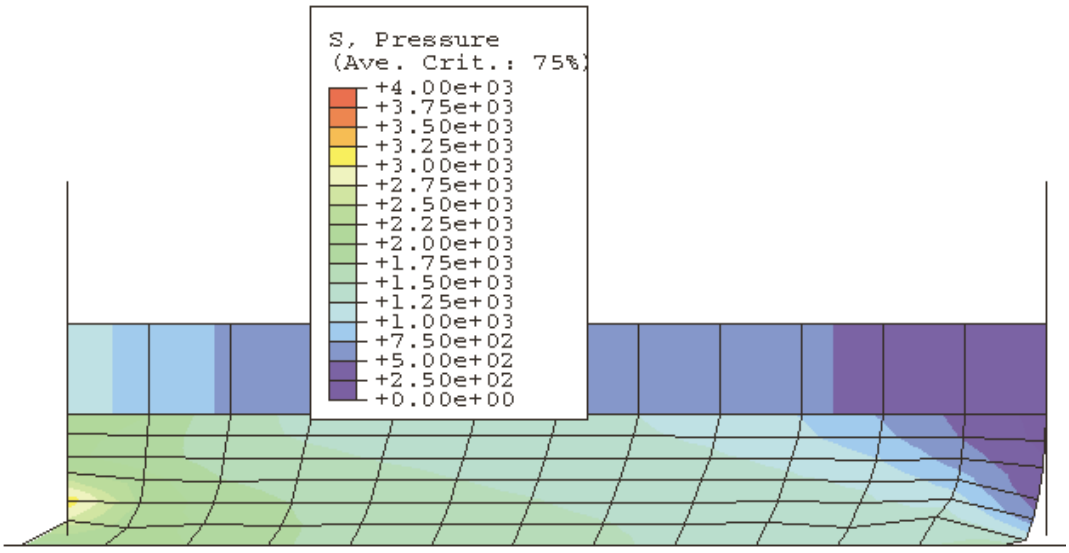

Figure 6.11. Confining pressure (kPa) for normally consolidated final bagasse, modified box geometry, displacement 13 mm, coarse mesh.

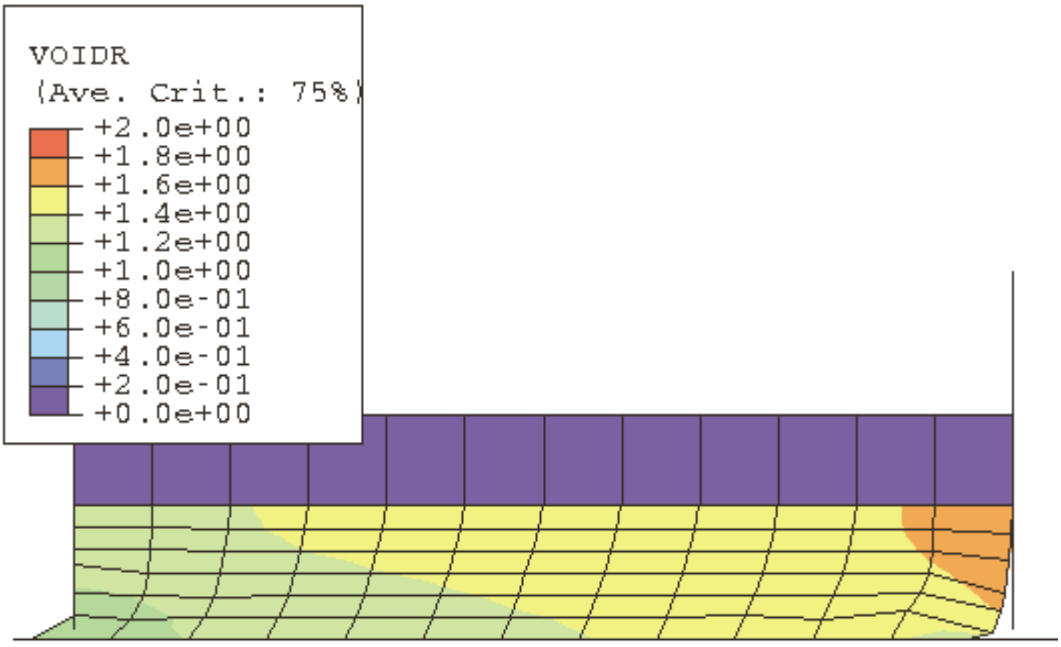

Figure 6.12. Void ratio for normally consolidated final bagasse, modified box geometry, displacement 13 mm, coarse mesh.

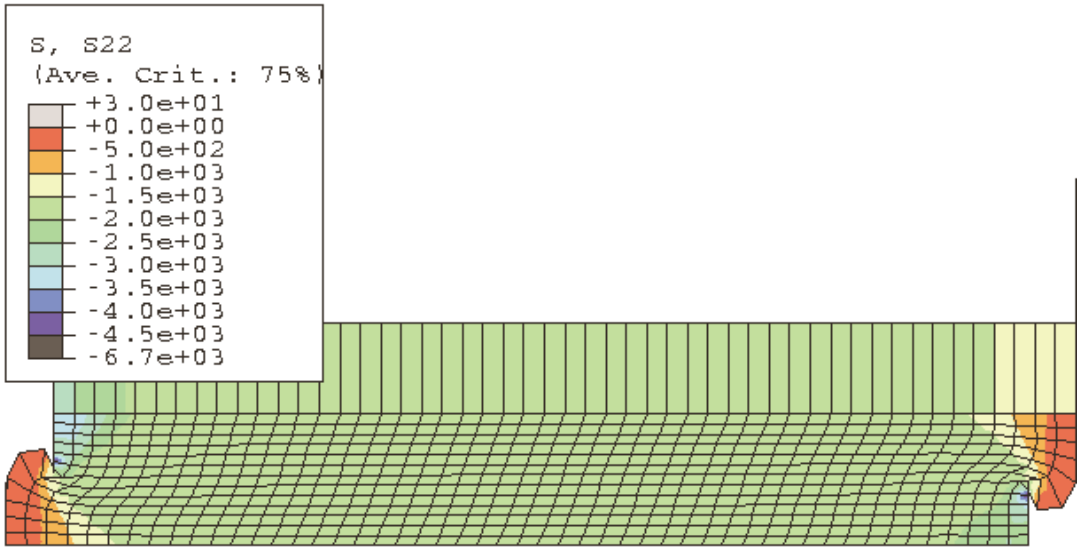

Figure 6.13. Vertical stress (kPa) for normally consolidated final bagasse, split box geometry, displacement 13 mm, fine mesh.

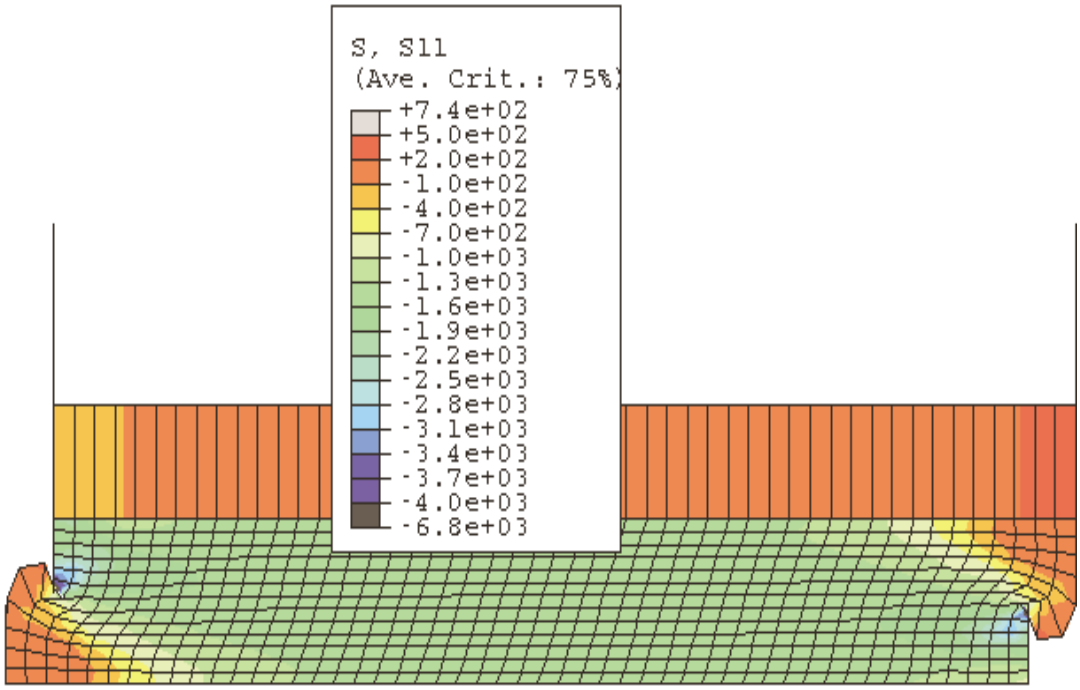

Figure 6.14. Horizontal stress (kPa) for normally consolidated final bagasse, split box geometry, displacement 13 mm, fine mesh.

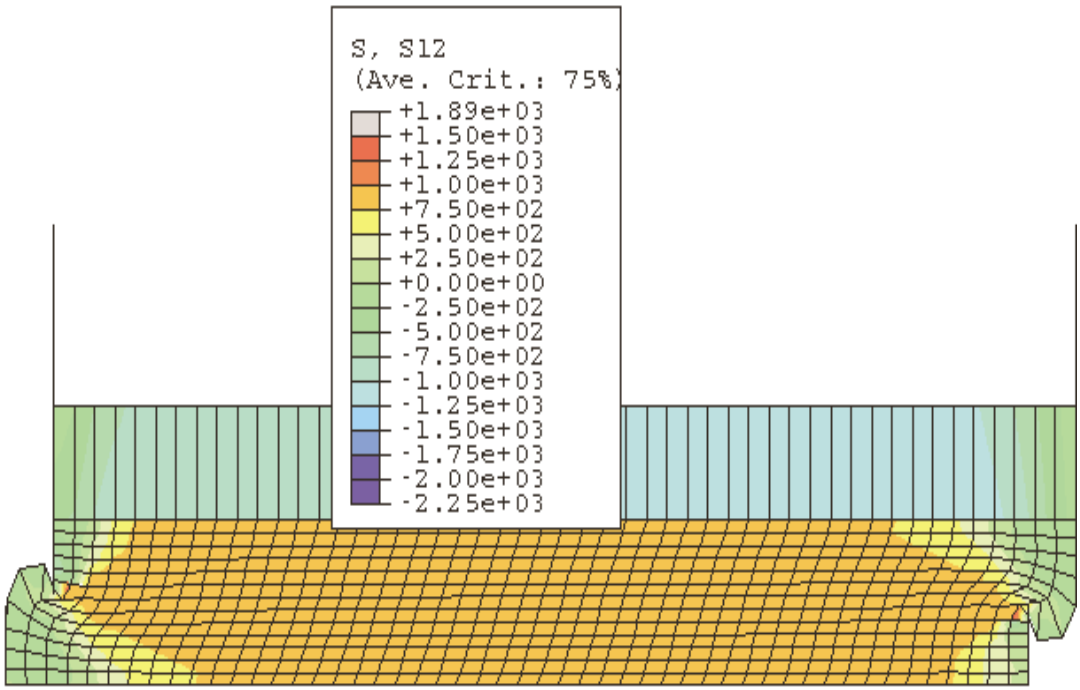

Figure 6.15. Shear stress (kPa) for normally consolidated final bagasse, split box geometry, displacement 13 mm, fine mesh.

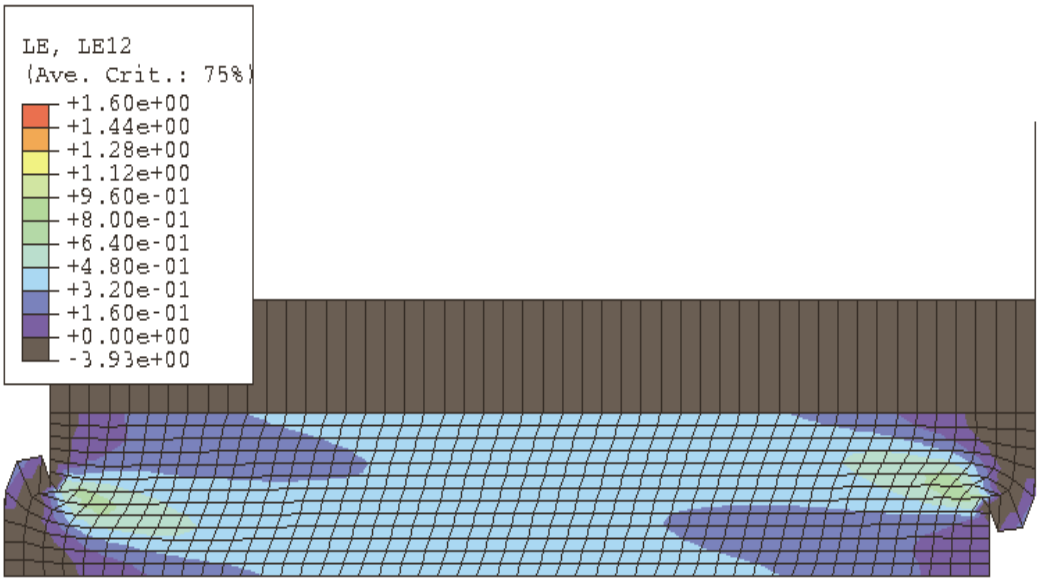

Figure 6.16. Shear strain for normally consolidated final bagasse, split box geometry, displacement 13 mm, fine mesh.

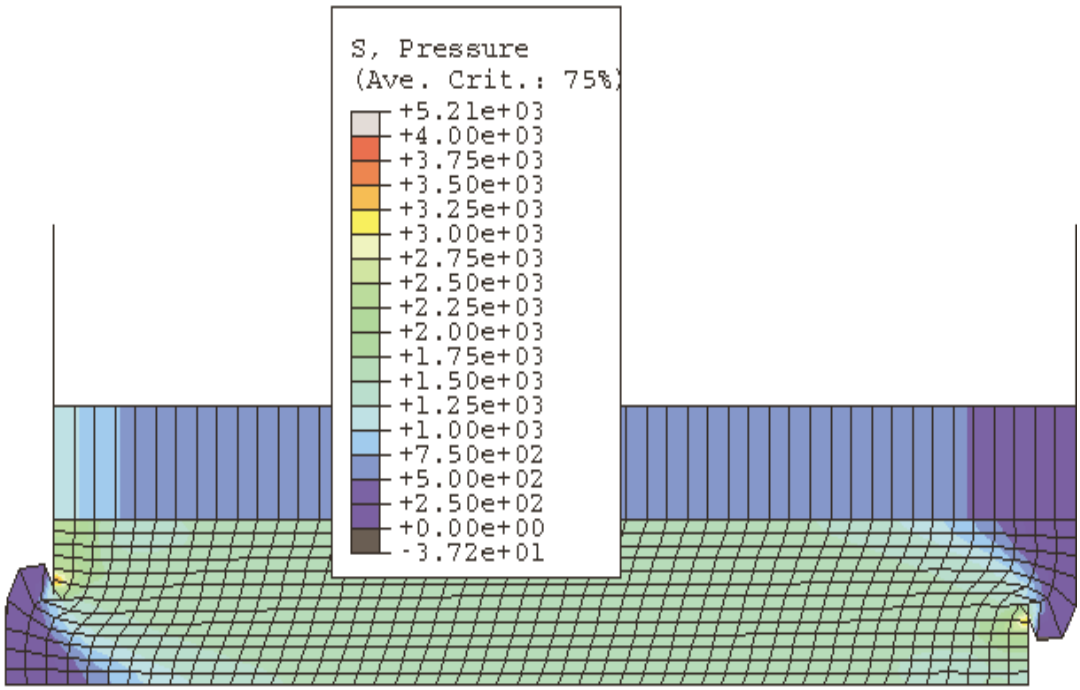

Figure 6.17. Confining pressure (kPa) for normally consolidated final bagasse, split box geometry, displacement 13 mm, fine mesh.

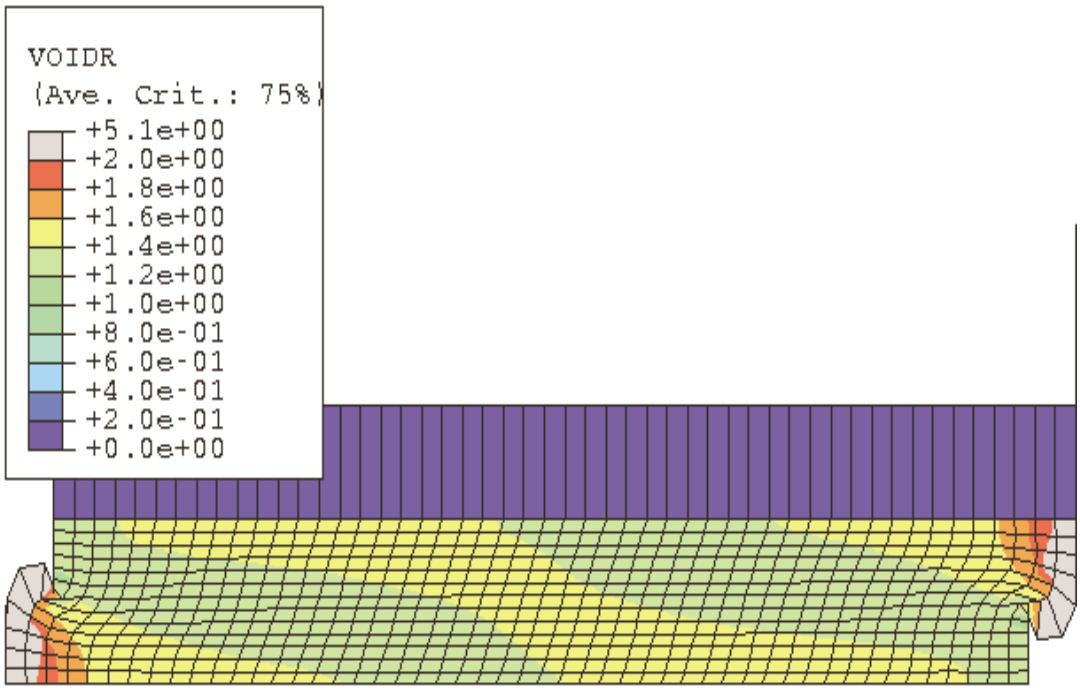

Figure 6.18. Void ratio for normally consolidated final bagasse, split box geometry, displacement 13 mm, fine mesh.

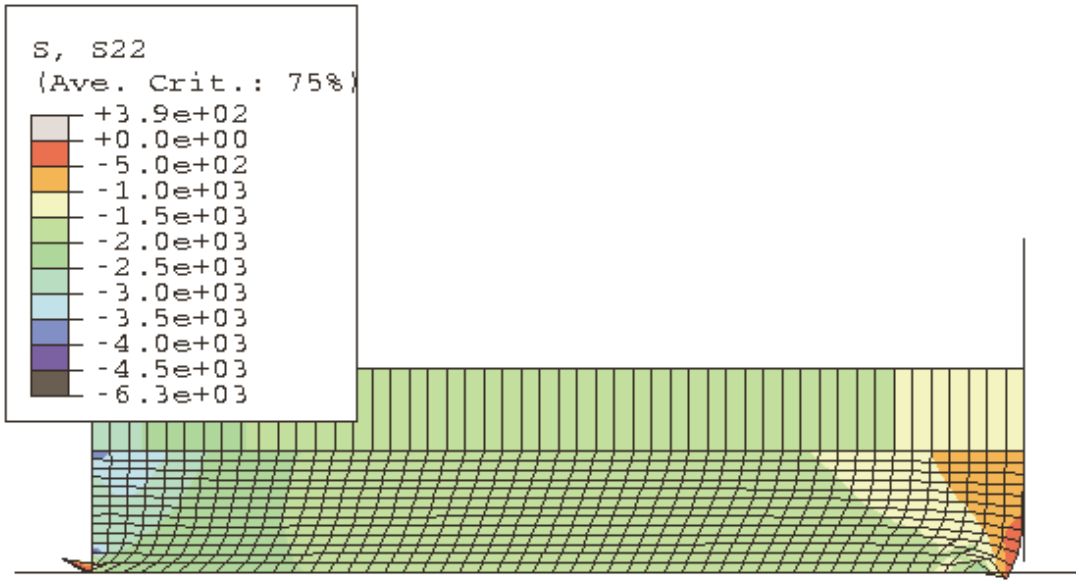

Figure 6.19. Vertical stress (kPa) for normally consolidated final bagasse, modified box geometry, displacement 13 mm, fine mesh.

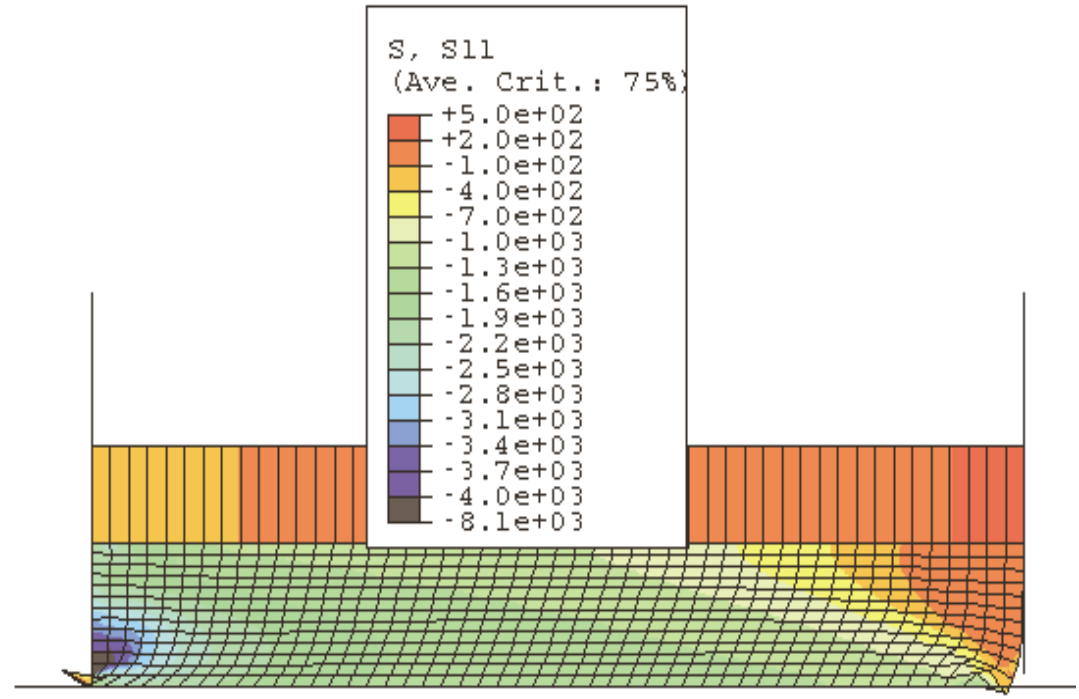

Figure 6.20. Horizontal stress (kPa) for normally consolidated final bagasse, modified box geometry, displacement 13 mm, fine mesh.

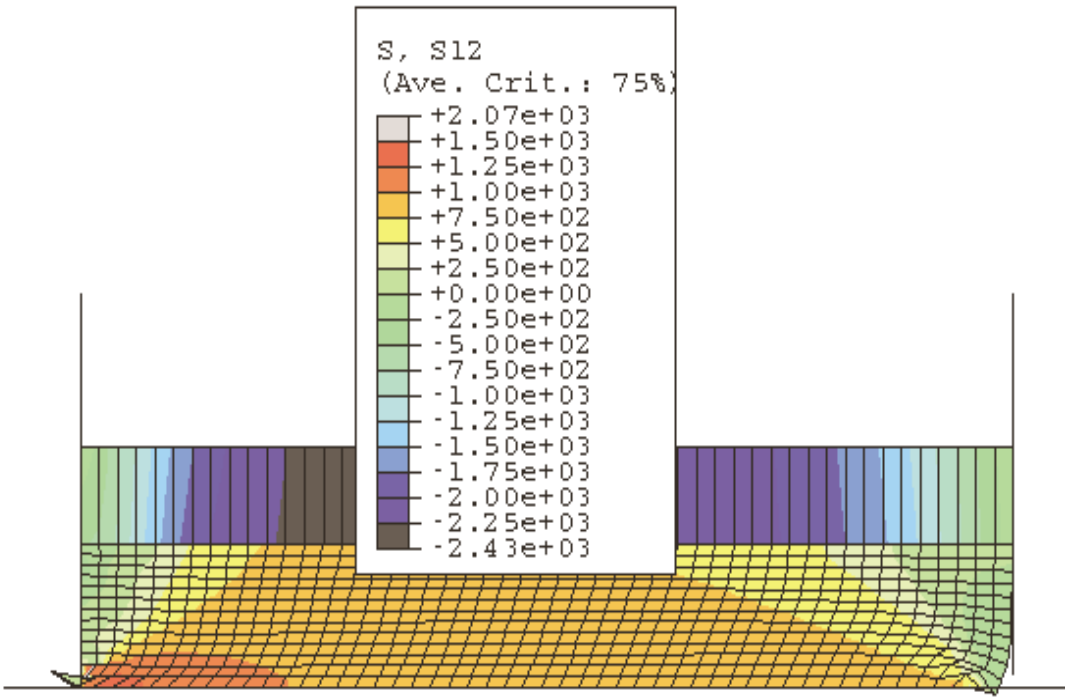

Figure 6.21. Shear stress (kPa) for normally consolidated final bagasse, modified box geometry, displacement 13 mm, fine mesh.

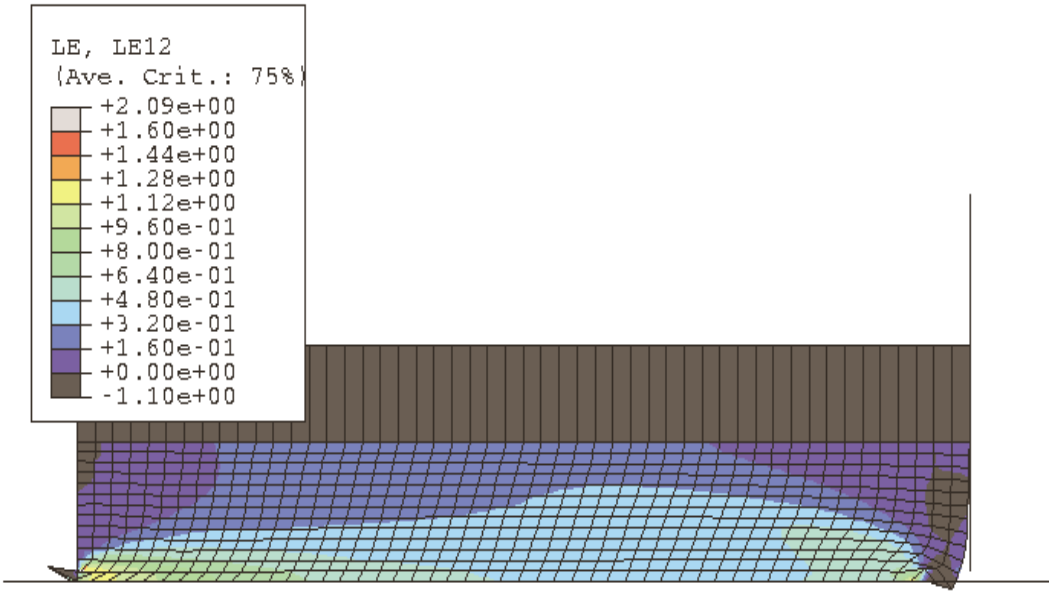

Figure 6.22. Shear strain for normally consolidated final bagasse, modified box geometry, displacement 13 mm, fine mesh.

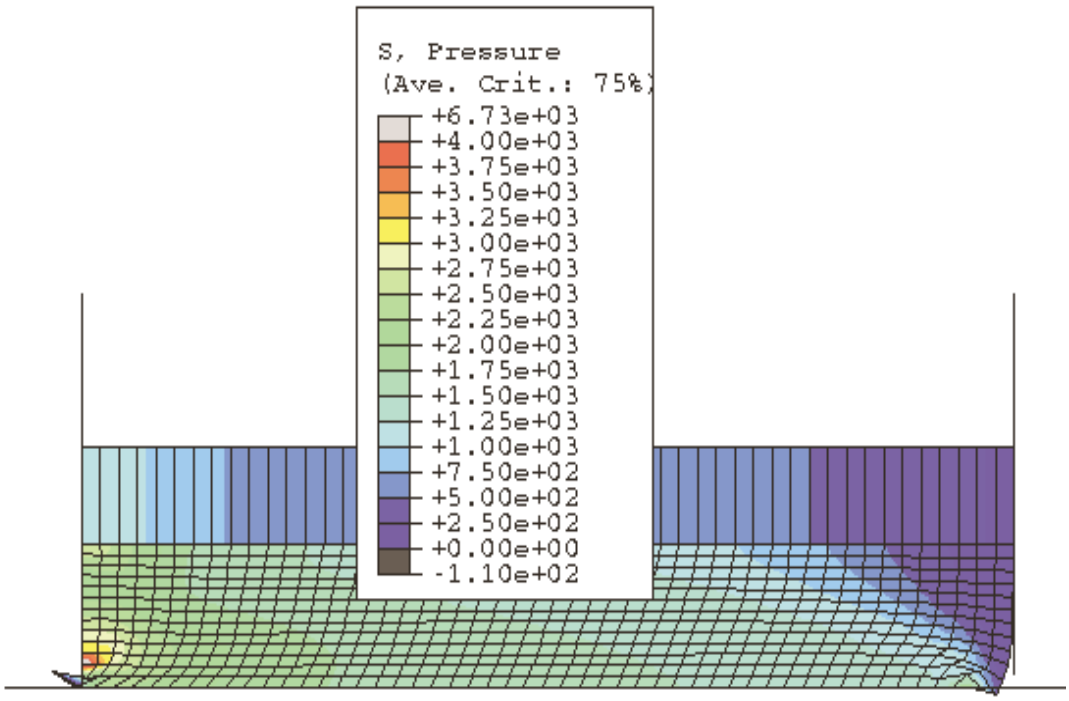

Figure 6.23. Confining pressure (kPa) for normally consolidated final bagasse, modified box geometry, displacement 13 mm, fine mesh.

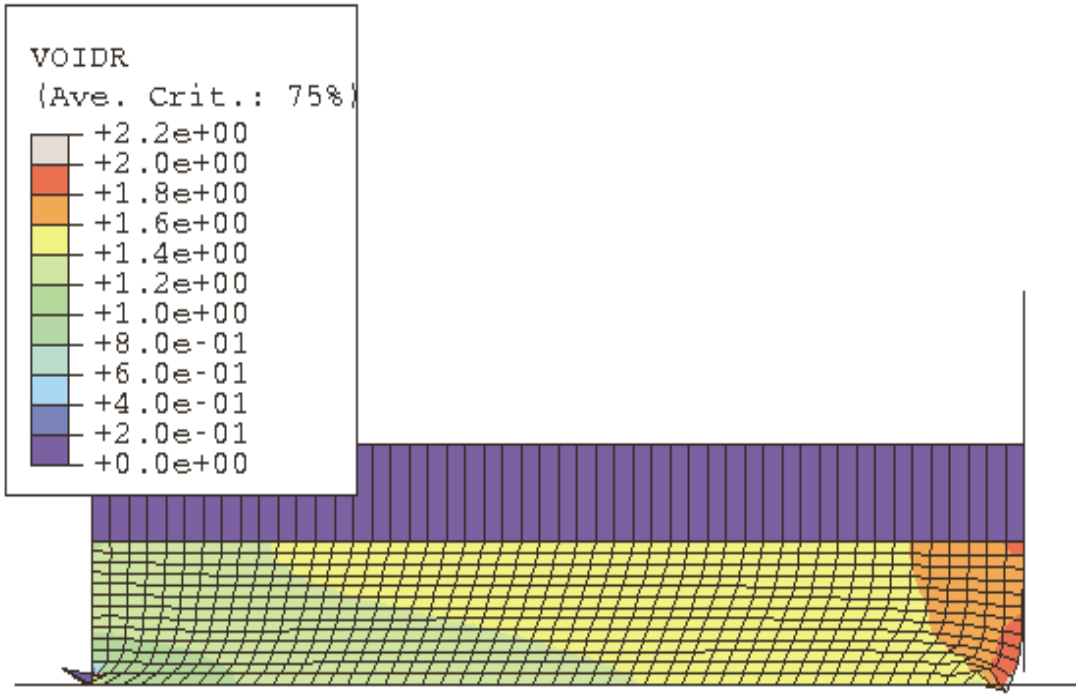

Figure 6.24. Void ratio for normally consolidated final bagasse, modified box geometry, displacement 13 mm, fine mesh.

The predictions from the quasi-analytical model are given in Table 6.2. Summaries of the overall predictions are given in Table 6.3 and in Table 6.4 for the split box geometry, for the coarse mesh and fine mesh, respectively. The predicted decrease in sample height, the sideways reaction force (shear force) per mm width, and the vertical force per mm width are given. The forces are split into the three rigid walls that make up the bottom part of the split box: W1 is the left wall, W2 is the bottom surface (with the sandpaper on it), and W3 is the right wall. Depending on the wall and applied direction of force (sideways or vertical) the forces are either compressive or shear. If desired, the corresponding stresses can be calculated using the corresponding wall dimensions. It is noted that the movement of the bottom part is from right to left. Similarly, summaries of the overall predictions are given in Table 6.5 and in Table 6.6 for the modified box geometry, for the coarse mesh and fine mesh, respectively.

The uniformity of the shear stress and shear strain throughout most of the split box sample is quite striking and looks much like that expected in simple shear (cf Potts et al., 1987). Non-uniformity is present only right at the sidewalls. The vertical stress, horizontal stress, confining pressure, and void ratio throughout the sample are also highly uniform. The predictions for the coarse mesh and for the fine mesh are almost identical, being significantly different only at the side walls of the split box. The behaviour of the bagasse sample right at the side edges for the fine mesh model, where the material expands when it becomes unrestrained and folds back towards the side walls of the box, is more realistic than for the coarse mesh, which does not allow such behaviour. The expansion and folding back behaviour of the bagasse has been observed in the experimental tests. However, the prediction of the behaviour at the sidewalls has little effect on the overall behaviour of the sample and its prediction is more of interest than of use: from a visual interpretation of the figures the coarse mesh seems to be adequate if the aim is to predict overall behaviour of the normally consolidated sample.

The shear stress, shear strain, vertical stress, horizontal stress, confining pressure, and void ratio throughout the sample in the modified box sample are also fairly uniform, but less so than the split box. The shear stress and shear strain are more pronounced towards the left side of the sample, and there are larger shear strains

predicted at the bottom of the sample than at the top. The predictions for the coarse mesh and for the fine mesh are again almost identical.

Table 6.2 Predictions of single element quasi-analytical model for a sideways displacement of 13 mm

Change in height (mm)	Shear force (N)	Vertical force (N)
-1.2	270	504

Table 6.3 Predictions of coarse mesh split box model for a sideways displacement of 13 mm

Travel of bottom node (mm)	Change in height (mm)	Sideways reaction force (N)	Vertical reaction force (N)
12.91	-0.93	W1 0.0	0.0
		W2 192.5	495.6
		W3 47.3	12.4
		Sum 240	Sum 508

Table 6.4 Predictions of fine mesh split box model for a sideways displacement of 13 mm

Travel of bottom node (mm)	Change in height (mm)	Sideways reaction force (N)	Vertical reaction force (N)
12.98	-1.06	W1 0.1	0.0
		W2 193.7	492.7
		W3 37.8	10.1
		Sum 231	Sum 503

Table 6.5 Predictions of coarse mesh modified box model for a sideways displacement of 13 mm

Travel of bottom node (mm)	Change in height (mm)	Sideways reaction force (N)	Vertical reaction force (N)
12.90	-0.86	255	513

Table 6.6 Predictions of fine mesh modified box model for a sideways displacement of 13 mm

Travel of bottom node (mm)	Change in height (mm)	Sideways reaction force (N)	Vertical reaction force (N)
12.98	-0.90	256	506

Before commenting on the overall predictions, it is noted that included in the split box and modified box summary tables are values of the travel of a node at the bottom surface of the bagasse sample (i.e. contacting the bottom surface) located halfway between the side walls. The travel of this node is a measure of the slip between the bagasse and the bottom surface. It is shown that the slip is negligible and that the input value of the coefficient of friction of 0.6 on this surface was adequate to prevent any significant slip. Both the split box and the modified box predict a smaller decrease in sample height (about 12% less for the split box fine mesh model) and a smaller shear force (about 14% less for the split box fine mesh model) than the single element. This can be explained because in a single element model every point is mobilised to the same degree, while in the split box and modified box there are always locations which are not participating. Following the same argument, it is not surprising to see that the modified box simulations predict a smaller decrease (about 15% less) in the sample height than the split box simulations, since the shear strains for the modified box sample are smaller towards the top of the sample. However, it is interesting to note that the predicted shear forces for the modified box are larger (by about 11%) than for the split box. It is also interesting that for the split box, the predicted sideways force provided by the side wall is between 15% to 20% of the total force, while the bottom rough surface provides 80% to 85%. The importance of the bottom and top rough surfaces is reinforced by the modelling, and provides a key role in minimising the extra compression of the bagasse next to the side walls noted previously by Cullen (1965) and shown in Figure 4 of Plaza and Kent (1997). The tendency for extra compression next to the side walls is shown in Figure 6.14, Figure 6.17, and Figure 6.18, and it is seen more clearly later in this chapter in the plot of void ratio for an over-consolidated bagasse sample (Figure 6.50).

It is noted that only one layer of elements was used to model the gap between the box and the bottom surface for the modified box geometry, and is probably insufficient to capture accurately the local detail of the deformation in this region. The effect of this local deformation on the overall response cannot be adequately assessed but is expected to be small.

The overall conclusion is that measurements carried out with the modified box are adequate for measuring bagasse behaviour. As noted in Chapter 2, the modified box has other perceived advantages, one important advantage being the ability to carry out material behaviour tests and friction tests on various surfaces using the same box. However, it was concluded that should further material behaviour testing be carried out, a split box with a rough surface both on the top and bottom surfaces would be trialed first. Such tests were carried out and are described in the next chapter.

6.3 Direct shear test simulations for normally consolidated final bagasse with a sideways displacement of 19.5 mm

In the previous section, simulations were carried out of direct shear tests with a bottom plate sideways displacement of 13 mm. It was difficult to carry out modelling with larger displacements since badly distorted unloading elements at the sidewalls prevented the solution from converging. In the experimental tests described in Chapters 3 and 4 the final sideways displacement of the bottom plate was approximately 76 mm. The results in Chapter 4 show that large displacements are required in order to get close to a critical state point where the shear stress is no longer increasing or decreasing while undergoing shear strain at constant vertical pressure. Schembri at al (1998) show in their Figure 1 the volume and shear strains for a test performed on an experimental three roll pressure feeder, and showed that shear strains in excess of 1.0 were present in the pressure feeder nip. It is therefore desirable to carry out direct shear tests at least up to a sideways displacement of 40 mm for a sample that is 40 mm high. A perceived advantage of the modified box over the split box is that the type of bottom surface remains constant for the modified box while the sideways displacement takes place. In contrast, the actual area occupied by the bagasse sample under the vertical load for the split box decreases (and therefore the vertical stress will increase).

To give an indication of whether this perceived advantage was real, the sideways displacement for the coarse mesh models was increased to 19.5 mm (a shear strain of about 0.55). The results of the simulations (vertical stress, shear stress, shear strain, and void ratio) are shown in Figure 6.25 to Figure 6.28 for the split box, and Figure 6.29 to Figure 6.32 for the modified box. A summary of the predicted

sample height changes and forces are shown in Table 6.7 to Table 6.9. The overall conclusion is, as in the previous section, that measurements carried out with the modified box are adequate for measuring bagasse behaviour, but the split box is better because of the more uniform conditions. The perceived advantage of the modified box over the split box, that the type of bottom surface remains constant for the modified box, is not likely to be correct, even at high displacements.

Table 6.7 Predictions of single element quasi-analytical model for a sideways displacement of 19.5 mm

Change in height (mm)	Shear force (N)	Vertical force (N)
-1.63	281	504

Table 6.8 Predictions of coarse mesh split box model for a sideways displacement of 19.5 mm

Travel of bottom node (mm)	Change in height (mm)	Sideways reaction force (N)	Vertical reaction force (N)
19.4	-1.47	W1 0.0	0.0
		W2 195.1	496.0
		W3 49.5	12.4
		Sum 245	Sum 509

Table 6.9 Predictions of coarse mesh modified box model for a sideways displacement of 19.5 mm

Travel of bottom node (mm)	Change in height (mm)	Sideways reaction force (N)	Vertical reaction force (N)
19.4	-1.31	266	514

As in the previous section, there was little slip predicted between the bagasse and the bottom surface. Because the shear stress increases by a relatively small amount after a large shear strain of 0.5, the measured coefficient of 0.6 for a vertical pressure of 1800 kPa, used as input to the model, is likely to provide good grip at all further shear strains (as was observed experimentally).

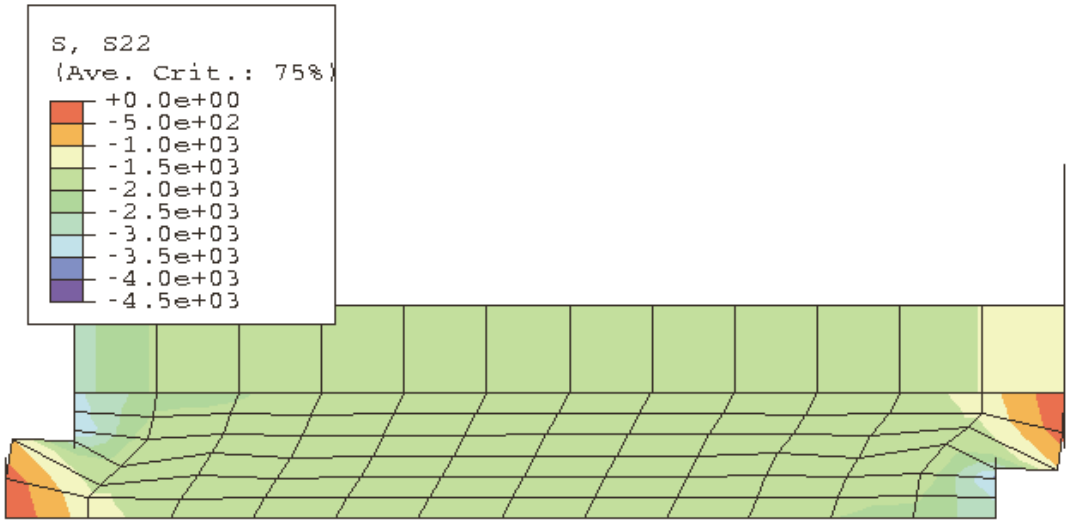

Figure 6.25. Vertical stress (kPa) for normally consolidated final bagasse, split box geometry, displacement 19.5 mm, coarse mesh.

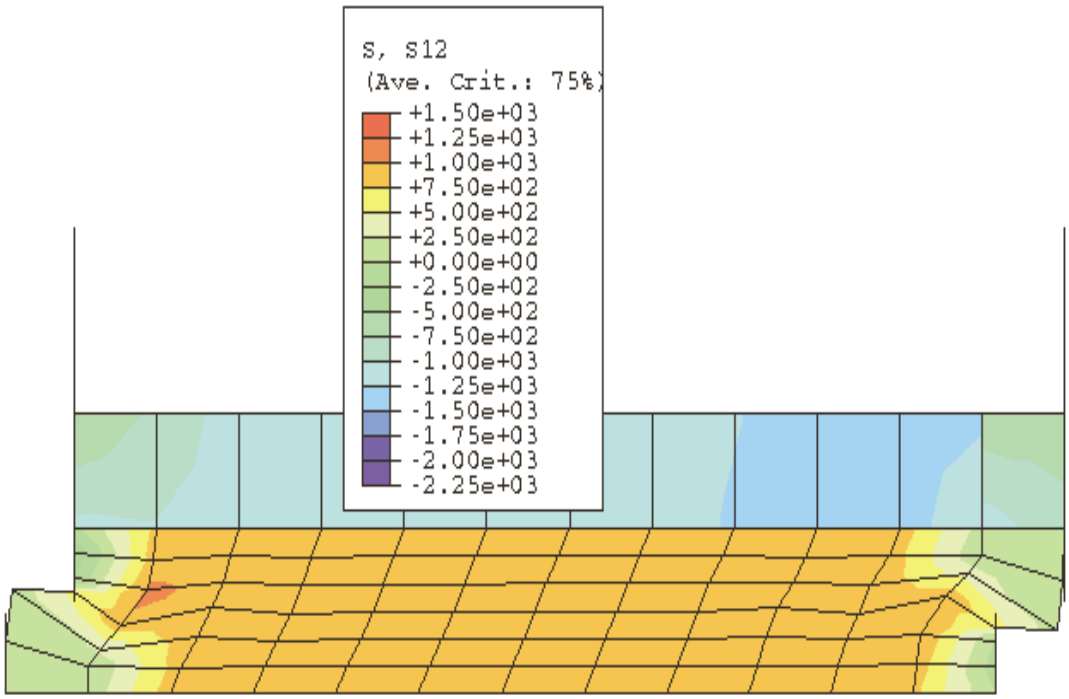

Figure 6.26. Shear stress (kPa) for normally consolidated final bagasse, split box geometry, displacement 19.5 mm, coarse mesh.

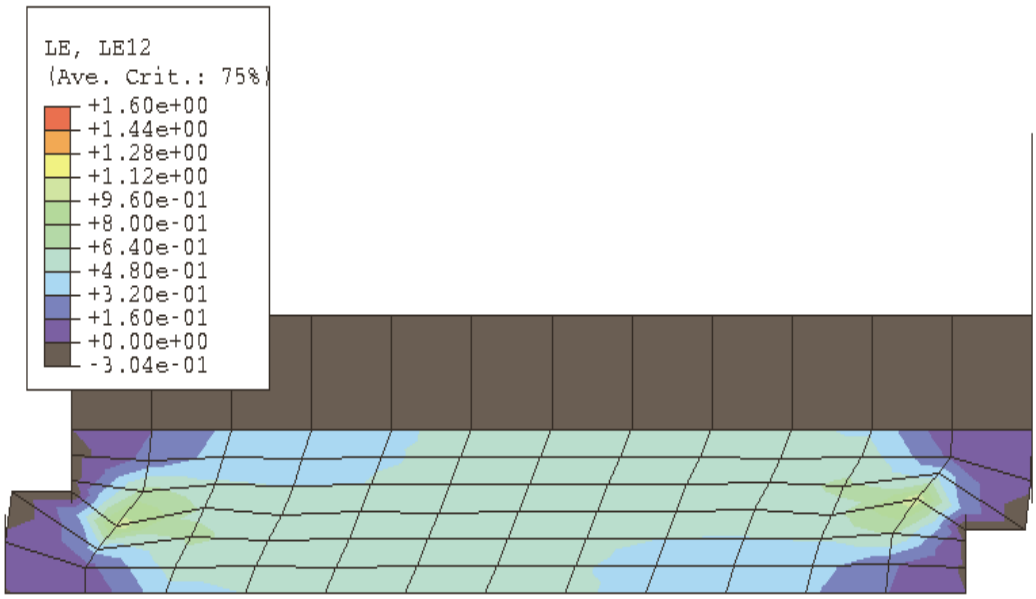

Figure 6.27. Shear strain for normally consolidated final bagasse, split box geometry, displacement 19.5 mm, coarse mesh.

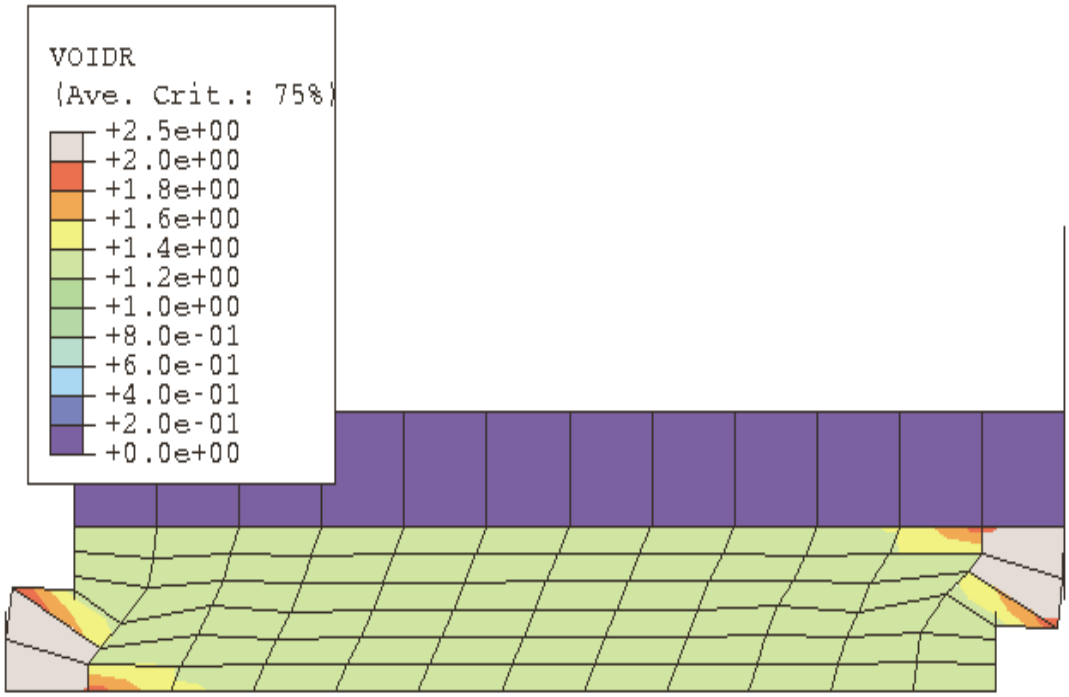

Figure 6.28. Void ratio for normally consolidated final bagasse, split box geometry, displacement 19.5 mm, coarse mesh.

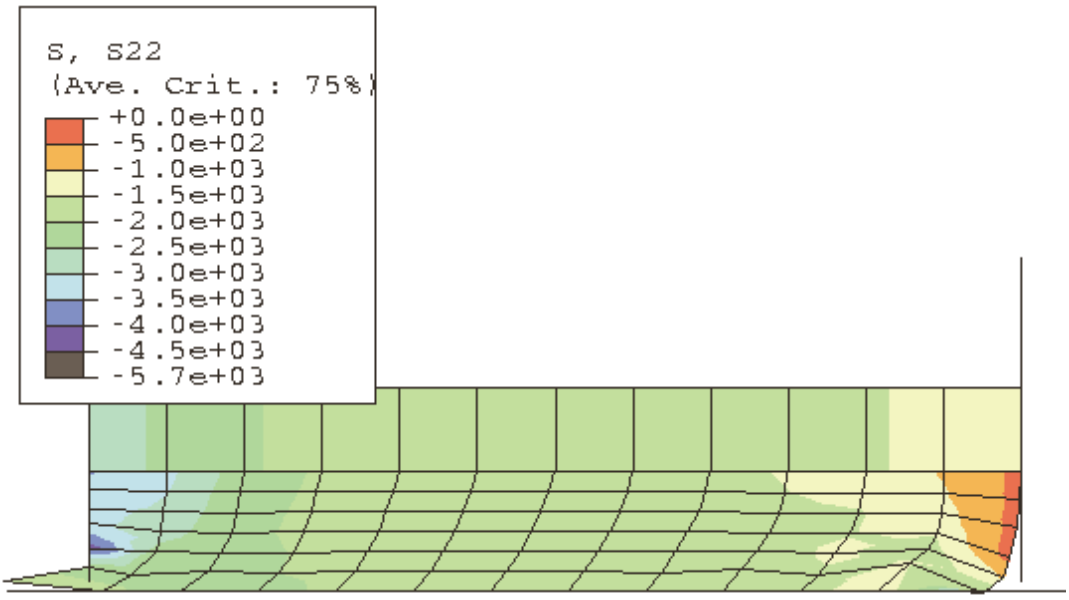

Figure 6.29. Vertical stress (kPa) for normally consolidated final bagasse, modified box geometry, displacement 19.5 mm, coarse mesh.

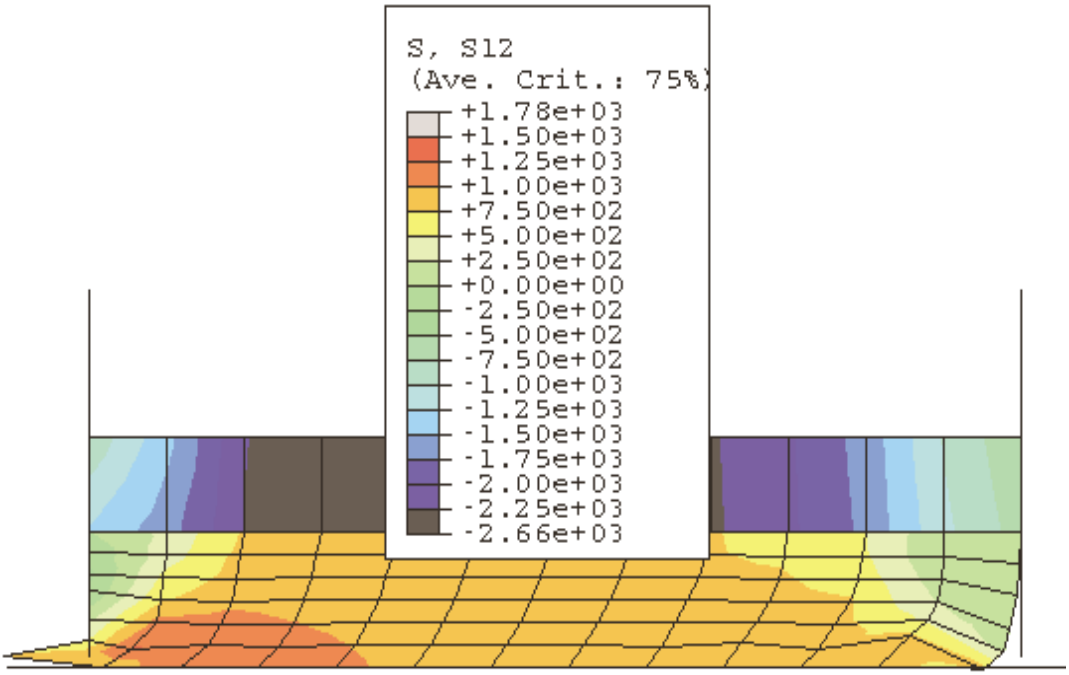

Figure 6.30. Shear stress (kPa) for normally consolidated final bagasse, modified box geometry, displacement 19.5 mm, coarse mesh.

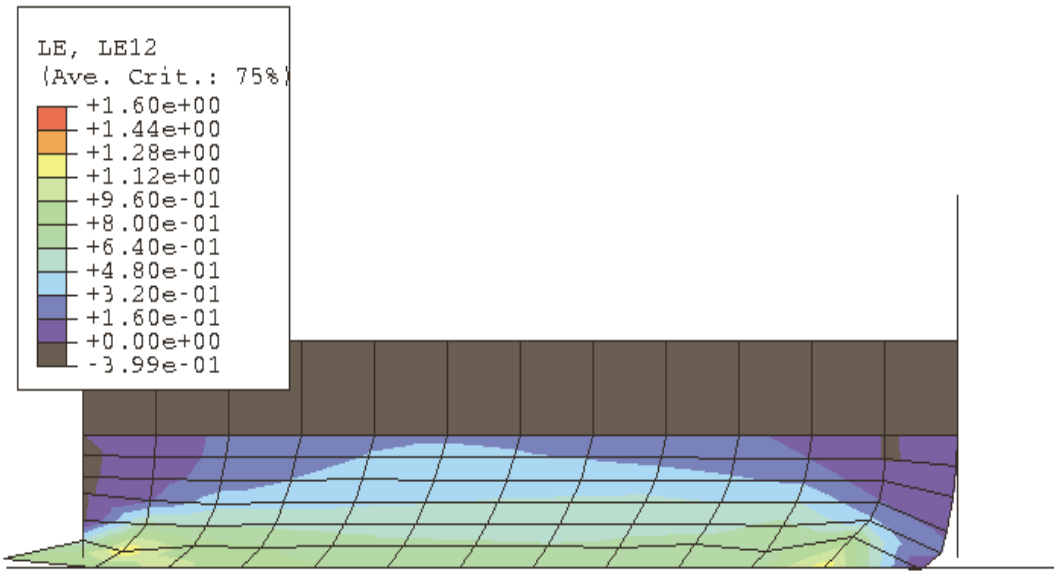

Figure 6.31. Shear strain for normally consolidated final bagasse, modified box geometry, displacement 19.5 mm, coarse mesh.

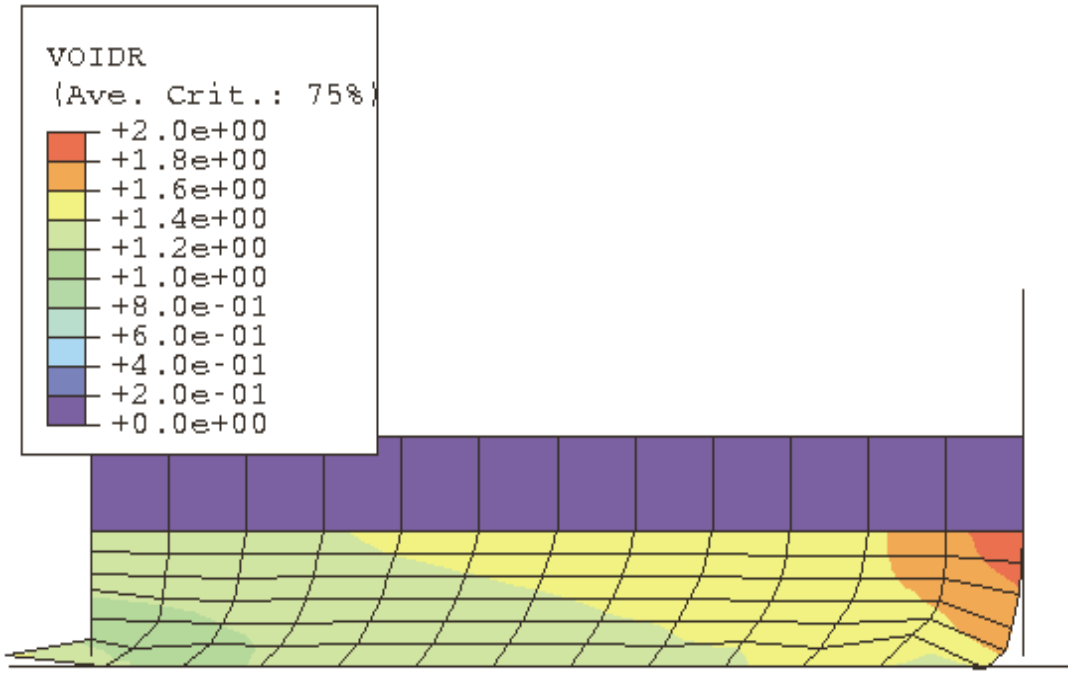

Figure 6.32. Void ratio for normally consolidated final bagasse, modified box geometry, displacement 19.5 mm, coarse mesh.

6.4 Direct shear test simulations for over-consolidated final bagasse with a sideways displacement of 16.0 mm

The material modelled was a sample of over-consolidated final bagasse 41 mm high. The over-consolidation ratio (OCR) was 5.3 (unloaded from 1800 kPa to 340 kPa, then sheared). The values of the input material parameters for the particular sample and initial stress conditions were the same as the normally consolidated sample modelled in the previous sections, except for the over-consolidation, and are shown in Table 6.1 (the vertical pressure during shearing was 340 kPa in this case). It is well established in the soil mechanics literature that over-consolidated soil has a higher value of K_o than normally consolidated soil. However there are no K_o measurements available for over-consolidated bagasse. In the absence of measurements, the value of K_o used in the modelling was kept at 0.2 (the value measured for normally consolidated bagasse). A similar mesh to the previous section's fine mesh for normally consolidated bagasse was used.

6.4.1 Coefficient of friction of 0.6

Initially, by an oversight, the surfaces of the top and bottom plates contacting the final bagasse were assigned a coefficient of friction of 0.6 (the same as for normally consolidated bagasse at 1800 kPa, data from Plaza and Kent, 1997). It was shown by Plaza et al. (2002) (as described in the next chapter) that over-consolidated bagasse with the stress conditions described above will achieve a coefficient of friction (actually a coefficient of shear) of between 1.1 and 1.2. In this section, results are presented first for a coefficient of friction of 0.6, to show the effect on the modelling of having too low a value (or having an inadequately rough surface in experimental tests). The coefficient of friction on the sidewalls (smooth mild steel) remained at 0.3 (where slip usually occurs). For the split box, Figure 6.33 to Figure 6.38 show the vertical stress, horizontal stress, shear stress, shear strain, confining pressure and void ratio, for a sideways displacement of the bottom part of the box of 16 mm. A summary of the results is shown in Table 6.10, which includes the travel of a node at the top of the bagasse and of a node at the bottom of the bagasse. A slip of 3.9 mm was predicted between the top steel elements and the bagasse, and a slip of 3.9 mm (16 minus 12.1 mm) between the bottom surface and the bagasse. There was therefore a large amount of slip predicted between the bagasse and the

top and bottom surfaces, with the sideways bagasse deformation being only 8.2 mm (12.1 minus 3.9 mm). The slip is apparent at the bagasse surface in contact with the top steel plate, where the grid does not line up. The result of the slip is that little shear strain and shear stress develop throughout most of the sample, while high horizontal stresses develop next to the pushing and restraining side walls, with a resulting increase in confining pressure and decrease in void ratio (increase in density) at these locations. In summary, tests carried out on a material with low stiffness such as bagasse with an inadequate roughness on the top and bottom surfaces would provide lower quality data.

Table 6.10 Predictions of fine mesh split box model for a sideways displacement of 16 mm for over-consolidated bagasse, coefficient of friction of 0.6

Travel of bottom node (mm)	Travel of top node (mm)	Change in height (mm)	Sideways reaction force (N)	Vertical reaction force (N)
12.1	3.9	0.84	W1 0.0	0.0
			W2 50.7	95.8
			W3 12.3	3.0
			Sum 63	Sum 99

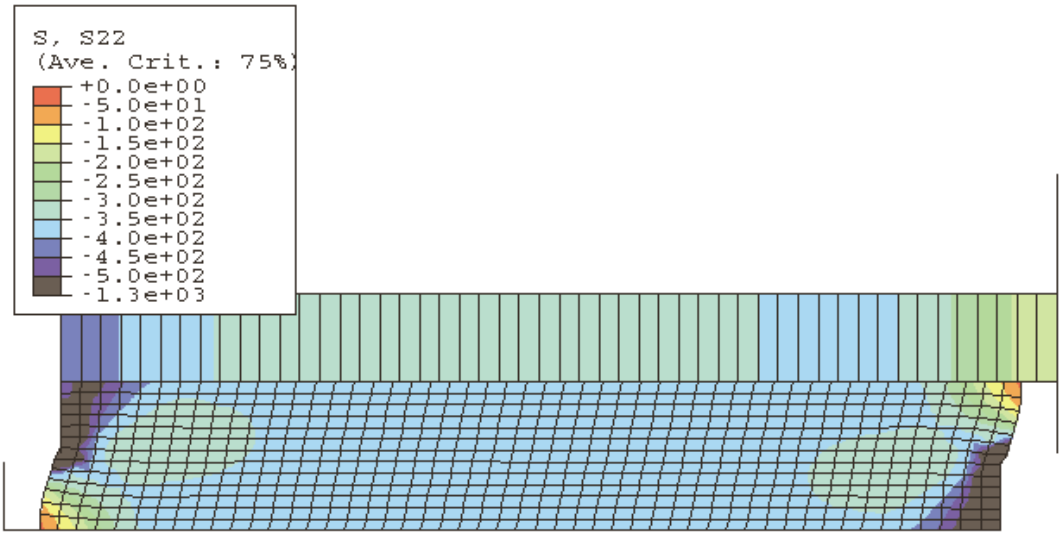

Figure 6.33. Vertical stress (kPa) for over-consolidated final bagasse, split box geometry, displacement 16 mm, fine mesh, friction 0.6.

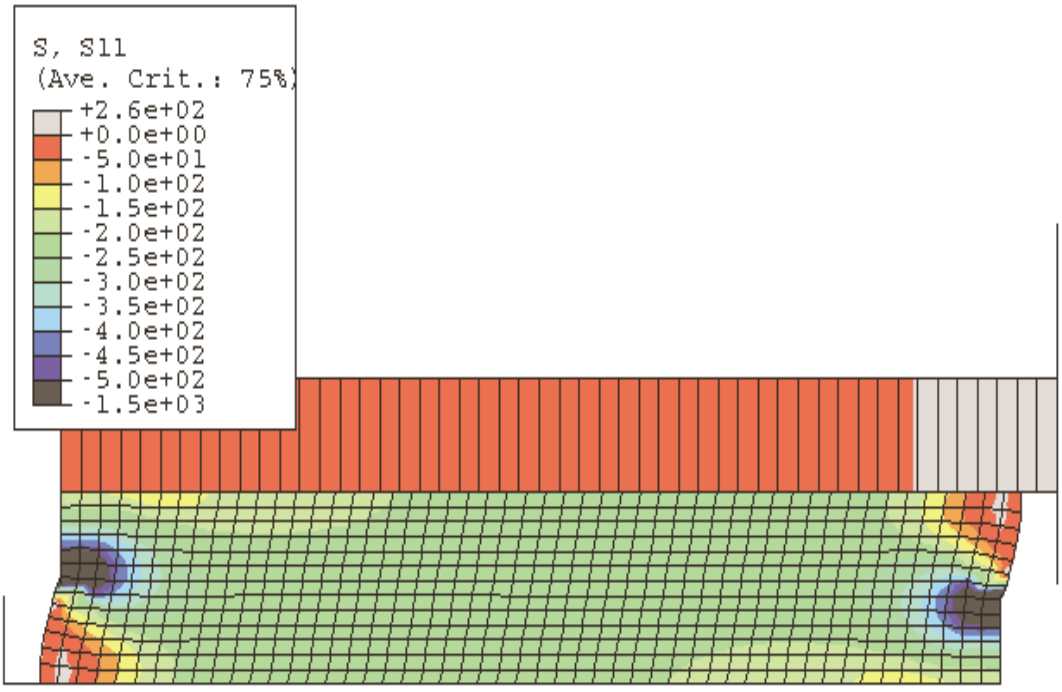

Figure 6.34. Horizontal stress (kPa) for over-consolidated final bagasse, split box geometry, displacement 16 mm, fine mesh, friction 0.6.

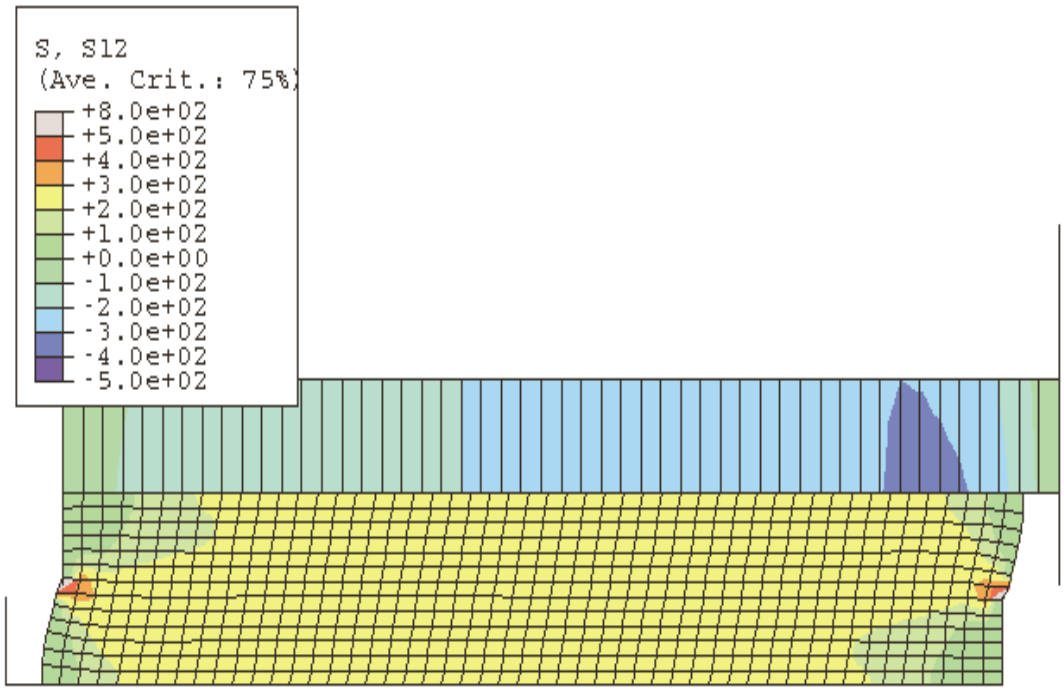

Figure 6.35. Shear stress (kPa) for over-consolidated final bagasse, split box geometry, displacement 16 mm, fine mesh, friction 0.6.

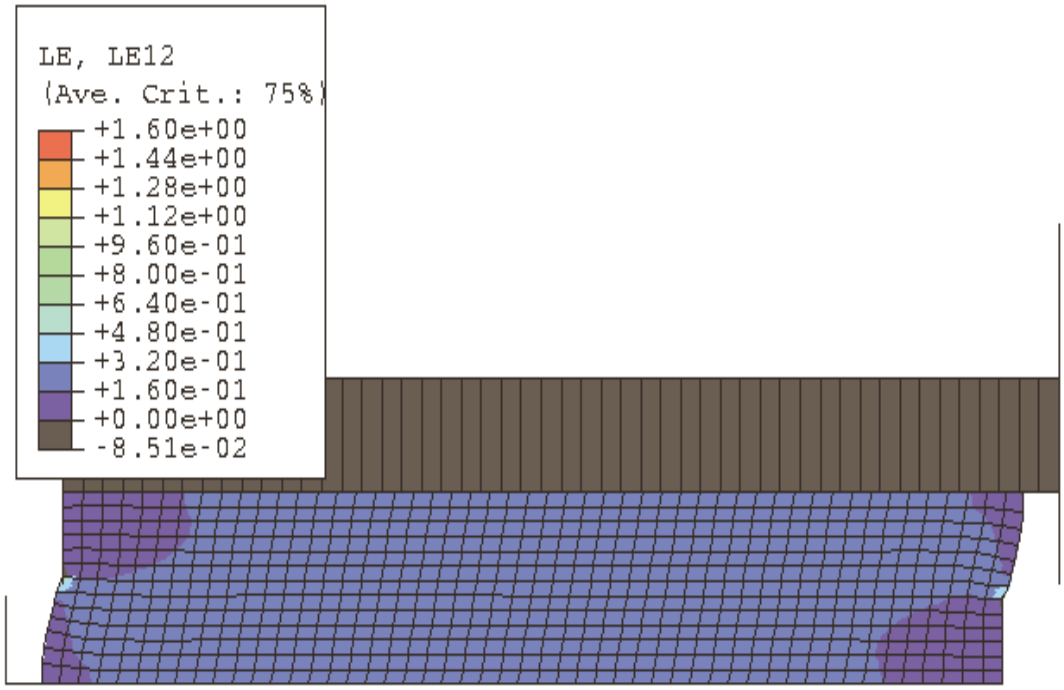

Figure 6.36. Shear strain for over-consolidated final bagasse, split box geometry, displacement 16 mm, fine mesh, friction 0.6.

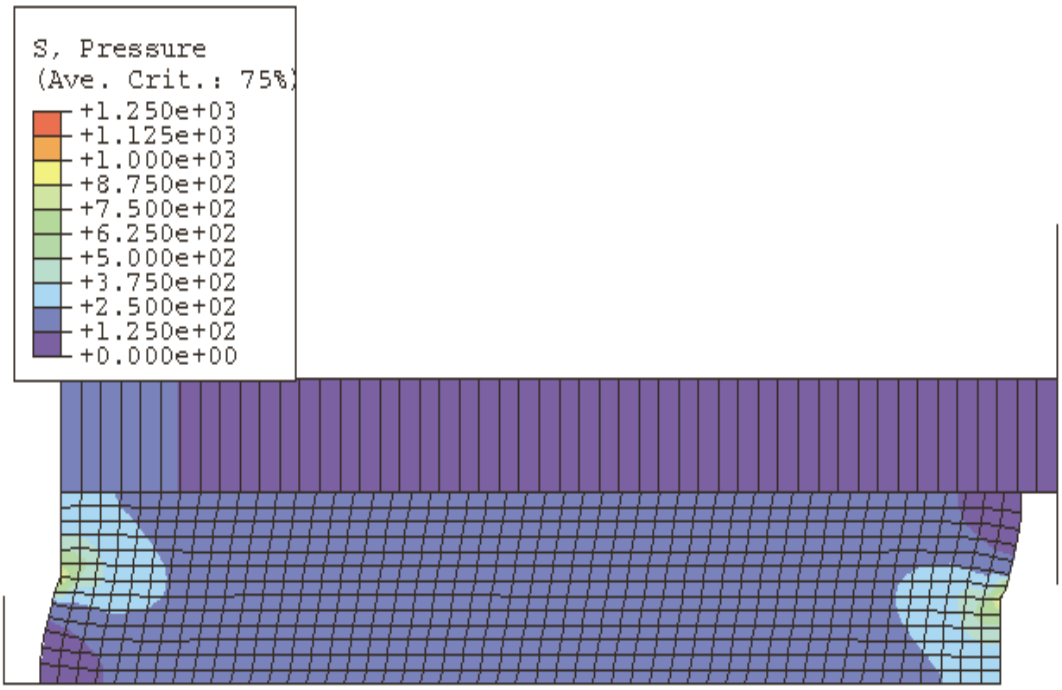

Figure 6.37. Confining pressure (kPa) for over-consolidated final bagasse, split box geometry, displacement 16 mm, fine mesh, friction 0.6.

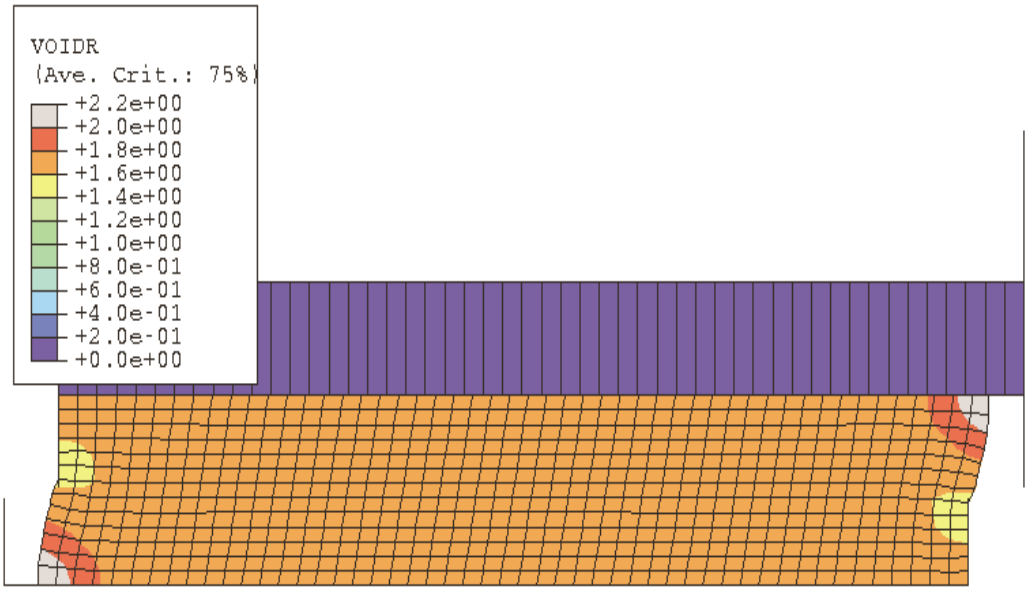

Figure 6.38. Void ratio for over-consolidated final bagasse, split box geometry, displacement 16 mm, fine mesh, friction 0.6.

6.4.2 Coefficient of friction to achieve good grip and formation of shear planes in over-consolidated bagasse sample

As shown by Plaza et al. (2002), a coefficient of friction (actually a coefficient of shear) of between 1.1 and 1.2 was measured for over-consolidated bagasse with the stress conditions described in the previous section. Simulations were carried out varying the coefficient of friction from 0.6 to 1.4. It was found that to get little slip between the bagasse and the top and bottom surfaces a coefficient of friction of at least 1.1 was required, which agrees well with the measured values of 1.1 to 1.2. Summaries for a simulation with a friction value of 1.1 are shown in Table 6.11. It is noted that calculating a coefficient of friction from the predicted values gives a value of 0.95, which is significantly less than 1.1. This implies non-uniformity in the sample and/or that the mesh is not fine enough.

Table 6.11 Predictions of fine mesh split box model for a sideways displacement of 16 mm for over-consolidated bagasse, coefficient of friction of 1.1

Travel of bottom node (mm)	Travel of top node (mm)	Change in height (mm)	Sideways reaction force (N)	Vertical reaction force (N)
15.97	0.03	1.2	W1 0.0	0.0
			W2 78.1	96.1
			W3 16.6	4.1
			Sum 95	Sum 100

A simulation with a coefficient of friction of 1.4 was found to achieve almost no slip. The results of the simulation with a coefficient of friction of 1.4 are shown in Figure 6.39 to Figure 6.44 for a displacement of 13 mm and in Figure 6.45 to Figure 6.50 for a displacement of 16 mm. Summaries of results are given in Table 6.12 for a single element model and in Table 6.13 for the fine mesh split box model. Quite uniform strains, increasing sideways forces on the box side walls, and increases in the sample height are predicted up to a displacement of about 13 mm. As the bottom part of the split box moves to the left, high shear stress zones are predicted to form at the top right and the bottom left of the sample. As localised shear planes having high shear strains form at these two locations (this point may be called failure since the stresses supported by the sample decrease after the formation of the

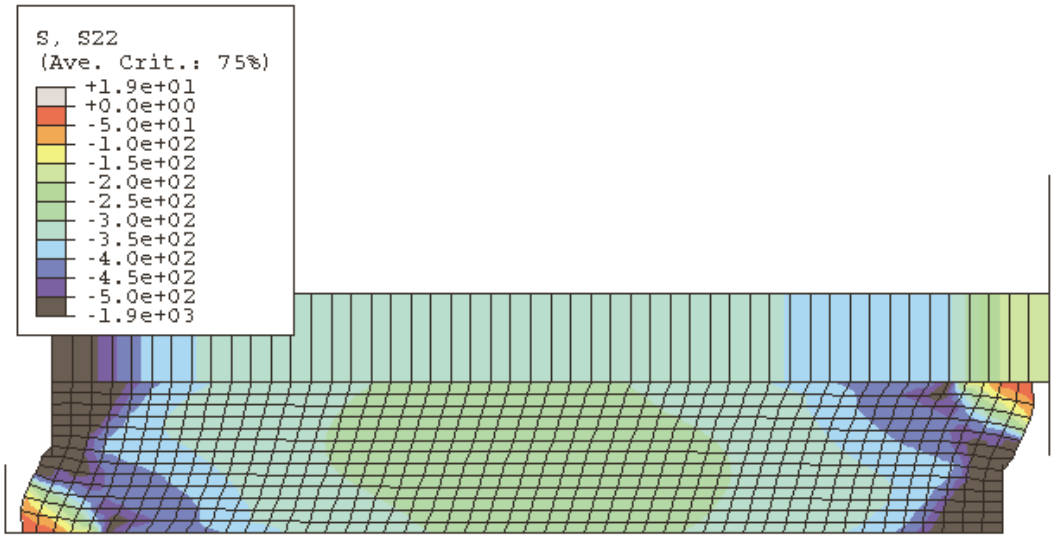

Figure 6.39. Vertical stress (kPa) for over-consolidated final bagasse, split box geometry, displacement 13 mm, fine mesh, friction 1.4.

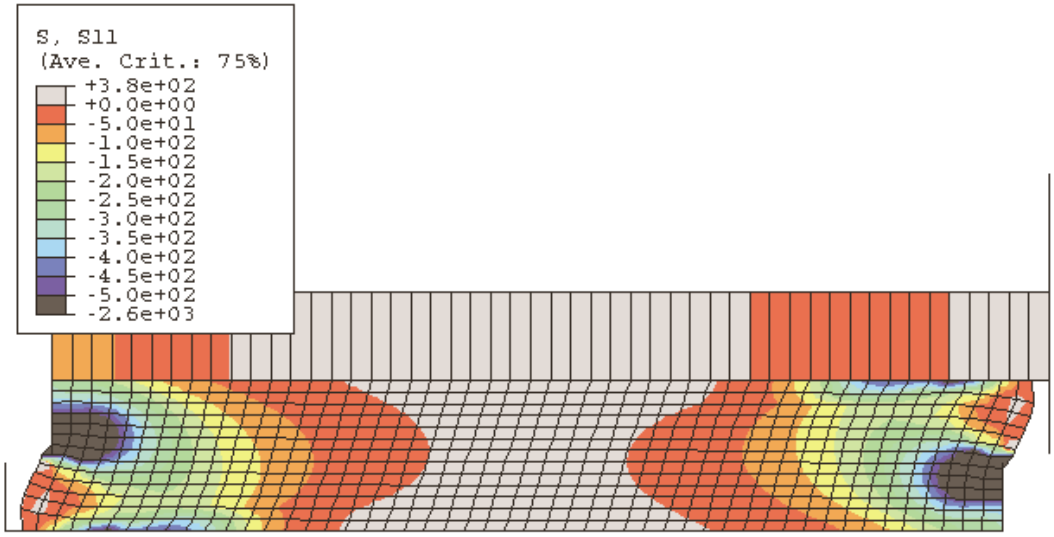

Figure 6.40. Horizontal stress (kPa) for over-consolidated final bagasse, split box geometry, displacement 13 mm, fine mesh, friction 1.4.

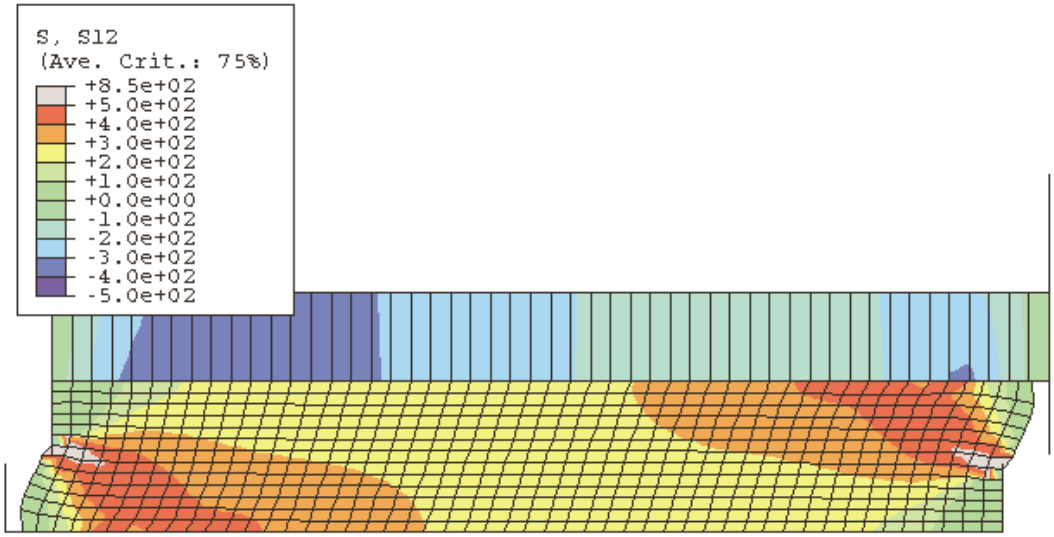

Figure 6.41. Shear stress (kPa) for over-consolidated final bagasse, split box geometry, displacement 13 mm, fine mesh, friction 1.4.

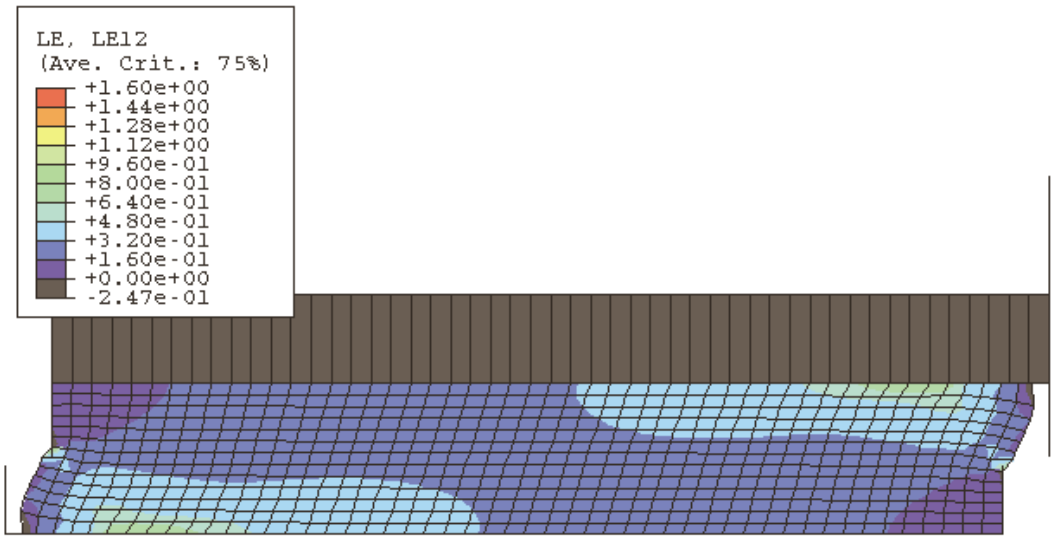

Figure 6.42. Shear strain for over-consolidated final bagasse, split box geometry, displacement 13 mm, fine mesh, friction 1.4.

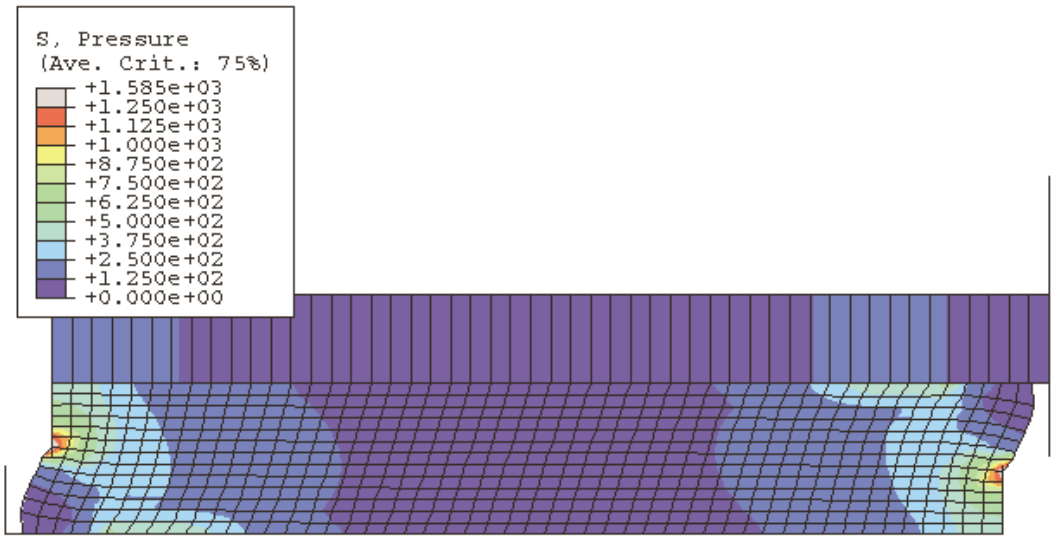

Figure 6.43. Confining pressure (kPa) for over-consolidated final bagasse, split box geometry, displacement 13 mm, fine mesh, friction 1.4.

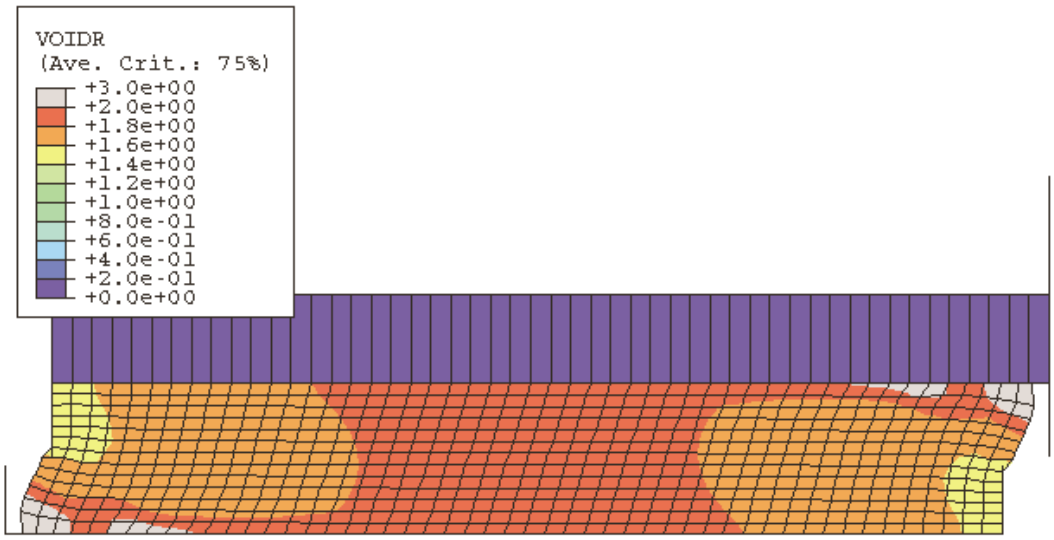

Figure 6.44. Void ratio for over-consolidated final bagasse, split box geometry, displacement 13 mm, fine mesh, friction 1.4.

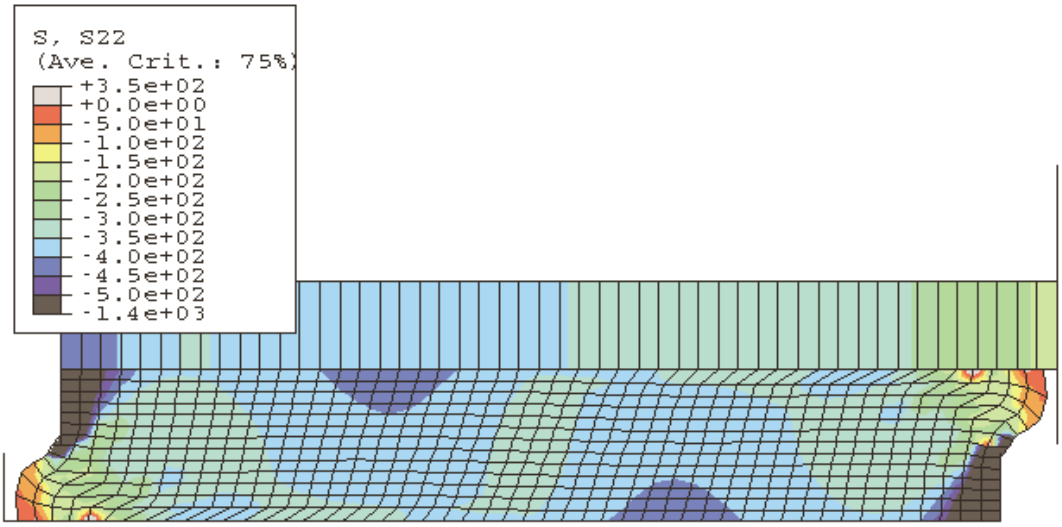

Figure 6.45. Vertical stress (kPa) for over-consolidated final bagasse, split box geometry, displacement 16 mm, fine mesh, friction 1.4.

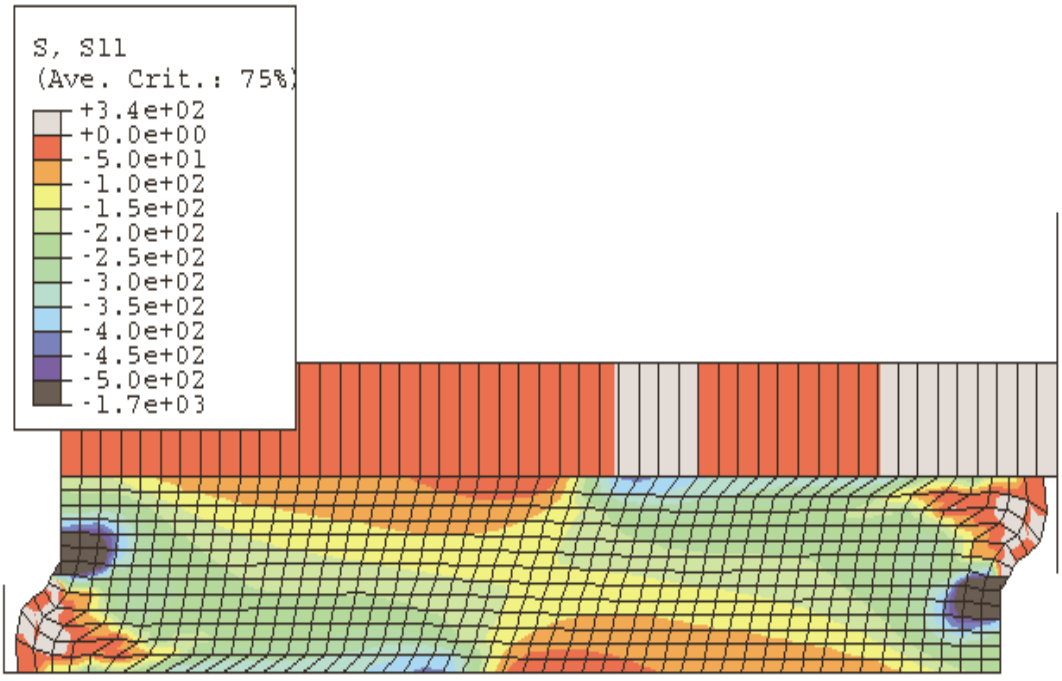

Figure 6.46. Horizontal stress (kPa) for over-consolidated final bagasse, split box geometry, displacement 16 mm, fine mesh, friction 1.4.

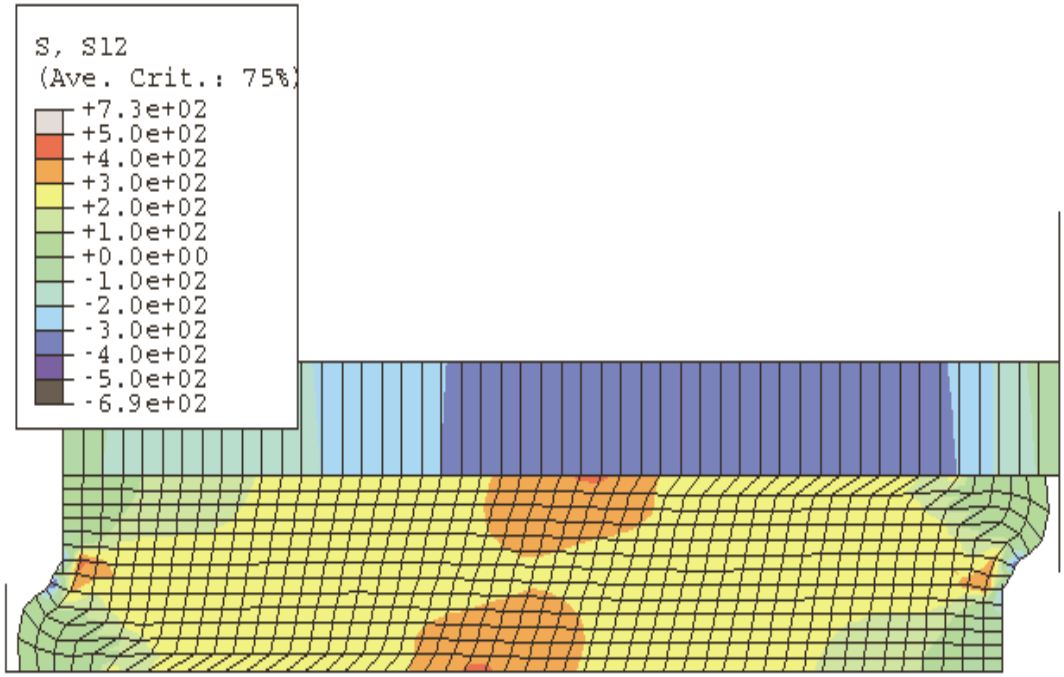

Figure 6.47. Shear stress (kPa) for over-consolidated final bagasse, split box geometry, displacement 16 mm, fine mesh, friction 1.4.

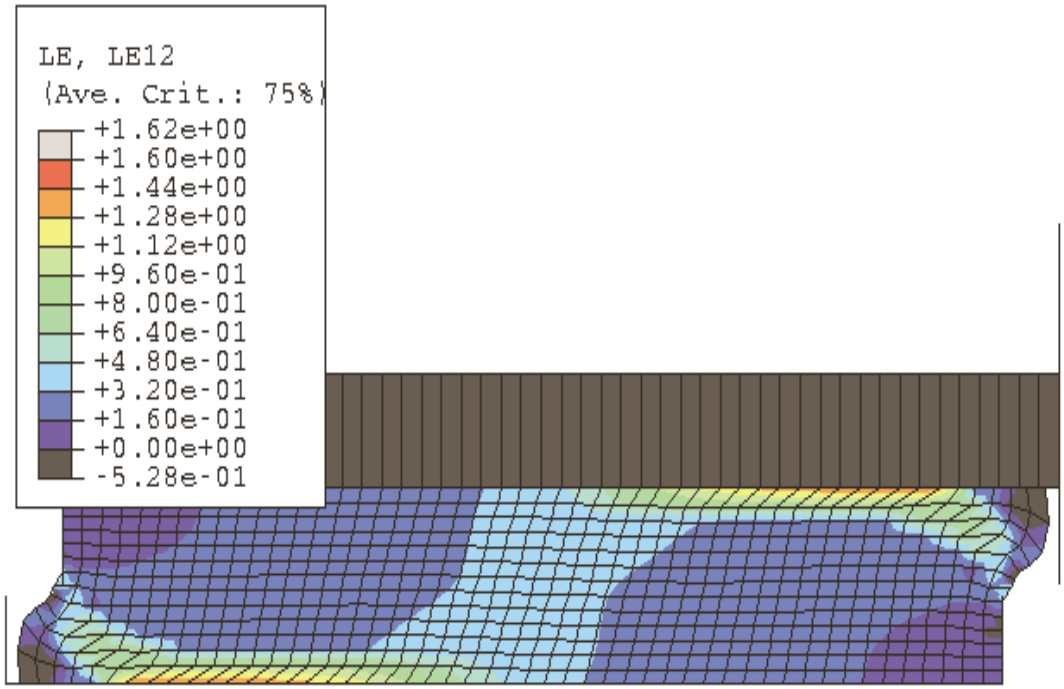

Figure 6.48. Shear strain for over-consolidated final bagasse, split box geometry, displacement 16 mm, fine mesh, friction 1.4.

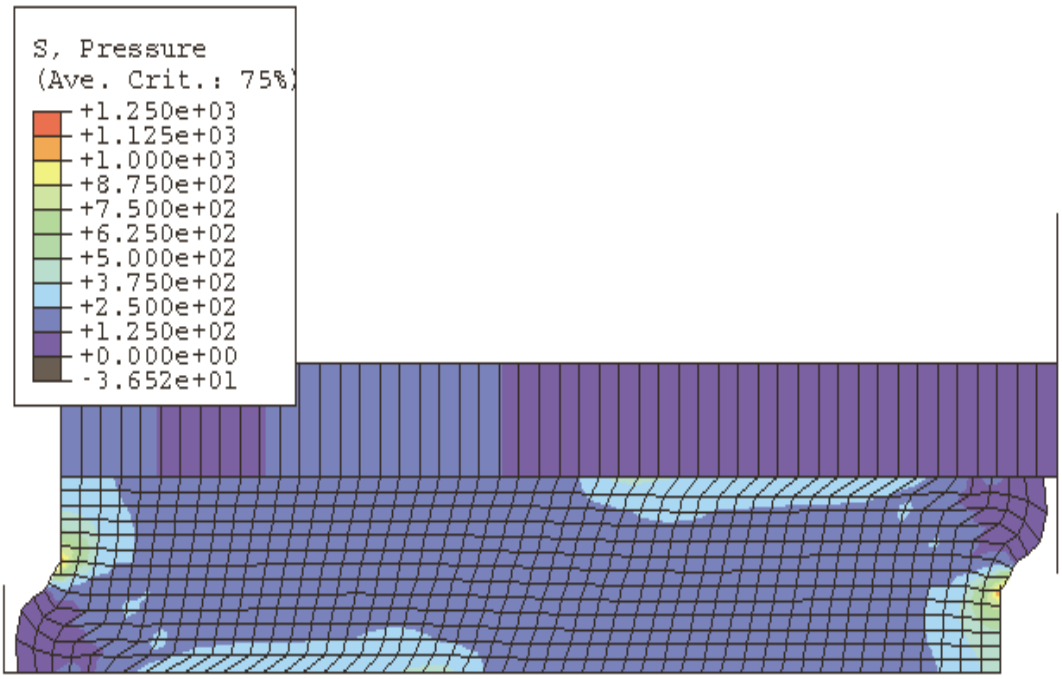

Figure 6.49. Confining pressure (kPa) for over-consolidated final bagasse, split box geometry, displacement 16 mm, fine mesh, friction 1.4.

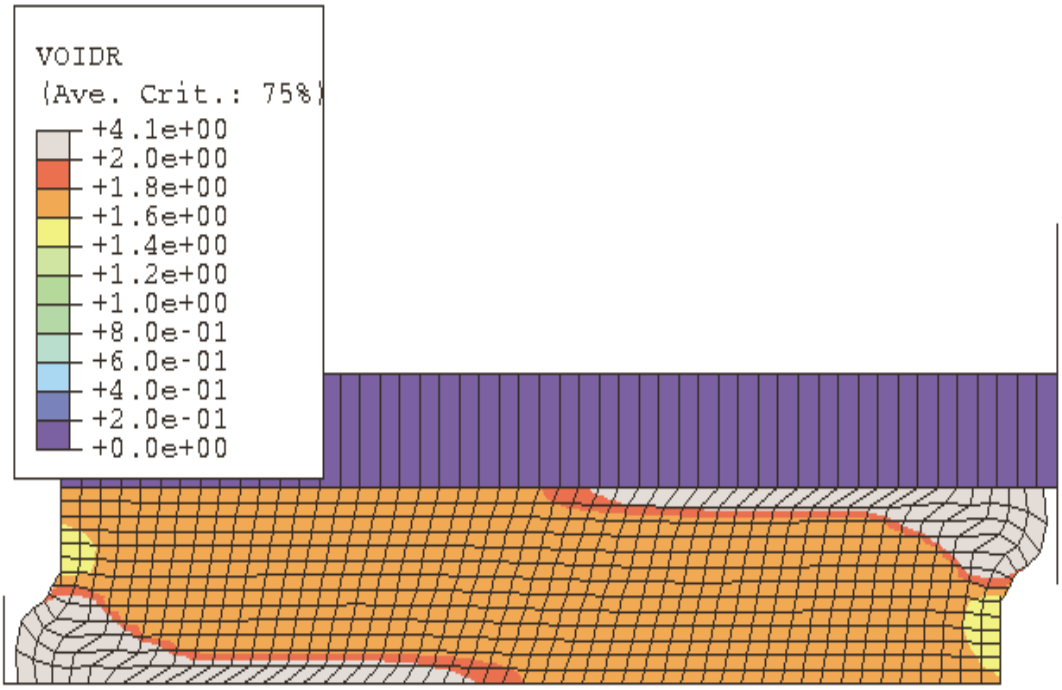

Figure 6.50. Void ratio for over-consolidated final bagasse, split box geometry, displacement 16 mm, fine mesh, friction 1.4.

localised shear planes), the high shear stress zones move towards the middle of the sample. As the localised shear planes are predicted to form, the sideways forces decrease while the overall sample keeps expanding. The locations of high shear strain expand while in the middle of the sample there is some reduction in volume.

Table 6.12 Predictions of single element quasi-analytical model for sideways displacements of 13 mm and 16 mm for over-consolidated bagasse

Sideways displacement (mm)	Change in height (mm)	Shear force (N)	Vertical force (N)
13	3.0	141	95
16	4.1	131	95

Table 6.13 Predictions of fine mesh split box model for sideways displacements of 13 mm and 16 mm for over-consolidated bagasse, coefficient of friction of 1.4

Travel of bottom node (mm)	Travel of top node (mm)	Change in height (mm)	Sideways reaction force (N)	Vertical reaction force (N)
Sideways displacement of 13 mm				
12.99	0.02	1.2	W1 0.0	0.0
			W2 74.9	95.4
			W3 18.2	5.3
			Sum 93	Sum 101
Sideways displacement of 16 mm				
15.98	0.02	1.8	W1 0.0	0.0
			W2 57.7	97.5
			W3 10.8	0.3
			Sum 69	Sum 98

The differences in the predicted distributions of the stresses and strains between a displacement of 13 mm and a displacement of 16 mm are quite striking. At 13 mm the shear strains throughout the sample are quite uniform. At 16 mm the shear strains are highly non-uniform. As shown previously in Chapter 5, the summary predictions from the single element model are very different from those of the fine mesh model. Because of the thin layers in which the shear planes form, a finer mesh than that shown would be desirable for a detailed study of the behaviour of an over-consolidated sample. A detailed comparison of the predicted and measured

deformations in a bagasse sample is not currently possible since in the experimental tests carried out and described in previous chapters (and the next chapter) the sample is hidden from view by the steel sides of the box. Even with clear side walls, a procedure similar to that carried out by Kirby (1994), where vertical layers of alternating colours were used to show the deformations in a normally consolidated clay sample and an over-consolidated clay sample, would be needed, and would be complicated by the large compressive deformations and the juice present.

The simulations for the modified box for a sideways displacement of 16 mm are shown in Figure 6.51 to Figure 6.56. Summaries of increase in sample height and forces are given in Table 6.14. For the modified box there is only one localised zone of high shear strain at the bottom and towards the left of the sample (the split box had two smaller zones predicted, one at the top right and one at the bottom left of the sample). The change in sample height predicted for the modified box is 11% smaller, while the sideways force is 4% higher. As in the simulations with the normally consolidated bagasse sample, the conclusion is that, although the split box is more uniform, the modified box is adequate.

The measured data for an over-consolidated final bagasse sample at an OCR of about 5.0 (Test G of the 1998 over-consolidated final bagasse tests) shows a maximum shear stress of 394 kPa (shear force of 110 N per mm width) at a sideways displacement of 8 mm and an increase in height of 0.5 mm (the same height sample was modelled). At a sideways displacement of 16 mm the shear stress decreases to 372 kPa (104 N per mm width) with an increase in sample height of 1.0 mm. Comparison of the measured values with the predictions in Table 6.13 and Table 6.14 shows that the predicted behaviour is less stiff than the measured behaviour, but that the predicted maximum shear force is only 15% less than the measured value. The values of measured and predicted changes in sample height are different, maybe by 80%, but when it is considered that for bagasse the change in volume due to compression forces is usually much larger than that due to shear forces, the differences are not seen as critical. The results give some confidence that the Modified Cam Clay material model (or a modification of it), in

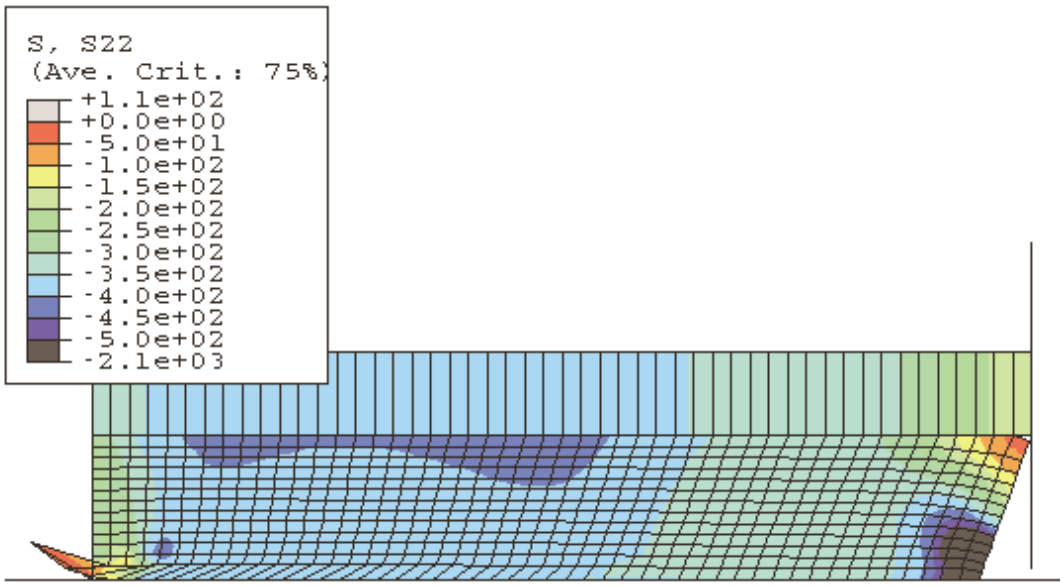

Figure 6.51. Vertical stress (kPa) for over-consolidated final bagasse, modified box geometry, displacement 16 mm, fine mesh, friction 1.4.

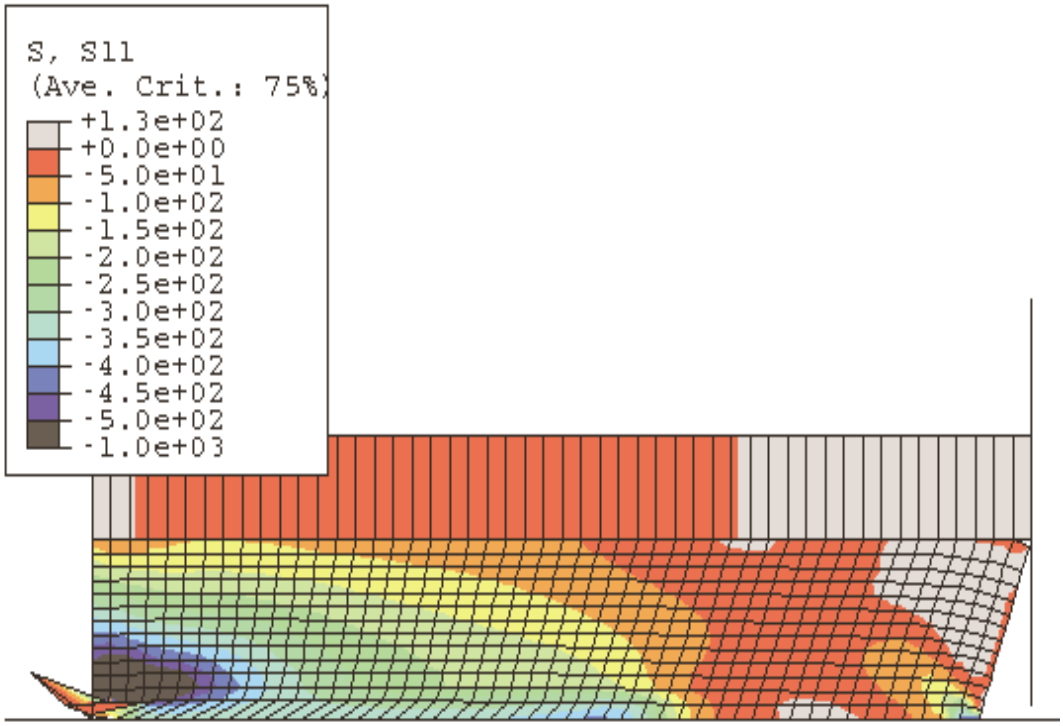

Figure 6.52. Horizontal stress (kPa) for over-consolidated final bagasse, modified box geometry, displacement 16 mm, fine mesh, friction 1.4.

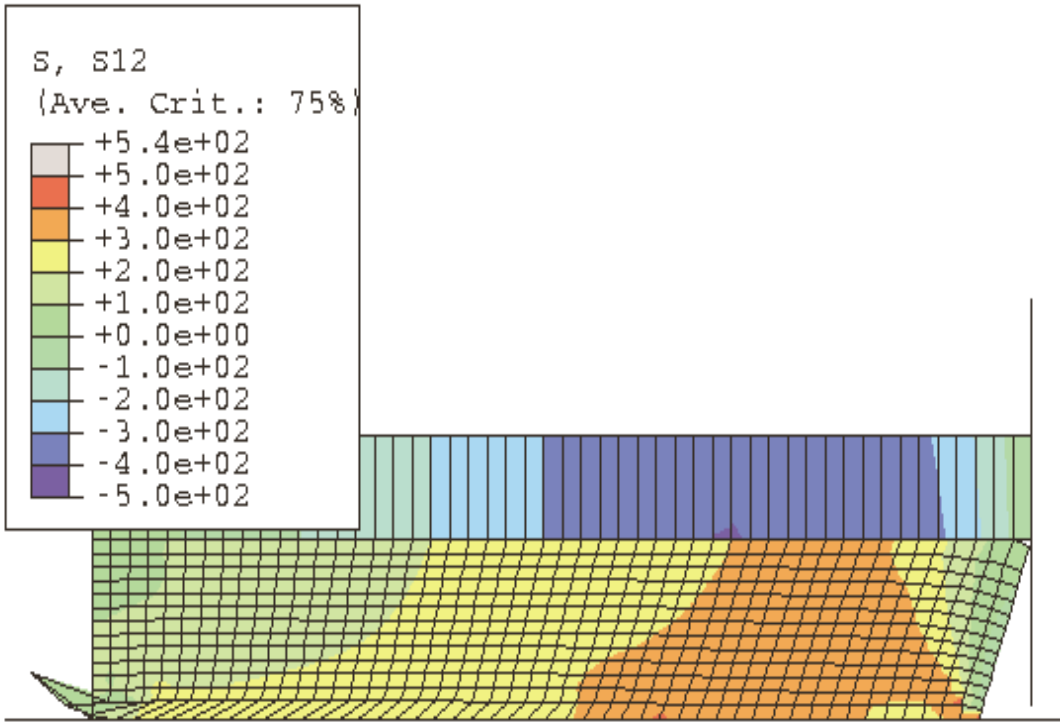

Figure 6.53. Shear stress (kPa) for over-consolidated final bagasse, modified box geometry, displacement 16 mm, fine mesh, friction 1.4.

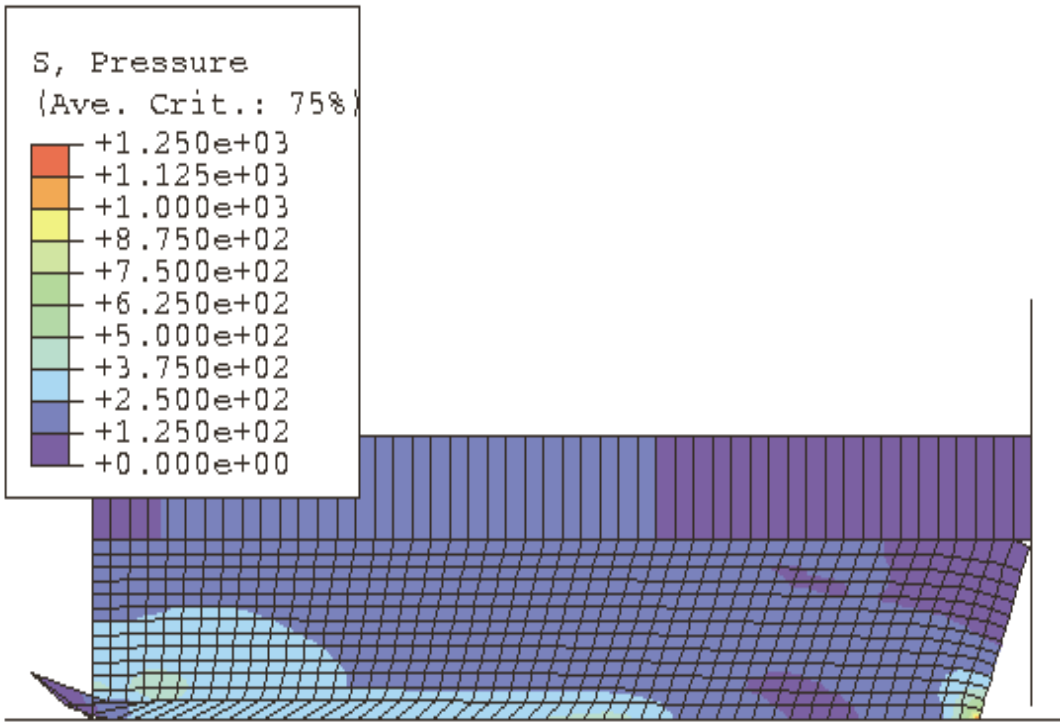

Figure 6.54. Confining pressure (kPa) for over-consolidated final bagasse, modified box geometry, displacement 16 mm, fine mesh, friction 1.4.

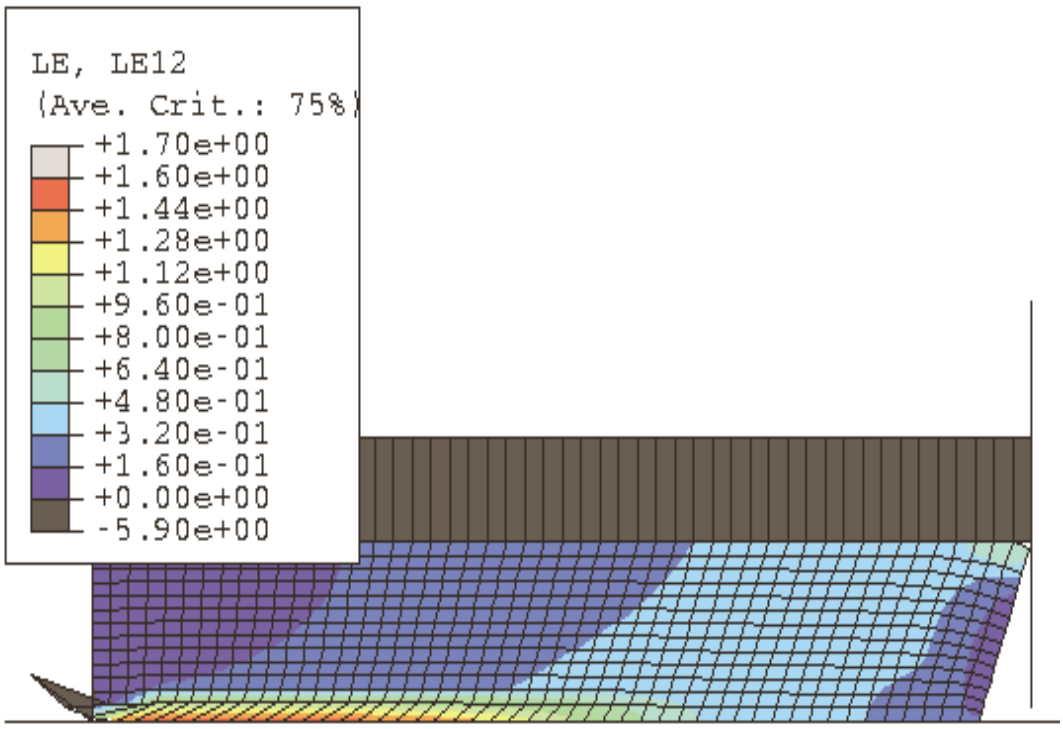

Figure 6.55. Shear strain for over-consolidated final bagasse, modified box geometry, displacement 16 mm, fine mesh, friction 1.4.

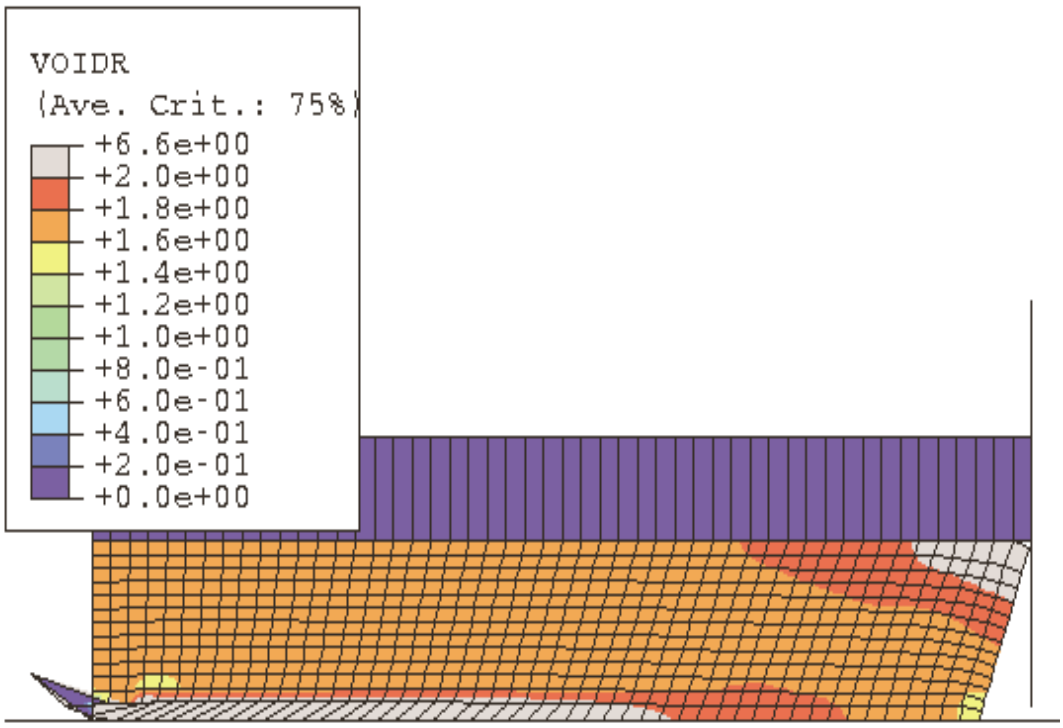

Figure 6.56. Void ratio for over-consolidated final bagasse, modified box geometry, displacement 16 mm, fine mesh, friction 1.4.

combination with an adequately finely meshed shear box, has a chance of predicting the shear behaviour of over-consolidated bagasse. The fact that the predicted coefficient of friction required as an input for the bottom and top surfaces of the split box and modified box to grip the final bagasse sample and prevent slip is very similar to the measured value, gives some strong confidence in the predictions carried out here using the Modified Cam Clay material model.

Table 6.14 Predictions of fine mesh modified box model for a sideways displacement of 16 mm for over-consolidated bagasse, coefficient of friction of 1.4

Travel of bottom node (mm)	Travel of top node (mm)	Change in height (mm)	Sideways reaction force (N)	Vertical reaction force (N)
15.99	0.01	1.6	72	98

6.5 Summary of Chapter 6

The modified direct shear test geometry that was used for the 1998 tests results in less uniform behaviour in the bagasse sample, compared to the classical split box geometry. However, the modified geometry has been concluded to be adequate for measuring bagasse behaviour, with the measurements being different to those from the split box by about 15%. For each geometry, the role and importance of the roughness on the top and bottom plates contacting the bagasse has been emphasised. Large shearing deformations are predicted to occur throughout all the sample for both the split box geometry and the modified geometry..

The modelling meshes used for the simulations of shearing of normally consolidated bagasse were adequate. The simulations have shown that both the coarse and fine mesh used are adequate for modelling the shear behaviour of normally consolidated bagasse in a direct shear box. Only the fine mesh is considered to be adequate for modelling the overall behaviour of over-consolidated bagasse. However, even the fine mesh may not be adequate to simulate the detail of the behaviour of over-consolidated bagasse, since thin localised shear planes are predicted to form.

The coefficient of friction required as a boundary input in order to prevent slip at the bagasse interface for the normally consolidated bagasse at the top and bottom surfaces was at least 0.6. For the heavily over-consolidated bagasse sample the value was at least 1.1. These values are in good agreement with the values of the internal coefficient of shear that were measured in the 1998 tests and this agreement is encouraging. Comparison of measurements and predictions have shown that the Modified Cam Clay model (or a modification of it), in combination with an adequately finely meshed shear box, has a good chance of predicting the shear behaviour of over-consolidated bagasse in a shear box (and therefore can be trialed with some confidence in modelling other geometries involving shearing). Similarly, Chapter 5 showed that there was a good chance of modelling the shear behaviour of normally consolidated bagasse. However, Chapter 5 also showed that there were major limitations in modelling the shear behaviour in combination with loading and unloading compression behaviour when using the Modified Cam Clay or similar critical state models. The inability to simultaneously model different loading combinations is seen as a major problem for modelling the crushing process in a milling unit, which is believed to involve complex loading conditions including both compression and shear.

7 Chapter 7 – Direct shear test measurements of bagasse behaviour at pressures occurring in the three main rolls

7.1 Introduction

The experimental tests carried out in late 1998 and described in Chapter 3 and Chapter 4 were carried out at pressures similar to those occurring at the pressure feeder of a milling unit. Direct shear tests were carried out at vertical pressures ranging from 200 kPa to 2000 kPa. The behaviour at the much higher pressures (up to about 20000 kPa) and compactions that occur at the three main rolls of a milling unit had not been measured. However, there were some previous measurements that intimated that the detail of the behaviour at the higher pressures may be different from that at lower pressures. In 1992, tests were carried out using a direct shear test rig (Plaza et al, 1993) with the aim of determining the required surface roughness to grip prepared cane and shear it internally. That limited set of measurements suggested that the magnitudes of the material parameters at the much higher pressures could be significantly different. For example, Figure 5.3 from Plaza et al (1993), reproduced in Figure 10 of Plaza and Kent (1997), showed the maximum shear stress plotted against vertical pressure for tests on normally consolidated prepared cane (the Mohr-Coulomb failure criterion). There are two distinct zones (one from about 200 to 4000 kPa, and one from about 6000 to 18000 kPa) in that plot with markedly different friction angles. The transition range between 4000 kPa and 6000 kPa where the friction angle changes greatly, matches with a similar transition range in a plot of compaction (or another measure of density) versus pressure.

In the second half of 2001 funding became available to carry out direct shear tests at the high pressures in the three main rolls, with the aim of measuring bagasse behaviour. The results of those tests are described in this chapter.

7.2 Test geometry and equipment

The equipment used for the higher pressure tests was very similar to that described in Chapter 4 for the tests at pressure feeder compactions. However, there were also some differences. The overall geometry is shown in Figure 7.1 while the arrangement of the top plate is shown in Figure 7.2.

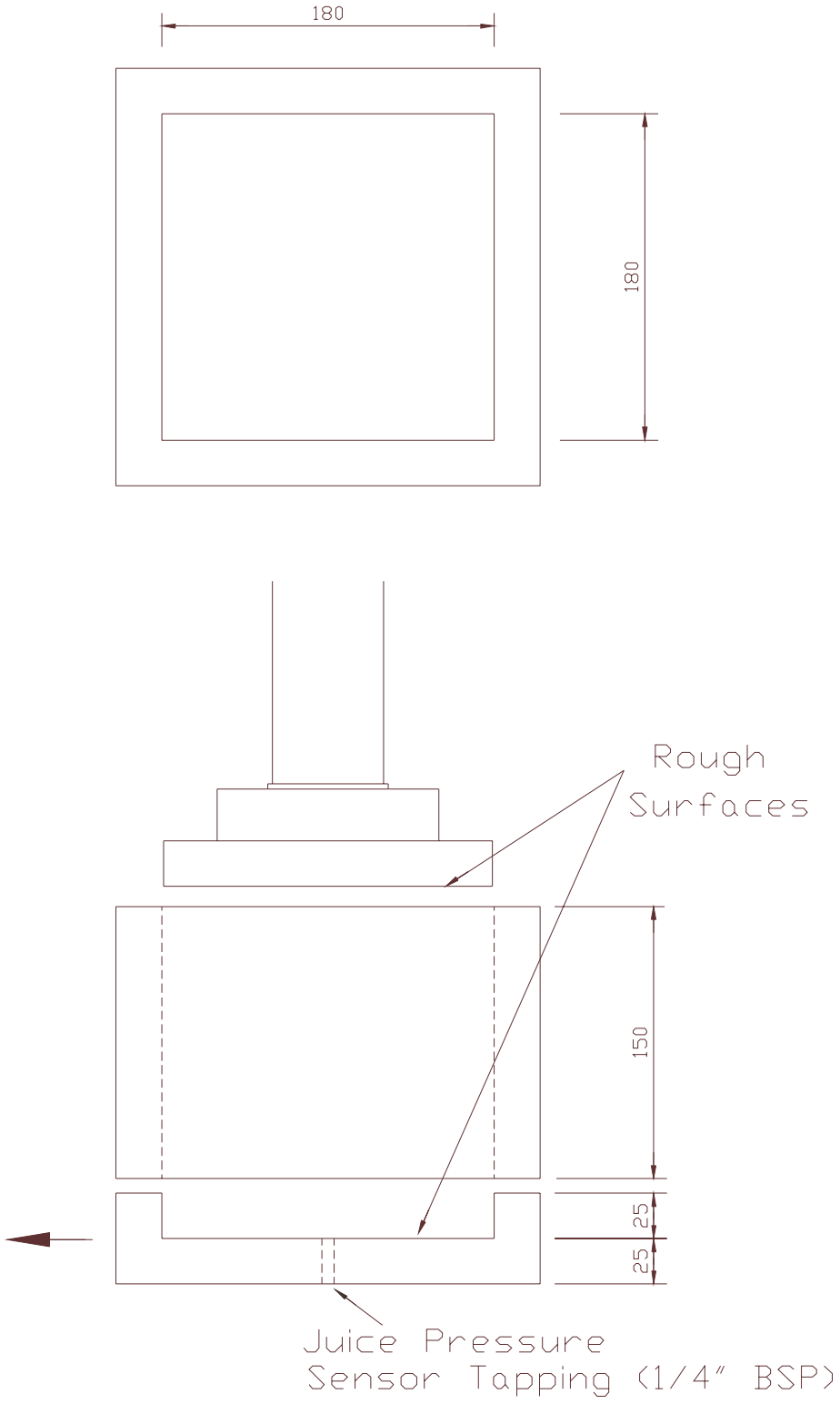

Figure 7.1. Overall geometry of direct shear test at higher pressures.

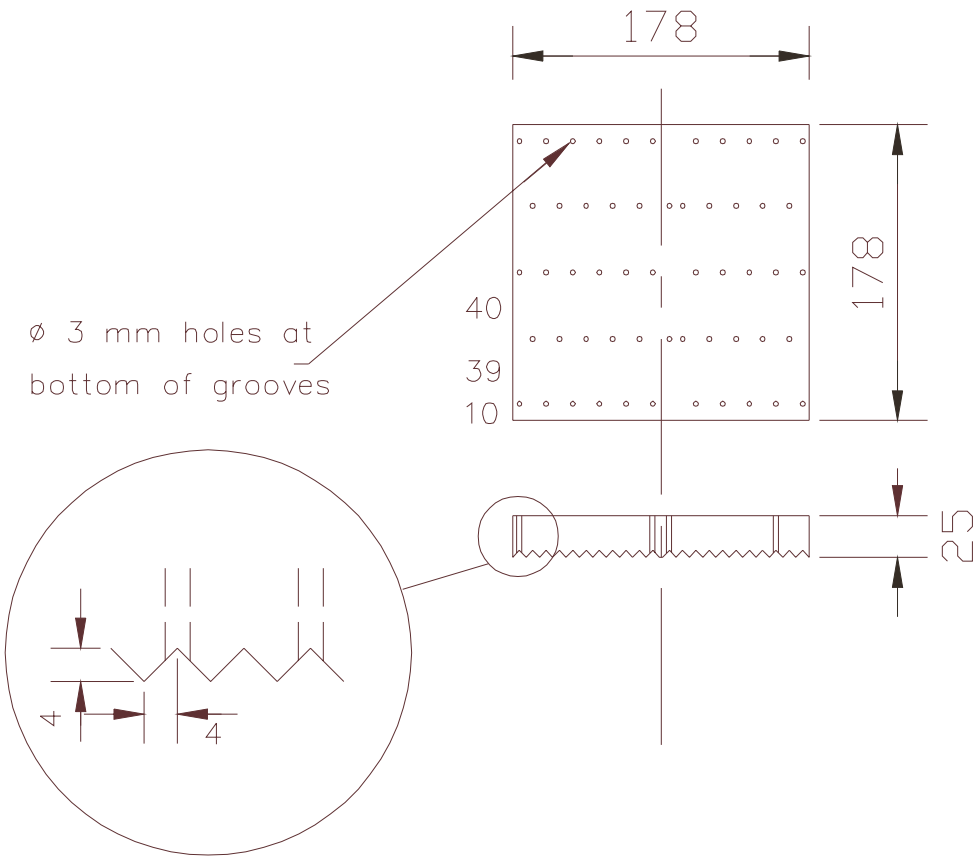

Figure 7.2. Arrangement of top plate and surface details for higher pressure tests.

Following the outcomes of the direct shear test geometry modelling described in Chapter 6, a classical split box geometry was used (instead of the modified geometry with the flat bottom plate which had been used for the tests at pressure feeder compactions). The box had internal dimensions 180 mm by 180 mm and was 150 mm high. The bottom plate still had a P24 (~1 mm diameter particles) closed coat sandpaper surface, and a 6.35 mm (1/4 inch) diameter hole at its middle through which water (juice) pressure was measured. The top plate still had 4 mm grooves with their axis perpendicular to the direction of sideways movement of the bottom plate. The grooves were drained to the top surface of the top plate through 3 mm diameter holes accessing the bottom of the grooves.

The vertical load on the top plate, the horizontal load on the bottom plate, the vertical displacement of the top plate, the horizontal displacement of the bottom plate, and the juice pressure at the middle of the bottom plate were logged.

7.3 Test procedure

The test procedure was similar to that described in Section 4.3 for the tests at pressure feeder compactions except for the following. A separate pre-compressor box, this time 270 mm high, was used to form a compound box in order to place enough prepared cane, first bagasse or final bagasse into the test box to be able to carry out the tests within the limited working height of the vertical press used. The sample was compressed into the test box in a separate large stroke/low pressure press and the test box containing the sample was then placed in the vertical press. Also, once the juice pressure had been reduced to a low level, the top plate was lifted off the cane then put back and increased to the target load, in readiness for the shearing stage (the second alternative used for the tests at pressure feeder compactions).

7.4 Test series at pressures in the main three rolls

The pressure range targeted was 1500 kPa to 16000 kPa. The tests were drained (but it is again noted that it is almost impossible to have zero water pressure during these kind of tests on bagasse), over-consolidated, constant total vertical pressure during shear tests. The over-consolidation ratios ranged from 1.0 to 10.0. The materials tested were variety Q124 prepared cane, first bagasse and final bagasse from Pleystowe Mill and Racecourse Mill. 67 tests were carried out and a summary is shown in Table 7.1. The test numbers show the order in which the tests were carried out each day. The sample masses and fibre contents are shown in Table 7.2. The fibre contents for prepared cane and final bagasse are averages for the mill for that week. The fibre content for first bagasse was determined from other tests not connected to this investigation.

A further 16 tests were carried out on prepared cane of different cane varieties. The prepared cane samples were normally consolidated to and sheared at a vertical pressure of approximately 1800 kPa and their description is shown in Table 7.3. The test numbers show the order in which the tests were carried out on the 17-10-2001. A duplicate test was carried out on a second subsample from the same sample collected from the mill for each cane variety. The mass of each subsample was 5 kg. The fibre content for Q124 was the mill average for that week. For

varieties Q135, Q136 and H56-752 from Pleystowe the fibre content was the average for the 17-10-2001 and was measured using a NIR (Near Infrared) machine. A value for Q117 of 15.58 % was also measured using the NIR machine. No fibre contents were available for H56-752 from Pleystowe and Q135, Q96, and Q117 from Racecourse.

Also included for comparison purposes in the results that follow are results from Chapter 4 for tests carried out at pressure feeder conditions.

7.5 General behaviour of bagasse at pressures in the main three rolls

The raw data for the tests is given in Appendix D. Also given in Appendix D are photographs of the equipment. The behaviour of prepared cane, first bagasse, and final bagasse at pressures ranging from 1500 kPa to 16000 kPa has been found to be similar to the behaviour measured in previous tests at pressures ranging from 200 kPa to 2000 kPa (pressure feeder compactions). An example of the behaviour is shown below for final bagasse.

Figure 7.3 shows the compression, unloading and reloading behaviour of final bagasse to and from a pressure (15000 kPa) close to delivery nip pressures (reproduced from Figure D.4.23 in Appendix D). The behaviour is very similar to Figure B.1.20 in Appendix B, where the bagasse was loaded to pressure feeder pressures. In Figure 7.3 the bagasse was initially loaded to an effective vertical pressure of about 15000 kPa. The initial loading line has two distinct sections. The first section is where the bagasse is reloaded to about 80 kPa (a pressure to which it was previously loaded during the initial test setup prior to transfer to main vertical press) at which time the normal compression line (NCL) is reached. During this time the specific volume is almost constant at about 7.6 with a slight decrease in volume that is barely discernible at the scale of the graph. The second section is along the NCL until a pressure of about 15000 kPa is reached. The normal compression line is not of high quality because it was reached by increasing the pressure manually (as the main objective of the tests was to be able to carry out shearing at constant vertical pressure).

Table 7.1 Summary of direct shear tests at pressures occurring in the three main rolls

Material type	Date	Mill	Test number	Nominal (or target) pressures and over-consolidation ratios		
				Maximum pressure (kPa)	Over-consolidation pressure (kPa)	Over-consolidation ratio
Final bagasse	11-10-2001	Pleystowe	1	8000.0	1600.0	5.0
			2		1600.0	5.0
First bagasse			1	12800.0	12800.0	1.0
			4		7680.0	1.67
			3		5120.0	2.5
			2		2560.0	5.0
			5		1543.0	8.3
Final bagasse	12-10-2001	Racecourse	4	16000.0	16000.0	1.0
			2		12800.0	1.25
			6		9600.0	1.67
			1		6400.0	2.5
			3		3200.0	5.0
			5		1600.0	10.0
Final bagasse	13-10-2001	Racecourse	4	4000.0	4000.0	1.0
			2		3200.0	1.25
			3		2345.0	1.7
			5		1850.0	2.16
			1		1600.0	2.5

Material type	Date	Mill	Test number	Nominal (or target) pressures and over-consolidation ratios		
				Maximum pressure (kPa)	Over-consolidation pressure (kPa)	Over-consolidation ratio
Final bagasse	14-10-2001	Racecourse	13	16000.0	16000.0	1.0
			10		12800.0	1.25
			8		6400.0	2.5
			11		4800.0	3.33
			9		3200.0	5.0
			12		1850.0	8.64
			4	10800.0	10800.0	1.0
			3		8640.0	1.25
			6		6480.0	1.67
			5		5400.0	2.0
			2		4320.0	2.5
			1		2160.0	5.0
			7		1230.0	8.75
			14	2685.0	2685.0	1.0
Prepared cane	15-10-2001	Racecourse	16	16000.0	16000.0	1.0
			17		9600.0	1.67
			13		6400.0	2.5
			14		3200.0	5.0
			15		2000.0	8.0

Material type	Date	Mill	Test number	Nominal (or target) pressures and over-consolidation ratios		
				Maximum pressure (kPa)	Over-consolidation pressure (kPa)	Over-consolidation ratio
			11	8000.0	8000.0	1.0
			9		6400.0	1.25
			8		3200.0	2.5
			10		2000.0	4.0
			12		1230.0	6.5
			7	4630.0	4630.0	1.0
			4		1230.0	3.75
			3	4000.0	4000.0	1.0
			6		3600.0	1.1
			1		3200.0	1.25
			2		2400.0	1.67
			5		1230.0	3.25
First bagasse	16-10-2001	Pleystowe	10	16000.0	16000.0	1.0
			9		9600.0	1.67
			7		6400.0	2.5
			11		4800.0	3.33
			6		3200.0	5.0
			8		2000.0	8.0
			4	10000.0	10000.0	1.0
			2		6000.0	1.67

Material type	Date	Mill	Test number	Nominal (or target) pressures and over-consolidation ratios		
				Maximum pressure (kPa)	Over-consolidation pressure (kPa)	Over-consolidation ratio
			1		4000.0	2.5
			5		3000.0	3.33
			3		2000.0	5.0
			15	6000.0	6000.0	1.0
			13		3600.0	1.67
			12		2400.0	2.5
			14		2000.0	3.0
			16		1230.0	4.86
			17	3000.0	3000.0	1.0
			18	1500.0	1500.0	1.0

Table 7.2 Sample masses for direct shear tests at pressures occurring in the three main rolls

Date	Maximum pressure (kPa)	Mass (kg) & Fibre content (%) (in brackets)		
		Prepared Cane	First bagasse	Final bagasse
11-10-2001	8000.0			2.5 (47.0)
	12800.0		2.5 (36.4)	
12-10-2001	16000.0			2.6 (46.0)
13-10-2001	4000.0			2.2 (46.0)
14-10-2001	16000.0			2.5 (46.0)
	8000.0			2.5
	2680.0			2.5
15-10-2001	16000.0	6.5 (14.8)		
	8000.0	6.0		
	4030.0	5.0		
	4000.0	5.0		
16-10-2001	16000.0		3.2 (36.4)	
	10000.0		2.6	
	6000.0		2.5	
	3000.0		2.5	
	1500.0		2.5	

Table 7.3 Summary of direct shear tests on different cane varieties carried out on 17-10-2001

Mill	Cane variety	Test number	Fibre content (%)	Comments
Pleystowe	Q124	4, 9	14.7	
	Q135	8, 13	15.97	
	Q136	3, 16	16.44	Stringy, large proportion of long fibres
	H56-752	6, 12	NA	
Racecourse	Q124	1, 10	15.2	Q124 from Racecourse is more finely prepared
	Q135	2, 14	NA	Q135 from Racecourse is more finely prepared
	Q96	5, 15	NA	
	Q117	7, 11	NA	

It is believed a high quality NCL can be measured by carrying out relatively slow constant speed compression tests, which should be very easy to carry out using computer control (some press machines already have that capability). Such tests should not be so slow such that creep behaviour becomes a factor. However, it was not possible to setup such tests in the limited time available for this investigation.

The sample was then unloaded fully and reloaded fully four times. The four data lines grouped at the bottom are the unload lines and their slopes (kappa, κ) are quite similar to the slope of the initial reload section where loading was carried out to 80 kPa. In the middle of Figure 7.3 are the four reload lines. They were expected to be located close to the unload lines. Their location is believed to be due to the bagasse sample being disturbed by the bagasse sticking to the top grooved plate and prising the sample apart as the plate lifted off the sample during each full unload. The sample has therefore being disturbed and is no longer at the same over-consolidation. The re-load lines are therefore higher than the unload lines. The reload lines converge on the position of the unload lines after a pressure of about 1500 kPa.

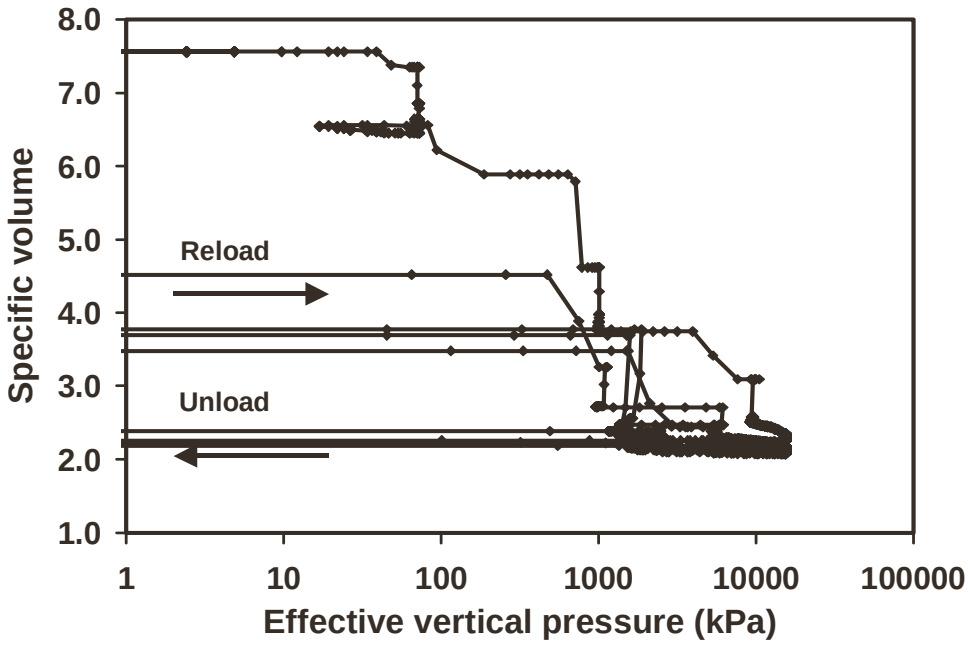

Figure 7.3. Compression behaviour of final mill bagasse loaded to a vertical pressure of 15000 kPa.

Shown in Figure 7.4 is a sample initially loaded to 15600 kPa, unloaded and sheared at a vertical effective pressure of 12200 kPa (a low over-consolidation ratio of about 1.26), with the final bagasse undergoing a decrease in volume during shearing (reproduced from Figure D.4.20 in Appendix D). The sample behaved in a similar way as the sample behaviour shown in Figure B.1.23 of Appendix B, a test carried out at much lower pressures.

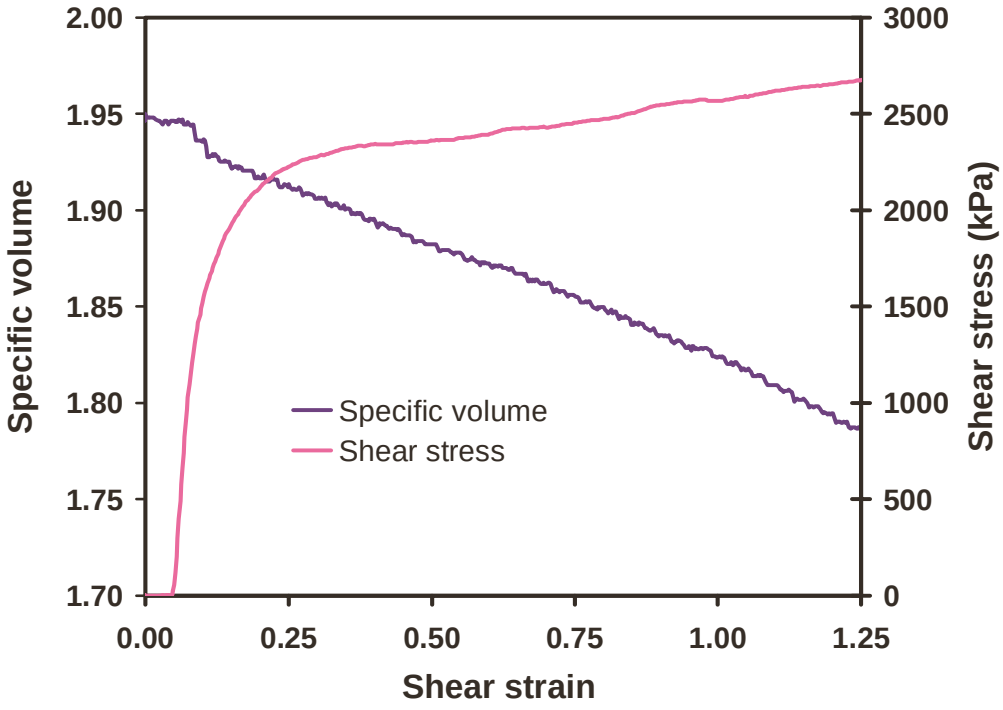

Figure 7.4. Shear behaviour of lightly over-consolidated final mill bagasse from a pressure close to that in a delivery nip.

The shear stress and specific volume behaviour of a final bagasse sample that was initially loaded to 15200 kPa, unloaded and then sheared at an effective vertical pressure of 1620 kPa (a high over-consolidation ratio of about 9.3) is shown in Figure 7.5 (reproduced from Figure D.4.24 in Appendix D). The bagasse undergoes a slight initial decrease in volume and then expands while being held under constant pressure. The sample behaved in a similar way to the sample shown in Figure B.1.29 of Appendix B, a test carried out at much lower pressures.

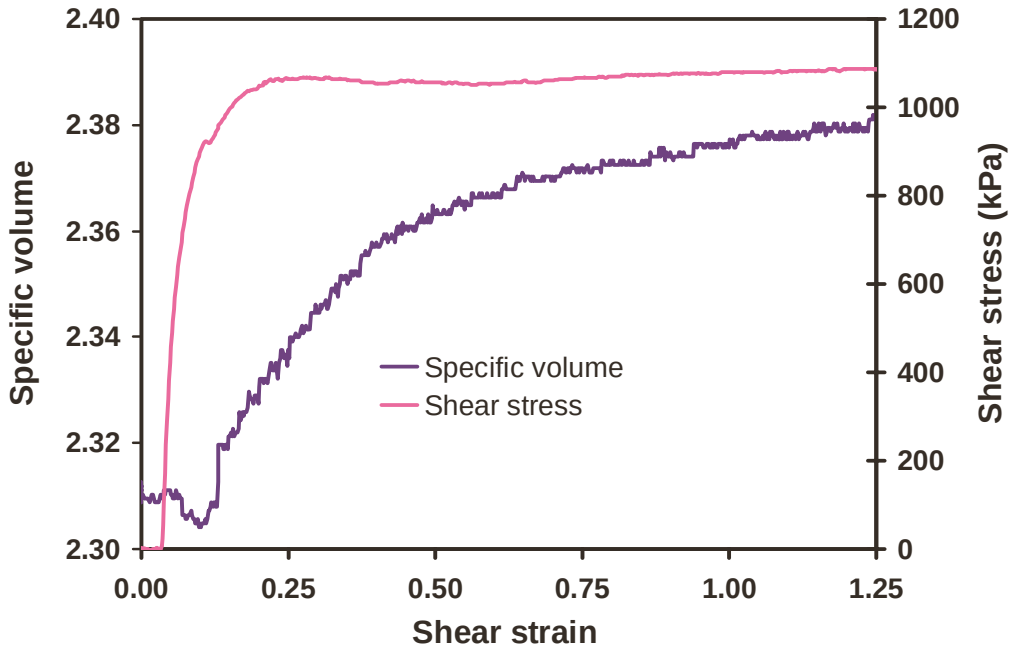

Figure 7.5. Shear behaviour of highly over-consolidated final mill bagasse from a pressure close to that in a delivery nip.

In summary, the measured general mechanical behaviour of final bagasse at pressures occurring in the main three rolls in a milling unit is similar to the behaviour of final bagasse at pressures occurring in the pressure feeder unit. It is critical state behaviour similar to that of soil. Similar behaviour has been measured for prepared cane and first bagasse. However, the next section shows that the detail of the behaviour is different as pressure increases.

7.6 Detail of material behaviour and magnitudes of material parameters

This section provides the detail of the measured behaviour and magnitudes of material parameters, both for the tests carried out at pressures occurring in the three main rolls and for the tests carried out previously at the pressures in the pressure feeder and described previously in Chapter 4.

7.6.1 Slopes of the normal compression line and elastic unloading-reloading line

The measured magnitudes of the slope of the normal compression line (lambda, λ) and the slope of the elastic unloading-reloading line (kappa, κ), are given in Table 7.4. As noted previously, the values of λ at pressures of 4000 kPa and above (the

2001 tests) are not accurate due to the poor quality of the measured NCL. The magnitudes of λ are much larger than the values of κ. The magnitudes of both λ and κ tend to decrease as pressure increases. The magnitudes of both λ and κ also tend to decrease as the cane material moves down the milling train, that is, from prepared cane to first bagasse and to final bagasse.

Table 7.4 Values of λ and κ for prepared cane, first bagasse, and final bagasse at pressure feeder and three main rolls pressures.

	Prepared Cane		First Bagasse		Final Bagasse	
Pressure (kPa)	λ	κ	λ	κ	λ	κ
1500 (1998)	2.19	0.23	1.28	0.18		
2000 (1998)	1.92	0.26	1.23	0.18	1.12	0.17
4000	0.84	0.039			1.36	0.068
6000			1.40	0.049		
8000	1.24	0.048				
10000			0.85	0.043		
10800					0.61	0.045
16000	1.36	0.039	1.05	0.046	0.74	0.038

7.6.2 Volumetric strain during shearing and position of critical state line with respect to normal compression line

In the previous section, two examples have been given of final bagasse: one, lightly over-consolidated, compressed during shearing, and one, heavily over-consolidated, expanded during shearing. The volumetric strain (the change of specific volume during shear divided by the specific volume just before shearing starts) was calculated for tests at different degrees of over-consolidation and unloaded from different maximum effective vertical pressures. The pressures were normalised by dividing by the maximum effective vertical pressure for each test. Figure 7.6, Figure 7.7 and Figure 7.8 show plots of volumetric strain against normalised effective vertical pressure for prepared cane, first bagasse, and final bagasse respectively. A positive volumetric strain means that the sample expanded, while a negative volumetric strain means the sample decreased in volume.

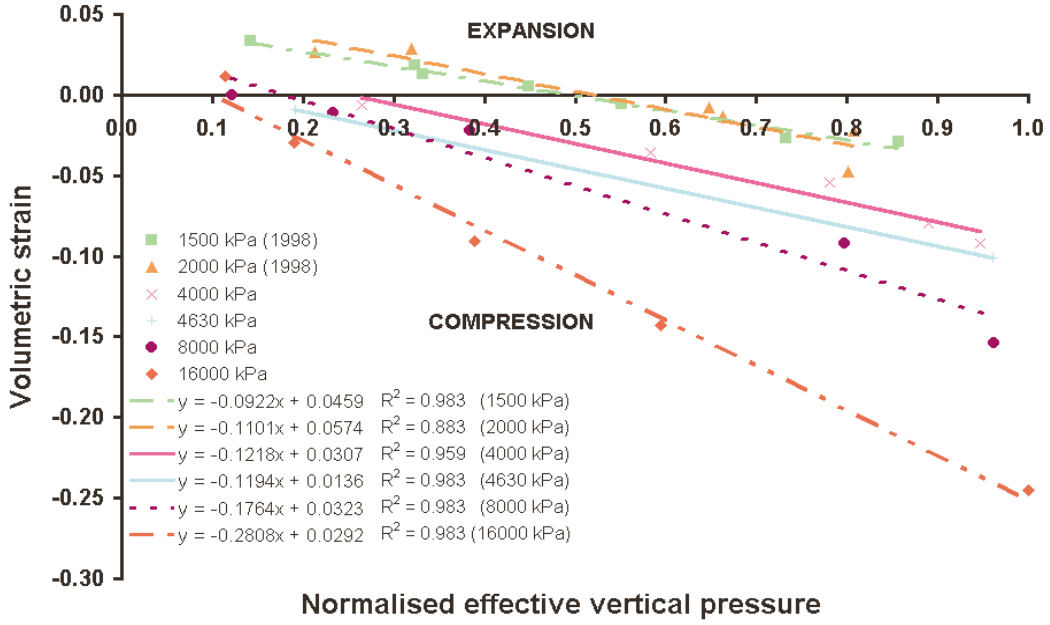

Figure 7.6. Volumetric strain during shearing for prepared cane.

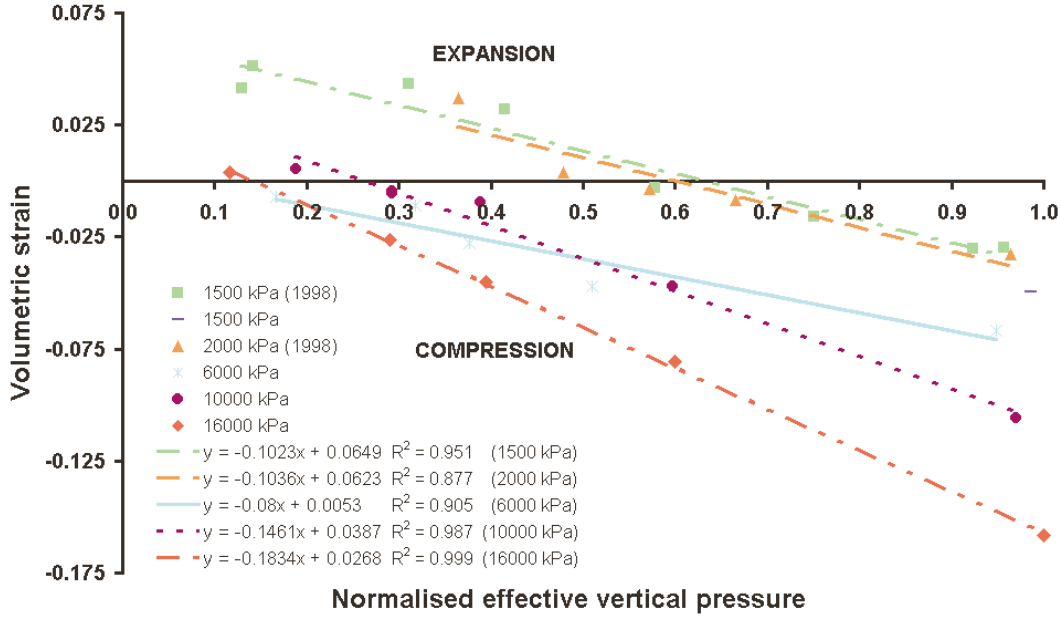

Figure 7.7. Volumetric strain during shearing for first bagasse.

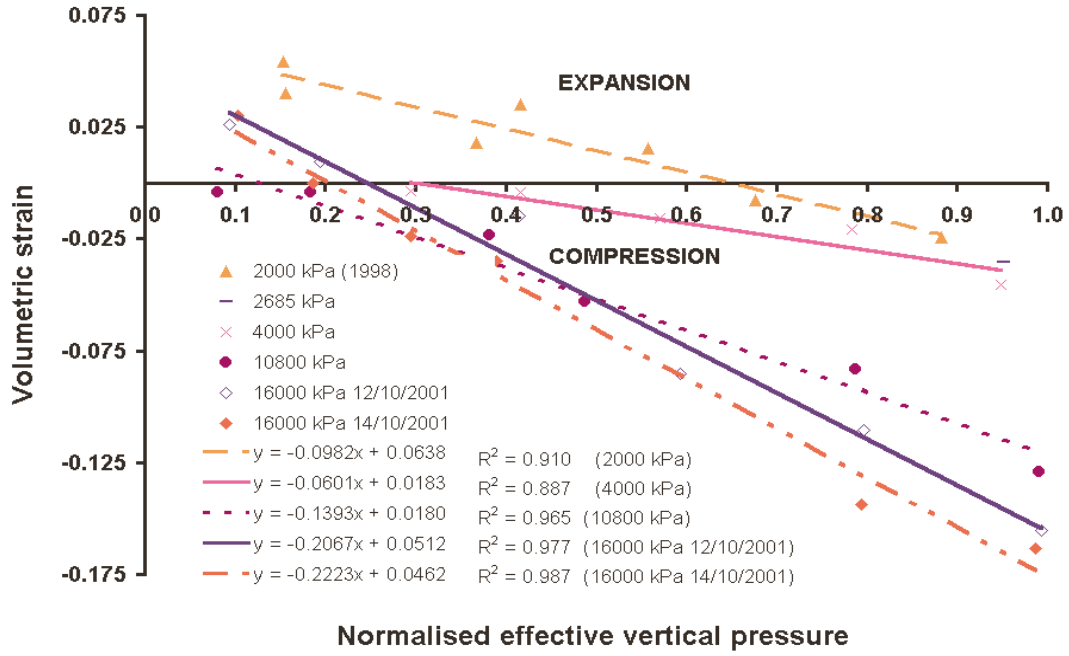

Figure 7.8. Volumetric strain during shearing for final bagasse.

A line of best fit is shown for each set of tests unloaded from a particular maximum vertical pressure. It is shown that, as the maximum vertical pressure increases from 1500 kPa to 16000 kPa, the measured values move further into the compressive region. This behaviour is well documented for soils, and is referred to as 'the suppression of dilatancy which accompanies an increase in effective normal stress' (Bishop, 1972).

One consequence of this 'suppression of dilatancy' behaviour is that the position at which the lines of best fit cross the horizontal axis is changed by a large amount. This position is that of zero volumetric strain during shear and it locates the critical state line with respect to the normal compression line. This is an important parameter for the description of a critical state model and is discussed in the next chapter, together with the likely effects for a material model that better reproduces bagasse behaviour. Here, the positions are detailed in Table 7.5 as the ratio of effective vertical pressure during shearing to the maximum effective vertical pressure. The reciprocal of this ratio (which is the over-consolidation ratio) is also shown. The effect of the overall movement of the values into the compression region as pressure increases is to move the position of zero volumetric strain (the position of the critical state line) further to the left. That is, the ratio of effective

vertical pressure to maximum effective vertical pressure decreases, and the over-consolidation ratio increases. It is also noted that for all three materials this trend is obscured at intermediate pressures from about 4000 kPa to 10000 kPa where the lines of best fit are significantly flatter than those at lower and higher pressures, and in general, the over-consolidation ratios at zero volumetric strain are similar to, or even larger than, the values at higher pressures. The reason for this behaviour is not known.

Table 7.5 Position of zero volumetric strain during shearing

Nominal maximum effective vertical pressure (kPa)	Ratio of pressure during shearing to maximum pressure (Over-consolidation ratio in brackets)		
	Prepared cane	First bagasse	Final bagasse
1500	0.50 (2.0)	0.63 (1.6)	
2000	0.52 (1.9)	0.60 (1.7)	0.65 (1.5)
4000	0.25 (4.0)		0.30 (3.3)
4630	0.11 (9.1)		
6000		0.07 (14.3)	
8000	0.18 (5.6)		
10000		0.26 (3.8)	
10800			0.13 (7.7)
16000	0.10 (10.0)	0.15 (6.7)	0.25 (4.0), 0.21 (4.8)

There is also a trend for the values of over-consolidation ratios at zero volumetric strain to decrease as the material tested changes from prepared cane to first bagasse and to final bagasse (that is, as the cane residue moves down the milling train). This trend is apparent at all pressures, both low and high, at which there are values for comparison.

7.6.3 Equivalent friction angle of the critical state line

Shown in Chapter 4 is a procedure for estimating the value of the equivalent friction angle of the critical state line, ϕ_{cs}, following Kirby (1991), and M, the slope of the critical state line, from the relation $M = 2 \sin \phi_{cs}$ (Naylor and Pande, 1981). The data for pressure feeder conditions were shown in Chapter 4. Those data are included in this section where the results for all pressures are shown for prepared cane, first bagasse, and final bagasse in Figure 7.9, Figure 7.10, and Figure 7.11,

respectively. The maximum and final shear stresses during the shearing part of a shear test are shown, normalised by the maximum effective vertical pressure, and plotted against the normalised effective vertical pressure. For the tests at pressure feeder conditions, values for ϕ_{cs} and M are given in Table 4.7 in Chapter 4. For example, values of 36.9^{o} and 1.2 respectively were estimated for first bagasse. Looking at Figure 7.10 for first bagasse, it is clear that at higher pressures, the slope of ϕ_{cs} is substantially smaller. The estimation of ϕ_{cs} is complicated by the presence of a transition in the test data (this transition is more clearly shown in the next section where non-normalised versions of Figure 7.9, Figure 7.10 and Figure 7.11 show that the friction angles at low pressure are much higher than at high pressure). Values of ϕ_{cs} and M of 14.5^{o} and 0.5 respectively at the higher pressures, or even as low as 3^{o} and 0.1 respectively at a maximum vertical pressure of 16000 kPa, look realistic for first bagasse. Similar values were determined for prepared cane and final bagasse. The decrease in the values of ϕ_{cs} and M is consistent with the much lower friction angle shown in Figure 10 of Plaza and Kent (1997) at pressures above 6000 kPa.

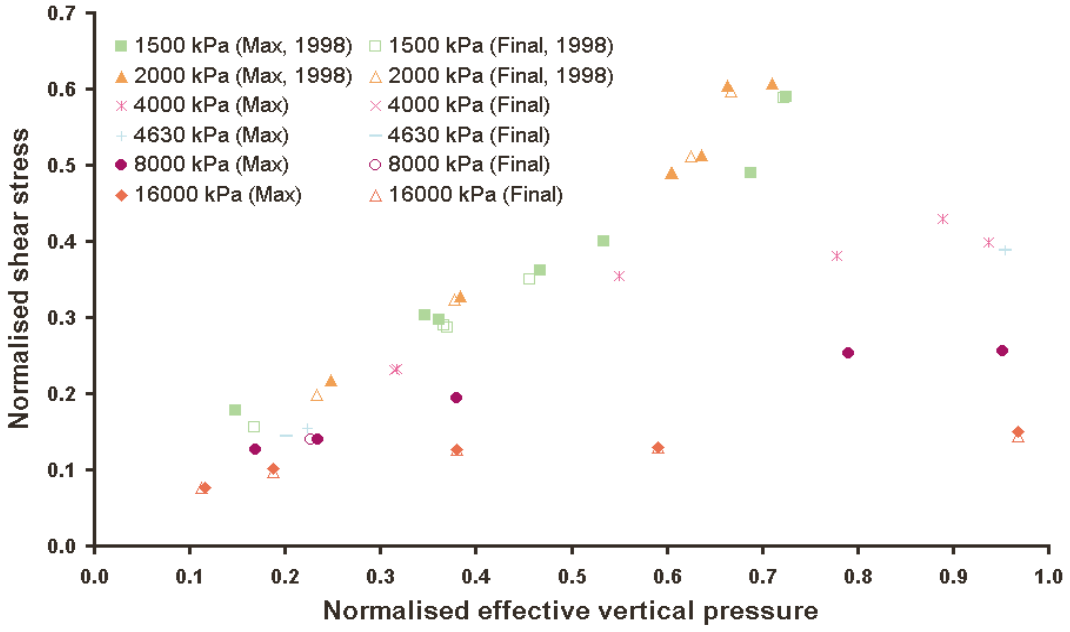

Figure 7.9. Normalised maximum and final shear stresses for prepared cane.

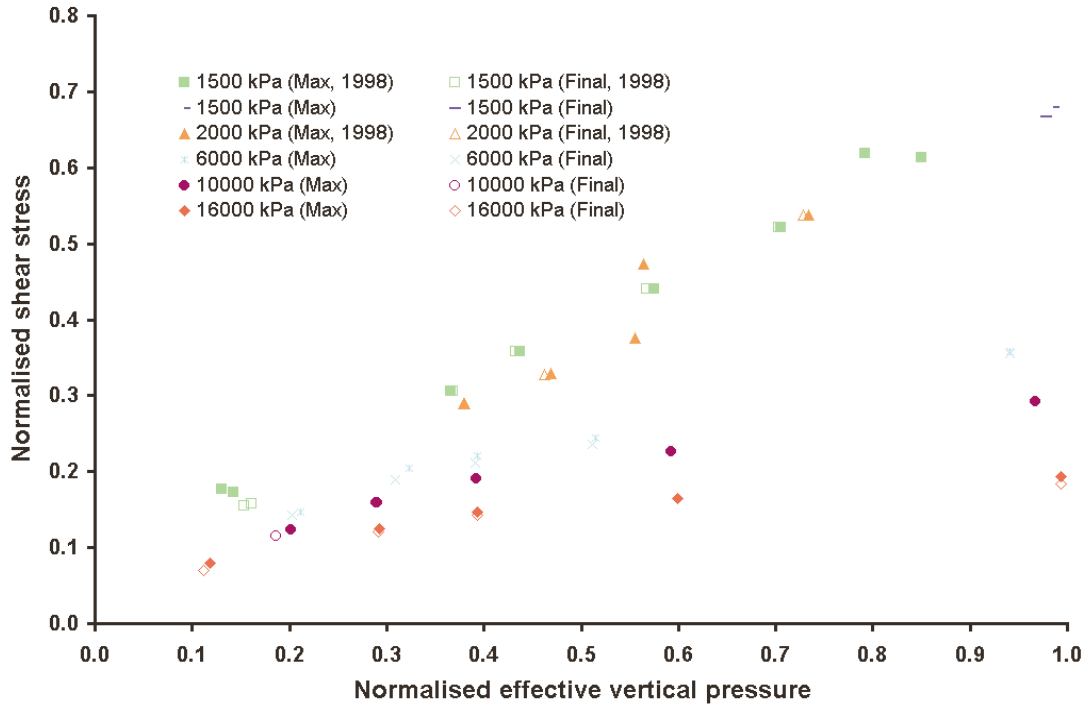

Figure 7.10. Normalised maximum and final shear stresses for first bagasse.

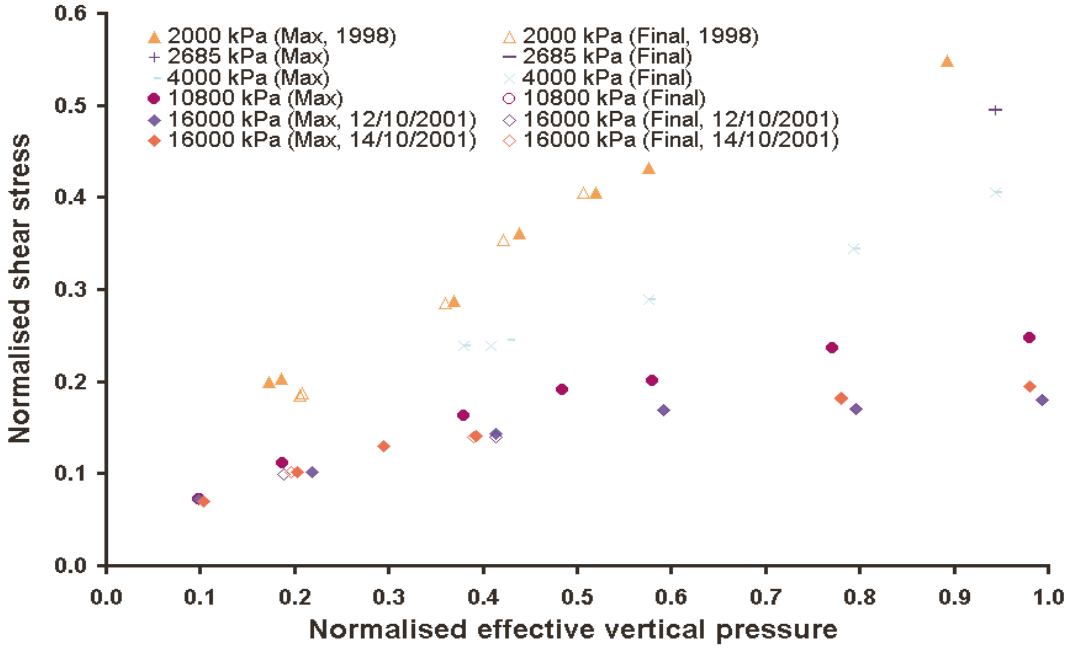

Figure 7.11. Normalised maximum and final shear stresses for final bagasse.

Included in Figure 7.10 (and Figure 7.7 of the previous section) are the results from a single test that was carried out in 2001 at the same maximum vertical pressure (1500 kPa) as one set of the 1998 tests. There is good agreement, even though the tests were three years apart, the test equipment was slightly different (the 1998 one being the modified geometry and the 2001 being the classical geometry with the insert), and the test box for the 1998 tests was significantly larger in area. The results confirm the conclusion from the computer modelling described in Chapter 6 that the overall experimental results from using a classical test geometry and a modified test geometry are expected to be similar.

7.6.4 An estimate of the dilatancy angle for bagasse.

No mention has been made in the previous chapters (apart from in the initial background description) of the dilatancy angle (ψ), primarily because it has not been required. This is because the computer modelling has been carried out using the Modified Cam Clay model, which is an associated material model (the yield surface and the potential surface are the same) where the dilatancy angle is the same magnitude as the friction angle in triaxial compression that corresponds to the value of M, the slope of the critical state line. A more detailed explanation of ψ and its relevance to reproducing bagasse behaviour is given in Chapter 8. Here an estimate is made of its magnitude in order to complete the material parameter measurements.

Dilatancy (ψ) is the change in volume during shearing (Craig, 1987). An estimate of the dilatancy angle can be made from the change in volume during shearing by following the method outlined in Section 8.3 of Muir Wood (1990) for simple shear. That is, $\psi = \tan^{-1}(dy/dx)$, where y is the height of the sample and x is the sideways movement. For each set of tests the dilatancy angles were estimated for a close to normally consolidated test (lightly over-consolidated) and a highly over-consolidated test (the other test results lie within these boundaries). For each test a maximum angle and a minimum angle were estimated. Shown in Figure 7.12, Figure 7.13, and Figure 7.14 are the boundaries for prepared cane, first bagasse, and final bagasse respectively. Positive values of the dilatancy angle indicate expansion. A summary of the dilatancy results is given in Table 7.6. At pressure feeder conditions the magnitudes of the dilatancy angle seem to be no larger than

about 6^{o}. At delivery nip conditions the magnitudes look to be as high as 25^{o}. In contrast, from the previous section, the magnitudes of the friction angle, ϕ_{cs}, range from about 37^{o} at pressure feeder conditions to about 3^{o} at delivery nip conditions. The dilatancy angles seem to be significantly different to the friction angles. What this implies is that, to reproduce bagasse behaviour more closely, the yield surface and the potential surface of a critical material model should be different, that is, the material model should be non-associated. The relationship between the dilatancy angle and the friction angle for bagasse is not known. It is noted that these measurements were undertaken with a direct shear test. A working triaxial test for bagasse would be more suitable to determine the shapes of the yield and potential surfaces. The description of material models will be progressed in the next chapter.

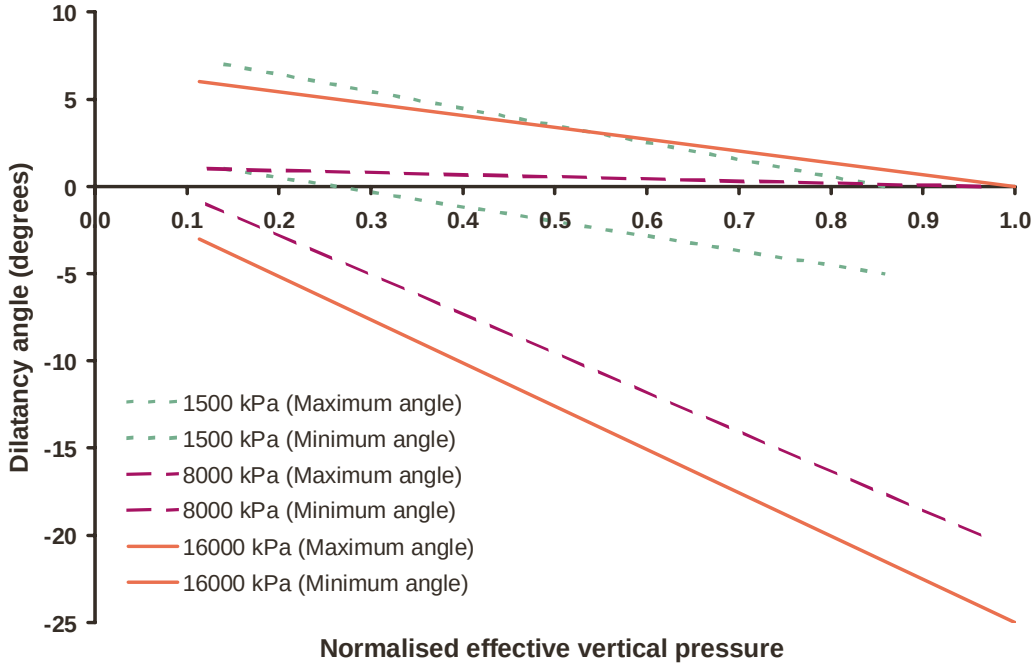

Figure 7.12. An estimate of the dilatancy angle for prepared cane.

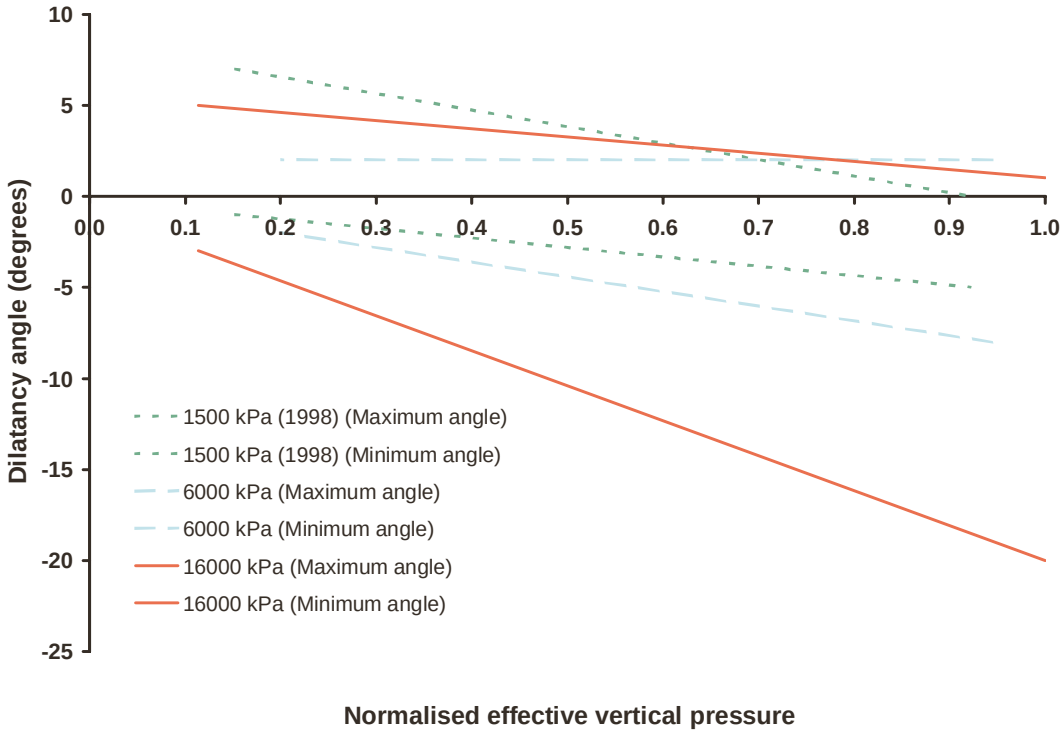

Figure 7.13. An estimate of the dilatancy angle for first bagasse.

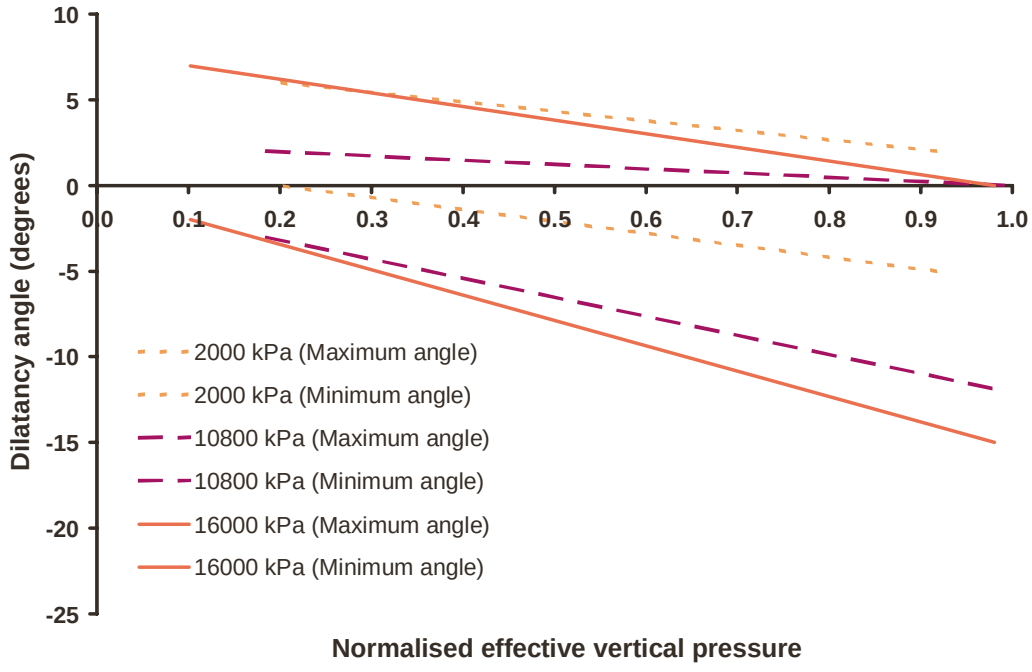

Figure 7.14. An estimate of the dilatancy angle for final bagasse.

Table 7.6 Estimate of dilatancy angles for cane residues

Nominal maximum effective vertical pressure (kPa)	Estimate of range of dilatancy angle (degrees)					
	Prepared cane		First bagasse		Final bagasse	
	HOC	LOC	HOC	LOC	HOC	LOC
1500	1 to 8	-5 to 0	-1 to 7	-5 to 0		
2000					0 to 6	-5 to 2
6000			-2 to 2	-8 to 2		
8000	-1 to 1	-20 to 0				
10800					-3 to 2	-13 to 0
16000	-3 to 6	-25 to 0	-3 to 5	-21 to 1	-2 to 7	-15 to 0

HOC= highly over-consolidated, LOC= lightly over-consolidated

7.7 The effect of pressure and over-consolidation on the grip of the roll surface on bagasse – friction and shear coefficients

As described in Chapter 1, the importance of roll roughness and feeding for milling performance is well established. For good feeding of prepared cane or bagasse between a pair of rolls, the roll surface needs to grip the material and the material must be strong enough to prevent internal shear failure. In the past few years, there have been considerable efforts to develop long life rough surfaces on the grooves of a roll. These efforts are described, for example, by Garson and Neill (1996) and Kroes (1999). The surface described by Kroes (1999), of tungsten carbide chips in a steel matrix, was observed to drag the bagasse 'around after the cane mat exits the nip. For many mill engineers, this dragging of the bagasse is used as an indicator for adequate roughness'. The attachment of bagasse to rough surfaces such as P24 sandpaper (1 mm diameter particles) has been noted by Plaza and Kent (1997, 1998) during direct shear tests and, in combination with the direct shear test data, was used to conclude that the tested surfaces were rough enough to grip prepared cane and shear it internally. That is, the maximum coefficient of friction of bagasse on rough surfaces that can be obtained for feeding is actually the coefficient of internal friction of the bagasse.

As the bottom part of the test rig was drawn horizontally from underneath the suspended box during the direct shear tests, it was observed that the prepared cane and bagasse were gripped well by the sandpaper surface. After unloading and

removing the suspended box, it was observed that the bagasse was still stuck to the sandpaper for all tests, implying that the bagasse sheared internally and that the measured coefficients represent the maximum coefficients of friction that could be obtained.

In this section the maximum shear stresses and corresponding coefficients of internal friction (called coefficients of shear) measured during the tests are presented.

7.7.1 Shear stresses

The maximum and final shear stresses for each test are plotted in Figure 7.15, Figure 7.16 and Figure 7.17 respectively for prepared cane, first bagasse, and final bagasse. The figures are the non-normalised versions of Figure 7.9, Figure 7.10 and Figure 7.11 from the previous Section 7.6.3. For each figure, the furthest data point to the right in each data series corresponds to the normally consolidated test. The remaining data points are the over-consolidated tests, which have been unloaded from the pressures shown in the legends, and then sheared at the pressures shown in the horizontal axis. Figure 7.15 shows the two regression lines from Figure 10 in Plaza and Kent (1997) for prepared cane, which shows 1992 test data where all tests were sheared at constant pressure while being normally consolidated (the Coulomb failure criterion line for soils). The discrepancies in the magnitudes of the shear stresses between the 1992 tests and the 1998/2001 tests for prepared cane are not surprising since, for the 1992 tests, the Q124 cane was harvested by hand, cleaned of trash and shredded with the SRI experimental shredder, while for the 2001 tests the prepared cane was obtained from Racecourse Mill and Pleystowe Mill. The prepared cane was obtained from the mill supply, and had been harvested and shredded as per normal mill operation. There were also differences in the test geometry and procedure.

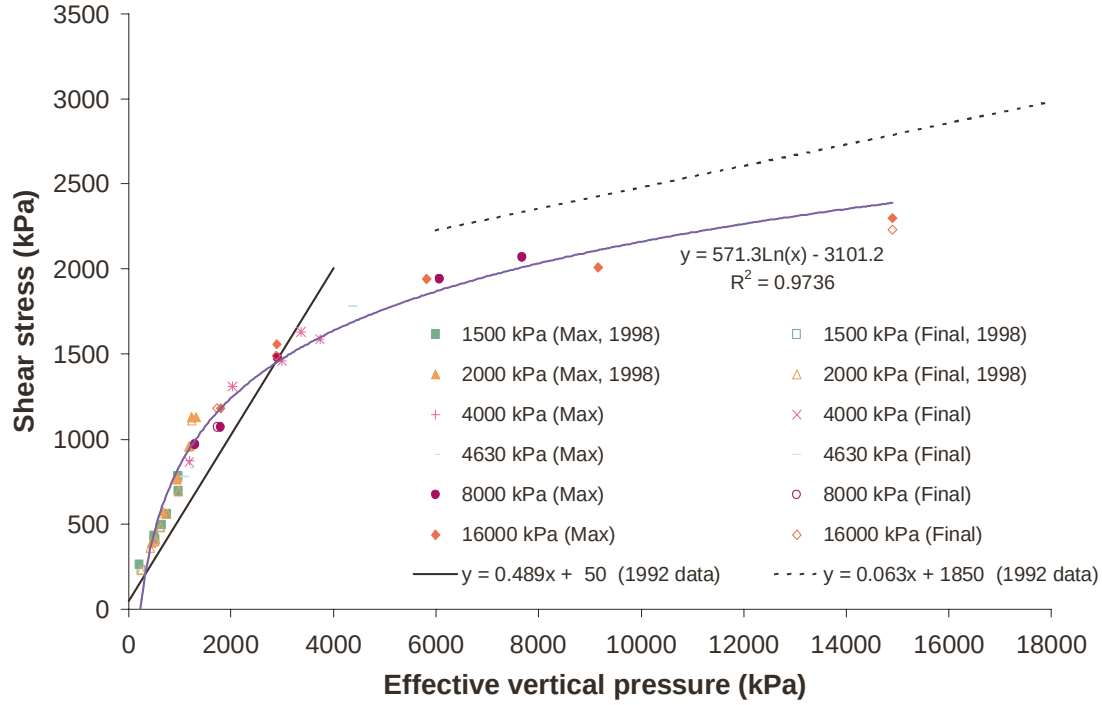

Figure 7.15. Shear stress versus effective vertical pressure for prepared cane.

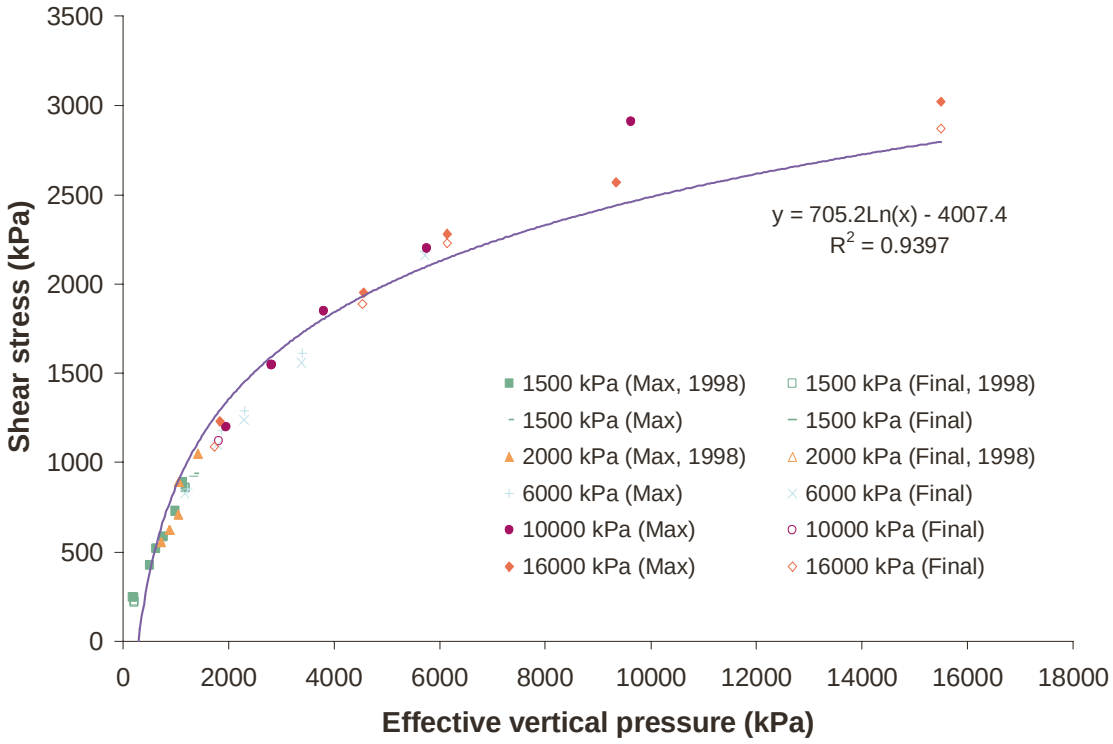

Figure 7.16. Shear stress versus effective vertical pressure for first bagasse.

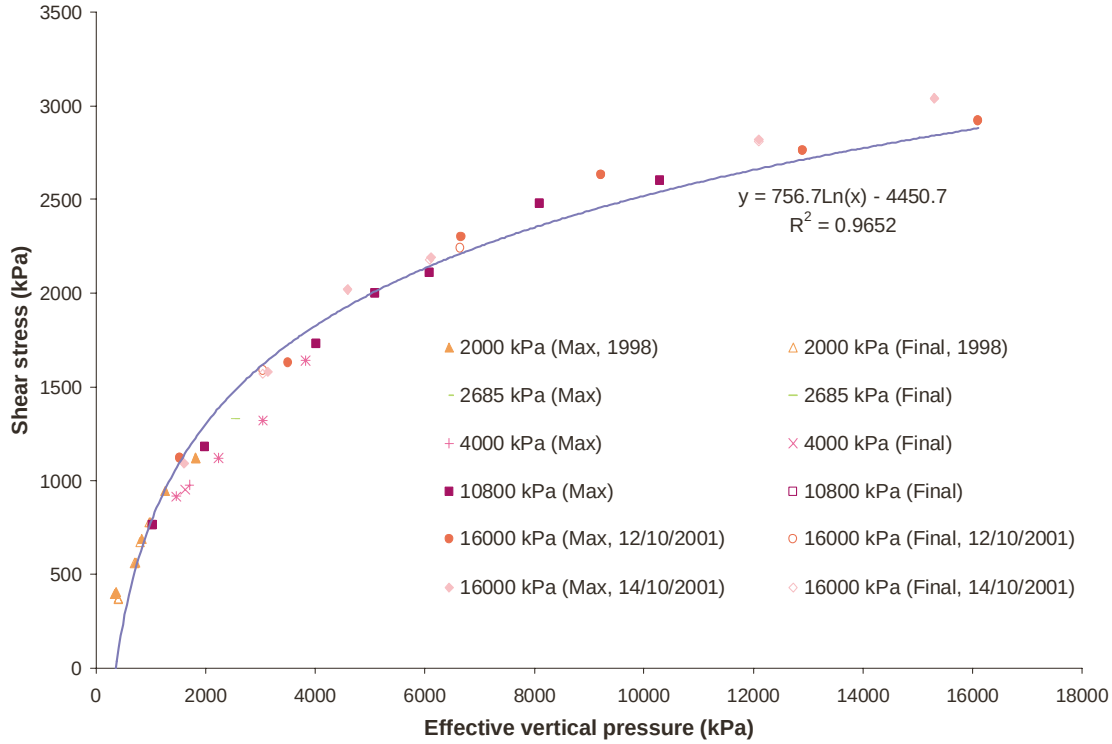

Figure 7.17. Shear stress versus effective vertical pressure for final bagasse.

It is shown that, for all materials, the friction angles at low pressures and at high pressures are quite different. At low effective vertical pressures, there is a relatively large increase in shear stress as pressure increases (a relatively large friction angle). At high effective vertical pressures, an increase in pressure results in a relatively small increase in shear stress (a relatively small friction angle). For ease of use the Coulomb failure criterion is usually held to be a straight line for a limited pressure range and Figure 7.15 shows the two regression lines from Figure 10 in Plaza and Kent (1997) for two pressure ranges, and a curved transition zone could be used in between. A similar transition zone is apparent when a measure of density such as fibre compaction is plotted versus vertical pressure (refer to Figure 3.2 of Chapter 3). However, in reality the full pressure range is curved and trends and equations have been given in the figures. Whichever is convenient can be used.

As noted by Carter (2003), 'the observation shown above that the failure envelope is curved in stress space, with the effective M (or ϕ, the friction angle) reducing with increasing mean pressure, is very common in frictional materials. It is also observed in the shearing of rock joints, where increasing normal stress on the

interface suppresses dilation. It would not be difficult to incorporate such a variation in a constitutive model for bagasse'.

7.7.2 Coefficients of internal shear

The data presented in Figure 7.15, Figure 7.16 and Figure 7.17 are presented in Figure 7.18, Figure 7.19, and Figure 7.20 respectively in a manner more familiar to milling technologists, where the coefficient of internal friction (labelled the coefficient of shear) is plotted versus effective vertical pressure. The coefficient of shear is simply the maximum shear stress divided by the corresponding effective vertical pressure.

The data for prepared cane, first bagasse, and final bagasse are similar. Previous investigations have shown that the magnitude of the coefficient of shear of prepared cane on rough surfaces is strongly pressure dependent (Cullen, 1965; Plaza and Kent, 1997); that is, as pressure increases, the magnitude of the coefficient of shear decreases. The results given above support that conclusion and show that it applies to first bagasse and final bagasse as well.

To a first approximation, the coefficients of shear for normally consolidated samples and over-consolidated samples seem to lie on the same line. That is, over-consolidation does not seem to affect the coefficient of shear, and this seems to be the case at most of the tested pressures. However, closer inspection at the relatively low pressures around 200 kPa to 800 kPa shows a few quite high coefficients of shear for all three tested materials, significantly higher than any which have been reported previously at similar pressures. The high values are shown in Figure 7.21. Values at these low pressures for normally consolidated samples are not available from the tests carried out in this investigation. Some coefficients for normally consolidated prepared cane are given in Plaza and Kent (1998) who used similar (but not split box geometry) direct shear test equipment and those data are also shown in Figure 7.21.

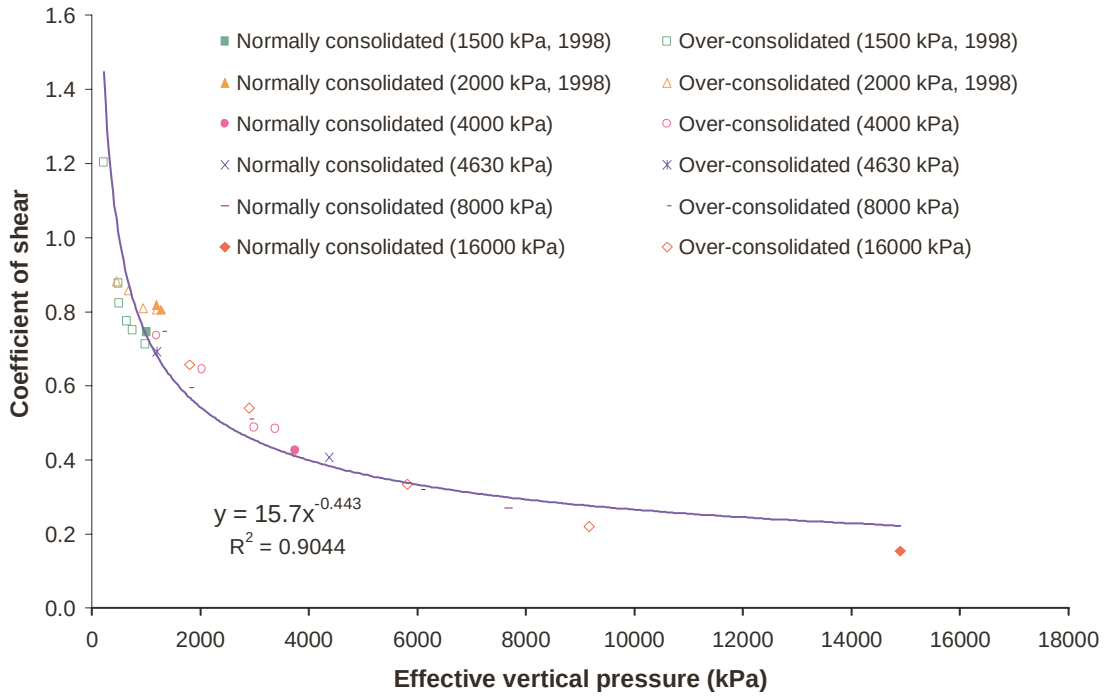

Figure 7.18. Coefficients of shear versus effective vertical pressure for prepared cane.

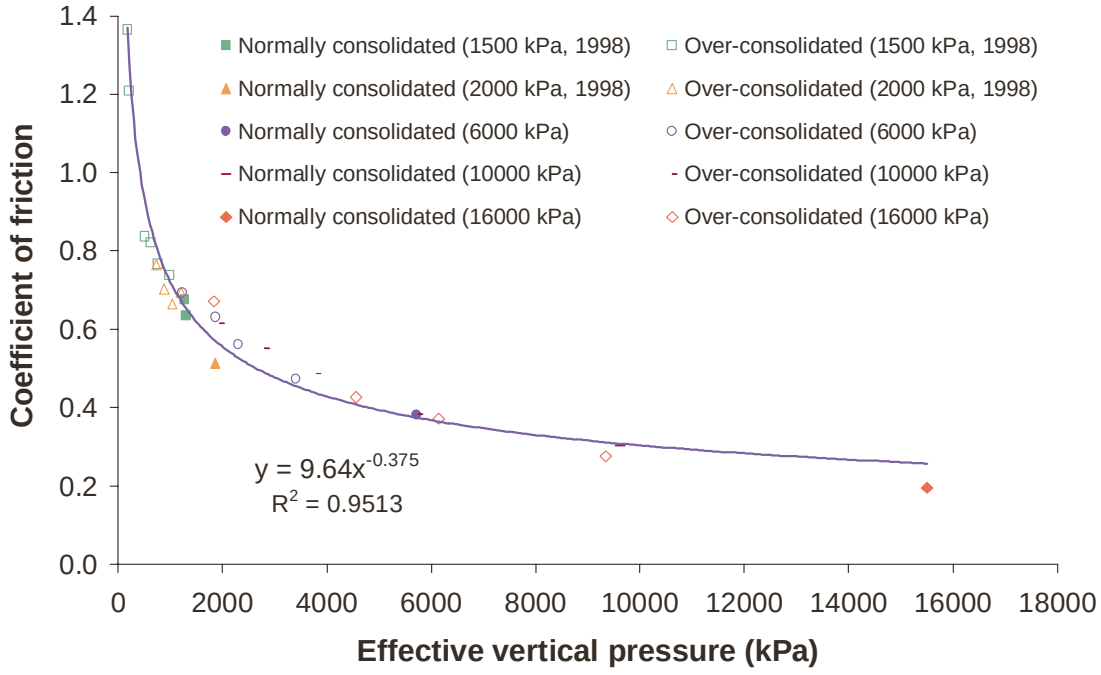

Figure 7.19. Coefficients of shear versus effective vertical pressure for first bagasse.

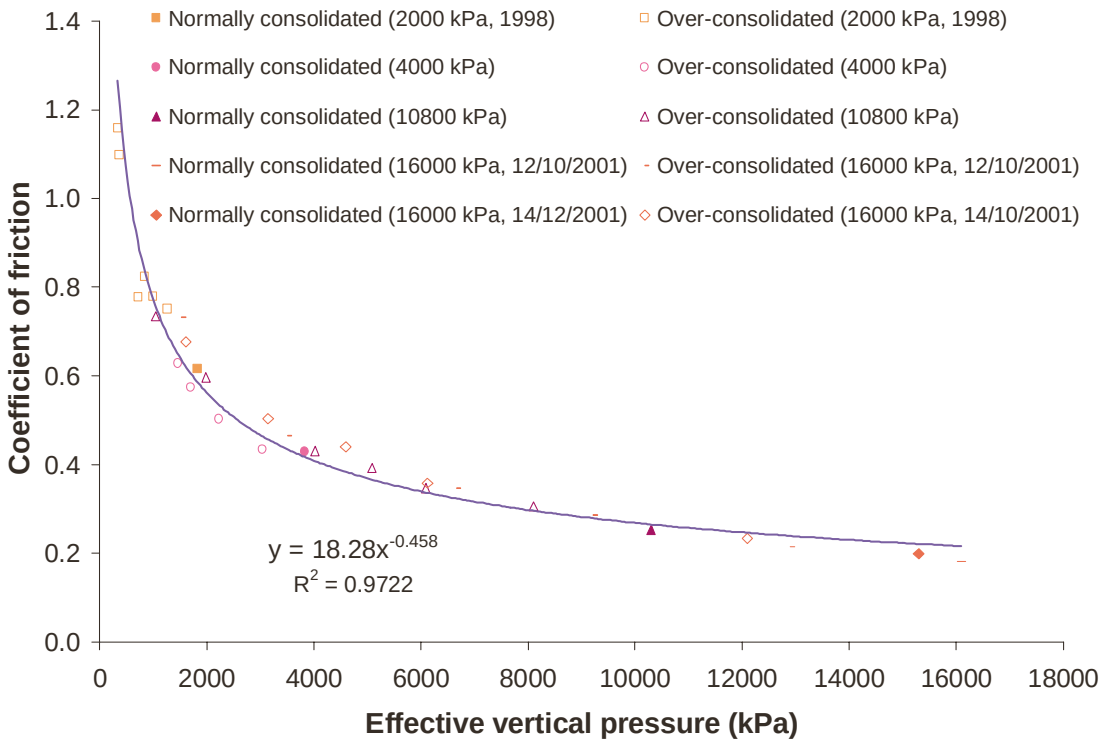

Figure 7.20. Coefficients of shear versus effective vertical pressure for final bagasse.

The magnitudes of the coefficients for the over-consolidated samples are similar or higher than the coefficients given in Plaza and Kent (1998) for normally consolidated prepared cane, but they occur at significantly higher pressures. For example, at 218 kPa, the coefficient of shear for an over-consolidated prepared cane sample is 1.20. At a similar pressure, 200 kPa, the values for normally consolidated prepared cane samples are 0.80 and 0.88. As noted previously, as pressure increases, the magnitude of the coefficient of shear decreases. Therefore, for an over-consolidated first bagasse sample with a coefficient of 1.36 at 181 kPa, and following the pattern shown, further over-consolidation (unloading) is likely to result in an even higher coefficient of shear. Such magnitudes are quite a deal higher than those reported previously in the literature for prepared cane, where typical values range from 0.3 to 0.6 (Crawford, 1955; Solomon and Murry, 1964).

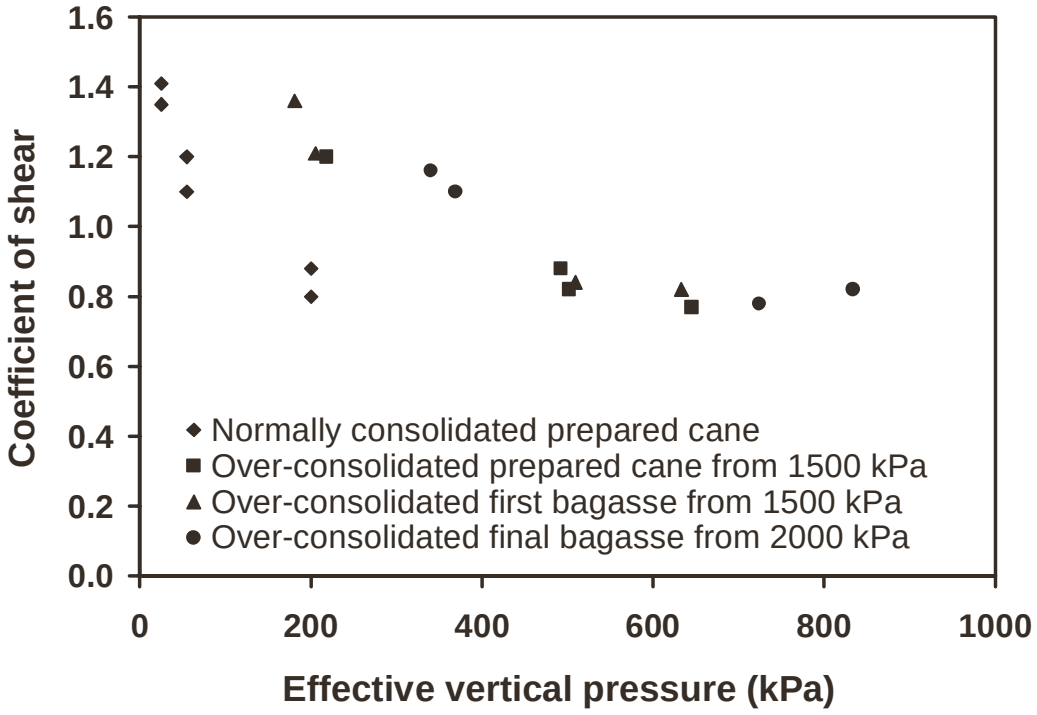

Figure 7.21. Coefficients of shear for normally consolidated prepared cane and over-consolidated prepared cane, first bagasse, and final bagasse.

In summary, the measurements suggest that, at pressures below about 800 kPa, bagasse which has been previously loaded to a higher pressure than its current state (i.e. the bagasse is over-consolidated) may exhibit a higher coefficient of shear (and therefore a higher coefficient of friction) than bagasse which has simply been compressed to the same pressure (the implication being that it will feed better). Further experiments should be conducted to confirm this result by testing both normally consolidated samples and over-consolidated samples at the same pressures in the same test series.

The concept of over-consolidated bagasse having a higher coefficient of shear (that is, being able to support a higher stress) than bagasse which is normally consolidated, while both being at the same vertical pressure, has a parallel in soil mechanics. It is well established that over-consolidated clay has a higher value of K_o than clay which is normally consolidated (Craig, 1987). The over-consolidated

clay will support significantly higher internal stresses than clay that is normally consolidated.

Over-consolidation is expected to occur after the underfeed nip, the pressure feeder nip, the feed nip, and the delivery nip. The over-consolidated bagasse may achieve a higher coefficient of friction when the bagasse contacts the arced surface on the next roll pair than it would if presented to the roll pair before consolidation. This increase in friction would provide an additional feeding benefit to complement the increase in feed compaction achieved by a previous roll pair. It is noted that the bagasse may not remain in an over-consolidated state if it is significantly disturbed (for example, by the action of the grooves and scrapers after the bagasse exits a nip). This may have implications for the design and positioning of scrapers, as well as the geometry of the grooves themselves.

7.8 Differentiation of cane varieties

As noted in Section 7.4, a limited number of direct shear tests was carried out in one day on different cane varieties from the Mackay region. The aim was to have a quick look at the variation in compression, shear, and volume behaviour for different varieties, and assess the likely performance of the modified direct shear test method in measuring the mechanical behaviour of different cane varieties. It is noted that the Bureau of Sugar Experiment Stations (BSES) uses a variation of the direct shear test (at a low vertical pressure of 50 kPa), as well as several other tests, to determine the likely performance of a new cane variety during the milling process.

Tests were carried out using prepared cane from Pleystowe Mill and Racecourse Mill with duplicate tests carried out on cane varieties Q124, H56, Q96, Q117, Q135, and Q136 (a more detailed description is given in Section 7.4). The compression, shear, and volume behaviour is presented here. Figure 7.22 shows, for prepared cane, the maximum shear stress measured at effective vertical pressures occurring in a six roll mill, together with regression lines from Figure 10 in Plaza and Kent (1997). It is shown that the values for the different varieties at 1800 kPa overlap the regression line from 0 to 4000 kPa. Figure 7.23 shows a close

up view of the maximum shear stresses for the different cane varieties at 1800 kPa. Figure 7.24 shows a corresponding plot of sample heights.

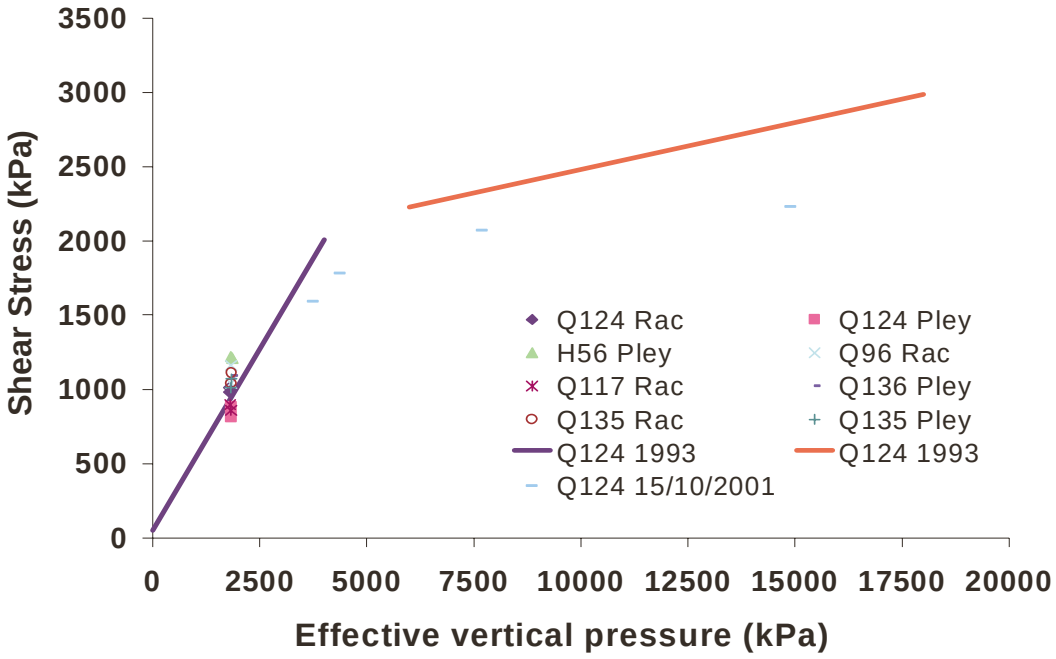

Figure 7.22. Maximum shear stress versus effective vertical pressure for prepared cane of different cane varieties.

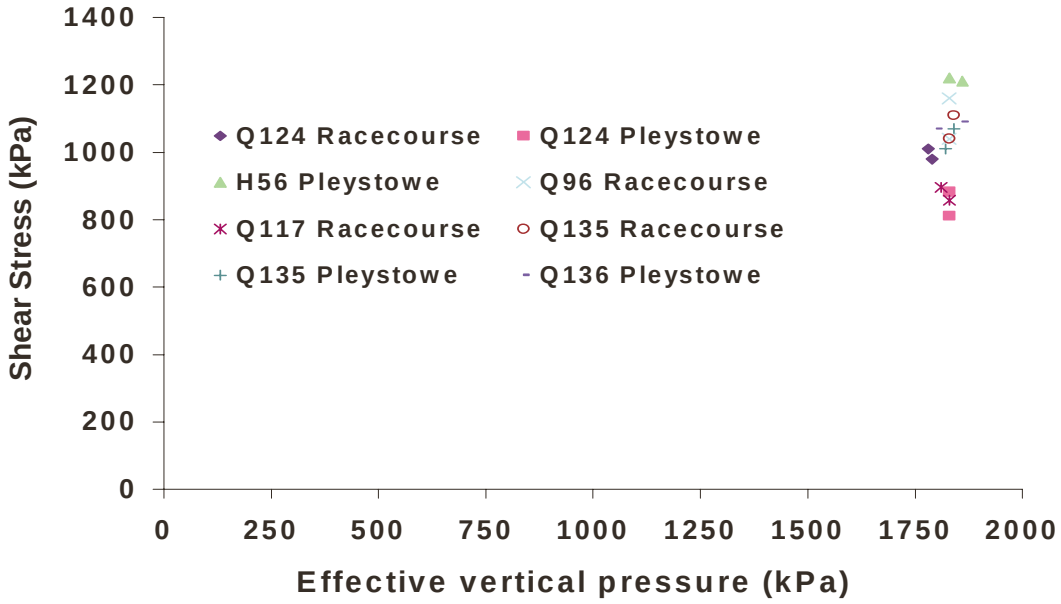

Figure 7.23. Maximum shear stress at an effective vertical pressure of approximately 1800 kPa for different cane varieties.

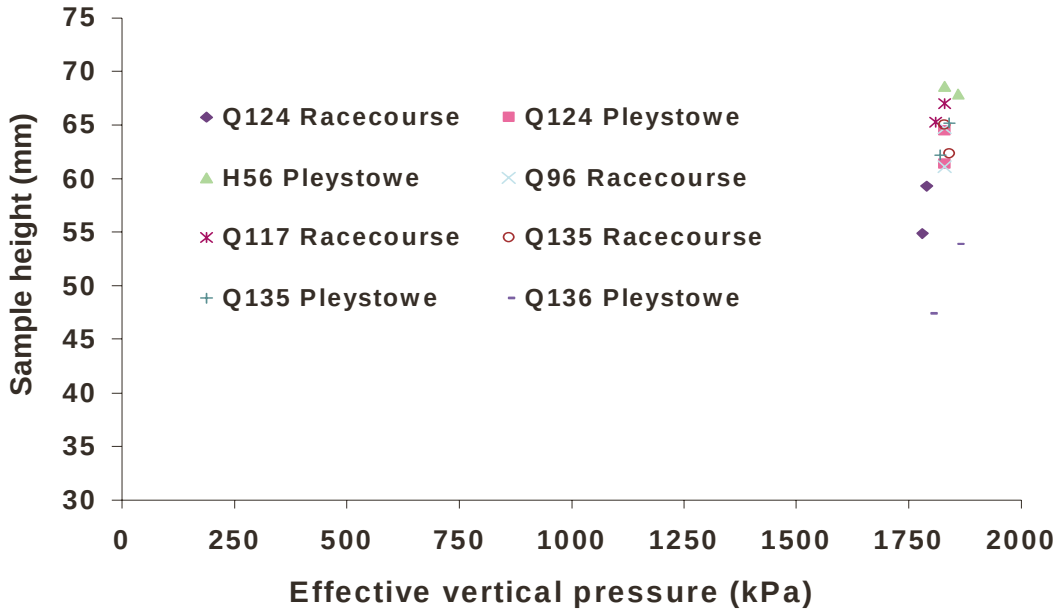

Figure 7.24. Sample height at an effective vertical pressure of approximately 1800 kPa for different cane varieties.

Some interesting values were noted: for the same vertical pressure, variety H56 had both the highest shear stress and volume while variety Q136, with one of the highest fibre levels, occupied the smallest volume.

The tests indicate (with the proviso that a total of only 16 tests were carried out) good reproducibility and differentiation between cane varieties. Further tests would be necessary to confirm this result, as well as measuring other cane varieties and varieties from different growing regions. A comparison of this direct shear test with that used by BSES (which uses a bed of nails as the gripping surface) may be useful and there is the strong possibility that the BSES direct shear test can be improved. For example, it may be desirable in the future that the test carried out routinely be able to supply data for use in computer modelling of the milling process of different cane varieties. Whether an improvement is necessary and for what purpose is a matter for the sugar industry to decide.

7.9 Summary of Chapter 7

The measured mechanical behaviour of prepared cane, first bagasse, and final bagasse at pressures present in the main three rolls and close to the compactions that occur in the delivery nip of a milling unit has been found to be similar to the behaviour at pressures occurring in the pressure feeder unit. It shows critical state behaviour similar to that of soil.

The magnitudes of the material parameters have been estimated from the test data: the slope of the normal compression line, the slope of the elastic unloading-reloading line, the position of the critical state line with respect to the normal compression line (that is, the over-consolidation ratio at which the materials do not change volume during shearing), the slope of the critical state line, and the dilatancy angle. It has been shown that there are marked differences in the magnitudes of these parameters across the range of pressures that occur in the milling process. The values of these parameters are of use in improving the understanding of bagasse behaviour, in the identification of a material model that can reproduce bagasse mechanical behaviour well, and as inputs for computer modelling of the milling process.

Plots of shear stress versus effective vertical pressure for prepared cane, first bagasse and final bagasse have shown that, for all three materials, the friction angle reduces markedly with increasing pressure. The magnitude of the coefficient of shear (the maximum coefficient of friction) of prepared cane, first bagasse and final bagasse is pressure dependent. Values spanning most of the pressure range in milling have been presented. The magnitudes of the coefficient of shear for the three materials are quite similar and are of use as coefficients of friction for feeding calculations and as boundary condition inputs to a milling model. Values of coefficients for over-consolidated prepared cane and bagasse suggest that, at least at relatively low pressures, the coefficient of shear of bagasse may be stress-history dependent. That is, bagasse which has been previously loaded to a higher pressure than its current state (over-consolidated) may exhibit a higher coefficient of shear than bagasse that has simply been compressed to the same pressure (the implication being that it will feed better). Over-consolidation is expected to occur after the underfeed nip, the pressure feeder nip, the feed nip, and the delivery nip. The over-

consolidated bagasse may then achieve a high coefficient of friction when the bagasse contacts the arced surface on the next roll pair.

A small number of direct shear tests on different cane varieties in the Mackay region measured the maximum shear stress and the volume at an effective vertical pressure of 1800 kPa. The results indicate (with the proviso that there were only 16 tests) good reproducibility and differentiation of those parameters between cane varieties. Further tests would be necessary to confirm this result, as well as measuring other cane varieties and varieties from different growing regions. A comparison of this direct shear test with that used by BSES (which uses a bed of nails as the gripping surface) may be useful and there is the strong possibility that the BSES direct shear test can be improved.

8 Chapter 8 – Development of improved material model for bagasse

8.1 Introduction

This chapter focuses on moving part of the way towards a material model that can reproduce bagasse mechanical behaviour well. The conclusions from Chapter 5, Chapter 6, and Chapter 7 relevant to this goal are discussed initially (and some are described in detail later in the chapter). Chapter 5 showed that the Modified Cam Clay model had a good chance of reproducing compression of a normally consolidated sample and re-compression. A similar conclusion was reached for shearing of a normally consolidated sample. Chapter 6 showed that a multi-element Modified Cam Clay model had a good chance of predicting shearing of an over-consolidated sample. However, this agreement could not be reached when using a single set of material parameters. That is, material models being used for mill modelling could not with a single set of parameter values successfully model all the loading and unloading conditions relevant to milling. Most importantly, compression and shear behaviour could not be reproduced with a single set of parameters. This is believed to be a key requirement in order to reproduce both roll load and roll torque in a milling unit.

Chapter 7 showed that there are major changes in the detail of the critical state behaviour of bagasse across the large range of pressures occurring in the milling process. This detail needs to be incorporated in a material model. It is stressed that there is much behaviour that has not been measured (such as the shear behaviour parallel to the direction of compression, as well as behaviour under triaxial conditions) which almost certainly would have a bearing on the makeup of a material model for bagasse. The position taken here is to work from the available data.

8.2 Desirable features of a material model for bagasse

8.2.1 M and K_o values

As described in Chapter 5 with reference to Brinkgreve et al, (1994), there is a notable limitation in the Modified Cam Clay (MCC) and Drucker-Prager Cap

(DPC) material models when modelling bagasse behaviour. When modelling compression a value for K_o is enforced based on the value of the material parameter M. For example, for M values of 1.1 and 3.8, K_o values of 0.69 and 0.108 are enforced respectively. That is, M and K_o are not independent. The magnitudes of these two parameters can have a large effect on the predictions from a model. Values of M of 1.1, 1.2, and 1.3 have been determined for final bagasse, first bagasse, and prepared cane respectively from direct shear test data at pressure feeder compactions, while values as low as 0.1 can be justified from the data at delivery nip compactions. Typical values of K_o for prepared cane and bagasse seem to range from 0.1 to 0.3 (Adam, 1997), although higher values have been quoted in the literature for different pressures, preparations, and measurement methods. Crawford (1955), for example, quoted a value of 0.35 for K_o. Since an M value of 1.1 corresponds to a K_o value of 0.69, the combinations of M of 1.1 and K_o of about 0.2 for bagasse are not allowed by the MCC and DPC models during normal compression. A material model that allows this combination of measured parameters is desirable in order to model bagasse crushing in a typical Australian three roll pressure feeder. A further development would be necessary to model the three main rolls with a value of M ranging from 1.0 to 0.1 and a K_o value of about 0.2.

8.2.2 Shapes of the yield and potential surfaces

The low values of K_o indicate that the bagasse solid skeleton can support relatively high internal shear stresses, when compared to, for example, a clay soil (typical K_o values for normally consolidated clay are 0.5 to 0.6). Some yield surface shapes can allow relatively high internal shear stresses to be supported and allow the position of the critical state line with reference to the normal compression line to be changed. The need to be able to change the position of the critical state line is shown in Figure 7.6, Figure 7.7 and Figure 7.8 of the last chapter, where it is shown that the position changes greatly as pressure increases from 2000 kPa (pressure feeder compactions) to 15500 kPa (towards delivery nip compactions). Therefore it would be an advantage to be able to change the shape of the yield surface in the material model. The MCC and DPC models in the ABAQUS finite element analysis software (Hibbitt et al., 2001) have this ability to a limited degree. It will

be shown in the next section that improved reproduction of bagasse measurements can be achieved by adopting this option in the MCC model in ABAQUS.

8.2.3 Non-associated flow

The plastic potential surface describes the relative amounts of volume and shear change occurring during plastic deformation. The MCC model has a plastic potential surface identical to the yield surface (a feature known as normality, or associated flow). The DPC model also has this feature in the right side (the compressing or 'wet' side) of the critical state line. There is some evidence that a potential surface different from the yield surface (non-associated flow) is required to reproduce some features of the material behaviour of bagasse. For example, Figure 5.36 in Chapter 5 shows that the predicted volume decrease during shearing is too large compared to the measured values, that is, that the ratio of volumetric strain to shear strain is too large. This implies that the magnitude of the dilatancy angle (ψ) should be different to the magnitude of the friction angle (ϕ_{cs}, from which M is estimated) in order to achieve a better fit. This observation is supported by the estimates of ϕ_{cs} and ψ made from experimental data on bagasse and shown in Chapter 7, where the magnitudes of the estimates of the two material parameters were quite different. The understanding of dilatancy has played a major role in soil mechanics. For example, Yu (1998) states that 'perhaps the most successful stress-dilatancy relation, which may now be considered to be one of the milestones in soil mechanics, is due to Rowe (1962)'. Applying different magnitudes of the dilatancy angle and the friction angle results in the potential surface being different to the yield surface, that is, non-associated flow.

As regards the yield surface, it is desirable to be able to change the shape of the plastic potential surface.

8.2.4 A note of caution

Although it is believed that the features for a material model described above are likely to lead to improvements in reproducing bagasse behaviour, some of the features may not be necessary and there may be other features that are required and have not been mentioned. For example, the tension behaviour of bagasse may need

to be modelled (Downing, 1999). It is again noted that bagasse behaviour in different loading directions (anisotropy) has not been measured in this investigation and may need to be included in a material model, or at the very least measured.

8.3 Improved predictions using an associated Modified Cam Clay model with a β extension

The previous section stated that in order to reproduce bagasse behaviour better, it was desirable to be able to change the shape of the yield surface and the position of the critical state line in a material model. These features are available to a limited degree in the extension of the Modified Cam Clay model provided in ABAQUS. Shown in Figure 8.1 is the yield surface (the plastic potential surface is the same since the MCC is an associated model) and its equation is given in 8.1.

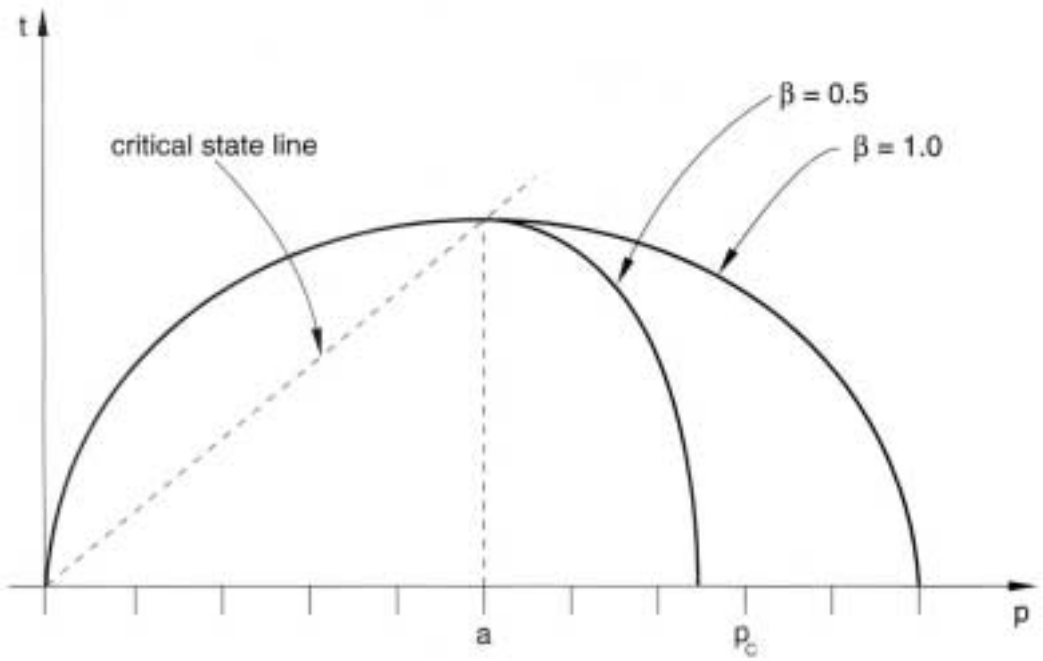

Figure 8.1. Clay yield surfaces in the p-t plane (after Hibbit et al, 2001).

$$\frac{1}{\beta^2}\left(\frac{p}{a}-1\right)^2+\left(\frac{t}{Ma}\right)^2-1=0 \qquad \textbf{(8.1)}$$

The confining pressure is shown as p and the deviatoric stress (q) as t (following ABAQUS definitions). P_c is the highest confining pressure the material has experienced previously, is also known as the pre-consolidation pressure, and is the pressure at the intersection of the current elastic loading reloading line with the normal compression line. The position of the critical state line is given by 'a'. The parameter β is a constant that is equal to 1.0 on the left (expanding, dry) side of the critical state line but may be different from 1.0 on the right (compressing, wet) side. A value of 1.0 results in the shape of the 'original' Modified Cam Clay model. By decreasing the parameter β a tighter cap is obtained as shown in Figure 8.1, that is, the normal compression line moves closer to the critical state line given the same value of M. It is assumed that the critical state line is parallel to the normal compression line. The locations of the normal compression line, elastic unloading-reloading line, and critical state line in the void ratio - confining pressure plane are shown in Figure 8.2.

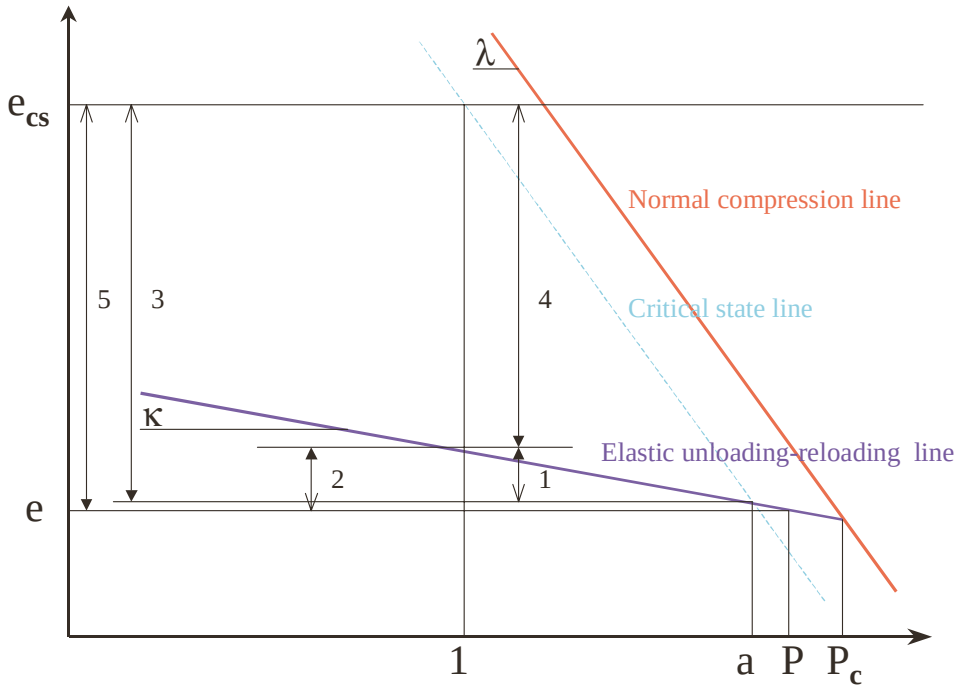

Figure 8.2. Locations of normal compression, elastic unloading-reloading, and critical state lines in void ratio – confining pressure plane.

The void ratio at a particular confining pressure is defined as follows:
e = void ratio,
P = confining stress (kPa),
e_{cs}=critical state void ratio at a pressure of 1 kPa,
P_c= pressure at intercept of elastic unloading-reloading line with normal compression line
The dimensions in Figure 8.2 are:

1) $\kappa \ln a$
2) $\kappa \ln P$
3) $\lambda \ln a$
4) $(\lambda - \kappa) \ln a$
5) $e_{cs} - e = (4) + (2) = (\lambda - \kappa) \ln a + \kappa \ln P$

Therefore the void ratio at a particular confining pressure is:

$$e = e_{cs} - (\lambda - \kappa) \ln a - \kappa \ln P \qquad \textbf{(8.2)}$$

and

$$P_c = a(1 + \beta) \qquad \textbf{(8.3)}$$

Recapping the conclusions from Chapter 5, simulating normal compression with the MCC model (which has a value of β equal to 1.0) and a value of M of 1.1 enforces a value of K_o of 0.69. Setting the value of β to 0.21 allows the value of K_o to be reduced to 0.4 (closer to the measured value of bagasse of about 0.2) and the stress state to remain on the 'wet' side of the critical state line. The simulations of the loading conditions (except for shearing of an over-consolidated sample) for final bagasse described in Chapter 5 were repeated with the modified MCC model and porous elasticity using a multi-element model in ABAQUS. The parameters used are given in Table 8.1. The shape of the yield surface is shown in Figure 8.3 at a vertical pressure of 149 kPa.

Table 8.1 Parameter values for modified MCC model simulation

λ	κ	M	ν	β	K_o
0.93	0.17	1.1	0.3	0.21	0.4

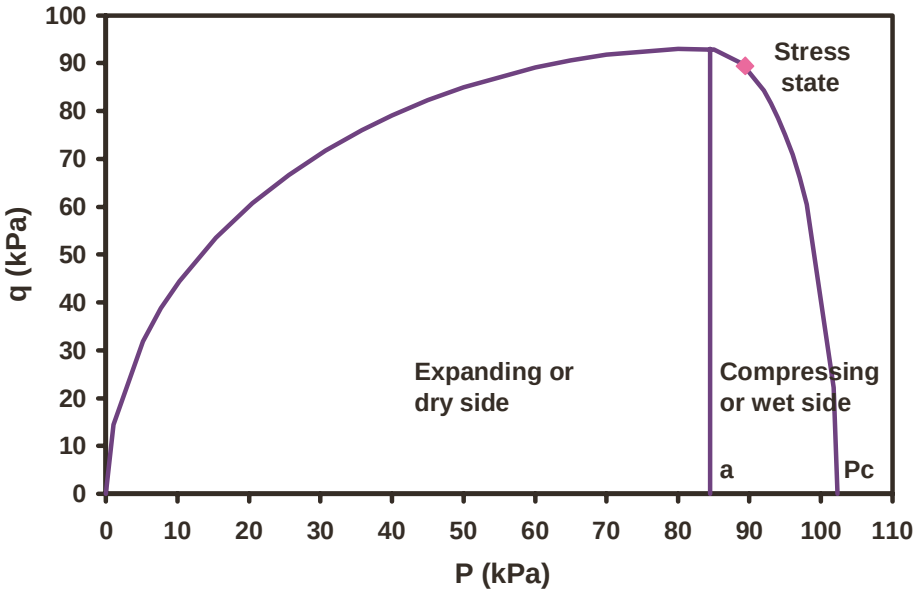

Figure 8.3. Shape of yield surface for extended Modified Cam Clay with M=1.1 and β=0.21.

A comparison of predicted and measured results for final bagasse is shown in Figure 8.4 to Figure 8.8. The predictions are compared to those shown in Chapter 5 using the MCC model with β=1.0.

Figure 8.4 shows the simulation for the initial compression of final bagasse to a vertical pressure of about 2000 kPa. The fit is excellent and as good as that shown in Figure 5.32 (shown in page 131) of Chapter 5 for a K_o of 0.69 using the MCC model with β=1.0. It is easy to achieve a good fit for initial compression.

Figure 8.5 shows the simulation for unloading of final bagasse from a vertical pressure of about 2000 kPa. The prediction is much improved compared to that shown in Figure 5.33 (shown in page 132). At a high degree of unload the prediction diverges from the experimental trend (that is, the slope of the line starts to become vertical). This behaviour seems to be typical of critical state models at a high degree of unload, and should be monitored/adjusted during modelling to avoid potential numerical problems.

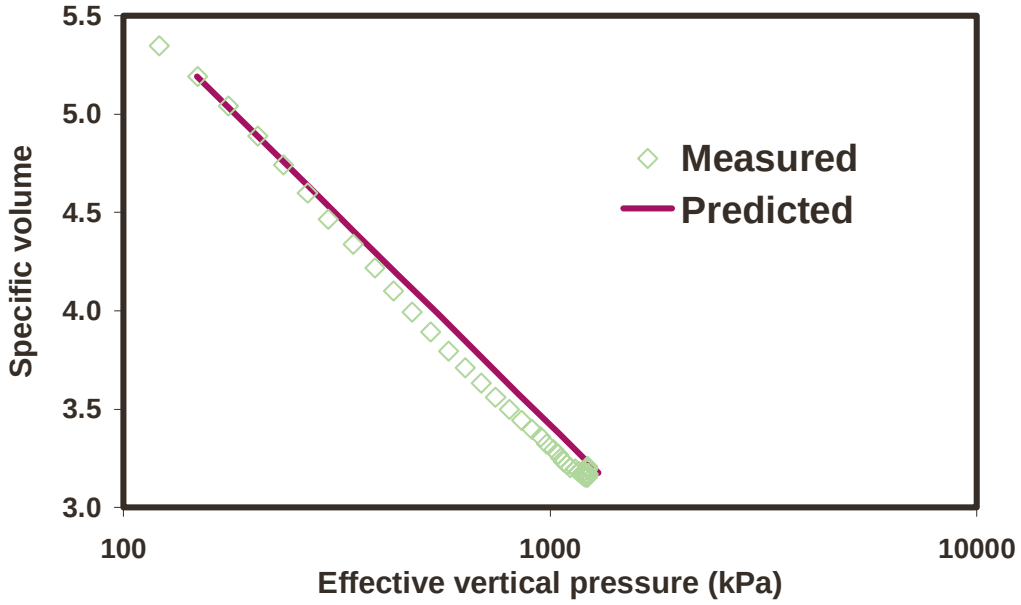

Figure 8.4. Reproduction of compression behaviour for MCC with β=0.21.

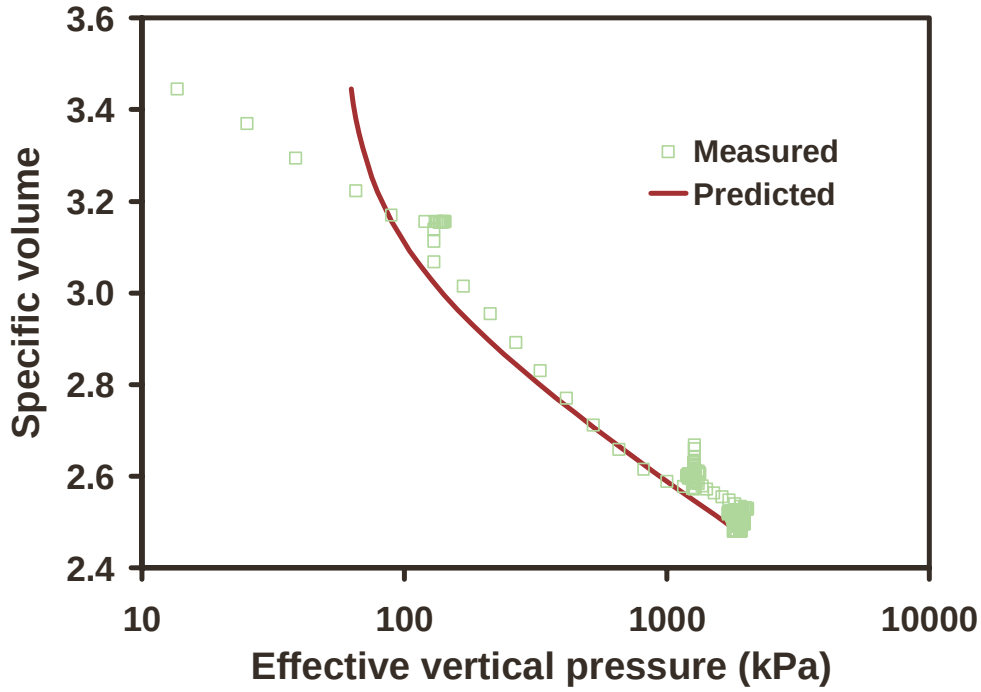

Figure 8.5. Reproduction of unloading behaviour for MCC with β=0.21.

Figure 8.6 shows the compression reloading behaviour of bagasse to 2000 kPa (which is basically identical to the unloading line shown in Figure 8.5). The prediction is an excellent fit to the measured data, as was the case for the prediction in Figure 5.34 (shown in page 132). Once the normal compression line is reached (at the maximum effective vertical pressure of 2000 kPa where the bagasse was initially loaded to and unloaded from), the prediction continues along the normal compression line.

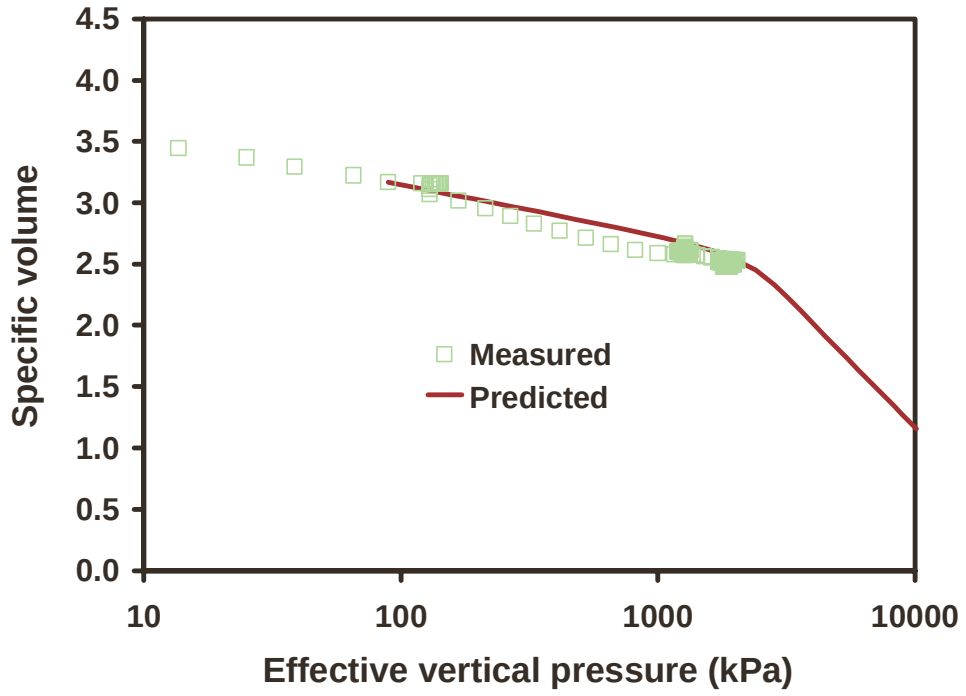

Figure 8.6. Reproduction of reloading behaviour for MCC with β=0.21.

Shown in Figure 8.7 and Figure 8.8 are the measured and predicted behaviour of normally consolidated final bagasse undergoing shearing at constant vertical pressure. Figure 8.7 shows the shear stress versus shear strain plot while Figure 8.8 shows the specific volume versus shear strain plot. The prediction of shear stress is significantly improved compared to the prediction in Figure 5.35 (shown in page 134). The prediction of the decrease in specific volume is still very poor (compare with Figure 5.36, also shown in page 134).

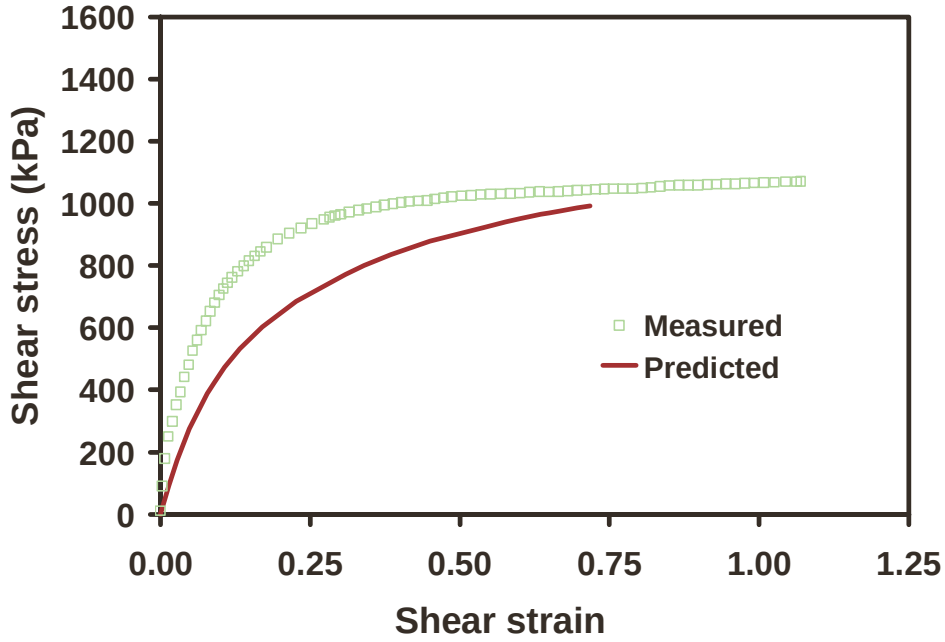

Figure 8.7. **Reproduction of shear stress versus shear strain for MCC with β=0.21.**

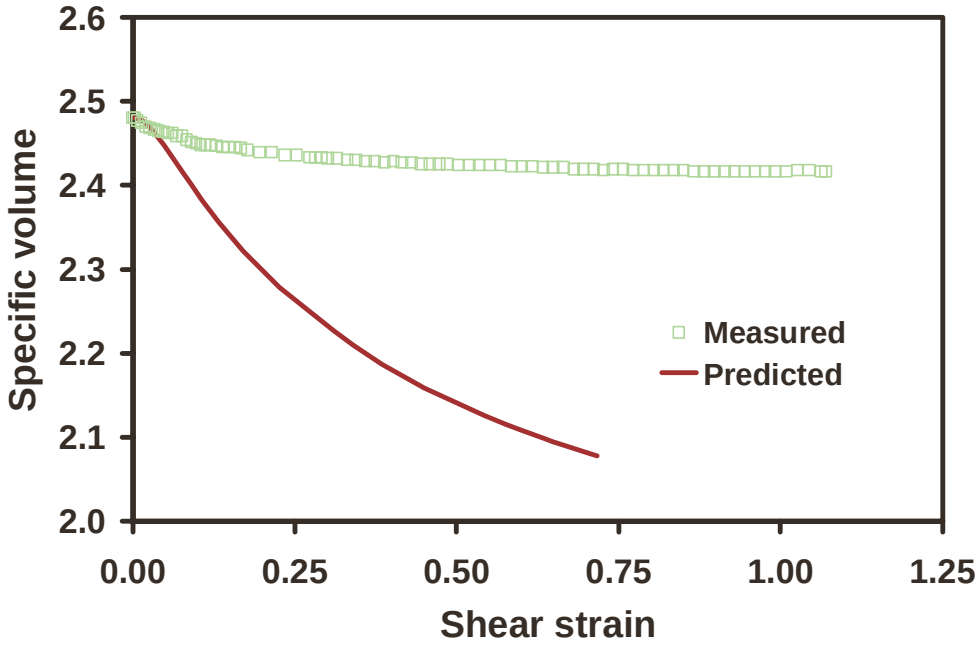

Figure 8.8. **Reproduction of specific volume versus shear strain for MCC with β=0.21.**

In summary, the use of a Modified Cam Clay model with β=0.21 resulted in improvements in the prediction of unloading behaviour and the shear stress during shearing, while the predictions during initial compression and during reloading remained just as good, but the prediction of the change in specific volume during shearing remained just as poor. Therefore there was an overall improvement in the predictions, while using a consistent set of input parameters that better reflect the magnitudes of measured parameters for bagasse (for example, a closer value of K_o to that measured). The results gave some confidence that some of the features of a better material model with which to reproduce bagasse material behaviour had been included and that this line of investigation should be pursued.

8.4 Predictions from a material model in the soil mechanics literature.

The search carried out for existing material models in the literature and its outcomes are detailed in Chapter 2. In summary, there seems to be a large number of material models that show promise, and most of them are in the soil literature. The material models detailed in the following publications are particularly interesting and were discussed briefly in Chapter 2. In alphabetical order, the publications are: Brandt and Nilsson (1999), Davies and Newson (1992), Gajo and Muir Wood (1999a, 1999b), Heshmati (2000), Houlsby and Sharma (1999), Kabirul (1999), Kumbhojkar and Banerjee (1993), Liu and Carter (2000), Manzari and Dafalias (1997), Molenkamp (1994), Molenkamp et al (1996), Oka et al (1999), Pestana and Whittle (1999), Sellmeijer (1994), Seung and Seboong (1995), Stallebrass and Taylor (1997), Thomas and He (1998), Topolnicki and Niemunis (1994), and Yu (1995, 1998).

The models described in the above publications have various degrees of complexity, require different numbers of material parameters, and have varied relevance to the features believed desirable in a material model for bagasse. In the time available, it was impossible to assess their performance by coding each of them into a single element model and comparing their predictions against the measured results. Also, some of the magnitudes of the material parameters required for some of the models were not available from the direct shear test results. The approach taken to advance

towards a material model for bagasse was to choose a model that included and extended the features available in the Modified Cam Clay with a β extension. Such a model is described by Yu (1995, 1998) and was adopted. The model described in Yu (1998) is attractive since it only requires two more material parameters than the classical MCC model. For modelling bagasse, a material for which there are large gaps in the experimental data, minimising the number of material parameters is an important consideration.

The Yu (1998) model is called CASM (Clay And Sand Model). Yu (1998) refers to Wroth and Basset (1965) and Been and Jefferies (1993) to introduce the state parameter concept. Yu (1998) states many reasons on why the state parameter is more useful than over-consolidation ratio for describing soil response. The state parameter ξ is defined as the difference between the specific volume at the current stress state and the specific volume at the critical state at the same effective stress (refer to Figure 1 of Yu (1998) reproduced here as Figure 8.9, which shows the specific volume (ν) and mean normal stress (or mean normal pressure, p or p', where water pressure is zero). ξ is zero at the critical state, positive on the 'wet' side and negative on the 'dry' side. As for the MCC model, the normal compression line and the critical state line are assumed to be parallel.

The yield surface is given as:

$$\left(\frac{q}{Mp'}\right)^n = 1 - \frac{\xi}{\xi_R} \qquad \textbf{(8.4)}$$

and can be expressed as:

$$F = \left(\frac{q}{Mp'}\right)^n + \frac{\ln\left(p'/p'_o\right)}{\ln r} = 0 \qquad \textbf{(8.5)}$$

The equation of the yield surface contains the two material parameters in CASM that are additional to the MCC model. The spacing ratio r (= p'_o/ p'_x) sets the position of the critical state line with reference to the normal compression line, using the over-consolidation ratio definition. The pre-consolidation pressure is p'_o,

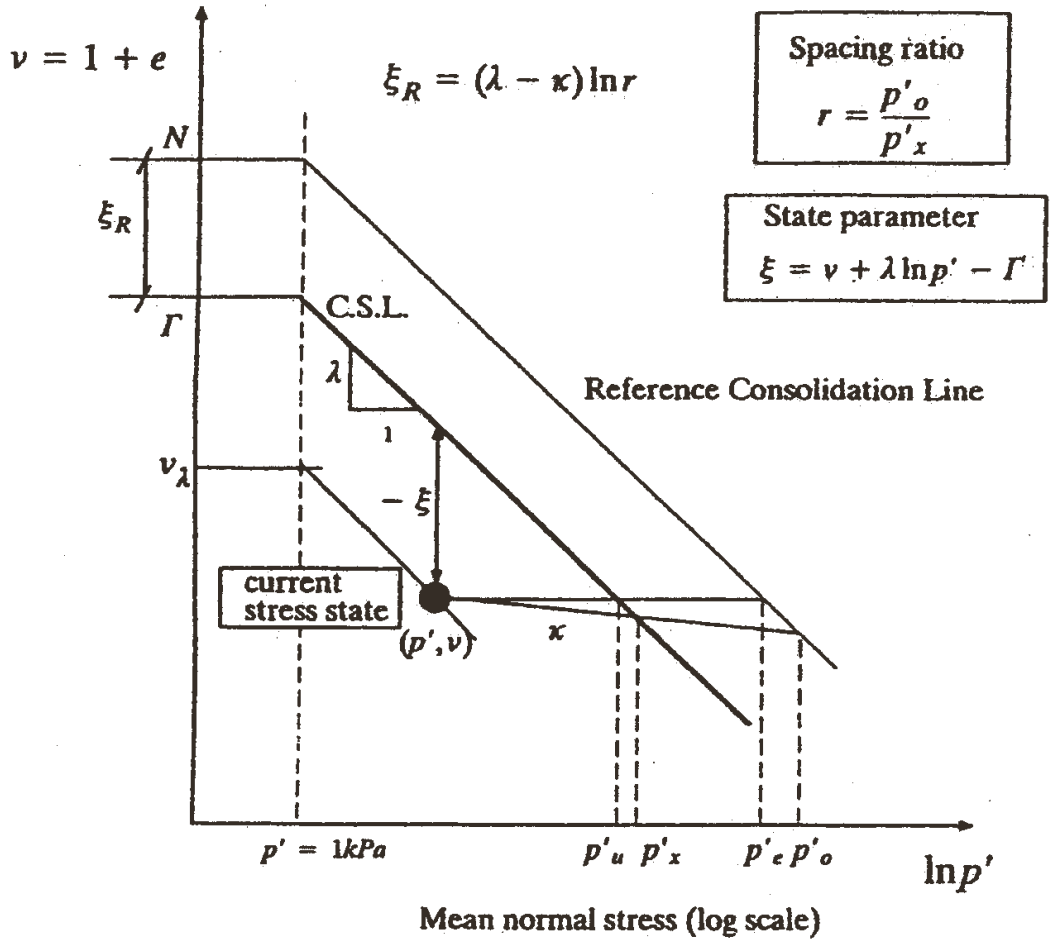

Figure 8.9. Definitions of state parameter and critical state constants for material model CASM (after Yu, 1998).

while the position of the critical state line is p'_x. The stress state coefficient n changes the height of the yield surface. The reference state parameter, ξ_R, denotes the vertical distance between the normal compression line and the critical state line, and is calculated from λ, κ and r.

Shown in Figure 8.10 are yield surfaces for the CASM model together with the yield surface for MCC. The yield surface for MCC with β=1.0 is plotted for a vertical stress of 149 kPa, M value of 1.1 and a K_o value of 0.69. The values of the spacing ratio r and the stress state coefficient n are 2.0 and 1.6 to obtain a close fit of the right hand side (the 'wet' side) of the MCC surface. Also shown in Figure 8.10 is the yield surface for CASM for a K_o value of 0.358, and r and n values of 1.04 and 9.0 respectively.

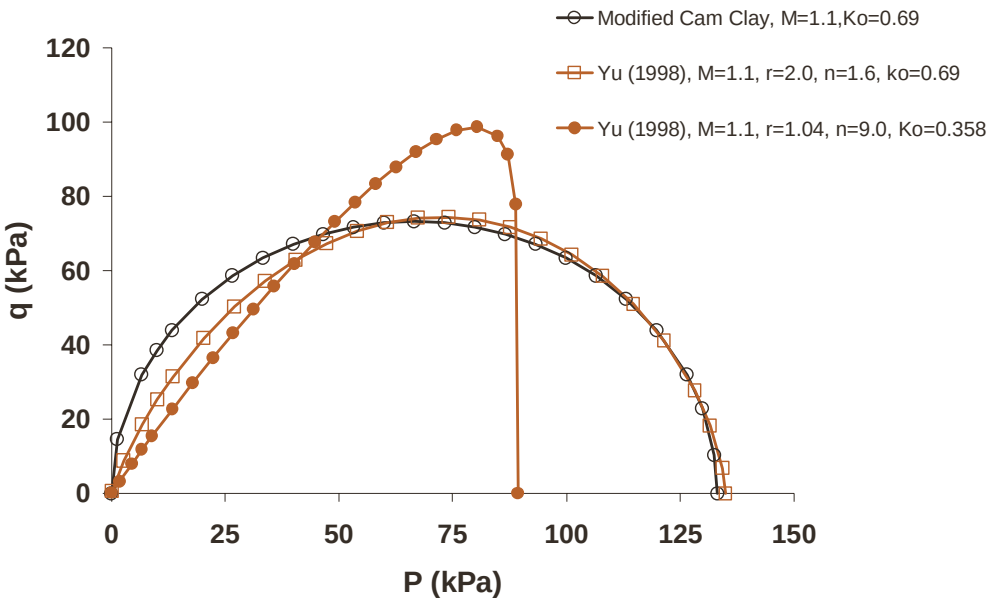

Figure 8.10. Yield surfaces for the MCC and CASM (Yu, 1998) material models.

By changing r and n, many different shapes for the yield surface can be obtained. The shape of the CASM yield surface offers a good deal of flexibility.

The CASM model is non-associated, since Yu (1998) adopted Rowe's (1962) stress-dilatancy relation as the plastic potential surface. Yu (1998) stated that 'Rowe's stress-dilatancy relation (either in its original or modified forms), which provides satisfactory results for most practical problems, has been widely accepted by the geotechnical community', and 'is perhaps the most successful stress-dilatancy relation, which may now be considered to be one of the milestones in soil mechanics'. However, no work has been done to show its applicability to bagasse. Indeed, although many papers have been published on mill modelling using critical state material models to describe the prepared cane behaviour, no mention of the term dilatancy seems to have been made.

The equation of the CASM plastic potential surface is given in (8.6) and the shape is shown in Figure 8.11 for values of M of 1.1, vertical stress of 149 kPa and K_o of 0.69, with the location of the stress state shown by a pink square. The shape is not variable like the yield surface, and is very similar to the plastic potential (and yield surface) of the original Cam Clay model.

$$Q = 3M \ln \frac{p'}{\beta} + (3 + 2M)\ln\left(\frac{2q}{p'} + 3\right) - (3 - M)\ln\left(3 - \frac{q}{p'}\right) = 0 \qquad \textbf{(8.6)}$$

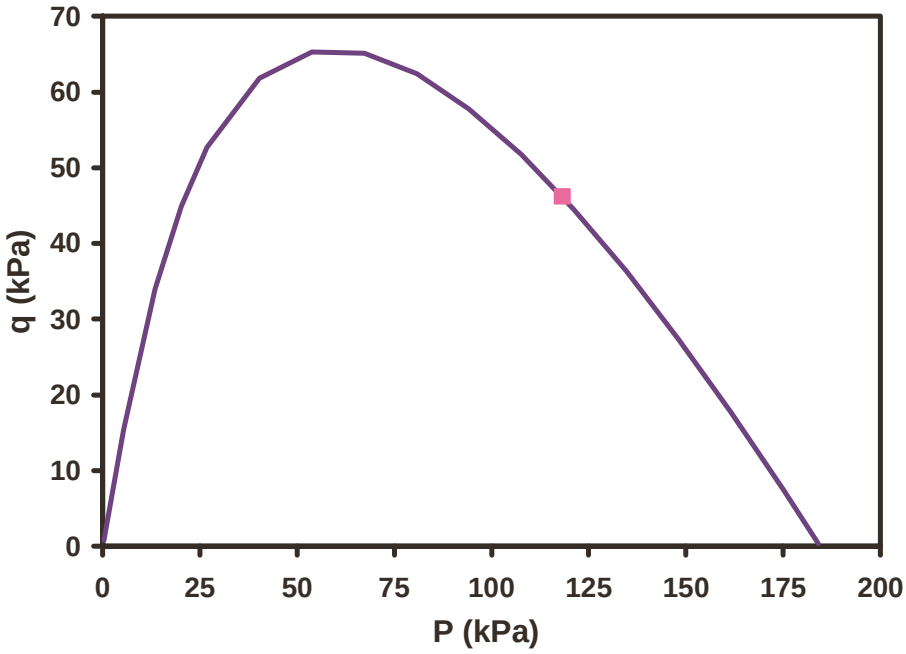

Figure 8.11. Potential surface for CASM material model.

The CASM model was coded into the previously used single element critical state model following the procedure outlined by Naylor and Pande (1981) and Naylor (1985) (and following some of the syntax from Yu, 1998) where the elastic-plastic matrix D_{ep} is used to determine the increments in stress from the increments in strain:

$$d\sigma = D_{ep} d\varepsilon \qquad \textbf{(8.7)}$$

For a two dimensional problem:

$$\begin{bmatrix} \partial\sigma_x \\ \partial\sigma_y \\ \partial\sigma_z \\ \partial\tau_{xy} \end{bmatrix} = \left[D_{ep}\right] \begin{bmatrix} \partial\varepsilon_x \\ \partial\varepsilon_y \\ \partial\varepsilon_z \\ \gamma_{xy} \end{bmatrix} \qquad \textbf{(8.8)}$$

where

$$D_{ep} = D_e - \frac{1}{\beta} b_q \left(b_f\right)^T \qquad \textbf{(8.9)}$$

$$b_f = D_e a_f \qquad \textbf{(8.10)}$$

$$b_q = D_e a_q \qquad \textbf{(8.11)}$$

$$a_f = \left[\frac{\partial F}{\partial\sigma_x}, \frac{\partial F}{\partial\sigma_y}, \frac{\partial F}{\partial\sigma_z}, \frac{\partial F}{\partial\tau_{xy}}\right] \qquad \textbf{(8.12)}$$

$$a_q = \left[\frac{\partial Q}{\partial\sigma_x}, \frac{\partial Q}{\partial\sigma_y}, \frac{\partial Q}{\partial\sigma_z}, \frac{\partial Q}{\partial\tau_{xy}}\right] \qquad \textbf{(8.13)}$$

$$\left[D^e\right] = \frac{E(1-\upsilon)}{(1-2\upsilon)(1+\upsilon)} \begin{bmatrix} 1.0 & \frac{\upsilon}{(1-\upsilon)} & \frac{\upsilon}{(1-\upsilon)} & 0.0 \\ \frac{\upsilon}{(1-\upsilon)} & 1.0 & \frac{\upsilon}{(1-\upsilon)} & 0.0 \\ \frac{\upsilon}{(1-\upsilon)} & \frac{\upsilon}{(1-\upsilon)} & 1.0 & 0.0 \\ 0.0 & 0.0 & 0.0 & \frac{(1-2\upsilon)}{2(1-\upsilon)} \end{bmatrix} \qquad \textbf{(8.14)}$$

$$\beta = H + \left(a_f\right)^T b_q \qquad \textbf{(8.15)}$$

$$H = -\frac{p_o^{'}}{\chi} \left[\frac{\partial F}{\partial p_o^{'}}\right] \left[\frac{\partial Q}{\partial p}\right] \qquad \textbf{(8.16)}$$

$$\chi = \frac{\lambda - \kappa}{\nu} = \frac{\lambda - \kappa}{1.0 + e} \qquad \textbf{(8.17)}$$

The plastic hardening modulus can be derived as (see equation 30 of Yu, 1998):

$$H = \frac{\nu}{(\lambda - \kappa)\ln r}\left[\frac{3M}{p'} - \left(\frac{6.0 + 4.0M}{2q + 3p'} + \frac{3 - M}{3p' - q}\right)\frac{q}{p'}\right] \qquad \textbf{(8.18)}$$

The CASM model was tested using the loading conditions in a direct shear test described in Chapter 5 for a normally consolidated final bagasse sample. Preliminary testing showed that the CASM model did not adequately reproduce the normal compression line, with the predicted slope being different to the measured slope. Also, some numerical instability was seen (non-associated models are less numerically stable than associated models). Based on these observations, and on the basis that using an associated MCC model with a β extension had shown promise, it was decided to develop a variation on the CASM model. It is emphasised that the behaviour of the CASM model in its original form was not fully tested and may be revisited in the future.

The selected variation of the CASM model removed Rowe's stress-dilatancy relation as the plastic potential surface and replaced it with Yu's yield surface equation. However, the material parameters controlling the shape for the yield surface (M1, r1, and n1) and the potential surface (M2, r2, and n2) were kept as separate parameters. This variation has been called modification 1 of the Yu (1998) model. The yield and plastic potential surfaces are given in equations (8.19) and (8.20) respectively.

$$F = \left(\frac{q}{M1\,p'}\right)^{n1} + \frac{\ln\left(p' / p_o'\right)}{\ln r1} = 0 \qquad \textbf{(8.19)}$$

$$Q = \left(\frac{q}{M2\,p'}\right)^{n2} + \frac{\ln\left(p' / p_o'\right)}{\ln r2} = 0 \qquad \textbf{(8.20)}$$

Again following the procedure outlined by Naylor and Pande (1981) and Naylor (1985), the elasto-plastic matrix was derived using the new potential surface and separate material parameters. The new plastic hardening modulus equation is shown in equation (8.21)

$$H = \frac{v}{(\lambda - \kappa)\ln r1}\left[-n2\,\frac{q^{n2}}{M^{n2}}\,p'^{-(n2+1)} + \frac{1.0}{p'\,\ln r2}\right] \qquad \textbf{(8.21)}$$

The material model modification 1 of Yu (1998) is perceived to have several desirable features with which to progress towards an improved material model for bagasse. One feature is the flexibility of being able to greatly change the shape of both the yield surface and the potential surface. The other related feature is that the shapes of the yield surface and the plastic potential surface can be modified independently simply by changing the magnitudes of the parameters in a particular simulation input file. This way, if the material parameters for the yield surface and the plastic potential surface are the same, an associated model is the result. If the parameters for the plastic potential surface are different, a non-associated model is the outcome.

These features allowed the following to be easily carried out. The modification was coded into a single element critical state model, and the shapes of the yield and potential surfaces of the Modified Cam Clay with β extension were closely reproduced. The simulations using modification 1 of Yu's (1998) model were checked against those provided by the MCC model already available in the commercial finite element package ABAQUS. This gave confidence that the coding of modification 1 of Yu's model had been carried out correctly. Then various shapes of the yield surface and potential surface, both associated and non-associated, were simulated and the effect of the shape modifications on the simulation results were judged against the measured direct shear test results.

Results of simulations carried out using a single element critical state model with modification 1 of Yu's (1998) model are presented below. As in Chapter 5 and previously in this chapter, the test data are for the loading conditions on normally consolidated final bagasse at pressure feeder compactions. The input parameters

used are given in Table 8.2. In choosing the input parameters, the approach taken was to leave the M value at the measured value of 1.1 and to reduce the K_o value to as low a value as possible within the limits of the model. The values of K_o used (0.358 and 0.37) are still slightly higher than those considered typical for bagasse (0.1 to 0.3). Two slightly different cases were modelled: case 1 in which the yield surface and the potential surface are identical (M1 equal to M2), that is, associated flow, and case 2 in which the surfaces were slightly different (by making M2 slightly smaller than M1, which also has the result of modifying the K_o value), that is, non-associated flow. The resulting yield surface for case 1 is shown earlier in Figure 8.10. The results of the simulations are shown in Figure 8.12 to Figure 8.16.

Figure 8.12 shows the plot of specific volume versus effective vertical pressure for the initial compression of final bagasse. For both simulated cases, excellent fits to the measured values of the normal compression line were obtained. The fits were just as good as shown in Figure 5.32 of Chapter 5 (page 131) using the MCC model with β=1.0 and in Figure 8.4 of this chapter using the MCC with β=0.21. The results again show that it is relatively easy to reproduce the normal compression line.

Table 8.2 Parameter values for modification 1 of Yu's (1998) single element model simulations

	λ	κ	E (kPa)[#]	G (kPa)[#]	ν	M1
Cases 1 and 2	0.93	0.17	76000	30000	0.3	1.1
	M2	r1	n1	r2	n2	K_o
Case 1	1.100	1.04	9.0	1.04	9.0	0.358
Case 2	1.065	1.04	9.0	1.04	9.0	0.370

[#]only at 2000 kPa

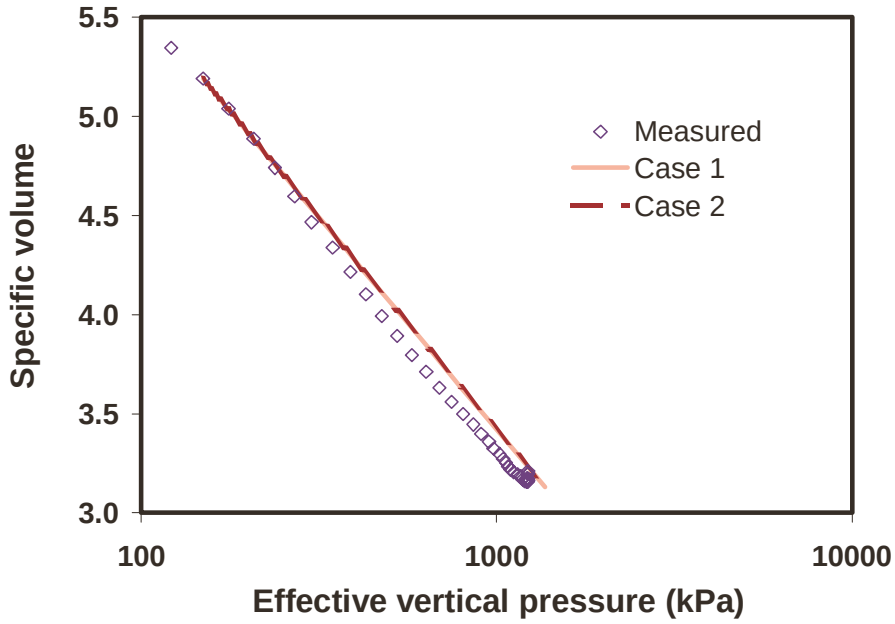

Figure 8.12. Reproduction of compression behaviour for modification 1 of Yu's (1998) model.

Figure 8.13 shows the specific volume versus effective vertical pressure relationship for final bagasse unloaded from a pressure of 2000 kPa. Quite good fits are obtained for both cases, and are much improved compared to the predictions shown in Figure 5.33 (page 132) using the MCC model with β=1.0, and are similar to the prediction shown in Figure 8.5 for the MCC model with β=0.21. For case 1, it is shown that, at a high degree of unload, the prediction diverges from the experimental trend (that is, the slope of the line starts to become vertical). As stated previously, this behaviour seems typical of critical state models at a high degree of unload, and should be monitored/adjusted during modelling to avoid potential numerical problems. Interestingly, case 2 with the slightly different potential surface does not show this tendency.

Figure 8.14 shows the compression reloading behaviour of bagasse (which is basically identical to the unloading line shown in Figure 8.13). Both simulated cases provided excellent fits to the reloading behaviour. This was also the case for the prediction shown in Figure 5.34 (page 132) using the MCC model with β=1.0, and the prediction shown in Figure 8.6 for the MCC model with β=0.21.

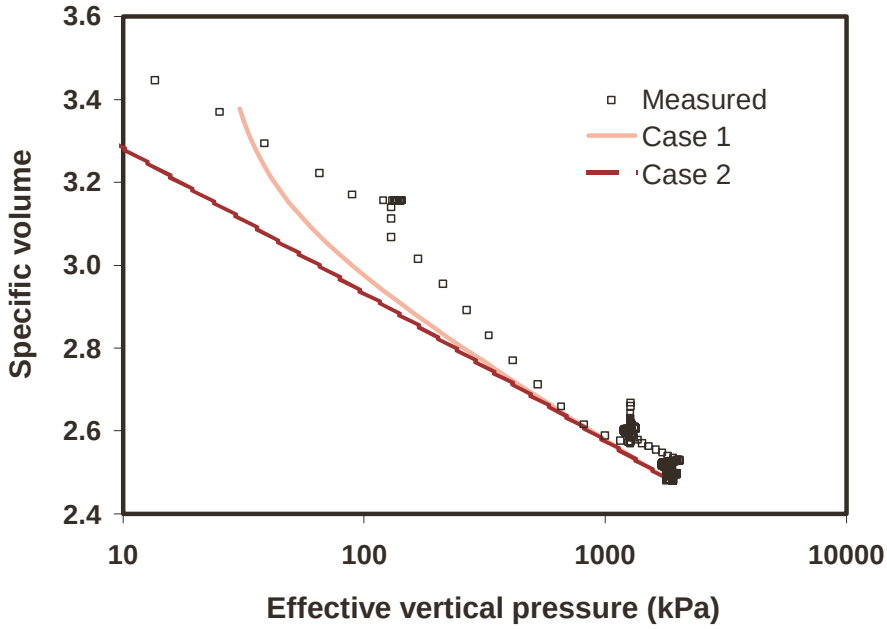

Figure 8.13. Reproduction of unloading behaviour for modification 1 of Yu's (1998) model.

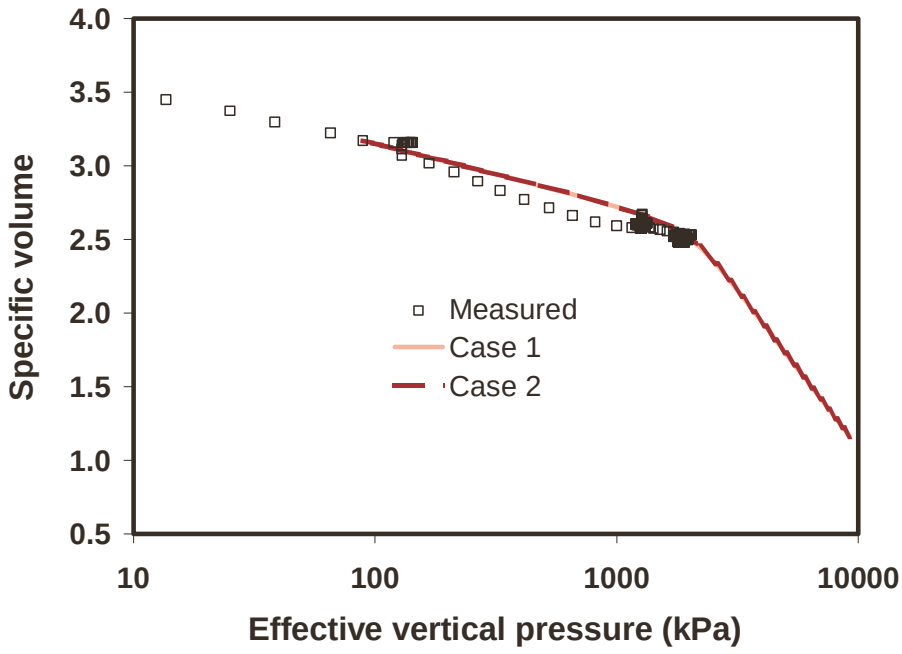

Figure 8.14. Reproduction of reloading behaviour for modification 1 of Yu's (1998) model.

Once the normal compression line is reached (at the maximum effective vertical pressure of 2000 kPa, where the bagasse was initially loaded to and unloaded from), the prediction continues along the normal compression line.

The measured and predicted shear behaviour for a normally consolidated final bagasse sample is shown in Figure 8.15 and Figure 8.16. Figure 8.15 shows the plot of shear stress versus shear strain. The predictions were excellent up to a shear strain of 0.5 and are quite good even up to a shear strain of 1.0. The prediction for case 2 is marginally better than that for case 1. Schembri et al. (1998) show in their Figure 1 the volumetric and shear strains for a test performed at SRI on a small-scale experimental three-roll pressure feeder, and showed that shear strains in excess of 1.0 were present in the pressure feeder nip. Therefore, the ability of a model to predict shear stress up to a shear strain of 1.0 is very desirable. The predictions for case 1 and 2 are much improved compared to that shown in Figure 5.35 (page 134) using the MCC model with β=1.0, and are also an improvement on the prediction shown in Figure 8.7 for the MCC model with β=0.21. Figure 8.16 shows the specific volume versus shear strain. The reproduction of the change in specific volume is still poorly predicted, similarly to the prediction shown in Figure 5.36 (page 134) using the MCC model with β=1.0, and the prediction shown in Figure 8.8 for the MCC model with β=0.21. Too much decrease in volume is predicted. This deficiency should be pursued in future work. However, the poor prediction of decrease in volume during shearing should be seen in the context that for prepared cane and bagasse, the change in volume due to compressive loads is much greater than those due to shearing. Therefore the poor prediction of volume change during shearing may not be of high consequence in many milling situations.

In summary, it has been shown that the modification 1 of the Yu (1998) material model produces improved reproductions of loading and unloading conditions relevant to milling compared to previously tested models, while using a single set of parameters that better reflect the magnitudes of measured material parameters of bagasse. The decrease in volume due to shear is still not predicted well, and should be pursued in future work, as well as pursuing a model in which the value of K_o can be reduced to 0.2 while keeping the value of M at 1.1. The model was numerically stable for the two input parameter cases modelled.

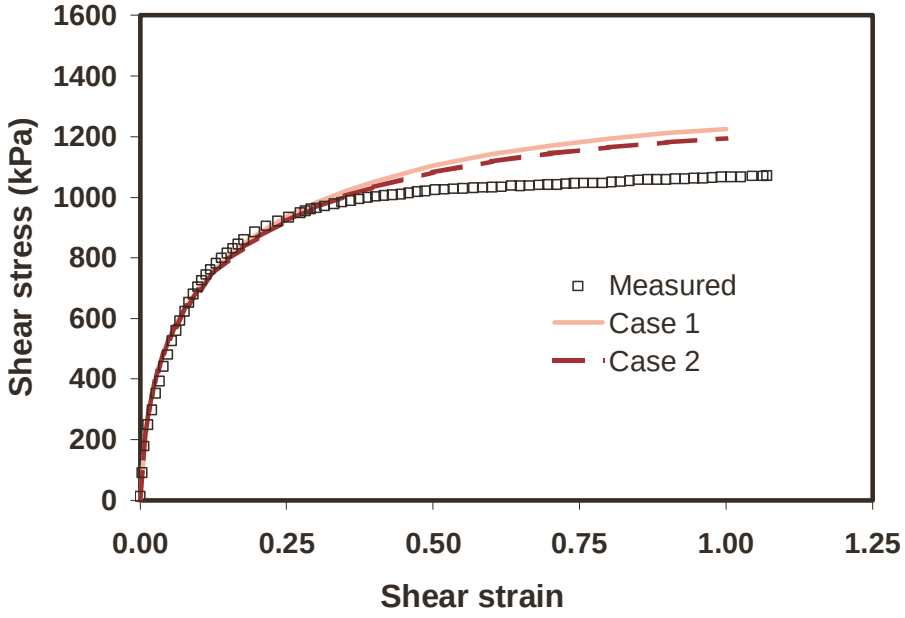

Figure 8.15. Reproduction of shear stress versus shear strain for Modification 1 of Yu's (1998) model.

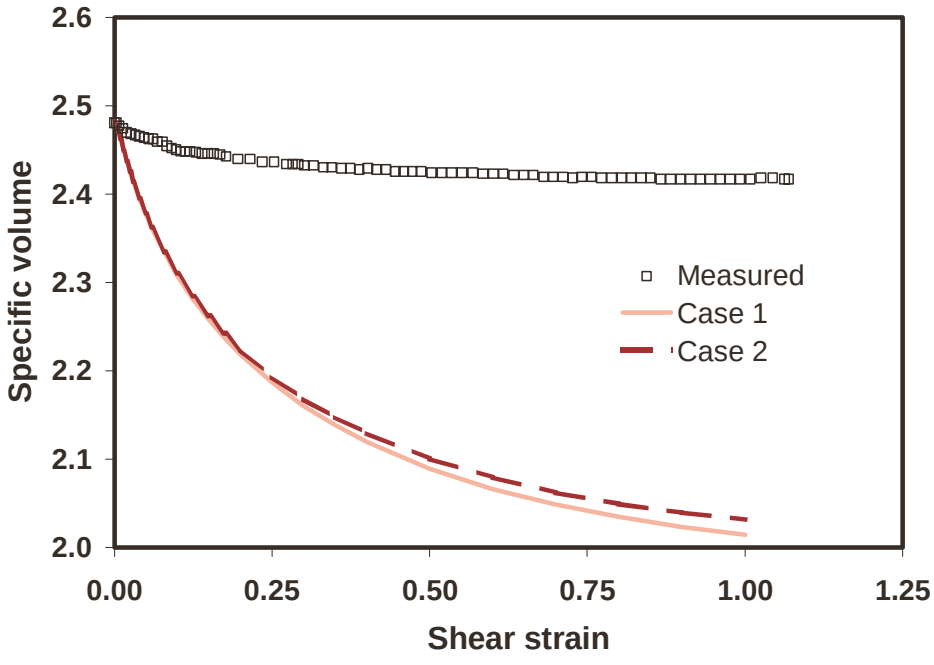

Figure 8.16. Reproduction of specific volume versus shear strain for Modification 1 of Yu's (1998) model.

The improvements achieved in reproducing bagasse behaviour are enough to justify the implementation of the material model into a commercial finite element package such as ABAQUS, and to test its performance in modelling parts of a milling unit (for example, the pressure feeder).

8.5 Summary of Chapter 8

Certain features desirable in a material model for predicting the behaviour of the solid skeleton (the fibre) of prepared cane and bagasse have been described.

A multi-element model in the finite element package ABAQUS, using an associated Modified Cam Clay model with a β extension and using porous elasticity, was exercised for five loading conditions on final bagasse at pressure feeder compactions. It was shown to achieve improved reproductions of loading and unloading conditions relevant to milling compared to previously tested models, while using a set of material parameters that better reflected the magnitudes of measured material parameters of bagasse.

A material model with its origins in the soil mechanics literature and having extended features to those of the Modified Cam Clay model with a β extension has been described. That model is the Clay and Sand Model (CASM) of Yu (1998). A modification of that model (modification 1 of Yu (1998)) has been shown to achieve a further improved prediction of loading and unloading conditions relevant to milling, while using a set of consistent parameters (i.e. K_o) that better reflect the magnitudes of measured material parameters of bagasse. The decrease in volume during shearing of a normally consolidated final bagasse sample is still not predicted well and that deficiency should be investigated further. The poor prediction of decrease in volume during shearing should be seen in the context that for prepared cane and bagasse, the change in volume due to compressive loads is much greater than those due to shearing. Therefore the poor prediction of volume change during shearing may not be of high consequence in many milling situations.

There are many other models in the soil mechanics literature with similar features to that of Yu (1998), although many may not be as simple to use. A modified Yu (1998) model forms a platform to work towards a material model that reproduces

bagasse behaviour adequately. It is stressed that there is much bagasse behaviour that has not been measured (such as the shear behaviour parallel to the direction of compression, as well as its behaviour under high quality triaxial tests) which almost certainly would have a bearing on the makeup of a material model for bagasse.

The improvements achieved in reproducing bagasse behaviour are enough to justify the implementation of modification 1 of Yu's (1998) material model into a commercial finite element package, and to test its performance in modelling parts of a milling unit (for example, the pressure feeder).

9 Chapter 9 – Application to mill modelling

9.1 Introduction

This investigation has focussed on showing that bagasse behaves like a soil and exhibits critical state behaviour, using the measured mechanical behaviour to determine material parameters for bagasse and working towards a material model that reproduces that behaviour more closely. The tool that has been used, both experimentally and numerically, is a version of the direct shear test used in soil mechanics. This chapter seeks to apply the improved material models, and the associated material parameters and boundary conditions, to the modelling of the first part of an Australian six roll mill, which is the pressure feeder. This is undertaken in two separate but related parts. The first part involves the calculation of loads and torques in the pressure feeder using measured data from direct shear tests and from theory available in the milling literature. The second part involves a similar calculation of loads and torques but using the commercially available finite element package ABAQUS, with the improved material parameters and material models, to simulate bagasse moving through the pressure feeder. In both parts there is an effort to compare the predictions with the available measurements from a sugar factory. It is noted that this exercise and its outcomes should be treated as a 'first look'.

9.2 Description of the Victoria mill B1 pressure feeder

The choice of experimental results to compare the predictions against was important. The following features in the experimental milling data were desirable:

1. The comparison of predicted material behaviour by the material models to the measured behaviour in direct shear tests was carried out at pressures ranging up to 2000 kPa. Simulation results above this magnitude have not been checked. It has also been shown that above 4000 kPa the detail of the behaviour of prepared cane, first bagasse, and final bagasse becomes significantly different to the behaviour below 4000 kPa. It would be difficult for existing material models to predict the different behaviour in the same simulation. Therefore a milling situation with pressures up to and including 2000 kPa (or a bit higher) was desirable.

2. There is a large difference in the coefficient of friction (and therefore feeding force) developed between a rough surface (such as the arced surface deposited on the grooves of a mill roll) and bagasse and between a smooth surface and bagasse. A rough surface on a roll allows feeding of bagasse at high contact angles (the angle between the contact point of the bagasse with the roll and a line connecting the centres of the rolls) and high self-feeding forces are generated. Although a large number of milling tests has been carried out over the last fifty years using laboratory scale equipment, most (if not all) tests were carried out using rolls with smooth surfaces (whether they had grooves or not). The result of having a smooth surface is that at high contact angles the bagasse slips on the roll. Therefore those tests were not believed suitable to carry out modelling simulations where the main task was to assess the performance of a material model. A situation where significant feeding forces were likely to occur was desirable in order to provide a severe test for the material model.

3. A milling situation where the development of juice pressures was not significant in comparison to the pressures on the solid skeleton (the fibre) of the bagasse (again to assess the performance of the material model, and not be complicated by an additional permeability model which may or may not be adequate).

4. Accurate measurements of the test geometry, operating conditions such as throughput, bagasse analysis, roll load, roll torque, and roll speed.

Available tests with the above features are rare. One such set of tests is that mentioned in Williams et al (2001), who carried out factory trials on a prototype two-roll mill operating as the second mill in a five mill train. However, the detail of those tests was commercially sensitive and was not available. Tests carried out by SRI staff during the 1997 crushing season at Victoria Mill were identified as having most of the features described above, except that loads were not measured. In particular, data was available for the pressure feeder of the number one mill of the B train. These tests were adopted for the exercise described here.

Victoria mill is the largest raw sugar factory in Australia and has two milling trains (A and B) operating in parallel. Each of the milling trains has five milling units. Shown in Figure 3.1 of Chapter 3 is a schematic of such a milling unit. The

pressure feeder is made up of the first three rolls in that unit, and may be considered to include the vertical feed chute at the entry point, and the pressure feeder chute at the exit point. The pressure feeder on the number one mill of the B train during the 1997 crushing season is shown schematically in Figure 9.1. The relative sizes and positions of the feed chute and the three rolls are to scale. The details of the geometry and available operating data are given in Table 9.1.

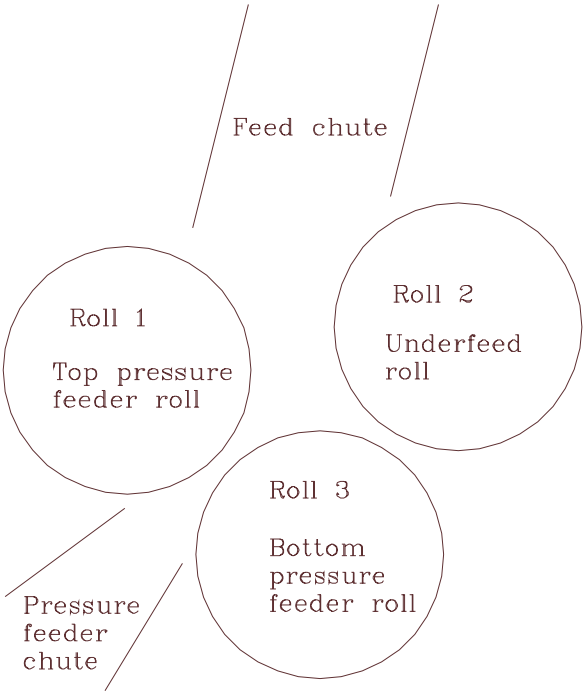

Figure 9.1. Pressure feeder of No 1 milling unit on B train at Victoria Mill.

As noted previously, the rolls have circumferential grooves. The mean diameter is measured to the middle of the grooves. The work opening at the nips is the smallest distance between rolls measured from the mean diameters. The underfeed roll is actually a roll with a smaller diameter (about 1200 mm) with steel plates welded to the roll such that the external diameter is similar to that of the pressure feeder rolls. The axis of the plates is parallel to the movement of bagasse. The plates are approximately 100 mm square, staggered, and spaced about 100 mm apart. The exercise here is carried out with an idealised underfeed roll which is identical to the pressure feeder rolls. It is noted that the underfeed roll is driven from the bottom pressure feeder roll and therefore the bottom pressure feeder roll torque includes the underfeed roll torque. The feed chute was about 1920 mm high (measured

vertically) and was inclined at an angle of about 76 degrees to the horizontal. A vertical chute is believed to be a (slightly) better geometry for feeding, however for reasons such as the current geometry being a modification from a previous geometry, and/or lack of space, there are many chutes in the sugar industry that are not quite vertical.

Table 9.1 Details of the geometry and available operating data for Victoria B1 pressure feeder

Parameter	Value
Cane variety	Q124
Crushing rate (t/hr)	543.0
Fibre content of cane (%)	12.77
Fibre rate (t/hr)	69.3
Roll mean diameter (m)	1.217
Groove depth (m)	0.060
Underfeed nip work opening (m)	0.433
Pressure feeder nip work opening (m)	0.132
Roll length (m)	2.54
Roll rotational speed (RPM)	3.49
Underfeed nip compaction (kg fibre/m^3)	79.0
Pressure feeder nip compaction (kg fibre/m^3)	258.0
Top pressure feeder torque (kNm)	149.0
Bottom pressure feeder torque (kNm)	139.0

9.3 Prediction of mill operating parameters using milling theory and direct shear test results

A method of predicting loads and torques is given in Section 3.2 of Murry and Holt (1967) based on considering the forces acting on a pair of rolls (shown here in Figure 9.2 reproduced from Figure 3.1 of Murry and Holt, 1967).

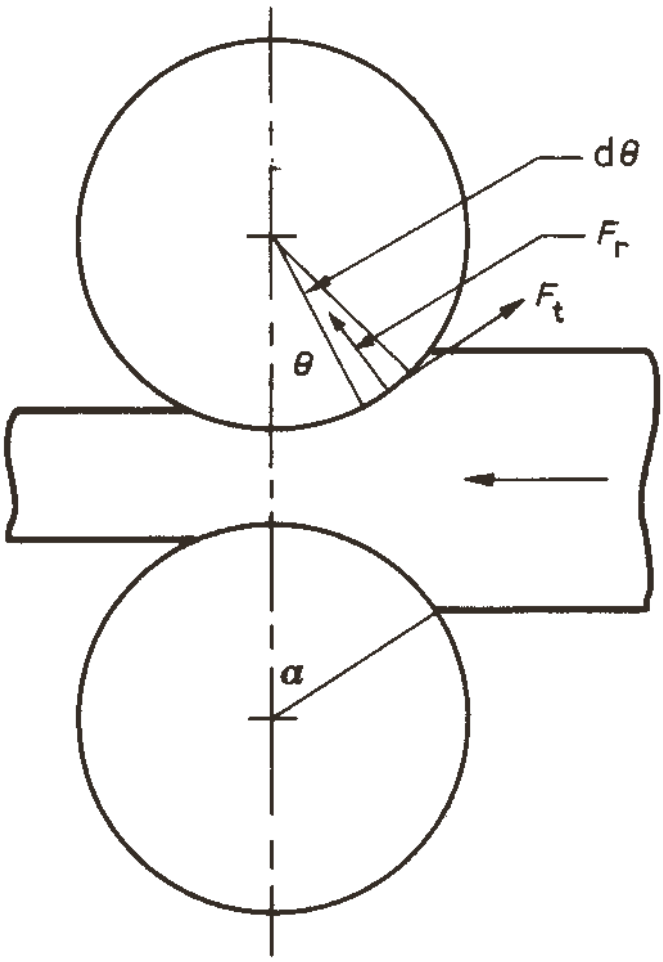

Figure 9.2. Forces acting on a pair of rolls (reproduced from Murry and Holt, 1967).

The total torque on one roll, G, is given by:

$$G = L\frac{D^2}{4}\int \mu p \, d\theta \qquad \textbf{(9.1)}$$

The separating force (vertical force in Figure 9.2), R, is given by:

$$R = L\frac{D}{2}\int p\left(\cos\theta + \mu \sin\theta\right) d\theta \qquad \textbf{(9.2)}$$

The horizontal force (parallel to the movement of bagasse), H, is given by:

$$H = L\frac{D}{2}\int p\left(\mu\cos\theta - \sin\theta\right) d\theta \qquad \textbf{(9.3)}$$

For the current exercise, L is the roll length, D will be assumed to be the roll mean diameter, p is the pressure acting perpendicular to the roll surface, and μ is the coefficient of friction acting on the roll surface. In order to solve these equations it is necessary to know p and μ as functions of θ, where p is usually determined in laboratory tests as the vertical pressure measured while compressing cane into a box. Murry and Holt (1967) related p to another method of representing density called the compression ratio (C). Previous investigations of the data required for this exercise also had this form and this form was adopted.

The compression ratio can be calculated from:

$$C = \gamma \left[\frac{\rho_j f + \rho_f (1 - f)}{\rho_f \rho_j f} \right] \qquad \textbf{(9.4)}$$

where γ is the compaction, ρ_f is the fibre density (1530 kg.m^{-3}), ρ_j is the juice density (1080 kg.m^{-3}), and f is the fibre content.

The vertical pressures were calculated as follows. Murry (1960) provided the quadratic shown in equation (9.5) to relate vertical pressure and compression ratio.

$$P = A\left((C + B1)^2\right) \qquad \textbf{(9.5)}$$

Loughran and McKenzie (1990) carried out compression tests for a large range of fibre contents and preparations for a pressure range from 3.5 to 80 kPa. Plaza et al (1993) found that, for their values of fibre content of Q124 cane given in Table 9.2, and using averaged parameters from Loughran and McKenzie (1990) also shown in Table 9.2, a good match of their results was obtained up to a compression ratio of 1.9. The curves are shown at low vertical pressures in Figure 9.3, while Figure 9.4 shows the match (reproduced from Figure E.1 and Figure E.2 in Plaza et al, 1993) at higher pressures. The calculations carried out here only involved the range at which there was a good fit to the data. It is noted that the data are not for the actual Victoria Mill cane, and this introduces an additional uncertainty.

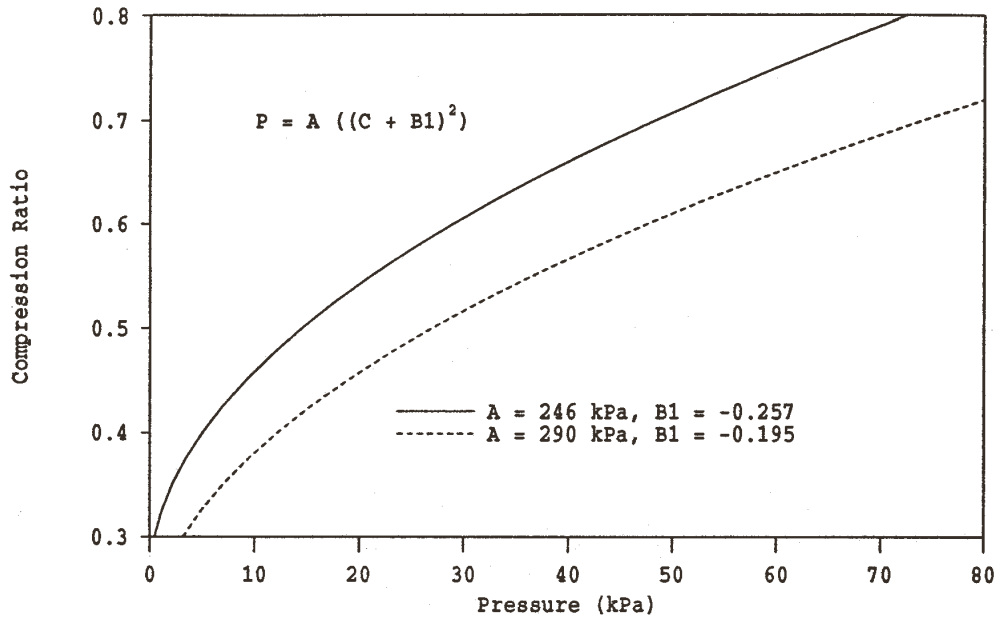

Figure 9.3. Loughran and McKenzie pressure vs compression ratio relationship.

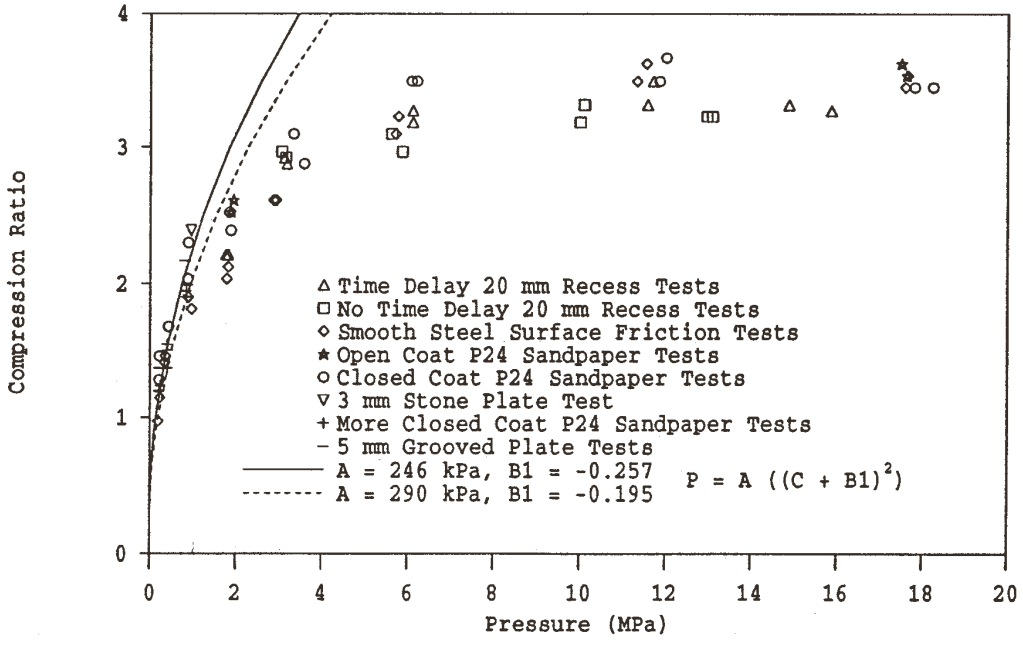

Figure 9.4. Fit to Plaza et al (1993) data of pressure vs compression ratio relationship given in Loughran and McKenzie (1990).

Table 9.2 Parameters for calculation of pressures for load and torque calculations

Fibre content (%)	Parameter A (kPa)	Parameter B1 (kPa)
11.6	246	-0.257
14.0	290	-0.195

The coefficients of friction adopted were actually coefficients of internal shear of the bagasse. As noted previously, a rough surface such as that on the arced surface on the grooves of a roll will provide enough grip to internally shear bagasse. The values are therefore the maximum that can be obtained at the surface. It is noted that, in reality, and as noted by Murry and Holt (1967), the values may not be realised at the roll surface since it may not be necessary to use the full available 'friction' force. The predicted loads and torques should therefore be higher than the measured values.

The coefficients of shear were calculated as follows. At pressures below 200 kPa, the values from Plaza and Kent (1998), measured for prepared cane using 4 mm high grooves with their axis perpendicular to the shearing motion, were adopted and the equation is shown in Figure 9.5. The coefficient of shear is simply the calculated shear stress divided by the corresponding vertical pressure. At pressures above 200 kPa, the values from Plaza and Kent (1997) using P24 sandpaper (~1 mm diameter particles) were used and the equations are shown in Figure 9.6.

The equations were coded into a Fortran program (shown in Appendix E) that summed the calculated forces from the contact angle with the prepared cane to the nip (the line connecting the centres of the two rolls being considered). Two angles were used for the calculations, 58^{o} and 43^{o}. The larger angle is that made by extending the feed chute until it contacts the top pressure feeder roll and the underfeed roll. The smaller angle is that which may be physically more realistic when the cane contacts the bottom pressure feeder roll. Both angles are used for all calculations to give a measure of the effect of the different angles on the predicted loads.

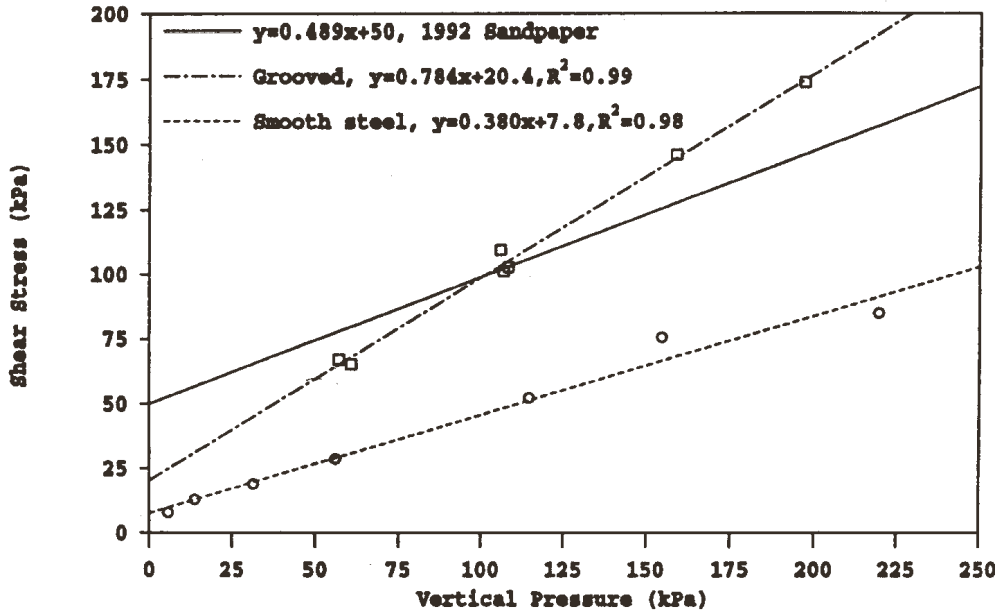

Figure 9.5. **Shear stress versus vertical pressure for prepared cane at low vertical pressures (reproduced from Plaza and Kent, 1997).**

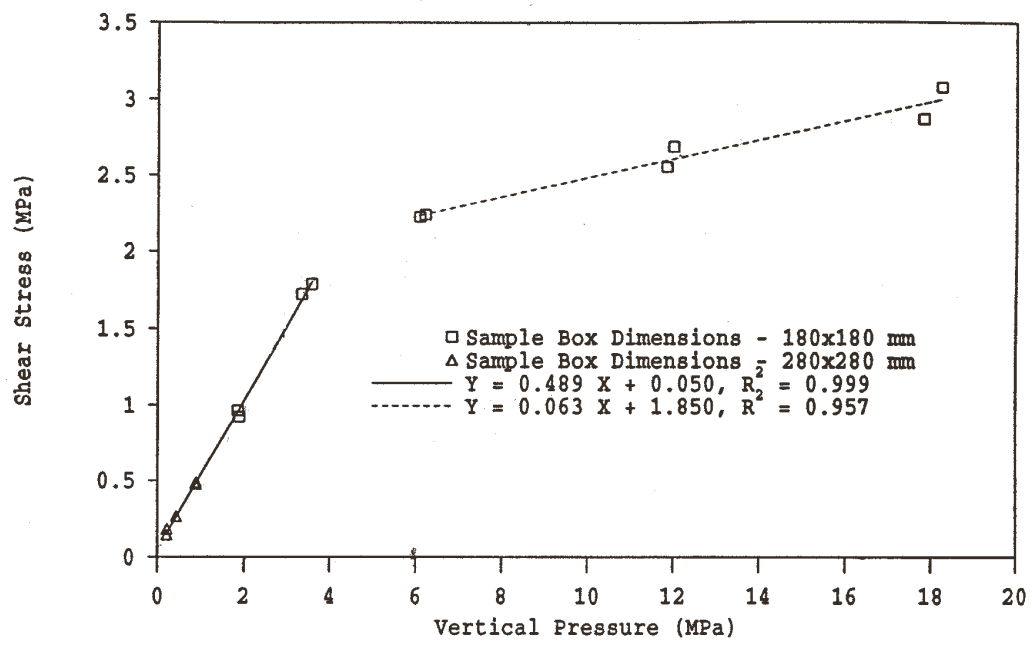

Figure 9.6. **Shear stress versus vertical pressure for prepared cane (reproduced from Plaza and Kent, 1998).**

The forces after the bagasse exits the nip and expands (and therefore remains in contact with the roll surface for an unknown distance) were not determined as they are much harder to define. This omission will introduce an error into the predictions and will reduce the magnitudes of loads and torques. The predictions are shown in Table 9.3 for the underfeed nip and in Table 9.4 for the pressure feeder nip.

Table 9.3 Predictions for one roll in underfeed nip

Fibre content (%)	Contact angle (^{o})	Separating force (kN)	Force at 90 ^{o} to separating force (kN)	Roll load (kN)	Torque (kNm)
11.6	58.0	38	33	50	29
	43.0	28	29	40	22
14.0	58	59	38	70	37
	43	44	35	56	29

Table 9.4 Predictions for one roll in pressure feeder nip

Fibre content (%)	Contact angle (^{o})	Separating force (kN)	Force at 90 ^{o} to separating force (kN)	Roll load (kN)	Torque (kNm)
11.6	58.0	367	101	381	121
	43.0	341	100	355	109
14.0	58	481	116	495	152
	43	444	117	459	135

The predicted torques for the underfeed roll are about 20 to 25% of those predicted for the pressure feeder rolls. Since the measured values given in Table 9.1 for the top pressure feeder torque includes the contributions from the underfeed nip and the pressure feeder nip, while the value of bottom pressure feeder torque includes the driven underfeed roll, the predicted values of torque for the underfeed nip and the pressure feeder nip were added together in Table 9.5 for comparison.

Table 9.5 Predicted torques for Victoria Mill no.1 pressure feeder configuration

Fibre content (%)	Contact angle (^{o})	Predicted top and bottom pressure feeder roll torque (kNm)
11.6	58.0	150
	43.0	131
14.0	58.0	189
	43.0	164

The magnitudes of the roll torque predictions spanned those that had been measured, being different by a maximum of approximately 28%. Considering the many uncertainties detailed previously, the results of the exercise gave some confidence that similar calculations can be used to link laboratory measurements to milling situations.

9.4 Prediction of mill operating parameters using multi-element modelling and direct shear test results

Chapter 8 identified two material models that reproduced bagasse behaviour better than material models previously used in mill modelling. The better prediction was obtained by using input parameters that better reflected measured values. The first material model was the extended Modified Cam Clay with a β value of 0.21. The application of this model to a milling situation is relatively straightforward, at least at first glance, since it is already available in the finite element package ABAQUS. The second material model, modification 1 of Yu (1998), showed further improvement in the reproduction of bagasse behaviour, and included features (such as the ability to be both an associated model or a non-associated model simply by changing a few values of input parameters) that are believed to facilitate even further improvement. There were no material models in the ABAQUS library with the features of the modification 1 of Yu's (1998) model. Therefore the modification 1 of Yu's (1998) material model needed to be coded in so that ABAQUS could access it. It was decided that it was worthwhile carrying out such an attempt.

9.4.1 Implementation of modified 1 of Yu's (1998) model into ABAQUS subroutine

As described in Chapter 8, the coding for the modification 1 of Yu's (1998) model was in the form of a quasi-analytical single element model in a fortran program. ABAQUS has a facility that allows the input of user defined mechanical material behaviour (i.e. the input of a user defined mechanical constitutive model) from an external Fortran subroutine. The subroutine is called UMAT. The UMAT subroutine is compiled automatically before any ABAQUS simulation that requires it. A short description of UMAT is given here, including the features in ABAQUS that affect its content and performance.

It is noted first that there are two versions of ABAQUS that could have been used for the simulations that are described in this section. The versions are Standard and Explicit. Standard has some features desirable for mill modelling that are not available in Explicit, such as being able to model permeability, and was the only version available (it was available because it was being used in a separate project). Standard was used for the modelling of the direct shear tests described in Chapter 5, Chapter 6, and Chapter 8. Explicit has improved procedures to deal with contact and convergence issues and it is believed that Explicit would have been a more suitable solver to use in mill modelling (at least initially), since as will be noted later, many contact and convergence problems were encountered during the modelling (and the permeability option was not required for this 'first look').

ABAQUS solves problems in time (or pseudo time). The user subroutine UMAT is called for each material point in an element at each iteration of every increment. Increments of strain are provided to the subroutine UMAT (or VUMAT in the Explicit version), as well as solution-dependent state variables such as P_c. UMAT or VUMAT update the stresses and the solution dependent state variables to their values at the end of the increment. This is the same procedure described in Chapter 8 for the single element critical state model. For ABAQUS Standard, UMAT is also required to provide the 'material Jacobian matrix', $\partial\Delta\sigma/\partial\Delta\varepsilon$, for the mechanical constitutive model. This is not necessary for Explicit. The elasto-plastic matrix, D_{ep}, shown in equation 8.8 and equation 8.9 of Chapter 8 (page 230), suffices as the 'material Jacobian matrix' and is able to provide the correct solution if convergence

is obtained. However, the rate of convergence, as well as whether convergence is obtained, can be affected. The calculation procedure shown in Chapter 8 after Naylor and Pande (1981), using the elasto-plastic matrix and implemented in UMAT for this exercise, is a form of forward Euler integration (Sawyer, 2002). ABAQUS uses the backward Euler method in its library of plasticity models, together with a 'material Jacobian matrix' consistent with this integration operator. Such an implementation of the modification 1 of Yu's (1998) material model in ABAQUS Standard was deemed to be beyond the scope of this work. If only for this reason, had Explicit been available, some initial simulations using ABAQUS Explicit would have been worthwhile for the purpose of testing the material model in a milling situation.

The modification 1 of Yu's (1998) material model was implemented in UMAT in ABAQUS Standard and its correct implementation was checked by comparing the predictions against the direct shear test loading conditions described in Section 8.4 of Chapter 8 in multi-element simulations. This checking was carried out successfully. A model describing the Victoria B1 pressure feeder was built. However, those simulations experienced significant numerical and convergence problems and a solution was not obtained. It is noted that, as described in the next section, significant numerical and convergence problems, although not as bad, were also experienced with material models already included in the ABAQUS library. It is also believed that the material models included in the ABAQUS library have additional code that stabilize the solution process and/or address some of the numerical weaknesses in the material models (such as numerical problems during large degrees of unload). That source code was not available externally. Some further work, with guidance from the providers of ABAQUS, would be required to bring the material model to the robust standard of the models available in the ABAQUS library. Simulations with the modification 1 of Yu's (1998) material model were stopped at this point.

9.4.2 Simulations of a three roll pressure feeder using a Modified Cam Clay model with β=0.21 and a corresponding Drucker-Prager Cap model

Simulations of the Victoria Mill B1 pressure feeder were carried out with material models already available in the ABAQUS library. The material models were an

extended Modified Cam Clay model with β=0.21 (which has been shown to achieve improved reproduction of bagasse behaviour) and a Drucker Prager Cap model with a similar yield surface and potential surface shape in the 'wet' side of the critical state line. In reality, prepared cane is the input material to the B1 pressure feeder. However, for these simulations, final bagasse was the input. There were two reasons for this: firstly, all of the direct shear test modelling that has been presented has been on final bagasse (although it is noted that the conclusions have been verified by carrying some first bagasse simulations) and it was desirable to continue that connection for a 'first look' at mill modelling. Secondly, it was found that it was easier to obtain a converged solution using the final bagasse material parameters (the magnitudes of the prepared cane parameters are quite similar to final bagasse, so this is just believed to be a coincidence).

The parameters for final bagasse for use with the Modified Cam Clay model are given in Table 8.1 of Chapter 8 (page 220). The given values of M of 1.1 and κ of 0.17 are reasonable for pressures ranging from 0 to 2000 kPa, given the measured data in Appendix B. The value of υ of 0.3 is reasonable, given that there is little data available in the literature. The approach follows that in the soil mechanics field (for example, see Kirby (1998b)). The value of λ of 0.93 is justified from a vertical pressure of 2000 kPa down to probably 100 kPa. However, there are data available that shows that at lower pressures the values of λ are probably much higher. Kent and McKenzie (2000) give values for λ ranging from 5 to 8 for pressures from 0 to about 80 kPa. The initial specification of the material in the feed chute requires the specific volume at a low pressure of about 3.0 kPa. In order to keep the modelling consistent and as simple as possible for a 'first look', the equation for a pressure range of 100 kPa to 2000 kPa was extrapolated down to determine the initial specific volume at the pressure of 3.0 kPa. In reality, the specific volume at low pressures is much higher. The effect of this simplification has not been quantified.

The parameters for the Drucker Prager Cap (DPC) model were a value of R of 0.23 (similar to the β value of 0.21 for the MCC model), and a β value of 42.3^{o} (different meaning to the β of the MCC model, it is actually a measure of the friction angle

and replaces M). The plastic hardening curve (an alternative method of representing the normal compression line with reference to the elastic unloading-reloading line) used by the DPC model is shown in Figure 9.7. The DPC Model has the option of setting a tensile strength for the material, which the MCC model does not, and a small value of 2.0 kPa was used. Such a value is reasonable given the direct shear test data in Figure 9.5 close to a vertical pressure of zero.

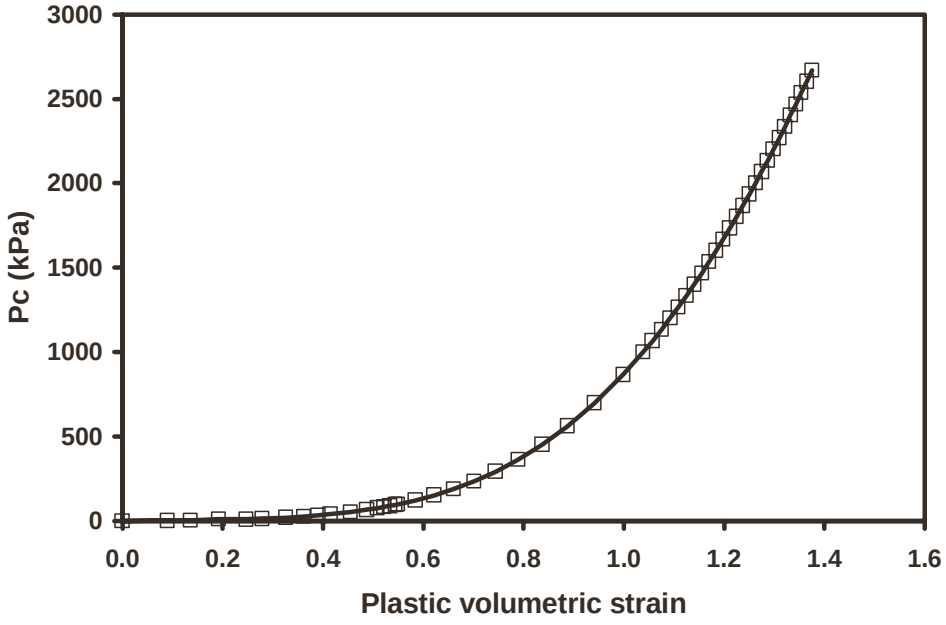

Figure 9.7. Plastic volumetric strain data for Drucker Prager Cap material model simulations.

An ABAQUS model of the pressure feeder and block of final bagasse prior to a simulation is shown in Figure 9.8. Two slightly different geometries were modelled. Since it was believed that the roughness on the top part of the grooves played an important part in feeding, and the roughness was present only in the top 30 mm of the 60 mm high grooves, the roll diameters modelled were 1247 mm (3/4 of the way to the tip of the grooves), and 1277 mm (actual roll diameter at the tip of the grooves). The resulting nip clearances between the rolls are given in

Table 9.6.

Table 9.6 Nip clearances for modelled roll diameters

Modelled roll diameter (mm)	Nip clearance (mm)	
	Underfeed nip	Pressure feeder nip
1247	432.8	94.9
1277	402.8	64.9

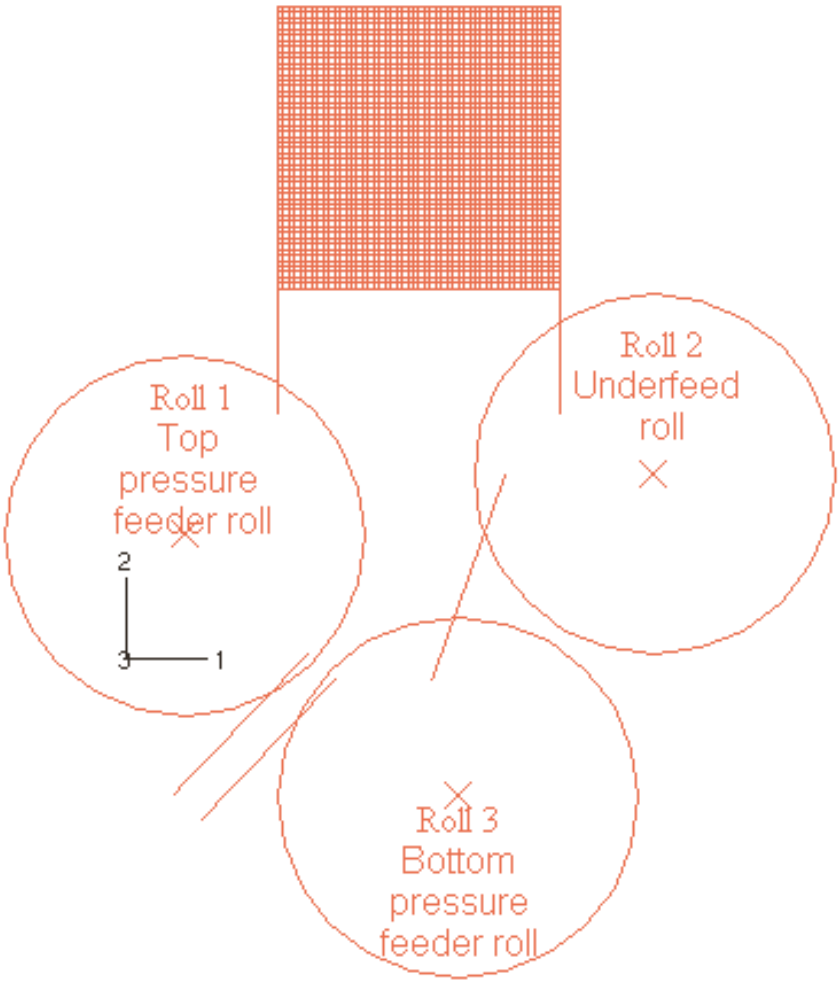

Figure 9.8. Initial model geometry for Victoria Mill B1 pressure feeder simulation

A coefficient of friction of 1.4 on the roll surface was used for all three rolls. The value was chosen as being the highest realistic value before internal shear of the bagasse occurred (again in order to have a severe test of the material model). The value was based on the measured maximum coefficients of shear shown in Figure 7.21 of Chapter 7 (page 209) and the conclusion in Section 6.4.2 of Chapter 6 (page 167) that, when simulating a direct shear test on over-consolidated bagasse, a coefficient of 1.4 was predicted to achieve almost no slip. It is noted (and will be shown later) that the predicted magnitudes of coefficient of friction at the roll surface are dictated by the material model (i.e. the stresses developed inside the bagasse) unless there is slip at the surface. The actual values will usually be lower than 1.4. When the magnitude reaches 1.4, slip is predicted on the roll surface and the shear stress inside the bagasse is limited to this value. The coefficient of friction on all other surfaces was assigned a value of zero.

The simulations were carried out using two-dimensional plane strain elements. The mesh was 50 x 50 elements and the elements were square with an initial side dimension of 20 mm. This mesh size was judged to be adequate for an initial set of simulations. The effect of mesh size on the solutions has not been quantified. The simulations were carried out on a Compaq Alpha workstation with a clock speed of 667 Megahertz and a memory size of 1.25 gigabytes. The simulations used about a fifth of the memory and took from 3.0 to 5.0 hours to complete. The initially undeformed block of final bagasse was modelled using a Lagrangian approach (the only approach available in Standard) where the block approached the rotating rolls and deformed gradually as contact was made.

Eventually the bagasse moved through both nips and exited through the pressure feeder chute. The modelled geometry has a plate (which is not present in reality) that guided the bagasse from the first set of rolls to the next set of rolls. A converged steady state solution was accepted when bagasse was both entering the first set of rolls at the bottom of the feed chute and also exiting the pressure feeder rolls and moving into the pressure feeder chute, and the predicted forces and torques on the rolls did not change. Significant problems were encountered during the simulations, particularly during the initial contact of the bagasse with the roll

surfaces and when the bagasse contacted or lost contact with the rolls, chutes and plate surfaces.

In general, the larger the value of the coefficient of friction on the roll surfaces, the greater were the convergence problems. These problems required many changes to the run settings (but no changes were made to the input material parameters) in order to progress the simulations. In general, the DPC model required significantly less increments to progress the solution. There were also major convergence problems when the bagasse exited each nip for both the Modified Cam Clay and Drucker Prager Cap models. These convergence problems were found to be mainly due to the unloading of some of the elements to a pressure close to zero. The convergence was greatly improved by having a plate pushing on and providing a small pressure (maximum values of 0.5 to 2.0 kPa) to the elements. The plate was pushed along as the bagasse moved forward. The mesh was also greatly deformed at some locations and sometimes caused convergence problems. The amount of bagasse material left to enter the first set of rolls when a steady solution was achieved was also quite small. For these reasons, it is emphasised that the results of the computer predictions described below should be verified with more extensive simulations (and checked against far more adequate experimental data) before making any practical judgements. However, importantly, these simulations showed that converged solutions of bagasse feeding through a pressure feeder could be obtained while using the MCC and DPC models and values of M close to 1.0 (which for the previous eight years had been claimed to be not possible).

Predictions carried out for the case where the modelled rolls had a diameter of 1277 mm, and using the Modified Cam Clay model, are shown in Figure 9.9 to Figure 9.24. The plot results for the smaller diameter rolls simulations, and also using the Drucker Prager Cap model, were similar overall. Table 9.7 gives a summary of the predicted forces and torques for simulations with roll diameters of 1247 mm and 1277 mm, and using the MCC and DPC models. The predictions are discussed below.

The bagasse was predicted to mainly stick to the rolls. For the top pressure feeder (roll 1) values of coefficients of friction ranging from 0.6 to 0.8 were predicted in

the underfeed nip region and values ranging from 0.2 to 1.4 were predicted in the pressure feed nip region. The higher coefficients correspond to the lower pressure (further from the nip) locations. For the underfeed roll the values ranged from 0.6 to 1.0, while for the bottom pressure feeder values ranging from 0.2 to 1.3 were predicted.

Figure 9.9 (page 262) shows the full deformed mesh and confining pressure plot while Figure 9.10 focuses on the underfeed nip and Figure 9.11 focuses on the pressure feeder nip and for clarity do not show the deformed mesh. Similarly, Figure 9.12 and Figure 9.13 show the predicted Von Mises stress, Figure 9.14 and Figure 9.15 show the vertical stress, Figure 9.16 and Figure 9.17 show the horizontal stress, and Figure 9.18 and Figure 9.19 show the predicted shear stress. The predicted shear strains (including the deformed mesh) are shown in Figure 9.20 and Figure 9.21, while predicted void ratios are shown in Figure 9.22 and Figure 9.23. Finally, Figure 9.24 shows (in red) the locations in the final bagasse predicted to be actively yielding.

A low compressive (negative) vertical stress of about 3.0 kPa is shown at the top of the bagasse mat, and is due to a plate pushing on the bagasse to enforce the condition that, with a feed chute full of wet bagasse, a vertical pressure of about 3.0 kPa is believed to be present at the bottom of the feed chute. Tension is predicted where the rolls draw the bagasse away from the feed chute (this is the point at which the contact angle is defined as described previously) and there is a corresponding increase in void ratio at these two locations (see Figure 9.16 and Figure 9.22). The action of the rolls in feeding and compressing the bagasse into the underfeed nip is predicted to be quite robust. This action can be seen in Figure 9.16 where high horizontal stresses are predicted next to the top pressure feeder roll and the underfeed roll just below the initial contact point with the bagasse. High shear stresses are shown in Figure 9.18 originating from these locations and developing further towards the underfeed nip (blue colours next to the underfeed roll and yellow colours next to the top pressure feeder roll).

Bands (coloured blue and red) of high shear strain are predicted to develop from both rolls, as shown in Figure 9.20, and appear to join at the middle of the bagasse

just before the underfeed nip. A small region of higher void ratio (i.e. less compaction) is predicted in Figure 9.22 just above this location (coloured orange). The predictions in this area are quite believable. For example, the small region of lower compaction can be explained by the material just below being drawn into the nip and material above it being self supported by bridging from both sides (the occurrence of bagasse bridging in chutes is well documented, for example, see Bernhardt (1994)). Similar predictions are discussed later in this chapter.

There are high shear strains predicted for the first layer of elements next to the top pressure feeder roll and next to the underfeed roll. This reflects the grip of the roll surface but also may indicate that the element mesh is not fine enough and should be graded close to the surface or that the predictions from the material model are not adequate in such highly stressed locations.

The level of stress decreases next to the underfeed roll after its nip and the corresponding increase in void ratio is shown in red in Figure 9.22. The feeding action of the bottom pressure feeder is predicted to result in a similar area of low compaction where the roll draws the bagasse away from the guide plate. All stresses increase greatly as the pressure feeder nip is approached. The confining stresses shown in Figure 9.11 at the pressure feeder nip are in the range of 400 kPa. However, the stresses at this location for a heavy pressure feeder should be in the order of 2000 kPa, that is, significantly greater than those predicted. Inspection of the shear strains at this location (Figure 9.21) show very large values. The magnitudes of the predictions for both stresses and strains at this location are believed to be unrealistic. The reasons for the poor predictions may be:

1. The use of final bagasse parameters and the assumption of a constant λ from low pressures may have affected the predictions.

2. The material model (Modified Cam Clay with β=0.21) is not adequate at this highly stressed region.

3. The simulation method requires improvement (i.e. the material behaviour has been detrimentally affected by its experiences when moving past the previous rolls).

The improvement of predictions at the pressure feeder nip is beyond the scope of this investigation.

The predicted roll loads and torques shown in Table 9.7 are now discussed. As expected, in all cases the forces predicted for the underfeed roll were much lower than those for the other two rolls, and the predicted forces were higher for the simulations with the larger rolls (smaller nip clearances). The predictions for the Drucker Prager Cap model followed the same trends as the Modified Cam Clay model predictions, but the magnitudes of the forces were lower for the DPC model. The reason for this is not known, but it is believed that the predictions should have been quite similar in magnitude, as the two models are quite similar (and the magnitudes of parameters used were similar, although not identical). The predicted torques for the pressure feeders are much smaller than the measured values given in Table 9.1, reflecting the previous discussion that the predicted stresses at the pressure feeder nip (which control the magnitudes of the forces on the pressure feeder rolls) are much lower than expected.

Since measured values for the underfeed roll were not available, the torque predictions carried out for a roll in the underfeed nip (see Table 9.3) in the first part of the chapter are compared here to the predictions shown in Table 9.7 for the underfeed roll. It is noted that the simple method achieved fairly good agreement for pressure feeder torques when compared against measured results. The values of the torque predictions carried out with a simple feeding model and direct shear test measurements range from 22 to 37 kNm. The values predicted using the multi-element models range from 9 to 13 kNm. Taking into account that the calculations carried out with the simple model are believed to be the maximum torques that can be achieved, the agreement was believed to be close enough to carry out further simulations with only the top pressure feeder and the underfeed roll present. Those simulations are shown in the next section.

It is also noted with reference to Figure 9.24 that, although the predictions of forces and torques were steady, the predicted actively yielding locations (in red) in the material are not fully consistent with a converged solution. The predicted locations undergoing yield include the elements close to the roll surfaces, the entry to the

underfeed nip where the high shear strain bands join together, and most of the pressure feeder nip. However, a large region to the right of the top pressure feeder is not yielding. Picturing bagasse moving into the underfeed nip and undergoing large decreases in volume, it is believed that this area should also be yielding. The feature in ABAQUS of plotting actively yielding regions should be useful in the future in understanding what is happening inside a mill.

Finally for this section, shown in Figure 9.25 and Figure 9.26 for the MCC and DPC models, respectively, are close ups of the final bagasse contacting the underfeed roll. Both models predict a large increase in void ratio at this location, while the Drucker Prager Cap model predicts the bagasse being drawn away from the sidewall of the feed chute. The difference is believed to be due to the small tensile strength of the material (2 kPa) in the DPC model, while the MCC model has none.

Since there is no accurate measurement of tensile strength of bagasse after it has been compressed to about 3.0 kPa, it is not known which is the better representation of bagasse behaviour.

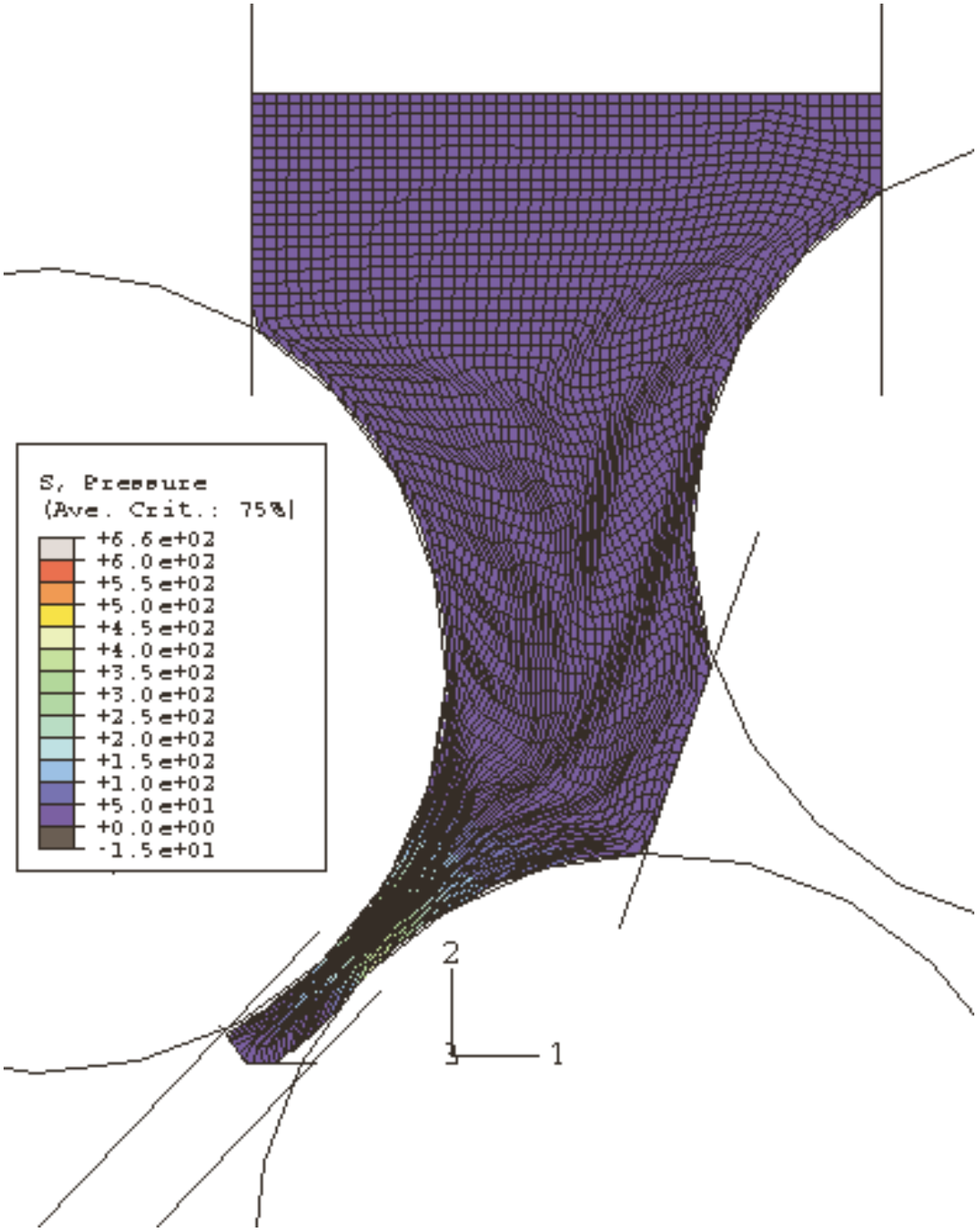

Figure 9.9. Predicted confining pressure (kPa) for the Victoria Mill B1 pressure feeder.

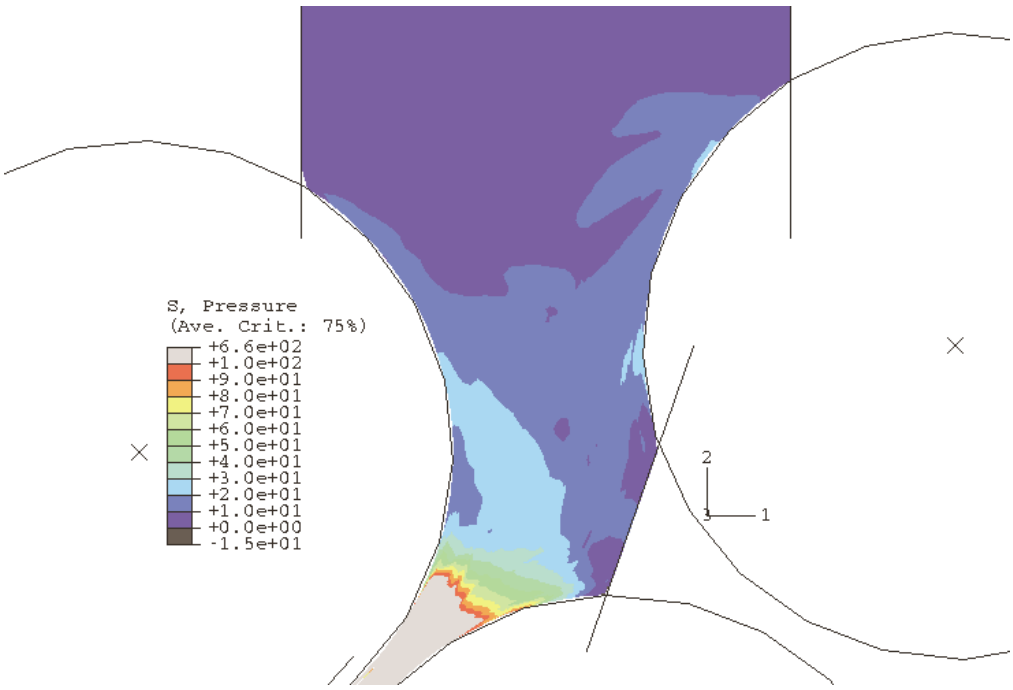

Figure 9.10. Predicted confining pressure (kPa) for the underfeed nip of the Victoria Mill B1 pressure feeder.

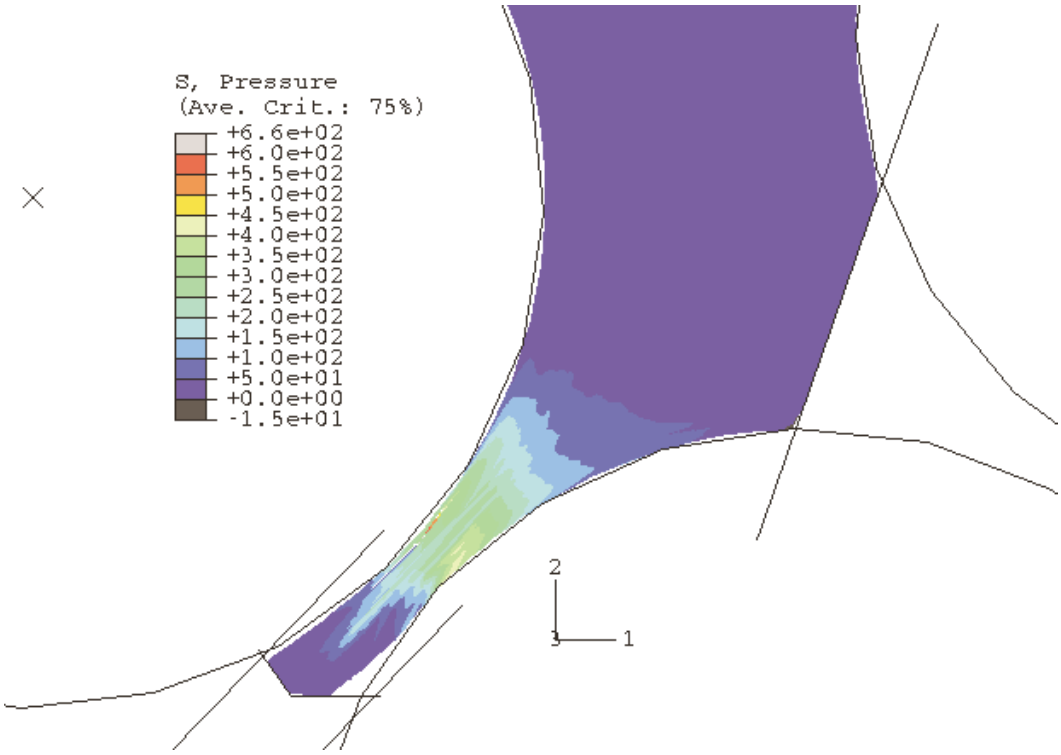

Figure 9.11. Predicted confining pressure (kPa) for the pressure feeder nip of the Victoria Mill B1 pressure feeder.

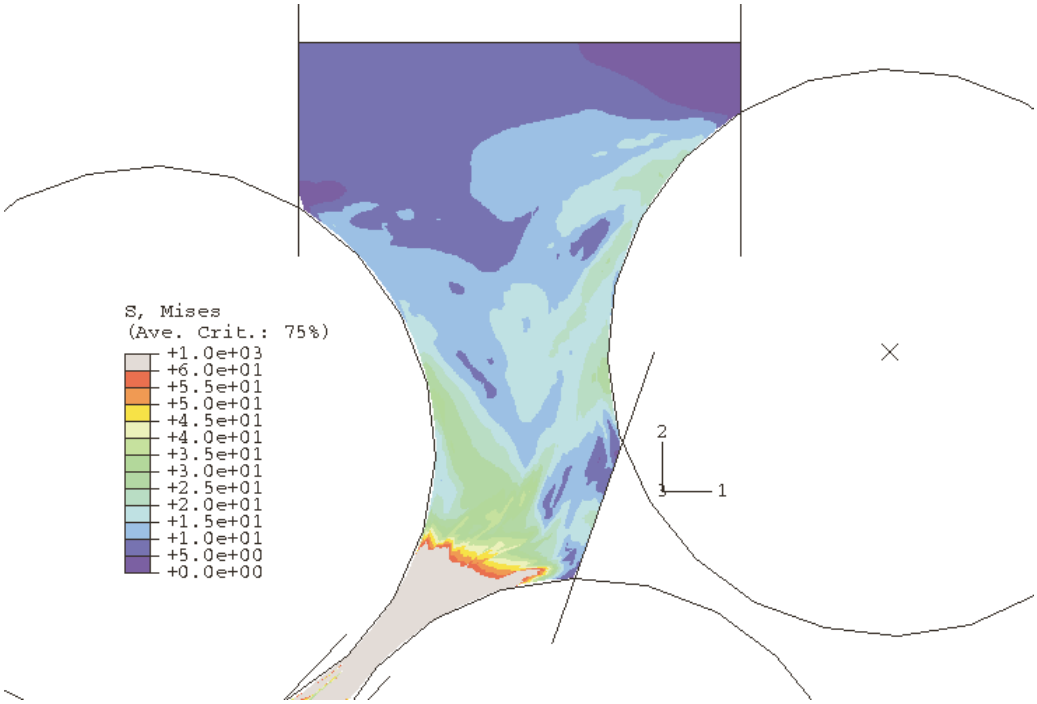

Figure 9.12. Predicted Von Mises stress (kPa) for the underfeed nip of the Victoria Mill B1 pressure feeder.

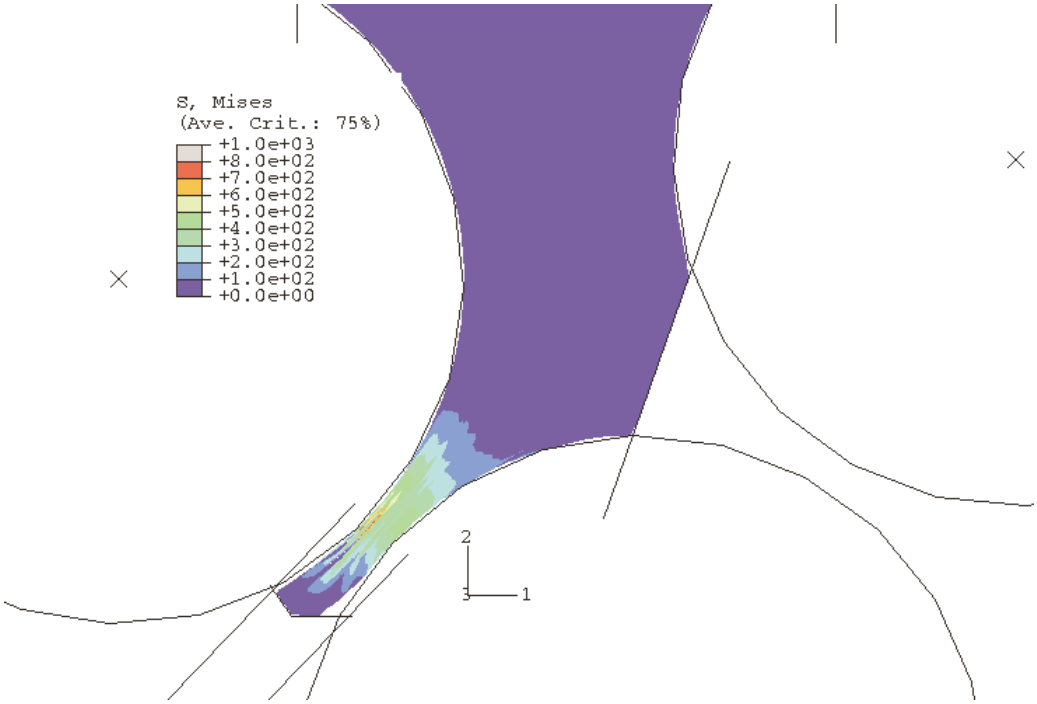

Figure 9.13. Predicted Von Mises stress (kPa) for the pressure feeder nip of the Victoria Mill B1 pressure feeder.

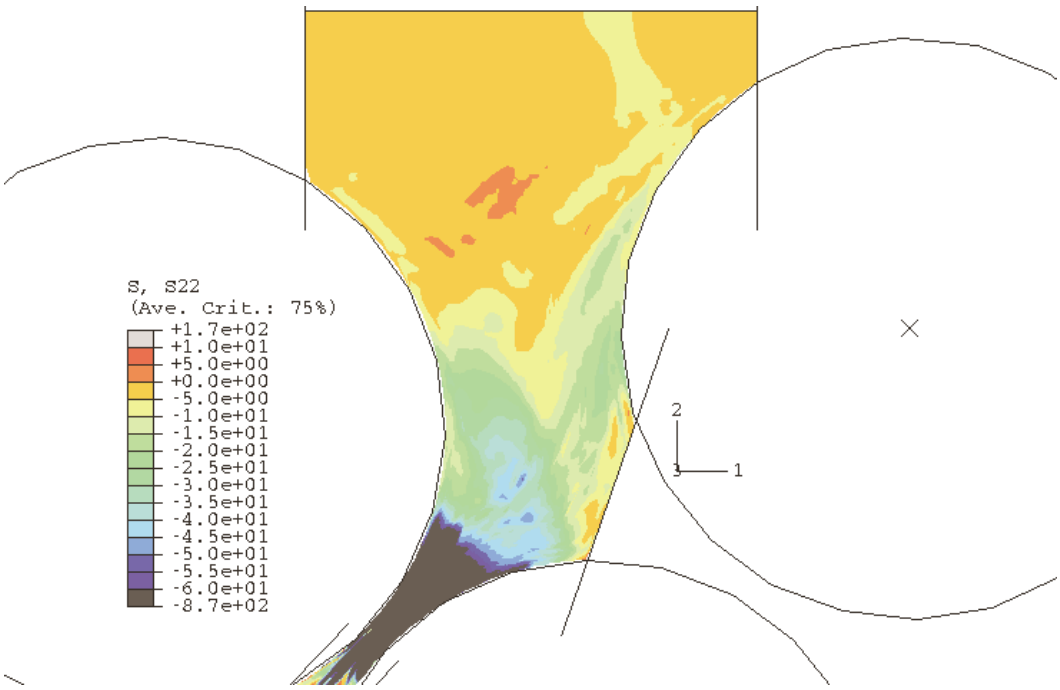

Figure 9.14. Predicted vertical stress (kPa) for the underfeed nip of the Victoria Mill B1 pressure feeder.

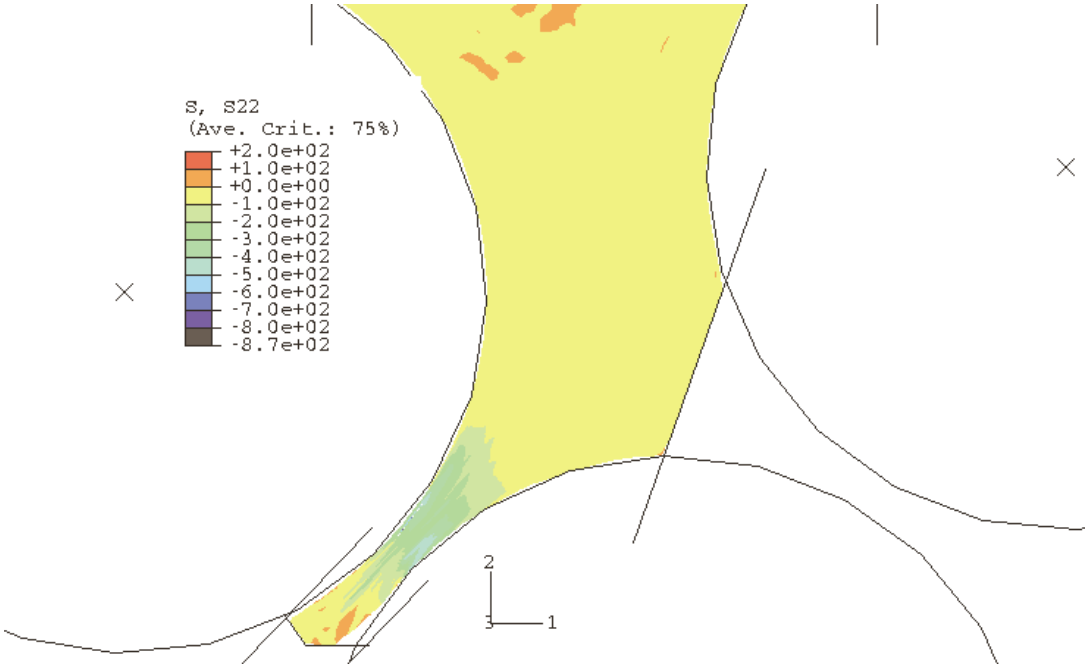

Figure 9.15. Predicted vertical stress (kPa) for the pressure feeder nip of the Victoria Mill B1 pressure feeder.

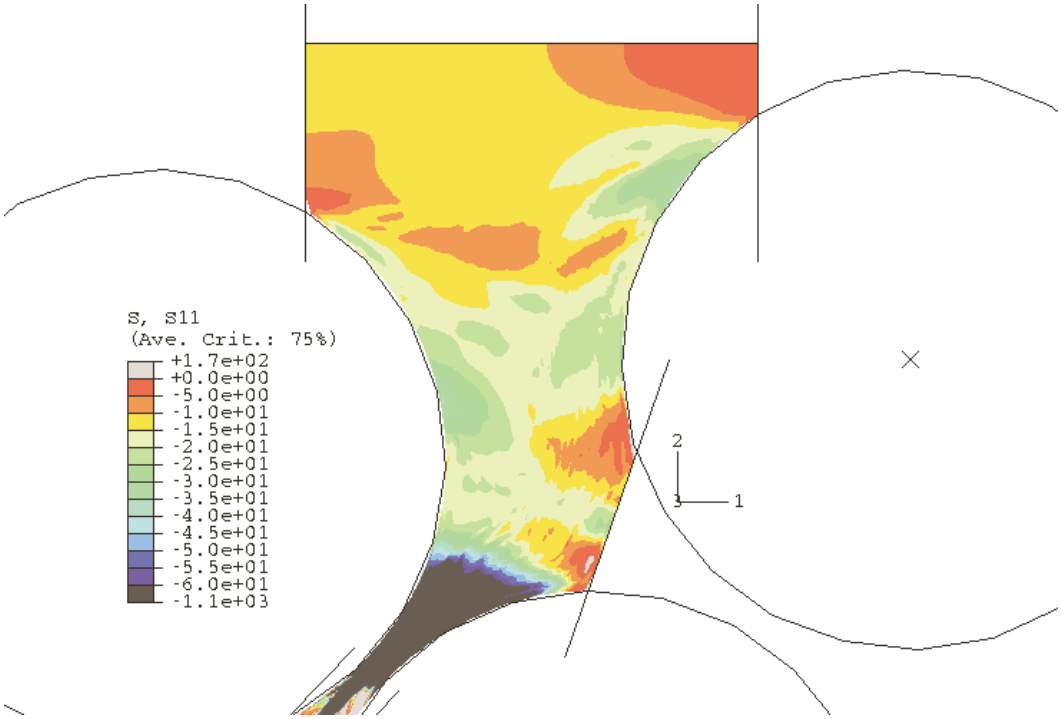

Figure 9.16. Predicted horizontal stress (kPa) for the underfeed nip of the Victoria Mill B1 pressure feeder.

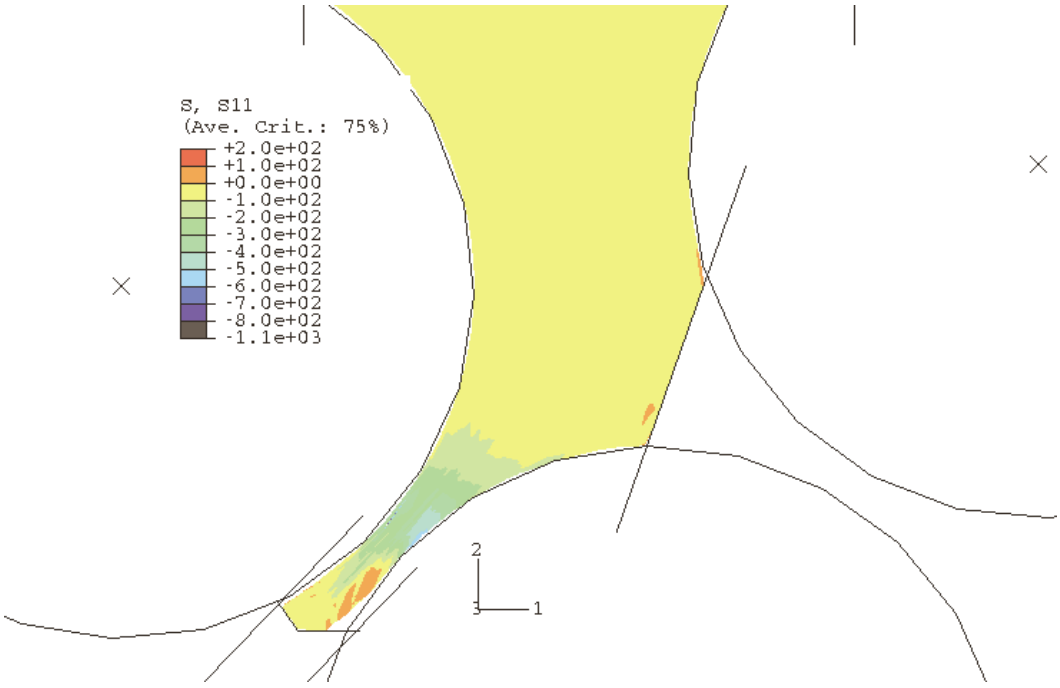

Figure 9.17. Predicted horizontal stress (kPa) for the pressure feeder nip of the Victoria Mill B1 pressure feeder.

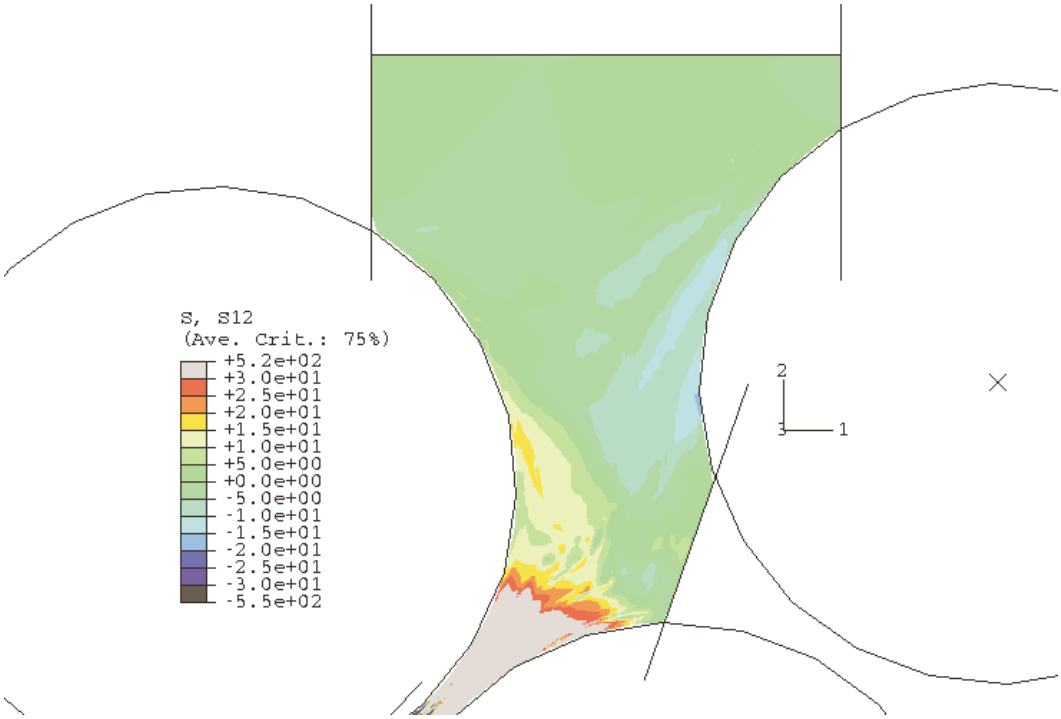

Figure 9.18. Predicted shear stress (kPa) for the underfeed nip of the Victoria Mill B1 pressure feeder.

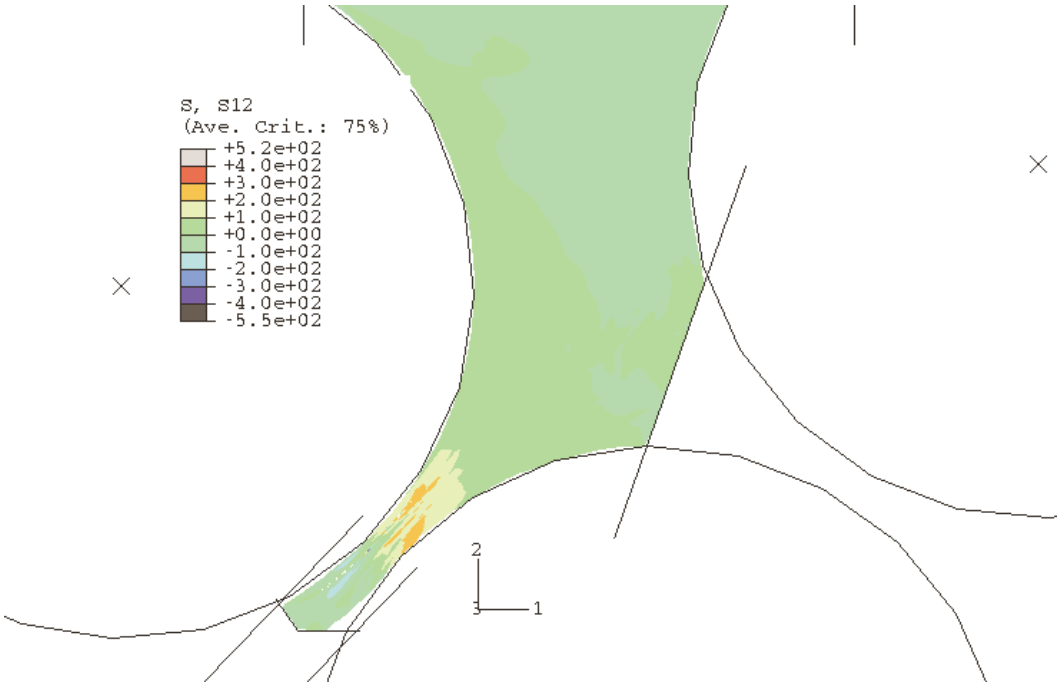

Figure 9.19. Predicted shear stress (kPa) for the pressure feeder nip of the Victoria Mill B1 pressure feeder.

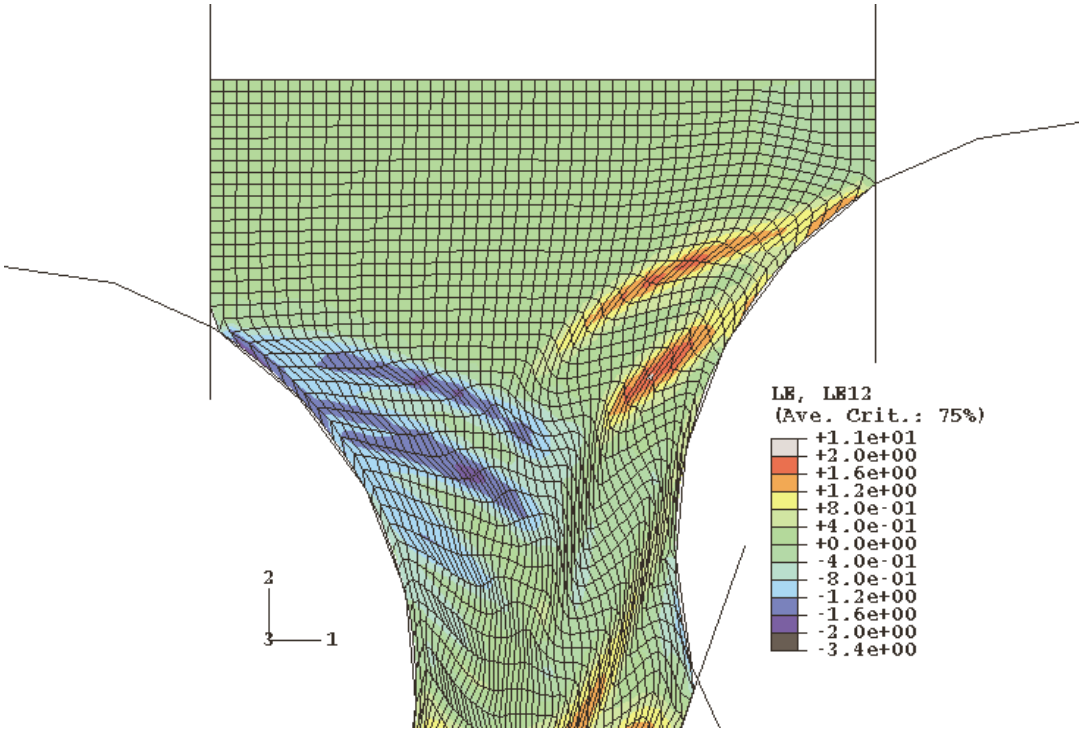

Figure 9.20. Predicted shear strain for the underfeed nip of the Victoria Mill B1 pressure feeder.

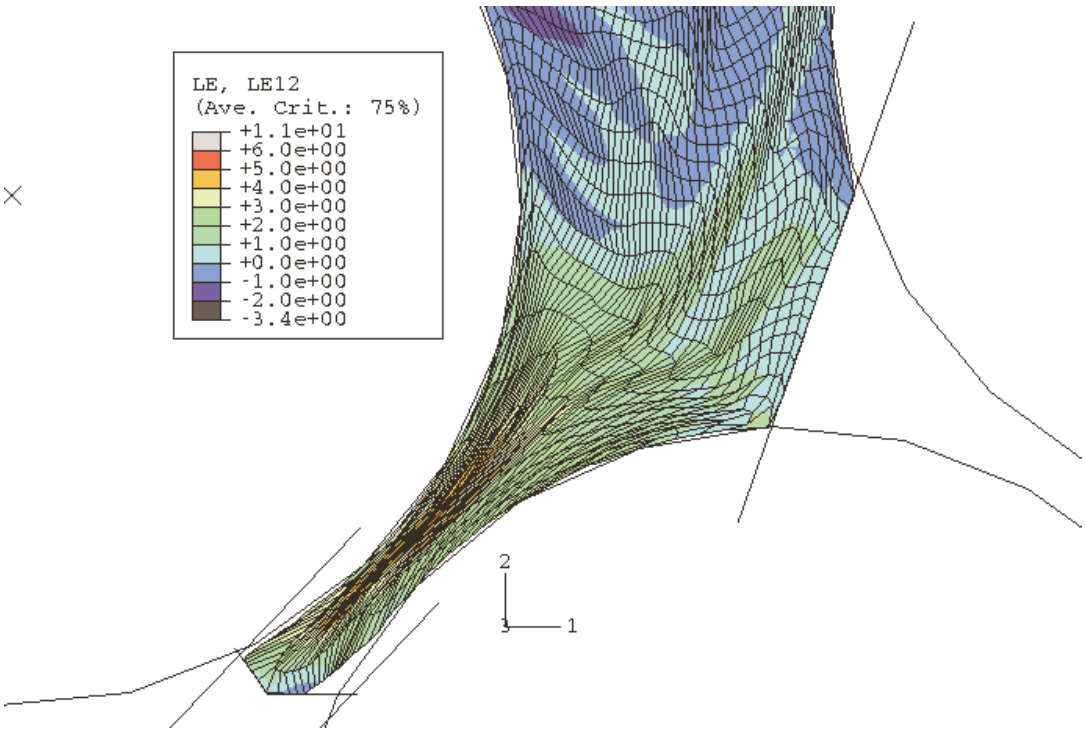

Figure 9.21. Predicted shear strain for the pressure feeder nip of the Victoria Mill B1 pressure feeder.

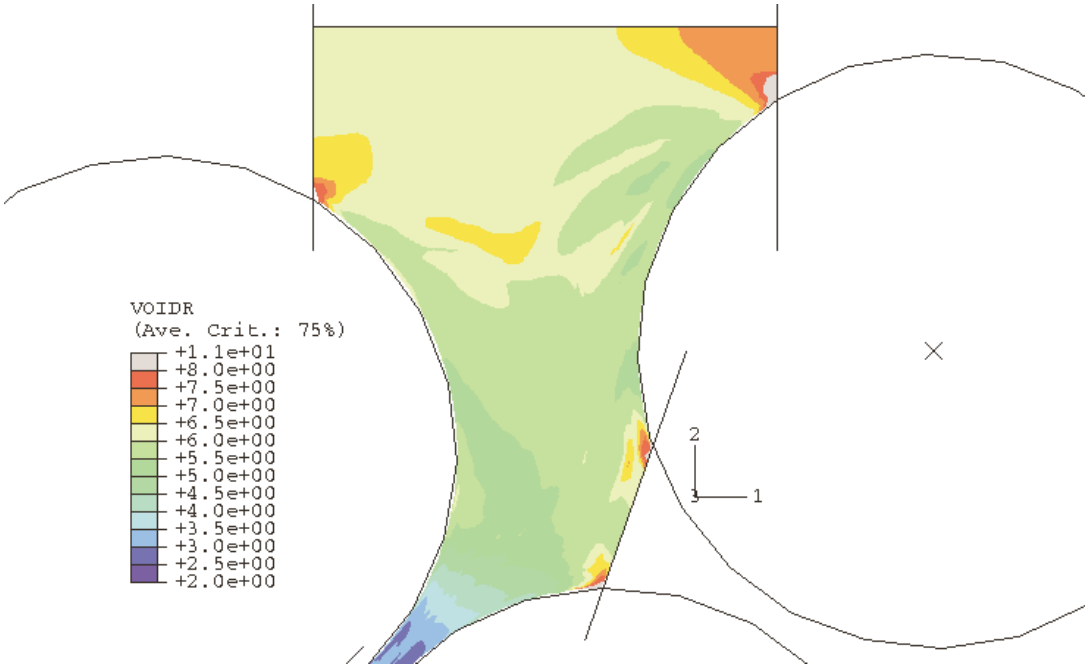

Figure 9.22. Predicted void ratio for the underfeed nip of the Victoria Mill B1 pressure feeder.

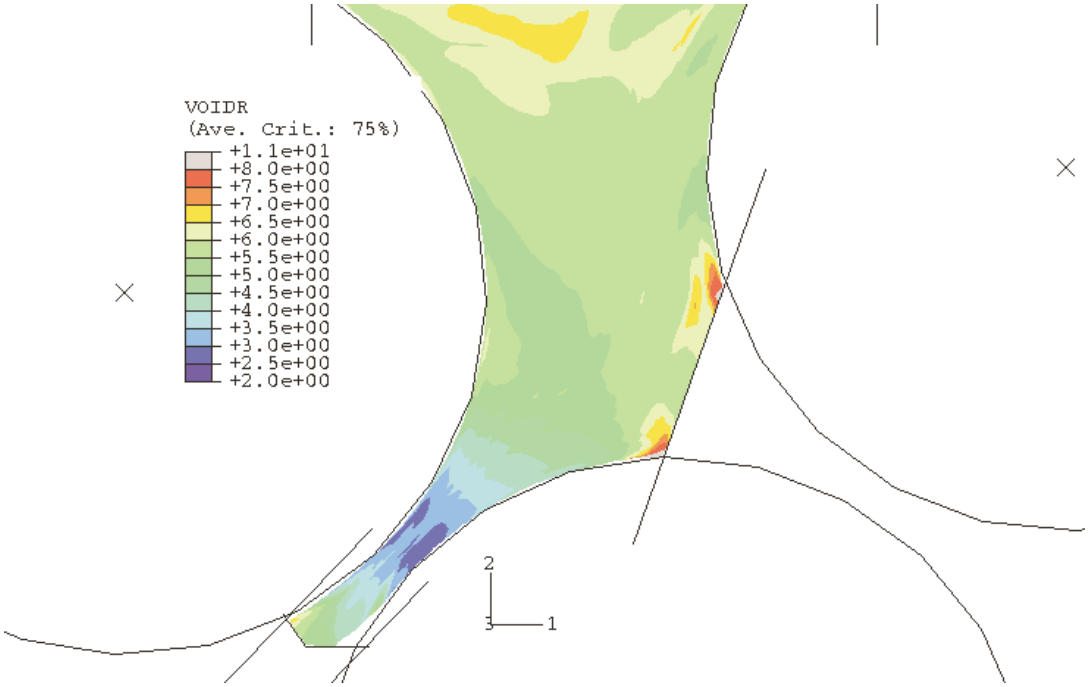

Figure 9.23. Predicted void ratio for the pressure feeder nip of the Victoria Mill B1 pressure feeder.

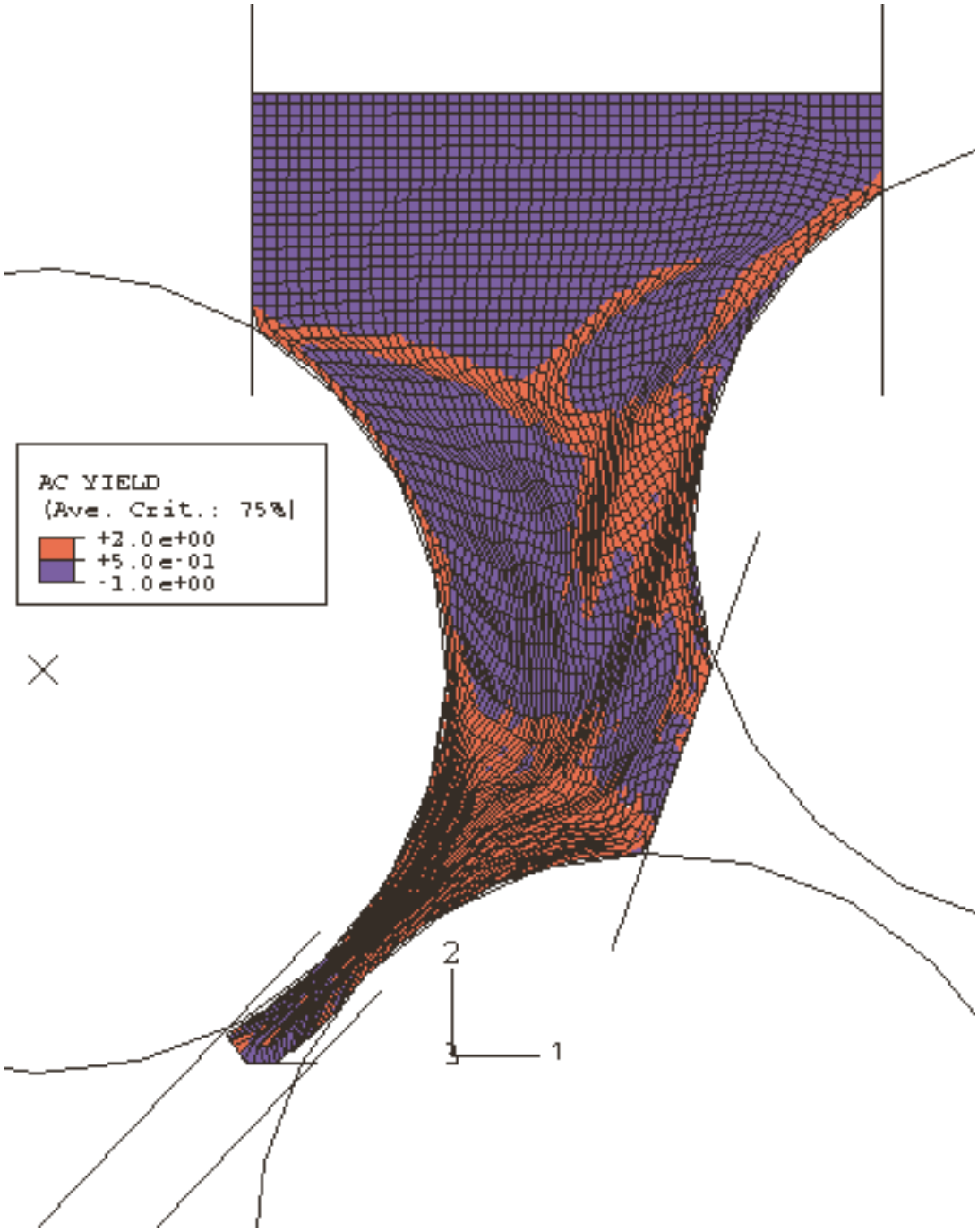

Figure 9.24. Predicted points where the material is yielding for the Victoria Mill B1 pressure feeder.

Table 9.7 Predicted roll loads and torques from three roll simulations

Simulation	Horizontal force (kN)	Vertical force (kN)	Roll Load (kN)	Torque (kNm)
Modified Cam Clay and roll diameter 1247 mm				
Roll 1 (TPF)	148	-115	187	-31
Roll 2 (UF)	-27	-8	28	12
Roll 3 (BPF)	-112	125	168	23
Drucker Prager Cap and roll diameter 1247 mm				
Roll 1 (TPF)	102	-66	121	-19
Roll 2 (UF)	-26	-5	27	9
Roll 3 (BPF)	-71	74	103	14
Modified Cam Clay and roll diameter 1277 mm				
Roll 1 (TPF)	268	-217	345	-42
Roll 2 (UF)	-38	-8	39	13
Roll 3 (BPF)	-224	230	321	32
Drucker Prager Cap and roll diameter 1277 mm				
Roll 1 (TPF)	166	-128	210	-27
Roll 2 (UF)	-28	-5	29	10
Roll 3 (BPF)	-138	138	195	22

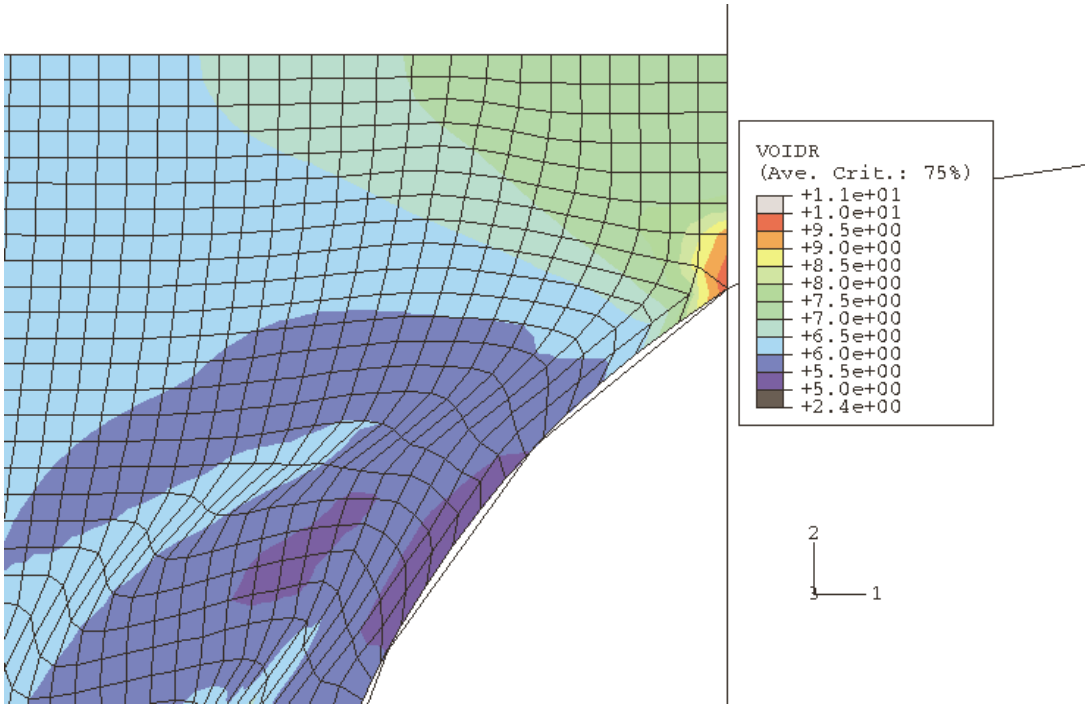

Figure 9.25. Predicted void ratio using the Modified Cam Clay material model at a close up of final bagasse next to the underfeed roll of the Victoria Mill B1 pressure feeder.

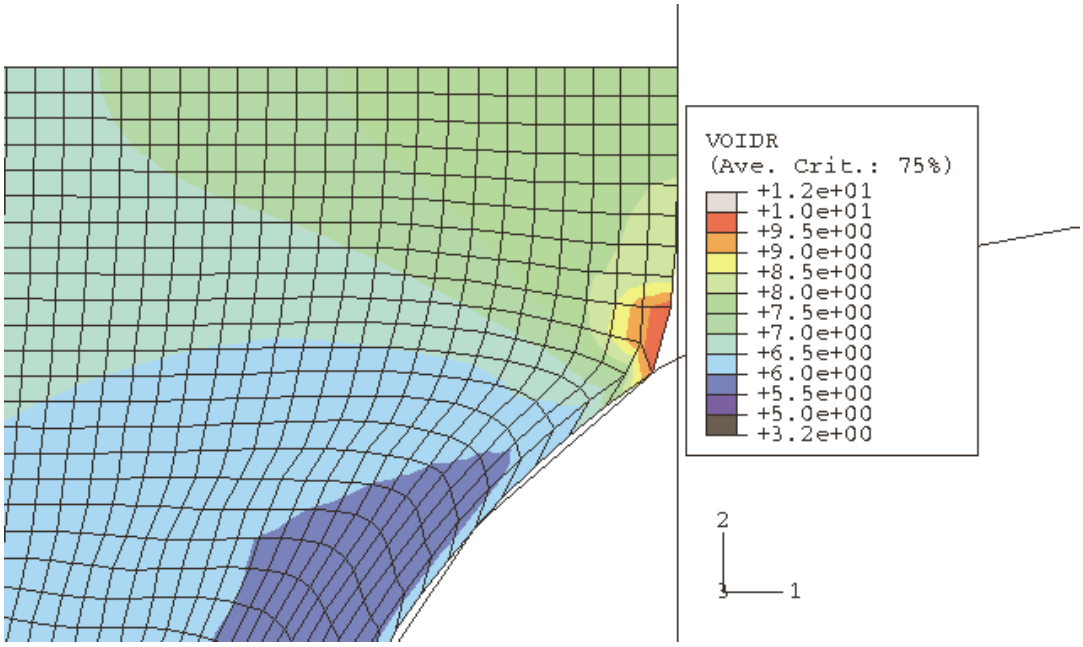

Figure 9.26. Predicted void ratio using the Drucker Prager Cap material model at a close up of final bagasse next to the underfeed roll of the Victoria Mill B1 pressure feeder.

9.4.3 Simulations of the first two rolls of the Victoria B1 pressure feeder using a Drucker-Prager Cap model with R=0.23

The top pressure feeder and underfeed roll were modelled for a roll diameter of 1277 mm and using the Drucker Prager Cap model with R=0.23, and the final bagasse material parameters and boundary conditions described in the previous section. As the bagasse exited the underfeed nip, it was constrained by a chute that allowed only a small amount of expansion. As in the previous three roll simulations, a plate (referred to here as a backstop) after the nip placed a small pressure on the unloading elements to allow convergence.

The overall predicted behaviour was similar to that shown previously for the three roll simulation at the same locations. The shear stresses and predicted yield points were modelled in two simulations. In the first simulation the bagasse is feeding through the nip, the bagasse is sticking to the rolls, and the bagasse is pushing the backstop downwards (Figure 9.27 and Figure 9.29). Values of coefficient of friction ranging from 0.6 to 1.0 for the top pressure feeder roll and 0.6 to 1.0 for the underfeed roll were predicted. In the second simulation, the backstop was fixed so that it could not move. Higher stresses were developed in the second situation until the rolls slipped on the bagasse at the coefficient of friction on the roll surface of 1.4. Figure 9.28 and Figure 9.30 show the situation where a steady state condition has been reached in which the rolls were slipping on the bagasse while the roll forces remained constant. A summary of the predictions is shown in Table 9.8.

Table 9.8 Predicted roll loads and torques from two roll simulations

Simulation	Horizontal force (kN)	Vertical force (kN)	Roll Load (kN)	Torque (kNm)
No back stop				
Roll 1 (TPF)	19	-5	20	-7
Roll 2 (UF)	-17	-3	17	7
With back stop				
Roll 1 (TPF)	21	-16	27	-15
Roll 2 (UF)	-21	-13	25	14

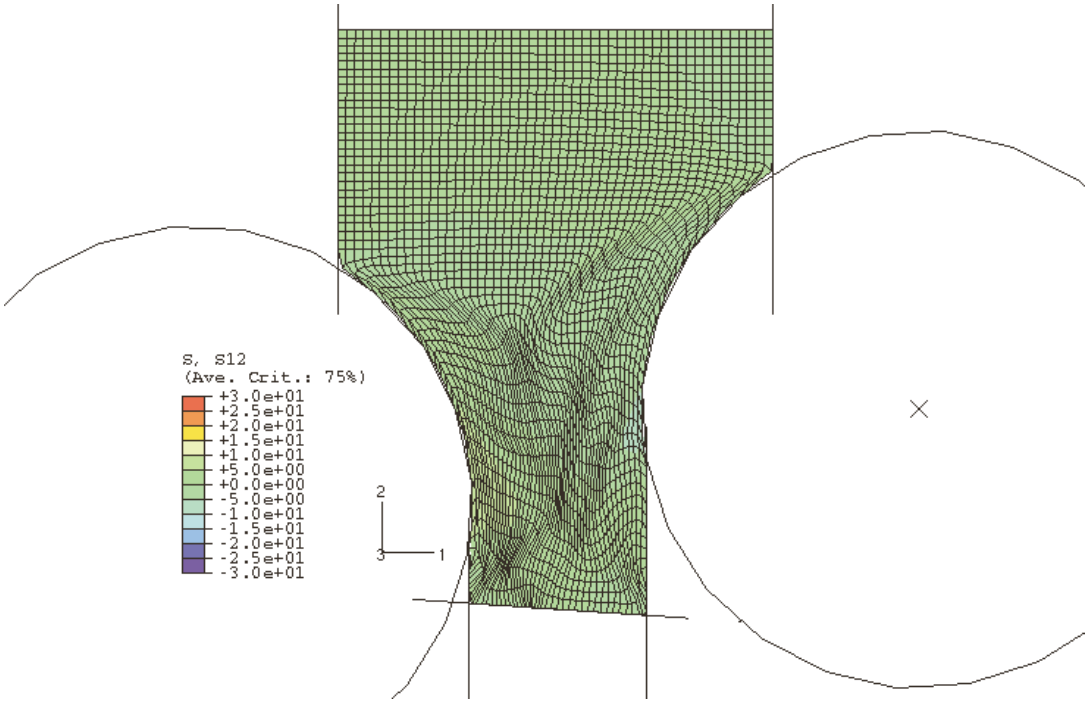

Figure 9.27. Predicted shear stress (kPa) for the top pressure feeder roll and underfeed roll of the Victoria Mill B1 pressure feeder with back stop not fixed.

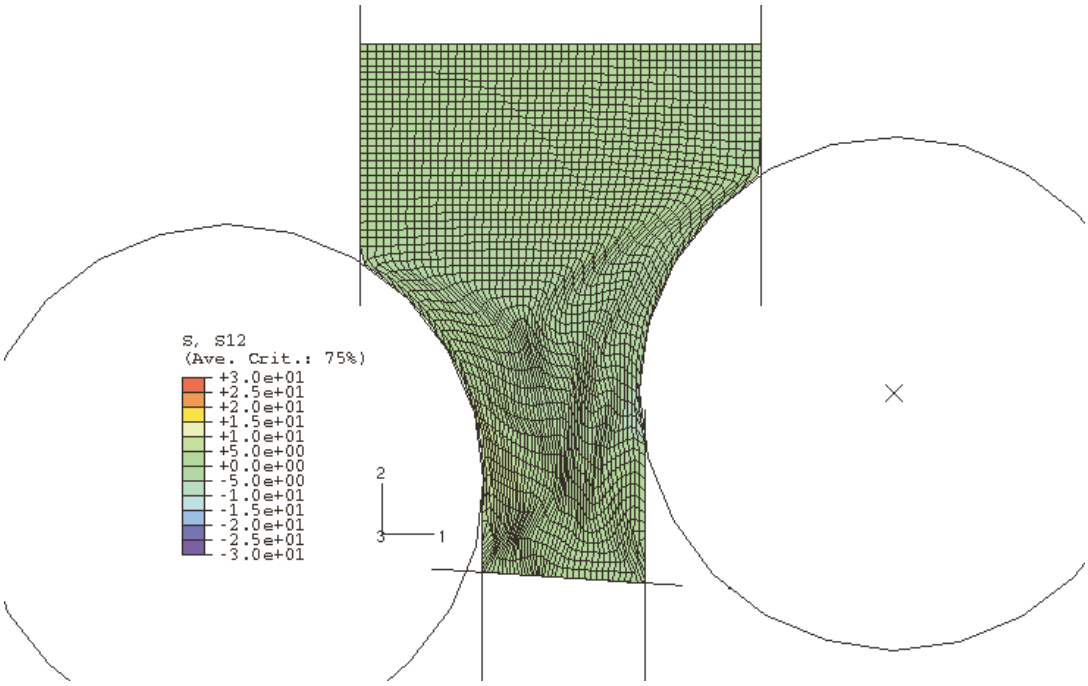

Figure 9.28. Predicted shear stress (kPa) for the top pressure feeder roll and underfeed roll of the Victoria Mill B1 pressure feeder with back stop fixed.

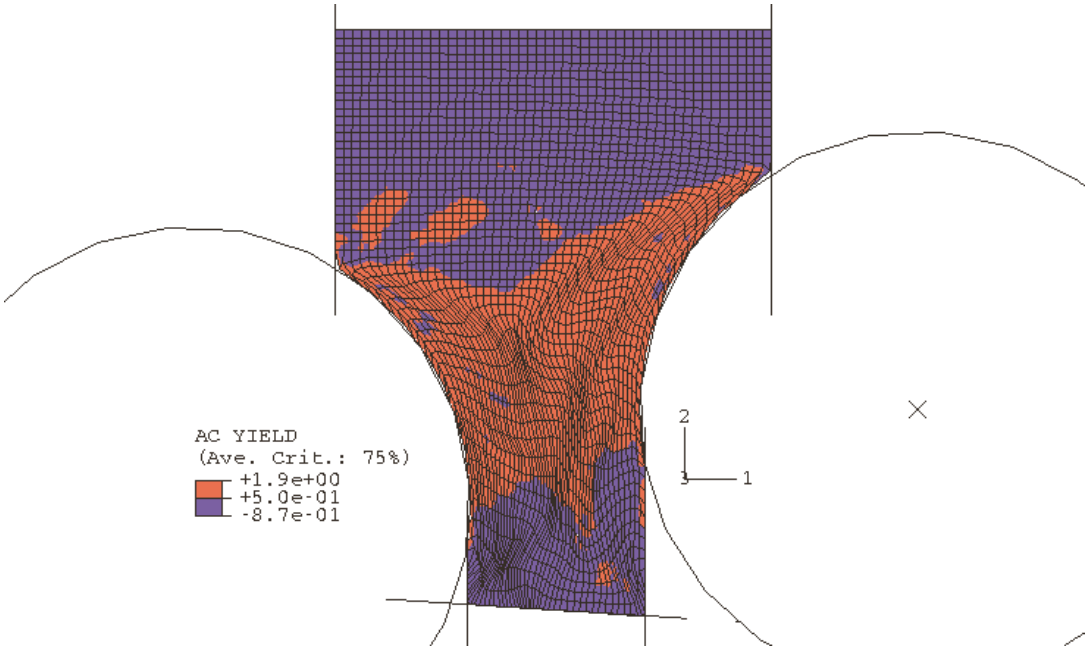

Figure 9.29. Predicted points where the material yielded for the top pressure feeder roll and underfeed roll of the Victoria Mill B1 pressure feeder with back stop not fixed.

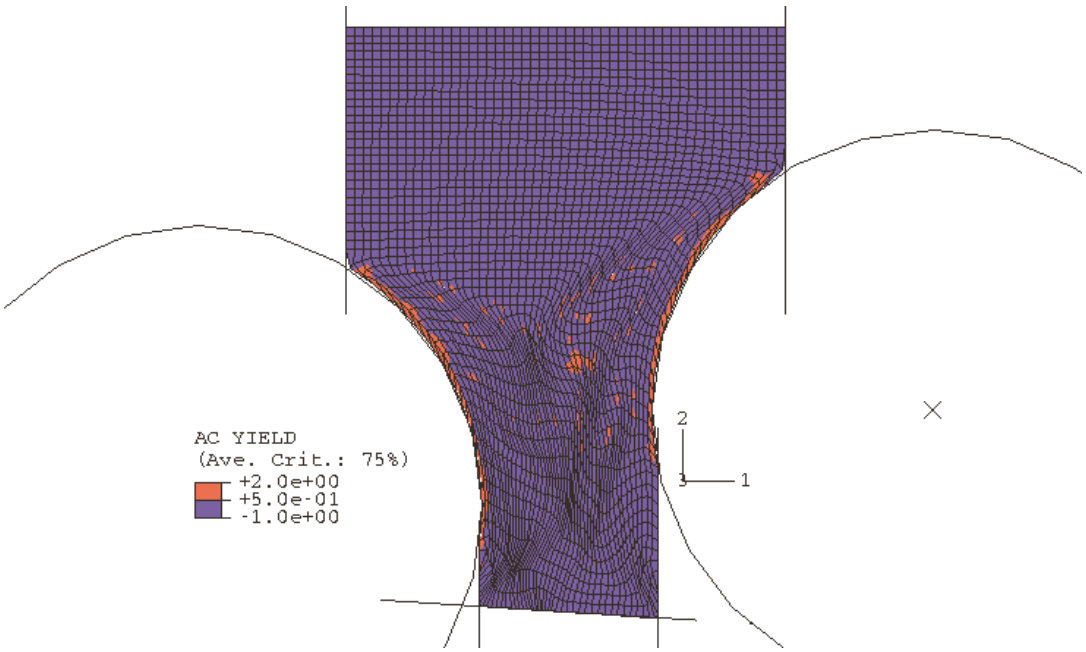

Figure 9.30. Predicted points where the material yielded for the top pressure feeder roll and underfeed roll of the Victoria Mill B1 pressure feeder with back stop fixed.

It is quite difficult to distinguish any difference between the shear stress plots for the two simulations. Close inspection shows that the magnitudes are higher for the case where the backstop is fixed and restraining the bagasse. However, the plots showing the locations of the final bagasse yielding are very different. For the first case where the backstop was not fixed the whole mat of material is yielding as it moves into the underfeed nip. For the case where the backstop is fixed and the bagasse is slipping on the rolls, most of the bagasse is no longer yielding, and the yielding is concentrated at the first layer of elements next to the roll surface. It is interesting to note that although the torque was predicted to double (and the vertical force increased by a factor of at least three) when the backstop was fixed, the increase in the horizontal force (which included most of the roll separating force) was significantly lower.

Measured values for the underfeed roll were not available. The multi-element predictions were compared against the previous predictions from the simple model (for the three roll pressure feeder, those torque predictions compared to measurements were out by a maximum of only 28%). As for the three roll simulations, the predicted torques were lower than the 'maximum' values predicted using the simple model (14 and 15 kNm compared to 22 to 37 kNm). Therefore, the multi-element torque predictions for the underfeed roll were 38% to 64% of those predicted using the simple method (the maximum possible torques when maximum shear stresses are developed throughout all the bagasse mat, which is not likely to happen in reality). The multi-element torque predictions for the underfeed roll were therefore quite realistic.

It can be stated with a significant degree of confidence that large compression and shear stresses and strains are experienced by the bagasse during the milling process, and their accurate prediction is important in order to predict the overall loads and torques in a milling unit. For example, with further verification of the predictions, the technique of using a modelled backstop to predict the maximum forces that an underfeed nip can generate under certain geometrical and operating conditions could be quite useful for evaluating different designs.

9.4.4 Simulations of the first two rolls (horizontally aligned) of the Victoria B1 pressure feeder using a Drucker-Prager Cap model with R=0.23

An attempt was made at predicting the effect of aligning the top pressure feeder and the underfeed roll horizontally, while keeping the nip clearance the same as in the previous section. However, these simulations were found to be quite difficult to carry out, with significantly greater convergence and numerical difficulties. Also, problems were encountered with the finite element mesh over-laying itself. Results from a non-steady solution are given for completeness in Figure 9.31 to Figure 9.38, where the confining pressure, Von Mises stress, vertical stress, horizontal stress, shear stress, shear strain, void ratio, and yielding locations are shown. As expected, the predictions are vertically symmetrical. The predicted behaviour of the material is quite similar to that described previously, such as tension occurring where the bagasse initially contacts the rolls and is drawn away from the surface of the feed chute, the bands of high shear strains meeting at the middle of the bagasse at the entry to the nip, and the high void ratio (low compaction) region just above this location. Above the high void ratio region, some bridging of the bagasse was predicted.

A summary of the forces is given in Table 9.9. They are significantly smaller than the values given in the previous section. This is most probably due to the fact that they are the result of a solution that is not properly converged. However, a contributing factor could be that un-aligned rolls are able to provide higher torques than vertically aligned rolls and this may be worth pursuing in future work.

Table 9.9 Predicted roll loads and torques from aligned two roll simulations

Simulation	Horizontal force (kN)	Vertical force (kN)	Roll Load (kN)	Torque (kNm)
Drucker Prager Cap, no back stop				
Roll 1 (TPF)	21	0.5	21	-5
Roll 2 (UF)	-21	0.4	21	5
Drucker Prager Cap, with back stop				
Roll 1 (TPF)	20	-6	21	-10
Roll 2 (UF)	-20	-6	21	10

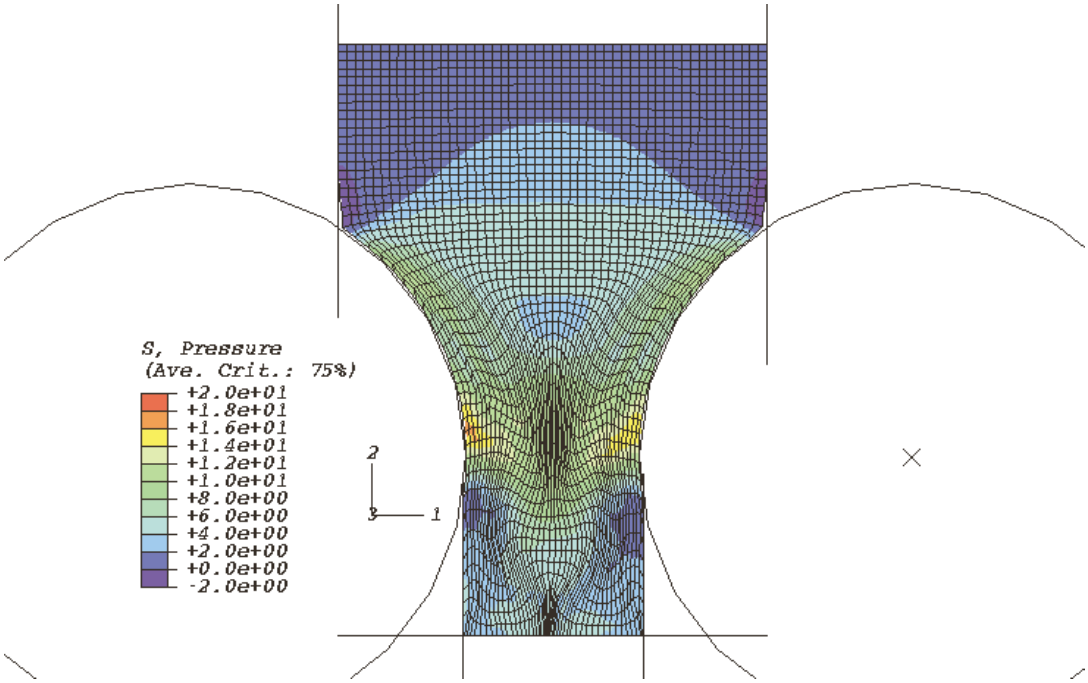

Figure 9.31. Predicted confining pressure (kPa) for aligned top pressure feeder roll and underfeed roll of the Victoria mill B1 pressure feeder.

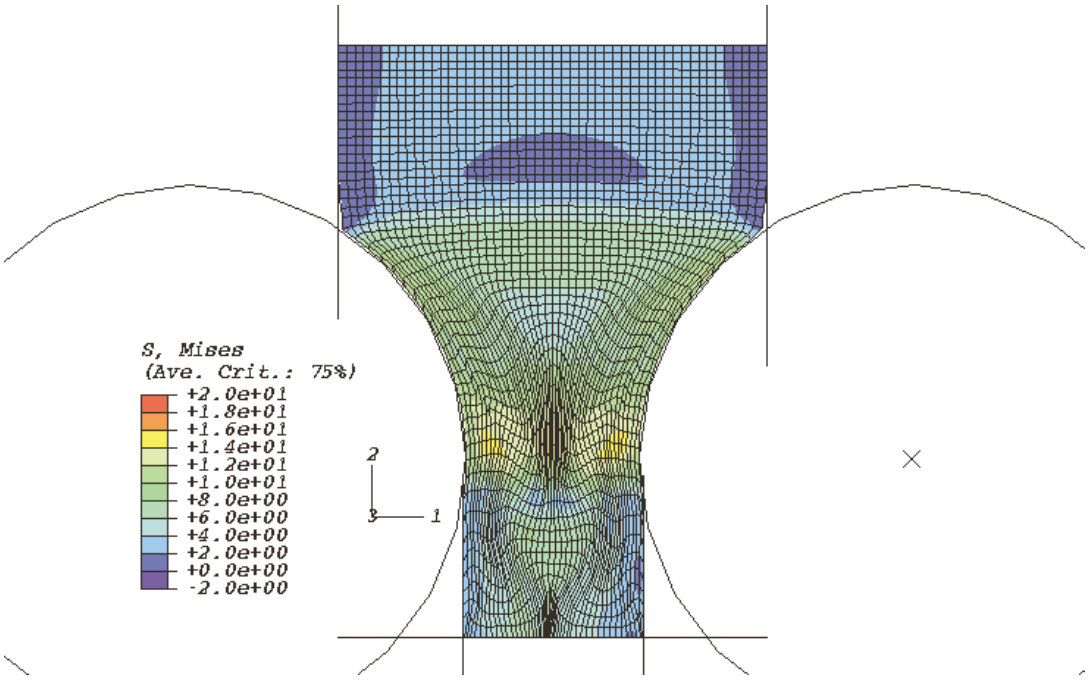

Figure 9.32. Predicted Von Mises stress (kPa) for aligned top pressure feeder roll and underfeed roll of the Victoria Mill B1 pressure feeder.

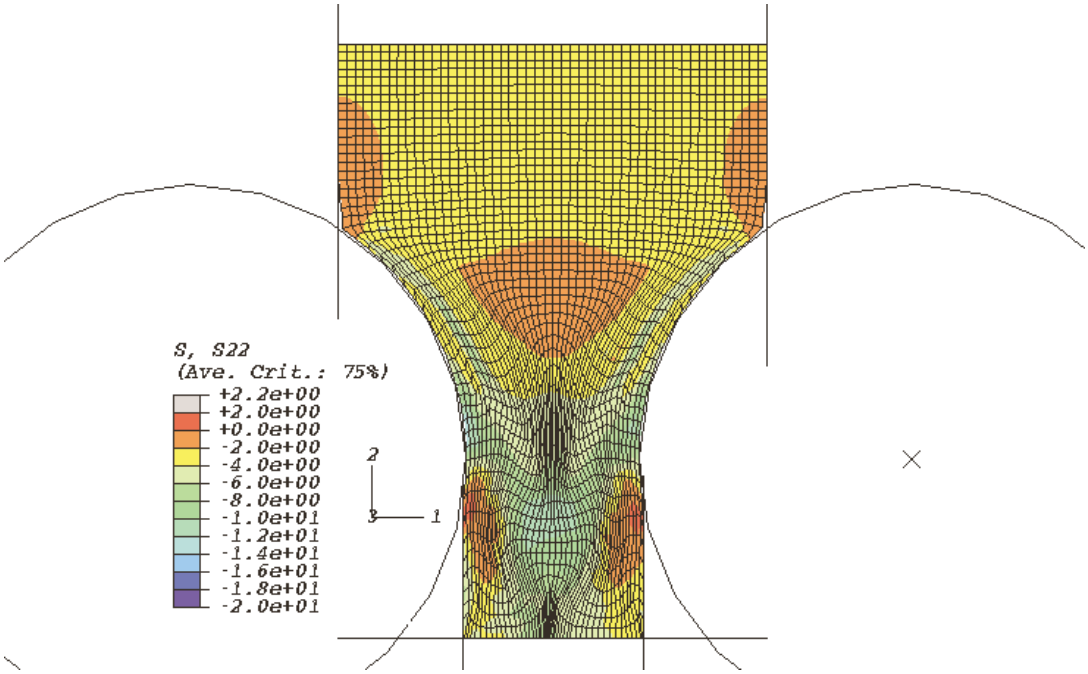

Figure 9.33. Predicted vertical stress (kPa) for aligned top pressure feeder roll and underfeed roll of the Victoria Mill B1 pressure feeder.

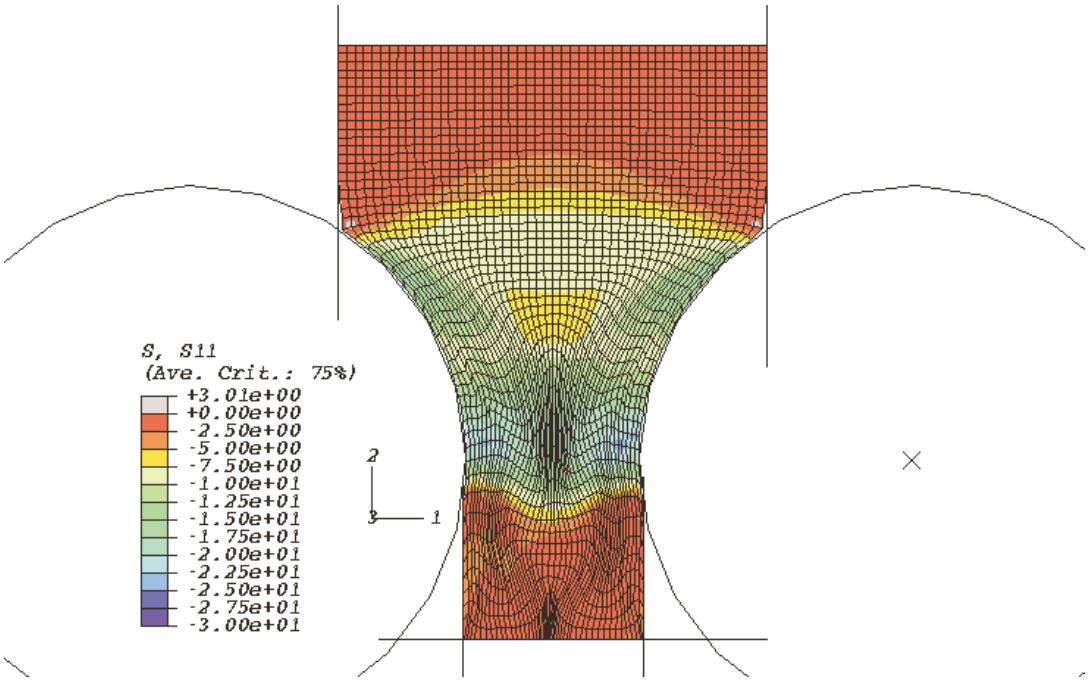

Figure 9.34. Predicted horizontal stress (kPa) for aligned top pressure feeder roll and underfeed roll of the Victoria Mill B1 pressure feeder.

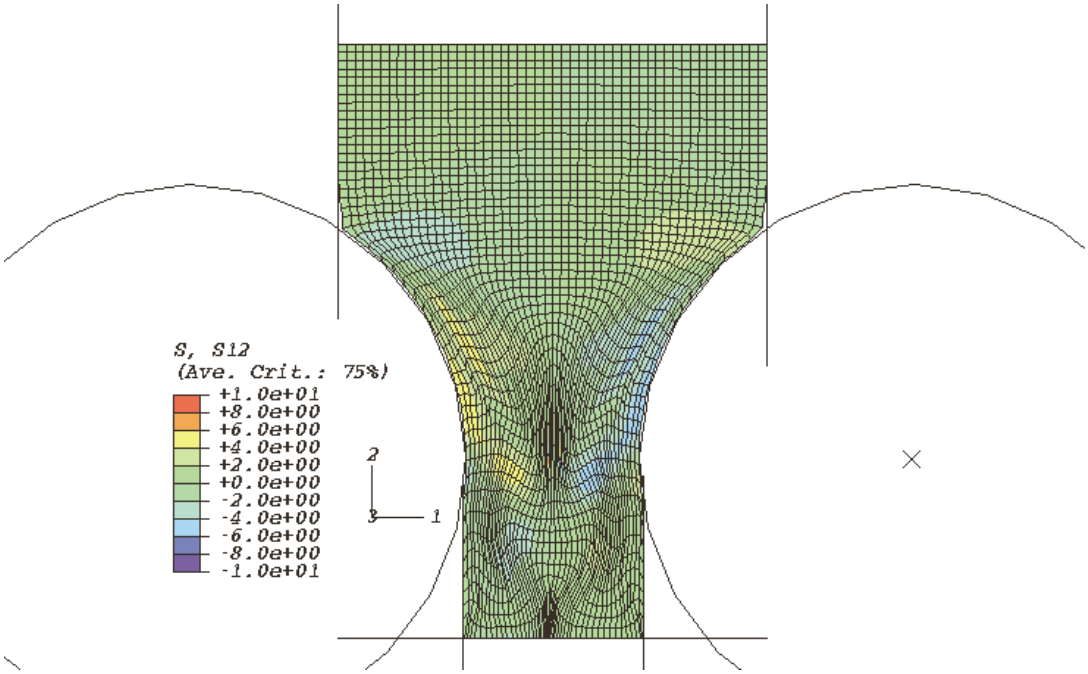

Figure 9.35. Predicted shear stress (kPa) for aligned top pressure feeder roll and underfeed roll of the Victoria Mill B1 pressure feeder.

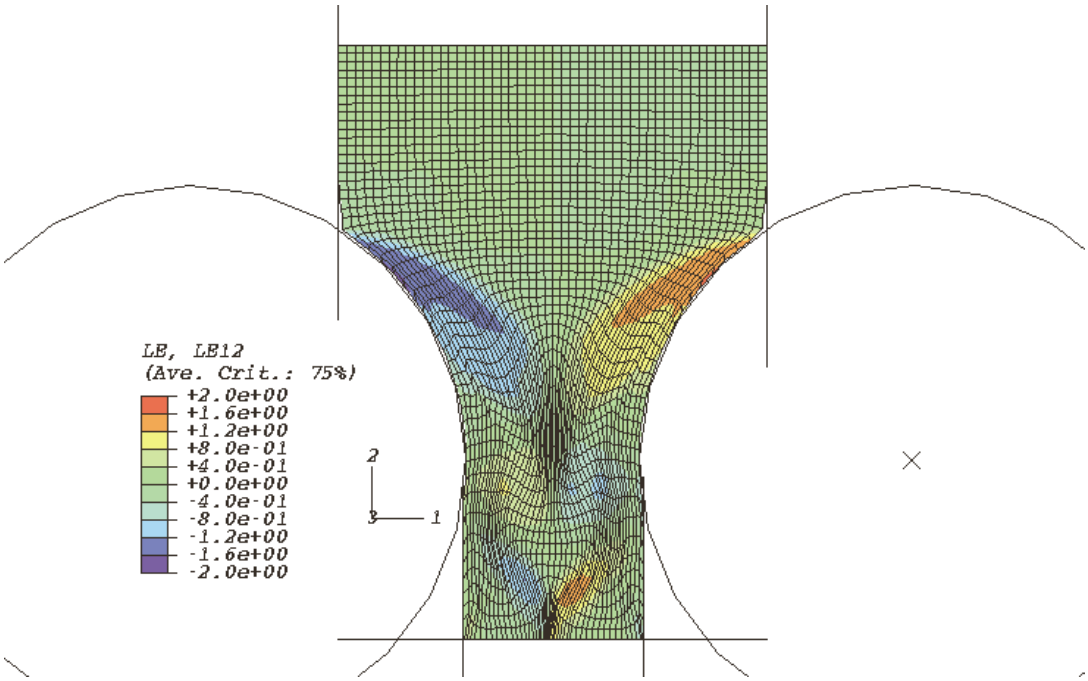

Figure 9.36. Predicted shear strain for aligned top pressure feeder roll and underfeed roll of the Victoria Mill B1 pressure feeder.

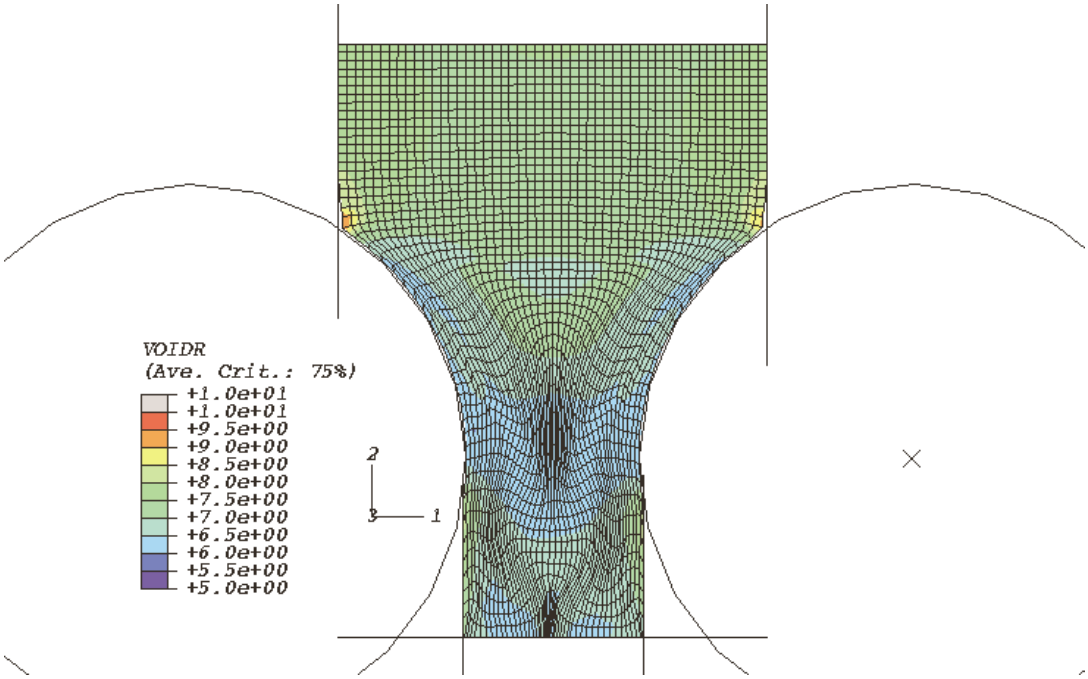

Figure 9.37. Predicted void ratio for aligned top pressure feeder roll and underfeed roll of the Victoria Mill B1 pressure feeder.

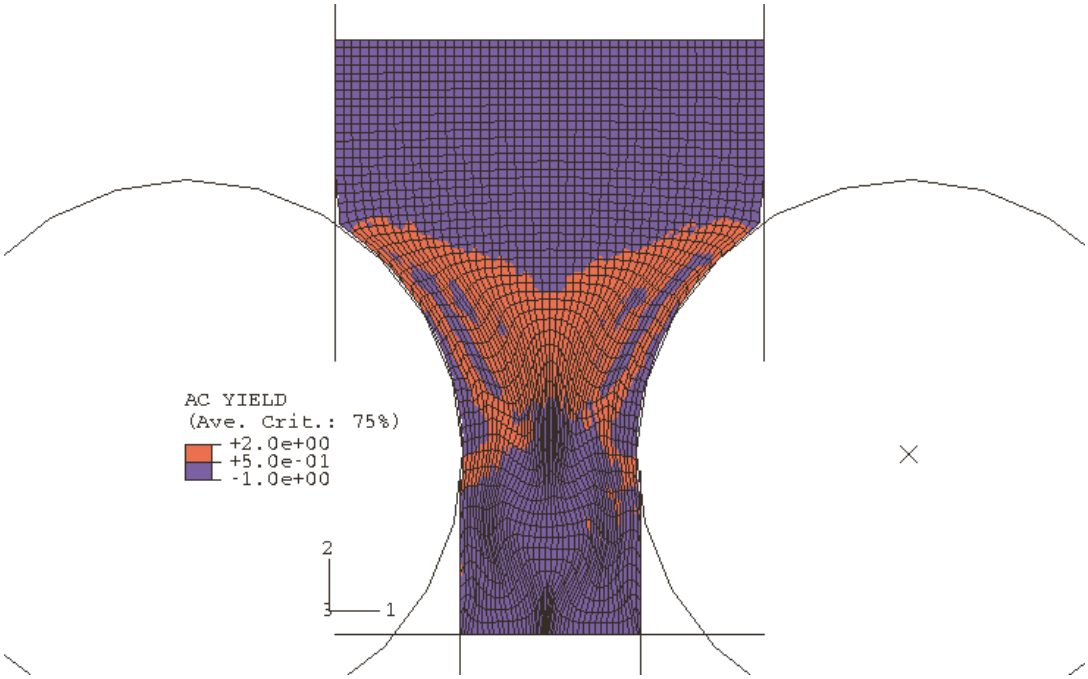

Figure 9.38. Predicted points where the material is yielding for aligned top pressure feeder roll and underfeed roll of the Victoria Mill B1 pressure feeder.

9.5 Summary of Chapter 9

A ‘first look’ has been carried out at modelling the first part of a milling unit, which is the pressure feeder. The modelling was carried out with input material parameters close to those measured for the bagasse using a direct shear test.

A simple theory described in the literature was used in combination with the direct shear test measurements to predict roll torques for a pressure feeder. The magnitudes of the roll torque predictions spanned those that had been measured, being different by a maximum of approximately 28%. The results give some confidence that similar calculations can be used to link laboratory measurements to milling situations.

Multi-element simulations of a pressure feeder were carried out. Initially an attempt was made to use a material model, modification 1 of Yu (1998), which had previously been shown to achieve better reproduction of bagasse behaviour. This material model was implemented as subroutines into a commercial finite element package and its predictions were checked against measured direct shear test data. However, it was subsequently found that the subroutine was not robust enough to achieve convergence during modelling of a pressure feeder.

Two other material models, already available in the finite element package, were previously shown, with particular parameters, to achieve improved reproduction of bagasse behaviour, although not quite as good as the predictions with the modification 1 of Yu’s (1998) model. Those two material models were used to predict stresses and strains experienced by bagasse in a pressure feeder and to predict overall forces. The results indicated that, during the crushing process, large compression and shear stresses and strains are experienced by the bagasse.

Importantly, these simulations showed that converged solutions of bagasse feeding through a pressure feeder could be obtained while using the MCC and DPC models and values of M close to 1.0 (which for the previous eight years had been claimed to be not possible).

The exercise identified that the predictions at the pressure feeder nip were not adequate and require improvement. The predicted pressure feeder roll torque values

(with a modelled pressure feeder nip) were significantly smaller (about 20%) than the measured values. The predicted pressures and shear stresses at the pressure feeder nip were much lower than expected. The reasons for the major discrepancies are not known, but could be due to the material model not being adequate at these higher pressures, or the simplifications made initially (such as assuming a constant λ).

Measured values for the underfeed roll were not available. The multi-element predictions were compared against the previous predictions from the simple model (for the three roll pressure feeder, those torque predictions compared to measurements were out by a maximum of only 28%). The multi-element torque predictions for the underfeed roll were 38% to 64% of those predicted using the simple method (the maximum possible torques where maximum shear stresses are developed throughout all the bagasse mat, this is not likely to happen in reality). The multi-element torque predictions for the underfeed roll were therefore quite realistic.

Some techniques were described with which to carry out future investigations to improve mill designs. As stated previously, modelling the pressure feeder was carried out as a first look into mill modelling using direct shear test results, to show that mill modelling solutions could be obtained using measured material parameters such as an M value of 1.1. Some extrapolation of the input data was carried out, and the available experimental data with which to verify the predictions was very limited. It is emphasised that the results of the computer predictions described should be verified with more extensive (and carried out with better defined input data) simulations (and checked against far more adequate experimental data) before making any practical judgements. This chapter provides an initial link between laboratory measurements and modelling the factory crushing process, as a platform to be used in better understanding and improving the milling process.

10 Chapter 10 – Summary, conclusions and recommendations

10.1 Summary and conclusions

Chapter 1 gave a brief introduction to the Australian cane sugar industry and its continuing need to reduce costs in order to maintain its financial viability. One avenue to achieve improvements is through computer modelling, which has resulted in major savings in several factory processes. The milling process is one area where significant work has been carried out, but progress in developing a suitable computer model has been limited. Chapter 1 gave a description of the investigations and the factors affecting the development of a model. One important factor was identified as being the lack of high quality experimental data of the mechanical behaviour of the cane material (prepared cane and bagasse) and the resulting poor understanding of the behaviour. The aims for the investigation were detailed as being the improved measurement of bagasse behaviour, the determination of material parameters and the development of a better model to reproduce the mechanical behaviour of bagasse. Previous work strongly indicated that a promising avenue to achieve these aims was through adopting and modifying soil tests and models for application to the milling process.

In Chapter 2 the description of literature searches carried out over the duration of the project was given, involving several related but distinct topics. A search for materials similar to bagasse was carried out. The material that most resembled bagasse was found to be peat soils referred to as Radforth and Sphagnum peats, which have a negligible content of mineral matter and consist mainly of organic fibrous particles such as stems and leaves. A review of available experimental test methods identified (or confirmed) three tests from soil mechanics that may result in improved measurements of bagasse mechanical behaviour. The tests were a direct shear test, a triaxial test, and a biaxial test. Interestingly, some of the first two types of tests had been carried out on peat with very similar problems to those encountered when testing bagasse. The literature also suggested variations of the tests that may result in improved results for bagasse. Finally, a review of available material models was carried out. It was found that most of the promising models (for modelling bagasse) originated in the soil mechanics literature. The discussion

of the model features was continued through the following chapters, particularly Chapter 7 and Chapter 8.

Chapter 3 described preliminary direct shear tests on bagasse with a progression of improved test procedures, geometries and equipment. These preliminary tests showed that bagasse exhibited critical state behaviour similar to that of soils.

Chapter 4 described direct shear tests carried out on prepared cane, first bagasse, and final bagasse at pressures occurring in the first part of a milling unit, which is the pressure feeder. The pressures ranged from 200 kPa to 2000 kPa. The direct shear tests were carried out with a modified geometry determined in the previous chapter that was significantly different from the classical split box geometry usually used in soil testing. The analysis of the results showed that the compression, shear, and volume behaviour of the three materials is very similar to that of a soil (sand or clay) despite their much higher moisture content and lower stiffness. As noted in the results of the previous chapter, it was critical state behaviour. The magnitudes of the material parameters required for a critical state model were determined by interpretation of the test results (within some limitations, since the direct shear test does not measure the full state of stress in a sample). It was also noted that the variation in the magnitudes of material parameters in loading situations where shearing is parallel to the direction of compression is still to be determined.

Shown in Chapter 5 are the results of a numerical modelling exercise of the loading steps in a direct shear test using an existing Modified Cam Clay material model. The predictions were compared against a set of measured results from the previous chapter. With reference to the description of a critical state model, it was shown that a single element model could be used to reproduce compression along the normal compression line, compression when unloading and re-loading along the elastic unloading-reloading line, and shearing of a normally consolidated bagasse sample. However, a multi-element model was required to predict the shearing behaviour of a highly over-consolidated (for example, an over-consolidation ratio of 5.0) bagasse sample, since the deformations were not uniform throughout the sample. The findings were in agreement with previous conclusions in the soil mechanics literature.

Material parameters were also determined by using the experimental results from a single direct shear test in combination with a single element Modified Cam Clay model and a parameter estimation package. There was good agreement with the magnitudes of the material parameters obtained in the previous chapter simply by inspection of the test results. The analysis also showed which material parameters could be confidently determined from each of the loading steps in a direct shear test: lambda (λ, the slope of the normal compression line) from compression, kappa (κ, the slope of the elastic line) from unloading (or reloading), and the slope of the critical state line (M) and Young's Modulus (E) from shearing. The loading steps are analogous to those that occur during the crushing of cane.

Chapter 5 also showed that material models that were being used for milling simulations at the time of this investigation could not with a single set of parameter values successfully model all the loading and unloading conditions relevant to milling. The Modified Cam Clay and Drucker-Prager Cap models can predict compression loading well by using particular combinations of parameter values but the predictions of unloading behaviour, shear behaviour and the change in volume due to shear are poor. This is likely to result in poor predictions when modelling the whole mill, which involves complex loading conditions. It was concluded that, for these circumstances, a material model was required which would model different loading conditions using the same experimentally measured material parameters.

In Chapter 6, an assessment of the modified direct shear test geometry was made using multi-element simulations. It was found that the modified geometry results in less uniform behaviour in the bagasse sample, compared to the classical split box geometry. However, the modified geometry was concluded to be adequate for measuring bagasse behaviour, with the measurements being different to those from the split box by about 15%. The simulations showed that both the coarse mesh and fine mesh used for the simulations were adequate for modelling the shear behaviour of normally consolidated bagasse in a direct shear box. The fine mesh was considered to be adequate for modelling the overall behaviour of over-consolidated bagasse. However, even the fine mesh may not be adequate to simulate the detail of

the behaviour of over-consolidated bagasse, since thin localised shear planes were predicted to form.

For both geometries, the role and importance of the roughness on the top and bottom plates contacting the bagasse was emphasised. The coefficient of friction required as a boundary input in order to prevent slip of normally consolidated bagasse at the top and bottom surfaces was at least 0.6. For the heavily over-consolidated bagasse sample the value was at least 1.1. These values are in good agreement with the measured values of the internal coefficient of shear and this agreement is encouraging. Comparison of measurements and predictions have shown that the Modified Cam Clay model (or a further modification of it), in combination with an adequately finely meshed shear box, has a good chance of predicting the shear behaviour of over-consolidated bagasse. Chapter 5 had already shown that there was a good chance of modelling the shear behaviour of normally consolidated bagasse, but that there were major limitations in modelling the shear behaviour in combination with loading and unloading compression behaviour when using the Modified Cam Clay or similar critical state models.

A further conclusion from Chapter 6 was that, even though the modified direct shear test geometry was judged to be adequate for testing bagasse, the classical split box geometry should at least be tried in any further experimental tests (while including the enhancements such as the testing procedure, the rough P24 sandpaper on the top and bottom surfaces contacting the bagasse, and the juice pressure measurement at the bottom surface).

Following the availability of some additional funding, further direct shear tests were carried out on prepared cane, first bagasse, and final bagasse from two sugar factories. The tests were carried out at vertical pressures ranging from 1500 kPa to 16000 kPa, with the highest pressures being close to those that occur at the delivery nip, which is the highest pressure location in a milling unit. The results of these tests were reported in Chapter 7. It was found that the behaviour at the much higher pressures was similar to the behaviour at pressures occurring in the pressure feeder unit. It is critical state behaviour similar to that of soil. The magnitudes of material parameters were estimated from the test data and it was shown that there are marked

differences in the magnitudes of the parameters across the range of pressures that occur in the milling process. The values of these parameters are of use in improving the understanding of bagasse behaviour, in the identification of a material model that can reproduce bagasse mechanical behaviour well, and as inputs for computer modelling of the milling process. A significant finding was that the suppression of dilatancy that occurs in soil due to an increase in effective normal stress also occurs in bagasse. The understanding of dilatancy has played a major role in soil mechanics and a similar understanding (to be obtained through consultation with soil researchers and further work) has significant potential for achieving improvements in the cane crushing process.

Plots of shear stress versus effective vertical pressure for prepared cane, first bagasse and final bagasse, have shown that for all three materials, the friction angle reduces significantly with increasing pressure. Values spanning most of the pressure range in milling have been presented. The magnitudes of the coefficient of shear for the three materials are quite similar and are of use as coefficients of friction for feeding calculations and as boundary condition inputs to a milling model. Values of coefficients of shear for over-consolidated prepared cane and bagasse suggest that, at least at relatively low pressures, the coefficient of shear of bagasse may be stress-history dependent. That is, bagasse that has been previously loaded to a higher pressure than its current state (over-consolidated) may exhibit a higher coefficient of shear than bagasse that has simply been compressed to the same pressure (the implication being that it will feed better). Over-consolidation is expected to occur after the underfeed nip, the pressure feeder nip, the feed nip, and the delivery nip. The over-consolidated bagasse may then achieve a high coefficient of friction when the bagasse contacts the arced surface on the next roll pair and therefore feed better and/or at a larger contact angle. Ideally, for relatively low pressures, the findings of the effect of stress-history dependence should be confirmed by testing both normally consolidated samples and over-consolidated samples at the same pressures in the same test series.

A small number of tests was carried out on different cane varieties in the Mackay region and indicated (with the proviso that there were only 16 tests) good reproducibility and differentiation between cane varieties. These results provide an

avenue for improved measurement and comparison of the mechanical parameters of different cane varieties. The conclusions need to be confirmed by a more extensive testing program.

Chapter 8 focussed on moving part of the way towards a material model that can reproduce bagasse mechanical behaviour well. The features desirable in such a material model in order to reproduce the behaviour of the solid skeleton (the fibre) were described. A multi-element model in the finite element package ABAQUS, using an associated Modified Cam Clay model with a β extension and using porous elasticity, was exercised for five loading conditions on final bagasse at pressure feeder compactions. It was shown to achieve improved reproductions of loading and unloading conditions relevant to milling compared to previously tested models, while using a set of material parameters that better reflected the magnitudes of measured material parameters of bagasse.

A material model with its origins in the soil mechanics literature and having extra features compared to those of the Modified Cam Clay model, with a β extension, was described. That model is the Clay and Sand Model (CASM) by Yu (1998). A modification of that model (modification 1 of Yu, 1998) was shown to achieve a further improved reproduction of loading and unloading conditions relevant to milling, while using a set of consistent parameters (i.e. K_o) that better reflected the magnitudes of measured material parameters of bagasse. The decrease in volume during shearing of a normally consolidated final bagasse sample is still not predicted well and that deficiency should be investigated further. The improvements achieved in reproducing bagasse behaviour were enough to justify the implementation of the modification 1 of Yu (1998) material model into a commercial finite element package, and to test its performance in modelling parts of a milling unit (for example, the pressure feeder).

It is emphasised that there are many other models in the soil mechanics literature with similar features to that of Yu (1998), although many may not be as simple to use, and there are models with different characteristics that may be useful for bagasse modelling. The Yu (1998) model and the variation selected form a platform to work towards a material model that reproduces bagasse behaviour

adequately. It is stressed that there is much behaviour that has not been measured (such as the shear behaviour parallel to the direction of compression, as well as adequate triaxial tests) which almost certainly would have a bearing on the makeup of a material model for bagasse. The effect of whether the presence of fibres in bagasse imposes a structure has not been addressed. It is only recently that attempts have been carried out to include the effects of structure in mechanical models for natural soils (that is, not reconstituted soil). By extension, one area of future research would be determining whether some of these newer soil models are appropriate for bagasse.

Chapter 9 described a 'first look' at modelling the first part of a milling unit, which is the pressure feeder. It is believed important to emphasise that the modelling has been carried out with input material parameters for bagasse that have been measured. It is also noted that the available actual milling unit experimental data with which to verify the predictions was very limited.

A simple theory described in the literature was used in combination with direct shear test measurements to predict roll torques for a pressure feeder. The magnitudes of the roll torque predictions spanned those that had been measured, being different by a maximum of approximately 28%. The results gave some confidence that similar calculations can be used to link laboratory measurements to milling situations.

Multi-element simulations of a pressure feeder were carried out. Initially, an attempt was made to use a material model, modification 1 of Yu (1998), which had been shown in Chapter 8 to achieve better reproduction of bagasse behaviour. This material model was implemented as subroutines into a commercial finite element package and its predictions were checked against measured direct shear test data. However, it was subsequently found that the subroutine was not robust enough to achieve convergence during modelling of a pressure feeder. Further work is warranted, with the assistance of the suppliers of the commercial finite element package, to enable the implementation of the model to the robust level of the already available materials models.

Two other material models, already available in the finite element package, had also been shown, with particular parameters, to achieve improved reproduction of bagasse behaviour, although not quite as good as the predictions with the modification 1 of Yu (1998) model. Those two material models were used to predict stresses and strains experienced by bagasse in a pressure feeder and to predict overall forces. The results indicated that, during the crushing process, large compression and shear stresses and strains are experienced by the bagasse. Importantly, these simulations showed that converged solutions of bagasse feeding through a pressure feeder could be obtained while using the MCC and DPC models and values of M close to 1.0 (which for the previous eight years had been claimed to be not possible).

The exercise identified that the predictions at the pressure feeder nip were not adequate and required improvement. The predicted pressure feeder roll torque values (with a modelled pressure feeder nip) were significantly smaller (about 20%) than the measured values. The predicted pressures and shear stresses at the pressure feeder nip were much lower than expected. The reasons for the major discrepancies are not known, but could be due to the material model not being adequate at these higher pressures, or the simplifications made initially (such as assuming a constant λ).

Measured values for the underfeed roll were not available. The multi-element predictions were compared against the previous predictions from the simple model (for the three roll pressure feeder, those torque predictions compared to measurements were out by a maximum of only 28%). The multi-element torque predictions for the underfeed roll were 38% to 64% of those predicted using the simple method (the maximum possible torques where maximum shear stresses are developed throughout the bagasse mat, which is not likely to happen in reality). The multi-element torque predictions for the underfeed roll were therefore quite realistic.

Some techniques were described with which to carry out future investigations to improve mill designs. The chapter provides a link between laboratory measurements of the mechanical behaviour of bagasse and modelling the factory

crushing process, as a platform to be used towards understanding and improving the milling process. It is emphasised that the results of the computer predictions described should be verified with more extensive (and carried out with better defined input data) simulations (and checked against far more adequate experimental data) before making any practical judgements. As stated previously, modelling the pressure feeder was carried out as a first look into mill modelling using measured direct shear test results. There is a strong possibility that the predictions can be improved by better modelling techniques (by further consultation with the suppliers of the modelling package), and by removing some of the simplifications that were adopted in order to carry out the initial modelling.

10.2 Recommendations

10.2.1 Experimental tests

The mechanical behaviour of prepared cane, first bagasse, and final bagasse is believed to be anisotropic. This investigation has not made any attempt to measure anisotropy. The experimental tests carried out in this investigation were direct shear tests where the direction of shear was perpendicular to the direction of compression of the sample. It has been noted that some fibres in bagasse become oriented perpendicular to the direction of compression. The effect of load and fibre orientation has not been considered. In order to determine the effect on material behaviour, on the magnitudes of material parameters, and on a material model for bagasse, the following tests could be carried out:

1. The sample in a direct shear test can be initially compressed then rotated 90°, recompressed, and sheared. Special sample preparation equipment would need to be built for this purpose. The results would provide a comparison between the two orientation extremes. The fibres could also be deliberately aligned in the direct shear test box.

2. Triaxial tests can be carried out, again with special sample preparation equipment to provide different sample orientations. Although previous attempts at this have had significant problems, it has been noted in Chapter 2 that at least on one occasion quite promising undrained triaxial tests were carried out on peat, a

material similar to bagasse. With this knowledge, and the experience obtained from the direct shear tests, greater success is expected.

3. Biaxial tests, again with special sample preparation and orientation equipment, which were carried out on peat.

Triaxial tests and biaxial tests could also be used to define the yield surface and the potential surface, and therefore provide further information with which to develop a bagasse critical state model.

The following investigations could be carried out with existing procedures and equipment:

1. For relatively low pressures, the effect of stress-history dependence on the coefficient of shear (and therefore on the coefficient of friction on a roll surface) should be confirmed by testing both normally consolidated samples and over-consolidated samples at the same pressures in the same test series.

2. A more extensive set of tests for improved measurement and comparison of the mechanical parameters of different cane varieties, and for determining how to obtain magnitudes of material parameters for mill modelling from only a few tests on each variety should be conducted.

3. A high quality normal compression line could be measured at pressures above 2000 kPa by carrying out relatively slow constant speed compression tests (but not too slow that creep becomes a factor. These tests should be very easy to carry out using computer control (some press machines already have that capability). This could be done particularly for first and final bagasse.

The need for detailed mill operating data (particularly individual roll loads and torques, as well as operating conditions such as speed and throughput) has been noted in order to verify and improve model predictions. The availability of such data is quite limited. It is desirable for testing a material model that the effect of juice flow (permeability) be largely removed in experimental tests. The importance of the measurement of effective stress has been shown in this investigation for laboratory direct shear tests but applies just as much to experiments in a milling

unit. It is also desirable that, at least initially, the effect of roll grooves be removed. It is believed that the following would provide valuable data for validation of model predictions:

1. Tests carried out in a two-roll mill where the rolls are flat (no grooves) and where the roll surface resembles P24 sandpaper. A surface with 1 mm diameter tungsten carbide particles would be adequate. The use of final bagasse as the test material would prevent the development of any large juice pressures. There are several two-roll mills available on which the tests could be done.

2. There are now quite a few pressure feeders in the Australian sugar industry where the rolls are individually driven by hydraulic motors, which allow the individual measurement of torque. It is believed that the addition of load cells to measure loads is not an onerous task and the measurement of both loads and torques would add significantly to validation data.

10.2.2 Improved material model for bagasse

Further work is warranted to enable the implementation of the Modification 1 of Yu's (1998) model into a commercial finite element package to a robust level similar to that of already available material models. This would provide a material model able to achieve a further improvement of the reproduction of the already measured bagasse behaviour. It also has the advantage of being able to closely reproduce the 'extended' Modified Cam Clay model (in order to compare and check predictions), as well as quite easily being able to change to a non-associated material model. Some evidence has been provided that a non-associated material model may be more appropriate for bagasse, such as the significantly different values of friction angle and dilatancy angle at particular pressures. Also, the poor prediction of the change in volume during shearing hints at the need for a non-associated model (but may also be due to an unknown deficiency). The implementation of the modification 1 of Yu's (1998) model would be a further step towards a more adequate material model, taking into account that there are many other models in the soil mechanics literature (many have been noted in Chapter 2) that should be closely scrutinised in any future material model development.

The dilatancy data obtained should be examined further and, if possible (there are limitations in that the data are from direct shear tests) tested to see whether they fit existing stress-dilatancy relations.

10.2.3 Improved modelling of the pressure feeder

There is a strong possibility that the pressure feeder predictions reported can be improved by better modelling techniques, and by removing some of the simplifications that were adopted in order to carry out the initial modelling, while using the currently available material models in the commercial modelling package. Adaptive remeshing may be required to overcome some of the problems associated with the large deformations.

11 Published technical papers

The following technical papers were published during the period of the candidature:

Plaza, F., Harris, H.D., and Kirby, J.M. (2000). A soil called bagasse. Proc. Aust. Soc. Sugar Cane Technol., 22: 429-435.

Plaza, F., Harris, H.D., and Kirby, J.M. (2001). Modelling the compression, shear, and volume behaviour of final bagasse. Proc. Aust. Soc. Sugar Cane Technol., 23: 428-436.

Plaza, F., Kirby, J.M., Langens, L.M., and Harris, H.D. (2002). Towards a material model for bagasse. Proc. Aust. Soc. Sugar Cane Technol., 24: 330-338.

Plaza, F., Langens, L.M., Kirby, J.M., and Harris, H.D. (2002). The effect of pressure and over-consolidation on the grip of the roll surface on prepared cane and bagasse. Proc. Aust. Soc. Sugar Cane Technol., 24: 367-373.

Plaza, F. and Langens, L.M. (2002). Some direct shear test results on cane varieties in the Mackay Region. Proc. Aust. Soc. Sugar Cane Technol., 24: 491. Poster paper.

Plaza, F., Langens, L.M., Kirby, J.M., and Harris, H.D. (2002). Measurements of bagasse behaviour at delivery nip compactions in a rolling mill – Final Report. Sugar Research and Development Corporation Project No. SRI 116. Research Institute Technical Report 2/02.

Plaza, F. (2003). Pressure feeder torque predictions using conventional milling theory and direct shear test data. Proc. Aust. Soc. Sugar Cane Technol., 25.

Plaza, F. (2003). Finite element modelling of a pressure feeder using direct shear test measurements. Proc. Aust. Soc. Sugar Cane Technol., 25.

Plaza, F., Kirby, J.M., and Harris, H.D. (2003). Modelling sugar cane bagasse behaviour in a modified direct shear test using an elastic-plastic critical state model. Proceedings of the ABAQUS Users Conference, Munich.

12 References

Adam, C.J. (1997). Application of computational porous media mechanics to the rolling of prepared sugar cane. PhD Thesis, James Cook University of North Queensland.

Adam, C.J., and Loughran, J.G., (1998). Application of computational mechanics to rolling of a saturated porous material. Simulation of Materials Processing: Theory, Methods and Applications, Huetink & Baaijens (eds), (Proc. NUMIFORM '98 Conf.) 503-508. Balkema, Rotterdam.

Adam, C.J., Loughran, J.G., and Owen, D.R.J. (1997a). Development of a computational tool for simulation of the rolling of prepared sugar cane. World Congress: Manufacturing Technology Towards 2000, Cairns, Australia, Sept. 1997, 271-280.

Adam, C.J., Loughran, J.G., and Owen, D.R.J. (1997b). Large strain analysis of a porous elasto-plastic material. Proc. Second Symposium on Computational Mechanics, Sydney, Australia. 2: 1-10.

Adams, J.I. (1961). Laboratory compression tests on peat. In Proceedings, 7th Muskeg research conference, NRC of Canada, Tech Memo No. 71, Ottawa, 36-54.

Adams, J.I. (1965). The engineering behaviour of a Canadian muskeg. In Proceedings, 6th International conference on soil mechanics and foundation engineering, Vol 1, University of Toronto Press, 3-7.

Atkinson, J.H., and Bransby, P.L. (1978). The mechanics of soils – An introduction to critical state soil mechanics. McGraw-Hill, London.

Anon., (1991). Laboratory manual for Australian sugar mills. Volume 2, BSES, Brisbane, Australia.

Been, K., and Jefferies, M.G. (1993). Towards systematic CPT interpretation. Predictive Soil Mechanics. Wroth Memorial Symposium. Thomas Telford, London, 121-134.

Bernhardt, H.W. (1995). A study of the phenomenon of bridging of sugar cane bagasse. PhD. Thesis, University of Natal.

Bishop, A.W. (1972). Shear strength parameters for undisturbed and remoulded soil specimens. In Stress-strain behaviour of soils, Roscoe Memorial Symp., Foulis, 3-58.

Bouazza, A. and Djafer-Khodja, S. (1994). Friction characteristics of a nonwoven geotextile and peat. Geotextiles and Geomembranes 13: 807-812.

Boulanger, R.W, Arulnathan, R., Harder Jr, L.F., Torres, R.A., and Driller, MW. (1998). Dynamic properties of Sherman Island peat. Journal of Geotechnical and Geoenvironmental engineering, pp12-20.

Brandt, J., and Nilsson, L. (1999). A constitutive model for compaction of granular media, with account for deformation induced anisotropy. Mechanics of cohesive-frictional materials, Vol 4, issue 4, 391-418.

Brinkgreve, R.B.J., Vermeer, P.A., and Vos, E. (1994). Constitutive aspects of an embankment widening project. In Proceedings, Advances in Understanding and Modelling the Mechanical Behaviour of Peat, den Haan, Termaat and Edil (eds), Balkema, Rotterdam, 143-158.

Britto, A.M. and Gunn, M.J. (1987). Critical state soil mechanics via finite elements. Ellis Horwood Limited.

Butterfield, R. (1979). A natural compression law for soils (an advance on e- log p'). Geotechnique, 29:469-480.

Carter, J.P. (2003). Private communication - assessment of PhD Thesis.

Casagrande, A., and Carillo, N. (1944). Shear failure of anisotropic material. Contributions to Soil Mechanics, Boston Society of Civil Engineers, pp. 122-135.

Craig, R.F. (1987). Soil Mechanics. Van Nostrand Reinhold (UK) CO. Ltd.

Crawford, W.R. (1955). Mill feeding – the basic factor in efficient cane milling, Proc. Qd. Soc. Sugar Cane Technol., 22:167-179.

Cullen, R.N. (1965). An investigation of the shear strength of bagasse. M. Eng. Sc. Thesis, University of Queensland, Australia.

Davies, M.C.R., and Newson, T.A. (1992). A critical state constitutive model for anisotropic soil. In G.T. Houlsby and A.N. Schofield (eds) Predictive Soil Mechanics. Proceedings of the Wroth Memorial Symposium, St Catherine's College, Oxford, 27-29 July, 219-229.

De Campos, T.M.P., and Carrillo, C.W. (1995). Direct shear testing on an unsaturated soil from Rio de Janeiro. Proc. 1st Int. Conf. Unsaturated Soils, Paris, 31-38.

Desai, C.S. and Siriwardane, H.J. (1984). Constitutive Laws for Engineering Materials with emphasis on geologic materials. Prentice-Hall Inc.

de Souza Neto, E.A., Zhao, S.Y., Owen, D.R.J., Peric, D., and Loughran, J.G. (1997). Finite element simulation of the rolling and extrusion of multi-phase materials. Computational Plasticity Fundamentals and Applications. Proc. Fifth Int. Conf. On Computational Plasticity, Barcelona, 1997, Part 2, pp. 1296-1304.

Dixon, T.F. and Plaza, F. (1995). Prediction of erosion in the convection tube banks of boilers. Proc. Aust. Soc. Sugar Cane Technol., 17: 307-324.

Downing, C.M. (1999). Investigation of the effects of soil contamination on the crushing of comminuted sugar cane. PhD Thesis, James Cook University of North Queensland.

Downing, C.M., Loughran, J.G., and Domanti, S.A. (1999a). Crushing soil contaminated sugar cane. Proc. Aust. Soc. Sugar Cane Technol., 21: 294-300.

Downing, C.M., Loughran, J.G., and Domanti, S.A. (1999b). Parameter estimation for highly deformable porous media. APCOM99, 4th Asian Pacific Conf. Computational Mechanics, 15-17 Dec 1999, Singapore.

Edwards, B.P., Kent, G.A. and Garson, C.A. (1995). An evaluation of the "Swansea" finite element model of cane crushing. Sugar Research Institute Internal Report.

Ekwue, E.I. (1990). Organic-matter effects on soil strength properties. Soil and Tillage Research, 16: 289-297.

Farrel, E.R., and Hebib, S. (1998). The determination of the geotechnical parameters of organic soils. Proceedings of the international symposium on problematic soils. Yanagisawa, Moroto & Mitachi (eds), Balkema, Rotterdam, 33-36.

Fry, J. (1996). A global perspective of the sugar industry, in Intensive sugarcane production: meeting the challenges beyond 2000, eds B.A. Keating & J.R. Wilson, CAB International, pp. 1-16.

Gajo, A., and Muir Wood, D. (1999a). A kinematic hardening constitutive model for sands: the multiaxial formulation. Int. J. Numer. Anal. Meth. Geomech., 23, 925-965.

Gajo, A., and Muir Wood, D. (1999b). Severn-Trent sand: a kinematic-hardening constitutive model: the q-p formulation. Geotechnique, 49, No. 5, 595-614.

Galvin, L.F. (1976). Physical properties of Irish Peats. Irish Journal of Agricultural Research, Vol 15, no.2: 207-221.

Garson, C.A. (1992a). Computer simulation of cane crushing between a pair of rolls. Final report submitted to the Sugar Research and Development Corporation as part of Grant SRI11S.

Garson, C.A. (1992b). 'Computer simulation of cane crushing between a pair of rolls'. Sugar Research Internal Report No. 13/92.

Hanrahan, E.T., Dunne, J.M., and Sodha, V.G. (1967). Shear strength of peat. In Proceedings, Geotechnical Conference, Oslo, Vol. I, 193-198.

Harris, H.D. (1998). Private communication.

Head, K.H. (1994). Manual of soil laboratory testing: Permeability, Shear Strength and Compressibility Tests. 2nd edition, Pentech Press, London.

Henkel, D.J. (1960). The shear strength of saturated remoulded clay. In Proceeedings of Research Conference on Shear Strength of Cohesive Soils. Boulder, Colorado, pp. 533-540.

Heshmati, A.A. (2000). Numerical simulation of properties of peat. PhD Thesis, University of Manchester Institute of Science and Technology (UMIST), United Kingdom.

Hibbitt, Karlsson, and Sorensen (2001). Abaqus: Standard user's manual, version 6.2. Hibbitt, Karlsson and Sorensen, Pawtucket, USA.

Houlsby, G.T., and Sharma, R.S. (1999). A conceptual model for the yielding and consolidation of clays. Geotechnique 49, No. 4, 491-501.

Jaeger, J. (1962). Elasticity, Fracture and Flow. 2nd edn. Methuen. London.

Jewell, R.A., and Wroth, C.P. (1987). Direct shear tests on reinforced sand. Geotechnique 37, No. 1, 53-68.

Kabirul, M.I. (1999). Constitutive models for carbonate sand and their application to footing problems. PhD Thesis, The University of Sydney, Australia.

Kent, G.A. (2001). Estimating material parameters for a critical state model from a uniaxial compression test. In Computational mechanics: New frontiers for the new millennium, eds S. Valliappan & N. Khalili, Elsevier Science Ltd, Oxford, United Kingdom, vol. 2, pp.1141-6.

Kent, G.A., and McKenzie, N.J. (2000). A laboratory investigation into feeding a pair of rolls. Sugar Research Institute Syndicated Project Report 1/00.

Kent, G.A., Schembri, M. and Watters, A.M. (1998). Validation of Zhao's cane crushing model solver 'elfeno'. Sugar Research Institute Internal Report.

Kirby, J.M. (1991). Strength and deformation of agricultural soil: measurement and practical significance. Soil Use and Management, 7 (4): 223-229.

Kirby, J.M. (1994). Simulating soil deformation using a critical-state model: I. laboratory tests. European Journal of Soil Science 45: 239-248.

Kirby, J.M. (1997). Can critical state models be used to analyse deformations of crushed cane? CSIRO Land and Water Report to Sugar Research Institute.

Kirby, J.M. (1998a). Private communication.

Kirby, J.M. (1998b). Estimating critical state soil mechanics parameters from shear box tests. European Journal of soil science, 49: 503-512.

Kirby, J.M., O'Sullivan, M.F., and Wood, J.T. (1998). Estimating critical state soil mechanics parameters from constant cell volume triaxial tests. European Journal of soil science, 49: 85-93.

Krieg, S., and Goldscheider, M. (1994). Some results concerning the development of K_o during one-dimensional creep of peat. Advances in understanding and modelling the mechanical behaviour of peat, den Haan, Termaat & Edil (eds), Balkema, Rotterdam, 71-75.

Kroes, S. (1999). Enhanced roll life. Proc. Aust. Soc. Sugar Cane Technol., 21:307-312.

Kubo, S. (1988). Inverse problems related to the mechanics and fracture of solids and structures. JSME Int. J., 31: 157-166.

Kumbhojkar, A.S., and Banerjee, P.J. (1993). An anisotropic hardening rule for saturated clays. Int. J. Plast., 9, 861-888.

Landva, A.O., and La Rochelle, P. (1983). Compressibility and shear characteristics of Radforth peats. In P.M. Jarret (ed) Testing of Peats and Organic Soils, pp 157-191, ASTM STP 820, American Society for Testing and Materials.

Leitch, C.J. (1996). An experimental investigation into the constitutive behaviour of prepared sugar cane, M.Eng.Sc. Thesis, James Cook University of North Queensland.

Leitch, C.J., Loughran, J.G. and Adam, C.J. (1997). Constitutive modelling of prepared sugar cane. Final report for project JCU8S, James Cook University.

Lewis, R.W., and Schrefler, B.A. (1987). The finite element method in the deformation and consolidation of porous media. John Wiley and sons, Chichester.

Liu, M.D., and Carter, J.P. (2000). On the volumetric deformation of reconstituted soils. Int. J. Numer. Anal. Meth. Geomech., 24, 101-133.

Loughran, J.G. and Adam, C.J. (1995). Modelling of the rolling of partially saturated highly compressible porous media. ABAQUS World Conference. Paris, France. 549-564.

Loughran, J.G. and Adam, C.J. (1998). Properties of prepared cane for computational crushing models. Proc. Aust. Soc. Sugar Cane Technol. 20:307-312.

Loughran, J.G. and Kannapiran, A. (2002). Finite element modelling of the crushing of prepared cane and bagasse. Proc. Aust. Soc. Sugar Cane Technol. 24:339-346.

Loughran, J.G. and McKenzie, N.J. (1990). An experimental investigation into the compression of prepared cane in a uniaxial test cell with biaxial juice flow. Sugar Research Institute Internal Report No. 1/93.

MacFarlane, I.C. (ed) (1969). Muskeg Engineering Handbook. University of Toronto Press.

MacFarlane, I.C., and Williams, G.P. (1974). Some engineering aspects of peat soils. Histosols: their characteristics, classification and use. SSSA Special Publication (No 6).pp.79-93.

Maniatty, A. and Zabaras, N. (1989). A method for solving inverse elastoviscoplastic problems. J. Eng. Mech. Div. ASCE, 115: 2216-2231.

Manzari, M.T., and Dafalias, Y.F. (1997). A critical state two-surface plasticity model for sands. Geotechnique 47, No. 2, 255-272.

Mehta, R.C., (1984). Numerical solution of nonlinear inverse heat conduction problem with a radiation boundary condition. International Journal for Numerical Methods in Engineering, 20: 1057-1066.

Molenkamp, F. (1994). Investigation of requirements for plane strain element tests on peat. In Proceedings, Advances in Understanding and Modelling the Mechanical Behaviour of Peat, den Haan, Termaat and Edil (eds), Balkema, Rotterdam, 181-202.

Molenkamp, F., Heshmati, A.A., and Lane, P.A. (1996). Analytical and numerical study to justify the application of a composite model to peaty type of soils. Proceedings of the Second Eccomas Conference of the European Community on Computational Methods in Applied Sciences. Numerical methods in engineering 96, Paris, 381- 387.

Muir Wood, D. (1990). Soil Behaviour and Critical State Soil Mechanics. Cambridge University Press.

Murry, C.R. (1960). The mechanics of crushing prepared cane. Ph.D Thesis, University of Queensland, Australia.

Murry, C.R., and Holt, J.E. (1967). The mechanics of crushing sugar cane, Elsevier Publishing Company.

Naylor, D.J. (1985). A continuous plasticity version of the critical state model. Int. J. Num. Meth. Eng, Vol. 21, 1187-1204.

Naylor, D. J., and Pande G.N. (1981). Finite elements in geotechnical engineering. Pineridge Press, Swansea.

Neill, S.W., McKinnon, S., and Garson, C.A. (1996). A library of cane transport and sugar factory images. Sugar Research Institute Internal Report 1/96.

Oka, F., Yashima, A., Tateishi, A., Taguchi, Y., Yamashita, S. (1999). A cyclic elasto-plastic constitutive model for sand considering a plastic-strain dependence of the shear modulus. Geotechnique 49, No. 5, 661-680.

Owen, D.R.J., and Zhao, S.Y. (Circa 1991). Modified model and numerical results of transient analysis. Swansea Research Report No. 5 to Sugar Research Institute.

Owen, D.R.J., Zhao, S.Y., and Loughran, J.G. (1994a). An overview of crushing theory investigations at Swansea. Part 1 – testing a constitutive relation. Proc. Aust. Soc. Sugar Cane Technol., 16: 264-270.

Owen, D.R.J., Zhao, S.Y., and Loughran, J.G. (1994b). An overview of crushing theory investigations at Swansea. Part 2 – modelling of a two roll mill. Proc. Aust. Soc. Sugar Cane Technol., 16: 271-277.

Owen, D.R.J., Zhao, S.Y., and Loughran, J.G. (1995). Application of porous media mechanics to the numerical simulation of the rolling of sugar cane. Engineering Computations, Vol. 12, 281-302.

Owen, D.R.J., de Souza Neto, E.A., Zhao, S.Y., Peric, D, and Loughran, J.G. (1998). Finite element simulation of the rolling and extrusion of multi-phase materials – Application to the rolling of prepared sugar cane. Computer methods in applied mechanics and engineering, 151:479-495.

Pestana, J.M., and Whittle, A.J. (1999). Formulation of a unified constitutive model for clays and sands. Int. J. for Numer. and Anal. Methods in Geomechanics, 23, 1215-1243.

Plaza, F., Kent, G.A., Everitt, P.G., and McKenzie, N.J. (1993). Coefficients of internal shear and surface friction for prepared cane. Sugar Research Institute Technical Report 03/93.

Plaza, F. and Edwards, B.P. (1994). Shear, friction, and the required roll roughness, Proc. Aust. Soc. Sugar Cane Technol., 16:244-247.

Plaza, F. and Kent, G.A. (1997). Using soil shear tests to investigate mill feeding, Proc. Aust. Soc. Sugar Cane Technol., 19:330-340.

Plaza, F. and Kent, G.A. (1998). A soil shear test to investigate feeding at the pressure feeder, Proc. Aust. Soc. Sugar Cane Technol., 20:327-333.

Plaza, F., Dixon, T.F., Dickinson, N.L., Fitzmaurice, A.L., and Owens, M. (1999). Performance of baffled boilers with redesigned convection banks. Proc. Aust. Soc. Sugar Cane Technol., 21:432-437.

Plaza, F., Harris, H.D., and Kirby, J.M. (2001). Modelling the compression, shear, and volume behaviour of final bagasse. Proc. Aust. Soc. Sugar Cane Technol., 23: 428-436.

Plaza, F., Langens, L.M., Kirby, J.M., and Harris, H.D. (2002). The effect of pressure and over-consolidation on the grip of the roll surface on prepared cane and bagasse. Proc. Aust. Soc. Sugar Cane Technol., 24: 367-373.

Popov, E.P. (1978). Mechanics of materials. Prentice-Hall, 2nd ed, New Jersey.

Potts, D.M., Dounias, G.T., and Vaughan, P.R. (1987). Finite element analysis of the direct shear box test. Geotechnique 37, No. 1, 11-23.

Rendulic, L. (1936). Pore-index and pore water pressure. Bauingenieur, 17, 559.

Roscoe, K.H. (1953). An apparatus for the application of simple shear to soil samples. Proc. 3rd Int. Conf. Soil Mech. Fdn Engng, Zurich 1, 186-191.

Roscoe, K.H., Schofield, A.N., and Wroth, C.P. (1958). On the yielding of soils. Geotechnique 8, 22-53.

Rowe, P.W. (1962). The stress dilatancy relation for static equilibrium of an assembly of particles in contact. Proc. R. Soc. A 269, 500-527.

Rowe, P.W. (1969). The relation between the shear strength of sands in triaxial compression, plane strain and direct shear. Geotechnique 19, No. 1, 75-86.

Saliklis, E.P, and Kuskowski, S.J. (1998). Constitutive modelling of paper accounting for rate of load and transient relative humidity effects. Tappi Journal, Vol 81, No 2, 181-188.

Sawyer, J.P.G. (2002). Private communication. Worley.

Sawyer, J.P.G., Jones, R., and McKinlay, P.R. (1996). An experimental description of paper. Journal of composite structures, Elsevier Applied Science, Oxford, 36, 101-112.

Sawyer, J.P.G., Jones, R., and McKinlay, P.R. (1998). A unified constitutive model for paper. Journal of composite structures, Elsevier Applied Science, Oxford, 42, 93-100.

Schembri, M.G., Kirby, J.M. and Kent, G.A. (1998). Describing the mechanical behaviour of prepared cane using critical state theory, Proc. Aust. Soc. Sugar Cane Technol., 20:313-319.

Schofield, A. & Wroth, P. (1968). Critical state soil mechanics. McGraw-Hill Publishing Company.

Schnur, D.S. and Zabaras, N. (1990). Finite element solution of two-dimensional inverse elastic problems using spatial smoothing. International journal for numerical methods in engineering, 33: 2039-2057.

Schreyer, H.L., Zuo, Q.H., and Maji, A.K. (1994). Anisotropic plasticity model for foams and honeycombs. J. Engineering Mechanics, 120 (9): 1913-1930.

Schwartzberg, H.G., Rebouillat, S., Humblot, J., Humblot, D., and Kim, K-H (1996). Analysis of juice expression from apples. Proceedings, 5th World Congress of Chemical Engineering, Vol II, San Diego, California, July 14-18, AIChE, 221-226.

Sellmeijer, J.B. (1994). Anisotropic peat model. In Proceedings, Advances in Understanding and Modelling the Mechanical Behaviour of Peat, den Haan, Termaat and Edil (eds), Balkema, Rotterdam, 211-229.

Seung, R.L., and Seboong, O.H. (1995). An anisotropic hardening constitutive model based on generalized isotropic hardening rule for modelling clay behaviour. Int. J. for Numer. and Anal. Methods in Geomechanics, vol 19, 683-703.

Shibuya, S., Mitachi, T., and Tamate, S. (1997). Interpretation of direct shear box testing of sands as quasi-simple shear. Geotechnique 47, No. 4, 769-790.

Solomon, T.J., and Murry, C.R. (1964). Low pressure feeding in the two roll mill. Proc. Qd. Soc. Sugar Cane Technol., 31:67-72.

Stallebrass, S.E., and Taylor, R.N. (1997). The development and evaluation of a constitutive model for the prediction of ground movements in over-consolidated clay. Geotechnique 47, No 2, 235-253.

Steindl, R.J. (1995). Optimum performance through CFD modelling of clarifier designs. Proc. Aust. Soc. Sugar Cane Technol., 17:207-215.

Steindl, R.J., Fitzmaurice, A.L. and Alman, C.W. (1998). Recent developments in clarifier design. Proc. Aust. Soc. Sugar Cane Technol., 20:477-483.

Termaat, R., and Topolnicki, M. (1994). Biaxial tests with natural and artificial peat. In Proceedings, Advances in Understanding and Modelling the Mechanical Behaviour of Peat, den Haan, Termaat and Edil (eds), Balkema, Rotterdam, 241-251.

Thomas, H.R., and He, Y. (1998). Modelling the behaviour of unsaturated soil using an elastoplastic constitutive model. Geotechnique 48, No. 5, 589-603.

Thun, R. and Rautalin, A. (1985). Applicability of the Jenike theory to the flow of peat. Proceedings – reliable flow of particulate solids. E.I. Conference No 07828.

Toolan, F.E. (1987). The engineering application of direct and simple shear testing. Geotechnique 37, No. 1, 1-2 (Preface).

Topolnicki, M., and Niemunis, A. (1994). Numerical simulation of stress-strain behaviour of peat for biaxial deformations at plane strain. In Proceedings, Advances in Understanding and Modelling the Mechanical Behaviour of Peat, den Haan, Termaat and Edil (eds), Balkema, Rotterdam, 253-266.

Valentin, B.F. (1999). Modelling paper strain in a calender nip. Tappi Journal, Vol 82, No 8, 183-188.

Watermark Numerical Computing (2000). Pest.

Wernick, E. (1977). Comparison and discussion of angles of shearing resistance measured in conventional shear tests and in pullout tests on piles. Proc. 5th Danube Conf. Soil Mech. Fdn Engng, Bratislava.

Williams, D.J. (2003). Private communication - assessment of PhD Thesis.

Williams, L.J., Garson, C.A., and Adam, C.J. (2001). Identification of mill feeding parameters. Proc. Aust. Soc. Sugar Cane Technol., 23: 451-456.

Wroth, C.P. (1987). The behaviour of normally consolidated clay as observed in undrained direct shear tests. Geotechnique 37, No. 1, 37-43.

Wroth, C.P. and Bassett, N. (1965). A stress-strain relationship for the shearing behaviour of sand. Geotechnique 15, No. 1, 32-56.

Xia, Q. S., Boyce, M.C., and Parks, D.M. (2002). A constitutive model for the anisotropic elastic-plastic deformation of paper and paperboard. International Journal of Solids and Structures 39(15), 4053-4071.

Yu, H.S. (1995). A unified constitutive model for clay and sand. Research Report No. 112.08.1995, Department of Civil Engineering and Surveying, University of Newcastle.

Yu, H.S. (1998). CASM: A unified state parameter model for clay and sand. Int. J. Numer. Anal. Meth. Geomech., 22, 621-653.

Zabaras, N. and Ruan, Y. (1989). A deforming finite element method analysis of inverse Stefan problems. International Journal for Numerical Methods in Engineering. 28: 295-313.

Zhao, S.Y. (1993). Finite element solution of saturated-unsaturated porous materials with application to the rolling of prepared sugar cane. PhD Thesis, University of Wales, United Kingdom.